TECTONOSTRATIGRAPHIC EVOLUTION OF THE WILLISTON BASIN

A Thesis Submitted to the College of
Graduate Studies and Research
in Partial Fulfillment of the Requirements
for the Degree of Doctor of Philosophy
in the Department of Geological Sciences
University of Saskatchewan
Saskatoon

By
Pál Rédly
Spring 1998

To Kathleen and Daniel

PERMISSION TO USE

In presenting this thesis in partial fulfilment of the requirements for a Postgraduate degree from the University of Saskatchewan, I agree that the Libraries of this University may make it freely available for inspection. I further agree that permission for copying of this thesis in any manner, in whole or in part, for scholarly purposes may be granted by the professor or professors who supervised my thesis work or, in their absence, by the Head of the Department or the Dean of the College in which my thesis work was done. It is understood that any copying or publication or use of this thesis or parts thereof for financial gain shall not be allowed without my written permission. It is also understood that due recognition shall be given to me and to the University of Saskatchewan in any scholarly use which may be made of any material in my thesis.

Requests for permission to copy or to make other use of material in this thesis in whole or part should be addressed to:

Head of the Department of Geological Sciences
114 Science Place
University of Saskatchewan
Saskatoon, Saskatchewan
CANADA S7N 5E2

ABSTRACT

In the Williston Basin five regional seismic profiles, covering ~3090 km were utilized for a comprehensive study of this complex geologic feature. 2300 km of field data were added to the existing 790 km long profile. The novel seismic information in conjunction with a sizeable number of wireline data and incorporation of stuctural and isopach maps provided a unique data environment for development of a new elaborate tectonostratigraphic model of this major continental depression.

Standard reflection seismic processing procedures were implemented with special emphasis on regional perspectives, including "Earth curvature correction", to generate images of the basin fill. The latter helped to reveal the true nature of this large scale cratonic basin. This novel information permitted new approaches in establishing the deformation styles in the Williston Basin.

Structural studies of the newly reprocessed regional seismic profiles revealed the compressional nature of the radially arranged tectonic elements in the center of the basin, and the extensional character of the peripheral regions. The results suggest that axisymmetric deformation controlled the early stages of the Williston Basin area, and was the causal factor of the oval shape of the basin.

In the first, "pre-Williston" phase, the region was uplifted by an axisymmetric lithospheric intrusion creating radial extensional signatures in the central zone and compressional structures in the surroundings. Erosion and thermal cooling and/or phase change of the mantle material led to the initiation of the basin subsidence.

Consequently, in the "intracratonic phase" (Sauk – Absaroka), the pre-existing radial and circumferentially arranged structures were periodically reactivated in the opposite sense. The active periods were unrelated to global orogenic events of the

continent. The exception is the Kaskaskia I (Devonian) interval, when the territory was tilted to the northwest and the axisymmetric cause of the subsidence was overprinted.

The subsequent "foreland phase" (Zuni – Tejas), was dominated by lateral forces of the Sevier and Laramide orogenies. This plate-margin-related major tectonic development was associated with the NNW-SSE elliptical elongation of the basin and the related highly prevalent NE-SW/NW-SE faulting and fracturing. Additional consequences of this process were offsetting and rotation of the pre-existing radial and circumferential structural features. These radial and circumferential structural features of the Williston Basin may be recognizable in comparable cratonic environments (e.g., Michigan Basin, Paris Basin).

Comprehensive seismic/sequence stratigraphy was developed throughout the basin. In the Sauk–Absaroka interval the sequence stratigraphic and the lithostratigraphic boundaries are generally identical. In the Zuni–Tejas interval, when the clastic sedimentation was dominant, the two subdivisions are not identical. In these younger strata 16 sequence stratigraphic units were identified. More detailed subdivision of the interval containing the Eagle Sandstone revealed that two major sources of the terrigenous sediments are directly recognizable on the seismic profiles, beyond 500 km east of the shorelines.

ACKNOWLEDGEMENTS

I am grateful for the advice and assistance of many people for the planning and preparation of this dissertation. I would like to acknowledge the invaluable guidance of my thesis adviser, Prof. Z. Hajnal, who devoted much time to organizing the collection of the enormous dataset and to providing a fertile research environment.

I am indebted to the other members of my committee. I had the honor to be their lab assistant. Prof. M. Stauffer's classes deepened my interest in structural problems on every scale. Prof. D. Gendzwill was always willing to stop to discuss the latest earthquakes. Dr. B. Pratt, from the "other side" of the geosciences with his colorful paleontological research, constantly reminded me that the "truth is down there".

Sincere thanks are expressed to Dr. B. Pandit for helping me to refine and clarify my model and to Dr. C. Zhu. Thanks are also extended to B. Reilkoff for his constant vigilance over the smooth operation of the computing system, and to Dr. M. Reeves for his assistance with the computers.

I am indebted to geoscientists in various governmental and corporate institutions for providing the fundamental data required in this thesis. Invaluablel contributions were made by Dr. D. Baird (Cornell University/Lawrence University), T. Heck (North Dakota Geological Survey), J. Halvorson (Montana Board of Oil and Gas), Dr. J. Dietrich (Geological Survey of Canada, Calgary) and K. Kreis (Saskatchewan Energy and Mines). Thanks are also extended to numerous colleagues I met at various conferences. Their criticism and our debates helped enormously to sharpen my ideas.

Special thanks are due to my fellow graduate student, B. Németh, who helped to develop some of the computer codes used in the study. Other graduate students, S. Bezdán, B. Benko, W. Gaskin, H. Ferdous, A. Polat, A. Peterhänsel, C. Hooge, etc.,

have provided me with many hours of science and friendship. Their help made the graduate student's life more bearable.

Special thanks are due also to Thomas and Patricia Bowman for proofreading parts of my thesis.

It would be unfair to leave out those colleagues and friends from Hungary who played some role in my coming to Saskatoon. Special thanks to Dr. I. Bérczi (Hungarian Oil Ltd./Hungarian Geological Society), Dr. F. Horváth (Eötvös University) and Dr. G. Tari (Amoco, Houston).

Finally, my deepest appreciation goes to my wife, Kathleen, who put up with all of the things required to work on a thesis: late nights, no weekends and holidays and the punishing and torturing job of reading the very first draft.

Scholarships were provided by Wascana Energy Inc. and the University of Saskatchewan. Additional financial assistance was received from the Geological Survey of Canada (Calgary).

TABLE OF CONTENTS

LIST OF FIGURES

LIST OF TABLES

CHAPTER 1

INTRODUCTION

The Williston Basin is an 'elliptical' cratonic basin located in North Dakota, Montana, Saskatchewan, Manitoba and South Dakota ***(Fig.1.1)***. The very definition of the extent of the basin throughout its history is problematic. This is partly because of the erosion, which is always much more severe on the cratonic platform areas, where the subsidence rate creating accommodation space for sedimentation is significantly lower (avg. ~ 10 m/M.a.) than other areas (e.g. passive margins, foreland ~40-100 m/M.a..). Erosion swept free large areas (hundreds of kilometers) of cratonic sediments making it difficult to reconstruct the areal extent of the sediments *(Sloss, 1996)*. The other reason for the difficulty in defining the basin's extent is that the area where the basin is located went through different stages in the Phanerozoic starting from a pericratonic environment going through a true intracratonic phase and ending up as part of the larger scale foreland basin. The term "Williston Basin" will be used in sensu lato, representing an area defined fundamentally by the oval shape of its Paleozoic intracratonic basin stage.

This thesis is fundamentally an answer to a call of the scientific community to analyze the regional context of local geological structures and stratigraphic features of the basin. The first step in this respect was done by Zhu *(1992)*, who compiled an 790-km-long east-west regional seismic line across the northern part of the Williston Basin. This pioneering work was probably the first regional seismic profile across the Phanerozoic portion of a cratonic basin. The main contribution of this mainly descriptive work was the subdivision of the Cretaceous succession of the basin into

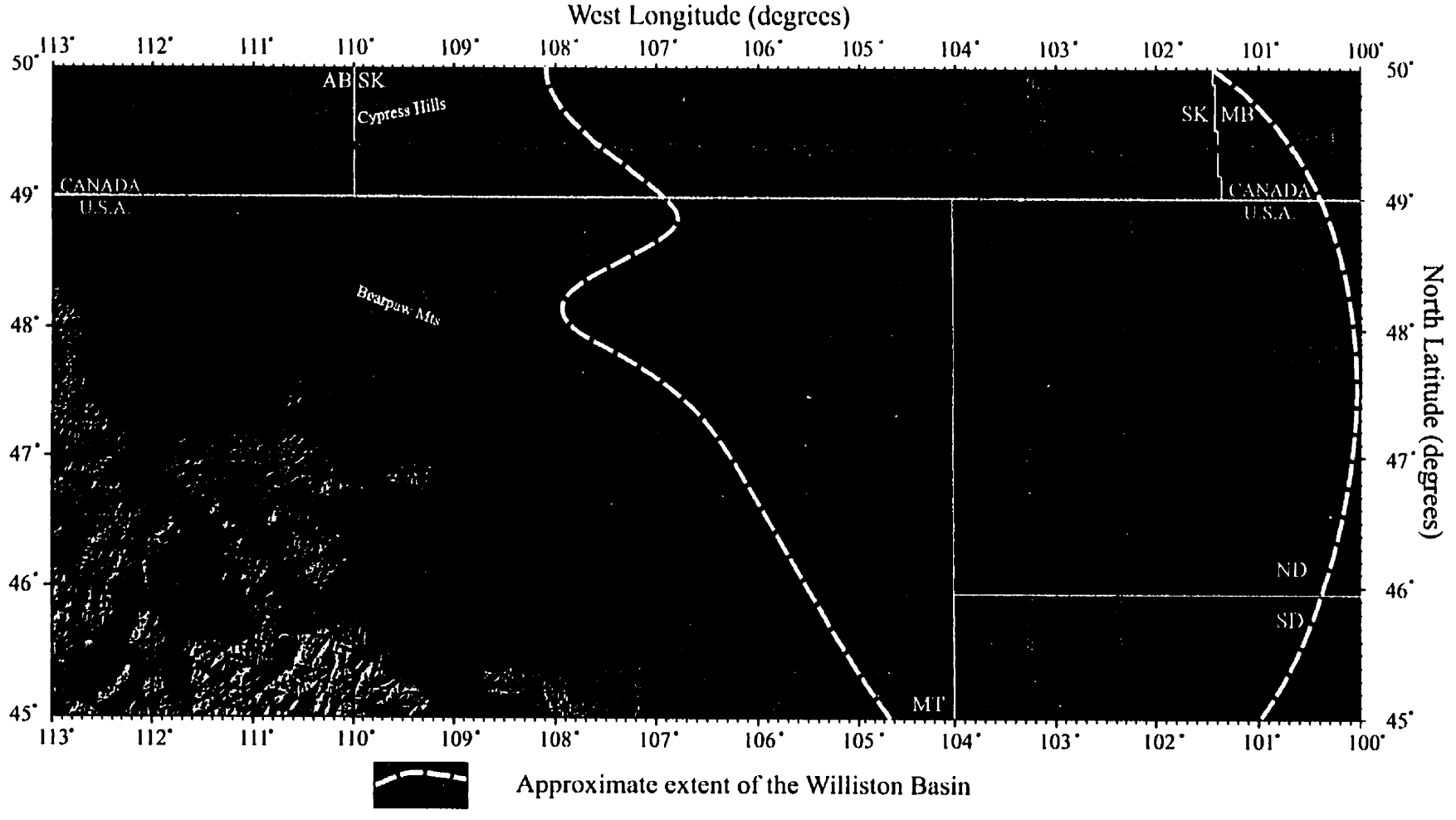

Fig. 1.1 Topography of the study area. (Map source: R. Steiner, John Hopkins University).

subsequences. Obviously, lacking the third dimension hampered this study's ability to deal with the evolution of the basin as a whole. In this thesis, three times more regional seismic data are available, providing both a qualitatively and quantitatively superior source of information for synthesis of this cratonic basin. This unique circumstance renders the rare opportunity to contribute to fundamental understanding of the Williston Basin and of cratonic basins in general.

This immense dataset has far more information than can be fitted into one doctoral thesis. During the course of work, it soon became obvious that this type of study can have nearly perpetual life expectancy. Given this large, new dataset, an attempt was made, therefore, to step back and to look at the Williston Basin from a fresh, new perspective. Following this line of thought, a fundamentally different view of the basin evolution was reached. During the regional interpretation phase special attention was paid to the local geological information compiled by excellent earth scientists during decades of research and exploration, but where the careful analysis of the dataset permitted, new, fundamentally different interpretations of the local structures and stratigraphy were put forward if demanded by the regional context.

The proposed model is not an all-inclusive process, but is believed to describe most phases of basin evolution with fewer contradictions than the existing models do. The thesis does not address the problem of the cause of the basin's initiation directly, but the Phanerozoic evolution of it. On the other hand, as the nature of the driving force behind the basin subsidence fundamentally defines the basin's architecture, based on the analysis of the Phanerozoic structural evolution of the basin, an assumption was made as to the possible primary cause of the basin subsidence.

This thesis is by no means the final answer to the fundamental questions relating to the evolution of the Williston Basin. On the contrary, similar to the demand for this regional seismic study, it is a new call for further research, to test the ideas presented here. Immediate further investigations in the area of more precise numerical modelling

with integration of additional regional data would be a welcome test of the present inferences.

The thesis is structured in the following manner: ***Chapter 2*** outlines the geological framework considering both lateral and vertical perspectives. ***Chapter 3*** reviews the subsidence history and tectonic evolution models of major cratonic basins, starting with the Williston Basin. The chapter ends with a critical summary and statements regarding the outstanding problems associated with the existing evolution models of the Williston Basin and cratonic basins in general. This section also presents the objectives of this thesis, as well as the means and methods used to achieve them. ***Chapter 4*** discusses the input data sets and the various processing steps applied to this basic information prior to interpretation and synthesis. ***Chapter 5*** explains the interpretation methods implemented to extract the necessary geological information from the geophysical dataset. ***Chapter 6*** is devoted to presentation of the detailed stratigraphic and structural interpretation of the regional seismic lines, with heavy reliance on the well established regional geology of the region. In ***Chapter 7***, the new, complex tectonostratigraphic model of the Williston Basin is introduced. ***Chapter 8*** discusses conclusions drawn from the new results and outlines directions for future research. Fundamental information concerning the data utilized for this study (seismic profiles, synthetic seismograms, well information, stratigraphic picks, etc.) is summarized in the ***Appendix***.

CHAPTER 2

GEOLOGY OF THE STUDY AREA

The overview of the geology of this continental-size structure requires a dual approach. First, a summary of the regional geology is provided of the Williston Basin in view of its relationship to the neighboring regions, primarily to the geologic settings to the west. Second, details of local geology are discussed in terms of the regional seismic profiles. This stratigraphic information related to the study area, along with regional geologic and structural information form the foundation of the basinwide quasi-3D analysis of the seismic profiles and development of the overall tectonostratigraphic evolution of the entire basin.

2.1 Regional Geology

2.1.1 Precambrian

The Williston Basin is bounded by three Archean (>2.5 Ga) cratonic provinces (the **Superior**, the **Hearn-Rae** and the **Wyoming** cratons) and underlain by the recently discovered Archean Dakota Block ***(Fig. 2.1)***. In general, reactivation is related in trend and intensity to the orogenic belts that frame the Archean provinces *(Hoffman, 1988)*. Many of the Proterozoic orogenic belts appear to represent collision zones between Archean provinces *(Hoffman, 1988; Williams et al., 1991)*. Two of these orogenies affected the Williston Basin area.

The Trans-Hudson Orogen (~1.7 Ga), running in a roughly north-south direction below the center of the basin, is the manifestation of the collisional event between the Hearn-Rae/Wyoming and the Superior provinces. The boundary between the Hearn-Rae and

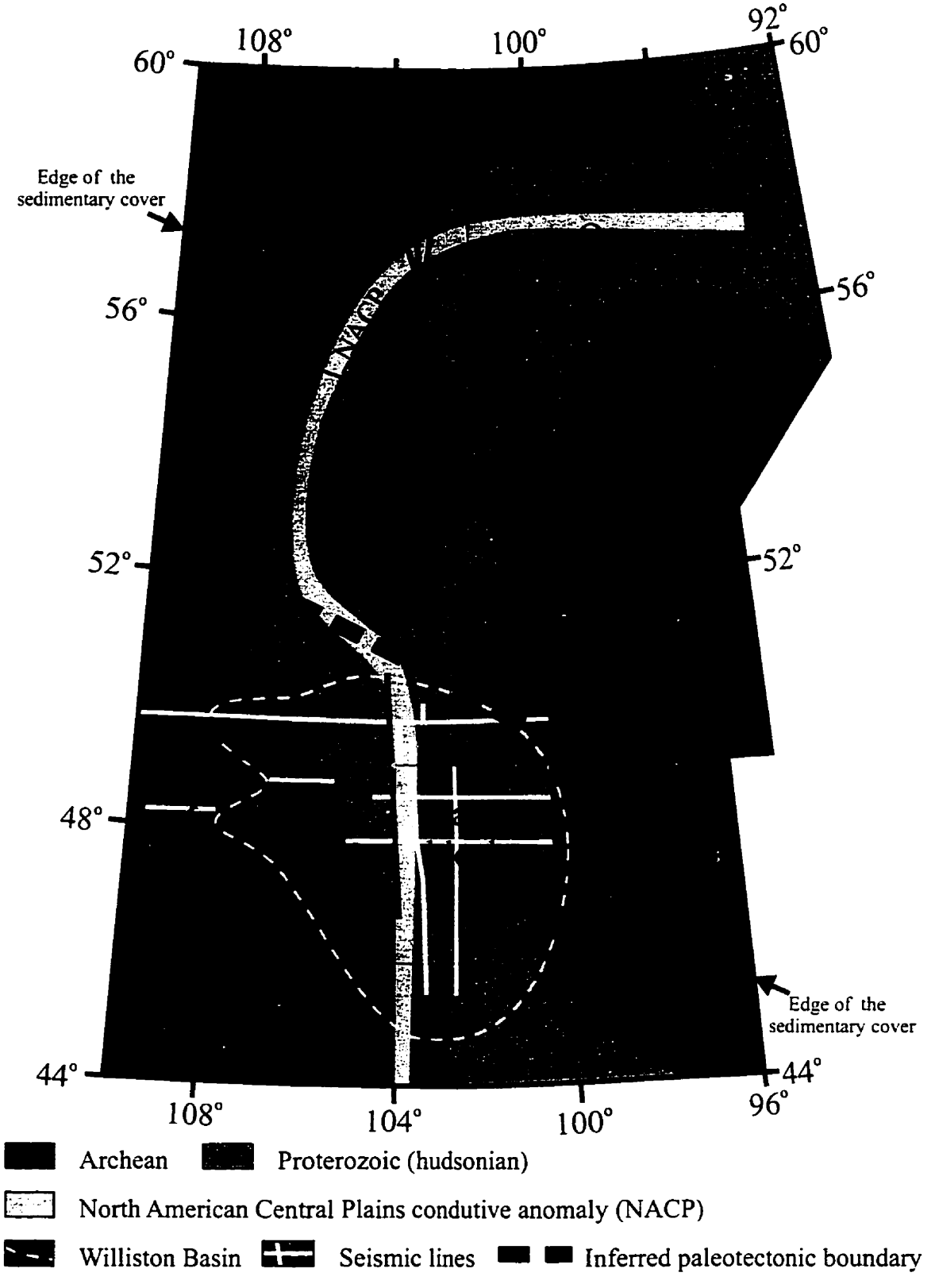

Fig. 2.1 Postulated basement structures around the Williston Basin (based on Baird et al., 1996).

the Wyoming cratons is more difficult to establish, because of the reworked Archean crust between them. The affinity of the "Medicine Hat Block" is not solved yet. The South Alberta Rift *(Kanasewich et al., 1969)* or Vulcan Low separating the Medicine Hat Block in the north from the Hearn-Rae craton is interpreted as the collision zone of the Hearn-Rae and the Wyoming cratons *(Thomas et al., 1987; Hoffman, 1988)*. Others place the Archean Medicine Hat Block in the Hearn-Rae province *(Ross and Stephenson, 1989; Ross and Parrish, 1991; Ross et al., 1991)* and consider the Great Falls Tectonic Zone *(O'Neill and Lopez, 1985)* as its southern limit. Recent seismic and magnetotelluric data underline the Hearn-Rae affinity of the Medicine Hat Block. These results revealed that the Vulcan Low is actually a south-dipping structural surface upon which the Medicine Hat Block was accreted to the Hearn Province.

New data have also added to our knowledge of the structural character of the western edge of the Superior Province. Earlier interpretation assumed that the Superior Craton subducted below the the Wyoming and Hearn-Rae cratons to the west *(Lewry et al., 1990; Klasner and King, 1990)*. Crustal seismic data of the LITHOPROBE and COCORP programs identified the Archean Sask Craton in the north and the Dakota Block in the south, below the Williston Basin in the Trans-Hudson Orogen system *(Andsdell et al., 1995; Baird et al., 1996)*. A problem remains with the western margin of the Superior Craton in the area between the two blocks in southeast Saskatchewan, where Lucas et al. *(1996)* interpreted west-dipping reflections of the Superior Boundary zone (or Thompson Belt) above the east dipping reflection of the Superior Craton. They suggested that the Superior craton extends westward beneath the low grade, eastern portion of the Thompson Belt. The problem of the tectonic affinity of this area is not solved satisfacorily and the structural position suggests that its evolution is related to the assumed structural line at the bend of the North American Central Plains conductive anomaly. Additonal north-south trending crustal seismic data could shed light on this structurally complex area.

2.1.2 Phanerozoic

The Phanerozoic stratigraphy of the North American intracratonic basins, the Williston Basin included ***(Fig 2.2)***, is examined in terms of "stratigraphic sequences", the most fundamental type being the cratonic tectonostratigraphic sequences of Sloss *(1963)* named after Native American tribes. The sequences represent major, continent wide transgressive-regressive cycles bounded by unconformities. These are the **Sauk Sequence** (Cambrian-Lower Ordovician), **Tippecanoe Sequence** (Middle Ordovician-Lowest Devonian), **Kaskaskia Sequence** (Devonian-Lower Carboniferous), **Absaroka Sequence** (Upper Carboniferous-Lower Jurassic), **Zuni Sequence** (Middle Jurassic-Paleocene) and **Tejas Sequence** (Eocene-Recent).

The following review heavily emphasizes the cyclic nature of sedimentation in the Williston Basin area punctuated by unconformities representing various scales of erosion or non-deposition. This approach was taken because the fundamentals of the seismic interpretation of the basin analysis are based on the chronologically significant unconformity surfaces. These surfaces are the basic building blocks of seismic/sequence stratigraphic interpretations. The sequence concept as an interpretive stratigraphic tool will be described briefly in ***Chapter 5***.

2.1.2.1 Sauk Sequence

Sauk Sequence ***(Fig 2.3.a)*** exhibits a time interval from the Cambrian to the Lower Ordovician. Sedimentation took place on a wide, shallowly inundated coastal shelf with a west-northwesterly slope *(Lochman-Balk and Wilson, 1967)* and on megascale it displays a pericratonic wedge. The sediments manifest a gradual eustatic sea-level rise, which included several small-scale transgressive-regressive periods *(LeFever et al., 1987b)*.

In the stratigraphic record from the west of the Williston Basin, the basal Flathead Formation, Middle Cambrian in age *(Peterson, 1988)*, represents the earliest transgression, followed by the Gros Ventre, Gallatin and Grove Creek Formations and

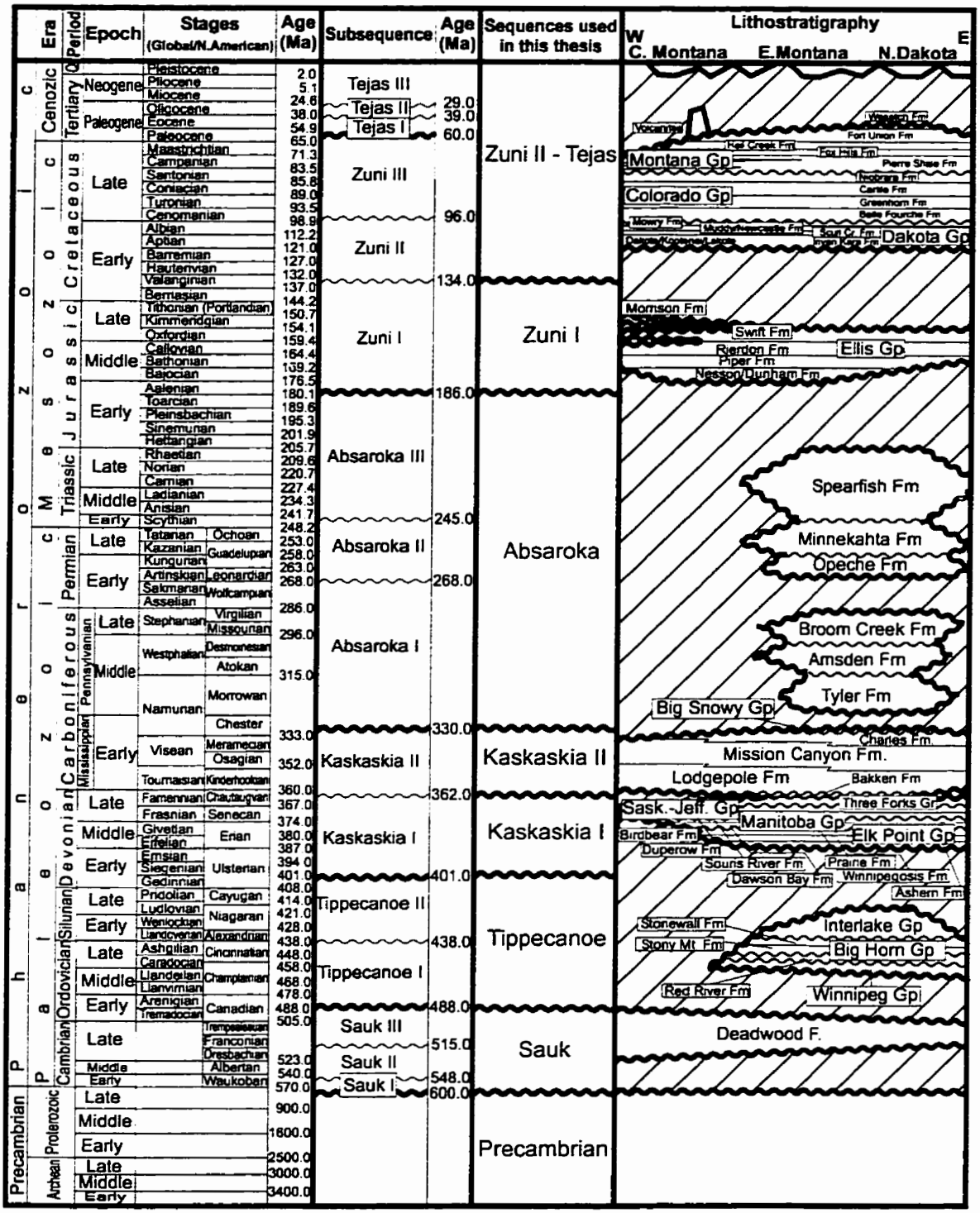

Fig. 2.2 Chrono-, sequence and lithostratigraphy of the study area (W-E approximately along lines WEII and WEIII); based on Bluemle (1981), Palmer (1983), AGAT Laboratories (1987), Sloss (1988b) and Gradstein et al. (1995).

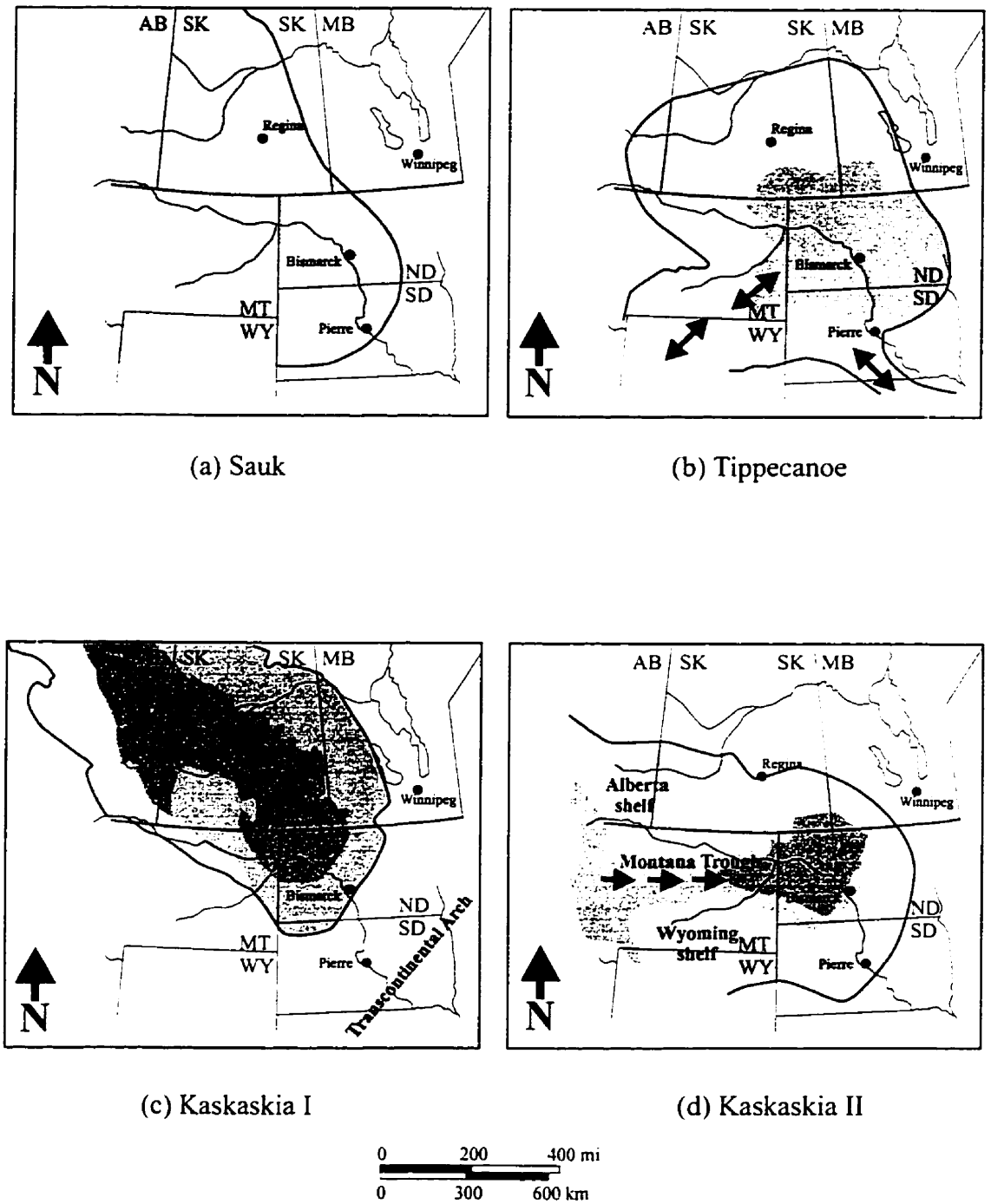

Fig. 2.3 Sauk, Tippecanoe, Kaskaskia I, and Kaskaskia II sequences in the Williston Basin area (based on Carlson and Thompson, 1987; Gerhard et al, 1982). Darker areas indicate deeper regions.

their equivalents (Emerson Formation). The transgression reached the Williston Basin area by the Upper Cambrian (Dreschbachian) and its stratigraphic expression is the Deadwood Formation. The Deadwood Formation consists of sandstones, shales and carbonates deposited over a highly irregular surface of Precambrian basement *(Carlson, 1960; Lochman-Balk and Wilson, 1967; Gerhard et al., 1982; Peterson and MacCary, 1987; Gerhard and Anderson, 1988)* in a marginal marine–inner shelf environment and reaches 300 m (~1000 ft) thickness in the central part of the basin.

The regional pattern of structural highs probably reflects the earliest tectonic history of the basin. The estimated relief of these "islands" *(Lochman-Balk and Wilson, 1967)* is in the range of 100 m *(Lochman-Balk, 1972)*. Major paleotopographic features, e.g., the Nesson Anticline, are associated with these early structural patterns *(Gerhard and Anderson, 1988)*. The Williston Basin as a new structural entity was established during the early Ordovician (Tremadocian) *(LeFever et al., 1987b)*. The regressive part of the sequence is largely missing due to the widespread post-Sauk erosion.

2.1.2.2 Tippecanoe Sequence

A second cycle of major transgression–regression comprises Middle Ordovician (transgressive) through Silurian–earliest Devonian (regressive) strata ***(Fig. 2.3.b)***. More than 760 m (~2500 ft) of sedimentary rock is preserved in the central part of the basin from this sequence. The circular shape and the depocenter of the Williston Basin in northwestern North Dakota became clearly defined, with openings to the southwest and to the southeast *(Gerhard and Anderson, 1988)*.

The sequence in the Williston basin in the Caradocian (Late Ordovician) began with deposition of overstepping basal siliciclastics of the transgressive Winnipeg Group (Black Island Formation - fluvial/deltaic sands and shales; Icebox Formation–deeper water marine shales; Roughlock Formation–argillaceous limes) *(LeFever et al., 1987b; Ellingson and LeFever, 1995)*. In the eastern part, due to the lithological similarities, it is difficult to place the Deadwood-Winnipeg boundary exactly, but in the west, in

Montana there is a sharp lithic contact between them *(Lochman-Balk and Wilson, 1967)*. The rest of the sequence is largely carbonate. The Winnipeg Group is conformably overlain by the Red River Formation. The cyclic Red River Formation indicates equatorial shelf and lagoonal environments *(Gerhard and Anderson, 1988)* and is overlain conformably or with minor disconformity by the cyclic carbonates-anhydrites of the thin Stony Mountain and Stonewall formations. The cyclic nature of the Ordovician sedimentation is attributed to several possible factors such as regional tectonism, continental glaciation, climatic changes *(Peterson and MacCary, 1987)*. The conformably overlying Silurian Interlake Group consists of three units representing two transgressive-regressive peritidal/shallow marine cycles *(LoBue, 1982)*. Regression after the Silurian resulted in widespread erosion and karstification at the top of the Interlake.

By the end of the deposition of the Tippecanoe sequence, all of the major structures of the basin were present (e.g., Billings, Little Knife, Antelope, Nesson, Cedar Creek anticlines) *(Gerhard et al., 1991)*. Major structural movements of the Nesson Anticline are documented from the Ordovician and the Silurian *(Famakinwa, 1989)*. During most of Late Silurian and Early Devonian time, the Williston Basin area was emergent.

2.1.2.3 Kaskaskia Sequence

In the Williston Basin area the Kaskaskia Sequence (Devonian-Lower Carboniferous) records two regional sea-level rises and an unconformity separates the older Kaskaskia I (Devonian) from the younger Kaskaskia II (Lower Carboniferous = Mississippian) sequences *(Sloss, 1988b; Gerhard et al., 1991)*.

Kaskaskia I (Fig.2.3.c)

Regional transgression from the northwest reached the study area by the Middle Devonian (Eifelian). Within this sequence three carbonate-evaporite cycles, reflecting smaller scale transgressive-regressive phases, can be distinguished.

The oldest one of these cycles is the lowermost, the Ashern Formation of the Elk Point Group, consisting of dolostone and shale. The depositional environment is not clear *(Rosenthal, 1987)*. Possibilities vary from transgressional infill of post-Silurian erosional surfaces through marine, tidal flat, coastal sabkha *(Lobdell, 1984)* to non-marine environments. With a brief hiatus this formation is followed by the second cycle.

Chow *(1991)* concluded that the Winnipegosis Formation, which is the lower part of the next cycle, grades laterally into the Elm Point Formation in Manitoba and in addition Day et al. *(1996)* put a subcycle boundary between them, indicating relative sea-level fluctuation. The Winnipegosis Formation has the widest extent in the Elk Point Group, and indicates the turnover from transgressive to regressive phase. The carbonates of the transgressive half are deposited in carbonate shelf and pinnacle reef environments. These reefs (mounds) are scattered throughout southeastern Saskatchewan *(Gendzwill and Wilson, 1987)*. They can reach 6 km in diameter and 100 m in thickness and can be mapped seismically *(Gendzwill, 1987; Martindale, 1991)*. Outcrop studies in Manitoba *(Kent and Minto, 1991)* indicate that their morpholgy is extremely changeable and they were formed on some irregular form on the sea floor. The regressive phase of the Winnipegosis Formation exhibits subtidal and intertidal depositional environments, expressed by increasing anhydrite deposition, which in turn, was capped by the halites of the Prairie Evaporite Formation *(Perrin, 1982)*. Activity on the Transcontinental Arch in the Middle Devonian caused the Elk Point Basin, consisting of the Williston and Alberta basins, to be tilted northwestward before basin restriction increased salinity and induced Prairie deposition. Based on intraformational correlation of anhydite/halite-potash successions, four shallowing-upward cycles can be identified (Ratner, Esterhazy, Belle Plain and Mountrail [Patience Lake] Members) *(Oglesby, 1991)* representing minor fluctuations in sea level. Dissolution of the Prairie salts occurred in a multiphase manner from after the deposition of the salts to the present time *(McTavish, 1991)*. Salt removal and collapse appear to be localized above the porous and permeable Winnipegosis mounds and above deep-seated (basement) structures *(McTavish and Vigrass, 1987)*.

The third cycle of the Kaskaskia I sequence overlies the Elk Point Group by an unconformity manifested by the presence of the Second Red Beds of the Manitoba Group. Water deepened again during the subsequent Dawson Bay deposition *(Gerhard et al., 1982)*. Evaporites of the Dawson Bay demonstrate shelf conditions in Saskatchewan *(Dunn, 1982)* and peritidal deposition in North Dakota *(Dean, 1982)*. The overlying First Red Beds indicate an unconformity. The following Souris River Formation consists of several depositional cycles of fine clastics grading into dolomite or limestone, capped by anhydrite. The southerly encroachment of the Late Devonian seas continued with a minor interruption through the deposition of the Saskatchewan-Jefferson Group and reached the maximum in the middle of Duperow time *(Altschuld and Kerr, 1982; Wilson and Piladzke, 1987)*. The Duperow Formation is characterized by about 12 cycles of shelf carbonates interbedded with peritidal rocks and anhydrite *(Wilson and Piladzke, 1987; Gerhard and Anderson, 1988)*. The final series of carbonate-evaporite cycles of the Devonian make up the Nisku (Birdbear) Formation. The Birdbear represents one transgressive-regressive cycle *(Halabura, 1982; Martiniuk et al., 1995)* in a shallow epicratonic sea exhibiting low-energy subdtidal and high-energy intertidal, lagoonal depositional environments in its lower and upper parts, respectively. Overlying the Birdbear (Nisku) Formation is the predominantly clastic marine and non-marine Three Forks Formation (Torquay and Big Valley in Saskatchewan). A major regression separating the Kaskakia I and the Kaskaskia II sequences occurred at the conclusion of the Three Forks deposition.

Kaskaskia II (Fig.2.3.d)

The disappearance of the northwestern connection via the Elk Point Basin reestablished the Williston Basin to a circular geometry similar to that controlling the Tippecanoe deposition. A reorientation of the seaway ushered in Mississippian sedimentation as the Williston Basin was opened to the west through the Central Montana Trough. The resulting unconformity separating the lower and upper Kaskaskia is extensive *(Gerhard and Anderson, 1988)*.

The basal transgressive unit of Kaskaskia II is the Bakken Formation (latest Devonian-lower Mississippian), which is composed of a tripartite organic black shale/siltstone - dolomitic siltstone – black shale succession. The depositional environment was interpreted by Smith et al. *(1995)* as a deep-marine – offshore/shoreface – deep-marine cycle; however, Sloss *(1996)* argued for a shallow water (lagoonal) origin as the initial deposits of transgressive seas.

The Bakken deposition was followed by a period of cyclic, shelf carbonate sedimentation of the Madison Group in the Lower Carboniferous (Mississippian). The continued transgression sustained limestone deposition of the Lodgepole Formation on the shelf. Isolated Lodgepole carbonate mudmounds are located in Montana and North Dakota along the margins of the structurally active Central Montana Trough *(Gerhard and Anderson, 1988; Precht and Shepard, 1989)*. The transgression reached its maximum at the end of the Lodgepole deposition or early in the deposition of the following Mission Canyon Formation *(Gerhard et al., 1982; Gerhard and Anderson, 1988)*. Mission Canyon rocks are typically shoaling-upward carbonates capped by anhydrite. Madison sedimentation came close with the deposition of the regressive evaporitic Charles Formation.

The Kaskaskia II sedimentary record finished with the deposition of a single depositional cycle, the dominantly clastic Big Snowy Group, of Chesterian age (Late Mississippian) reflecting the influence of the Antler/Cariboo orogenic events. The shales, silts and sandstones with a thin but widespread carbonate marker of the Kibbey Formation indicate near-shore origin. The Otter Formation consists of marine – tidal-flat shales and carbonates, while the severely eroded organic shales, lime and sandstones and gypsum of the Heath Formation are the manifestations of a restricted marine environment *(Peterson, 1984; 1988)*.

2.1.2.4 Absaroka Sequence

The deposits of the next 150 M.a. (latest Mississippian – Early Jurassic) known as the Absaroka Sequence ***(Fig. 2.4.a)***, accumulated under dramatically different conditions from those prevailing during earlier cratonic episodes. They record the most complex and longest Phanerozoic tectonostratigraphic evolution of the craton *(Sloss, 1988b)*. Contrary to its complexity and timespan, in the Williston Basin area, the remnants of the sequence are rather thin and restricted mostly to the central and southern parts of the basin. The Absaroka sequence can be subdivided in the area into three subcycles separated by widespread erosional surfaces.

Sediments of the first subcycle (latest Mississippian – Early Permian) were deposited on a severely eroded surface; however, in the Central Montana Trough the depositional hiatus is minimal. The transgressive Tyler Formation of the Late Carboniferous (Pennsylvanian) Amsden Group is also tricyclic *(Sturm, 1978; Maughan, 1984)*, and exhibits alternating fluvial/deltaic – marine/near-shore environments, mirroring a fluctuating sea and an oscillating shoreline. The Tyler Formation is overlain by shales and sandstones of the Amsden Formation which was deposited in a more restricted environment. The subsequence is capped in places by the severely eroded Broom Creek Formation.

The sediments of the second subcycle of the Absaroka Sequence (middle Permian – late Permian) were deposited under episodic hypersaline conditions exhibited by the red shales of the overlying Opeche Formation and the carbonates of the Minnekahta Formation, and are limited to the central part of the basin.

The final Absaroka subsequence, with the regressive Triassic Spearfish Formation consists of red shales and sandstones with some halite beds (e.g., Pine and Saude [=Lower Watrous in Saskatchewan and Lower Amaranth in Manitoba] salts). This succession represents the conclusion of the Absaroka sequence. The higher

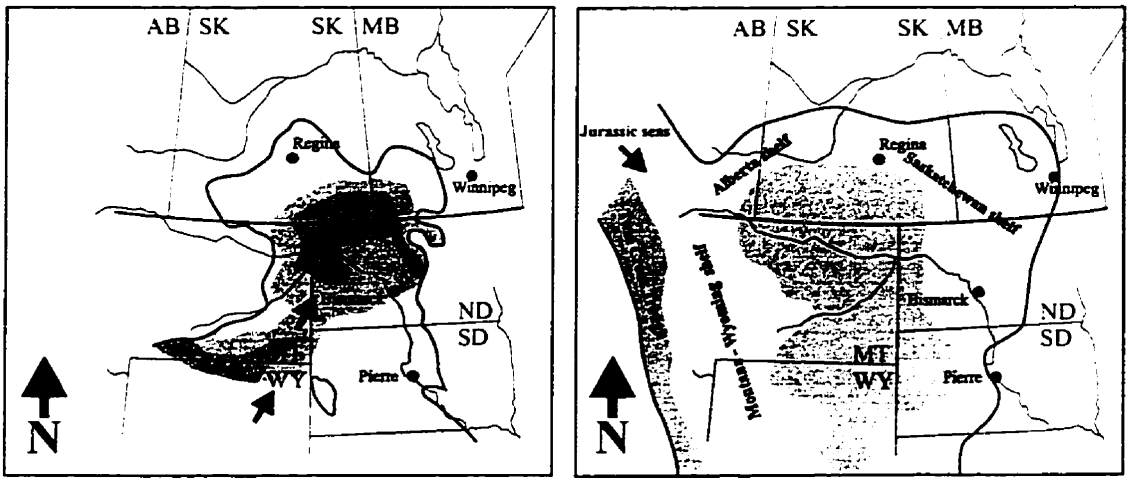

(a) Absaroka

(b) Zuni I

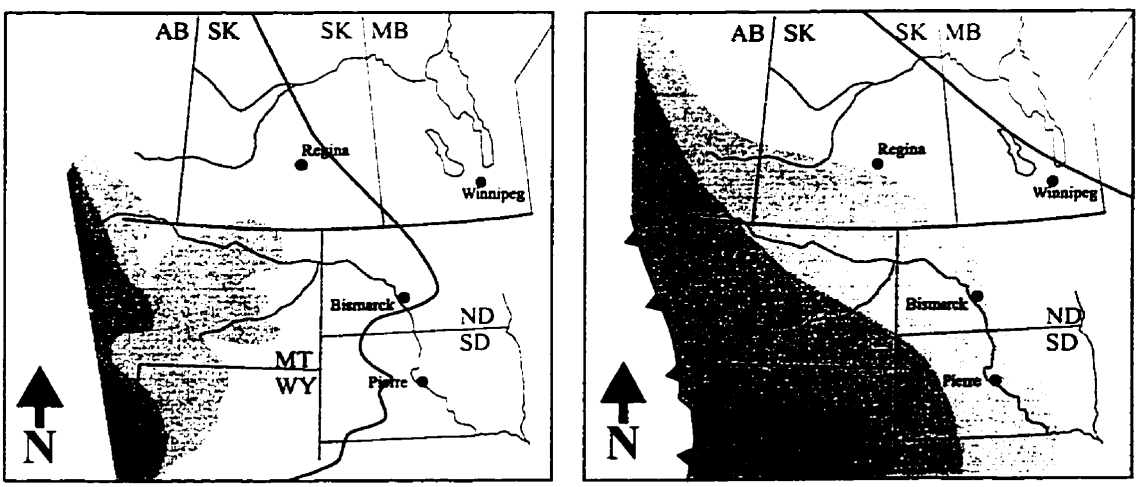

(c) Zuni II

(d) Zuni III

Fig. 2.4 Absaroka, Zuni I, Zuni II, and Zuni III sequences in the Williston Basin area (based on Gerhard et al., 1982; Langtry, 1982; Sloss, 1988; Beaumont et al., 1993). Darker areas indicate deeper regions.

sandstone content of the Spearfish Formation in the eastern part of the basin indicates fluvial deposition drained from uplifted eastern sources.

2.1.2.5 Zuni Sequence

The Zuni Sequence in the Williston Basin comprises a single large cycle of sedimentation and represents more than half of the preserved sediments of the area. The sediments were deposited in a new structural entity of the craton, in the north-south trending Western Interior Seaway. The extent and marine connections of the seaway changed continuously during the Zuni Sequence. Although an unconformity due to the severe post-Absaroka erosion is present between the Absaroka and Zuni sequences, the lithologies on either side of the unconformity are similar *(Gerhard et al., 1982)*, making it difficult to differentiate them in some areas. This sequence can also be subdivided into three subsequences *(Sloss, 1988b; Shurr et al., 1989a)*, separated by unconformities reflecting the changing nature of the sedimentation.

Zuni I (~ Jurassic; Fig. 2.4.b)

The Zuni I (Stage I and II of *Peper, 1993*) is sometimes referred to as the "great transgressor" *(Peterson, 1988)*. Sloss *(1988)* compared it to the Sauk Sequence, based on its similarity in showing pulsating and progressive expansion of areas subsiding below the depositional base level. The Zuni I subsequence exhibits a smaller scale transgressive-regressive cycle of the "Sundance Sea", which is lithologically expressed by the Ellis Group. This cycle in turn also shows smaller-scale cyclicity. The basal part comprises the corresponding Nesson (central part), Gypsum Spring (SE Saskatchewan) and Gravelbourg (SW Saskatchewan) formations overlain by the red beds and evaporites of the Piper Formation in the central part of the basin, by the sandstones of the Sawtooth Formation in the northwest and by the Melita Formation in the northeast. This succession is followed by the shallow marine shales and carbonates of the Rierdon Formation. The Oxfordian (Late Jurassic) renewed marine transgression indicates the initiation of the Sevier Orogeny *(Sloss, 1988b)* and the corresponding uplift of the Sweetgrass Arch in the west. The increased clastic sediment supply is manifested partly

by the sandstones of the Swift Formation (Vanguard Formation in SW Saskatchewan) and by the non-marine clastic sediments of the regressive Morrison Formation. The remnants of the Zuni I subsequence are fairly thin all over the study area because of the subaerial erosion. This unconformity is attributed to the global lowering of the sea level in earliest Cretaceous time and represents 10 M.a. of erosion and/or nondeposition *(Sloss, 1988b)*; however, Gerhard and Anderson *(1988)* prefer relatively small emergence of the basin with a 26 M.a. time gap in the sedimentary column.

Zuni II (~Lower Cretaceous; Fig. 2.4.c)

The Zuni II subsequence (Stage III of *Peper, 1993*) is relatively uniform in thickness across the basin. Sedimentation commenced with the transgressive Inyan Kara Group (~Dakota Group, Mannville Group). The non-marine rocks of the lower part (Kootenai Formation in the east, Lakota Formation in the central parts and the lower parts of the Dakota Formation in the south and east) are capped by a minor unconformity. The post-Kootenai Zuni rocks were deposited in six main transgressive-regressive cycles.

The first, "Skull Creek" cycle *(Peterson, 1988)*, started with the marine sandstone beds of the Fall River and First Cat Creek Formations. The transgression reached its peak during the deposition of the overlying Skull Creek Formation (~Joli Fou Formation in Saskatchewan).

The second, "Mowry cycle", started with a sea level low *(Dolson et al, 1991; LeFever and McCloskey, 1995)* during the increasingly transgressive marginal and shallow marine deposition of the Newcastle Formation (Muddy Sandstone Formation in South Dakota, Viking Formation in SE Saskatchewan, Bow Island Formation in southern Alberta). This cycle reached its maximum extent during the deposition of the marine Mowry Shale. The top of the Mowry Shale (Fish Scale Zone in Saskatchewan, Fish Scale zone of Ashville Formation in Manitoba, top of Blackleaf Formation at the Sweetgrass Arch area) indicates the end of the Early Cretaceous, Zuni II sedimentation.

Zuni III (~ Upper Cretaceous – Paleocene; Fig. 2.4.d)

The sediments of the Zuni III subsequence (Stage IV and V of *Peper, 1993*) show the combined effects of the increasing activity of the Laramide Orogeny and of the fluctuating, high worldwide sea-level, due to accelerating sea-floor spreading. The Colorado Group confines the sediments of the third and fourth Zuni cycles.

The third, "Greenhorn cycle", commenced with a relative sea level drop during the deposition of the Belle Fourche Formation *(Schröder-Adams et al., 1996)* (Colorado Shale in SW Saskatchewan and Alberta, Graneros Shale in South Dakota). The sea level during this cycle reached its maximum during the deposition of the Greenhorn Formation (Second White Speckled Shale in Saskatchewan and Alberta and Favel Formation in Manitoba) and a basin-wide drop was recorded at the end of it *(Schröder-Adams, et al., 1996)*. The Greenhorn Shale (with its equivalents) is the best marker in the Zuni sequence, due to its sharp, characteristic log profile and strong seismic response. It is widely used as a datum as in this thesis. The overlying Carlile Shale is considered to be the concluding part of this cycle *(Shurr et al., 1989a)*.

The fourth, "Niobrara cycle", above an unconformity, started with the calcareous Niobrara Formation (First White Specks in Canada). The rest of the cycle and the rest of the Cretaceous are part of the Montana Group. The regressive phase of the Niobrara cycle was caused by the tectonism and volcanism in western Montana and exhibits the growing clastic influx from the west. In the western part of the area, closer to the source, this phase is represented by the deposition of the Telegraph Creek and successive Eagle Formation (Milk River Formation in Alberta and SW Saskatchewan), and in the east by the Gammon Shale part of the Pierre Shale Formation. The end of the cycle, above the Eagle Formation, is marked by the Ardmore Bentonite Bed, which is the deposit of the ashes of the volcanoes in the Elkhorn Mountains to the west.

The transgressive part of the fifth , "Claggett cycle", is the Claggett Shale in the west (Pakowski Formation and Lea Park Formation in Alberta and in Saskatchewan) and the middle part of the Pierre Shale in the east (lower part of the Riding Mountain Formation in Manitoba). The regressive part of this cycle is represented by the Judith River Formation (upper Two Medicine Formation west of the Sweetgrass Arch *(Horner, 1984)*, Foremost Formation and Oldman Formation of the Belly River Group in Alberta, upper part of the Riding Mountain Formation in Manitoba). The regression of the Claggett cycle was more advanced and the strandline was running north-south somewhere around the 107^{th} parallel at the end of the cycle *(Gill and Cobban, 1973)*.

The beginning of the sixth, "Bearpaw cycle", indicates recurrent tectonism in the west, accompanied by explosive volcanism shown by the bentonite beds in the transgressive Bearpaw Formation. The subsequent regression marks the final retreat of the Western Interior Seaway from the study area. The regressive sediments of the Fox Hills Formation indicate the advance of the "Sheridan delta" from the southwest into the central part of the basin. The "Mosby embayment", open to the north, in central Montana was located between the delta and the western shores of the seaway *(Gill and Cobban, 1973)*. The equivalent formations are the Horsethief Formation, west of the Sweetgrass Arch, St. Mary River Formation in Alberta and Eastend Formation in Saskatchewan. The overlying Hell Creek Formation (Willow Creek Formation in Alberta and Frenchman Formation in Saskatchewan) was followed by the last marine sediments of the Paleocene Cannonball Formation part of the Fort Union Group. The sediments of the rest of the group (Ravenscrag Formation in Alberta and Saskatchewan, Turtle Mountain Formation in Manitoba) are deposited in a fluvial/deltaic environment. The extensive quantities of detritus originated from further uplift, erosion and volcanism in the Laramide Rockies in the west *(Gerhard et al., 1982)*.

2.1.2.6 Tejas Sequence (late Paleocene – Present)

There are few remnants of the Tejas Sequence in the Williston Basin area. The Williston Basin became inactive, although deposition of terrestrial sediments continued.

The Fort Union Group is overlain by lacustrine and fluvial clastics of the Golden Valley and White River formations (Cypress Hills Formation in Alberta and SW Saskatchewan). Laramide Orogeny-related volcanism of the Central Montana Alkalic Province, which started in the Late Cretaceous (69 M.a.), continued into this sequence up to the Oligocene (27 M.a.) *(Marvin et al., 1980)*. Unnamed remnants of the Miocene and Pliocene consisting mostly of lacustrine-fluvial deposits and minor limestone are present in the Williston Basin. Continental Pleistocene glacial sediments cover most parts of the basin.

2.2 Geology beneath the regional seismic lines

Local geology of only a few township-wide strips will be discussed here. The following review will be conducted with the help of cross-sections drawn across 48 wells along the seismic lines ***(Fig. 2.5)***. The location, the stratigraphic picks of the wells and the abbreviations of the lithostratigraphic intervals can be found in the ***Appendix***. Special emphasis will be put on the local structures and structural evolution. The thesis incorporates the results of Zhu's *(1992)* study which was constructed utilizing a regional, 790 km long, west-east line in Canada (WE I in ***Figs. 1.1 and 2.5***). The detailed descriptions of local structures and the identified new structures that were presented by Zhu *(1992)* will not be discussed here. Two east-west (WE II and WE III) and two north-south (NS I/CA I and NS II) lines ***(Fig. 2.5)*** were composed from the most recent industrial data contributions. South of the international border NS I and CA I lines will be discussed together. All reviews will be presented from west to east and from north to south.

2.2.1 WE II line

WE II line is the longest profile, reaching over 1000 km in length between the very eastern edge of the Disturbed Belt of the Rockies and north-central North Dakota. Because of this extended length, the relevant geology was broken into a western and an eastern half ***(Fig. 2.5)***.

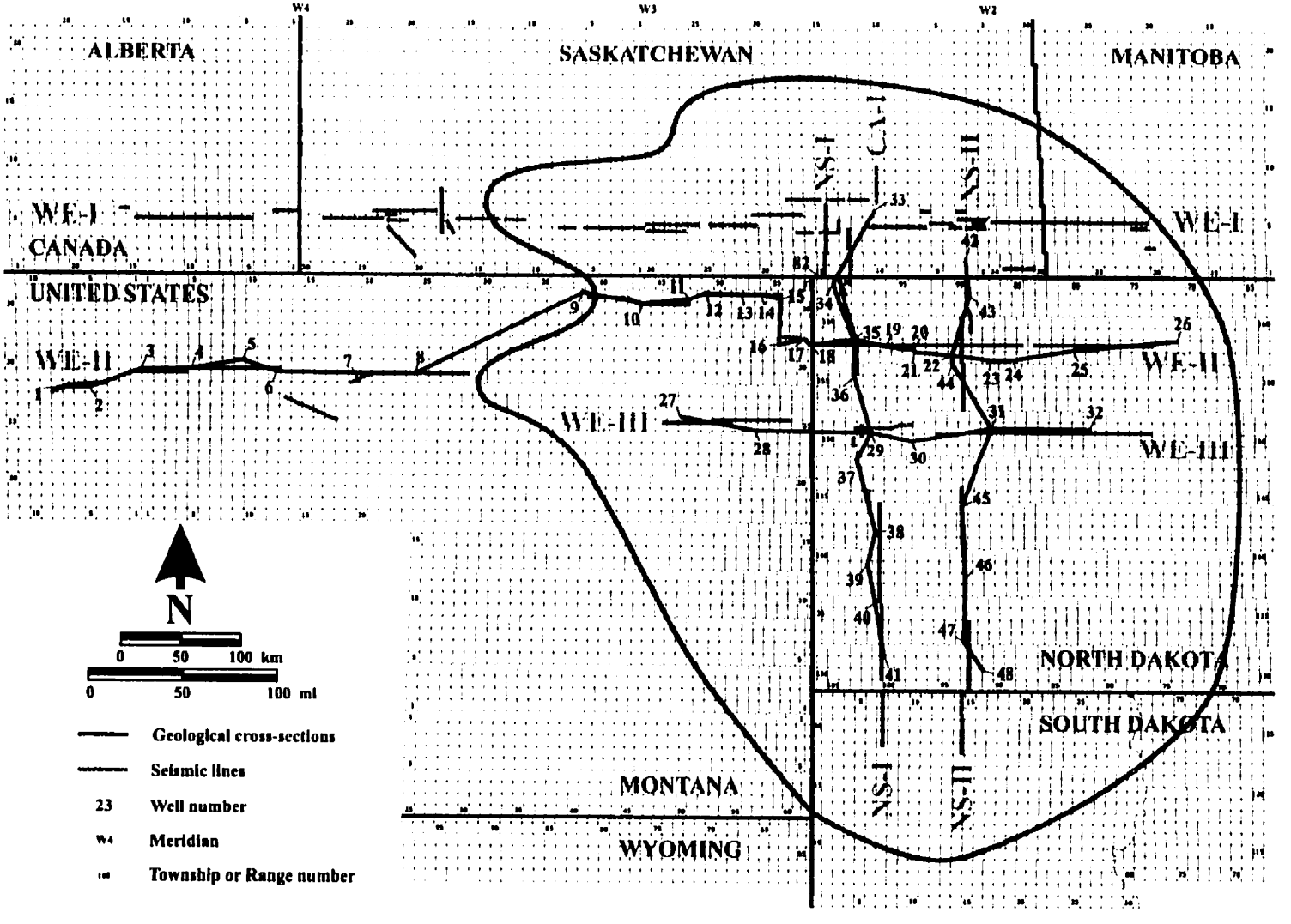

Fig. 2.5 Geological cross-sections.

2.2.1.1 Western part

The western part ***(Fig. 2.6)*** covers the ***Foothills***, ***Sweetgrass Arch***, ***Bearpaw Mountains*** and ***Bowdoin Dome*** areas. It starts at T28N, R8W, Sec. 28 (Well 1) location between the Sheep Creek and the 'Blackleaf Bird and Game Refuge', in Pondera County, Montana.

The ***Foothills*** region lies east of the Knowlton trend in the area between Well 1 and Well 2 ***(Fig. 2.7.a)***. Thrust sheets of the Laramide deformation involve Upper Cretaceous through Cambrian strata *(Napier, 1982)*. Reverse faults dominate the area; however, a major, NE-SW striking normal fault with strike-slip is present (Pendroy Fault), contributing to the trapping of hydrocarbons at the Gipsy Basin Field *(Chamberlain, 1985)*.

All the formations dip steeply to the west. The thickness and lithology of the Cambrian strata are uncertain due to the lack of deep borehole penetrations. The overlying Devonian (~Kaskaskia I) succession consists of a 350-400 m thick Souris River - Three Forks series; however, the whole Elk Point Group is missing. The Mississippian (~Kaskaskia II) section is around 400 m thick *(Johnson, 1984)*, where the series above the Bakken Formation comprises the Madison Lodgepole - Mission Canyon - Sun River (Charles equivalent) units. Both Kaskaskia subsequences have uniform thickness between the two wells. The unconformably overlying thin Jurassic (~Zuni I) Ellis Group gently thins from 100-150 m in the west to 60 m in the east. The overlying Zuni II-Tejas sediments exhibit a large foreland wedge thinning from 1350 m in Well 1 to 820 m in Well 2. Most of the thinning is attributed to the uplift in the Sweetgrass Arch to the east.

The ***Sweetgrass Arch*** traverses the cross section roughly between Well 2 and Well 6 ***(Fig. 2.7.b)***. The structures on and around the area are closely related to the tectonic history of the Sweetgrass Arch, which is composed of two northwest-southeast striking antiforms, the North Arch (Kevin-Sunburst Dome) and the South Arch, offset

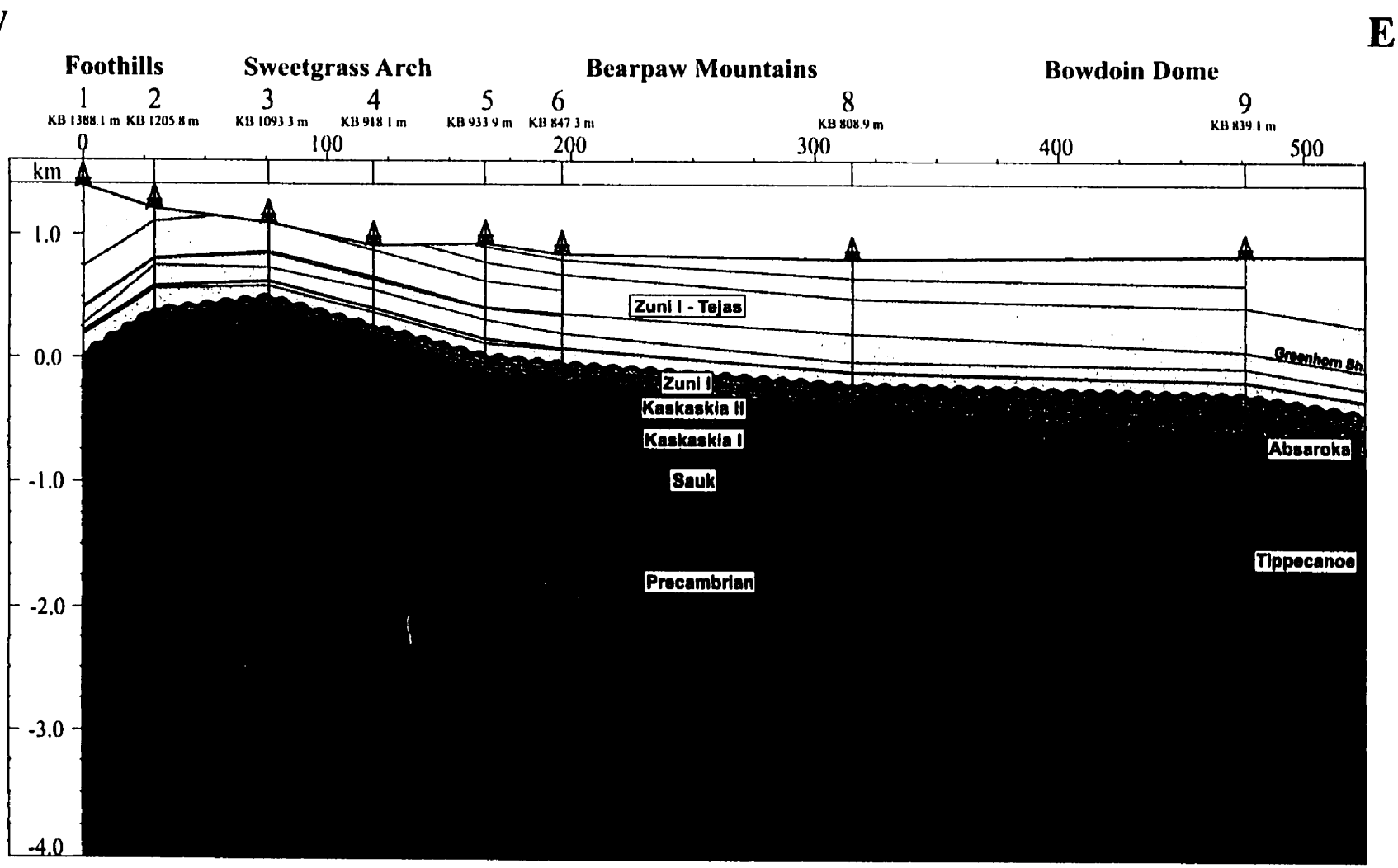

Fig. 2.6 Geological cross-section - Line WE II, Western Part.

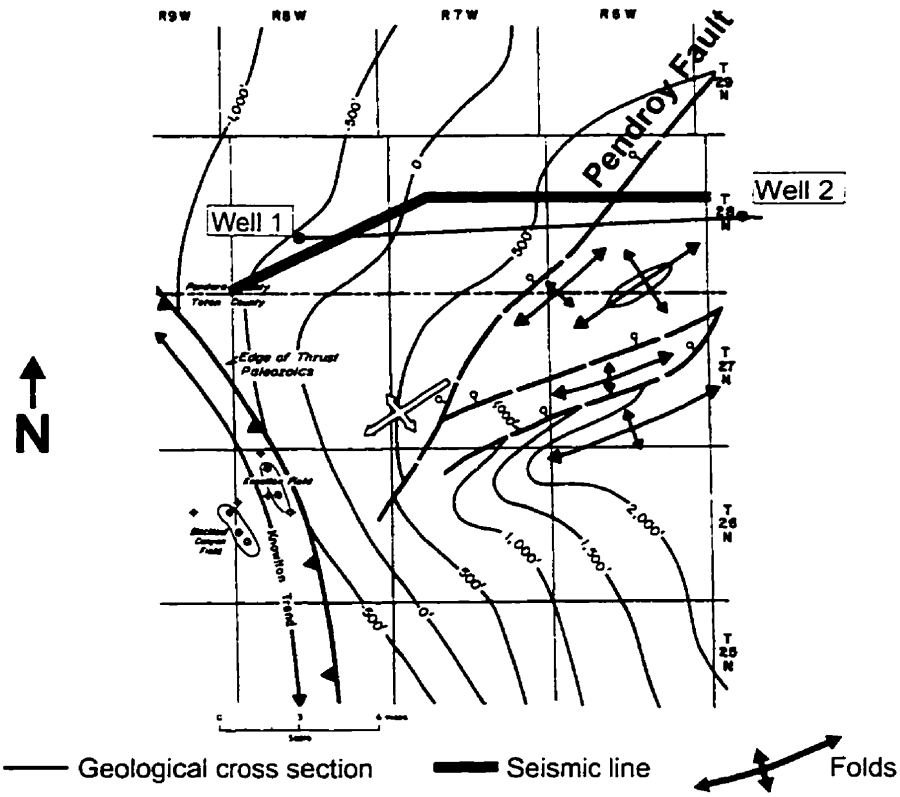

Fig. 2.7.a Structural map of the Foothills area between Well 1 and 2 (Napier, 1982) (top of Sun River dolomite).

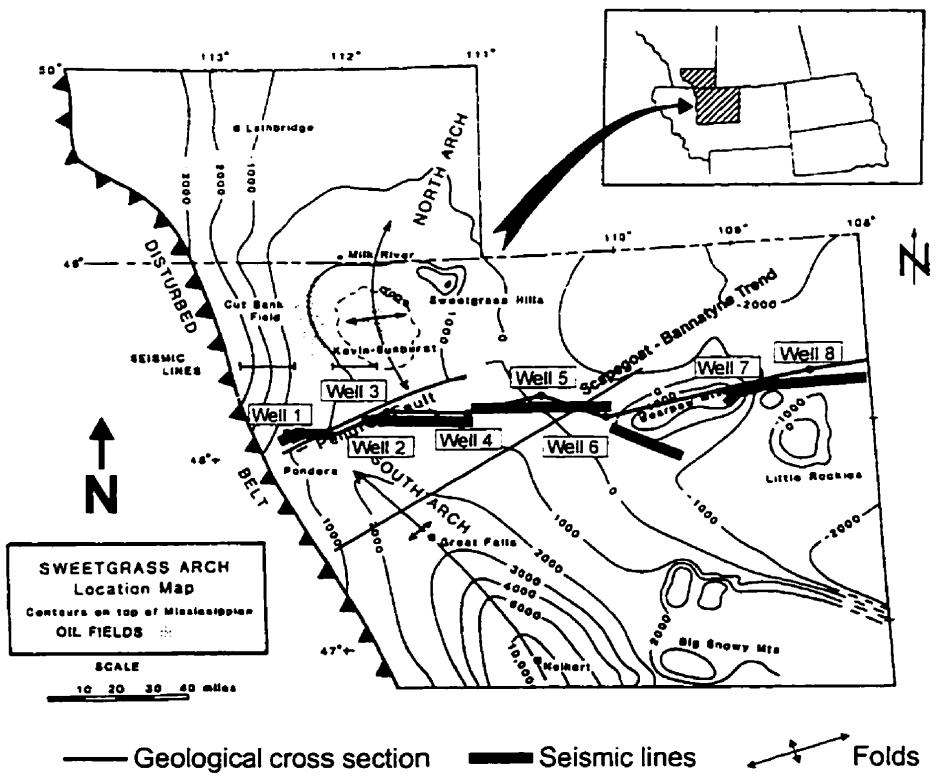

Fig. 2.7.b Map of the Sweetgrass Arch (Shepard and Bartow, 1986).

by the right lateral Pendroy Fault *(Lorenz, 1982)* ***(Figs. 2.7.a and b)***. The feature had its inception in the Cambrian or Late Precambrian and underwent regional pre-Devonian uplifts and consequent truncation, possibly in the Middle Cambrian, Silurian, Upper Mississippian and perhaps in the Pennsylvanian - Triassic periods *(Lorenz, 1982)*. In the mid-Mesozoic the regional tectonic pattern changed due to the Sevier Orogeny and the arch was uplifted again from the Middle Jurassic. The present structural configuration of the arch is the by-product of the Laramide Orogeny. Lorenz *(1982)* puts the main uplift to its early stage (Late Cretaceous–Paleocene), but Shepard and Bartow *(1986)* prefer the later phase (post-Eocene) due to a lack of thickness and facies changes on the east and west sides of the Arch during the Late Cretaceous – early Tertiary interval ***(Fig. 2.6)***.

Structurally, the Arch is interpreted as a forebulge of the thrust belt; however, it did not migrate with the recurrent thrust load *(Lorenz, 1982)*. At the eastern part of the segment, around Well 6 (Laredo Field, T29N, R12E) the NE-SW striking, SE dipping reverse faults (Butterfield, 1985) are probably related to the regional Scapegoat-Bannatyne Trend ***(Fig. 2.7.b)***.

There is evidence of thinning of Cambrian (~Sauk) sediments over the arch *(Lochman-Balk and Wilson, 1967)*. Thin sediments (0-20 m) of the Red River Formation of the Tippecanoe Sequence exist on the eastern side of the arch and thickening occurs to the east. Both Kaskaskia sequences are 350-375 m thick in the west and thinning over the arch to 225-250 m in the east. The overlying Jurassic formations (Ellis Group, Morrison Formation) of the Zuni I sequence are thin on the crestal part of the arch and thicken again toward the east, showing the effect of the Sevier Orogeny. The accompanying pre-Cretaceous unconformity bevels in some places into the deeper Mississippian strata *(Dolson et al., 1993)*. The thickness of the lower part of the overlying Zuni II – Tejas interval is fairly uniform, but the upper part is (~Tejas) thin and mostly eroded above the crest of the arch (Well 2 – Well 4) showing the effects of

the late Laramide (~post-Eocene) uplift. Around Well 3 at the Ledger Field (T30N, R1W), the surface formation is Upper Cretaceous Colorado Shale *(Ballard, 1985)*.

The segment between Well 6 and Well 8 is the ***Bearpaw Mountains*** area ***(Fig. 2.8.a)***. Well 7 is not on the cross-section because its immediate vicinity was affected by magmatic intrusion; thus it is not representative in the regional sense. The Bearpaw Mountains lie within the Great Falls Tectonic Zone *(O'Neill and Lopez, 1985; Best, 1991; Lopez, 1995)* which marks the northwest boundary of the Archean Wyoming Province. West of the Bearpaw area, a localized layering at a depth of 72 km, in the upper mantle, the "Lonesome Lake Complex", is associated with the development of the Bearpaw Mountains *(Best, 1991)*. On the surface, the Bearpaw Mountains are an erosional remnant of Tertiary igneous intrusions that occupy a circular area of about 55 km in diameter *(Reeves, 1953)*. The main volume of the Bearpaw Mountains consists of mafic phonolite and latite flows. The igneous activity occurred during the early Eocene (55 to 50 M.a.) *(Marvin et al., 1980)*.

The hypothesis of the structural history of the area, originated by Reeves *(1924, 1925, 1946)* early in the century, has not changed much; however, some problems still remain *(Reeves, 1953)*. According to this model ***(Fig. 2.8.b)***, a doming and subsequent erosion of the sedimentary rocks in the present mountain area were followed by periods of new volcanic activity when extrusive rocks accumulated in the mountain area. Later, during the more explosive phases, a plainsward sliding took place down the flanks of the mountain arch along the bentonite beds of the Upper Colorado strata, producing circularly arranged belts of thrust faults in the adjacent plains. This phase in the central region was accompanied by the formation of a rift, with the intrusion of dikes. At the close of the volcanic activity or after it, normal faulting occurred around the margins of the mountains. Similar, but smaller structures, attributed to the same mechanism were identified by Shouldice *(1963)* at the Bowes Dome, a couple of kilometers to the north, and by Lopez *(1995)* in the Sweet Grass Hills further to the northwest.

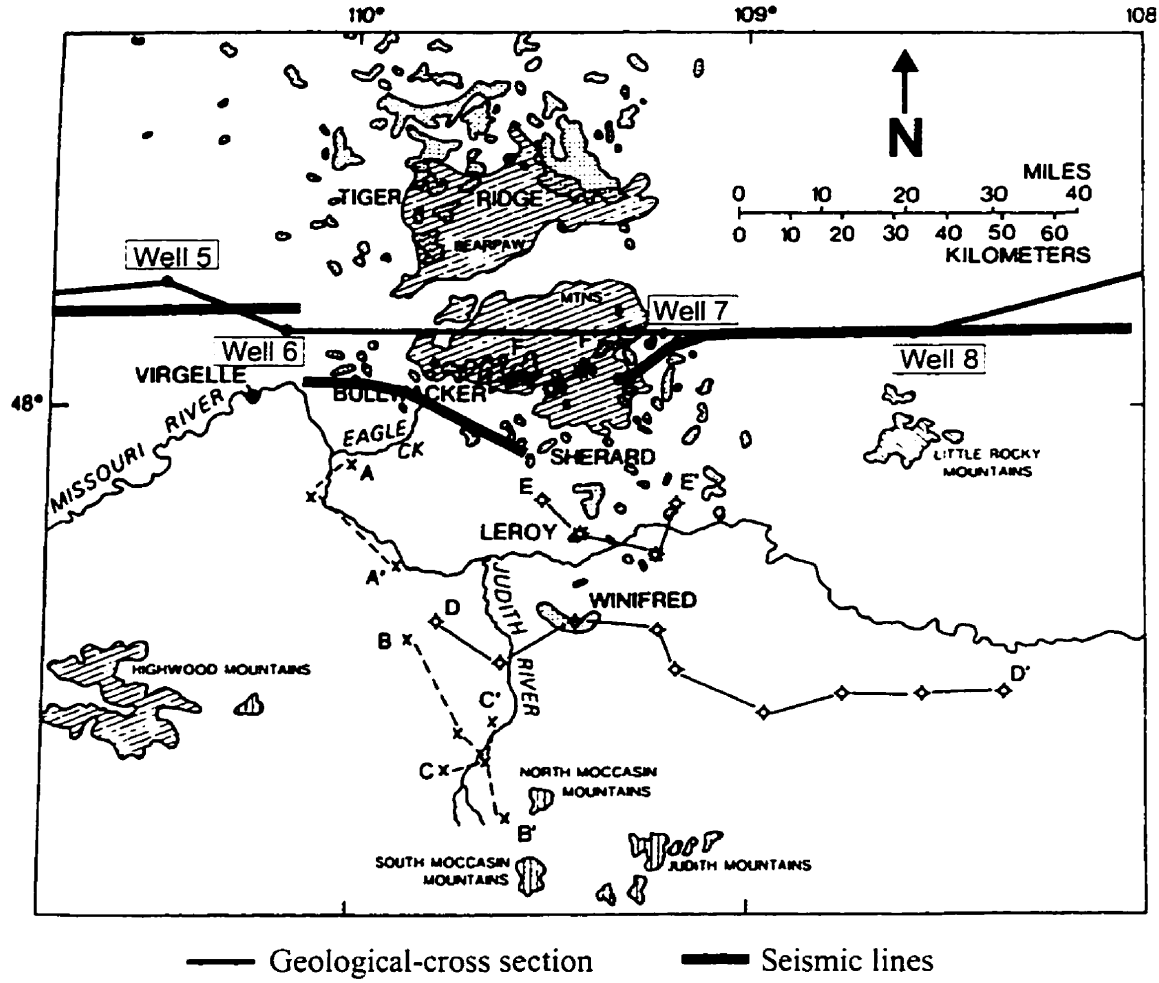

Fig. 2.8.a Map of the Bearpaw Mountains (Rice, 1980).

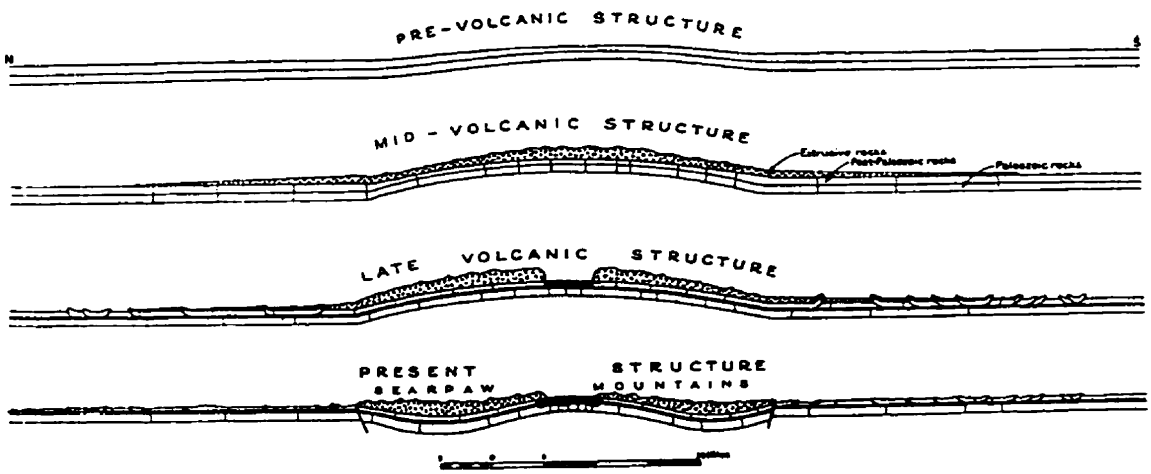

Fig. 2.8.b Structural development stages of the Bearpaw Mountains (Reeves, 1946).

Between Well 6 and Well 8 and further to the east, toward the Williston Basin, the sedimentary sequences generally thicken, with the exception of the Sauk Sequence. At the Bearpaw Mountains proper, below the Cretaceous layers, Devonian (Three Forks, Birdbear, Duperow) and Silurian (Red River) strata are in a high tectonic position (not indicated in the cross-section) due to the structural deformation during the magmatic intrusion; however, the structural features at the contact were never investigated closely (e.g., by the seismic method).

Between Well 8 and Well 9 the cross-section continues to the northeast, traversing the ***Bowdoin Dome*** in central Montana (no seismic coverage). The Bowdoin Dome structurally belongs to the marginal elements of the Williston basin. The Bowdoin Dome is a NW-SE striking arch broken by local arches, saddles, noses and by several NE-SW striking faults *(Nydegger et al., 1980)*. The structure was active throughout the Phanerozoic; however, the recent, major domal structure is a product of the Laramide Orogeny *(Nydegger et al., 1980)*.

Across the Bowdoin Dome the Sauk Sequence thins slightly; however, the rest of the sedimentary columns exhibit general thickening to the east. The Tippecanoe Sequence reaches 250 m in thickness and apart from the Red River Formation of the Big Horn Group, sediments of the Winnipeg Group and the Silurian Interlake Group appear in the under- and overlying layers, respectively. The lowest part of the Kaskaskia I subsequence exhibits thin Elk Point Group (Ashern, Winnipeg and Prairie formations) sediments. The rest of the subsequence shows a full Williston Basin succession of the Madison and Saskatchewan-Jefferson groups and the Three Forks Formation. Similarly, the Kaskaskia II subsequence exhibits Williston Basin affinity with the Bakken Formation, and a more extensive Lodgepole — Mission Canyon – Charles series of the Madison Group. The Big Snowy Group is still missing in this area. The first, thin (~35 m) appearance of the upper part of the Absaroka Sequence (Spearfish Formation) is observable. The Zuni I Ellis Group thickens considerably, reaching over 300 m thickness in this area. Even more dramatic is the thickening of the Zuni II - Tejas

interval from 900 m in the west to 1300 m in the east; however, the main contributor to this thickening is the uppermost part of the succession.

2.2.1.2 Eastern part

The eastern part of the WE II cross section ***(Fig. 2.9)*** covers the entire Williston Basin, from Well 10 in northeast Montana, to the T158W, R72W, Sec. 1 (Well 26) location in Pierce County, north-central North Dakota. Following the regional seismic line, the cross section is offset by a 30 km north-south segment between Well 15 and Well 16 in Montana ***(Fig. 2.5)***. The intersections with other regional cross sections are indicated ***(Fig. 2.9)***. Four subregions can be designated: the ***Williston Basin Margin*** (Fort Peck Reservation area, northeast Montana), the ***West-Central***, the ***Nesson Anticline***, and the ***Eastern Flank***. The cross section between Well 9 and Well 15 runs parallel to the northern edge of the Fort Peck Indian Reservation, an area of well-documented exploration.

Williston Basin Margin

Monson and Lund *(1991)* subdivided the Fort Peck Reservation area into three tectonic regimes. These are from west to east "Central Block", "Transition Zone" and "Williston Basin Element" ***(Fig. 2.10)***. The extension of the Central Block and of the Transition Zone is represented by the interval between Well 9 and Well 11 on the regional line.

The Central Block is practically the extension of the Bowdoin structure, confining the Wolf Creek Nose and the Poplar Dome *(Monson, 1995)*. Together they represent the major northwestern marginal structural element of the Williston Basin. Due to the proximity of the Poplar Dome to Line WE III, the discussion of its structure will be addressed there. Larger structures (Bowdoin Dome, Poplar Dome) in the Central Block were active tectonically throughout the Phanerozoic, while smaller features (e.g., Wolf Creek Nose) experienced at least one episode of tectonic reversal *(Shurr and Monson, 1995)*. A noticeable dip reversal occurs between the elevated Central Block

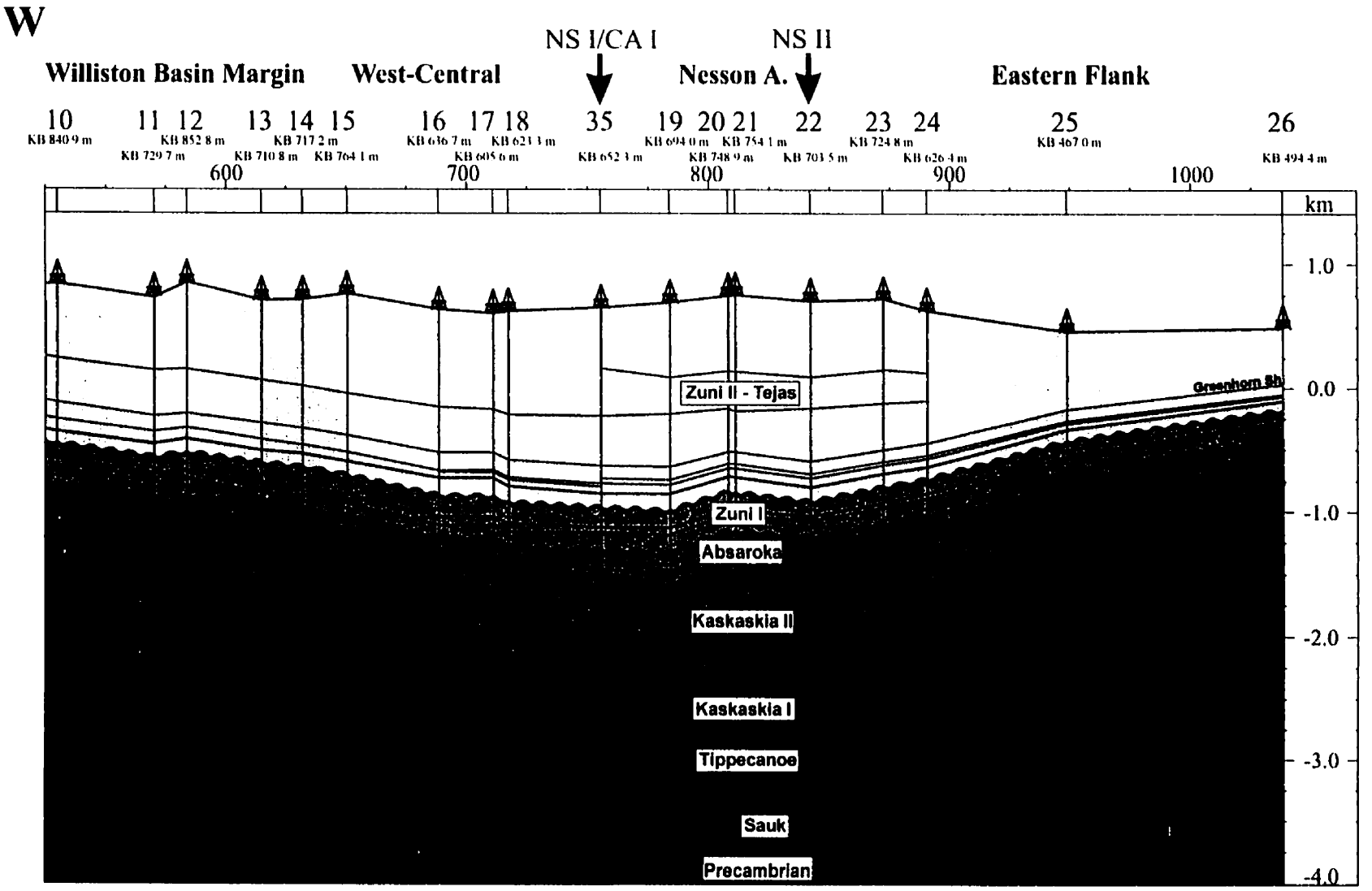

Fig. 2.9 Geological cross-section - Line WE II, Eastern Part.

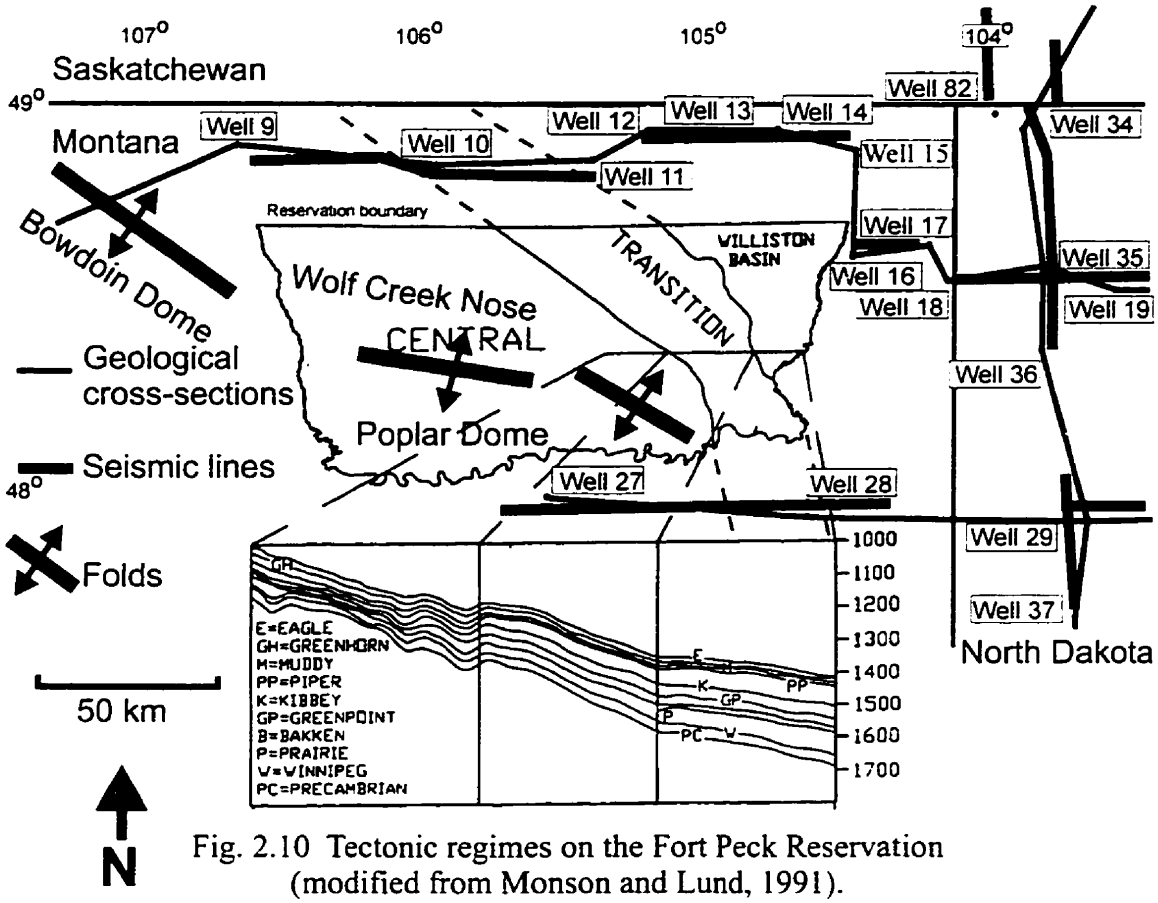

Fig. 2.10 Tectonic regimes on the Fort Peck Reservation (modified from Monson and Lund, 1991).

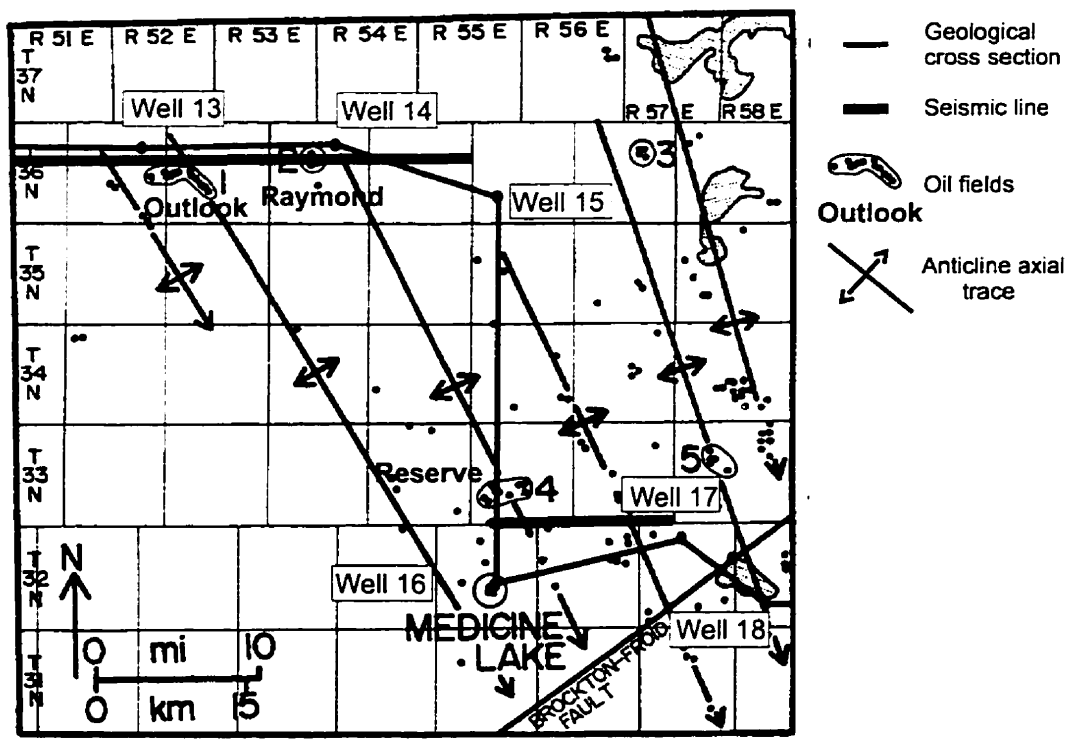

Fig. 2.11 Structure of the Sheridan County, Montana (Indorf and Norwood, 1987).

and the neighboring Transition Zone, which in turn with a steeper gradient "rolls" over into the Opheim Syncline [or the Smoke Creek Syncline] *(Monson, 1991)*.

The Transition Zone is the area of widespread fault activity observed in the fractured Bakken Formation and also marks the approximate limit of the Prairie Evaporite *(Monson, 1995)*; however, on the cross-section, the Prairie Evaporite is present from Well 9 (8 m thickness) to the east.

West-Central

The less steep area, east of the Transition Zone, starts with the Smoke Creek anticline, which belongs to the Williston Basin element ***(Fig. 2.10)***. This segment is represented in the cross section by the interval between Well 12 and Well 19. Between Well 15 and Well 16 the regional line is offset by 30 km from the north to the south.

Just 3 kilometers south of Well 13, in the Outlook Field (T36N, R52E), salt removal and collapse of the Prairie Evaporite and subsequent thickening of the overlying Duperow and Three Forks formations were detected *(Parker, 1967; Basinski, 1985)*.

Further to the east, at Well 14, the cross section passes through the Raymond Field (T36N, R53E). The field is situated on two southeast trending noses, forming together a NE-SW striking structural step. The structure is probably controlled by NW-SE striking faults. Low-relief structures were present from the Ordovician through the Mississippian *(Parker and Powe, 1982)*. Intermittent tectonic activity along basement faults caused fracturing in a number of formations *(Parker and Powe, 1982)*.

In the northeast corner of Montana ***(Fig. 2.11)***, between Well 15 and Well 16, the structural dip steepens toward the center of the basin. The tectonic activity in the area is governed by NW-SE striking faults in the western part, and NNW-SSE striking faults toward the eastern part, which possibly originated in the Precambrian and were

rejuvenated in Phanerozoic times, especially during the Laramide Orogeny. The younger, NE-SW striking secondary fault directions were developed during the Laramide Orogeny *(Andrew et al., 1991)*.

In the southern part ***(Figs. 2.10 and 11)***, between Well 16 and Well 18, the overall structural directions are similar and their Precambrian origin was emphasized by Indorf and Norwood *(1987)*. The presumed "Brockton-Froid Fault" does not offset these structural directions *(Indorf and Norwood, 1987)*. This part of the cross section traverses numerous stuctural noses with basin-center-trending axial traces. These structural noses are locations of numerous oil fields (e.g., Reserve, Colored Canyon, Katy Lake, Dagmar, Fishook, Clear Lake, Dwyer fields [T32-34N, R54-58E]). The trends of these noses are getting closer to north-south toward the east, closer to the deeper, central part of the basin. The cross section intersects the NS I/CA I line(s) at Well 35.

The WE II geological cross section reaches its maximum sedimentary thickness further to the east at Well 19 ***(Fig. 2.9)***. Here the thickness of the Sauk Sequence (Deadwood Formation) is around 200 m. The Tippecanoe Sequence with full Winnipeg, Big Horn and Interlake Groups reaches a thickness of 670 m. The overlying Kaskaskia I (Devonian) sequence, is represented by 570 m of sediments of the Elk Point, Manitoba, Saskatchewan-Jefferson Groups and the Three Forks Formation. The subsequent Kaskaskia II sequence exhibits full Bakken Formation overlain by the complex Madison Group and capped by the Big Snowy Group totalling 820 m of preserved sediments. The significant, 270-m thick Absaroka Sequence represents all the three subsequences: the Minnelusa Group (Pennsylvanian), the Opeche and Minnekahta formations (Permian) and the Spearfish Formation (Triassic). The Ellis Group of the Zuni I sequence reaches 320 m, while the rest of the Zuni Sequence and the Tejas Sequence (Inyan Kara, Colorado and Montana Groups) top the sedimentary column with a considerable 1690 m thickness.

Nesson Anticline

The next area to the east, between Well 19 and Well 22, is the Nesson Anticline ***(Fig. 2.12)***. This major north-south-trending structural feature in the basin is even more pronounced toward the south, where it is traversed by the WE III cross section. Structurally, the Anticline comprises at least six tectonic blocks, which are bounded by the major West Temple and West Nesson faults in the west and by the East Temple and East Nesson faults in the east *(Famakinwa, 1989)*. The role of the presumed numerous "regional lineaments" in the structural evolution of the anticline is not clear. The bounding faults have been present and active since Precambrian times *(Gerhard et al., 1987)*. Major structural movements are documented in the Ordovician, Silurian, Devonian, Mississippian, Pennsylvanian, Permian and Triassic periods *(Famakinwa, 1989)*. The role and position of the Nesson Anticline were interpreted differently by various authors; however, no model describes these adequately in the context of the basin's evolution as a whole. This thesis gives a new perspective on the Nesson Anticline that is in accordance with the regional and local constraints in space and in time.

Eastern Flank

The area from Well 22, where the line crosses the NS II geological cross section, to the end of the line (Well 26) ***(Fig. 2.5)***, represents the eastern flank of the Williston Basin ***(Figs. 2.9, 2.13 and 2.14)***. The area is dominated by structures trending toward the basin center (NE-SW in the west and more ENE-WSW towards the east) ***(Figs. 2.13 and 2.14)***. The geological profile just passes the SW Aurelia Field (T157N, R88-87W) east of Well 23 and bisects the Heartland Field (T157N, R84W) northeast of Well 24, while the seismic profile traverses the Mackobee Coulee Field (T158-159N, R85W) farther to the north. Northwest of Well 25, the line extends over the Glenburn Field (T158-159N, R82-81W). All of these fields are located within NE-SW (basin center) trending structural noses.

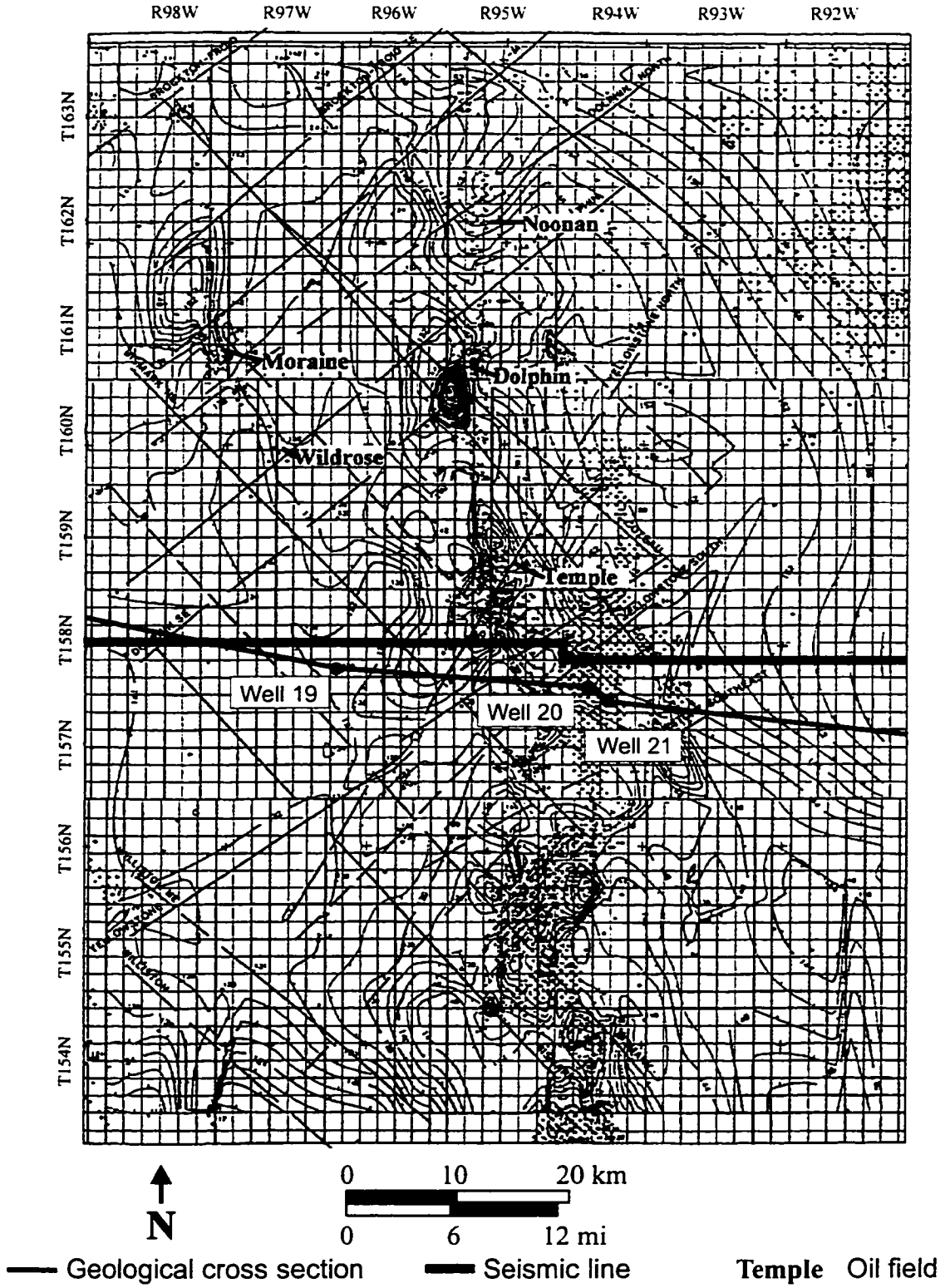

Fig. 2.12 Dawson Bay isopach map of the northern Nesson Anticline . (Inden and Burke, 1995).

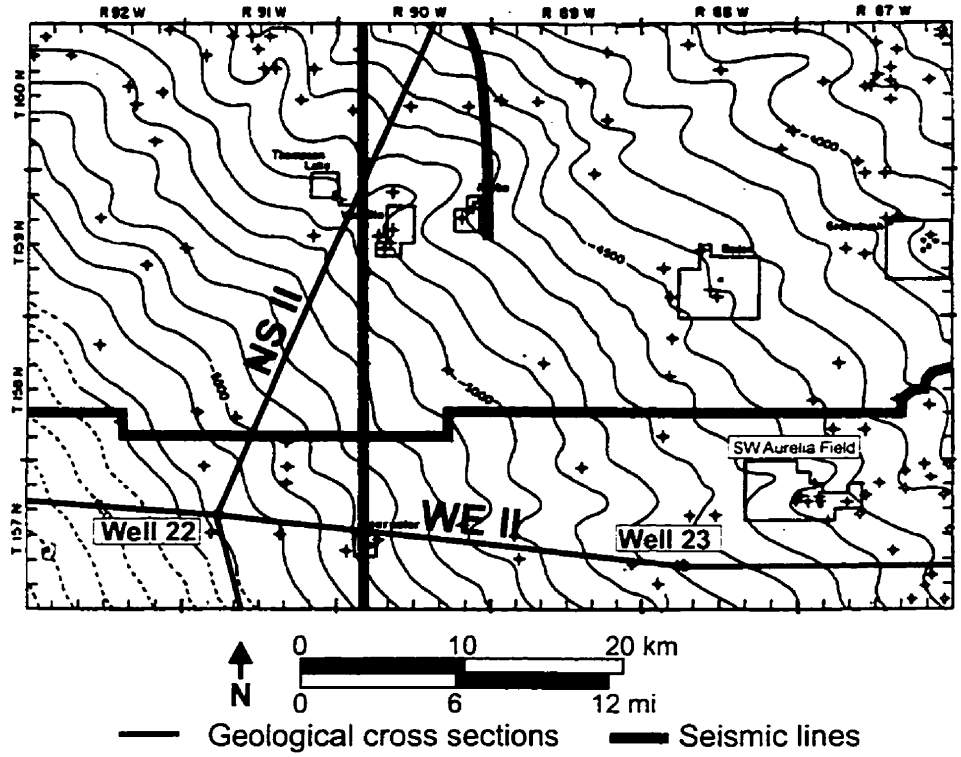

Fig. 2.13 Structure of the Coteau (Mississippian) interval in northern North Dakota (Burke, 1991).

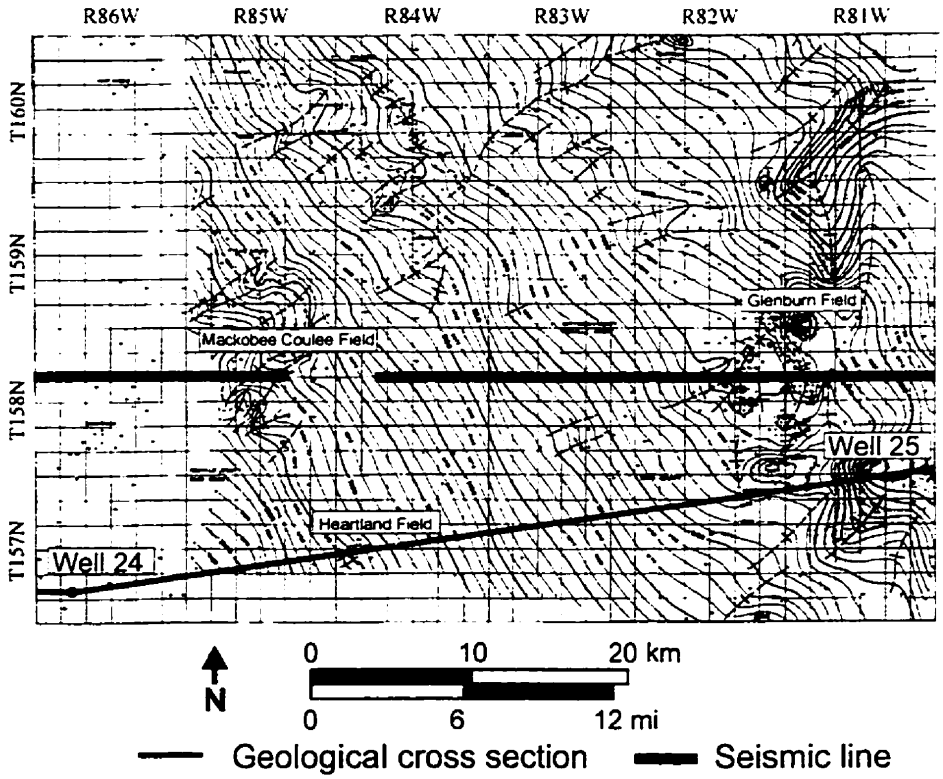

Fig. 2.14 Structure of the State "A" Marker bed in northern North Dakota (LeFever and Anderson, 1986).

The strata generally thin and/or wedge out to the east. The Deadwood Formation of the Sauk Sequence almost reaches its erosional edge and shows only 8 m preserved thickness. The Tippecanoe Sequence thins to 325 m, but all of the formations are present at the end of the line. The overlying Kaskaskia I thins by more than half between Well 22 (620 m) and Well 26 (255 m). The Prairie Evaporite pinches out between Well 24 and Well 25. The thickness of the Kaskaskia II sequence drops from 740 m to 120 m. The Bakken Formation disappears between Well 25 and Well 26. Formations of the Madison Group wedge out successively between Well 25 and Well 26. The Big Snowy Group vanishes between Well 24 and Well 25. The subsequent Absaroka Sequence, similarly to the Sauk Sequence, almost reaches its erosional edge and at the end of the line exhibits a bare 17 m total thickness. The lower and middle parts of this sequence disappear before Well 22 and Well 23, respectively. The Ellis Group of the Zuni I Sequence thins only 16% between Well 22 and Well 26. The lower part of the following Zuni II - Tejas interval preserves most of its thickness toward the east; however the upper part is progressively eroded in that direction.

2.2.2 WE III line

The geological cross section along the second seismic line starts at T26N, R48E, Sec. 29 (Well 27) in McCone County, Montana and ends at T151N, R80W, Sec. 22 (Well 32) in McHenry County, North Dakota ***(Figs. 2.5 and 2.15)***. This and the rest of the lines, with lengths ranging from 350 to 400 km, are half of the lateral extent of the WE II and do not extend beyond the Williston Basin proper. This west-east striking WE III profile ***(Fig. 2.5)*** with a length of 360 km, crosses the deepest portion of the basin and is located some 67 km (42 mi) south, and parallel to WE II. Similarly to the eastern part of WE II, structurally WE III can be subdivided into four portions: the ***Williston Basin Margin***, the ***West-Central***, the ***Nesson Anticline*** and the ***Eastern areas***.

Williston Basin Margin

The westernmost section, from Well 27 to Well 28, is parallel with the southern limit of the Fort Peck Indian Reservation (Missouri River) ***(Fig. 2.10)***. The area is

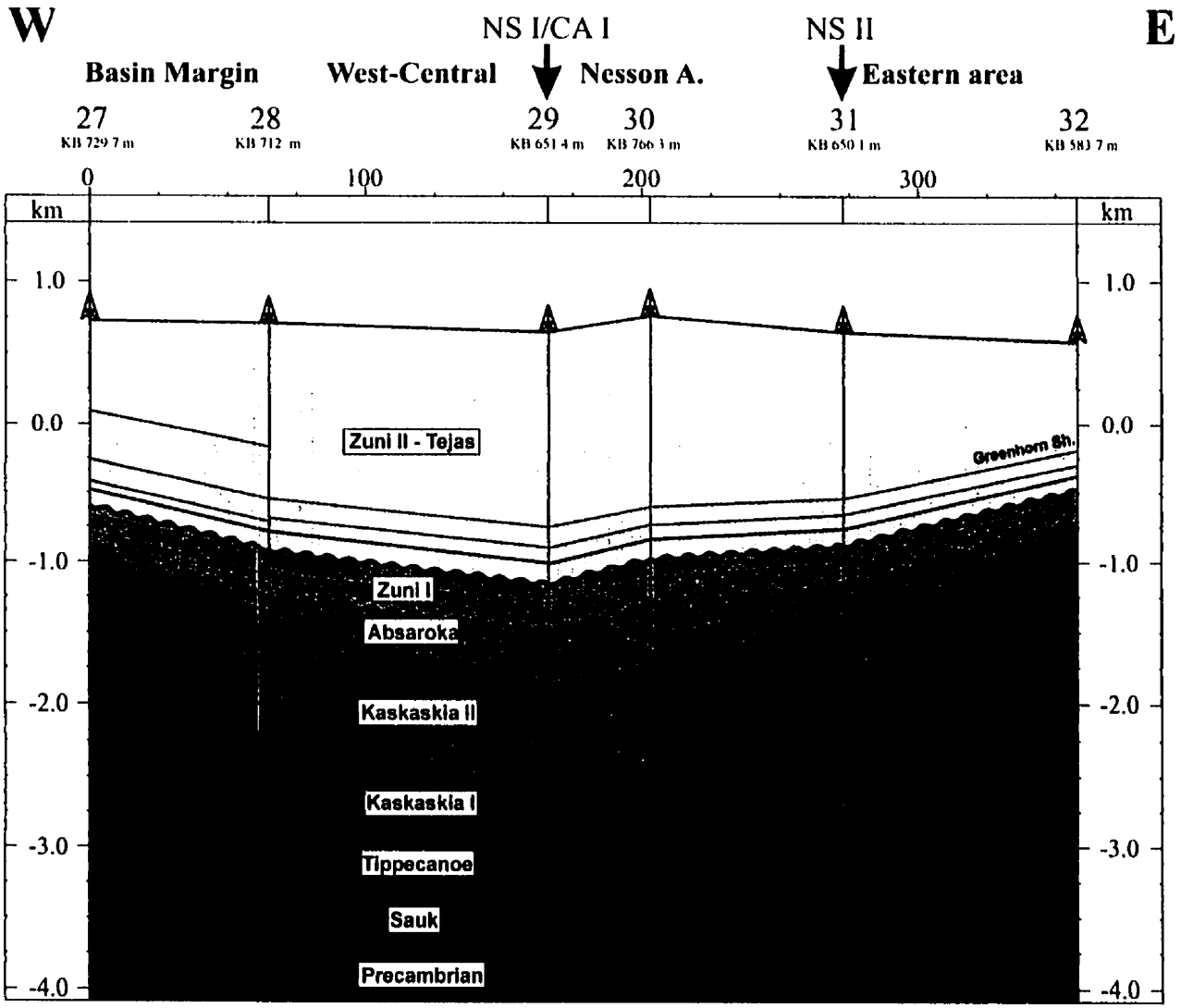

Fig. 2.15 Geological cross-section - Line WE III.

dominated by the presence of the southeastern extension of the Poplar Dome. The Poplar Dome is an elongated structural nose trending NW-SE toward the basin center. The steepest dip occurs along a flexure on the northeastern and eastern sides of the dome *(Orchard, 1987)*. The Poplar Dome was active throughout the Paleozoic. Its paleotectonic expression was detectable during the Upper Kaskaskia (Mississippian), Absaroka and Zuni II sequences *(Shurr and Monson, 1995)*. The major uplift, leading to the present-day structural configuration, occurred in the post-Paleozoic Laramide Orogeny *(Orchard, 1987)*.

West-Central area

Covering an area east of the Poplar Dome to Well 29 ***(Fig. 2.15)***, this portion of the basin is noted for a generally high density of small, low-relief, deep-seated structures *(Hill, 1985)*. These structural noses trend toward the center of the basin (in directions ranging from SE to E). Numerous oil fields are located in the area traversed by the cross section (e.g., Charlie Creek North, Stampede, Andes, Middle Sioux Pass, Otis Creek fields in Montana and Glass Bluff Field in North Dakota).

Between Well 27 and Well 29 there is no direct information about the thickness of the Sauk Sequence (Deadwood Formation). However, based on regional maps, it is in the range of 200-250 m and thickening toward the east. Most of the sequences reach their maximum thickness at or near Well 29, the deepest well of the study. The Tippecanoe Sequence along this 160-km interval more than doubles from about 280 m to 625 m. Similarly Kaskaskia I increases its thickness from 270 m to 480 m. The Kaskaskia II already has considerable thickness (670 m) in Well 27, due to the fact that it is located in the Big Snowy Trough area. The sequence thickens somewhat toward the center of the basin to 840 m. The Absaroka Sequence is represented in Well 27 by a bare 64 m of sediments and expands to 390 m in Well 29. The thickness of the Zuni I subsequence is fairly uniform in the range of 300-325 m. The lower part of the Zuni II - Tejas interval is also uniform, but the upper part thickens toward the center of the basin.

Nesson Anticline

East of Well 29, the next ~70 km of WE III line traverses the north-south striking Nesson Anticline and also records the deepest part of the basin ***(Fig. 2.16)***. The structure is bounded by the north-south striking, steep West and East Nesson faults. The Nesson Anticline has higher amplitude and is narrower at this portion than at its northern part; however, further south it splits into smaller secondary folds *(LeFever et al, 1987a)*. The cross section traverses three blocks of the Nesson Anticline across the Dimmick Lake, Clear Creek and Blue Buttes fields. The greatest uplift of these blocks occurred during the Devonian, Early Mississippian and Pennsylvanian *(LeFever et al., 1987a)*.

Eastern areas

East of the Nesson Anticline to the end of the line is the Eastern flank of the basin ***(Fig. 2.17)***. Like in the corresponding section of the WE II, the structural noses trend toward the center of the basin (WSW and W in this area) (northeast part of ***Fig. 2.17***) and the sedimentary sequences are gradually thin or wedge out to the east.

By the end of the line, the Sauk Sequence is reduced to some 50 m thickness. The Tippecanoe Sequence from 650 m in Well 31 shrinks to 44 m in Well 32. Similarly, on this ~100 m distance, the Kaskaskia I Sequence thins from 500 m to 320 m. The Kaskaskia II Sequence also thins from 710 m to 500 m in such a way that no sediments of the Big Snowy Group are present in Well 32. Approaching its erosional edge, the Absaroka Sequence is reduced to 60 m. Even the overlying Zuni I subsequence thins toward the east, however, not as dramatically as the sequences below (280 m - 220 m). The complex Zuni II - Tejas interval by the end of the line is thinned by a third from 1540 to 1060 m.

2.2.3 NS I / CA I lines

To emphasize the regional context of the geological features of the two major, parallel, north-south lines, two regional seismic profiles and geological cross sections

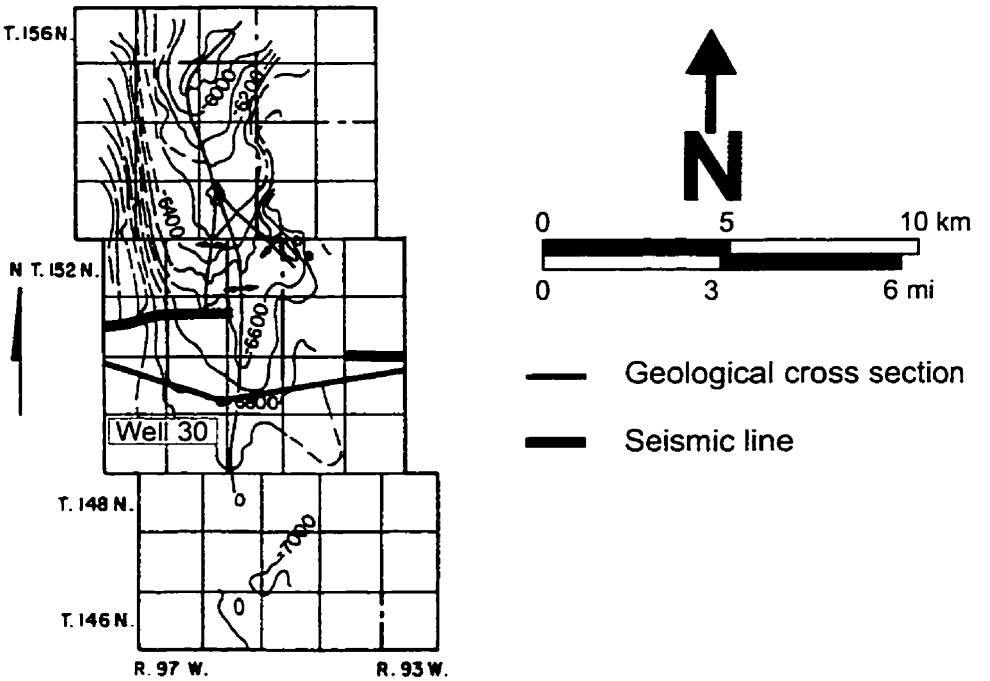

Fig. 2.16 Structural map of the top of the Mission Canyon Formation, southern part of the Nesson Anticline (LeFever et al, 1987a).

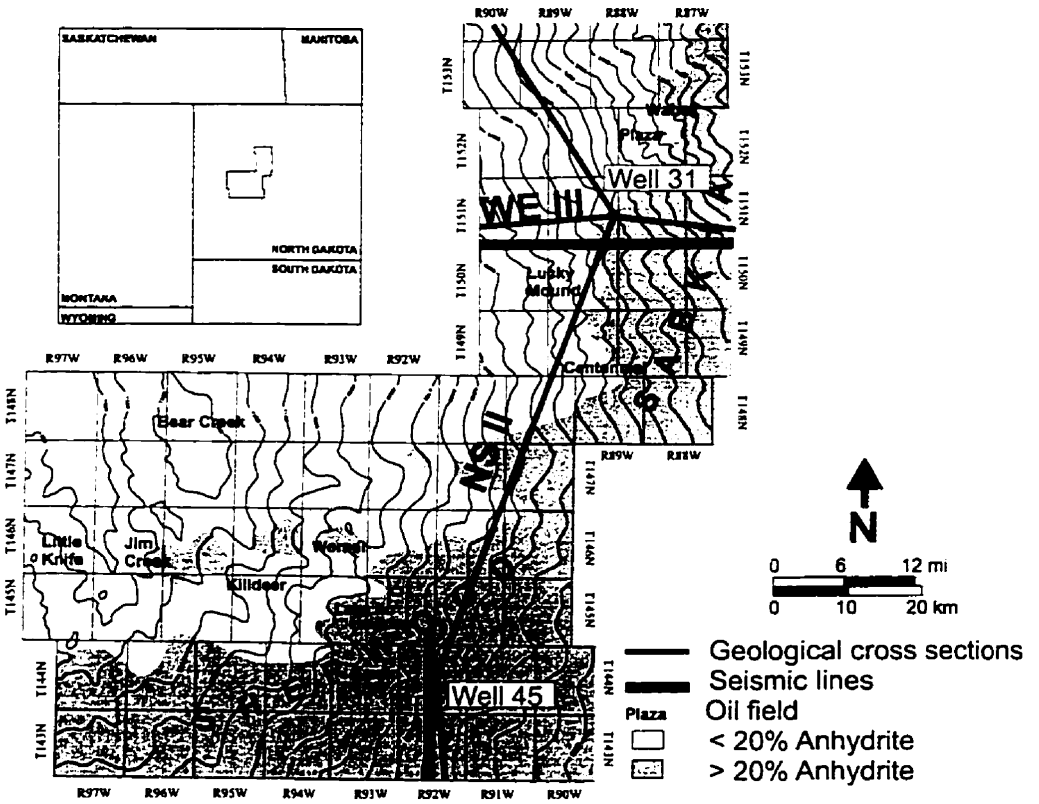

Fig. 2.17 Sherwood subinterval (Mission Canyon Formation) structure, McLean, Mountrail and Dunn counties, North Dakota (McClellan, 1995).

were constructed (NS I and CA I lines) ***(Fig. 2.5)***. Since only Well 33 provides additional information along line CA I, no new geologic section was generated for this line. Well 33 was incorporated into the geological information of NS I ***(Fig. 2.18)***. The NS I (CA I) geological cross section starts at 6-10-6-10W2 in the Midale area of Saskatchewan and ends at 6-131N-100W in Bowman County, North Dakota. The seismic line extends some 45 km to the south into South Dakota. The CA I geological cross section runs in a north-south direction across the deepest part of the Williston Basin, covering 400 km. The basin in this section exhibits a slightly asymmetric pattern, steeper dips on the northern side and more moderate trends on the southern flank as a consequence of the line crossing the axis of the basin (~NNW-SSW) at an angle. Subsequently, the section can be subdivided into a ***northern section*** (Well 33 - Well 29) and a ***southern interval*** (Well 29 - Well 41).

Northern part

The northern part incorporates the Canadian section of the line ***(Figs. 2.18 and 19)***, an area of gently dipping, basin-center-trending structural noses (SSE, S in this area). Numerous oil fields are located on or around the line on these noses (e.g., Bromhead [T3, R13-12W2], Oungre [T2, R14W2] and Hoffer [T1, R15W2] fields).

The structurally important NW-SE trending Hummingbird Trough is situated west of the area. In the trough region, Prairie Salt dissolution and accompanying collapse have taken place at different times, ranging from the Upper Devonian through the Cretaceous *(Hartling et al., 1982)*. From the international border to Well 36, where the line runs parallel with the Nesson Anticline, the stratigraphic dip is fairly uniform and no major structure is encountered. The segment between Well 36 and Well 29 comprises the deepest portion of the geology. The region is characterized by east-to-southeast trending structural noses *(Dean, 1987)* pointing toward the geometric center of the basin, which is located just east of Charlson, ND and Keene, ND *(Ahern and Mrkvicka, 1984)*. These noses were active throughout the Phanerozoic *(Mayer, 1987;*

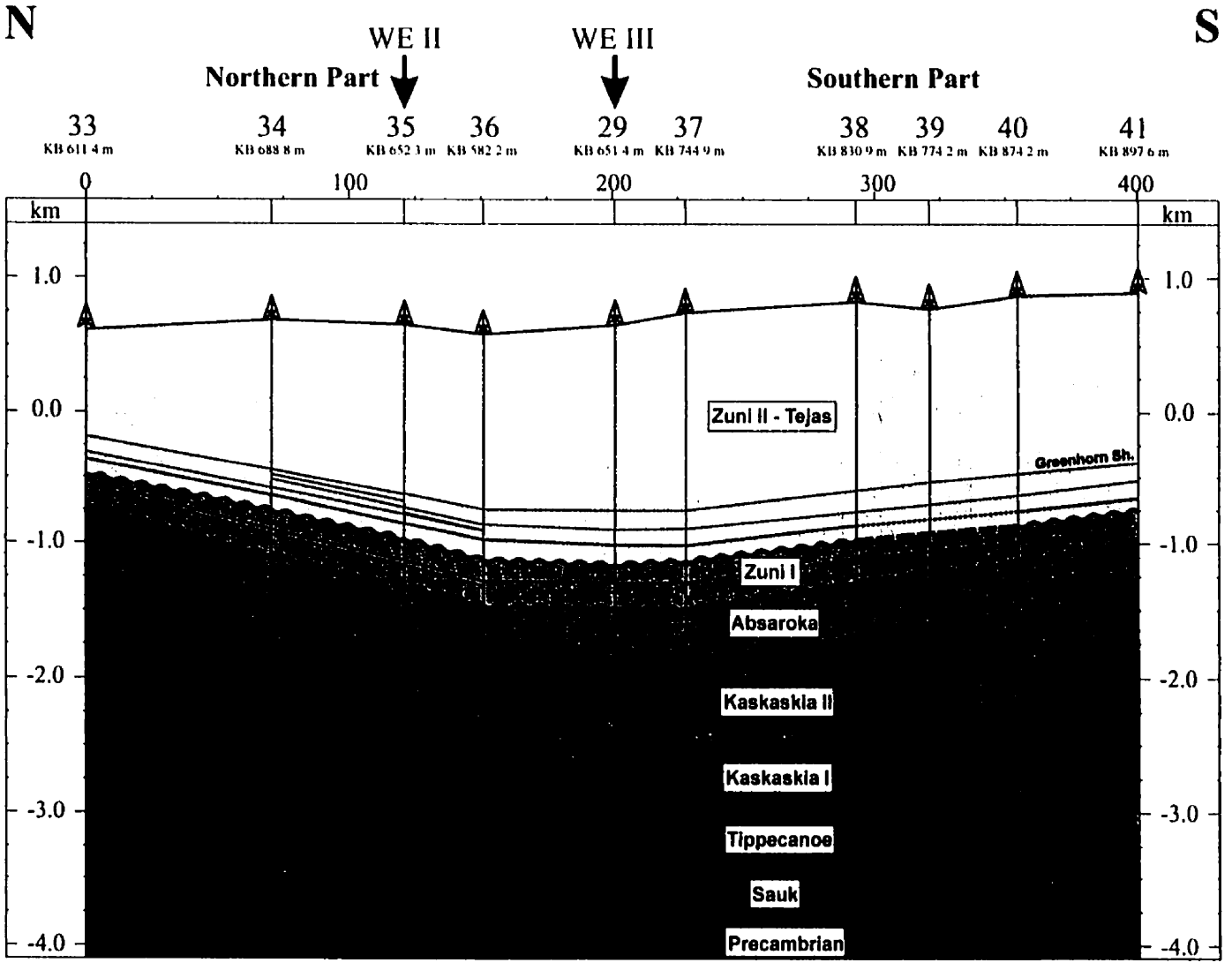

Fig. 2.18 Geological cross-section - Line NS I (CA I).

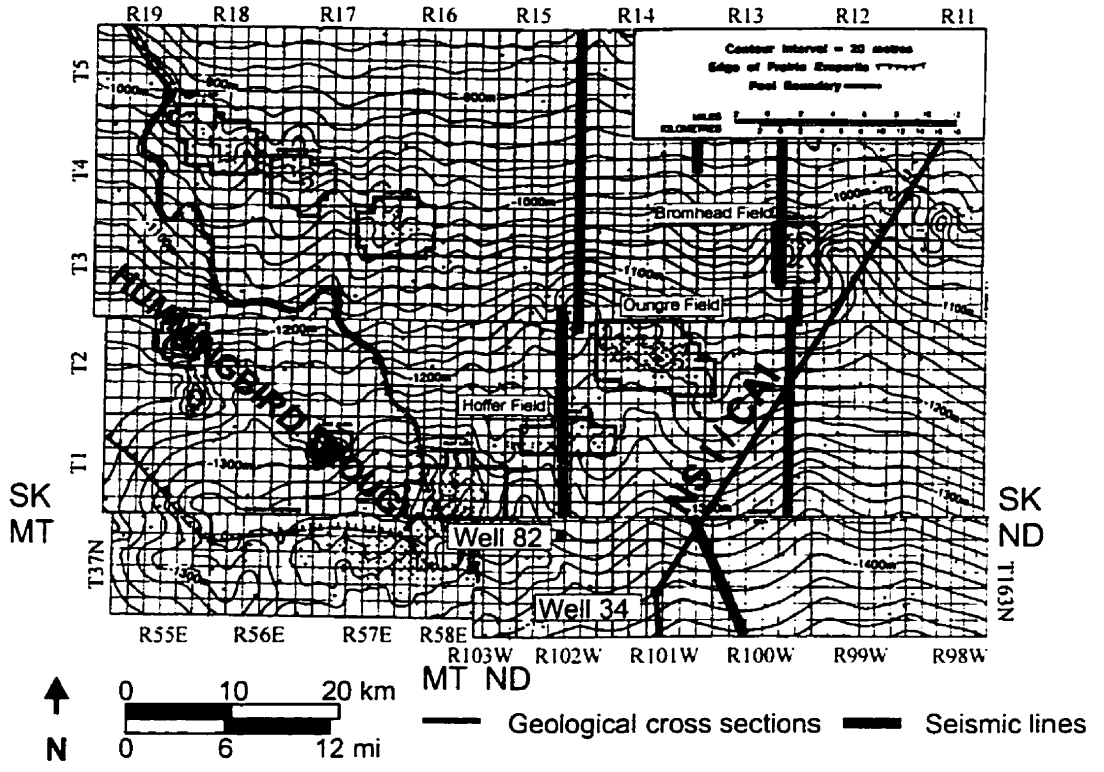

Fig. 2.19 Structure map on the top of the Oungre Zone (Charles Formation), in southern Saskatchewan and adjacent areas (Hartling et al., 1982).

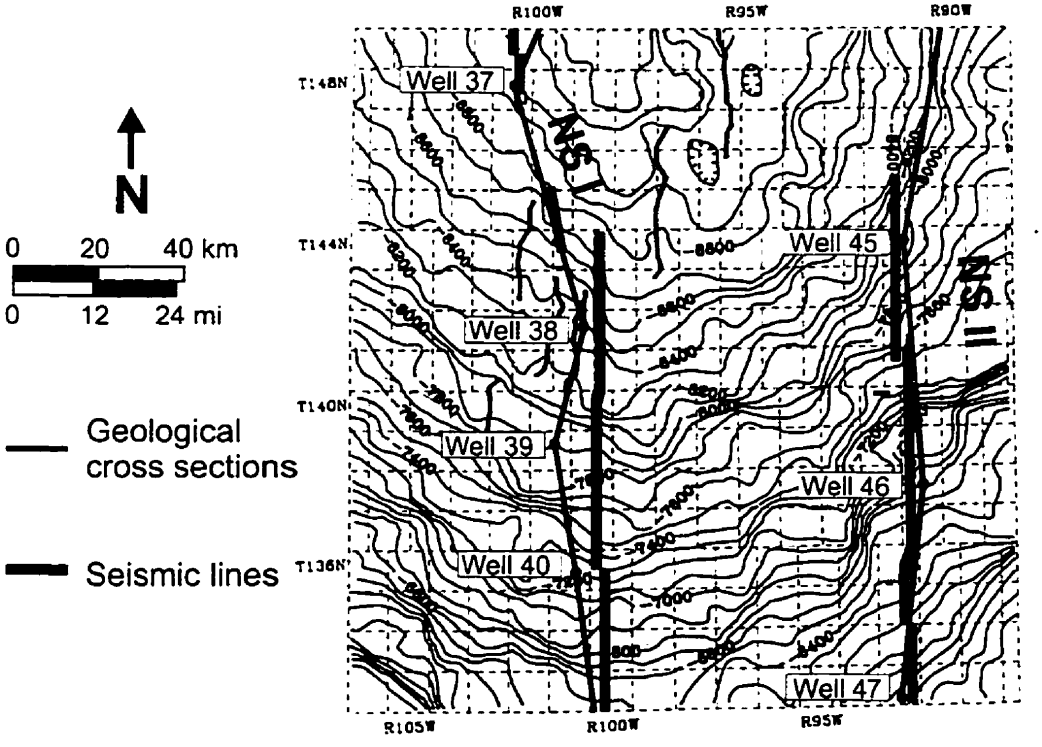

Fig. 2.20 Structure map on the top of the Duperow Formation (Devonian) in southwestern North Dakota (LeFever and Crashell, 1991).

Dean, 1987) are the locations of the Rosebud, Baker, Trenton, Hardscrabble, Camp and Indian Hill oil fields.

From north to south, between Well 33 and Well 29, the Sauk Sequence thickens from 100 m to about 250 m. The Tippecanoe thickens from 420 m to 625 m in the same interval. The overlying Kaskaskia I Sequence, representing the deposits of the structurally different Elk Point Basin, thins southward from 612 m to 480 m. The southward thickening of the stratal pattern reappears in the Kaskaskia II Sequence (390 m - 840 m). The Absaroka Sequence thickens in this interval from 85 m to 390 m. The thickness of the Zuni I subsequence, only 200 m in Well 33, is otherwise in the range from 320 to 350 m between Well 34 and Well 29. The lower part of the Zuni II - Tejas has fairly uniform thickness along this 200 km, while the eroded upper part thickens toward the south.

Southern part

The gently dipping interval between Well 29 and Well 41 is in the southern flank of the basin ***(Figs. 2.18 and 20)***. The area is represented by structural noses trending toward the basin center. This means that the noses trend to the east in the northern part, to the northeast in the central part, and to north in the southern part of the segment ***(Figs. 2.18 and 20)***. The largest structures are the NNE-trending Billings nose and the N-trending Little Knife nose, bounded by steep faults. The Billings nose and Little Knife area with the adjacent structural noses are sites of numerous oil fields (e.g., Tree Top, Whiskey Joe, West and East Fryburg, Medora, Four Eyes, Big Stick, T-R, Rough Rider, Elkhorn Ranch, Little Knife, Knutson and Square Butte fields). The structures behaved independently of each other throughout time *(LeFever and Crashell, 1991)*, although the structural activities on them were more or less coeval. Active periods took place presumably from the early Paleozoic; however, only the later ones (Devonian, Mississippian and Late Cretaceous) were documented *(LeFever and Crashell, 1991)*. A post-Mesozoic, NE-SW and NW-SE set of fractures has been observed in the Little Knife area *(Narr and Burrus, 1984)*.

Two local, circular structural anomalies along the line can be distinguished on almost all maps. The northern one is the Red Wing Creek "concentricline" at T148N, R101E ***(Fig. 2.21)***, once attributed to meteorite impact (astrobleme) *(Bridges, 1978)* and later reinterpreted as a result of a multi-stage tectonic movement along intersecting strike-slip faults *(Bridges, 1987)*. To the south, the Cold Turkey Creek structure at T130N, R102W, originally also believed to be of a meteoritic origin, is similarly reinterpreted as a tectonically controlled feature *(Gerhard et al., 1995)*.

From the central part of the basin to the end of the line, the Sauk Sequence thins somewhat from ~250 m to ~200 m. Thinning of the Tippecanoe Sequence is more pronounced (625 m - 390 m). The Kaskaskia I subsequence thins dramatically to the south from 480 m to 150 m, in such a way that that the Elk Point Group wedges out between Well 39 and Well 40 and only a few meters are preserved from the Souris River Formation of the Manitoba Group in Well 41. The thickness of the Kaskaskia II subsequence drops from 840 m to 510 m. The Bakken Formation pinches out between Well 38 and Well 39. The Absaroka Sequence is fairly uniform along this 200 km line in the range of 360-430 m. The Zuni I subsequence thins gradually toward the south (320 m - 230 m). The eroded Zuni II – Tejas interval is progressively reduced in thickness from 1810 m to 1650 m.

2.2.4 NS II line

The last, 370-km long north-south cross section starts at 13-24-2-3W2 on the Canadian side of the border and ends at T130N, R91W, Sec. 7 in Adams County, North Dakota ***(Fig 2.22)***. Similarly to the NS I / CA I line, its northern flank is steeper than its southern one. The apparently higher structural position of Well 31 is the consequence of its location, 25 km (15.5 mi) east of the north-south axis of the line ***(Fig. 2.5)***. Nevertheless this well is the informal boundary of the ***northern*** and ***southern*** parts of the line.

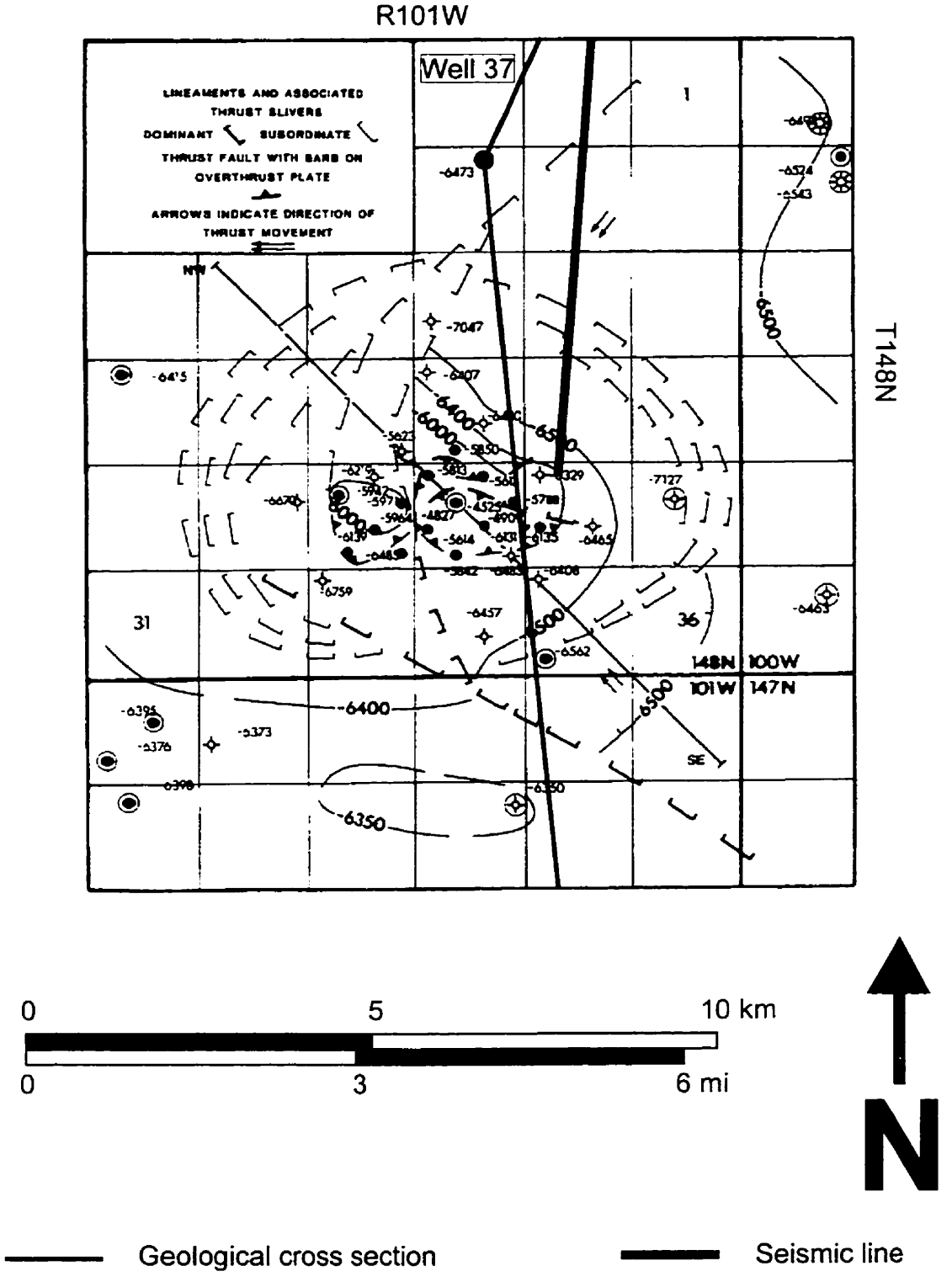

Fig. 2.21 Structure map of the Charles Formation (Mississippian), Red Wing Creek area, North Dakota (Bridges, 1987).

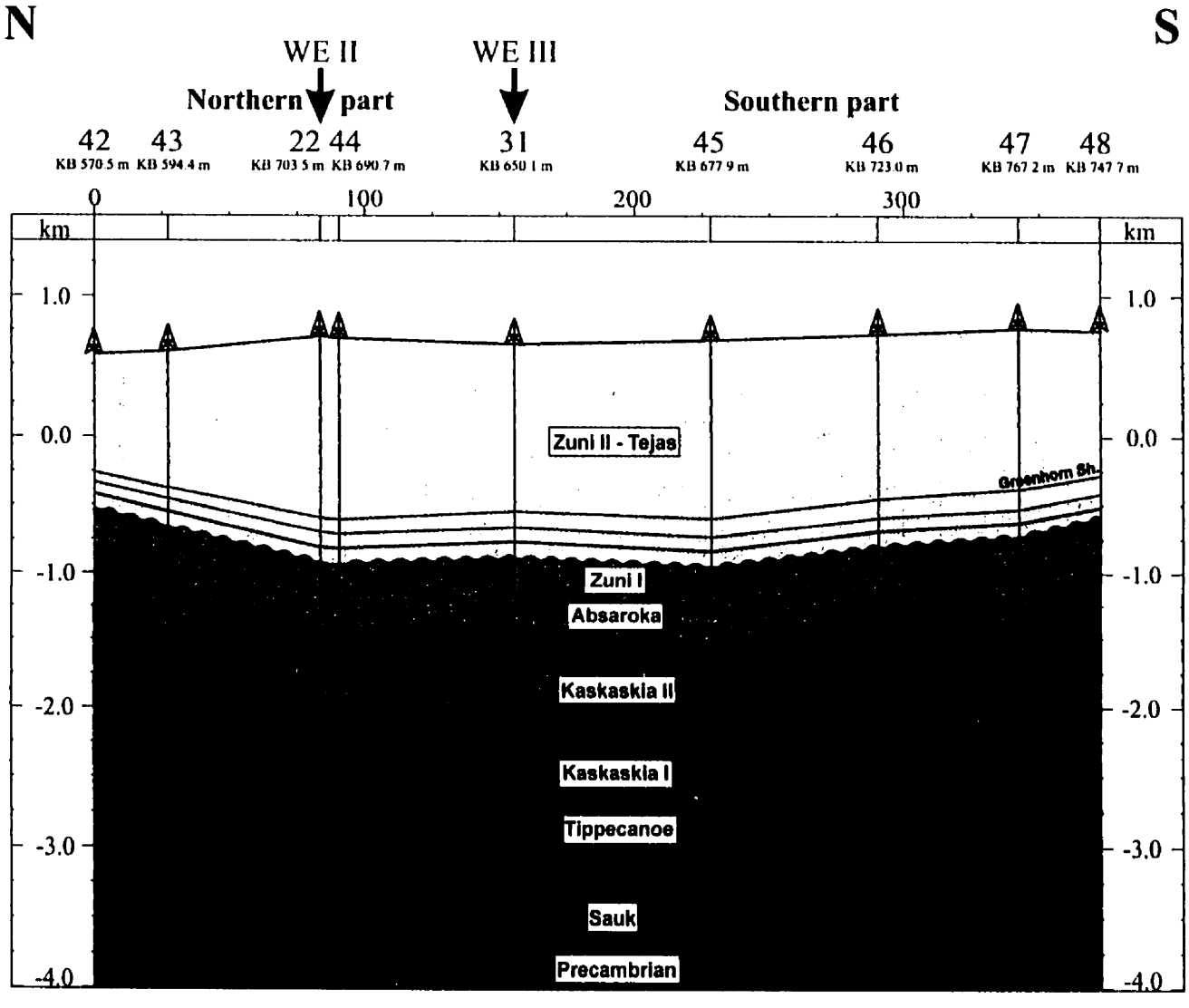

Fig. 2.22 Geological cross-section - Line NS II.

Northern part

The northern part crosses only a few kilometers of Canadian territory; the rest runs south of the international border ***(Figs. 2.23, 2.13, and 2.17)***. The line crosses structural noses trending toward the basin center. Proceeding from north to south, the noses trend SW in the northernmost part ***(Fig. 2.23)***, WSW in the central part ***(Fig. 2.13)*** and W in the southern part ***(Fig. 2.17)*** of this interval. Most of these noses trap significant amounts of hydrocarbons (e.g., Entry, Stony Run, Bowbells, Thompson Lake, Vanville, Clearwater fields).

The Sauk Sequence in the northern part thickens from ~200 m to ~250 m toward the south. Similar, gradual thickening is observed on the Tippecanoe thickness (490 m - 710 m). The Kaskaskia I subsequence, thickens by only 60 m (560 m - 620 m) between Well 42 and Well 44. The Kaskaskia II almost doubles its thickness (400 m - 760 m) in the same interval. Even more dramatic is the thickness change of the Absaroka Sequence (60 m - 215 m) along this 90 km stretch. The Zuni I subsequence moderately increases its thickness toward the south (250 m - 300 m). A similar, gradual thickness change is observed in the Zuni II - Tejas interval (1100 m - 1625 m).

Southern part

The strata on the southern flank of the line, between Well 31 and Well 48, dip gently to the north. In this interval the structural noses also trend toward the basin's center, to the W and WNW on the northern segment ***(Fig. 2.17)*** and to the NW and NNW on the southern segment ***(Fig. 2.20)***. Similarly to the southern part of NS I /CA I, recurrent structural activity during the Paleozoic and Mesozoic was documented on these structures *(LeFever and Crashell, 1991)*. In this part the line also traverses important oil fields, located on the structural noses (e.g., Lucky Mound, Halliday, Buffalo Creek).

Between Well 45 and Well 48 the Sauk Sequence thins from ~250 m to 115 m. The thickness of the Tippecanoe Sequence is reduced from 670 m to 380 m. The

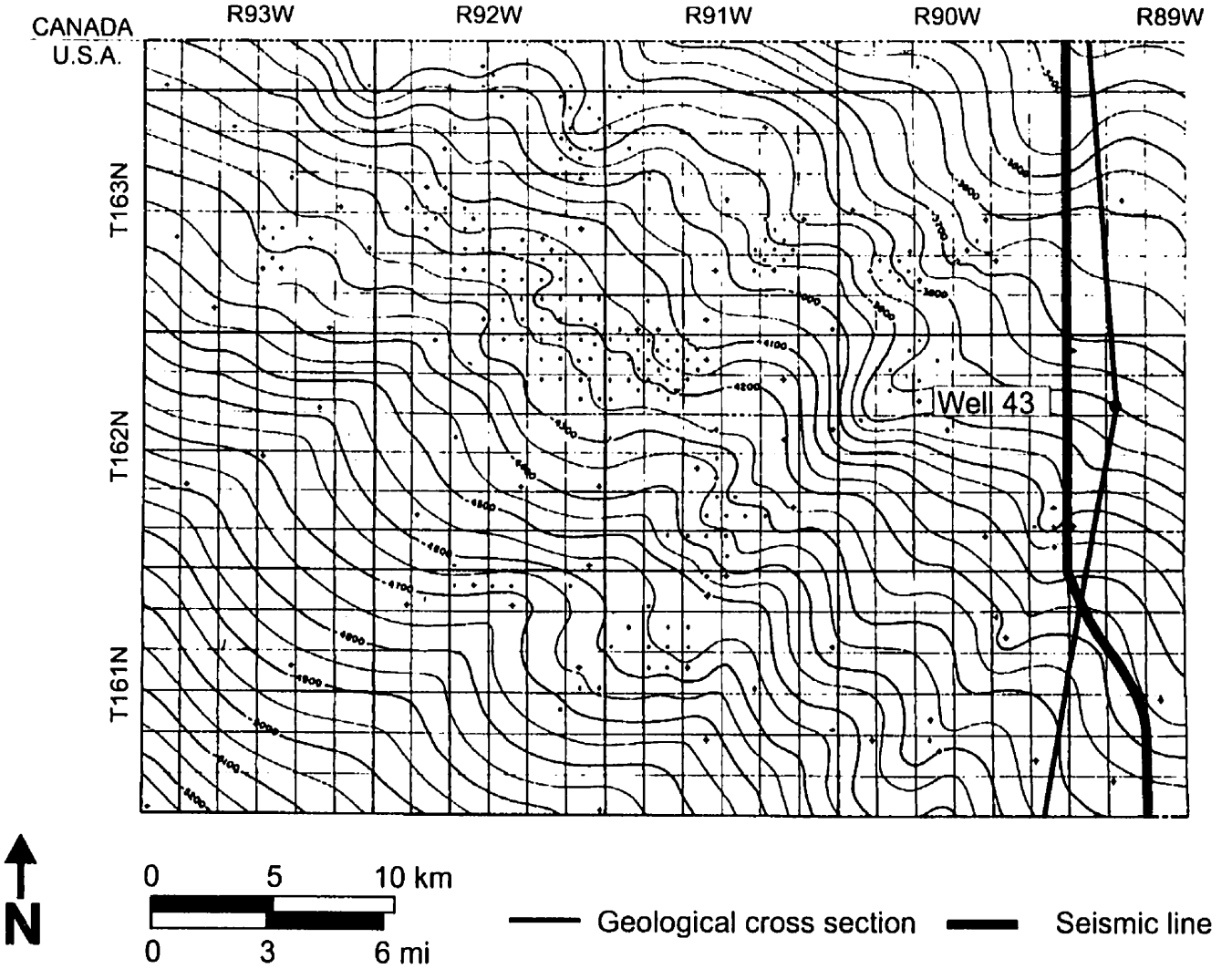

Fig. 2.23 Structure of the Rival subinterval of the Mision Canyon Formation (Mississippian) in north-central North Dakota (Anderson et al., 1960).

Kaskaskia I thickness drops to less than half, from 400 m to 170 m. Sediments of the Elk Point Group wedge out between Well 45 and 46. The Kaskaskia II subsequence thins from 750 m to 475 m along this 150 km stretch. The Bakken Formation wedges out between Well 46 and Well 47. The Absaroka Sequence thickens gradually from 370 m to 200 m. The Zuni I subsequence undergoes a similar decrease in thickness toward the south (280 m - 185 m). A relatively small thinning of the Zuni II – Tejas interval is observed (1630 m - 1340 m).

CHAPTER 3

CRATONIC BASINS AND BASIN EVOLUTION MODELS: CRITICAL REVIEW AND PROBLEM STATEMENT

Before the discussion of evolution models and structures of cratonic basins, the definition of "craton" and "cratonic basin" should be given.

"Cratons" are synonymous with extensive regions of thick continental crust, suggesting that cratons extend oceanward as far and as long as the presence of continuous thick continental crust is indicated for the time span in question *(Sloss, 1988a)*. Phanerozoic cratonic boundaries therefore shift with time, a principle accepted in the interpretation of Precambrian history. Consequently, the eastern, Appalachian margin of North America became "cratonized" in the Mesozoic and remained so, while the western margin was "de-cratonized" since the Sevier and Laramide orogenies *(Sloss, 1988a)*.

Accordingly, "cratonic basins" are basins located either on cratonic margins (pericratonic basins) or in the interiors of cratons (intracratonic basins). Here, only the latter, intracratonic type of cratonic basins will be addressed as analogues to the Williston Basin, since throughout its history, the Williston Basin was situated in cratonic interior areas.

3.1 Cratonic basin evolution models

The "deceptively simple" cratonic basins *(Bally, 1989)* remain stubbornly enigmatic. No model suggested to date has been able to describe satisfactorily every

aspect of their initiation, location, structure and evolution. Most of the subsidence models try to produce subsidence curves, which are constructed from well information (thickness, lithology). These curves basically plot sediment age versus depth, corrected for sediment compaction, variation paleobathymetry and isostatic amplification effects of sediment load *(Steckler and Watts, 1978)*. Obviously, a resulting subsidence curve is sensitive to the input parameters used (e.g., sea-level changes, compaction coefficient, etc.) and can vary from place to place within a basin due to the structural position of a given well. Generally, wells from the central part of a basin are used as representative of the basin's subsidence. Different basin modelers have viewed the same subsidence curve differently, which has resulted in different interpretations of various controlling factors on basin subsidence. Hypotheses on the origin of a cratonic basin can vary widely in different aspects:

Duration of subsidence. Disagreement pertaining to various basins exists about when the basins actually formed and how long they lasted as cratonic basins, since the areas in question can have different basinal history before and/or after the cratonic basin evolution.

Pattern of subsidence. Theories show one or two exponentially decreasing or increasing, linear patterns of subsidence.

Periodicity. Types of periodicity invoked in the models are: one, two or multiphase; continuous or episodic subsidence.

The theories can be put into categories; however, these categories are not mutually exclusive, since each theory has relative strengths and weaknesses.

3.1.1 Models based on lithospheric stretching and thermal contraction

The most popular thermal model invokes a heating event below the basin, followed by thermal contraction. As Quinlan *(1987)* pointed out, heating and cooling in

itself would not produce a basin; therefore, subcrustal thinning, subaerial erosion or phase change is required for subsidence.

Certain thermal models suggest a sigmoidally decreasing subsidence curve. This implies a slower initial subsidence phase, e.g., for the early Williston Basin evolution *(Ahern and Mrkvicka, 1984; Ahern and Ditmars, 1985)*. This approach assumes a heat source within the lithosphere below the basin (hot intrusive body), which was heated, uplifted, eroded and which then subsided isostatically due to the cooling and contraction of the heat source *(Nunn and Sleep, 1984)*. Some of these models emphasize the axial symmetry of the cratonic basin as could be expected from a point or disc-shaped heat source and point out that the location of maximum subsidence (location of the lithospheric load) would not change significantly during subsidence. This is more obvious if the data are corrected for tilting of the basin caused by tectonic effects in the neighboring orogenies *(Ahern and Dikeou, 1989)*. Where the heating event and related uplift and erosion are not obvious (Michigan Basin), the theory suggests that the heat source or thermal anomaly was at a great depth and did not reset the "thermal clock" *(Nunn et al., 1984)*. Observed periods of rapid/slow subsidence, which deviate from the exponentially decreasing subsidence rate consistent with thermal contraction, were interpreted as multiple heating events *(Cercone, 1984)*, changes in sediment supply *(Nunn and Sleep, 1984)*, or the consequence of periods of free thermal convection in the underlying rift *(Nunn, 1994)*; however, no explanations were given for the cause of this.

Others *(Klein and Hsui, 1987; Klein, 1991)* analyzing the subsidence curves from cratonic basins, concluded that they have a simple, exponentially decreasing pattern reflecting three phases of subsidence. These are the (a) initial, rapid fault-controlled subsidence (rift reactivation); (b) rapid thermal subsidence; and (c) slow thermal subsidence coupled with isostatically uncompensated mass. The problem remains, that not every cratonic basin is underlain by rifts, and even if it were, there is no evidence of reactivation. Klein and Hsui, *(1987)* and Klein *(1991)* accounted for a

second episode of subsidence in response to flexural foreland deformation in North American cratonic basins (Michigan, Illinois and Williston).

Another thermal model by Burke and Dewey *(1973)* and Burke *(1977)* is similar and suggests triple-junction rifting associated with a thermal plume as cause of the subsidence. Again, the problem remains in the case of basins without a rifted basement. In areas where they exist, they rarely exhibit triple-junction configurations. Nevertheless, this model could tackle the problem of axisymmetric character of most intracratonic basins.

3.1.2 Models based on crustal and mantle phase changes, metamorphism and intrusion

The phase-change model is based on the hypothesis that the Mohorovičić discontinuity is a phase boundary between gabbro and eclogite. The phase-change model supplies an alternative cause to subaerial erosion.

Haxby et al. *(1976)* proposed that cratonic basin formation involved mantle diapirs. According to this model, the hot asthenospheric mantle rocks intruded into the lithosphere and heated the lower crust, where metastable lower-density gabbro transformed into high-density eclogite. As the mantle rocks cooled, the cratonic basin subsidence began under the crustal load of the eclogite. A two-stage phase-change model has been proposed by several authors, emphasizing that subsidence of cratonic basins accelerates some time after it is initiated.

Ahern and Dikeou *(1989)* suggested that phase change is produced by heating during thermal rejuvenation, combined with the predicted thermal contraction following rejuvenation.

Middleton *(1980)* theorized that subsidence due to deep crustal metamorphism (greenschist to amphibolite) occurs during the latter part of the heating period, and is

followed immediately by subsidence due to thermal contraction during the cooling period.

According to Marechal and Lee *(1983)*, subsidence is caused by the superposition of the motion of a phase boundary and of the flexure of the elastic lithosphere in response to the loading of the Earth's surface by sediments, applying changes in pressure to describe the initial stages of the basin's subsidence.

Hamdani et al. *(1991)* reasoned that two-stage subsidence is the consequence of delayed phase change which causes accelerated subsidence after a time, on the order of 20 M.a. The delay is because of the time required for cooling at the lithosphere–asthenosphere boundary. They concluded that the phase-change mechanism is the dominating effect of the late stage of subsidence; however, they emphasized that the model can not be applied readily to cratonic basins with an extremely long subsidence history (e.g., the Williston Basin). In the Williston Basin, Hamdani et al. *(1994)* accounted for a longer delay (~ 40 M.a.) and a drop in the heat flow at the lithosphere-asthenosphere boundary.

Naimark and Ismail-Zadeh *(1995)* suggested that a cratonic basin was formed due to the subsidence of a heavy eclogite lens in the asthenosphere. They indicated a different time from other authors for the start of subsidence in the case of North American cratonic basins.

Stel et al. *(1993)* invoked a two-stage development model for intracratonic basins implying magmatic underplating as the governing factor of their evolution. The initial phase involves an incipient crustal dome, formed by asthenospheric upwelling, associated with basaltic underplating, and a migration of the induced lower-crustal melts to upper-crustal level causing a phase change of the dioritic melt to a denser mafic layer. The domal-style axial symmetry of the uplift is emphasized. Furthermore, they assume active rift involvement along "pre-existing" shear zones. Subsidence occurs in the

absence of crustal extension with an initial high rate due to crystallization of gabbro at the Moho, followed by low subsidence attributed to solid state cooling. The second phase of accelerated subsidence is related to the transformation of the gabbroic underplate to heavier eclogite.

Fowler and Nisbet *(1985)* considered a linear and continuous pattern for the subsidence curve of the Williston Basin resulted from the phase-change mechanism. Deviation from the linear trend is attributed to effects of episodic sea-level changes.

Bally *(1989)* warned that the main disadvantage of phase-change models is that they can not be used in a predictive sense and are used as a refuge, in ad-hoc mode, when all other explanation fails.

3.1.3 Models based on changes of in-plane stress and tectonic rejuvenation

In-plane-stress and tectonic-rejuvenation models suggest a multi-stage evolution of the cratonic basin with recurrently applied external forces; however, they can not resolve a basic problem of how lateral forces can cause oval-shaped intracratonic basins. Moreover, the external forces are vaguely termed as "far-field stresses", rarely quantified, and are just referred to as tectonic effects on the plate margins.

DeRito et al. *(1983)* theorized that they are related to successive cycles of intraplate stress application and removal in a temporal range of about 0.1 M.a. These intraplate stresses, according to them, were applied to the pre-existing lithospheric flexure, which, in turn, was due to the load of older rift-related features beneath the basin.

Similar effects from lithospheric stresses on intracratonic basins are expected by Karner *(1986)* and Cloetingh *(1988)*.

Bond and Kominz *(1991)* and Kominz and Bond *(1991)* broke up the general subsidence curve into shorter exponential intervals suggesting cycles of acceleration and decelaration of subsidence. They proposed a model in which basin reactivation is a consequence of compressive intraplate stresses developed during periods when the lithosphere passes over zones of cool mantle downwellings.

Also commenting on the episodic nature of the subsidence, and intervals with higher and lower subsidence rates, many authors have related the initiation of cratonic basins to the breakup of supercontinents in the Cambrian and in the Late Jurassic to Early Cretaceous *(Klein and Hsui, 1987; Klein, 1991; Hartley and Allen, 1994)*. However, many cratonic basins have different times of initiation.

Loup and Wildi *(1994)* also suggested stress-induced acceleration and decelaration of subsidence having originated in extrinsic causes. They identified coeval and contradictory stress regimes (rifting at plate margins and compression in the center), the cause of which remains unexplained.

A similar scenario puzzled Fisher et al. *(1988)* in the case of the Michigan Basin, where a high density of compressional folds was observed in the central part of this oval-shaped cratonic basin, while no apparent deformation was detected on the basin's margin. Admitting the contradiction, they retained the lateral force as the control on subsidence and uplift on the folds.

The idea that lateral force is involved in episodic subsidence of cratonic basins was repeated by Quinlan and Beaumont *(1984)* and Howell and van der Pluijm *(1990)* in the case of the Michigan Basin and suggested by Daly et al. *(1992)* for the Congo Basin.

LeFever and Crashell *(1991)* conducted an extensive mapping of the south-central part of the Williston Basin and prepared numerous subsidence curves. They did

not comment on the general shape of the subsidence curves, but subdivided the Paleozoic part of it into four events. Each of them began with a high rate of subsidence, and declined to a relatively slow subsidence. The average timespan of these intervals is 50-90 M.a. and the subsidence events do not coincide with major orogenic events in North America.

Tectonic rejuvenation of older structures was proposed by Gerhard et al. *(1982)* for the origin of the Williston Basin and by De Brito-Neves et al. *(1984)* for Brazilian basins.

Gerhard et al. *(1982)* suggest that the Williston Basin is a large scale "pull-apart" basin formed at the time of Sauk-Tippecanoe sequence boundary, between megascale NE-SW trending left-lateral faults zones (Fromberg and Colorado–Wyoming fault zones).

3.1.4 Models with convective instabilities

This type of model tries to overcome the heating problem by replacing it with heat withdrawal from the lithosphere by convective downwelling of the asthenosphere (descending plume), showing the converse of active rifting *(Middleton, 1989)*. The model also explains the uplift at the end of subsidence, which occurs when the downward pull of the plume vanishes and thermal recovery (heating) of the lithosphere occurs. The radial pattern of the subcrustal stresses related to these types of mantle downwellings (and upwellings) was emphasized by Liu and Bostrom *(1980)*.

3.1.5 Passive models

Porter et al. *(1982)* emphasized the equal importance of the uplift and erosion of the arches around the Williston Basin between transgressive-regressive cycles in the evolution of the basin to its differential subsidence. Uplift of the marginal elements around the Michigan Basin (e.g., Kankakee, Findlay, Algonquin arches) is also considered important to its evolution.

Burke *(1976)* indicated that the Chad Basin originated in response to peripheral uplifts and suggested that this basin is a recent model for the evolution of the Paleozoic Michigan Basin.

3.1.6 Geometric consideration of cratonic basin evolution

Dallmus *(1958; 1964)* pointed out that the shape of a cratonic basin on the face of the earth is like that of a watch glass with the convex side upward ***(Figs. 3.1.a, b and 3.2)***. He concluded that during the subsidence a basin under this geometric setting would result in the generation of compressive forces in the shallow crust. Compression would build up in the central region of the basin, between the inflection points (point on the basin profile where the profile became less or more convex than the curvature of the earth). This approach challenges the general perception based on conventional cross-sectioning (i.e., sea-level as horizontal). The model predicts that basin subsidence leads to compression, folding, uplifts, reverse movements in the central part of the basin, while extension at the flanks ("dynamic rim").

Scherer *(1973)*, Sloss and Scherer *(1974)*, Sloss *(1987; 1991)* pointed out the shortcomings of the subsidence curves used in basin evolution models. They indicated that the one- or quasi-two-dimensionality of those datasets fails to tackle the problem of basins with shifting loci of maximum subsidence (i.e. shifting center of the basin). They considered that sedimentary volumes are integrations of thicknesses and represent the amplitude of subsidence throughout a basinal area. Taking an analogy from land subsidence over mine workings, they approached the cratonic basin with an inverted, bivariate normal probability, or Gaussian surface ***(Fig. 3.3.a)***. Using digitized thickness maps of the Michigan, Elk Point (Devonian Williston Basin) and Moscow basins, they analyzed the subsidence of these basins by monitoring the sediment volume, basin width (radius at inflection locus) and slope (dip of base unit at inflection locus), calculated from the variables of the bivariate Gaussian function ***(Fig. 3.3.b)***. They excluded the thickness values affected by erosion at the flanks of the basin. No attempt was made to

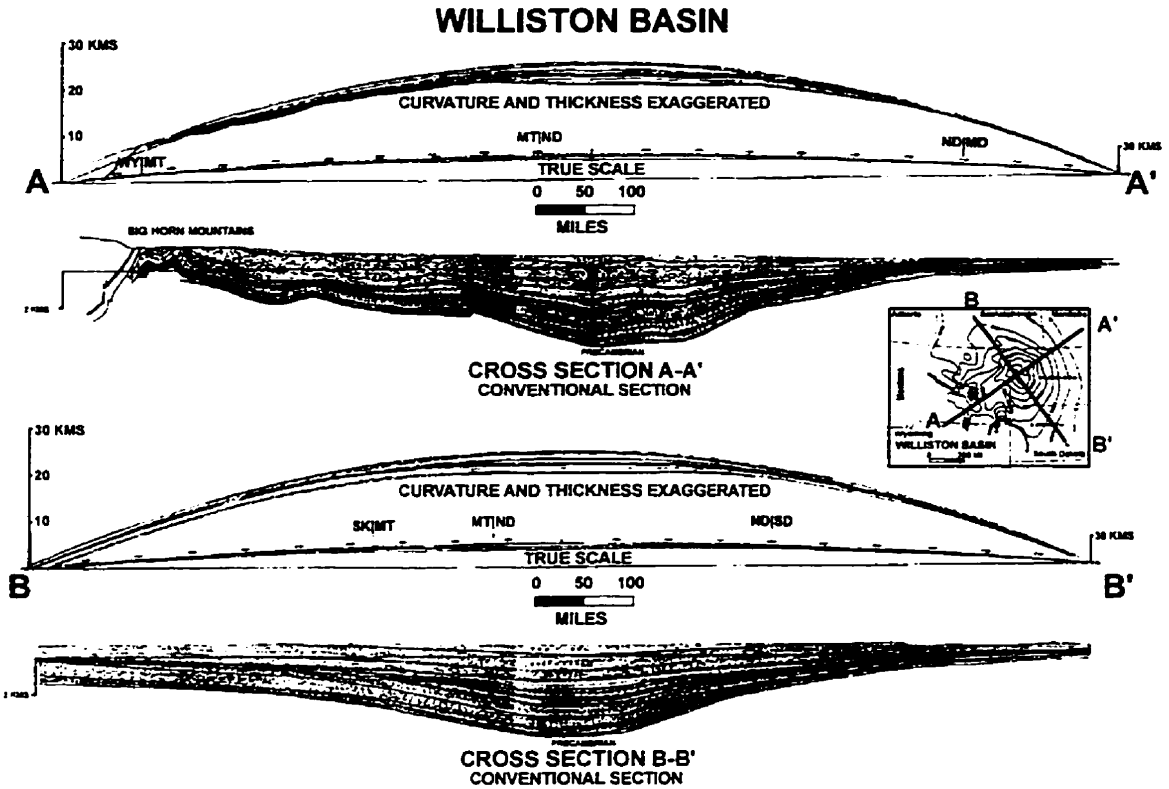

Fig. 3.1.a Cross-sections of the Williston Basin (Dallmus, 1958).

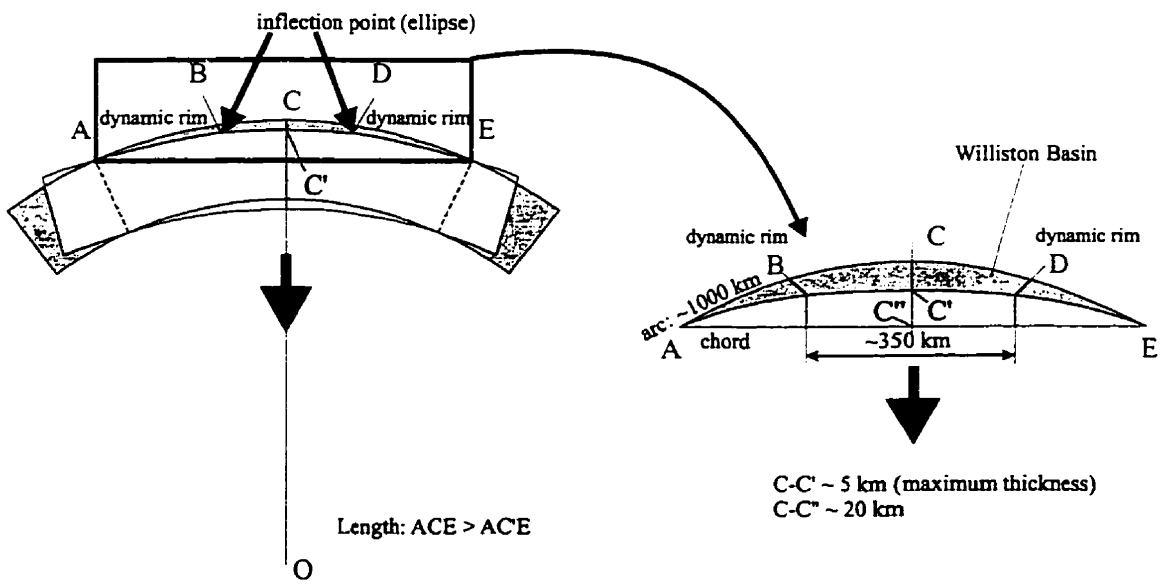

Fig. 3.1.b Geometry of a subsiding basin. (modified from Dallmus, 1958).

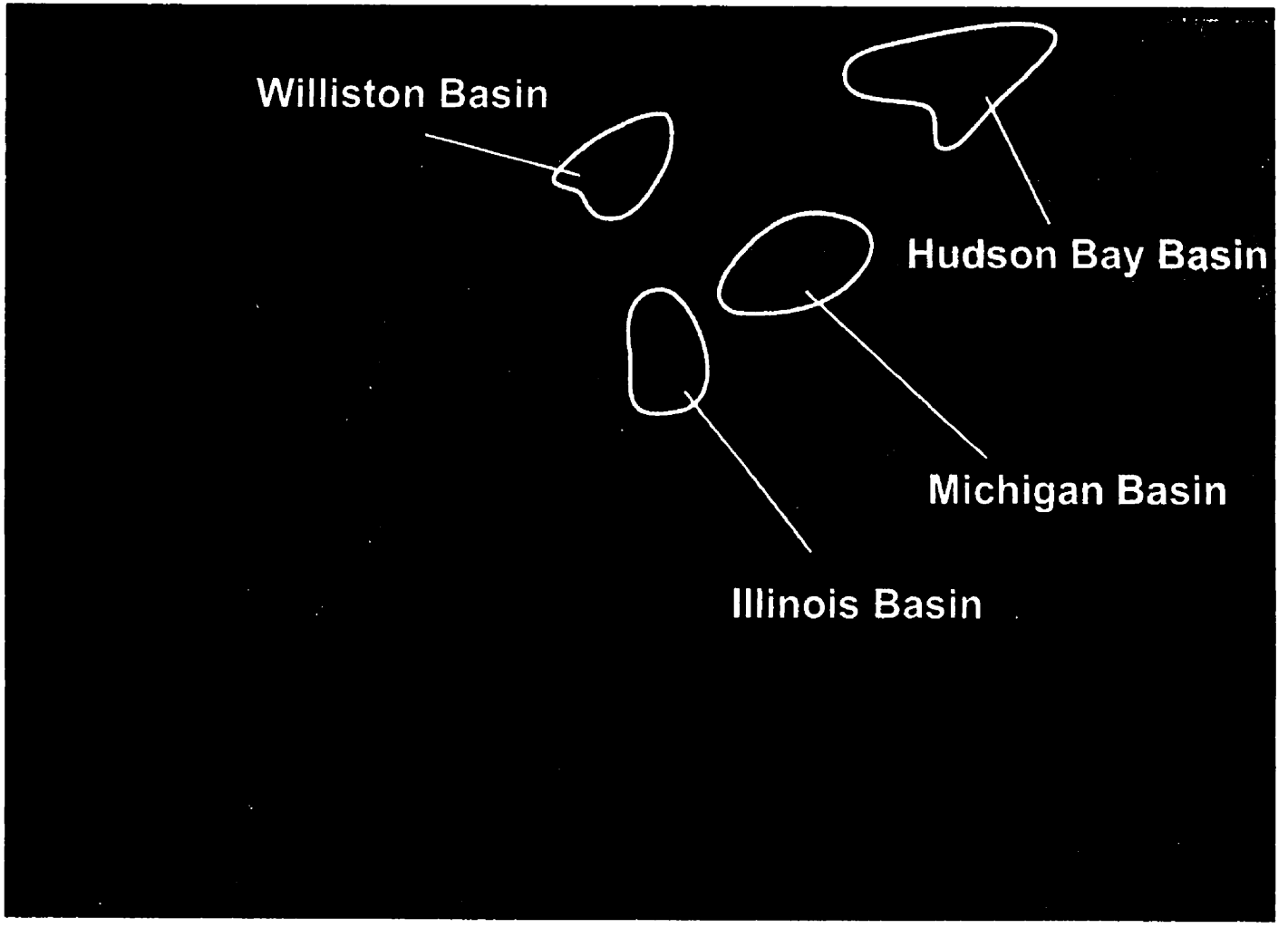

Fig. 3.2 North American cratonic basins in global perspective. Photo source: Bill Brown, USACERL.

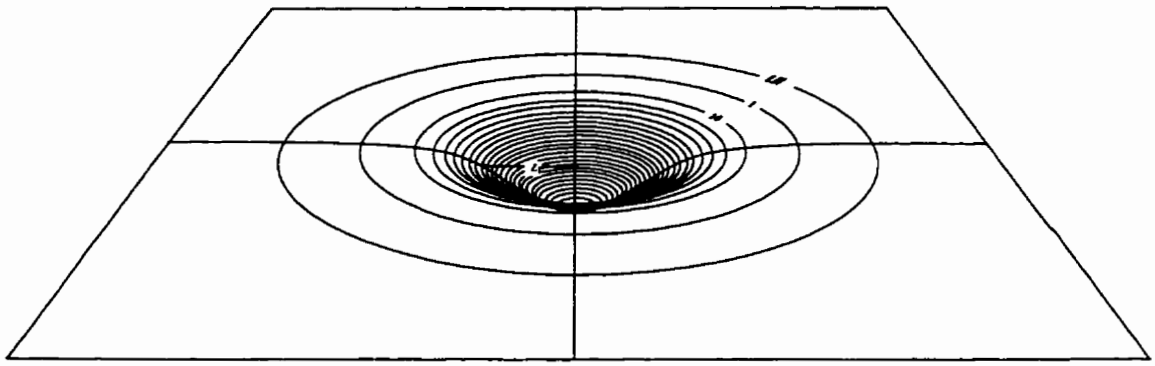

Fig. 3.3.a Perspective view of a sedimentary basin simulated by the bivariate-normal function (Sloss, 1991).

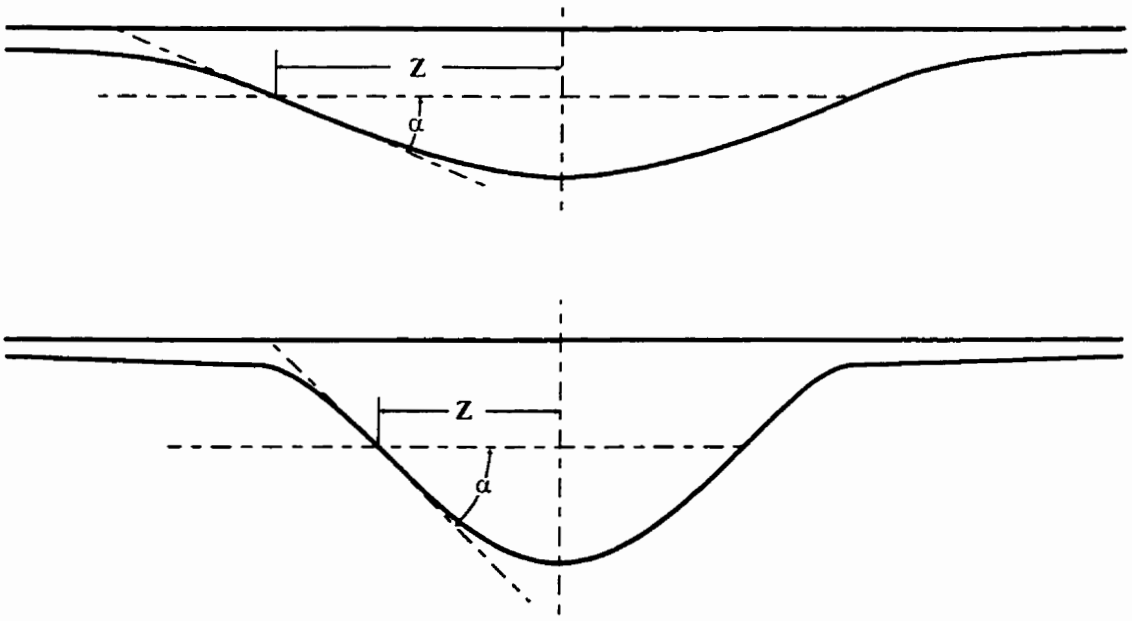

Fig. 3.3.b Modeling parameters.
z: basin width;α: basin slope (Sloss and Scherer, 1974).

include general tilting of the basin unrelated to the subsidence. They concluded that the subsidence history of the three basins, especially those of the Elk Point and Moscow basins, are very similar, suggesting a global control on their subsidence.

The shapes of the Williston and Michigan basins were also modeled by Ahern and Mrkvicka *(1984)* and Ahern and Dikeou *(1989)* using an approach based on flexural deformation of elastic plate. They corrected for regional tilt and concluded that in both basins the geometric center did not migrate significantly during subsidence, evidenced by their circular shape and axial symmetry.

3.2 Tectonic evolution and structure of cratonic basins

Apparent similarities of various intracratonic basins on the Earth could give valuable insights into the structural evolution and subsidence history of the Williston Basin. It is therefore necessary to review some of them briefly, to draw conclusions as to the similarities and differences in their structure and evolution.

3.2.1 North American cratonic basins

There are four major cratonic basins located on the North American continent: the ***Williston Basin***, the ***Michigan Basin***, the ***Hudson Bay Basin*** and the ***Illinois Basin***.

3.2.1.1 Williston Basin

Since the stratigraphic aspect of the Williston Basin was reviewed in ***Chapter 2***, here its regional tectonic and internal structural pattern will be addressed.

The Williston Basin is an elliptical structural depression of approximately 345,000 km^2 *(Gerhard et al., 1991)**(Figs. 3.2 and 3.4.a)***. The basin is underlain by an Archean crustal fragment (Dakota Block) caught up in the terminal collision of the the Superior and Wyoming cratons *(Baird et al., 1995; 1996)* ***(Fig. 2.1)***. Deep seismic studies have showen that the crustal thickness beneath the northern part of the basin

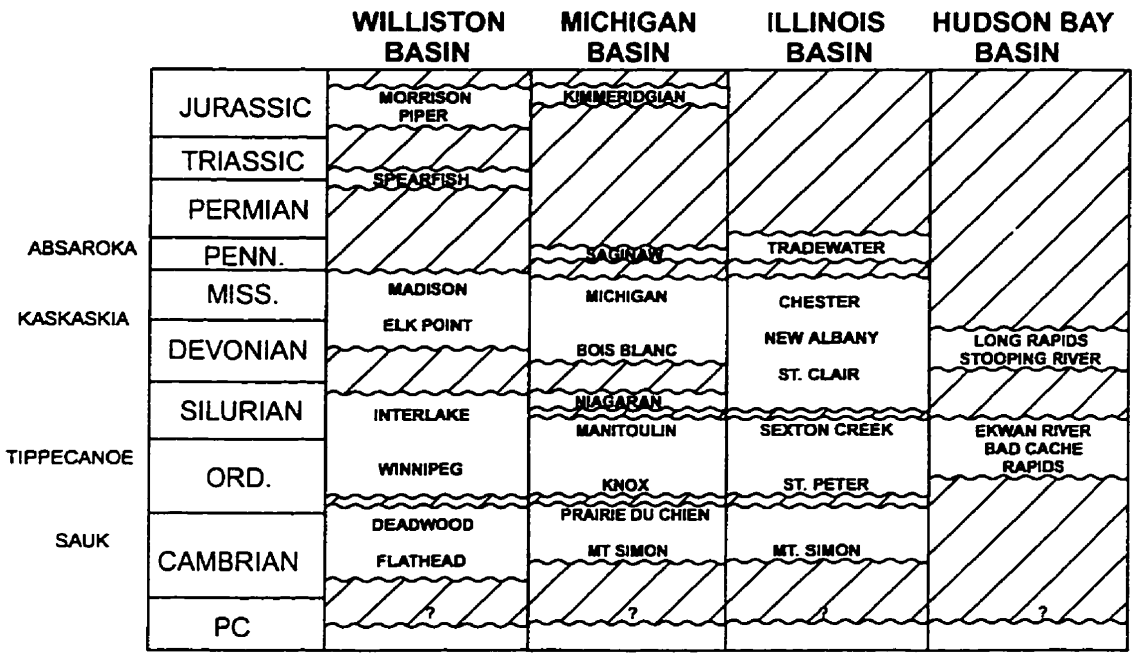

Fig. 3.4.a Simplified stratigraphy of North American cratonic basins (Quinlan, 1987)

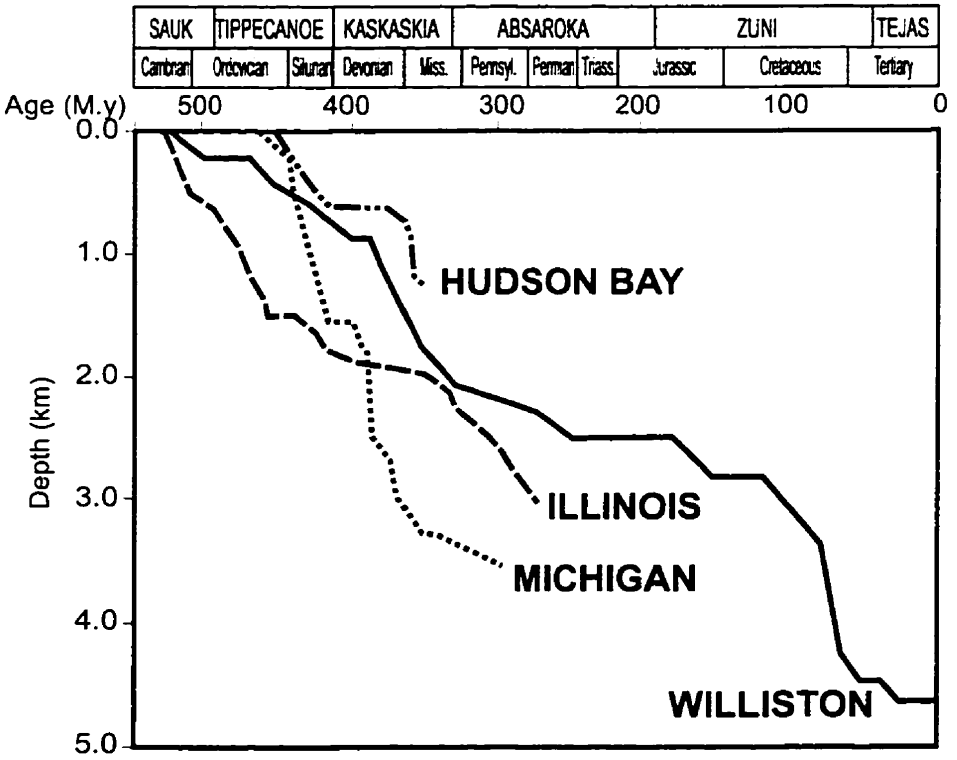

Fig. 3.4.b Subsidence curves of North American cratonic basins (Hamdani et al,, 1994)

ranges from 35 to 50 km and can reach 54 km below the central portion of the basin *(Hajnal et al., 1984; Kanasewich et al., 1987; Morel-a-l'Hussier et al., 1987)* and presumed that it could have been even 60 km before the erosion preceding the basin's subsidence *(Kanasewich et al., 1987)*.

The fault directions within the basement are not clear. One assumption postulates major north-south structural trends in the basin. The major Precambrian Tabbernor Fault is postulated to extend from northern Saskatchewan to south of the international border and to have been reactivated several times during the Phanerozoic *(Elliott, 1996)*. Other presumed structural directions in the basement were interpreted based on air and satellite photos. This NW-SE/NE-SW conjugate set of faults and joints, which are well documented in surface *(Stauffer and Gendzwill, 1987)* and subsurface studies *(Narr and Burrus, 1984)*, reflects Sevier-Laramide deformation paths. An assumption was made that these directions are "pre-existing" weakness zones in the basement which originated in Precambrian times, and were active throughout the Phanerozoic *(e.g. Thomas, 1974; Brown and Brown, 1987)*. No plausible proof or structural explanation is given for this argument.

There is considerable debate over many aspects of the evolution of the Williston Basin. Fundamental differences among theories are based on disagreements about its time of initiation, and the pattern and duration of its subsidence, which has resulted in various hypotheses regarding the major controlling factor of the subsidence. The Williston Basin is one of the most investigated intracratonic basins of the world. For this reason and because the subsidence history of the Williston Basin is more complex and longer than that of other North American cratonic basins *(Hamdani et al., 1994; Naimark and Ismail-Zadeh, 1995)* ***(Fig. 3.4.b)***, the Williston Basin is the testing ground for all the types of cratonic basin models detailed above.

At least 3 km of pre-subsidence uplift and erosion from the Early Cambrian has been recorded based on fission-track analysis by Crowley et al. *(1985)*. Based on

thickness information the basin was initiated about 495 M.a. ago during the Tremadocian (Ordovician) *(LeFever et al., 1987b; LeFever and Crashell, 1991)*. Circular symmetry of the basin was emphasized by Ahern and Mrkvicka *(1984)* and Ahern and Ditmars *(1985)* as part of their thermal model with a continuous, sigmoidally decreasing subsidence pattern.

Fault reactivation in the underlying rift zone followed by continuous, thermal subsidence was invoked to explain the initiation of the basin by Klein and Hsui *(1987)* and Klein *(1991)*.

A model of continuous subsidence due to gabbro-eclogite phase change was applied by Fowler and Nisbet *(1985)* and the linear trend of the subsidence was emphasized.

Another phase change model was proposed by Hamdani et al. *(1994)*, and Naimark and Ismail-Zadeh *(1995)*. LeFever and Crashell *(1991)* recognized four separate Paleozoic events, starting with higher and followed by lower subsidence rates.

Similar, episodic subsidence postulated by Bond and Kominz *(1991)* and Kominz and Bond *(1991)* was attributed to compressive intraplate phases.

A theory of shorter intraplate stress fluctuation was invoked to describe the continuing subsidence of the basin *(DeRito and al., 1983)*.

Gerhard et al. *(1982)* suggested that the Williston Basin is a large scale "pull-apart" basin formed between the Fromberg and Colorado-Wyoming fault zones.

Porter et al. *(1982)* contemplated a passive evolution model for the Williston Basin implying the uplift and erosion of the arches around the basin.

3.2.1.2 Michigan Basin

The oval shaped Michigan Basin occupies an area of 207,000 km^2 mostly in the state of Michigan *(Catacosinos et al., 1991)* ***(Fig.3.2)***. The basin is underlain by the Keweenawan structure, a divergent arm of the Midcontinental Rift System, whose age is about 1.1 G.a. *(Zhu and Brown, 1986; Klein and Hsui, 1987; Fisher et al., 1988)*.

Burke and Dewey *(1973)* proposed the concept of a triple junction in the eastern part of Lake Superior, with the Kapuskasing Fault Zone trending northeast as the third arm; however, this arm is located further to the north. The basin is filled with a 4.5-km thickness of sediments, which consist predominantly of carbonate rocks and evaporite rocks with subordinate shale and sandstones *(Fisher et al., 1988)*. The sedimentary fill ranges in age from Cambrian through Carboniferous and is capped with Jurassic red shales. All six cratonic sequences of Sloss *(1963)* have been recognized ***(Fig. 3.4.a)***. The bulk of the subsidence in the Michigan Basin occurred from the middle Ordovician through Devonian time; however, the basin existed in embryonic form from the Late Cambrian *(Fisher and Barratt, 1985)* and continued to subside in the Mesozoic ***(Fig. 3.4.b)***.

The structures observed in the basin are primarily the product of vertical movements of basement blocks activated by regional stresses *(Fisher and Barratt 1985; Fisher et al. 1988)*. The majority of the folds are located near the center of the basin; whereas no major compressional features are known in the marginal areas. Furthermore, anticlines in the basin become tighter at depth *(Fisher et al., 1988)*. The horst and graben blocks of the Precambrian basement, moving along high-angle normal and reverse faults, moved up or down in response to regional stresses, demonstrating that these faults have been periodically active since the Precambrian and that structural inversion occurred frequently *(Fisher and Barrett, 1985)*.

Seismic evidence demonstrates that the faults in the Precambrian rocks beneath the basin die out upward and, generally with few exceptions, do not extend above the Middle Devonian formations *(Fisher and Barratt, 1985)*.

Recently, Prouty *(1986, 1988)* demonstrated by Fourier analysis the radial pattern of the faults and folds in the basin and suggested shear movements along these radial elements ***(Fig. 3.5.a)***.

There is no agreement on the cause and style of subsidence in the case of the Michigan Basin. Similar subsidence models have been proposed to describe the initiation and evolution of the Michigan and Williston basins.

Thermal models with single or multiple heating events were suggested by several authors *(e.g., Sleep et al., 1980; Nunn and Sleep, 1984; Nunn et al., 1984; Cercone, 1984, Nunn 1994; Coakley et al., 1994)*.

A rift-reactivation/thermal-subsidence model was invoked by Klein and Hsui *(1987)* and Klein *(1991)*.

Variations on phase-change models were applied for the Michigan Basin by Haxby et al. *(1976)*, Middleton *(1980)*, Mareschal and Lee *(1983)*, Ahern and Dikeou *(1989)*, Hamdani *(1991)* and Naimark and Ismail-Zadeh *(1995)*.

Laterally transmitted in-plane stresses from the Appalachian orogenies during the evolution of the basin were emphasized by Quinlan and Beaumont *(1984)*, Howell and van der Pluijm *(1990)*, Bond and Kominz *(1991)* and Coakley et al. *(1994)*.

Subsidence above convective downwelling was implied by Middleton *(1989)*.

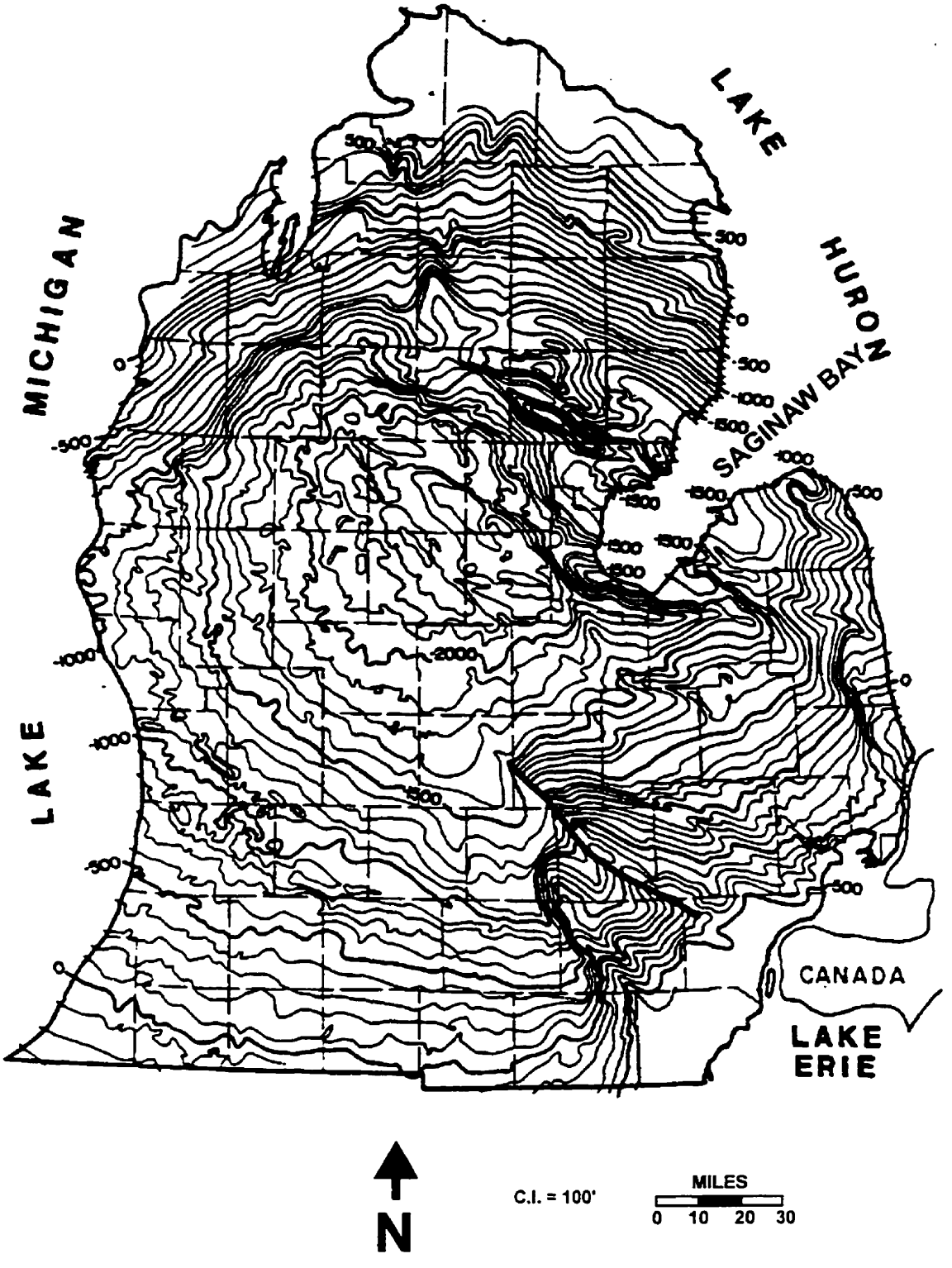

Fig. 3.5.a Structure contour map on the Traverse Limestone (Devonian) in the Michigan Basin area (Fisher et al, 1988).

3.2.1.3 Illinois Basin

The Illinois Basin is an oval-shaped depression that covers approximately 155,000 km^2 (60,000 mi^2) in parts of Illinois, Indiana and Kentucky *(Buschbach and Kolata, 1991)* ***(Fig.3.2)***.

The basin is surrounded by arches and domes (Kankakee, Wisconsin, Mississippi River, Cincinnati, Pascola arches, Nashville and Jessamine domes, Ozark Uplift). A sedimentary thickness of 6 km accumulated within the basin during Paleozoic time from the Middle Cambrian to the Early Permian *(Hedilauf et al., 1986; Klein, 1991)* ***(Fig. 3.4.a)***. The Illinois Basin was located approximately 300 km north of the margin of the craton during this period *(Collinson et al., 1988)*.

The center of the basin is located above the end of the failed arm (Reelfoot Rift or Mississippi Embayment) of the Jackson aulacogen *(Burke and Dewey, 1973)*, where the rift breaks into a three-arm rift system (Rough Creek Graben, St. Louis arm and Southern Indiana arm), exhibiting together a rare four-armed rift configuration with thinned crust *(Braille et al., 1982, 1986)* ***(Fig. 3.5.b)***. This complex rift system affected the structural evolution of the Illinois Basin and is still an active, seismogenic zone *(Braille et al. 1982)*. Trends of internal faulting and folding in the basin are related to these four main rift directions. Major deformations and repeated structural activity throughout the evolution of the basin are detected from the central part of the basin in the La Salle anticlinal belt, the Du Quoin monocline, and the Cottage Grove, and Rough Creek-Shawneetown fault systems *(Buschbach and Kolata, 1991)*.

Despite the simpler subsidence pattern of the Illinois Basin, it does not lack for theories of its evolution ***(Fig. 3.4.b)***.

Usually, thermal models require two heating events to describe the subsidence *(Sleep et al., 1980)*. Some authors consider the second phase the result of the tectonic

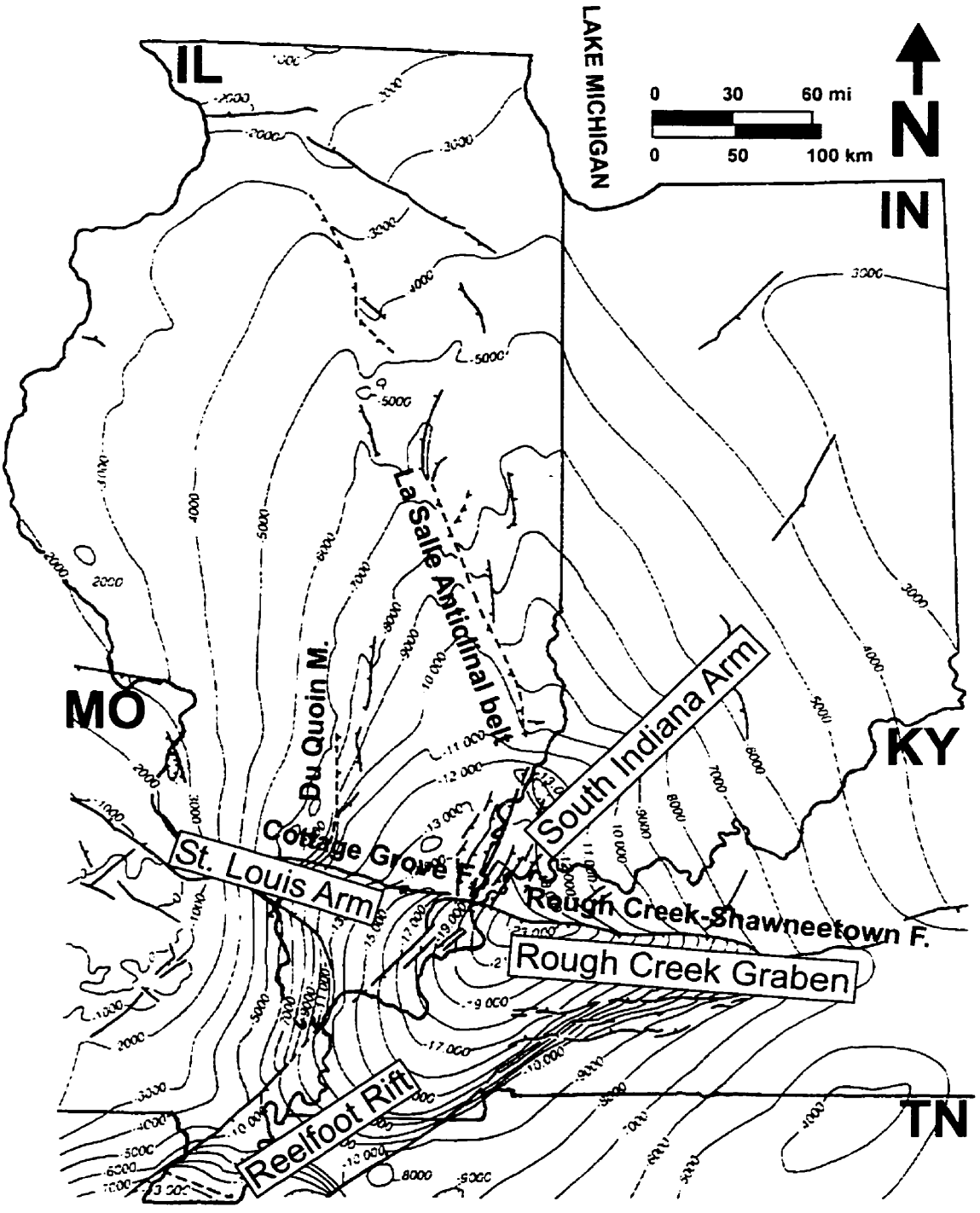

Fig. 3.5.b Structural map of the Precambrian basement in the Illinois Basin area (Buschbach and Kolata, 1991).

effects of the Appalachian orogeny *(Quinlan and Beaumont, 1984; Heidlauf et al., 1986; Klein, 1991; Bond and Kominz, 1991)*.

Obviously, due to the underlying rifts, models suggesting rift reactivations accompanied by thermal subsidence are also applied *(Heidlauf et al., 1986; Klein and Hsui, 1987; Klein, 1991)*.

Phase-change models for the Illinois Basin were suggested by Middleton *(1980)* and Naimark and Ismail-Zadeh *(1995)*.

3.2.1.4 Hudson Bay Basin

The Hudson Bay Basin is the least explored North American cratonic basin with the shortest subsidence history. It is situated in the northern part of the craton ***(Fig. 3.2)***, bounded by the Severn, Transcontinental, Keewatin and Boothia-Bell Arches ***(Fig. 3.6.a)***. It covers some 1.2 million km^2, more than half of which is covered by water *(Sanford, 1987)*.

Apparently no rift exists under the basin and probably this is why Leighton *(1991)* considered the Hudson Bay Basin as "problematic". The basin is filled with approximately 1800 m of sediments, which range in age from Late Ordovician to Late Devonian ***(Fig. 3.4.a)***.

The basement structure of the Hudson Bay Basin is complex. The main structural feature in the basin is the NW-SE trending horst system in the central portion ***(Figs. 3.6.a and b)***. The up and down movements on this horst system and other, differently oriented structures appeared in a recurrent manner throughout the history of the basin ***(Fig. 3.6.b)***.

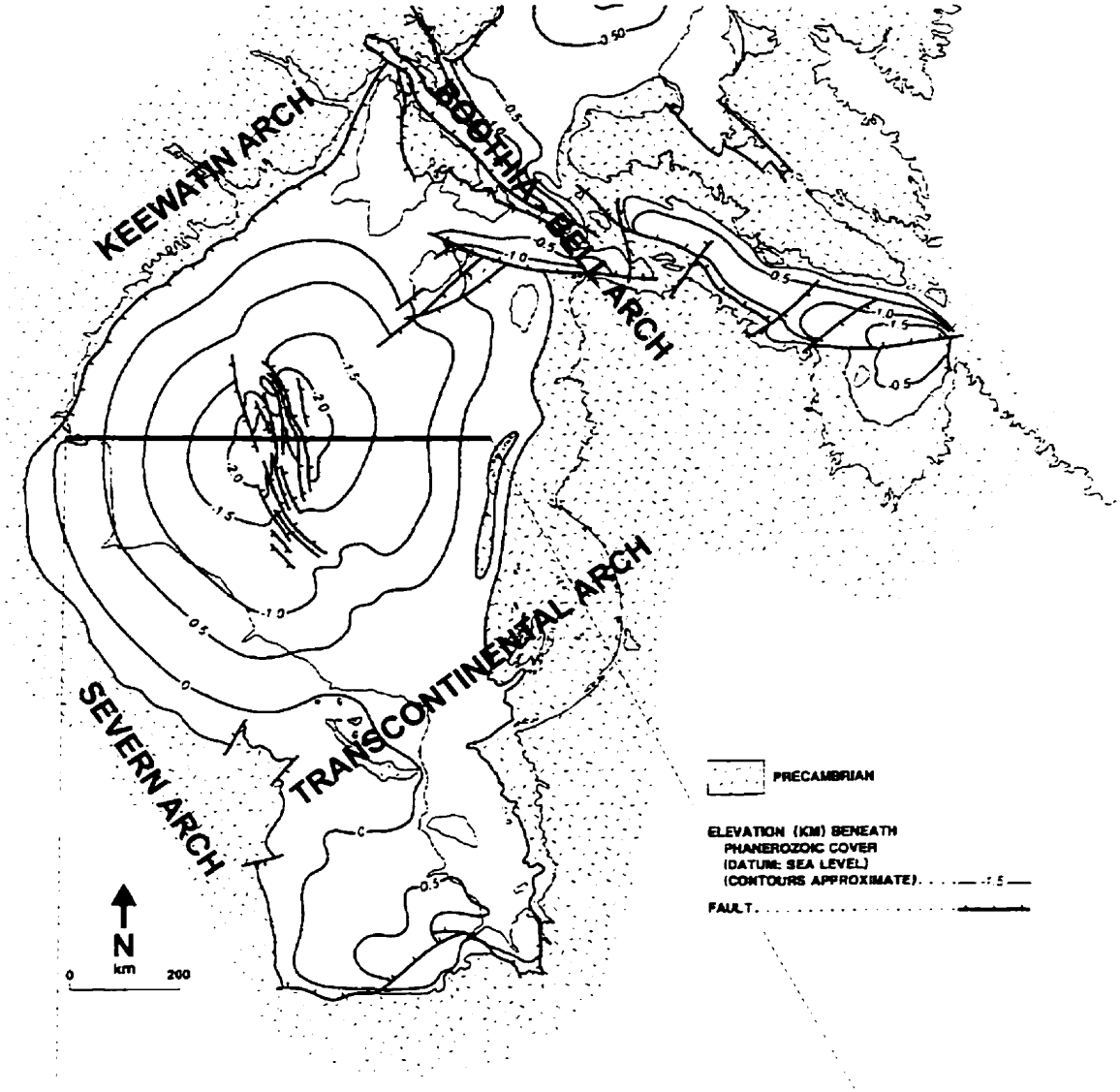

Fig. 3.6.a Structure on the Precambrian basement, Hudson Bay Basin (Sanford, 1987).

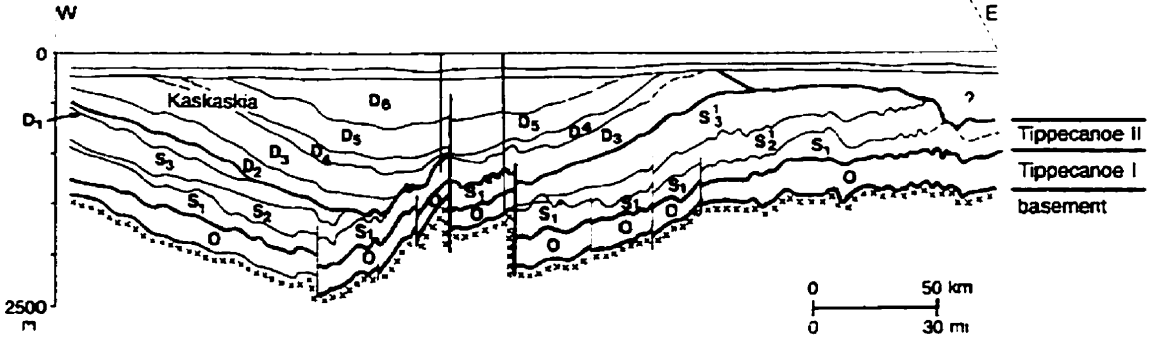

Fig. 3.6.b Structural cross section across the Hudson Bay Basin (Roksandic, 1987).

There is some debate about when the Hudson Bay Basin started to subside, since the basin acquired its circular identity only during the Middle and Upper Devonian *(Bally, 1989)*.

Klein *(1991)* proposed the rift reactivation/thermal contraction model; however, the lack of rift beneath the basin makes this model untenable.

Roksandić *(1987)* emphasized the importance of the Precambrian structures and the tectonic activity of the surrounding regions, while Sanford *(1987)* underlined the significance of the effects of the plate-margin forces on the basin subsidence.

3.2.2 Selected cratonic basins from other continents

After reviewing the structure and tectonic history of the four major North American cratonic basins, some selected cratonic basins will be briefly discussed below, since they are probably less relevant analogs for the Williston Basin.

3.2.2.1 South American cratonic basins

There are three major cratonic basins in the South American continent, all of them located in Brazil ***(Fig. 3.7)***. These are the ***Amazon Basin***, the ***Paranaiba (Maranhaõ) Basin***, and the ***Paraná Basin***. Similarly to those on the North American continent, the principal evolutionary stages are interpreted by craton-wide tectonosedimentary sequences *(Soares et al., 1987)*. These sequences are: ***α Sequence***, ***β Sequence*** (Ordovician-Silurian), ***γ Sequence*** (Devonian-early Carboniferous), ***δ Sequence*** (late Carboniferous-Late Permian), ***δ-A Sequence*** (Middle Triassic-Jurassic), ***ϵ Sequence*** (Cretaceous-early Tertiary) and ***ζ Sequence*** (Tertiary) ***(Fig. 3.8)***. These sequences correspond well with the North American cratonic sequences in the Paleozoic; however, later they show some differences.

The elongated ***Amazon Basin*** is covered by 7 km of Paleozoic, Mesozoic and Cenozoic sediments, and actually consists of three subbasins ***(Fig. 3.7)***. The large,

Fig. 3.7 South American cratonic basins.

Geologic period	West African cratonic sequences	Brazilian cratonic sequences	North American cratonic sequences
Tertiary	Dosso	ζ	Tejas
Cretaceous	Azaouak	ϵ	Zuni
Jurassic	Damergou	δ-A	
Triassic		δ	Absaroka
Permian			
Carbonifeous	Djado	γ	Kaskaskia
Devonian			
Silurian	Telimele	β	Tippecanoe
Ordovician	Taoudeni	α	Sauk
Cambrian			
Precambrian			

Fig. 3.8 Comparision of West African, Brazilian and North American cratonic sequences.

circular Solimões Basin (Upper Amazon), and the smaller Middle and Lower Amazon basins are bounded by large structural arches. The Solimões Basin shows shallow, basement involved Jurassic–Early Cretaceous reverse faulting, apparently without a strike-slip component, in its central part *(de Matos and Brown, 1992)*.
Stress analysis concluded that the maximum horizontal stresses showed no preferred orientation in the Solimões Basin *(Lima et al., 1997)*.

The ***Paranaiba (Maranhaõ) Basin (Fig. 3.7)***, located close to the Atlantic margin in northern Brazil, exhibits a large circular shape and is connected to the Amazon Basin in the northwest. It contains 3 km of Paleozoic–Mesozoic sediments. The basin is only mildly deformed before the Jurassic. Jurassic intrusives, probably related to the opening of the Atlantic, significantly altered the local structure of the basin and masked the deformations of any earlier events *(Mesner and Woolridge, 1964)*.

The oval shaped ***Paraná Basin*** is the largest South American cratonic basin ***(Fig. 3.7)***, filled predominantly with siliciclastic sedimentary and volcanic rocks that range in age from Ordovician to Cretaceous, deposited in three subsidence phases (Silurian-Devonian, Permian-Carboniferous, late Jurassic-Early Cretaceous) *(Zalán et al, 1991)*. The present basin represents the superposition of three different basins that developed in different tectonic regimes. The recent N–S elongated shape of the basin and the NW–SE, NE–SW basement fault systems reflect recurrent pulses of the subduction on the plate margin during the Late Cretaceous–Tertiary.

Similarly to the Solimões Basin, the maximum horizontal stresses show no significant trend. Zalán et al. *(1991)* questioned the existence of a rift below the basin. They suggested several variations for a thermal mechanism explaining the basin's subsidence (e.g., crustal stretching, elliptical mantle dome) and stressed the importance of the older structures. This later opinion was emphasized by De Brito-Neves et al. *(1984)* for all three Brazilian cratonic basins.

3.2.2.2 African cratonic basins

There are four major cratonic basins on the African continent. Three of them, the ***Taoudeni***, ***Iullemmeden*** and ***Chad basins***, are located in the Saharan region; while the ***Congo Basin*** is in the equatorial area ***(Fig. 3.9.a)***. Six unconformity-bounded stratigraphic sequences are recognized in the Paleozoic of the west African part of the craton *(Petters, 1979)*. These sequences are the ***Taoudeni Sequence*** (late Precambrian-Ordovician), the ***Télimélé Sequence*** (Ordovician-Silurian), the ***Djado Sequence*** (Devonian-early Carboniferous), the ***Damergou Sequence*** (Late Carboniferous-Early Cretaceous), the ***Azaouak Sequence*** (Late Cretaceous-Early Tertiary) and the ***Dosso Sequence*** (Tertiary). These sequences are correlatable in the Paleozoic with the North American and Brazilian cratonic sequences; however, later the three cratonic areas exhibit differences ***(Fig. 3.8)***.

The ***Taoudeni Basin*** is roughly oval shaped, covers 2 million km^2 and comprises Upper Proterozoic to Late Devonian sediments 2-4 km thick, covered by a thin veneer of Mesozoic and Cenozoic deposits ***(Fig. 3.9.b)***. The central and northern parts of the basin are characterized by a negative regional gravity anomaly, suggesting thickened crust and graben structure *(Bronner et al., 1980)*. The subsidence is attributed to a Late Precambrian orogenic event *(Bronner et al., 1980)*.

East of the Taoudeni Basin lies the ***Iullemmeden Basin (Figs. 3.9.a and b)***. This basin contains 1.5-km thick Late Jurassic-Tertiary sediments, exhibits a pentagonal shape and is surrounded by uplifted terranes *(Kogbe, 1991)*. The Iullemmeden lacks any clear Bouguer gravity anomalies and does not appear to overlie any buried rifts *(Sahagian, 1993; Hartley and Allen, 1994)*.

Subsidence took place in two fast–slow phases. Generally the cause of the subsidence is considered to be thermal; however, in the case of the second subsidence phase, uplift on the surrounding regions is suspected *(Sahagian, 1993)*.

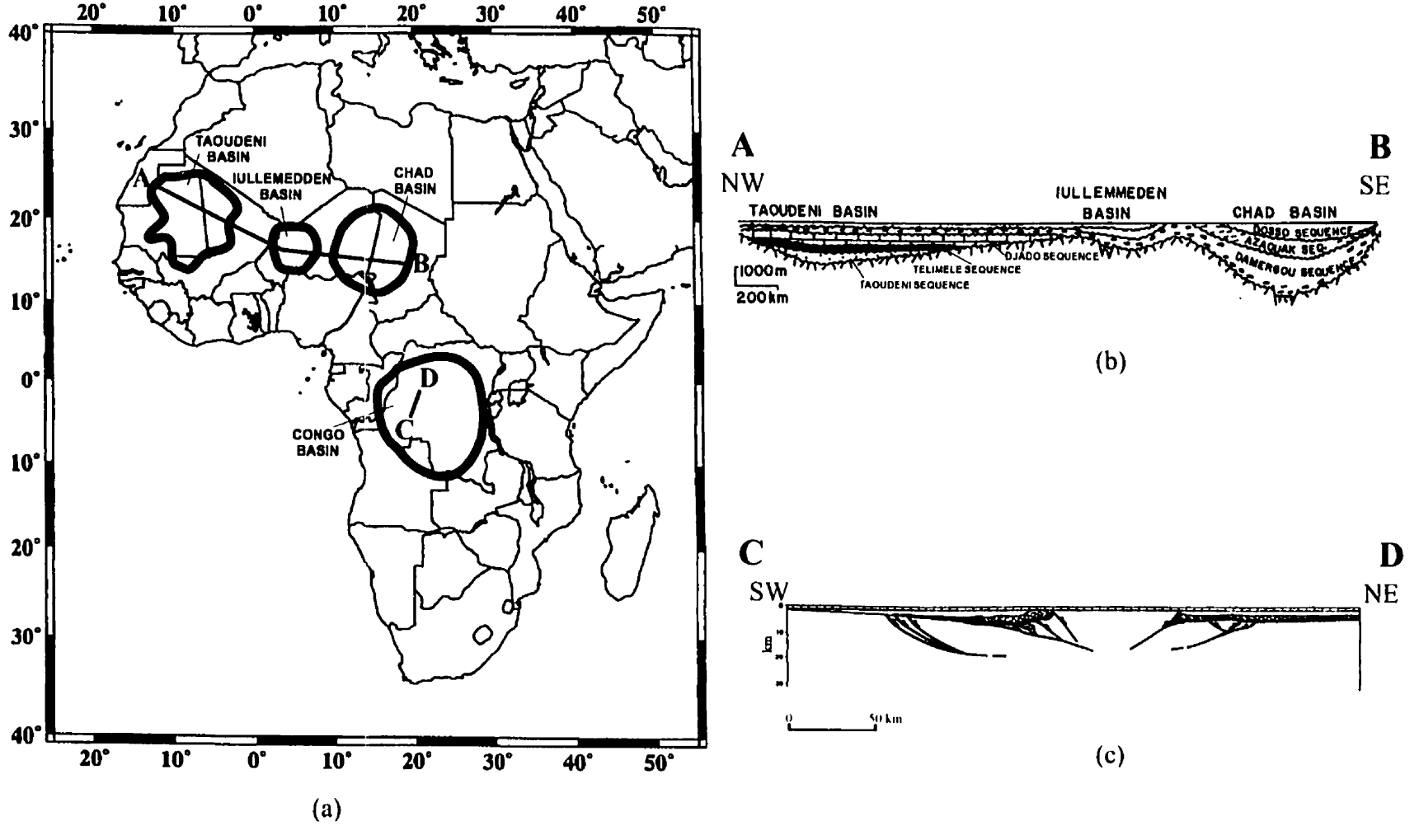

Fig. 3.9 African cratonic basins. (a) Location; (b) Cross section across the Taoudeni, Iullemedden and Chad basins; (c) Cross section across the central part of the Congo Basin. (Sahagian, 1993; Petters, 1979; Daly et al., 1992).

Further toward the east, the larger ***Chad Basin (Figs. 3.9.a and b)*** is also encircled by domal structures of hotspot swells *(Hartley and Allen, 1994)*. The basin is located at the end of the Benue Aulacogen and underlain by deep rift systems. The estimated elastic thickness of the lithosphere beneath the basin is 20-25 km *(Hartley and Allen, 1994)*. The rifting period in the Early Cretaceous is followed by a simple, linearly accelerating subsidence, resulting in 4 km of Late Cretaceous-Recent sediments. An increase of the amplitude and frequency of folds in a basinward direction was observed in the southwest part of the basin *(Avbovbo et al., 1986)*.

The origin of the basin is attributed to rift-related thermal subsidence *(Hartley and Allen, 1994)* or to the emergence of the peripheral uplifts *(Burke, 1976; Sahagian, 1993)*. The recent evolution of the Chad Basin can supply an analog for the Paleozoic Michigan Basin *(Burke, 1976)*.

The oval-shaped ***Congo Basin***, covering 1.2 million km^2, is the largest cratonic basin in Africa, occupying one tenth of the continent. It is surrounded by uplifted areas *(Daly et al., 1992)* ***(Fig. 3.9.a)***. It contains a 9-km thickness of Late Proterozoic-Recent sediments. The basin is located on the stable Archean Congo Craton, one of the cores of the African plate. The lithosphere beneath the Congo Basin has an estimated elastic thickness in the range of 100 km *(Hartley and Allen, 1994)* and does not show any rift structure. All of the six West African cratonic sequences can be recognized in this area *(Hartley and Allen, 1994)*. Based on very limited dataset, high, horst-style NW-SE trending blocks bounded by reverse faults ***(Fig. 3.9.c)*** are detected in the central part of the basin. There are records of other anticlinal directions from that area.

The subsidence pattern of the basin is fairly uniform throughout its history. The basin's origin is attributed to rift related crustal stretching and thermal relaxation *(Lawrance and Makazu, 1988; Daly et al., 1992)* despite the absence of rifts. Other theories evoke uplifts of the surrounding areas *(Sahagian, 1993)* and a convective

downwelling "cold spot" below the basin *(Hartney and Allen, 1994)*. The importance of orogenic activities on the cratonic margin was also emphasized *(Daly et al., 1992)*.

3.2.2.3 Eurasian cratonic basins

There are numerous cratonic basins in the European and Asian continents. Only the ***Paris Basin***, the ***West Siberian Basin*** and the ***Sichuan Basin*** will be discussed, representing different structural styles.

The ***Paris Basin*** covers a 110,000 km^2, roughly circular area in France *(Perrodon and Zabek, 1991)* ***(Fig. 3.10.a)***. The Triassic-Tertiary sediments reach a 3-km maximum thickness in the central portion of the basin ***(Fig. 3.10.b)***.

A triple-junction rift system is centered below the basin, and the tectonic features show a distinct radial pattern accordingly. During the main subsidence period (Jurassic-Cretaceous) the depocenter of the basin shifted only about 60 km *(Megnien and Pomerol, 1980)*. The subsidence of the basin clearly took place in a polyphase manner. A thermal model, implying rifting, heating, crustal thinning and subsequent cooling was considered by Perrodon and Zabek *(1991)*. A similar model was applied by Loup and Wildi *(1994)* and the deviation of the subsidence curve from the ideal thermal relaxation pattern was considered as short-lived compressive stresses from orogenic events.

The problem of coeval, but contradictory stress regimes in and outside of the basin remained unexplained. Megnien and Pomerol *(1980)*, considering a linear subsidence pattern, suggested the origin of the Paris Basin was due to lithospheric flexure by sedimentary loading. A phase change mechanism was proposed by Marechal and Lee *(1983)*.

The ***West Siberian Basin*** with its 3.5 million km^2 is the world's largest cratonic basin *(Peterson and Clarke, 1991)* ***(Fig. 3.11.a)***. The basin contains 6 km of Triassic–

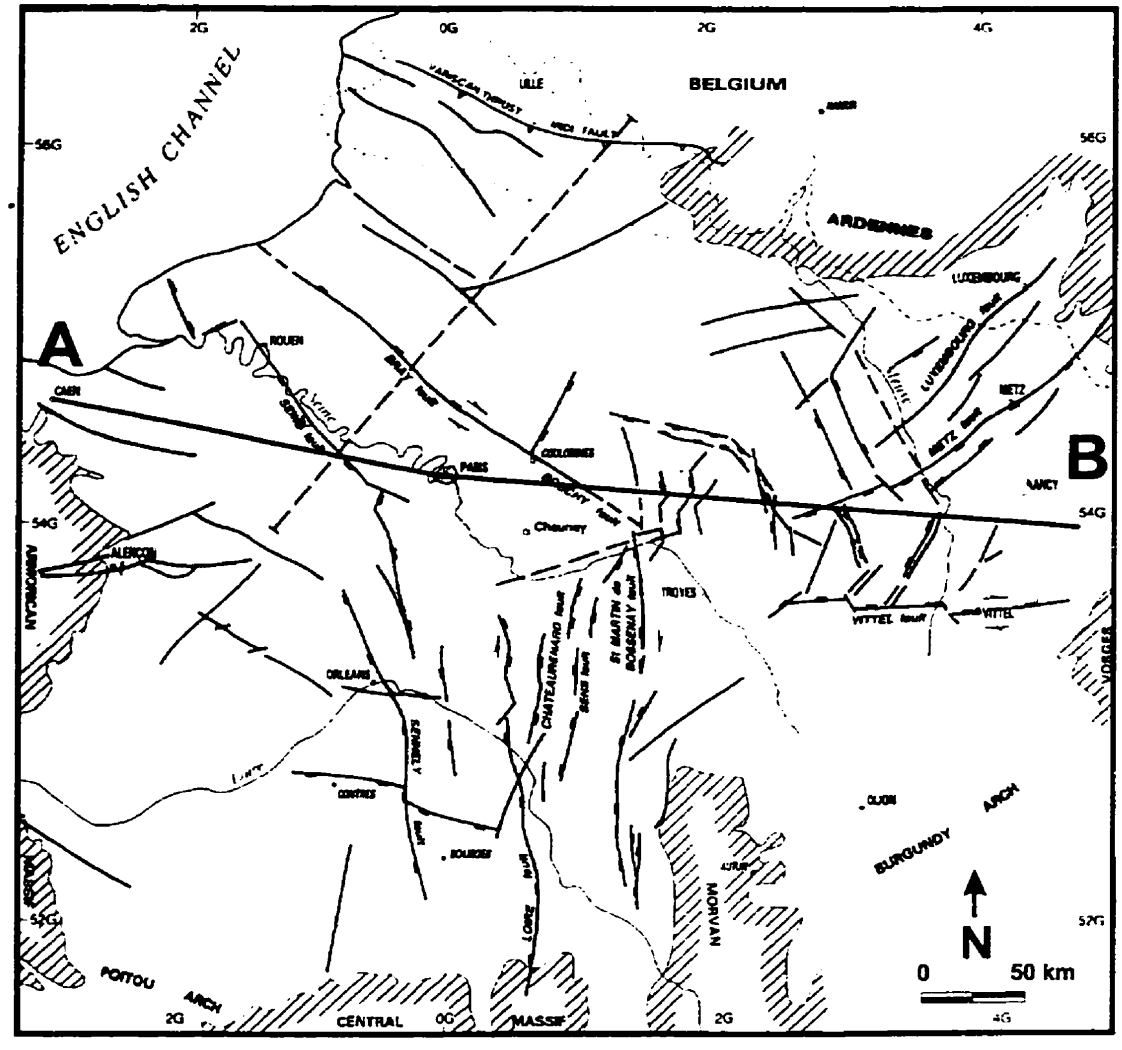

(a)

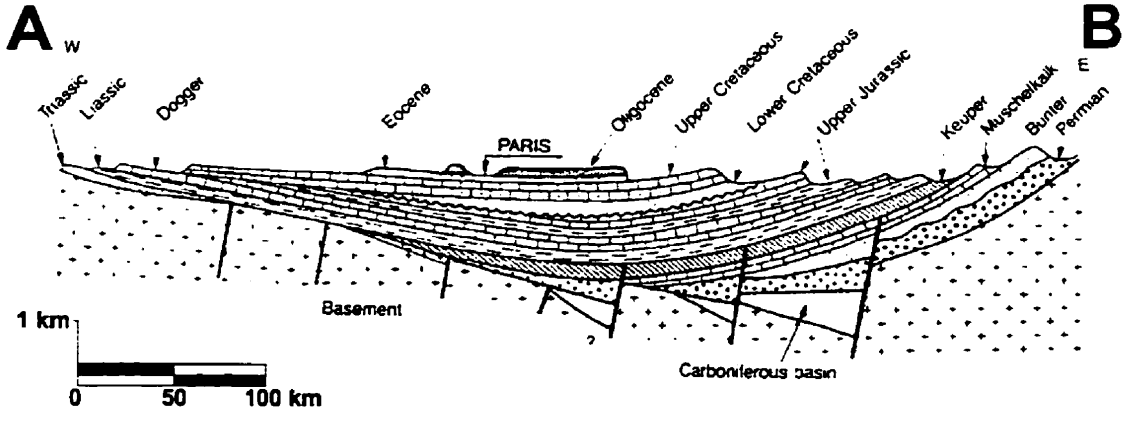

(b)

Fig. 3.10 Paris Basin (Perrodon and Zabek, 1991).

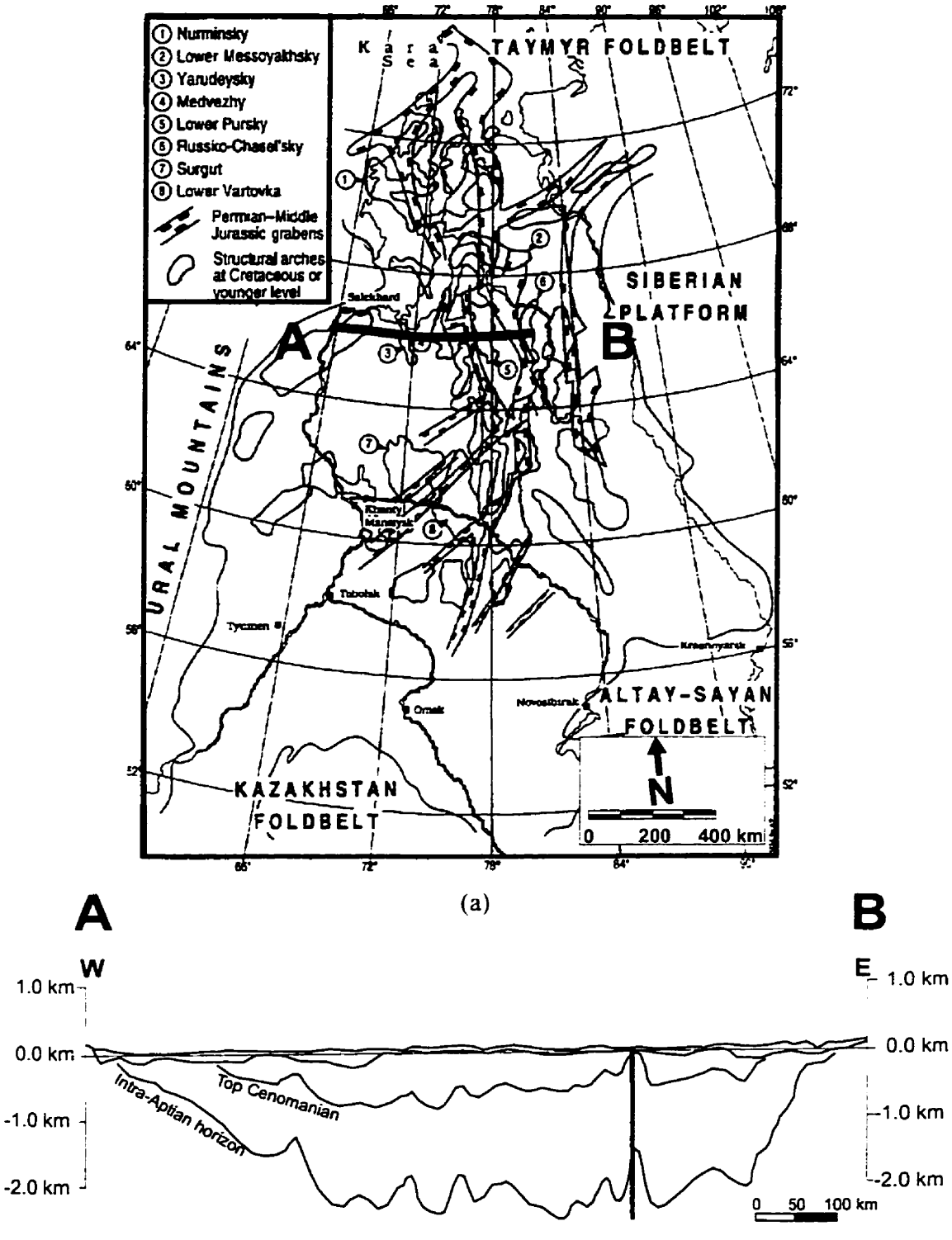

Fig. 3.11 West Siberian Basin (James, 1995).

Recent sediments in its deepest parts. The Moho is generally elevated beneath the basin. The basin was formed on a megasuture and the basement consists of accreted Paleozoic terrains.

The structural trend of the underlying rift system is mostly N-S, but other directions also exist. The largest structures are in the central part of the basin *(Peterson and Clarke, 1991)*. Basin-wide compression accompanied by folding and reverse faulting was reported by James *(1995)* in the post-Jurassic time ***(Fig. 3.11.b)***. The fold directions and fault trends have no preferred orientation. This fact and the existence of the compressive structures in the basin in an extensive megaregional environment remain a fundamental problem *(James, 1995)*.

Peterson and Clarke *(1991)* suggested that the basin was formed due to Triassic rifting, which was followed by a Jurassic sagging period with fault reactivation. Similarly, a Triassic thermal anomaly was invoked as the primary cause of the subsidence by Ziegler *(1988)*. Three phases of higher subsidence rates were observed by Aleinikov et al. *(1980)*.

The ***Sichuan Basin*** is located in southwest China on the cratonic South China Block *(Korsch et al., 1991)* ***(Fig. 3.12.a)***. The basin contains a 3-km section of Late Proterozoic-Recent sediments. The basin is now part of a foreland basin, due to the latest Mesozoic–early Cenozoic thrusting from the NE ***(Fig. 3.12.b)***. Until the Permian, the central part of the basin was a paleohigh *(Korsch et al., 1991)*.

The subsidence started 750 M.a. ago and is the result of crustal thinning, thermal cooling and loading; however, there is no evidence of rifting events in the basin *(Korsch et al., 1991)*. The basin subsided clearly in a polyphase manner, with periods of alternating faster and slower subsidence, which is attributed to plate tectonic events.

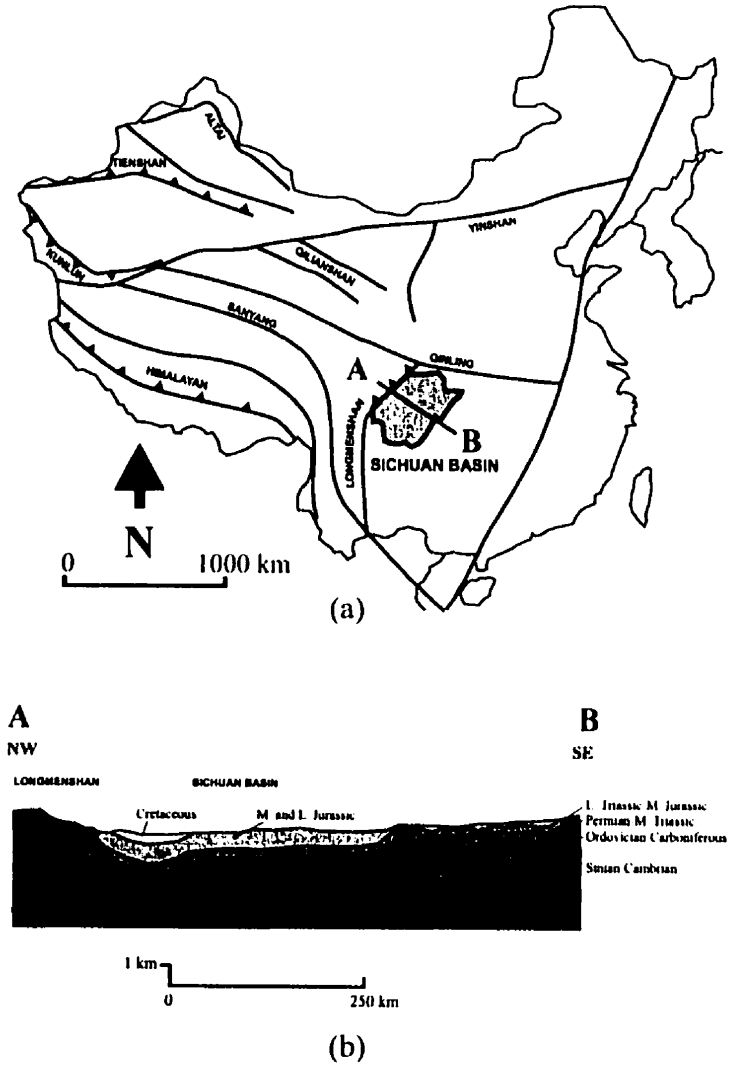

Fig. 3.12 Sichuan Basin (Korsch et al., 1991).

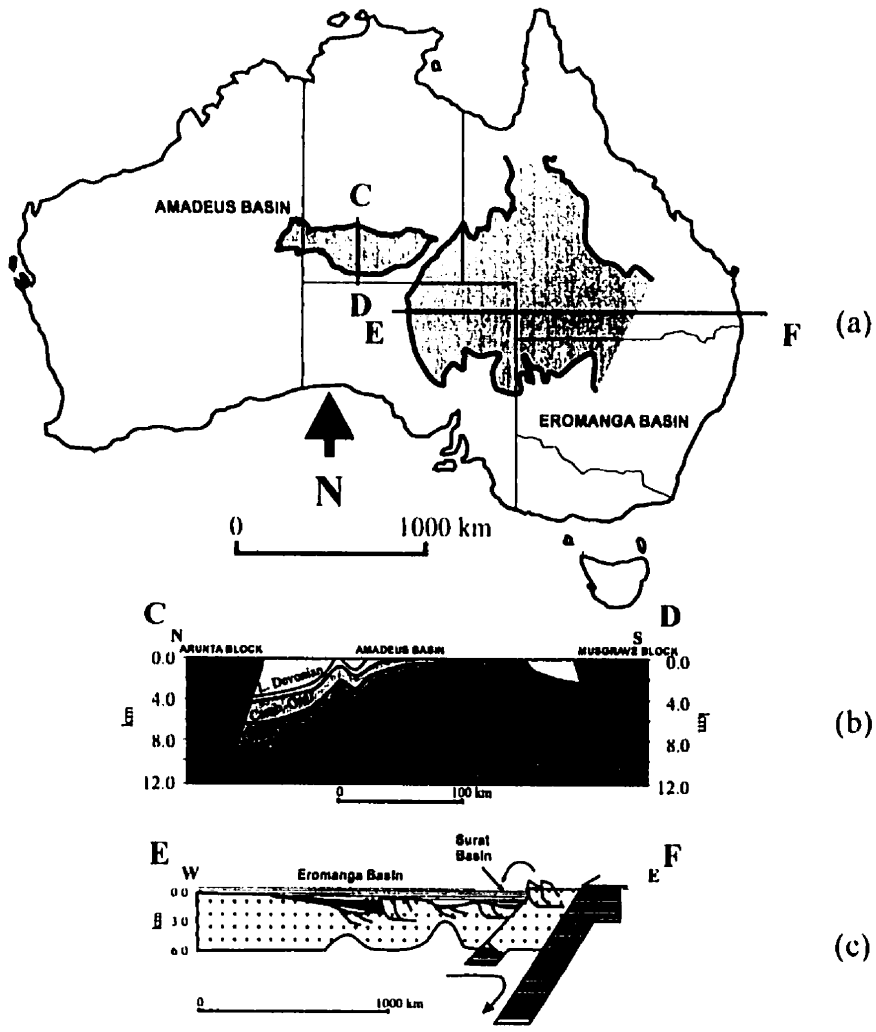

Fig. 3.13 Amadeus and Eromanga basins (Lambeck, 1983; De Caritat and Brun, 1992).

3.2.2.4 Australian-Antarctic cratonic basins

From the numerous cratonic basins from the Australian continent, only two, the ***Amadeus***, and the ***Eromanga*** basins, will be sampled. An important structure in Antarctica will be mentioned.

The central part of Australia is dominated by a series of parallel intracratonic basins which are elongated in an east-west direction, and whose history spans in time from the Late Proterozoic to the Carboniferous. The largest, ***Amadeus Basin***, locally contains 14-km of sediments *(Lindsay and Korsch, 1989)* ***(Figs. 3.13. a and b)***. Folding occured several times during the evolution of the basin. The dominant structures are trending in an E-W direction.

A thermomechanical subsidence model was proposed by Lambeck *(1983)*, suggesting that the basin was formed on the crust buckled by long-lasting horizontal compression causing increasing subsidence and sedimentation rates with time. Lindsay and Korsch *(1989)* supplied an alternative three-stage model, which predicts rift-related crustal extension and thermal subsidence in the first two stages (900-400 M.a.), and complex overthrusting and syntectonic deposition in the third (400-350 M.a.) (foreland basin) stage.

The ***Eromanga Basin*** is located in the eastern part of the continent ***(Fig. 3.13.a)***. It has a circular shape and contains a 2.7 km column of Jurassic–Cretaceous sediments *(Gallagher and Lambeck, 1989)* ***(Fig. 3.13.c)***. The basin is underlain in the lower crust by dense, high-velocity lenticles *(Finlayson et al., 1989)*. The basin subsided above several non-marine Permo-Triassic basins, and represents the final, platformal stage (extensional, foreland, platform) of vertically stacked basins formed behind the eastward retreating subduction zone *(De Caritat and Braun, 1992)*. After the Jurassic formation of the basin, in the Early Cretaceous, a second, faster subsidence rate is observed.

Models suggest that this pattern is the consequence of the effect of a high global sea level on the otherwise thermally subsiding basin *(Gallagher and Lambeck, 1989)* or a phase-change mechanism *(Middleton, 1980)*.

The region of the ***Gamburchev Mountains*** in Antarctica is postulated to be an inverted intracratonic superbasin, which is underlain by a thick crust *(Veevers, 1994)*. Similar to its recent configuration, the ice flow pattern in the Permian was radial, originating from the central parts, suggesting structural control in these directions.

3.3 Problems of existing basin-evolution models and lack of a comprehensive structural model for the Williston Basin

3.3.1 Cratonic basins

One of the most important conclusions of the preceding review is that the "simple" cratonic basins have complex histories. Any attempt to put their evolution into one category or describe them with one mechanism is misleading. Nevertheless, it is worthwhile to summarize the major differences and similarities in their evolution.

Age of the initial subsidence

Despite the claim that cratonic basins are related to the break-up of continents (e.g., Cambrian and Triassic-Jurassic), cratonic basins were formed at other times before and after these periods (Late Proterozoic – Sichuan, Amadeus, Taoudeni, Congo; Late Jurassic – Iullemedden Basin; Late Cretaceous – Chad Basin). Within the North American craton, the Hudson Bay Basin started to subside in the Late Ordovician.

Character of the basement

Some theories rely heavily on the assumption that cratonic basins are underlain by rifts, or rift triple junctions, and attribute the cratonic basin subsidence to rift reactivation and thermal effects. Not all basins are underlain by rift zones and even fewer by rift triple junctions. For example, there is no evidence of rifts below the

Congo, Sichuan, Paraná and Iullemmeden basins. Even where an earlier rift was detected, the last rifting event or orogenic activity was sometimes 1 billion years earlier than the cratonic subsidence (Michigan, Williston basins).

A fundamental problem is how linear rift features produce subcircular basins and why other portions of the same rift fail to do so. This could be solved by triple junctions. but only a few cratonic basins are underlain by this type of structure (Illinois, Paris basins). The age of the underlying basement also varies from basin to basin (Archean-Proterozoic: Williston, Michigan, Amadeus, Sichuan basins etc.; Carboniferous-Permian: Paris Basin; Permian-Middle Jurassic: West Siberian Basin).

Position on the craton in time and in space, tectonic environments before and after the intracratonic basin phase

Due to the longevity of cratonic basins and the continuous evolution of the craton (cratonization–decratonization), different basins can go through different phases of evolution. Some basins are situated throughout their history in intracratonic position (Williston, Hudson Bay, Congo basins), while others lie closer to the cratonic margins (Illinois Basin).

Many basins became part of a foreland basin as the active plate margin approached (decratonization), e.g., Williston, Sichuan and Paraná basins. or in the opposite way a cratonic basin was stacked on top of foreland basin due to retreating subduction (Eromanga Basin). The Amadeus Basin experienced significant compressive phases ending up with a rare elongated configuration.

Effect of neighboring tectonic regimes, "far-field" stresses

Some hypotheses invoke the effects of structural activity in the neighboring tectonic regimes (e.g., subduction at plate margins) as a source of subsidence. These forces are transmitted in the lithosphere laterally, and again it is questionable how they could cause oval shaped, sometimes uniaxially subsiding cratonic basins (Williston,

Michigan). The same "far field" stress effects are suggested also for the episodicity in the basin's evolution.

No apparent coincidence with orogenic events on the neighboring areas was found for the Williston Basin in the Paleozoic. Most of the basins exhibit their largest amplitude of intrabasinal deformation (folds, horsts) in the basin center. This pattern is also contradictory to the notion of laterally applied forces. These far-field stress models in cratonic basin environments are many times conjectural, rarely quantified convincingly.

Parallel evolution

Apparent similarities in sedimentation patterns in cratonic basins in different continents (Williston Basin – Moscow Basin) lead to the assumption of a world-wide cause of the evolution of cratonic basins. It became obvious in the case of the African, North American and South American continents, that even the unconformity bounded sequences are not correlatable after the Paleozoic ***(Fig. 3.8)***, suggesting individualization of cratonic evolution after the break-up of Pangea.

Cratonic basins subside generally in an episodic pattern; however, frequently the evolutionary intervals can not be correlated from basin to basin even within the North American craton. Consequently, episodicity is in the very nature of cratonic subsidence and must therefore be the result of something inherent in the basin and unrelated to global effects or tectonic activity in neighboring areas.

Circular shape of cratonic basins, three-dimensional considerations of cratonic basin evolution

One of the few patterns which characterizes almost all cratonic basins, at least at some point in their history, is their enigmatic circular shape in map view. Very few theories address the three-dimensionality of basins of this type and their internal deformation patterns.

This three-dimensionality is more important in basins with proven pre-subsidence uplift (Williston Basin), which is virtually uninvestigated. Similarly, the active role of the basin margin uplifts as part of the subsidence process is mostly unaddressed and unsolved (observe the contradictory stress states in the Michigan, Paris, and West Siberian basins).

Models applying subsidence curves usually use wells from the central part of the basin as representative of the basin's evolution. Even if a given theory is extended into three dimensions, the models, with few exceptions, are based on 1D assumptions from the basin center. They disregard the temporarily and spatially changing subsidence patterns of other parts of the basin and the importance of internal structural features on its evolution, which are considered as "noise" in some models.

Finally, all cratonic basins are analogs in either origin, character, timing, age, subsidence pattern, or primary cause. There are no two cratonic basins with the same history and parallel evolution. A mixture of the existing models or some new ones could properly describe their evolution. In either case, any theory can be substantiated based on a dataset which explores the given basin in time and space. Unfortunately, until now, even the most investigated North American cratonic basins were lacking this type of comprehensive dataset.

3.3.2 Inconsistencies of recent structural interpretations of the Williston Basin

3.3.2.1 Southern extent of the Tabbernor Fault

The N-S trending Tabbernor Fault in Saskatchewan is a Precambrian structural feature that was active even in Phanerozoic times. The fault can be clearly traced south to the 50th parallel ***(Fig. 3.14)***. Some interpretations claim that it continues at least to the international border or even south of it, based on satellite data. Interpretations of the COCORP lines in North Dakota show indications of the fault. However, there is not any

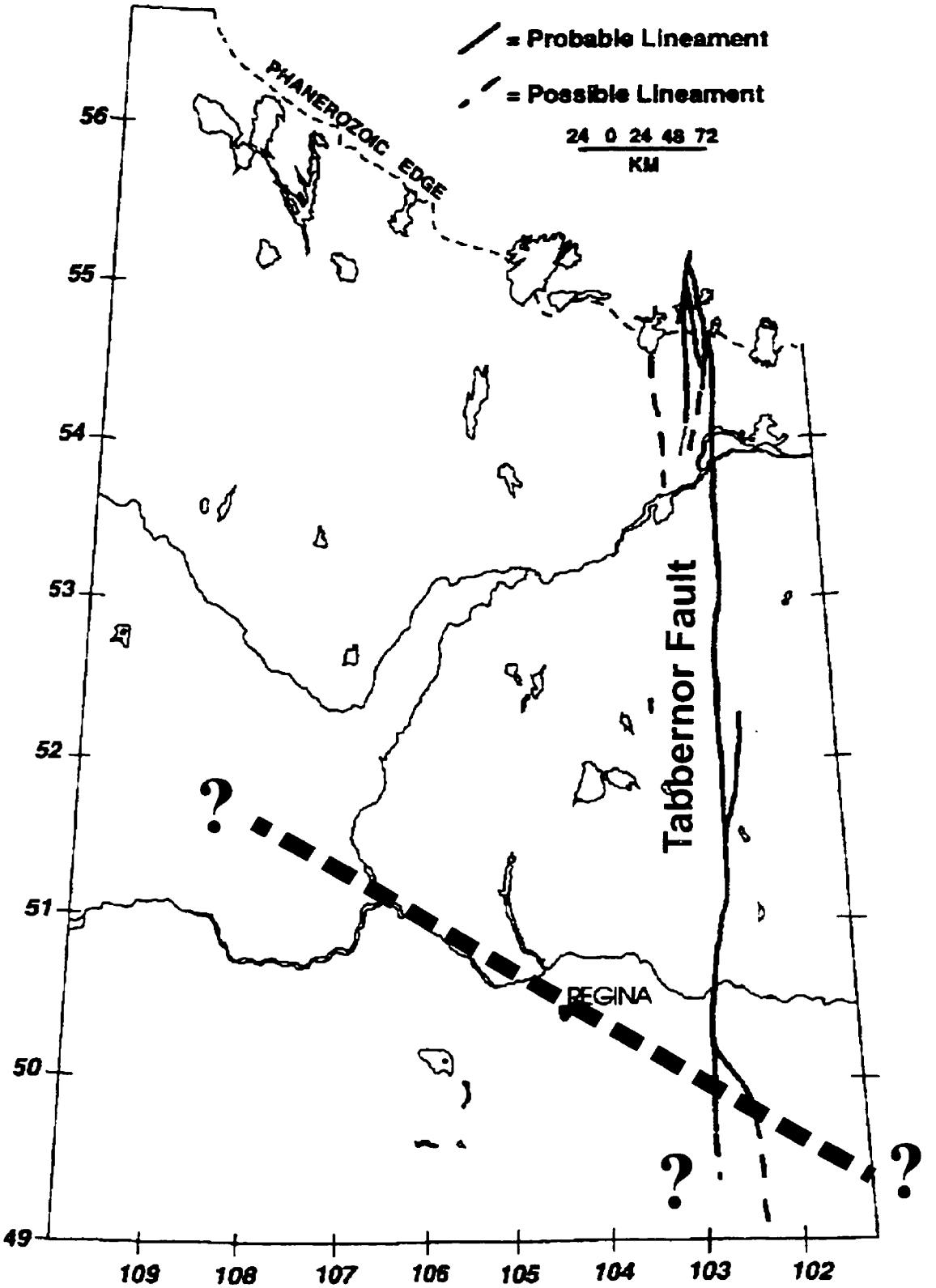

Fig. 3.14 Southern extent of the Tabbernor Fault in Saskatchewan (adapted from Giroux, 1995).

sign of faulting and the location is purely hypothetical based on the projection of the fault line to the south. Clearly, the fault in southeasternmost Saskatchewan can not be traced. However, there is an apparent structural boundary in southern Saskatchewan, trending approximately NW-SE roughly coinciding with the "Midale–Weyburn trend". This feature continues into the southwesternmost corner of Manitoba and can be identified on magnetic maps. In light of the recent discovery of the Archean Dakota Block south of this line beneath the Williston Basin, the area of the Basin is assumed here to have a separate structural grain or tectonic environment from the areas north of it and suggests different kinematic behavior ***(Fig. 2.1)***. This regional structural trend is probably also related to the bend in the North American Central Plains conductive anomaly, the origin of which has not yet been properly addressed. The Tabbernor Fault, as suggested here, is terminated by this regional feature or flattens into it. If the Tabbernor Fault is offset by this line its continuation to the south can be expected east of the Williston Basin.

3.3.2.2 The problem of the lineament block tectonics interpretations in the Pre-Zuni of the Williston Basin, contradicting air and satellite photo interpretations

One of the earliest lineament interpretations of the Williston Basin area was given by Thomas *(1974)*. In this model, based on photogeologic data, it was suggested that the E–W compressive forces of the Laramide Orogeny acted on vertical NW–SE/NE–SW trending fault bounded basement blocks ***(Fig. 3.15.a)***. It was also assumed that these structural trends are of early Precambrian origin and the that Paleozoic deformation of the basin can also be attributed to them; however, no proof was given for this assumption.

Later, this unproven premise became the prevailing line of thought, and remote sensing methods (air and satellite photos) became the leading tools in interpreting basement tectonics. The idea was carried on mostly by geoscientists of Cretaceous geology, for which system these structural directions are well documented. Later,

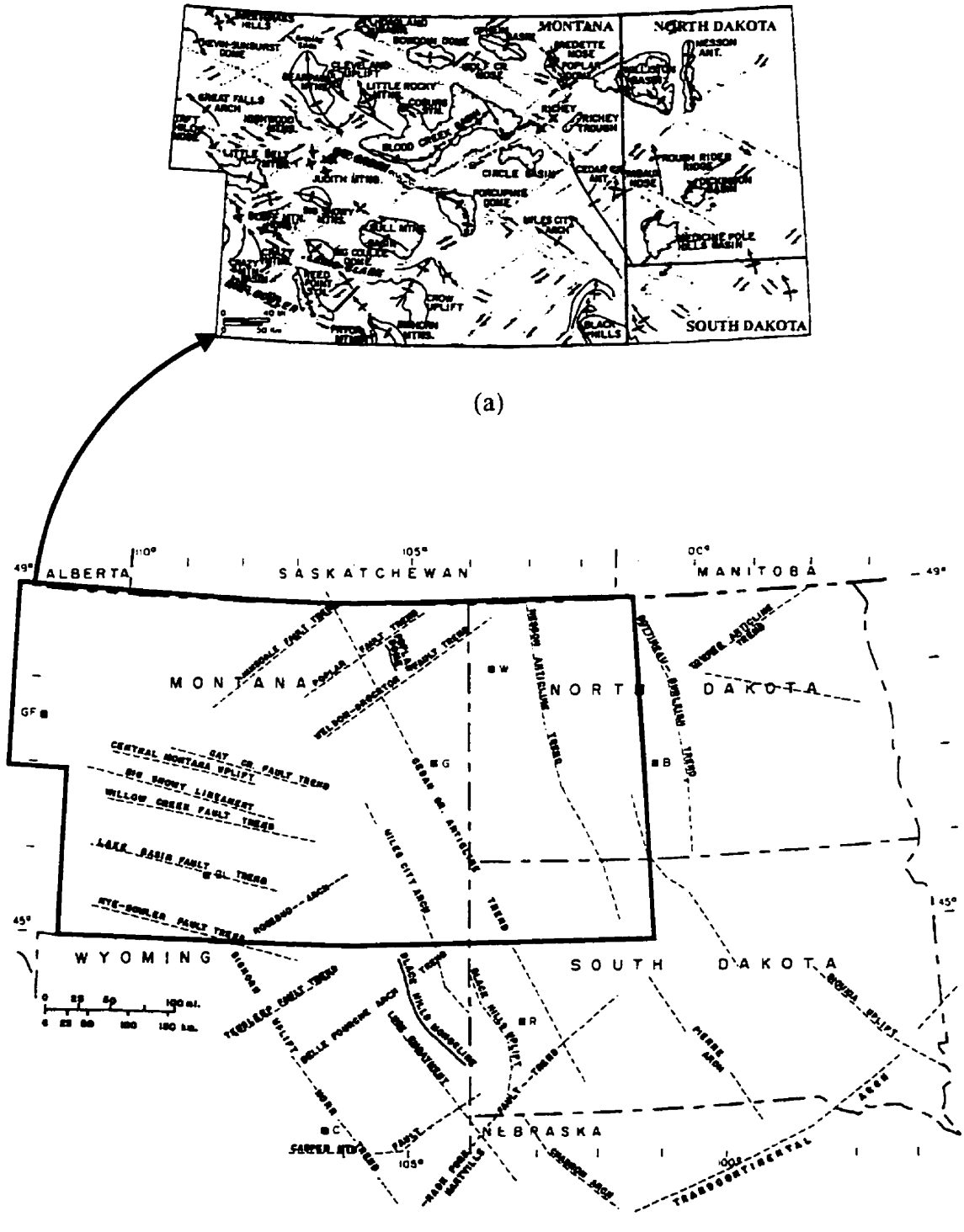

Fig. 3.15 Various lineament interpretations in the Williston Basin area ([a] Thomas, 1974; [b] Peterson and MacCary, 1987).

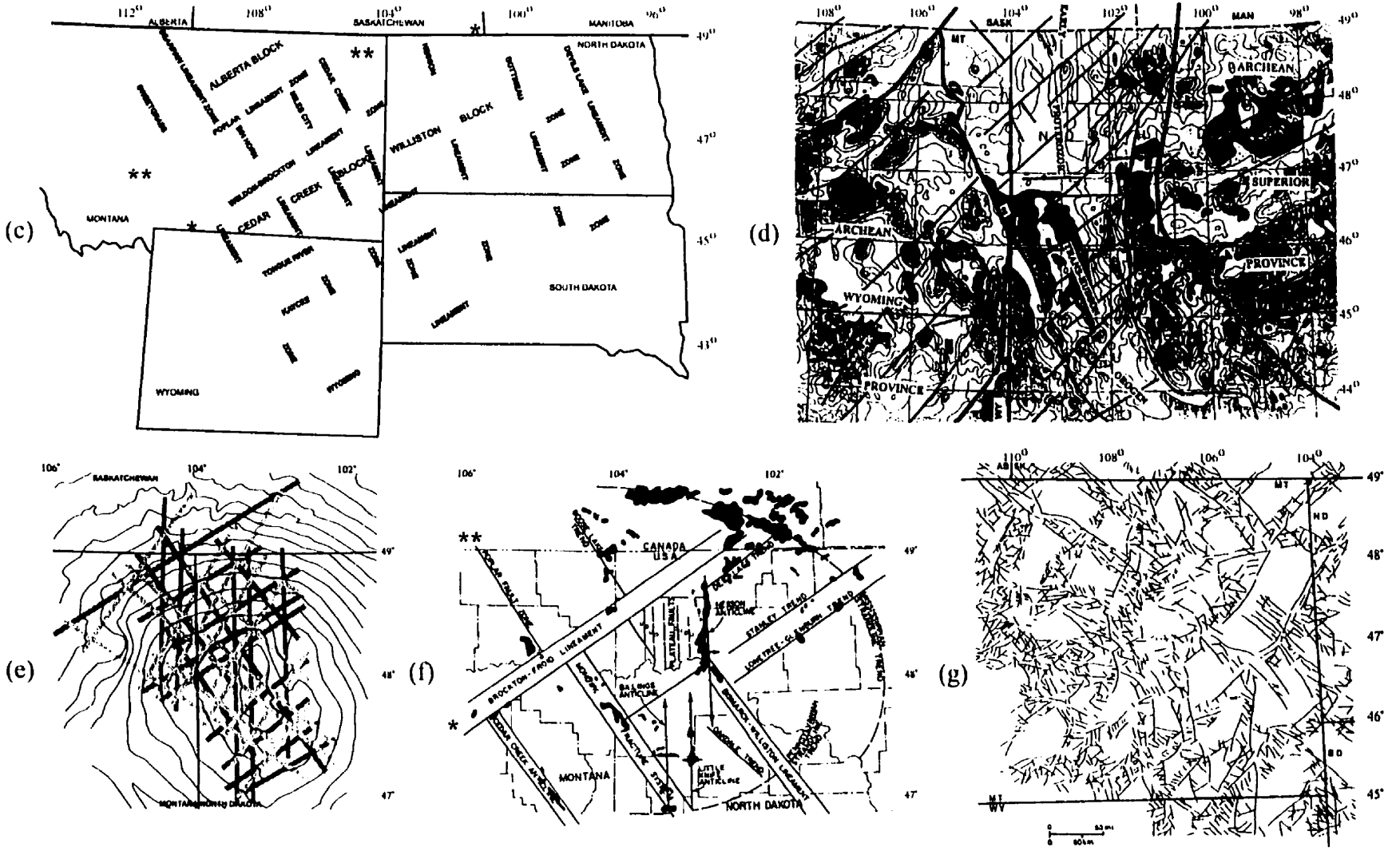

Fig. 3.15 Various lineament interpretations in the Williston Basin area [continued] ([c]Brown and Brown, 1987; [d] Gibson, 1995; [e] Mollard, 1987; [f] Gerhard et al., 1991; [g] Shurr et al., 1989b).

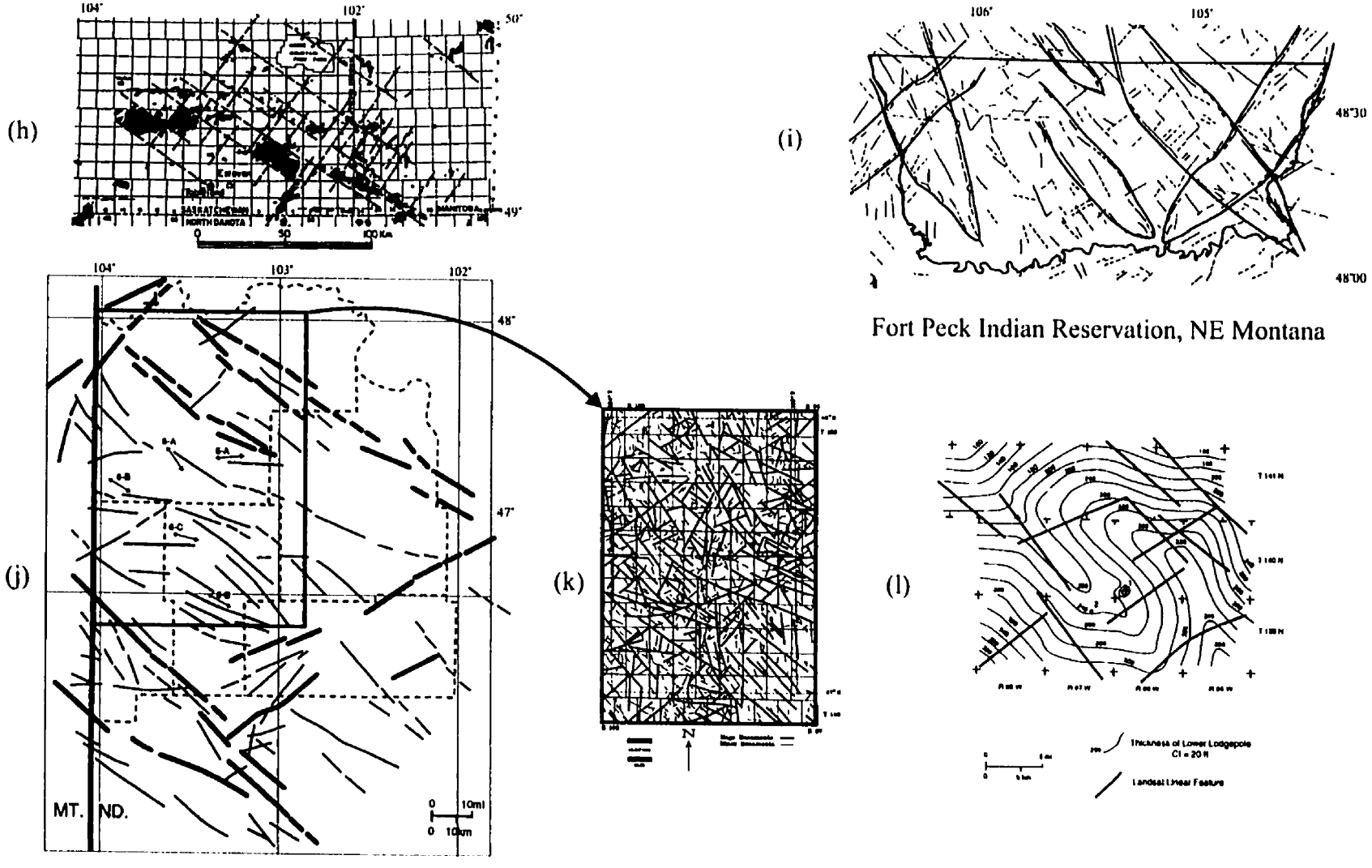

Fig. 3.15 Various lineament interpretations in the Williston Basin area [continued] ([h] Mollard, 1987; [i] Monson and Lund, 1991; [j] Shurr et al., 1995; [k] Freisatz, 1995; [l] Shurr et al., 1995).

interpretation of Paleozoic structures in the basin also followed this model, even if most of the time the observed structural features did not comply with the theory.

Part of the problem lies in the remote sensing methods and their applicability in deep subsurface interpretations. Since the advent of aircraft and cameras, aerial information became popular. This trend is enhanced from the 60's onward by vast numbers of satellite photos. On these types of datasets, lineament interpretation became easier. These lineaments in most cases were readily interpreted as structural directions and surface expressions of various subsurface features. Even at the beginning there was considerable debate over what these linear features on the remotely sensed data meant (photolineament vs. tectonic lineament) *(Kupsch and Wild, 1958; O'Leary et al., 1976, 1978; Allum, 1978)*. An early warning against claims that surface fracture patterns, as seen on aerial photographs in unconsolidated deposits, can reveal subterranean reef-bioherms *(Rumsey, 1971)* was largely disregarded.

There are numerous lineament initerpretations in the Williston Basin area are mostly inconsistent ***(Figs. 3.15. a-l)***. Not only did the interpretations exhibit fundamentally different structural directions ("basement weakness zones"), but the lineaments with the similar name sometimes ran 20 km away ("Weldon-Brockton Lineament" * in ***Figs. 3.15. c and f***) or in different directions ("Poplar Lineament Fault Zone" ** in ***Figs. 3.15. c and f***).

Later interpretations based on "pre-existing" lineament preconceptions led to, e.g., the pull-apart basin model. It is difficult to imagine how jostling blocks could produce an axisymmetric, circular basin in the Paleozoic. If this were the case, the area would have shown a block-faulted pattern in the Paleozoic, with no specific regional depocenter. In this case the Williston Basin would be a minor sub-basin west of the Nesson Anticline as the Thomas *(1974)* map suggests for the Laramide deformation ***(Fig. 3.15.a)***.

Unfortunately, even if various data types were applied together, the interpreterations were "model-based" and lineament were interpeted, where other directions could have been more obvious ***(Fig. 3.15. d)***. Model-based interpretations frequently contradicted existing maps and forced structural features in order to fit the model (e.g. Little Knife Field, Billings Anticline in ***Fig. 3.15.f***). Without disregarding entirely the importance of the indirect information about the subsurface deduced from air and satellite photos. As O'Leary et al. *(1978)* stated *some* lineaments could represent *some* faults.

It is emphasized here that the problem with most of the lineament interpretations are built on the premise that they are "pre-existing" Precambrian weakness zones in the basement, reactivated throughout the history of the basin. Some of these "weakness zones" are not found with other, independent methods.

The origins of these assumed weakness zones are still ambiguous, and no model discusses them adequately. Despite these legitimate concerns, photo and satellite geology are fundamentally important and *all* lines on these data types have *some* meaning, not necessarily basement and structurally related, however. Photo and satellite geology is extremely useful in neotectonics, engineering and Quaternary geology and can be applied with reliability on the late, Sevier-Laramide deformations. Extreme care should be taken when applying these data sources to deeper geology.

Satellite and photogeologic information should constitute supporting datasets and not the main source of interpretation in these problems. For deeper subsurface studies, the vast amount of direct geologic data (well logs, structure, isopach maps), compiled meticulously by generations of excellent geoscientists from both sides of the border should be used. Adding to this huge dataset, information from the third dimension is required from regional seismic studies, such as presented in this thesis, to put the geological information into a basin-wide tectonic context. Disregarding these fundamental data types can lead to model-driven interpretation.

The late L.L. Sloss warned *(1991)* that the beauty of algorithms of theory-based numerical models can give a false impression of credibility that disregards the frailty and inadequacy of the database employed — prophetic words that should be taken seriously. This opinion was reiterated by Bally *(1982)*, who cautioned that our ability to invent models is moving much faster that the capacity of geologists and geophysicists to aquire the critical high-quality information to unambiguously support these models. Sloss *(1991)* suggested that any conjectural models should be supported by the most up-to-date stratigraphic synthesis in order to test their real-life validity.

These words are taken as the guidelines of this thesis, which is an attempt to conduct not a "model-driven", but an observation-based theory about the evolution of the Williston Basin. The unique new dataset of the thousands of kilometers of regional seismic lines of this thesis gives qualitatively and quantitatively new basic information about the internal stratigraphy and structure of the Williston Basin. This new information, together with the vast amount of public domain regional and local scale data, should be a reliable starting point for any future model.

3.4 Outstanding issues, problems to solve

The most important unresolved issues are the three-dimensionality of the basin's structure, the directions associated with intrabasinal features, and their evolution throughout the history of the basin. Regional seismic profiles can shed light on the actual structural characters of the tectonic features (strike, dip directions), adding an extra dimension to the well-based interpretations. Based on the new dataset, contributions are expected to be made in three areas:

Pre-Zuni structure of the basin

- The lineament theory for the pre-Zuni history of the basin is considered inadequate.
- Model-independent interpretation of basement structural trends is fundamentally important.

- The pre-Zuni stratigraphy of the basin is well established, and fundamental new results in this basin-scale study cannot be expected. Due to the platform type of sedimentation in this period, the litho- and sequence stratigraphic boundaries are identical in regional scale.

Zuni stratigraphy of the basin

- Contrary to those for pre-Zuni times, the Zuni structural interpretations of the basin are reliable, and models tracing the effects of the Sevier and Laramide orogenies in the study area are applicable.
- It is the stratigraphy of Zuni times which requires a more regional interpretation. Principles of sequence stratigraphy are fundamental to setting the spatial and temporal framework of the basin during this period.
- Zhu's *(1992)* subdivision of the Zuni sequence in the northern part of the basin will be extended to other parts of the basin. Renaming of the subdivisions is necessary, since, unfortunately, existing lithostratigraphic names were given for sequence stratigraphic units, which can cause confusion.

New basin evolution model

- Based on the structural and stratigraphic interpretation of the new dataset, a new basin-evolution model will be presented, one that is in harmony with the existing and new datasets.

CHAPTER 4

SEISMIC DATA

This thesis is based primarily on seismic data. Four additional regional lines were added to Zhu's *(1992)* east-west section ***(Fig. 4.1)***. Two of the new regional lines, WE II and WE III trend east-west, and two others, NS I and NS II are directed north-south. An additional line segment, CA I is a part of the Canadian data but its southern extension in the U.S. is identical with NS I. Wireline information from 49 wells along these lines was incorporated in the essential geophysical data to combine the geologic information with the seismic results through synthetic seismograms. The processing steps of these two data types will be discussed separately. Since this investigation is essentially a basin analysis study, the theoretical aspects of seismic data processing steps will not be addressed in great detail. Elaborate definitions are supplied by excellent books on this topic *(e.g., Yilmaz, 1987; Telford et al., 1990; Sheriff, 1991)*. Synthesis of the data and interpretation will be conducted in ***Chapter 6***.

4.1 Seismic profiles

The seismic data were obtained by various means. The sedimentary portions of the COCORP Montana and North Dakota datasets were donated by Cornell University. Other data were contributed by petroleum companies or data brokerage firms. *All* seismic data were reprocessed from field tapes in order to achieve comparable regional seismic images required for basin analysis.

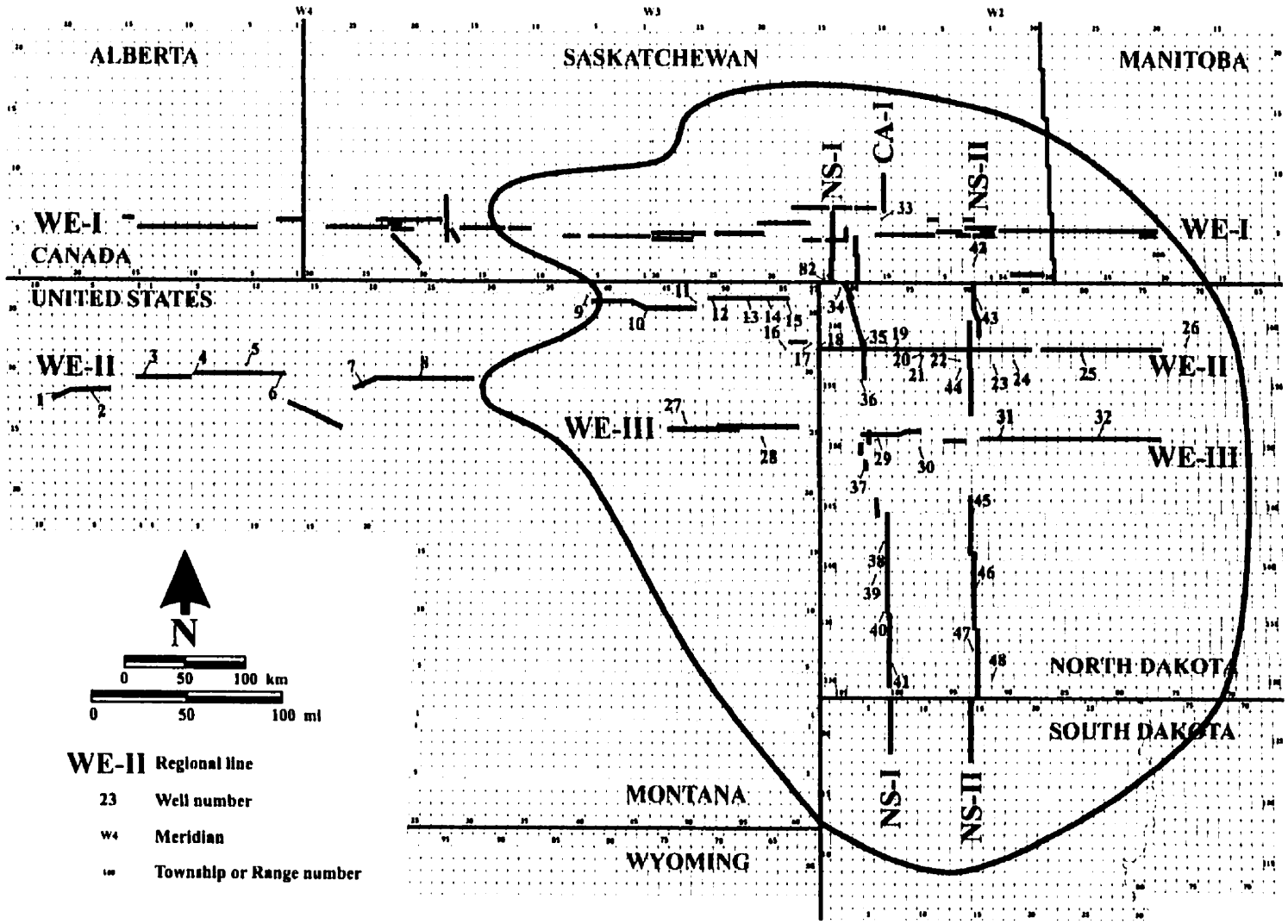

Fig. 4.1 Location of seismic lines and wells used for synthetic seismograms.

4.1.1 Acquisition parameters

All together 40 seismic profiles were reprocessed ***(Fig. 4.1; Table 4.1)***. The whole dataset covers ~1900 line km, which, with gaps represents a total subsurface coverage of ~2300 km. The lengths of the longest gaps are: 103 km on WE II, 52 km on WE III and 62 km on NS II. Efforts were made to minimize the gaps; however, lack of available data made 100% coverage impossible. This minor deficiency did not hamper the basin analysis. Contrary to Zhu's *(1992)* study, where the regional profile was compiled from many short survey line segments, the individual profiles in this study are quite long and only 7 out of 40 are shorter than 20 km. This more extensive coverage made interconnection of regional lines a less cumbersome process. Digitally, these **40 lines** represent **9,795 shot gathers** and over **1.2 million seismic traces**. This vast amount of data had to be subjected to a good number of processings steps, requiring extended computer time and disk space.

The quality of the field data ranges from good to excellent. Complete listings of acquisition parameters are given in ***Table 4.1***. Most of the data were acquired in the 80s and late 70s with state-of-the-art instrumentation and field techniques of the time.

Station intervals vary from 25 m to 134 m. Low number of channels per spread (20, 24) were used on three lines from the 70's, but the majority of the surveys utilized 48 channels. Higher numbers of channels (94, 120, 240, 355, 400) were used occasionally, especially by the COCORP crustal project.

Depending on the number of channels and shot spacing, data coverages of varying fold was achieved. With the exception of the lowest (4) and the highest (100) nominal folds, the survey multiplicity ranged from 6 to 48.

Both explosive and vibrator energy sources were used in the lines. Explosive sources were used in 23 out of 40 lines but the Vibroseis™ data cover a longer distance.

Table 4.1 Seismic lines, acquisition parameters.

Line #	Regional line	Line code	Original line #	Company	Length (km)	Township-Range	State / Province	Date shot	Station int. (m)	Shot int. (m)	Channels	Fold	Source (Dyn/Vib)	Instrument type	Rec length (s)	Sample rate (ms)
1	**WE II**	we01	MT-3	COCORP	50	27N-08W - 28N-03W	MT	Jun-86	100.60	100.60	96	48	V	MDS-10	16	4
2		we02	MT-4	COCORP	45	29N-01W - 29N-05E	MT	Jun-86	100.60	100.60	96	48	V	MDS-10	16	4
3		we03	MT-5	COCORP	72	30N-05E - 30N-13E	MT	Jun-86	100.60	100.60	96	48	V	MDS-10	16	4
4		we04	MT-6	COCORP	52	27N-13E - 25N-18E	MT	Jul-86	100.60	100.60	96	48	V	MDS-10	16	4
5		we05	MT-7	COCORP	110	28N-19E - 30N-29E	MT	Jul-86	100.60	100.60	96	48	V	MDS-10	16	4
6		we06	MT-8	COCORP	85	36N-39E - 35N-48E	MT	Aug-86	100.60	201.20	96	24	V	MDS-10	16	4
7		we07	MT-10	COCORP	62	36N-49E - 36N-55E	MT	Aug-90	50.00	100.00	400	100	V	SGR-IV	20	4
8		we08	MT-11	COCORP	17	32N-56E - 32N-58E	MT	Jul-90	50.00	200/400	355	44/22	V	SGR-IV	20	4
9		we09	ND-1w	COCORP	170	158N-103W - 158N-85W	ND	Jul-90	50.00	200.00	400	50	V	SGR-IV	20	4
10		we10	ND-1e	COCORP	95	158N-84W - 158N-74W	ND	Sep-90	50.00	200.00	400	50	V	SGR-IV	20	4
11	**WE III**	kn01	600-10	Pacific West	56	25N-46E - 25N-52E	MT	Dec-81	50.29	201.16	96	12	D	SN338HR	4	2
12		kn02	RMA 18	Pacific West	66	25N-51E - 25N-57E	MT	Aug-80	67.05	268.22	48	6	D	MDS-10	5	2
13		kn03	M-1	Pacific West	52	151N-101W - 151N-96W	ND	Dec-80	67.05	268.22	48	6	D	SN338HR	5	2
14		kn04	100-8W ext	Marathon	18	151N-93W - 151N-92W	ND	Sep-74	67.05	268.22	48	6	D	Sercel	4	2
15		kn05	100-8	Pacific West	43	151N-90W - 151N-85W	ND	Oct-77	67.05	268.22	48	6	D	SN338B	4	2
16		kn06	100-8A	Pacific West	56	151N-85W - 151N-80W	ND	Feb-79	50.29	301.75	48	4	D	SN338B	4	2
17		kn07	100-8 ext	Pacific West	48	151N-79W -151N-75W	ND	Nov-78	67.05	268.22	48	6	D	SN338B	4	2
18	**CA I**	ca01	CBT-20/WB-F-20	Union Oil	29	T10-R10W2 - T7-R10W2	SK	Oct-79	67.05	134.10	48	12	V	MDS-10	4	2
19		ca02	EBN-12	Union Oil	11	T5-R13W2 - T4R13W2	SK	Oct-85	27.00	108.00	120	15	D	DFS-V	3	2
20		ca03	CBS-11/WB-LC-11	Union Oil	16.5	T5-R13W2 - T3R13W2	SK	Sep-79	67.05	134.10	48	12	D	DFS-V	3	2
21		ca04	CBS-07/WB-LC-07	Union Oil	22.5	T3R13W2 - T1R13W2	SK	Sep-79	67.05	134.10	48	12	D	DFS-V	3	2

Table 4.1 Seismic lines, acquision parameters (continued).

Line #	Regional line	Line code	Original line #	Company	Length (km)	Township-Range	State / Province	Date shot	Station int. (m)	Shot int. (m)	Channels	Fold	Source (Dyn/Vib)	Instrument type	Rec length (s)	Sample rate (ms)
22	**NS I**	ns01	33-05	Shell Can.	41	T7-R15W2 - T2R15W2	SK	Aug-77	67.00	134.00	48	12	D	DFS-V	3	2
23		ns02	33-04	Shell Can.	20	T3-R15W2 - T1R15W2	SK	Aug-77	67.00	134.00	48	12	D	DFS-V	3	2
24		ns03	NCW-270 N	StratSeis	12.5	164N-101W - 162N-100W	ND	Jun-85	34.28	67.05	120	30	V	DFS-V	3	2
25		ns04	NCW-270 M	StratSeis	43	163N-100W - 158N-99W	ND	Jun-85	34.28	67.05	120	30	V	DFS-V	3	2
26		ns05	NCW-270 S	StratSeis	32	159N-100W - 156N-100W	ND	Jun-85	34.28	67.05	120	30	V	DFS-V	3	2
27		ns06	66-25-70	Conoco	13	151N-100W - 150N-100W	ND	Mar-70	134.11	134.11	20	10	V	?	5.5	4
28		ns07	65-25-70	Conoco	9.5	150N-100W - 149N-100W	ND	Mar-70	134.11	134.11	20	10	V	?	5.5	4
29		ns08	8-ND-91	Conoco	9.5	149N-100W - 148N-101W	ND	Feb-90	25.14	75.43	240	40	V	DFS-V	5	2
30		ns09	LM 1-15	PGC	14	146N-100W - 144N-100W	ND	Aug-78	134.11	268.22	24	6	D	?	4	2
31		ns10	A	STM Corp.	82	144N-99W - 136N-100W	ND	Aug-78	100.58	402.33	48	6	D	?	4	2
32		ns11	A(a)	STM Corp.	61	136N-100W - 129N-101W	ND	Sep-80	67.05	268.20	48	6	D	SN338HR	4	2
33		ns12	SPEC-9	E.Gunderson	45	23N-07E - 18N-07E	SD	Aug-75	67.05	268.20	48	6	D	DFS-IV 9T	4	2
34	**NS II**	ed01	WBR-10 (L-10)	PGC	46	164N-90W - 159N-90W	ND	Jan-78	100.58	402.33	48	6	D	?	3	2
35		ed02	100-15	Pacific West	38	160N-90W - 157N-90W	ND	Nov-78	67.05	268.22	48	6	D	DFS-V	4	2
36		ed03	180-25	Pacific West	38	156N-91W - 153N-91W	ND	Jun-81	67.05	268.22	48	6	D	SN338B	4	2
37		ed04	D-8	STM Corp.	48	146N-92W - 141N-92W	ND	Sep-85	67.05	268.22	48	6	D	SN338B	4	2
38		ed05	NPN 22-B	Pacific West	67	141N-92W - 135N-93W	ND	Jan-77	100.58	402.33	48	6	D	DFS-IV 9T	4	2
39		ed06	NPN 14	Pacific West	48	134N-92W - 129N-93W	ND	Jan-76	100.58	402.33	48	6	D	DFS-IV 9T	4	2
40		ed07	SP-3	Pacific West	50	23N-14E - 18N-14E	SD	Apr-76	67.05	268.22	48	6	D	SN338B	4	2

Record lengths depend on the purpose of the aquisition. The COCORP crustal seismic lines have total record lengths of 16 and 20 seconds; however, only the uppermost, sedimentary portions were considered for this study. The hydrocarbon-exploration field information had 3, 4, 5, and occasionally 5.5 second recording lengths.

The sampling rate of the records is 4 ms for the COCORP and for two other profiles, while the rest of the data were recorded with at 2 ms digitization steps.

4.1.2 Seismic data processing

The primary goal of the processing is to assemble seismic section with the clearest possible signal images. To achieve the highest comparability between individual sections of a regional line, processing steps were kept as similar as possible with data of different vintages and acquisition parameters.

All of the profiles were processed by execution of routines of the INSIGHT seismic processing system, a product of Landmark/Inverse Theory and Application (ITA) Inc.

The processing steps can be subdivided into four main groups: ***Preprocessing (Edit procedures); Parameter selection tests / prestack processing; Poststack processing,*** and ***Special applications (Fig. 4.2***). The first three groups constitute a standard processing operation, while the fourth involves special steps required because of the regional line construction and basin analysis.

4.1.2.1 Preprocessing (Edit procedures)

All of the profiles were reprocessed from demultiplexed field data. *Field data* were received on magnetic medium either in SEG-B or in SEG-Y format.

For processing the field information was reformatted into ITA format.

PREPROCESSING (EDIT PROCEDURES)

Field tapes
Reformatting
Vibroseis correlation ⇐ *sweep**
*Resampling**
Geometry ⇐ Observer notes, survey file
Gain recovery/adjust
Energy equalization
Editing (bad trace killing)
First break picking, field statics calculation
Muting
Field statics (datum, refraction/uphole time statics)

PARAMETER SELECTION TESTS / PRESTACK PROCESSING

Spectral analysis, autocorrelation
Deconvolution (*zero phasing**, spiking, predictive)
Bandpass filtering
Velocity analysis
Sorting into CDPs
Normal moveout correction, mute ⇐ velocity file
Residual static corrections
Stacking

POSTSTACK PROCESSING

Gain recovery
Bandpass filtering
Deconvolution
Migration (time, depth)

SPECIAL APPLICATIONS

Data alignment (reflection dejaggling/*flattening**)
Horizontal stacking
Data merging
Energy balancing
*Earth-curvature corrections**

*Note: * step not required on all data*

Fig. 4.2 Generalized processing sequence of seismic data.

Some Vibroseis™ data were uncorrelated; consequently Vibroseis™ cross-correlation of the data with the input sweep trace was performed on them. A raw, unprocessed record is shown in ***Fig. 4.3***.

Since some of the data were acquired with a 2 ms, others with a 4 ms sampling rate, part of the data had to be resampled. The 4 millisecond sample rate was chosen to save computation time and disk space.

Most of the field observer notes and survey files were on paper copy, consequently all of these data had to be entered manually. Proper *geometric* and acquisition information was put into individual trace headers.

The next step was the gain recovery/adjust (AGC = Automatic Gain Control) and energy equalization. This process was necessary to eliminate or at least minimize the amplitude loss due to signal attenuation (e.g., spherical divergence,). An example of a raw data record with only AGC applied is shown in ***Fig. 4.4***. This representative record exhibits bad traces, low-velocity ground roll, static busts, multiples, etc. Removal of these unwanted characteristics is essential to achieving a geologically meaningful seismic profile. Subsequent processing steps attempt to achieve this goal by maximizing the positive effects of the individual processing steps.

Bad traces (noisy traces, monofrequency signals, polarity reversals) had to be killed or corrected in order to avoid a decrease in the final data quality. First breaks were picked on the datasets to calculate the structure and velocity of the layers above a chosen datum.

After this, the first-break parts of the records had to be muted (excluded from the stack), because they interfered with shallow arrivals.

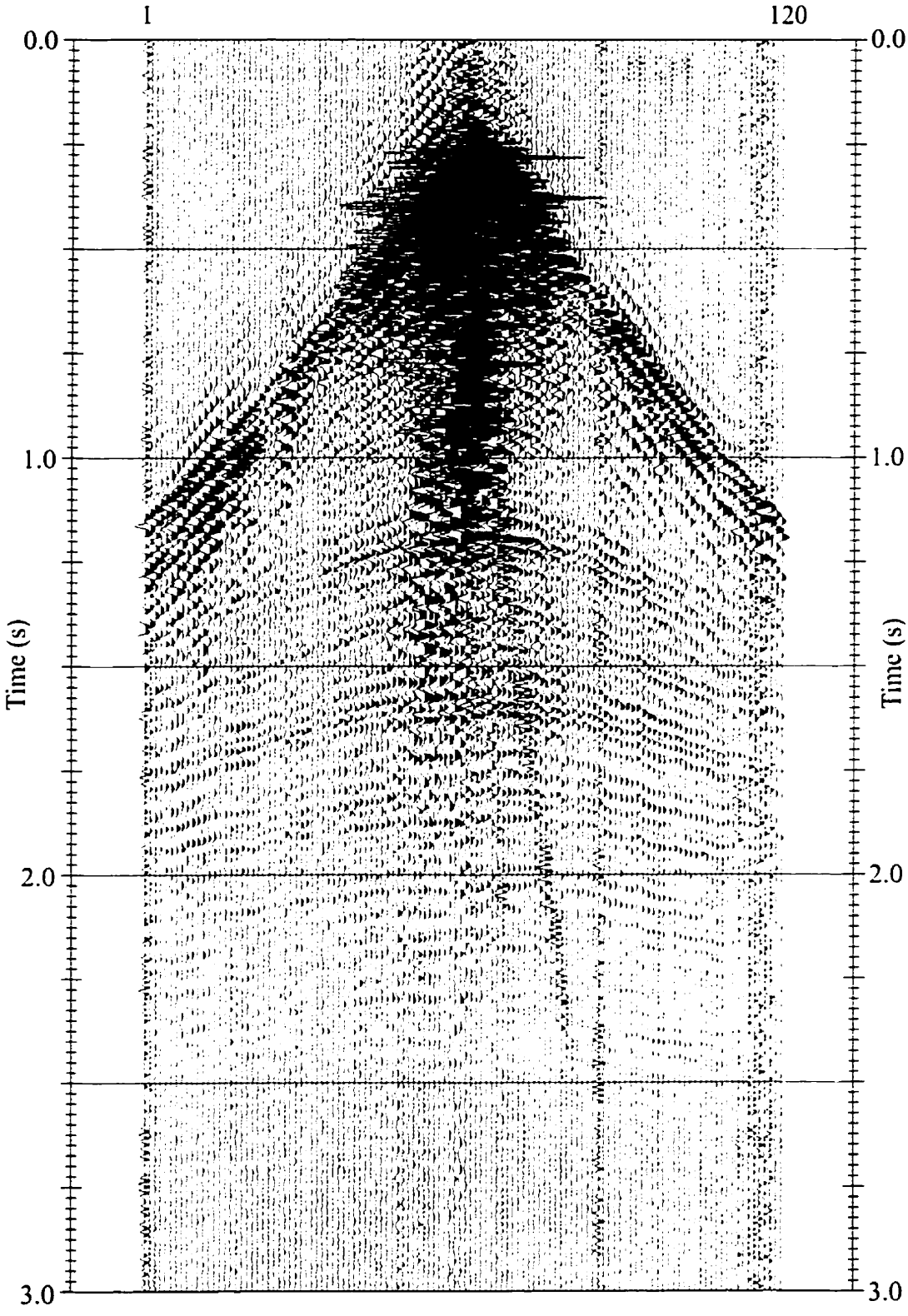

Fig. 4.3 A raw shot gather.

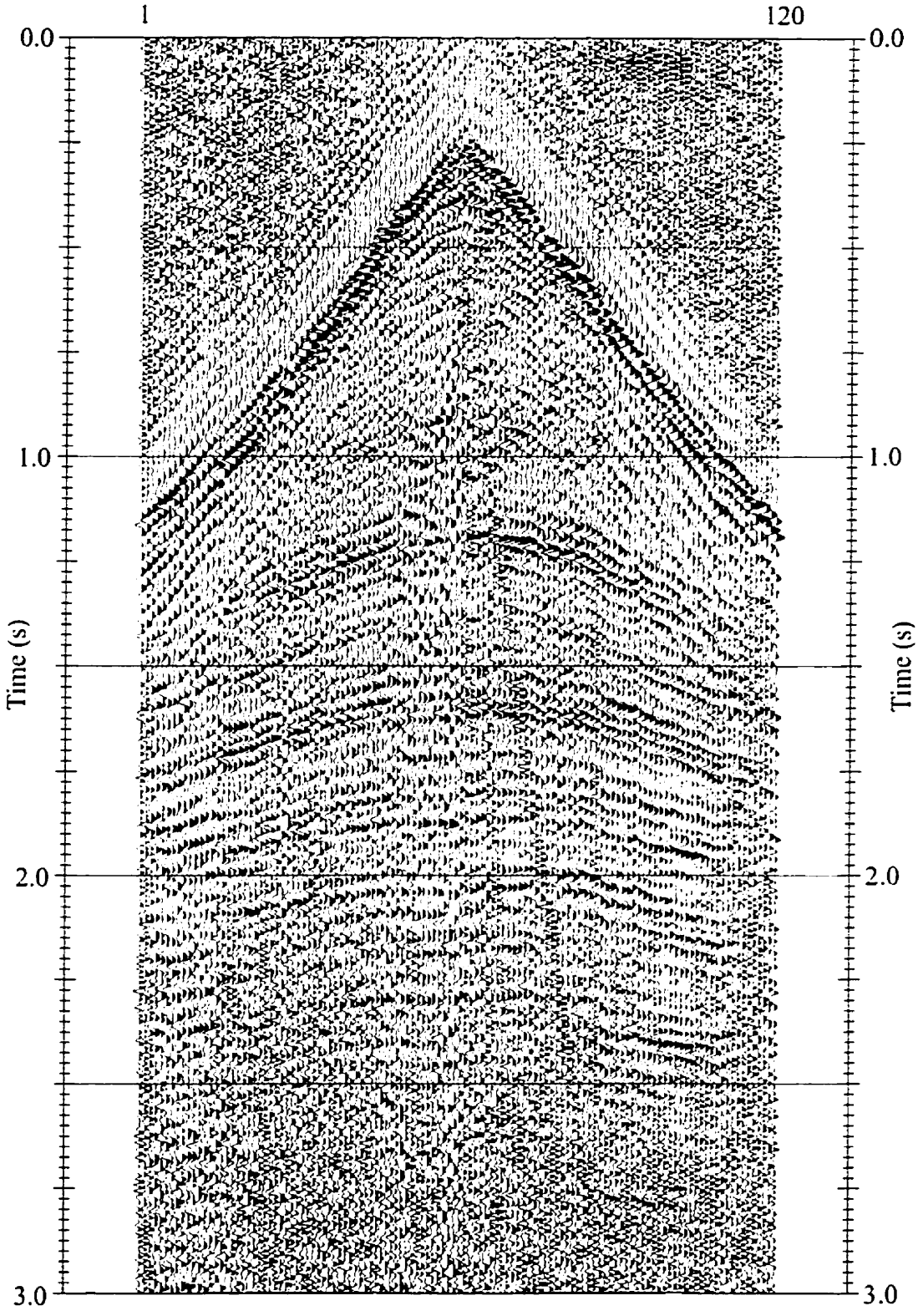

Fig. 4.4 A raw shot gather with AGC
(same shot as Fig. 4.3).

Subsequently, field static corrections (datum, refraction/uphole time statics) were applied to the data. The choice of refraction versus up-hole-time statics depends on the data type (dynamite or Vibroseis™) and on which method provides better results. The magnitude of these corrections is based on the chosen datum and the values calculated from first-break information or supplied by the up-hole time measurement. The corrections were necessary to compensate for the effects of variations in elevation, weathering thickness and weathering velocity above the datum level.

4.1.2.2 Parameter selection tests / prestack processing

After the preprocessing steps, spectral analysis was performed (frequency, phase) and autocorrelation functions were calculated. Explosive records with minimum-phase signal characteristics had to be converted to zero-phase records to be compatible with the zero-phase Vibroseis™ measurements.

Two deconvolution steps were performed, one to improve the temporal resolution of the seismic data (spiking deconvolution) the other to eliminate multiple reflections (predictive deconvolution). Prediction parameters were determined from the autocorrelation functions calculated earlier. Frequency filtering operations were designed to attenuate undesirable high and low frequencies (e.g., ground roll). An attempt was made to keep the frequency bands on different lines as close as possible. An example of the effectiveness of the above signal enhancement steps is given in ***Fig. 4.5***.

After the deconvolution/frequency filtering, velocity analysis was performed. The semblance method was used during the processing. Preferably the velocity analysis is performed on common-depth-point (CDP) sorted data; however, low fold coverage in some areas led to uncertain results. To counterbalance this problem, velocity values were computed utilizing both shotgathers and CDP data and computations were carried out in increased distance intervals. Given the rather unchanging character of the local stratigraphy, low dips, and almost horizontal strata, this approach did not hamper the quality of the final sections.

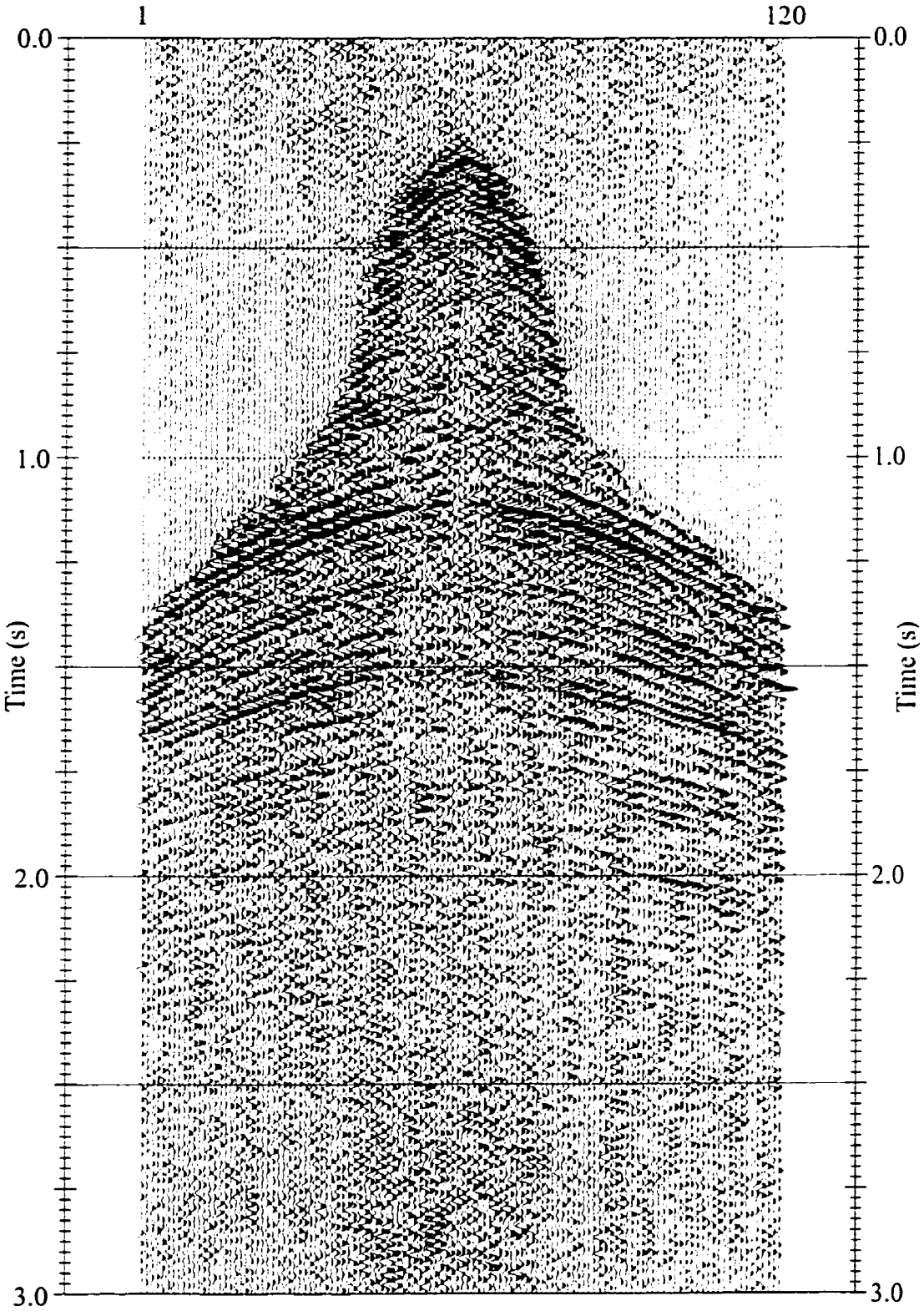

Fig. 4.5 A shot gather after initial processing [deconvolution, frequency filtering, mute] (same shot as Fig. 4.3).

Following the velocity-depth determinations, normal moveout (NMO) corrections were performed, applying the velocity functions determined during the velocity analysis. Parallel with this process, additional muting was performed to exclude the distorted, low-velocity part of the traces due to the "NMO-stretch".

Prior to stacking, a residual statics calculation was performed on the CDP gathers, and corrections were made to maximize the stack energy.

After this stacking was performed, leading to the seismic cross section ***(Fig. 4.6)***. Stacking is also a tool for suppressing multiple reflection and increasing signal-to-noise ratio. It also involves filtering suppression of higher frequencies because of occasional timing errors or wavelet shape differences among the elements being stacked. In order to minize these errors, the processing steps from velocity analysis to stacking were repeated until the best stacked section was achieved.

4.1.2.3 Poststack processing

Some additional fine tuning was required on the stacked sections, to improve the quality of the seismic profiles.

AGC was applied again to enhance the deeper reflections.

Bandpass filtering was performed additionally to cut the low frequencies.

Wave-shaping deconvolution was implemented to further enhance the temporal resolution and the signal-to-noise ratio and balance waveforms throughout the section. These steps were performed iteratively until the best result was achieved ***(Fig. 4.7)***.

Migration represents the final steps in the conventional data processing sequence. Both time and depth migrations were applied on the data. Time migration did

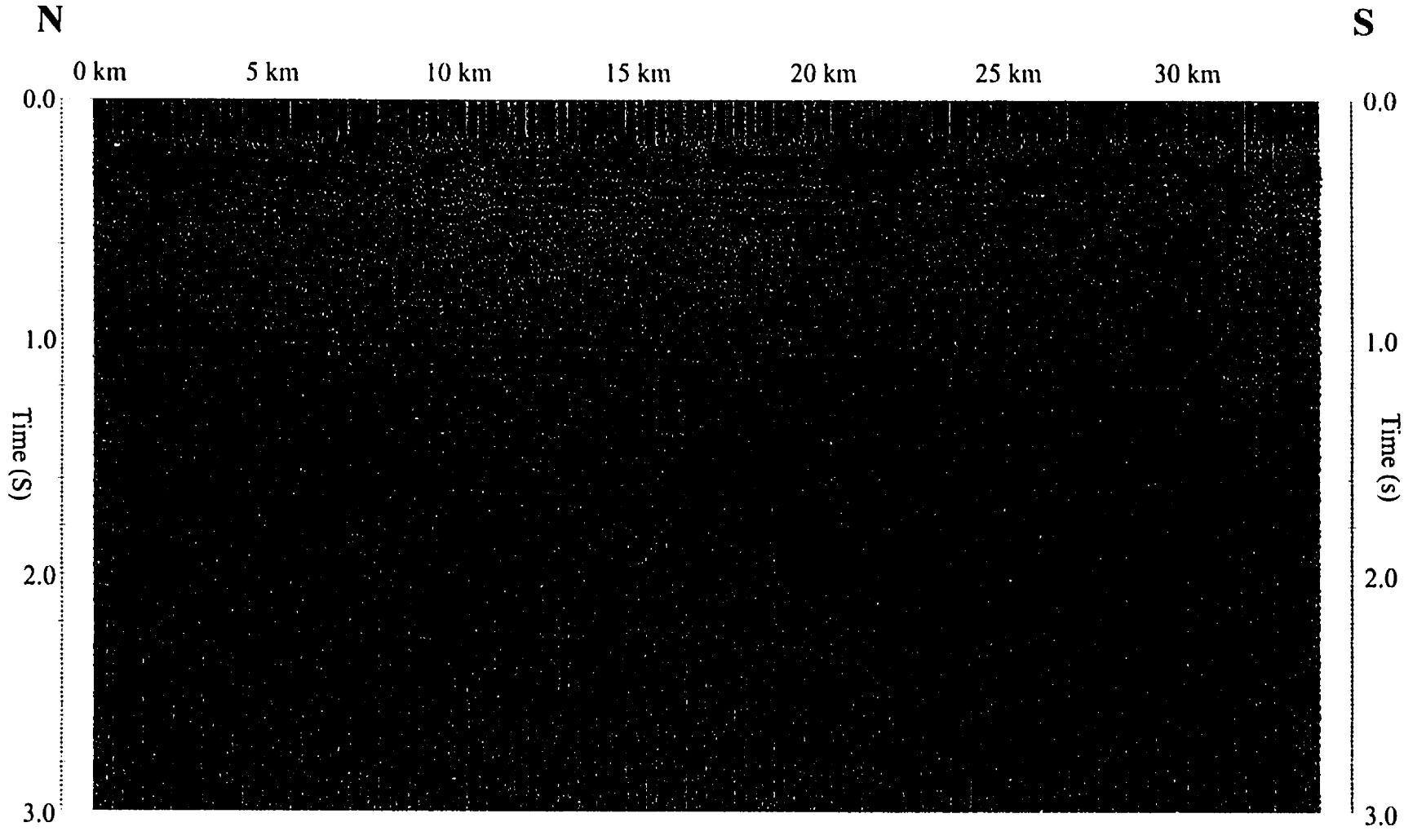

Fig. 4.6 Stacked section before poststack processing (Line ns05).

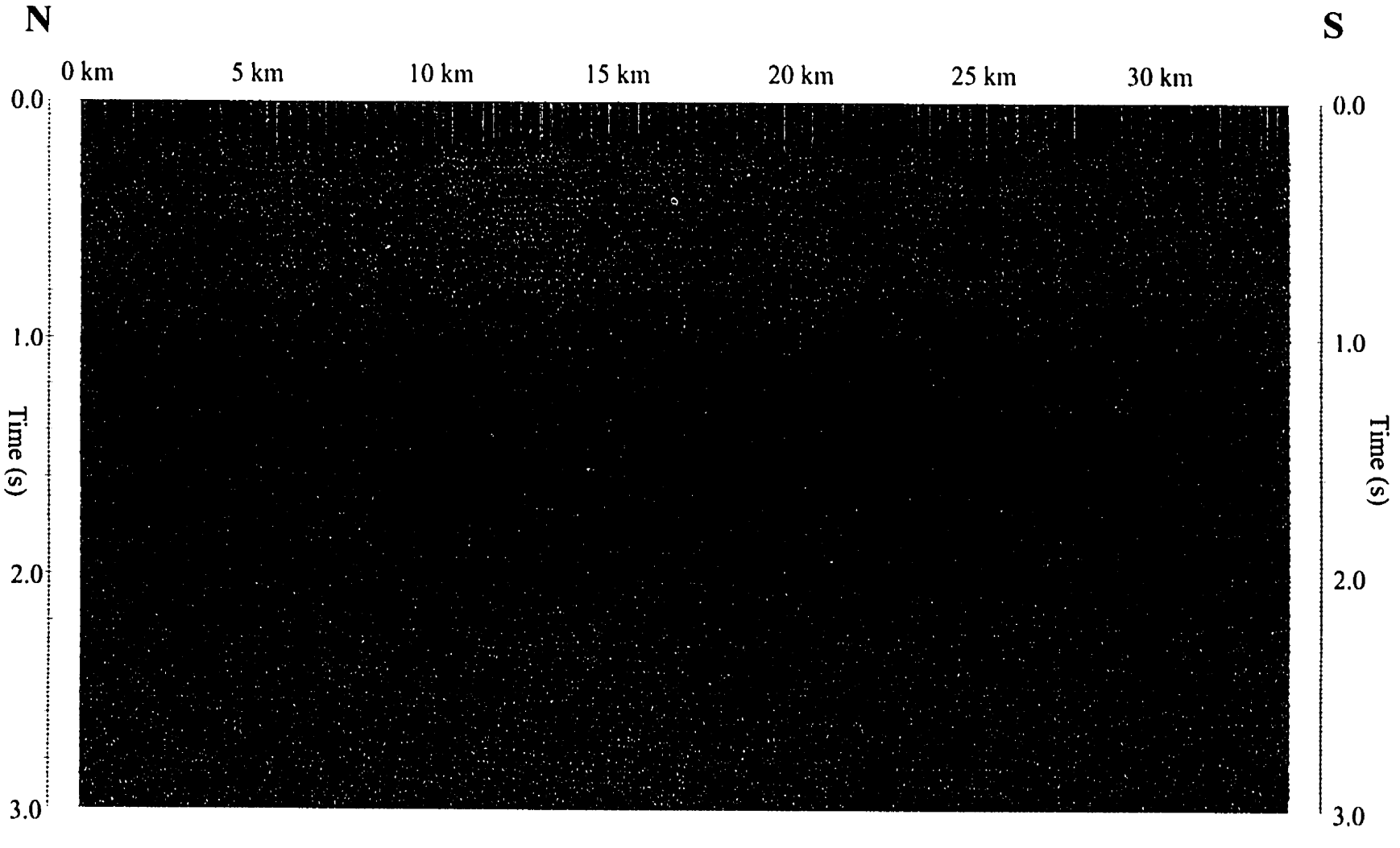

Fig. 4.7 Stacked section after poststack processing (Line ns05) [AGC, deconvolution, band-pass filtering].

not produce dramatically different results, due to the virtually horizontal layering in the study area. Depth migration, needed for special regional considerations, was performed in the frequency-space domain. However the velocity estimation required for migration, based on seismic and other data, is always limited in accuracy; therefore, depth conversion is not completely accurate *(Yilmaz, 1997)*. Keeping in mind the purpose of the study (i.e., basin analysis), the resulting lines were satisfactory for helping in the regional scale interpretation.

4.1.2.4 Special applications

The following supplementary processing steps were done to achieve comprehensive, comparable regional seismic lines. Different data alignment procedures were carried out.

One type of aligning technique is minimizing the occasionally still present short-wavelength bursts (dejaggling), and enhancing the larger-scale structures.

Another type of aligning is essentially datuming (flattening) to a chosen horizon. This horizon is the Cretaceous Greenhorn Shale (Second White Speckled Shale, in Canada), because this layer is practically the only formation present in the whole area with excellent reflection characteristics. This step was necessary to compare the results of this study with Zhu's *(1992)* regional seismic line, which was flattened to this reflector.

It was necessary to execute various amounts of decimation on the individual lines, since the station spacing was different in each line. This process was achieved through "horizontal stacking". This step improved the reflections, but obviously reduced the lateral resolution. This later degradation did not hamper the regional scale interpretation.

After the trace intervals in each line were uniform, the individual lines were merged into regional cross sections. Acquisition gaps had to be padded out with the proper numbersof empty traces.

On the compiled regional lines, energy balancing had to be performed to achieve a uniform energy level and comparable, continuous reflections. These steps were done on both time and depth sections. On the datum-flattened regional sections, the Zuni-Tejas seismic/sequence stratigraphy can be interpreted more easily than on the unflattened sections. These sections can be found in the Appendix ***(Figs. A.1-6)***

One additional, special step needed for the depth sections was correcting for the Earth's curvature. This is required in regional cross sections, to achieve realistic spatial relationships of the megascale structures (i.e., basin). Detailed analysis and discussion of this topic is found in ***Chapter 7***. The Earth-curvature corrected regional cross sections are attached to this thesis and can be found in the back pocket of this manuscript ***(Attachment 1-5)***.

4.2 Synthetic seismograms

Synthetic seismograms are the links between the well-based geological subsurface information and the seismic profiles. The connecting constituent is the continuous velocity information of the sonic-log curves, which couples the depth values of geological interfaces to arrival times of seismic reflections representing them. The fundamental pieces of information required to create comparable synthetic seismograms are *sonic velocity (V)*, *geological picks (x)* and, preferably, *formation density (ρ)* values. The product of velocity and density at *depth i* is the **acoustic impedance**:

$$Z_i = V_i \cdot \rho_i \qquad \text{(Eq. 4.1)}$$

The **reflection coefficient** for normal incidence on an interface separating two intervals with different acoustic impedance values (Z_{i+1}, Z_i) is:

$$R = (Z_{i+1} - Z_i) / (Z_{i+1} + Z_i) \qquad \text{(Eq. 4.2)}$$

The magnitude of the reflection coefficient is the manifestation of differences in the physical properties of the formations below and above the interface. In case of a lack of density information, the velocity data usually gives satisfactorily good results, since the effect of density is minor in many cases. Calculation of reflection coefficients for the entire well results in the reflectivity series. The generation of synthetic seismograms is, in fact, a mathematical convolution of a wavelet with the reflectivity series. For the best match, the wavelet used for convolution was always extracted from the seismic traces recorded closest to the well in question.

Synthetic seismograms were generated from 48 wells relatively evenly distributed along the regional seismic sections. An attempt was made to compile the deepest wells, closest to the lines, to maximize the information extracted from them ***(Table 4.2)***. Fortunately, from most of the wells (37) both sonic and density logs were available. The SynView module of the GeoQuest IES software was adopted to generate the synthetic seismograms. All the final results were compiled in the Appendix ***(Figs. A.7-54)***. The compilations contain the velocity, density (if available), calculated reflection coefficient series, the extracted wavelet, 5 synthetic traces and 5 traces from the nearest seismic line for comparison, as well as the depth picks of the major stratigraphic horizons. Only the primary reflections were included in the synthetic panel.

Most of the stratigraphic information (formation picks) are courtesy of Thomas Heck (North Dakota Geological Survey) and James Halvorson (Montana Department of Natural Resources and Conservation). Stratigraphic picks are displayed in ***Table A.1*** in the Appendix in both SI and imperial scales. This table also contains sequence- and lithostratigraphic subdivisions and abbreviations of the names of lithostratigraphic units used throughout the thesis.

Table 4.2 Well data.

Well #	API #	Township	Range	Section	Q1,Q2,Q3/Lsd	State/Province	County	Operator	Well name	Oil field	KB (m)	GL (m)	TD (m)	Formation at TD	Logs:Son,Den
1	25-073-21567	28N	8W	28	NE,NE,C	MT	Pondera	Imperial Oil	Mobil-Matchett 1-28	Wildcat	1388.1	1384.1	2162.0	DSD	S,D
2	25-073-21734	28N	5W	20	NE,NW,SE	MT	Pondera	Smokey Oil	H&W Ranch 31-20	Wildcat	1205.8	1202.7	1620.9	COD	S,D
3	25-073-05469	30N	1W	36	SE,NE,C	MT	Pondera	Farmers Union	1 State 6444-61	NE Ledger	1093.3	1090.3	1362.8	COD	S
4	25-051-21197	30N	5E	32	SE,SE,NW	MT	Liberty	Tesoro Petr.	Tiber-Federal 1	Wildcat	918.1	915.6	810.8	MMM	S
5	25-041-22339	30N	9E	2	NW,NE,SE	MT	Hill	Louisiana Land	Anderson 12-2	Wildcat	933.9	929.9	1616.4	COD	S,D
6	25-015-21630	29N	12E	2	SW,SW,NE	MT	Chouteau	Louisiana Land	Federal 14-2	Wildcat	847.3	843.1	1575.2	COD	S,D
7	25-005-21041	29N	19E	14	SW,NE	MT	Blaine	Superior Oil	Kuhr 1	Wildcat	1218.0	1214.9	581.9	OBR	S
8	25-005-21833	29N	24E	11	NW,SE,W2	MT	Blaine	Montana Power	Tribal 8-11-29-24	Wildcat	808.9	806.2	1206.4	MMM	S,D
9	25-105-21114	36N	39E	7	SW,SW,C	MT	Valley	Getty Oil	1 Federal 7-13	Wildcat	839.1	833.9	2496.0	COD	S,D
10	25-019-21074	35N	44E	4	NW,SW	MT	Daniels	Anschutz Corp.	Wilson 5-4	Wildcat	840.9	836.4	2499.4	SI	S,D
11	25-019-21047	36N	48E	28	NE,SW,C	MT	Daniels	Reading & Bates	Hughes 1-28	Wildcat	729.7	724.8	2824.0	OBR	S,D
12	25-019-21054	36N	49E	2	SW,SW,NE	MT	Daniels	Kirby Expl. Co.	Berger Carl 1	Wildcat	852.8	849.8	2977.9	OBR	S,D
13	25-091-21087	36N	52E	11	SW,NE,C	MT	Sheridan	American Miner.	Radons 1	Wildcat	710.8	707.4	3020.3	OBR	S
14	25-091-21047	36N	54E	10	NE,NE,C	MT	Sheridan	Sinclair O&G	Myers 1	Wildcat		717.2	3161.7	OBR	S
15	25-091-21622	36N	56E	29	SW,SW,SE	MT	Sheridan	Slawson	Lee 1-29	Wildcat	764.1	760.5	3337.6	OBR	S,D
16	25-091-21247	32N	56E	22	NE,NE,N2	MT	Sheridan	Sunmark/Synatec	Erdahl 1	Medicine Lk.	636.7	630.6	3783.5	PC	S,D
17	25-091-21457	32N	58E	3	NE,SW	MT	Sheridan	Nucorp Energy	Christensen 1	Wildcat	605.6	599.2	3541.8	OBR	S,D
18	25-091-21577	32N	59E	29	NE,SW	MT	Sheridan	Arco Oil & Gas	Turtle Mt 1/Willie B.	Dwyer	623.3	617.2	3680.5	OBR	S,D
19	33-105-27000	158N	97W	27	SE,NW	ND	Williams	Arco Expl. Co.	Simpson 1	Wildcat	694.0	687.3	4399.2	COD	S,D
20	33-105-36000	158N	95W	36	SW,NW	ND	Williams	Amerada Petr.	N.D.C."B" 9	Tioga	748.9	744.6	4397.0	PC	S
21	33-061-00378	157N	94W	6	NW,SE	ND	Mountrail	Amerada Hess	Knoshaug 6-22	Tioga	754.1	748.6	4264.2	COD	S,D
22	33-061-00261	157N	91W	17	SW,SW,C	ND	Mountrail	True Oil Co.	Kuster 14-17	Wildcat	703.5	697.7	3936.8	OBR	S,D
23	33-061-00336	157N	88W	29	NE,NW	ND	Mountrail	Challenger Min.	Alvstad 31-29	Wildcat	724.8	721.2	3198.0	SI	S,D
24	33-101-00278	157N	86W	29	SE,SE	ND	Ward	Incxco Oil Co.	Erickson 1-18	Wildcat	626.4	622.7	2831.0	SI	S,D

Table 4.2 Well data (continued).

Well #	API #	Township	Range	Section	Q1,Q2,Q3/Lsd	State/Province	County	Operator	Well name	Oil field	KB (m)	GL (m)	TD (m)	Formation at TD	Logs:Son,Den
25	33-075-00910	158N	81W	36	SE,SW	ND	Renville	Apache Corp.	Watne 36-1	Wildcat	467.0	463.3	1859.3	DMS	S,D
26	33-069-00043	158N	72W	1	NE,SE	ND	Pierce	Chapman Expl.	Selvig 1	Wildcat	494.4	490.7	1657.2	PC	S,D
27		26N	48E	29	SW,SW,NE	MT	McCone	Callaway, W.O.	E. C. Casterline 1	Wildcat	729.7	726.3	2861.8	OBR	S
28		25N	54E	35	NW,NE,SW	MT	Richland	McAlester Fuel	N. P. Vaira B-2	Spring Lake	712.6	709.1	3707.3	COD	S
29	33-053-01071	151N	99W	33	NE,NE,N2	ND	McKenzie	Texaco/Missouri	Torstenson 1	Wildcat	651.4	643.7	4504.6	COD	S,D
30	33-053-02224	150N	96W	25	NW,NE,SE	ND	McKenzie	Sun Expl./Oryx	Delmer Rink 1	Wildcat	766.3	759.9	4614.7	COD	S,D
31	33-061-00218	151N	89W	24	NE,SE	ND	Mountrail	Bass Enterpises	Robert V. Andes 41-1	Wildcat	650.1	645.3	4107.8	PC	S,D
32	33-049-00127	151N	80W	22	NE,NE	ND	McHenry	Arco Expl. Co.	Wunderlich 1	Wildcat	583.7	580.3	2679.8	PC	S,D
33	1800610W200	6	10W2	18	6	SK		Shell Can.	Midale A	Midale	611.4	606.6	2906.6	PC	
34	33-023-00210	163N	101W	16	SE,SE	ND	Divide	Conoco Inc.	State 16-1	Wildcat	688.9	682.8	3505.2	COD	S,D
35	33-105-00853	158N	100W	2	SE,NW	ND	Williams	Depco Inc.	Smith 33-2	Wildcat	652.3	645.9	4074.3	OWB	S,D
36	33-105-00768	155N	100W	5	SW,SW	ND	Williams	Lamar Hunt Flb	Shaide 1	Wildcat	582.2	576.4	4334.6	COD	S,D
37	33-053-01220	148N	101W	10	NE,NW	ND	McKenzie	Hunt/Broschat	Larson 1	Wildcat	744.9	737.6	4590.0	COD	S,D
38	33-007-00590	142N	100W	23	NW,SW	ND	Billings	W.H.Hunt Trust	Anna Osadchuk B1	Tree Top	830.9	823.6	4401.3	PC	S,D
39	33-007-00054	139N	101W	10	SW,NE	ND	Billings	Amerada Pet.Co.	Fryburg Unit 8	Scoria	774.2	769.6	4191.0	PC	S
40	33-087-00011	136N	101W	23	NW,NE,SW	ND	Slope	H.L. Hunt	NPRR "A" 3	Wildcat	874.2	870.2	3532.0	OBR	S
41	33-011-00382	131N	100W	6	NE,NW	ND	Bowman	Placid Oil Co.	Cornell 6-2	Wildcat	897.6	891.2	3299.2	COD	S,D
42	2400203W200	2	3W2	24	13	SK		Shell Can.	South Oxbow		570.5		3002.6	PC	S,D
43	33-013-00869	162N	89W	8	SW,SW	ND	Burke	Monsanto/BHP	Melby 1	Wildcat	594.4	590.4	3331.5	COD	S,D
44	33-061-00282	156N	92W	1	NW,SW	ND	Mountrail	Gulf Oil	Juma 1-1-1D	Wildcat	690.7	684.9	4252.0	COD	S,D
45	33-025-00274	144N	92W	16	NW,SE	ND	Dunn	Getty/Texaco	Halliday 16-6	Wildcat	677.9	672.1	4130.0	COD	S,D
46	33-089-00246	138N	92W	21	NW,NE	ND	Stark	Gulf/Equitable	Leviathan 1-21-1B	Wildcat	723.0	716.3	3724.1	PC	S,D
47	33-041-00015	133N	93W	26	SE,SW	ND	Hettinger	Amoco Prod. Co.	Charles Rokusek 1	Wildcat	767.2	762.0	3287.0	PC	S,D
48	33-001-00006	130N	91W	7	SW,NE	ND	Adams	Energetics,Inc.	Soelberg 23-7	Wildcat	747.7	743.7	2921.2	PC	S,D
82	33-023-00280	164N	102W	33		ND	Divide		Angedal 33-4		682.1	676.1	3269.9	COD	S

CHAPTER 5

THEORY AND METHOD OF SEISMIC INTERPRETATION

This chapter addresses the fundamentals of the interpretation processes of the seismic method. This rather vast subject will be discussed at a depth required by regional scale, i.e., basin analysis studies.

5.1 Nature and characteristics of seismic reflections and resolution of seismic method

The most basic question of seismic interpretation: is what do seismic reflections represent geologically. Seismic reflection occurs when some of the energy in a wave coming from a seismic source is bounced back or reflected from an acoustic-impedance contrast. Acoustic impedance, as discussed in ***Section 4.2***, is the product of seismic velocity and formation density. Different lithologies have different seismic velocities and densities. Geological formations can therefore be characterized by representative acoustic impedance values. Acoustic impedance can vary significantly for the same rock type because of fluid content, porosity variations, fractures, etc. Nevertheless, seismic reflections emanate from surfaces separating rocks with different physical properties. The larger the difference in physical properties of these rocks, the larger the amplitude of the seismic reflections recorded from the reflecting surface. From this, it would be natural to expect that reflections are generated from lithological boundaries. Another, equally fundamental requirement is that the surface of sharp impedance contrast must be laterally continuous to be resolved by the seismic wave and the interpreter *(Cross and Lessenger, 1988)*.

Many times, however, lithological boundaries do not appear in a laterally continuous manner; consequently, no coherent reflection can be detected from them. Such considerations are tied up with the horizontal resolution of the seismic method.

The seismic analog of the Fresnel zone in optics can be used to determine the limit of **horizontal resolution** ***(Fig. 5.1.a)***. As a waveform reaches a reflecting interface, part of it will be reflected. As ***Fig. 5.1.a*** shows, the region, called the first Fresnel zone, is a 1/4 wavelength behind the wavefront, tangent to the reflector.

The major contribution to the reflected signal comes primarily (not completely) from this zone. Energy from the periphery of the first Fresnel zone will reach the detector at the source location a 1/2 wavelength later than the first reflected energy, allowing for two-way time. All the energy reflected from the first Fresnel zone will arrive within a third of a wavelength; therefore, will interfere constructively. The radius of the first Fresnel zone is

$$R_f \sim [(\lambda \cdot h_0)/2]^{1/2} = (v/2) \cdot (t/f)^{1/2} \qquad \text{(Eq. 5.1)}$$

where, h_0 is the depth of the reflector, t is the arrival time, v is the average velocity, λ is the dominant wavelength and f is the dominant frequency *(Sheriff and Geldart, 1982)*.

Obviously, for higher frequency, shorter wavelength, or decreasing depth, the Fresnel zone will be smaller, and consequently the lateral resolution will be better ***(Fig. 5.1.a)***. Accordingly, impedance contrasts over diffuse boundaries or surfaces shorter than the Fresnel zone generate either weak or no reflection *(Neidell, 1977)*. Coherent, continuous reflection, is therefore a result of a geological process affecting a larger area, a process involved changes in sedimentation patterns.

Changes in sedimentation patterns are manifested in bedding surfaces or unconformities, which are expressions of erosion and/or non-deposition, with

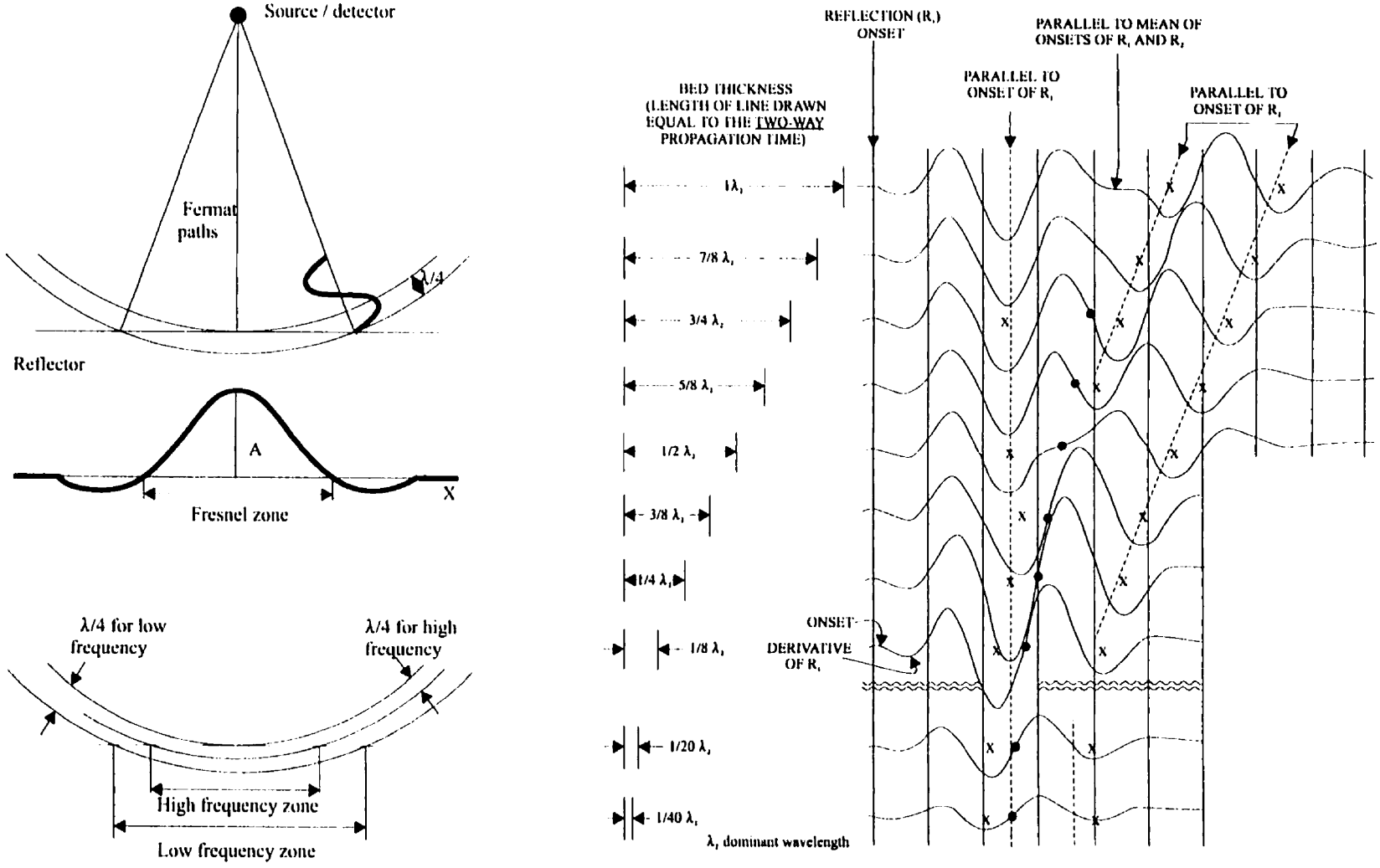

Fig. 5.1 Principles and constraints of lateral (a) and vertical (b) resolution of the seismic method ([a] Emery and Myers, 1996; [b] Widess, 1973).

chronostratigraphic significance. In many depositional settings, where there is little or no topographic relief (e.g., cratonic platform basins), the beds are essentially horizontal and continuous. In these cases sedimentary facies and lithological boundaries correspond with bedding surfaces; therefore, impedance contrasts from bedding surfaces coincide with lithological boundaries.

In depositional settings with topographic relief (shelf margin, reef margin, etc.) sedimentary facies and lithologies transgress bedding surfaces/unconformities (i.e. are "time transgressive") ***(Fig.5.2.a)***. In these circumstances, lithological boundaries are diffuse, and consequently do not exhibit a continuous reflection pattern. On the contrary, due to their lateral continuity, bedding surfaces/unconformities are reflecting surfaces ***(Fig. 5.2.b)***. Thus reflections are "time lines" *(Vail et al., 1977b)* and represent unconformities or isochronous surfaces *(Sheriff, 1980)*. Reflection amplitude, however, can vary along a continuous reflection due to the different acoustic impedance contrasts ***(Fig. 5.2.b)***.

Recently, some authors emphasized that, in special circumstances or in the case of improved seismic resolution with higher frequencies, lithological boundaries could produce coherent seismic reflections *(Badley, 1985; Tipper, 1993)*. This can occur also if a series of discontinuous lithologic units, thin in comparision to the seismic wavelength, create continuous reflections *(Thorne, 1992)*. Here, therefore the vertical resolution of the seismic method should be addressed.

Vertical resolution involves the ability to identify individual reflections from the top and bottom of a thin bed. The principle of vertical resolution is quite complex; however, generally, the resolution is about 1/8 to 1/4 of a wavelength ***(Fig. 5.1.b)*** *(Widess, 1973)*. "Resolution" should be differentiated from "detection", which is the recording of a composite reflection without considering that the composite wavelet can be resolved into two or more wavelets: in this way an event that is detectable is not necessarily resolvable *(Kallweit and Wood 1982)*. (E.g., the Bakken Formation in the

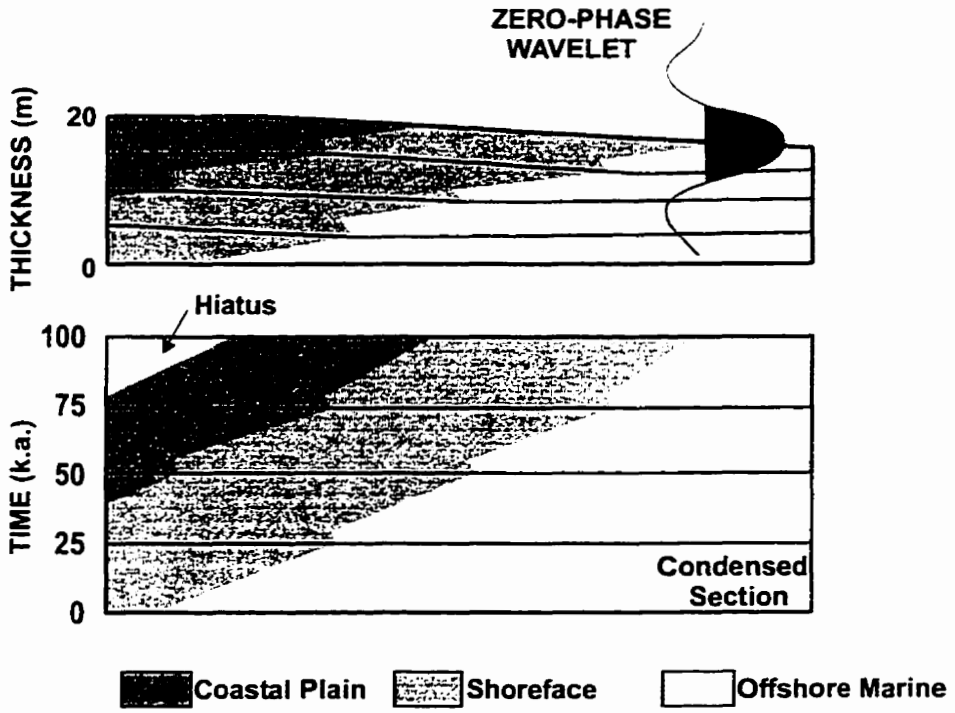

(a)

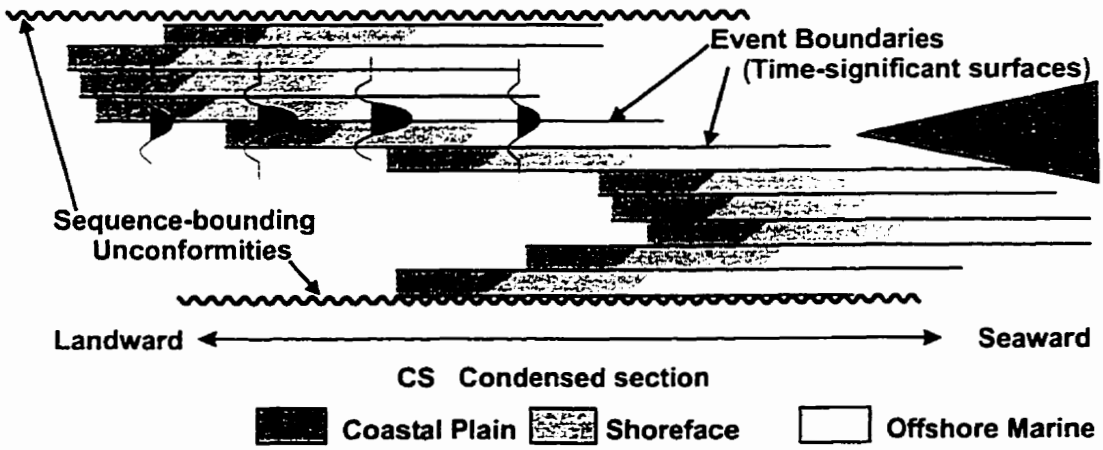

(b)

Fig. 5.2 Time-transgressive lithologic boundaries and temporal significance of seismic reflections (from Cross and Lessenger, 1988).

Williston Basin is easily detectable, but its upper and lower limits are not easily resolvable).

Migration can improve the horizontal resolution dramatically. Post-migration Fresnel diameter is more like $\lambda/4$ than $\lambda/2$ and applies only if the trace spacing is no more than $\lambda/2$ at the highest frequency of importance (Lindsey, 1989). Under ideal conditions after migration, horizontal and vertical resolution are comparable.

Considering the limits of resolution of the seismic method and the purpose of this study, it can be concluded that given the scale of interest (regional, basin scale), the limitation of the methods does not hamper the interpretation. The premise that reflections represent time lines (bedding surfaces/unconformities) holds true on this scale of interpretation. Seismic profiles therefore supply the temporal framework of deposition in a given area, which is the fundamental information of basin studies.

5.2 Seismic stratigraphy

The basic premise of seismic stratigraphy is that reflection relationships (e.g., reflection terminations) can be used to deduce chronology, whereas reflector configuration and attributes can be used to infer lithology and depositional settings (seismic facies analysis).

5.2.1 Reflection terminations

The first and most important step in seismic stratigraphic interpretation is to determine the temporal relationships between the reflections by recognizing reflection termination patterns.

A reflection termination against another reflection on seismic sections is indicated conventionally with an arrow ***(Fig. 5.3)***. A set of seismic stratigraphic terms has been widely adopted to describe reflector relationships *(Mitchum et al., 1977a;b)*. Two basic types of reflection termination can be differentiated: *lapout* and *truncation*.

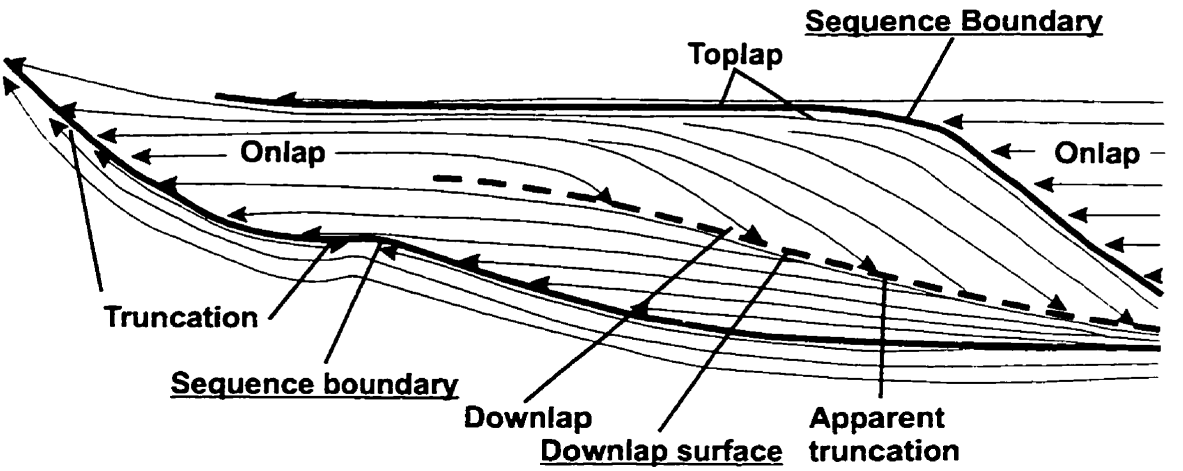

Fig. 5.3 Stratal termination patterns (Vail, 1991).

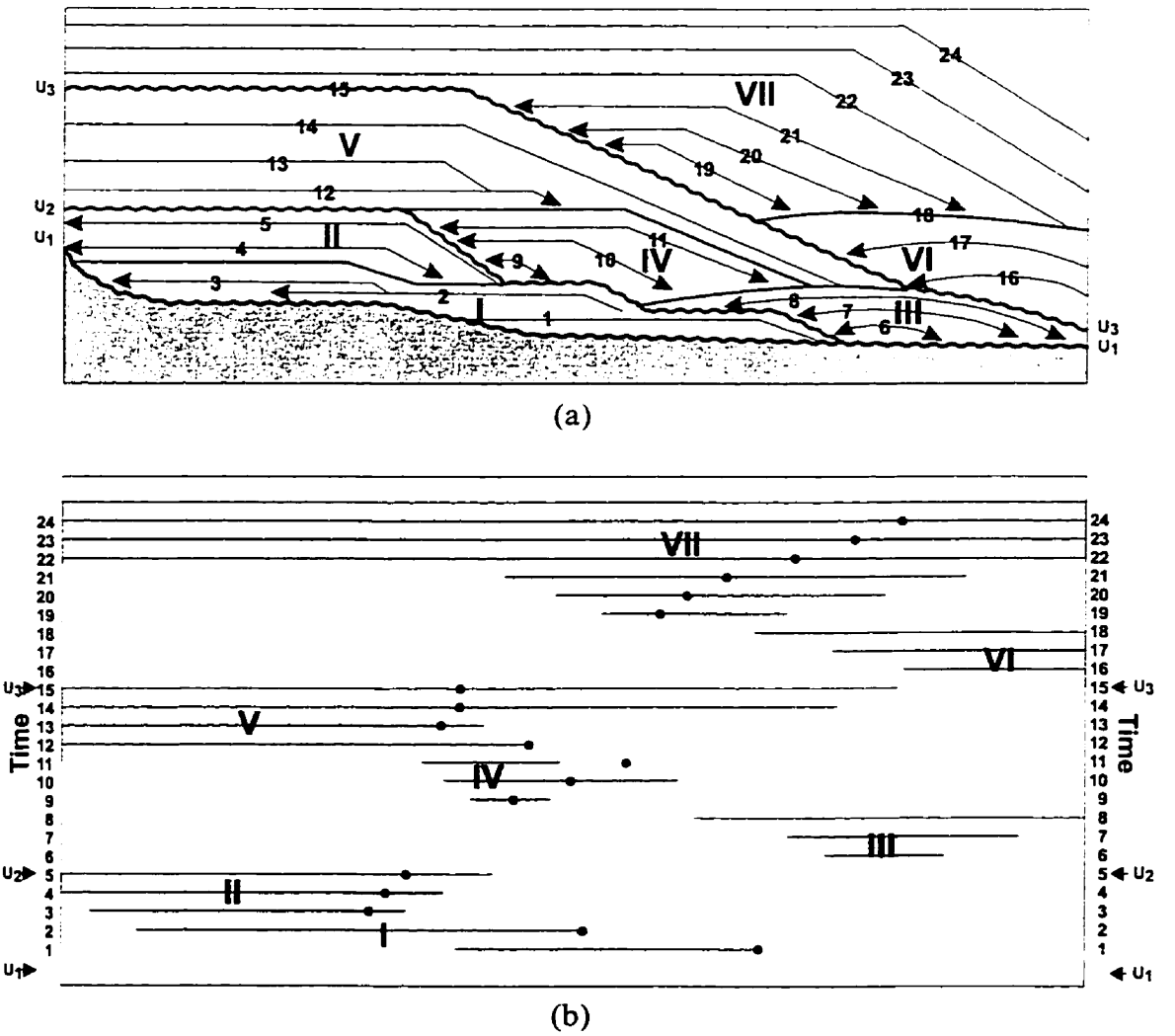

Fig. 5.4 (a) Identification of seismic stratigraphic surfaces and units; (b) deduced chronologic information (Emery and Myers, 1996)

Lapout is the lateral termination of a reflection. Based on their position within a seismic stratigraphic unit (i.e., "sequence", defined later), reflection lapouts can be baselap (lower boundary) and toplap (upper boundary) ***(Fig. 5.3)***. An initially subhorizontal reflection lapping out against a reflection with a greater inclination is called onlap, while an inclined reflection lapping out against a subhorizontal reflection is termed as downlap. Later structural complications (e.g., postdepositional tilting) may make it difficult to differentiate between these two types of baselaps *(Badley, 1985; Thorne, 1992)*.

Two types of onlap (marine, coastal) can be recognized according to the depositional environment they represent. Toplap configuration appears at the upper boundary of a seismic stratigraphic unit (sequence) ***(Fig.5.3)***. Generally, toplap is caused by non-deposition, and each reflection of the toplapping succession pinches out in a landward direction *(Hardage, 1987)*.

Truncation is a lateral reflection termination caused by erosion, which appears at the upper boundary of a seismic stratigraphic unit ***(Fig. 5.3)***. Sometimes truncation can resemble toplap due to limited vertical resolution *(Badley, 1985; Thorne, 1992)*. Limited resolution can exhibit apparent truncations. These can appear when the reflection terminations represent distal, seaward depositional limits (or thinning below seismic resolution). Apparent truncation also occurs when the inclined reflectors become horizontal and thin landward and exhibit as a single, apparent upper boundary ("pseudo-toplap") *(Stafleu and Schlager, 1993)*.

5.2.2 Seismic surfaces

Seismic reflection termination is due to the termination of the bedding plane/unconformity, or the thinning of the bedding to below the seismic resolution. A seismic surface therefore represents a facies change from sedimentation to non-sedimentation or erosion *(Emery and Myers, 1996)*. Seismic surfaces are identified by

connecting consecutive reflection terminations ***(Fig. 5.4.a)***. These seismic surfaces represent unconformities or fault planes.

5.2.3 Seismic packages and sequences

Seismic surfaces bound seismic packages (Roman numerals in ***Fig. 5.4***), which are the building blocks of seismic stratigraphy. Genetically related seismic packages represent a seismic sequence. The seismic sequence is the fundamental unit of seismic stratigraphy. Seismic sequences are bounded by seismic surfaces representing unconformities (U_1, U_2, U_3 in ***Fig. 5.4***) or bedding planes.

5.2.4 Definition of temporal framework

Seismic sequences, due to their chronological significance, can be transferred into chronostratigraphic charts to deduct spatial and temporal information required to analyze the evolution of a given area ***(Fig. 5.4.b)***. Other types of information can be added to these charts, e.g., well data. Biostratigraphic information can help to put a more exact temporal constraint on sequence boundaries.

5.2.5 Seismic facies analysis

Analysis of external and internal reflection characteristics (seismic facies analysis) of seismic packages can help to interpret geological depositional environments and facies ***(Fig. 5.5)***. By combining the analysis of stratal relationships with the attributes of individual reflection, it is often possible to build up a detailed picture of the subsurface geology. The following several seismic-reflection parameters can be used to identify depositional environments *(Mitchum et al., 1977b)*:

Seismic reflection configuration ***(Fig. 5.5.a)*** can help to identify geologic bedding, depositional processes, erosional surfaces, paleotopography, and sedimentary environment.

Seismic reflection continuity shows bedding continuity and depositional processes.

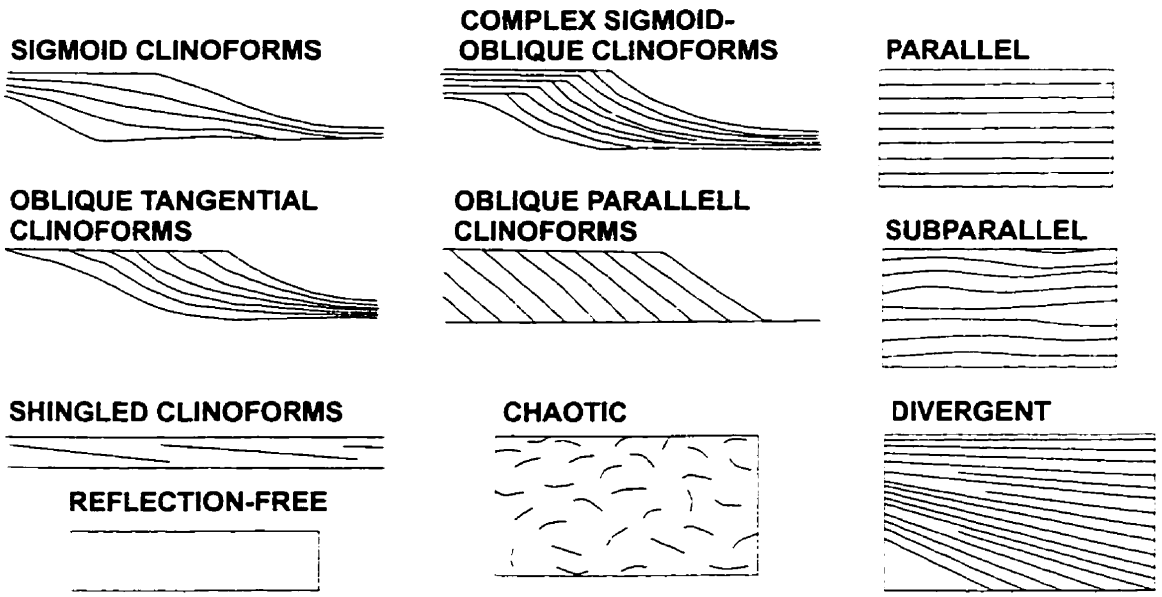

(a)

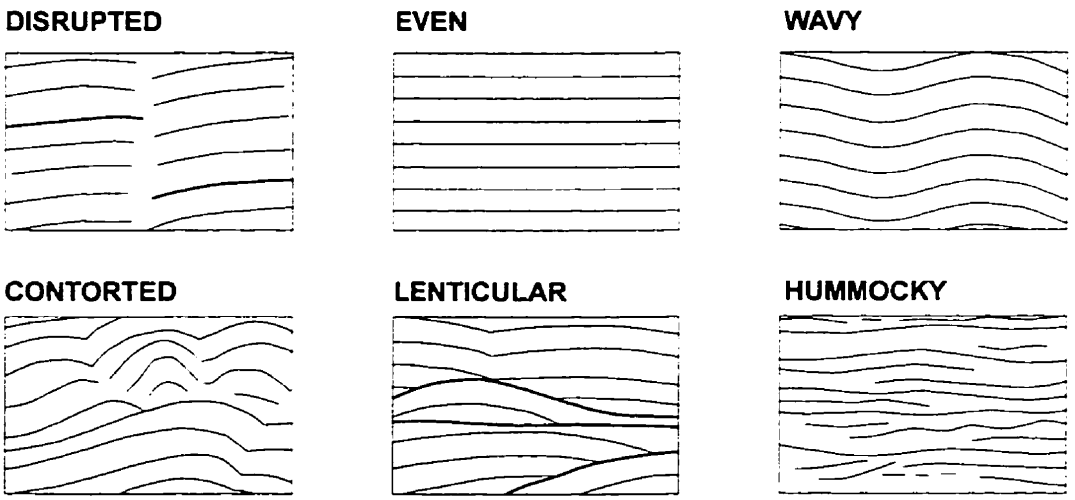

(b)

Fig. 5.5 Seismic facies patterns. (a) primary patterns; (b) modifing patterns (modified from Mitchum et al., 1977a; Sangree and Widimer, 1977).

Seismic reflection amplitude reveals velocity–density contrast, fluid content, and bed spacing.

Seismic reflection frequency shows bed thickness and fluid content.

Interval velocity is a function of lithology, porosity and fluid content.

External form and spatial association of seismic facies units shows the gross depositional environment, sediment source and overall geological setting.

5.3 Sequence stratigraphy

Sequence stratigraphy is one of the most dynamic fields in the geosciences nowadays. Sequence stratigraphy is the study of rock relationships within a chronostratigraphic framework of repetitive, genetically related strata bounded by surfaces of erosion or non-deposition or their correlative conformities *(Van Wagoner et al., 1988)*.

The fundamental basics of the sequence stratigraphic approach are not new. Concepts of geochronology, global cycles, "law of superposition", etc., have a considerable past; although, probably the most important contribution was given by Sloss *(1963)* with the introduction of cratonic sequences ***(Fig. 5.6)***. **Stratigraphic sequence** was defined as a rock-stratigraphic unit, traceable over major areas of a continent and bounded by unconformities of interregional scope. The full-fledged application of sequence stratigraphy can be dated from 1977, from the publication of the AAPG Memoir 26 *(Payton, 1977)*. This was possible because of the advancement of seismic methods from the 50s, which resulted in vast amounts of seismic information. The quality and quantity of the new seismic datasets led to the development of modern sequence stratigraphy.

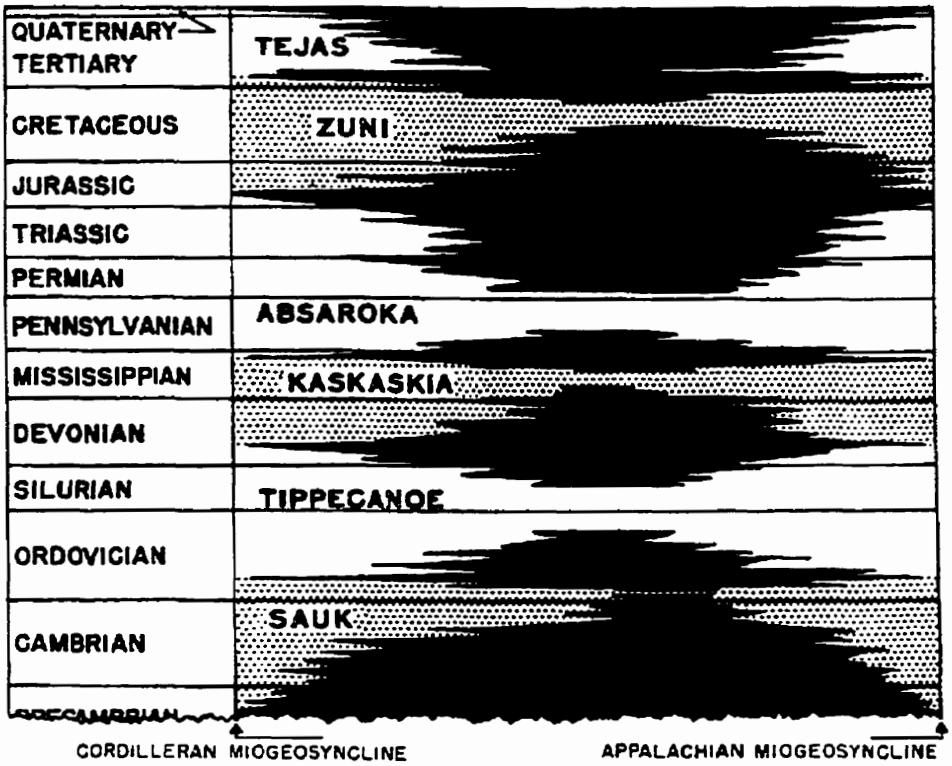

Fig. 5.6 North American cratonic sequences (Sloss, 1963).

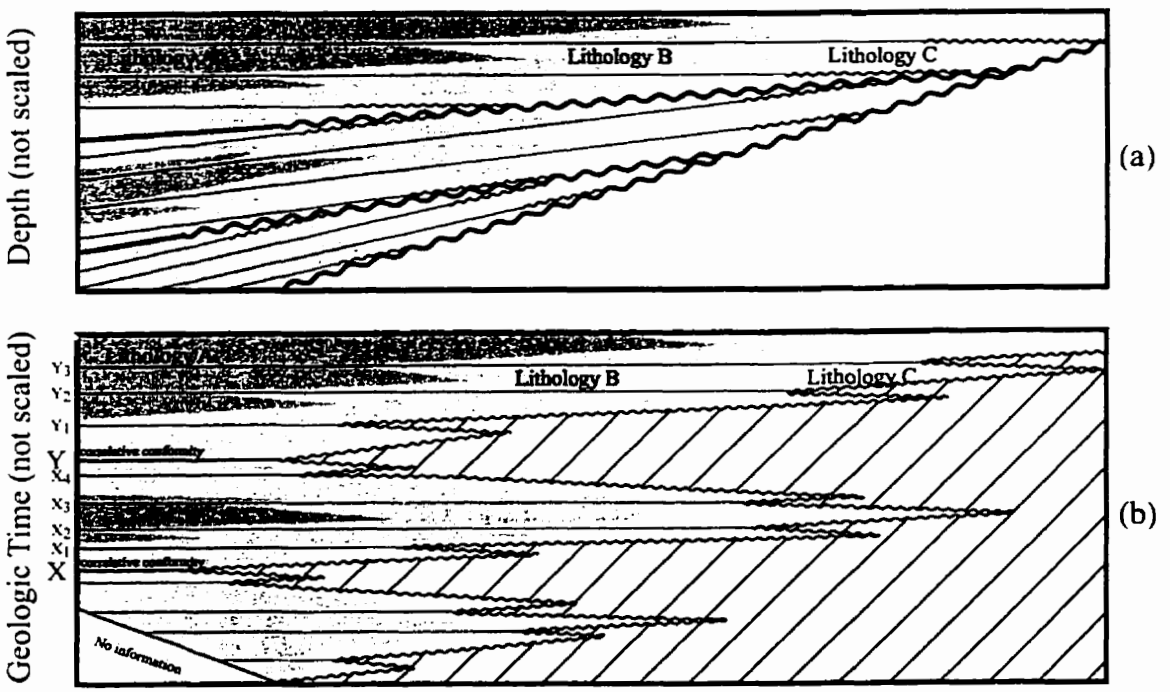

Fig. 5.7 Chronostratigraphic significance of unconformities in sequence stratigraphy. (a) Stratigraphic cross section. (b) Chronostratigraphic chart.

It is not surprising then, that sequence stratigraphy borrows most of its basic definitions from seismic stratigraphy. The term "sequence" was slightly redefined, with some temporal and spatial connotations being attached to its meaning.

The **sequence** is the fundamental unit of sequence stratigraphy, being bounded by unconformities and their correlative conformities. Due to their temporal range, the Sloss-type sequences were considered "supersequences".

Other stratigraphic approaches, similar to those of sequence stratigraphy, also appeared in the last decades. "Allostratigraphy" defines its units with bounding discontinuities, similarly to sequence stratigraphy *(North American Commission on Stratigraphic Nomenclature, 1983)*. In an alternative sequence model, the basic unit is the "genetic stratigraphic sequence", bounded not by unconformities, but by surfaces of maximum flooding *(Galloway, 1989)*. The sequence stratigraphic approach is strongly related to unconformities and to the cyclic nature of sedimentary records and further basics can be understood within this context.

5.3.1 Unconformities and their correlative conformities

It was stated above that stratigraphic sequences are bounded by unconformities and their correlative conformities.

An **unconformity** is a geological surface separating younger from older strata, along which there is evidence of subaerial erosional truncation (or correlative submarine erosion), with a significant hiatus indicated *(Van Wagoner et al., 1988)*.

A **conformity** also separates younger from older strata, without a significant hiatus. The importance of hiatus depends on the scale of interest (see later).

Unconformities and their correlative conformities therefore, have temporal significance ***(Fig. 5.7)***. There is a notable but rare exception to this basic premise of

sequence stratigraphy. Christie-Blick et al. *(1990)* showed that strong, along-shore marine currents can produce a *diachronous unconformity* ***(Fig. 5.8)***. Unconformities occur over many geographical and temporal scales, from local to continent-wide and from a few hours to millions of years, reflecting the cyclic nature of the sedimentary record. Due to its applicability in a wide temporal and spatial range, the sequence stratigraphic approach is scale-independent. Progressing from the descriptive stage to the interpretative level, the governing causes of different scales of unconformities should be addressed.

5.3.2 Cyclic nature of the sedimentary record

Recognition of the cyclic nature of the sedimentary record has a considerable past. The fundamental question is the governing factors of the different scales of depositional cycles. The dominant part of sedimentation takes part in marine environments; consequently, the controlling factors are of marine sedimentation have primary importance. This problem leads to the concept of **"accommodation"**, which is the space available for sedimentation *(Jervey, 1988)*.

Obviously, changes in the accommodation space/potential reflect changes in a governing factor or composite effects of governing factors. Ultimately the relative change of sea level produces accommodation space for sedimentation ***(Fig. 5.9)***.

Relative change of sea level is the result of the interaction of tectonism and eustacy.

Eustacy refers only to the position of the sea surface with reference to a fixed datum, such as the center of the Earth, and is therefore independent of local factors.

Relative sea level incorporates local subsidence and/or uplift by referring to the position of the sea surface with respect to the position of a datum (e.g., basement).

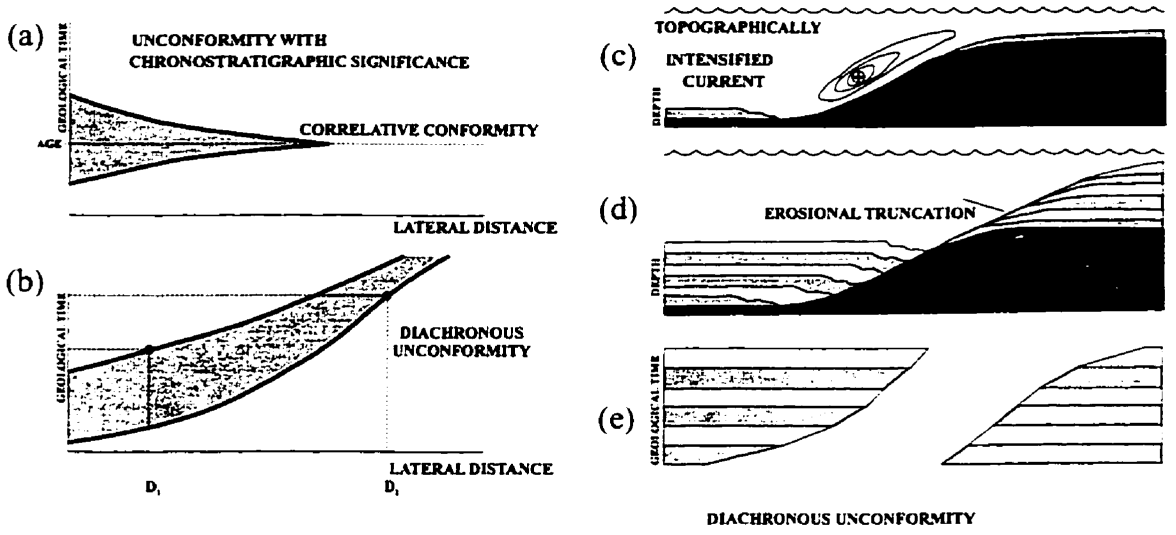

Fig. 5.8 Unconformities in chronostratigraphic framework (Christie-Blick et al., 1990). (a) Unconformity with chronostratigraphic significance; (b) Unconformity with a diachronous unconformity; (c)-(e) Development of a diachronous unconformity.

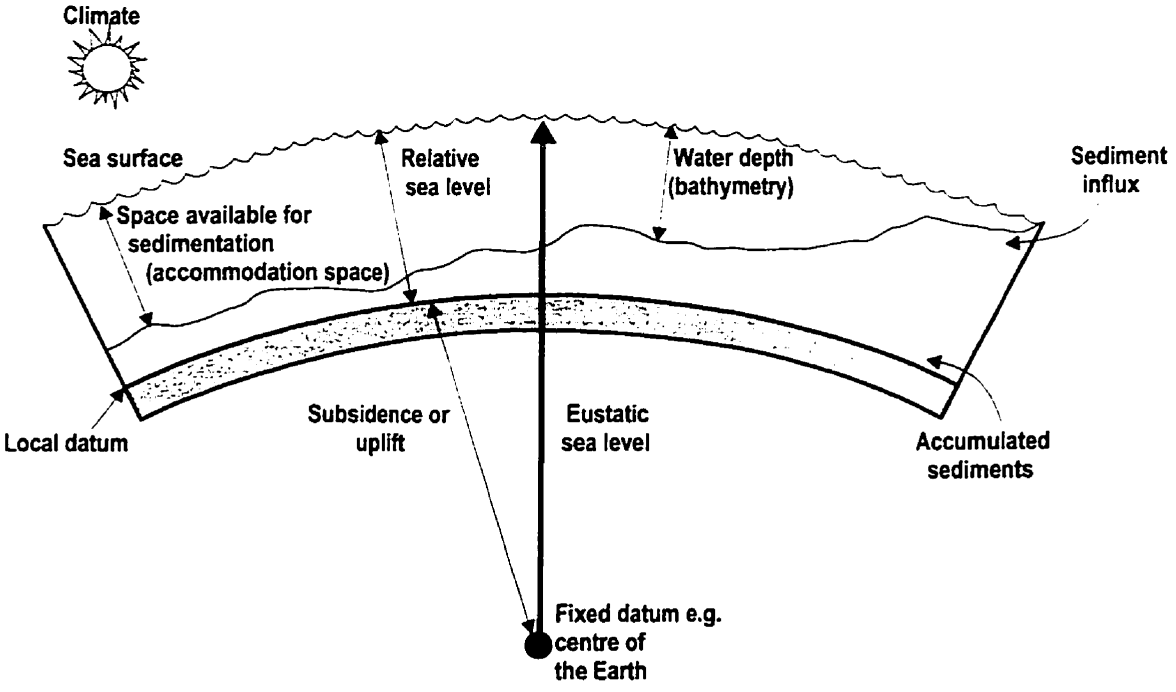

Fig. 5.9 Simplified model of the controlling factors of sedimentary cycles (based on Vail and Cramez, 1990; Emery and Myers, 1996).

Stratigraphic features or signatures in a given rock, are the results of combined tectonic, eustatic, sedimentary and climatic factors. The two most important criteria to separate these factors are the spatial and temporal distribution of their effects on the accommodation space. Controlling factors have hierarchy based on their temporal distribution:

Order	Time (M.a.)
1st	>50
2nd	5–50
3rd	0.5–5
4th	0.1–0.5
5th	0.01–0.1
6th	<0.01

First-order sedimentary cycles and their stratigraphic expressions, first-order sequences (megasequences), are the results of global tectonic events (supercontinent cycles) and accompanying eustatic sea level changes (tectonoeustacy). During the Phanerozoic times two megasequences can be identified ***(Fig. 5.10)***. These large changes were recognized independently and much before the advent of sequence stratigraphy. Ultimately, these large-scale changes effect the sediment accommodation potential on a global scale.

Second-order tectonic events, such as major orogenies with their non-periodic nature, act on a global or continental scale. The second-order tectonoeustatic events produce second order changes in the accommodation potential on a continental scale, expressed in second-order sequences (supersequences) ***(Fig. 5.10)***. The Sloss-type North American cratonic sequences ***(Fig. 5.6)*** are in fact second-order sequences, and can be related to orogenic events.

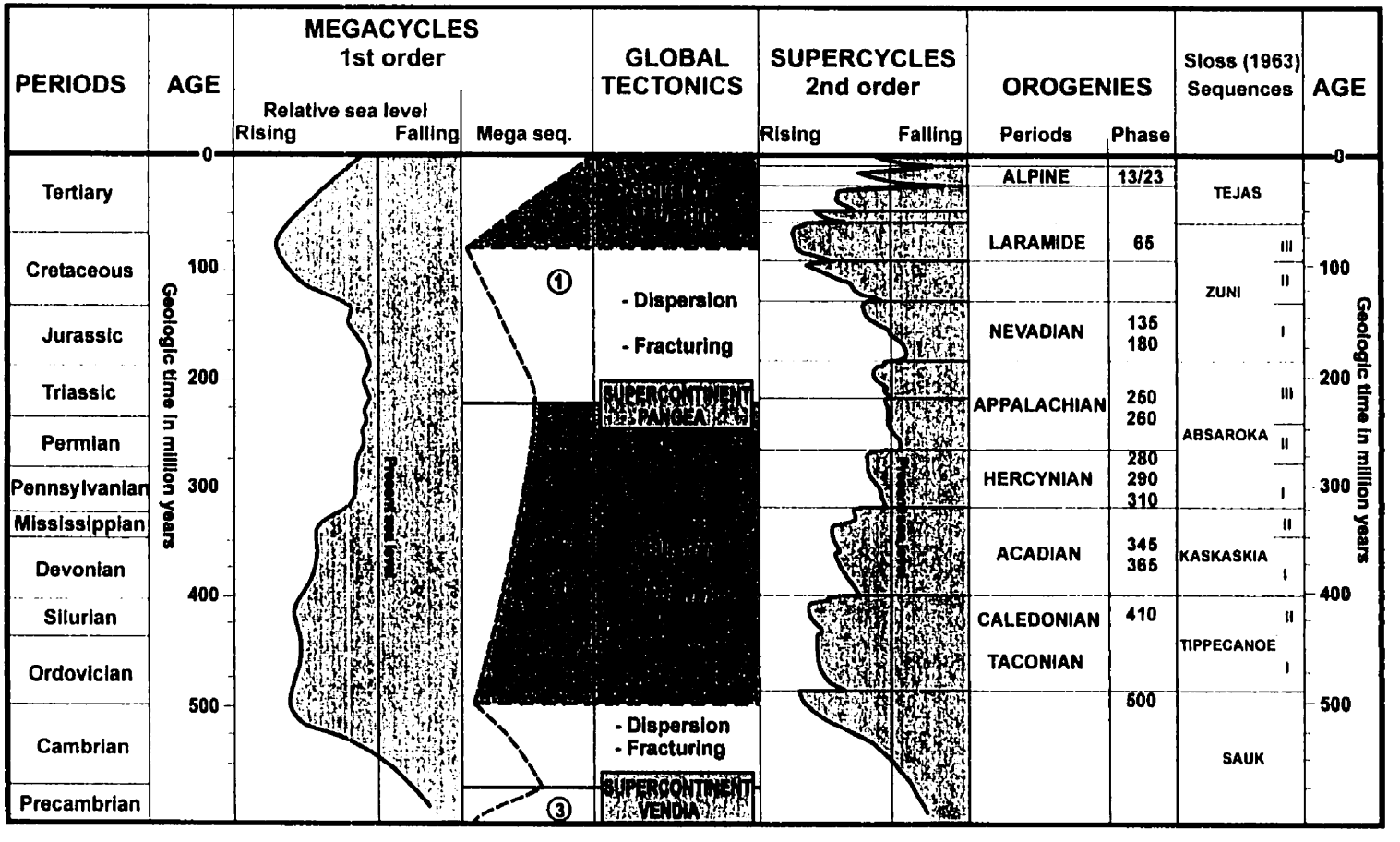

Fig. 5.10 First and second order sequences and relative sea-level changes during the Phanerozoic (modified from Vail and Cramez, 1990).

Sequence as a term, defined previously, has **third-order** spatial and temporal connotations. **Higher-order sequences** (parasequence sets, parasequences, bedsets, beds, lamina sets and laminae) also refer to temporal and spatial distribution. The scale of interest defines the appropriate exploration tool to investigate these sequence stratigraphic units ***(Fig. 5.11)***. The conventional exploration seismic method can resolve fourth-order sequences (parasequence sets).

There is an ongoing debate over the governing factors of the third and fourth order sequences. The classical school attributes them explicitly to changes in eustatic sea level due to the melting and freezing of polar ice *(glacioeustacy)*. In this scenario, tectonic effects are not governing, but only modifying factors. Based on this premise a worldwide sea level curve was compiled, indicating third- and fourth-order global sea-level cycles and globally correlatable unconformities *(Vail et al., 1977; Haq et al., 1988a)*. Although this sea-level curve is widely used in the industry, there are serious theoretical and empirical reservations about this theory.

Burton et al. *(1987)* showed the impossibility of deducing an absolute sea level curve (eustatic) from the geologic record. They pointed out that it is possible to obtain only the sum of the tectonic and sea level variations. Eustatic curves assume some simplistic behavior of tectonism and sediment accumulation.

Mathematical modeling showed that intraplate stress changes, without eustatic sea level change, acting on a third order temporal level can create considerable accommodation space *(Cloetingh, 1986; 1988)*. Interestingly enough, some cycles on the curve are shorter than the temporal resolution of existing biostratigraphic tools.

Miall *(1992; 1997)* went even further, pointing out additional inconsistencies of the eustatic sea level curve, and concluding that the sea level curve is misleading, too flawed to be fixed and should be discarded altogether.

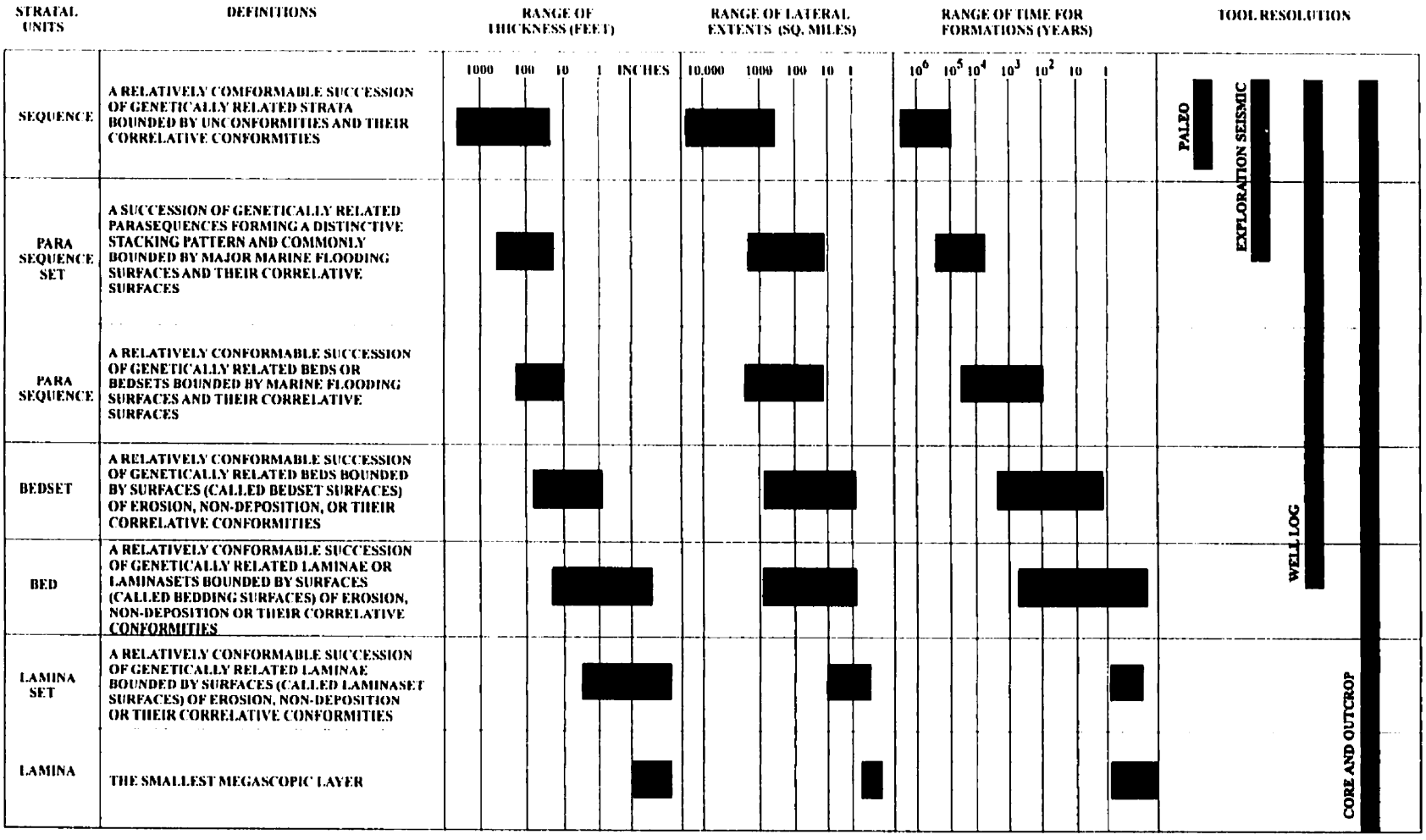

Fig. 5.11 Stratal units in hierarchy; definitions and characteristics (Van Wagoner et al., 1990).

The eustatic curve, practically speaking an averaged curve, was produced primarily from data of the Atlantic, passive margin areas. Probably it can be used, with some caution, in those areas; however, in other tectonic environments and geological times, third- and fourth-order sea-level curves can lead to erroneous interpretations. Nevertheless, the principles of sequence stratigraphy are independent of the questionable theory behind the third and fourth order sea level curves.

5.3.3 Sequence architecture

The practical implementation of the sequence stratigraphic interpretation is based on the recognition of changes in the accommodation potential of the given area. Two distinct types of sequences can be defined as a product of the changes of the relative sea level.

Type-1 and **Type-2 sequences** are defined by the sequence boundary below ***(Fig. 5.12)***. Thus, a type-1 sequence ***(Fig. 5.12.a and b)*** is bounded below by a type-1 sequence boundary, and type-2 sequence ***(Fig. 5.12.c)*** is bounded below by a type-2 sequence boundary. Based on the physiography of their depositional environment, type-1 sequences are somewhat different in areas with shelf break and with ramp margin.

The nature of sequence boundaries depends on the magnitude of the relative sea level drop at the **depositional shoreline break**. This is the position on the shelf, landward of which the depositional surface is at or near the base level (usually sea level), and seaward of which the deposition is below sea level *(Van Wagoner et al., 1988)*. This point is different from the shelf break, which is a physiographic province in the basin defined by a change in dip from shelf to slope *(Van Wagoner et al., 1988)*.

Based on the position of the relative sea level during one depositional cycle, the sequence can be subdivided into system tracts, which are bounded by secondary surfaces. These system tracts are: the *lowstand system tract*, the *transgressive system tract* and the *highstand system tract*. The lowstand system tract is replaced by the *shelf*

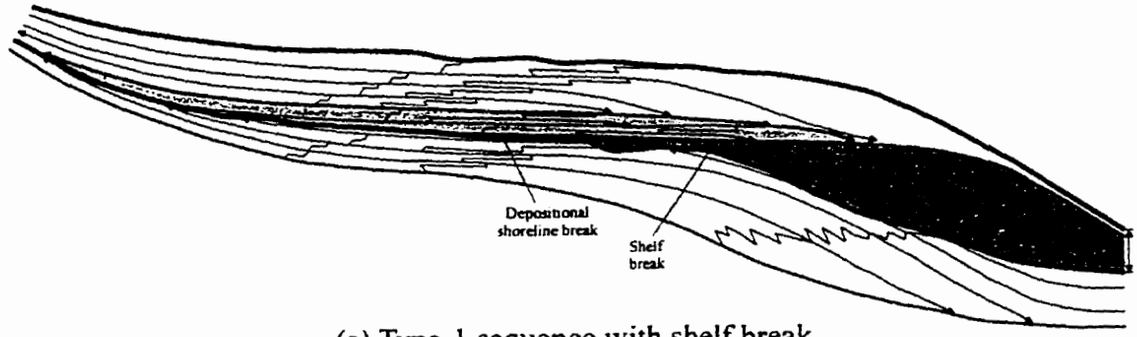

(a) Type-1 sequence with shelf break

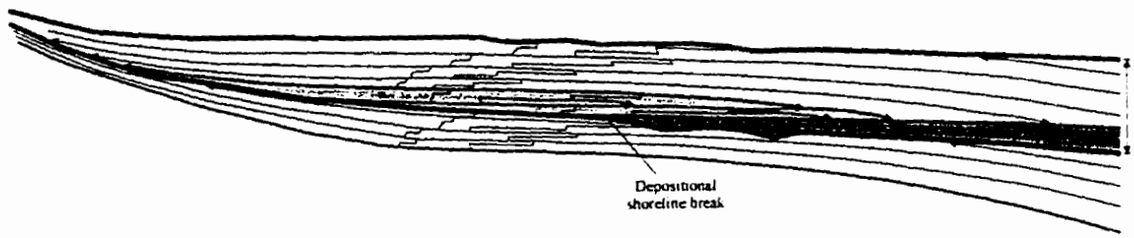

(b) Type-1 sequence with ramp margin

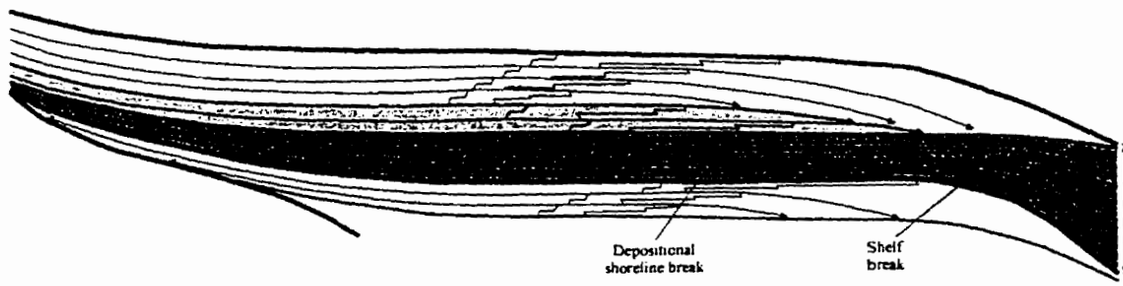

(c) Type-2 sequence

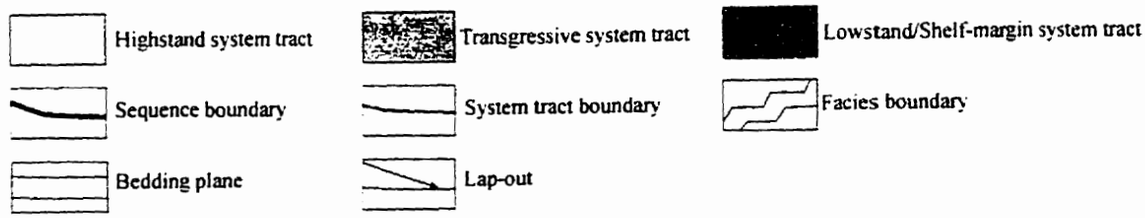

Fig. 5.12 Sequence types (adapted from Van Wagoner et al., 1988).

margin system tract in Type-2 sequences. Each system tract can be recognized by its internal structure. This topic will not be discussed because it is beyond the scope of this thesis.

Although sequence stratigraphy was introduced in siliciclastic environments, the physical basics of it can be readily applied to carbonate environments. Obviously, due to the fundamentally different nature of carbonate sedimentation, the recognition and interpretation of the physical surfaces in this environment require special considerations.

Ultimately, the accommodation space determines the sequence evolution. While in the siliciclastic environment accommodation space is created primarily by the interaction of relative sea level and sediment supply; in the carbonate environment it is the result of relative sea level change and carbonate growth *(Schlager, 1992)*. The carbonate growth obviously depends on other factors. The differences can be enhanced by physiographic dissimilarities (e.g., reefs, rimmed platforms). The timing of maximum sedimentation can deviate from that in siliciclastic environments *(Schlager, 1992)*.

5.3.4 Sequence stratigraphy in intracratonic areas

Sequence stratigraphic analysis in cratonic/platform areas, on a regional scale, requires special considerations. In the Williston Basin area the Sauk–Absaroka sedimentation is primarily carbonatic; while in the Zuni–Tejas interval, when the basin is part of a foreland basin, the siliciclastic deposition is prevalent ***(Chapter 2)***.

The scale of tectonic activity, rate of sedimentation and erosion are significantly different in platform areas than in other sedimentary environments. Sloss *(1996)* emphasized that the area and environment where the sequence stratigraphic method was developed (clastic passive margin) are markedly different from the cratonic interior/platform areas (e.g., Paleozoic Williston Basin).

Due to the physiography of these areas, only a few clinoforms and shelf breaks can be found. In sequence stratigraphic framework, Sloss *(1996)* considered the intracratonic platform basin areas as "basins with ramp margins". On a larger scale, however, the whole area can be considered as rimmed shelf region ***(Fig. 5.13)***. Few clinoforms can be found at flanks of wave-resistant structures (reefs and mounds) ***(Fig. 5.14)***.

In platform areas, like in the Paleozoic Williston Basin, covered by shallow water, a relatively minor sea level drop can expose sediments over hundreds of kilometers. A consequence of this is that lowstand system tracts can not be found in platform areas, or if they can, only in very limited thickness ***(Fig. 5.13)***. The type of sequence can not be identified based on cratonic strata; however, in these areas it does not have much relevance. Most of the existing records are part of transgressive or highstand system tracts. In cratonic areas third to fifth order depositional cycles can be traced for hundreds of kilometers *(Sloss, 1996)*. Fine details of the sequence stratigraphic jargon have limited applicability in these areas, since facies changes appear in the range of hundreds of kilometers. To overcome this problem, the application of regional seismic profiles is extremely useful.

Seismic/sequence stratigraphic analysis in platform areas (Sauk–Absaroka interval in the Williston Basin area) is fairly simple, since the sensitivity of the sedimentary record for the sea level changes expressed in unconformities most of the time correspond to lithological changes. This means that sequence boundaries (unconformities) are commonly identical with lithostratigraphic boundaries.

During the Zuni–Tejas times, the Williston Basin area was part of a foreland basin. A vast amount of siliciclastic sediment was eroded from the area to the west ***(Chapter 2)***. The classical siliciclastic sequence stratigraphy is the prime tool in the interpretation of this segment of the sedimentary record, since the unconformities and

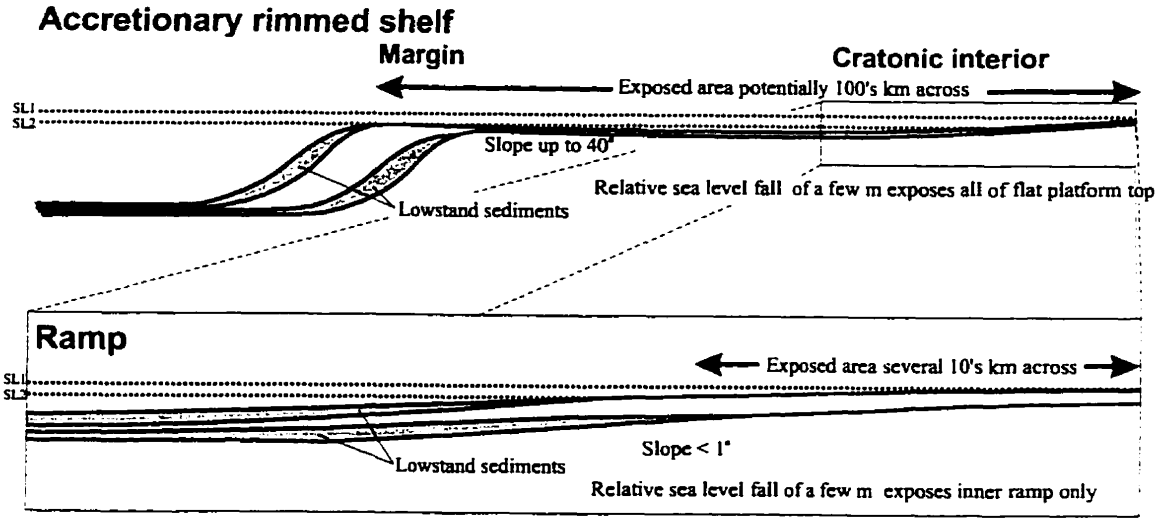

Fig. 5.13 Effects of minor changes of relative sea level on rimmed shelf and on ramp (modified from Burchette and Wright, 1992).

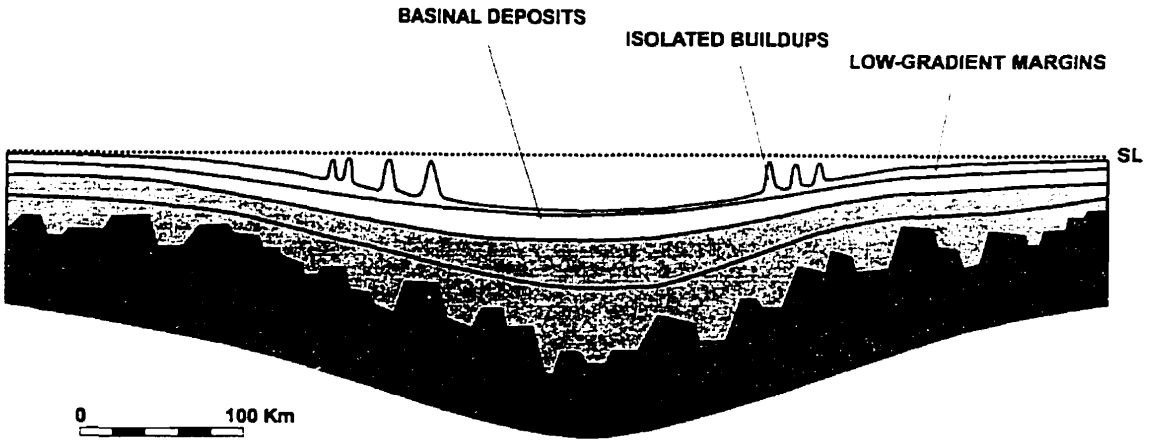

Fig. 5.14 Locations of carbonate ramps in cratonic basins (after Burchette and Wright, 1992).

lithostratigraphic boundaries are generally not identical. Numerous clinoforms can help the identification of changes in the accommodation potential in the area.

5.4 Special considerations in regional seismic profiling

Regional profiling, such as regional seismic sections, is fundamental to recognizing large scale lapouts and erosional surfaces.

On a regional scale, unconformities represented by seismic reflections on a seismic profile have chronostratigraphic significance. Diachronous unconformity ***(Fig. 5.8.b)***, related to significant along-shore current, postulated by Christie-Blick et al. *(1990)* is expected neither in the Paleozoic, nor during the later periods in the Williston Basin's history. Leckie and Krystinik *(1989)* found that the along-shore current activity was minor compared to the orthogonal current activity in the Cretaceous Western Interior Seaway, part of which was occupied by the Williston Basin area.

Regional seismic studies, due to the decreased lateral resolution, resolve only third order sequences. It does not hamper the interpretation, since the scale of interest does not extend below this level.

A regional seismic profile usually uses extreme vertical exaggeration to enhance the subtle structures. Special attention should be paid when interpreting structures on scale exaggerated seismic profiles *(Stone, 1991)*.

CHAPTER 6

INTERPRETATION OF THE REGIONAL SEISMIC LINES

In this chapter all the currently reprocessed regional seismic lines will be interpreted, using the seismic stratigraphic method. Due to the considerable extent of the lines, interpretation and description of seismic stratigraphic features will be conducted in shorter (100-250 km) intervals.

The longest, WE II line will be discussed in four segments; while the rest of the lines (WE III, NS I, NS II and CA I) will be broken into two segments for interpretation. The scale of each individual segment of the regional seismic lines used for detailed interpretation was kept the same. Nevertheless, since the purpose of the thesis is a regional scale synthesis, all the compiled regional seismic profiles will be displayed at the beginning of each section. Except for the long WE II line, the scales of all five regional lines are the same for easier comparison and correlation. Due to the fundamentally different nature of the Zuni sedimentation in the Williston Basin area, the interpretation of this part of the geological record is more apparent in the datumed versions of the regional profiles ***(Figs. A.1-6)***.

As noted earlier, the Greenhorn Shale (Second White Speckled Shale in Canada) was chosen to be the datum due to its excellent seismic characteristics throughout the study area. The datum-flattened versions of the regional sections, together with Zhu's *(1992)* regional section (WE I), are displayed in the Appendix ***(Figs. A.1-6)***.

6.1 WE II line

The longest regional seismic line, WE II, exhibits two overlapping megatectonic units along the 900+ km of its length ***(Fig. 6.1)***. These two units are the **"Rocky Mountains Foreland"** in the west and the **"Williston Basin"** in the east. The important overlapping area of the two units is unfortunately not covered fully by seismic data here. This area lies in the region of the Bowdoin Dome.

The western, Rocky Mountains Foreland area, on a large scale, displays a complex pattern. The westernmost part is the ***"Foothills–Sweetgrass Arch"*** area. In this region the general characteristics of the strata are changing from an apparently westerly dip to an apparently easterly dip. The uplifted and deeply eroded ***Sweetgrass Arch*** dominates this region. East of this area lie the ***Bearpaw Mountains***. The general apparent dip is still easterly; however, to a smaller degree. The structures of this interval are less dramatic, although the major characteristics of the Bearpaw Mountains could not be imaged in great detail because of the irregular basaltic layers at the surface.

The **Williston Basin** side of this regional profile displays a "bowl"-shaped form; however, the basin is tilted slightly to the west in this section. This part of the section is fairly symmetric with a generally easterly dip in the ***Western part*** and a westerly dip in the ***Eastern part***. Smaller-scale folds can be observed in the Williston Basin part of the section. The largest-amplitude folds appear to be in the central part, while away from the basin's center the amplitudes of the folds decrease.

6.1.1 Foothills–Sweetgrass Arch area

This area is dominated by the antiformal feature of the Sweetgrass Arch ***(Figs. 6.2.a, b)***.

The lower seismic sequence boundary of the *Sauk Sequence* (top of the Precambrian basement), can be identified only with limited certainty. No clear reflection of this surface is present; however, based on reflection characteristics some assumptions

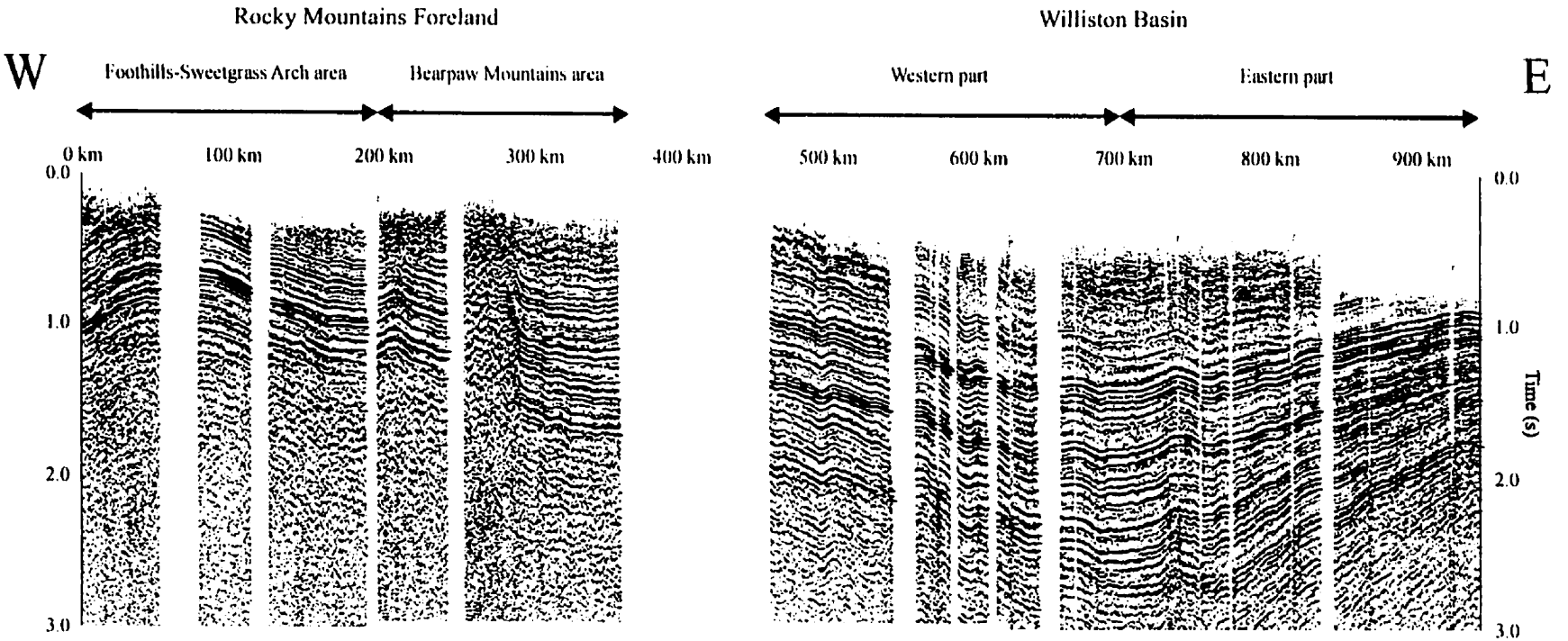

Fig. 6.1 WE II line.

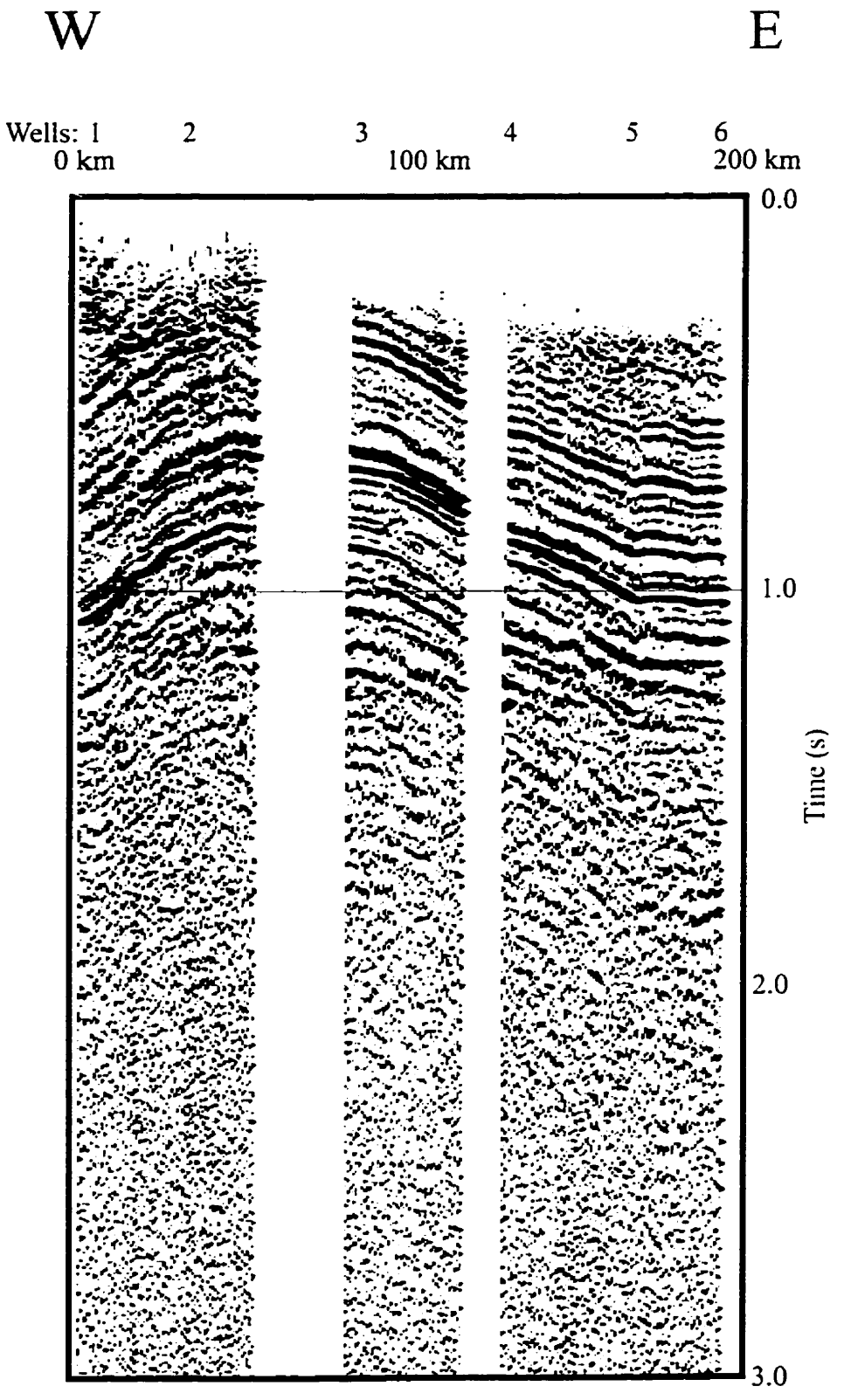

Fig. 6.2.a Line WE II, Foothills - Sweetgrass Arch area, uninterpreted section.

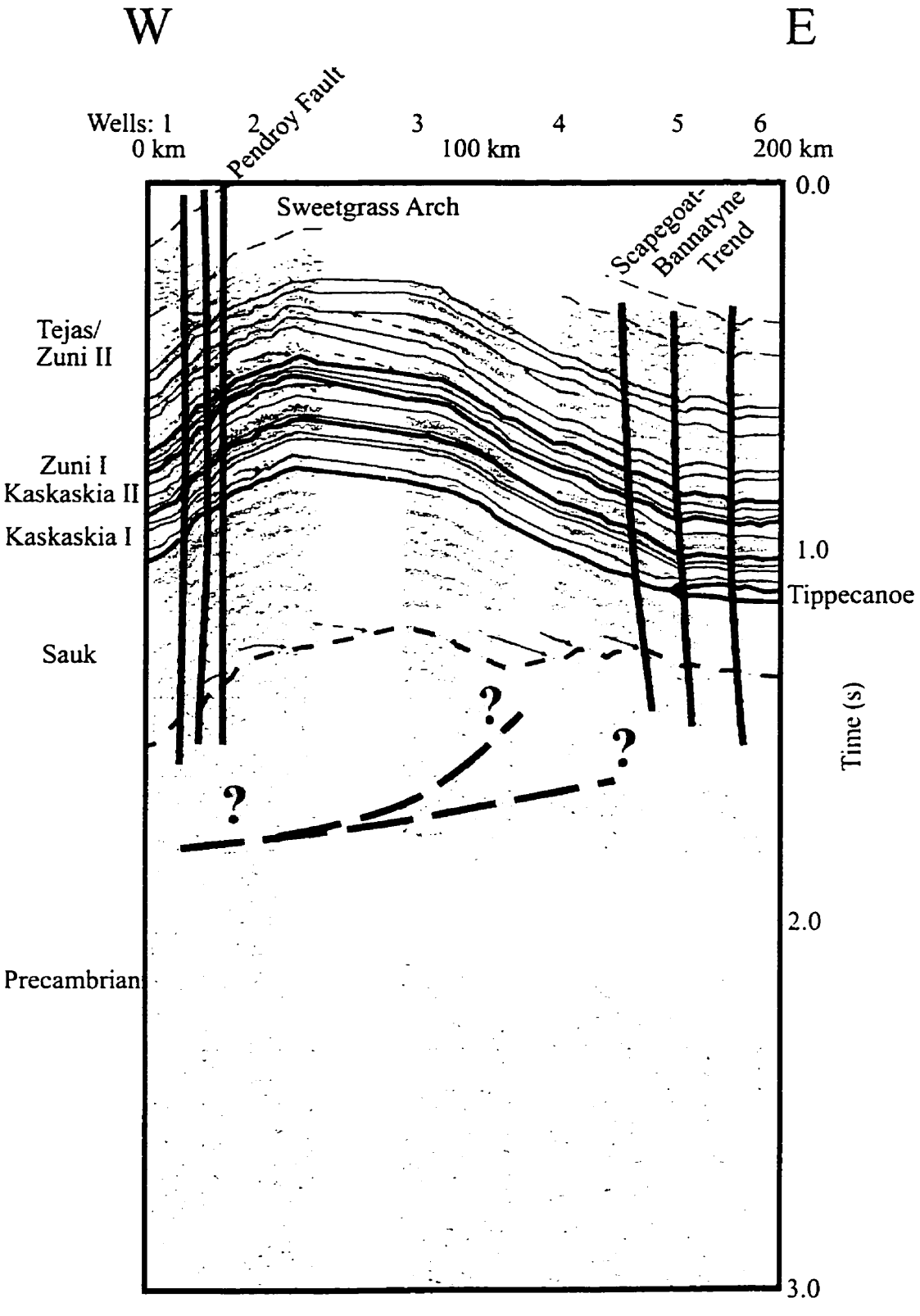

Fig. 6.2.b Line WE II, Foothills - Sweetgrass Arch area, interpretation

can be made. As expected from its regional geology, the sequence is fairly thick in the west and thins gradually to the east. The subparallel, highe- amplitude reflections of this sequence can be differentiated from the rather chaotic basement reflections. The basement can ultimately be defined by the progressively onlapping reflection terminations of the lowermost Sauk reflections. This part of the record reflects a transgressive series advancing toward the east, in accordance with the geological history of the area. Unfortunately, the wells obtained from this area did not penetrate the full Sauk Sequence and the wells from the neighboring areas in general also fail to do so, making it difficult to achieve a subdivision of the sequence.

The *Tippecanoe Sequence* is present only in the easternmost extremities of this area, with ~20 ms thickness which represents ~10-15 m here. Due to its limited thickness, the internal structure of the sequence can not be identified. The sequence itself onlaps against the upper boundary of the Sauk Sequence exhibiting a westerly advancing transgressive series.

In the following *Kaskaskia I Sequence*, four continuous reflections can be differentiated. These reflections are subparallel and reflection terminations can be observed only in a few places. The lowermost reflection represents the top of the Souris River Formation of the Manitoba Group. The next two reflections indicate the tops of the Duperow and Birdbear (Nisku) formations of the Saskatchewan–Jefferson Group. Some onlapping reflection terminations can be identified against the reflection representing the top of the Souris River Formation. The upper boundary of the Kaskaskia I Sequence is the top of the Three Forks Formation, which appears as a strong negative reflection on the seismic profile. An erosional surface can be suspected based on some indication of a truncation type upper sequence boundary.

The lowermost part of the *Kaskaskia II Sequence* contains the Bakken Formation. The top of this formation is still within the strong negative reflection and its downlap termination is assumed to be where the reflection becomes narrower between

Well 3 and Well 4. Two more major reflections can be identified within the Kaskaskia II Sequence in this area. The lower, negative one is somewhat discontinuous and delineates approximately the top of the Lodgepole Formation. The upper, weak positive reflection terminates against the upper boundary of the Kaskaskia II Sequence with erosional truncation between Well 2 and Well 3. The reflection demarcates the top of the Mission Canyon Formation. The interval between this reflection and the upper sequence boundary, west of Well 3 is occupied by the Charles Formation.

No remnants of the *Absaroka Sequence* are present in this area.

Two subparallel reflections can be identified within the *Zuni I Sequence*. No obvious reflection terminations can be found in this area.

The *Zuni II – Tejas* interval in general exhibits a subparallel reflection configuration. The lowermost reflections in the west terminate progressively toward the east, delineating the lower sequence boundary. This configuration probably indicates the direction of transgression. Further up, an erosional truncation type of upper reflection termination delineates a sequence boundary. This reflection pattern shows an easterly prograding sedimentation and indicates a westerly source. The sequence was terminated by a rearranged tectonic environment. Two more subparallel reflections can be identified above this sequence boundary. Further above, the reflections are somewhat contorted or in some places are chaotic; no continuous reflection or reflection termination can be identified with great certainty. Moreover, there are no reflections in this interval around the hinge of the Sweetgrass Arch. Nevertheless, the contorted reflection pattern, especially in the Foothills segment suggests rapid, easterly prograding terrigenous sedimentation from a westerly source.

The **structure** of the area is quite complex. The thrust faults in the Foothills segment are clearly detectable. The Pendroy Fault with normal displacement, can be identified. The downthrown side of the fault is on the west, which is in accordance with

the field observations. The strike-slip component attributed to this fault can not be determined from this section alone.

By analogs, below the Sweetgrass Arch a major detachment fault can be assumed to exist, from which the thrust faults splay upward. In the eastern part of the interval, east of the Sweetgrass Arch, easterly dipping reverse faults are interpreted. These faults are related to the regional Scapegoat–Bannatyne Trend, which is considered transpressive in this area.

6.1.2 Bearpaw Mountains area

The next ~170 km interval covers the Bearpaw Mountains ***(Figs. 6.3.a, b)***. The first 50 km actually run circumferentially with the circular region of the mountains *(Figs. 2.8.a and 4.1)*. Across the Bearpaw Mountains, the reflections exhibit a divergent pattern, which shows a general thickening toward the east, in the direction of the Williston Basin.

Due to the lack of deep wells, the position of the *basement–sediment* contact in this area was defined by extending the interpretation from the previous interval. This important horizon can be traced with some certainty within a positive, high-amplitude reflection across the area, except in the Bearpaw Mountains where the chaotic nature of the reflections did not allow any reliable interpretation.

Subparallel reflections in the *Sauk Sequence* have moderate to high amplitudes, good continuity and in some places show eastward onlapping reflection terminations, which probably represent the transgressive nature of the remnants of the Sauk Sequence.

The *Tippecanoe Sequence* is still fairly thin; however, it thickens continuously to the east. One major reflection can be identified within the sequence, which terminates with a westward onlap against the upper sequence boundary of the Sauk, east of the mountains. This clearly shows that the Tippecanoe transgression arrived from the east.

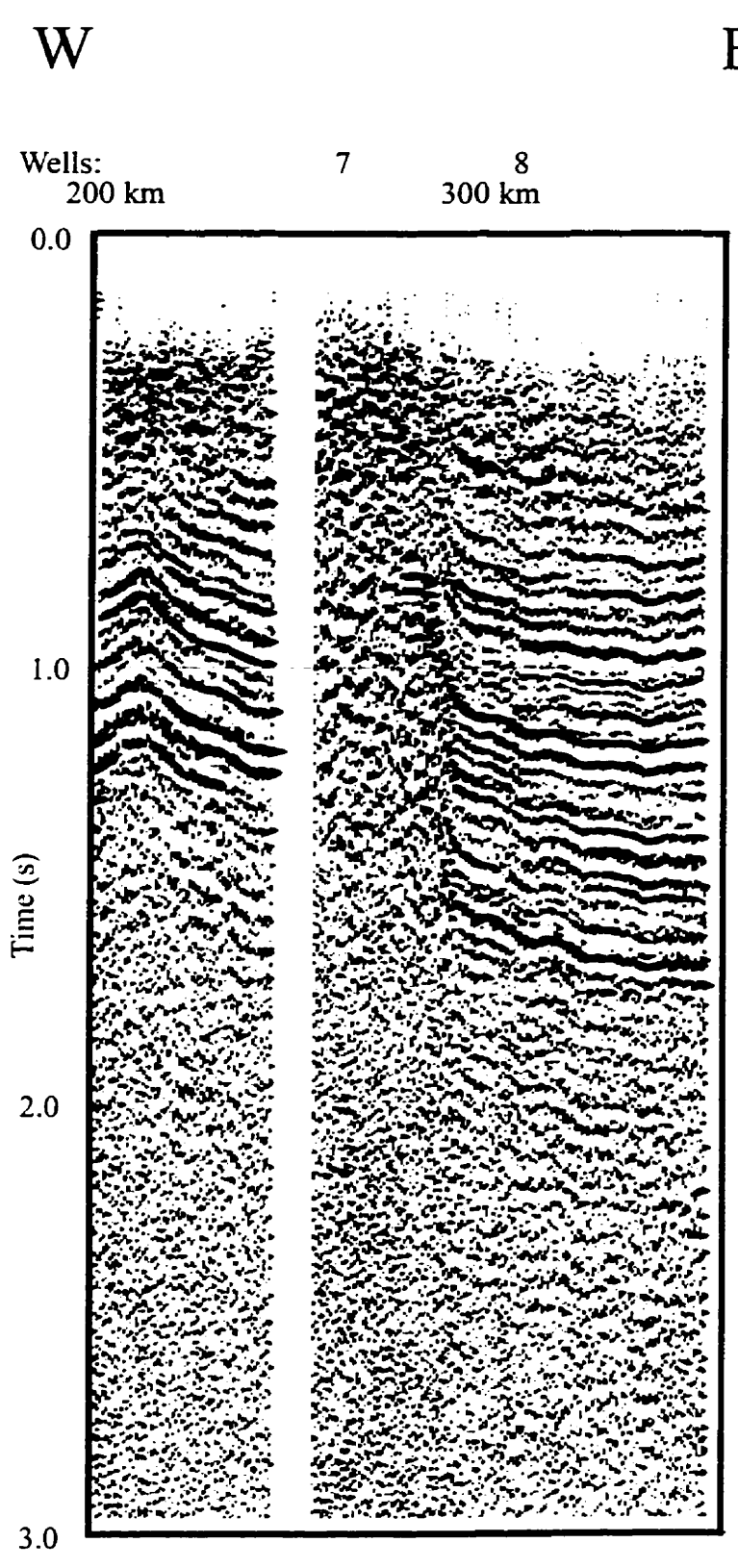

Fig. 6.3.a Line WE II, Bearpaw Mountains area, uninterpreted section.

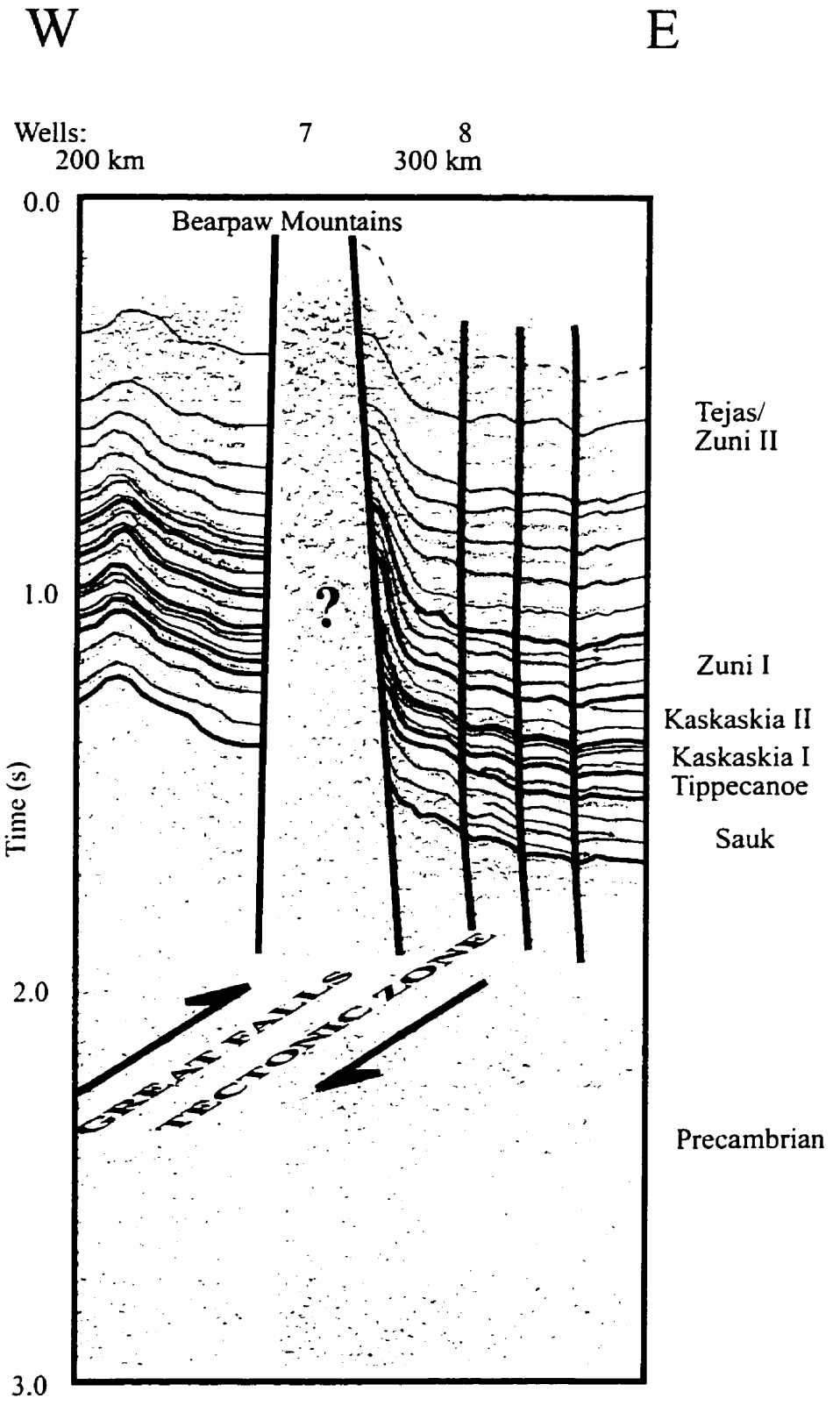

Fig. 6.3.b Line WE II, Bearpaw Mountains area, interpretation.

The reflections of the successive *Kaskaskia I Sequence* are subparallel, with good continuity and high amplitudes. The lower sequence boundary can not be identified by reflection terminations, because of paraconformity. This configuration suggests that reflection terminations can be expected in the cross section more or less perpendicular to the strike of this section. Geologically, it means transgression ocurred in this perpendicular direction, which is in harmony with the general pattern of sedimentation in the Devonian Elk Point Basin.

The overlying *Kaskaskia II Sequence* shows a more complex internal picture. The reflections are only moderately continuous and the amplitudes are variable, reflecting a more irregular internal character of this sequence. This is the seismic expression of the lateral facies changes in the Mississippian succession. Some truncation of reflection terminations can be observed against the upper sequence boundary of the Kaskaskia II, indicating a significant erosion after the Kaskaskia II deposition.

Remnants of the *Absaroka Sequence* are missing in this area.

The successive *Zuni I Sequence* is more complex, reflecting its progressively complicated geological history. The lower part, with subparallel, high-amplitude, continuous reflection suggests a low-energy environment. Above this, with a sharp contrast in seismic facies, easterly dipping clinoforms indicate progressively terrigenous sedimentation from a westerly source. Geologically the lower part refers approximately to the Piper–Rierdon series of the "Sundance Sea", while the upper part corresponds to the Swift–Morrison interval.

The *Zuni II – Tejas* interval comprises more than half of the sedimentary succession in this area. In the lower part, high-amplitude reflections with good continuity alternate with reflections with moderate continuity and amplitude. No clear reflection termination can be identified. This part corresponds to sheet-like deposition in

a marine or marginal marine environment. The upper part in the west does not allow precise interpretation and in the east some uncertainties also are exhibited due to aquisition and processing limitations. Nevertheless, based on the general character of the interval, some subparallel reflections with clinoforms can be inferred.

Structurally, the area is dominated by the presence of the Bearpaw Mountains. The western part of the section, as mentioned above, is circumferential with the mountains, and the apparent high-amplitude fold is actually the western extension of the intrusives in the mountains.

The central part is the main area of the intrusives and the general structure is certainly not like the profile suggests. Due to the presence of the uneven surface volcanic layer, it is extremely difficult to image the layering below the mountains in great detail with the seismic method. Nevertheless, on the eastern flank of the mountain, there is clear indication of pull-up and dragging of strata due to the forces accompanying the magmatic intrusion.

Further toward the east, indication of folding and faulting is apparent. The Bearpaw Mountains are located in the vicinity of the NE-SW trending Great Falls Tectonic Zone, which separates the Archean Medicine Hat Block from the Archean Wyoming Craton. The folding and faulting can be associated with the presumably transpressive deformation along this major tectonic feature. There is no clear indication of plainsward (eastward in this section) sliding of strata above an Upper Colorado layer in the close vicinity of the mountains, as suggested by Reeves *(1946)*. Identifying this type of shallow structure and corroborating the theory would require special seismic acquisition around the Bearpaw Mountains.

6.1.3 Williston Basin, western part

This part of the regional seismic section is ~240 km long, crossing the Williston Basin from its western flank to its central part ***(Figs. 6.4.a, b)***. The line is offset by 32

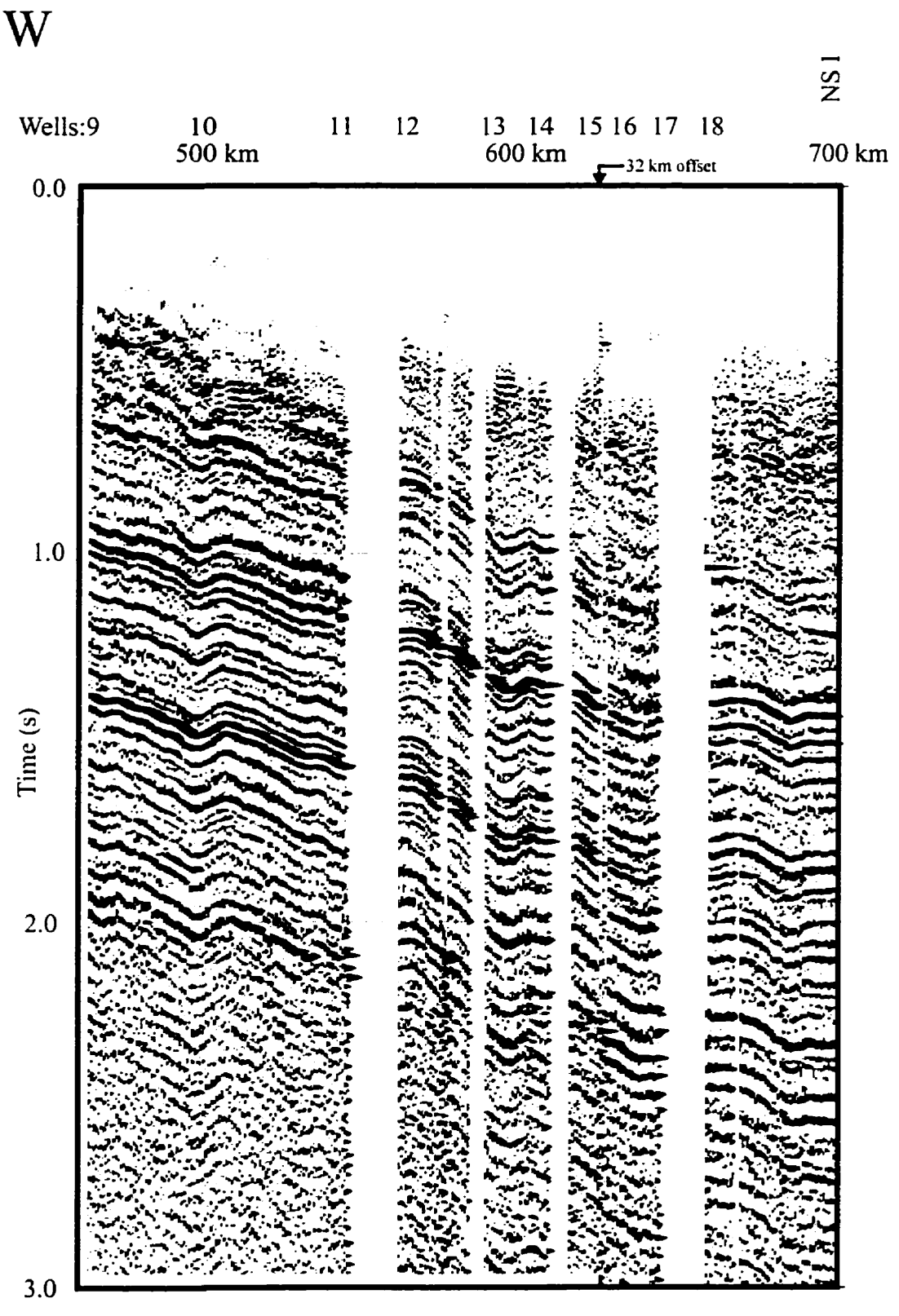

Fig. 6.4.a Line WE II, Williston Basin - western part, uninterpreted section.

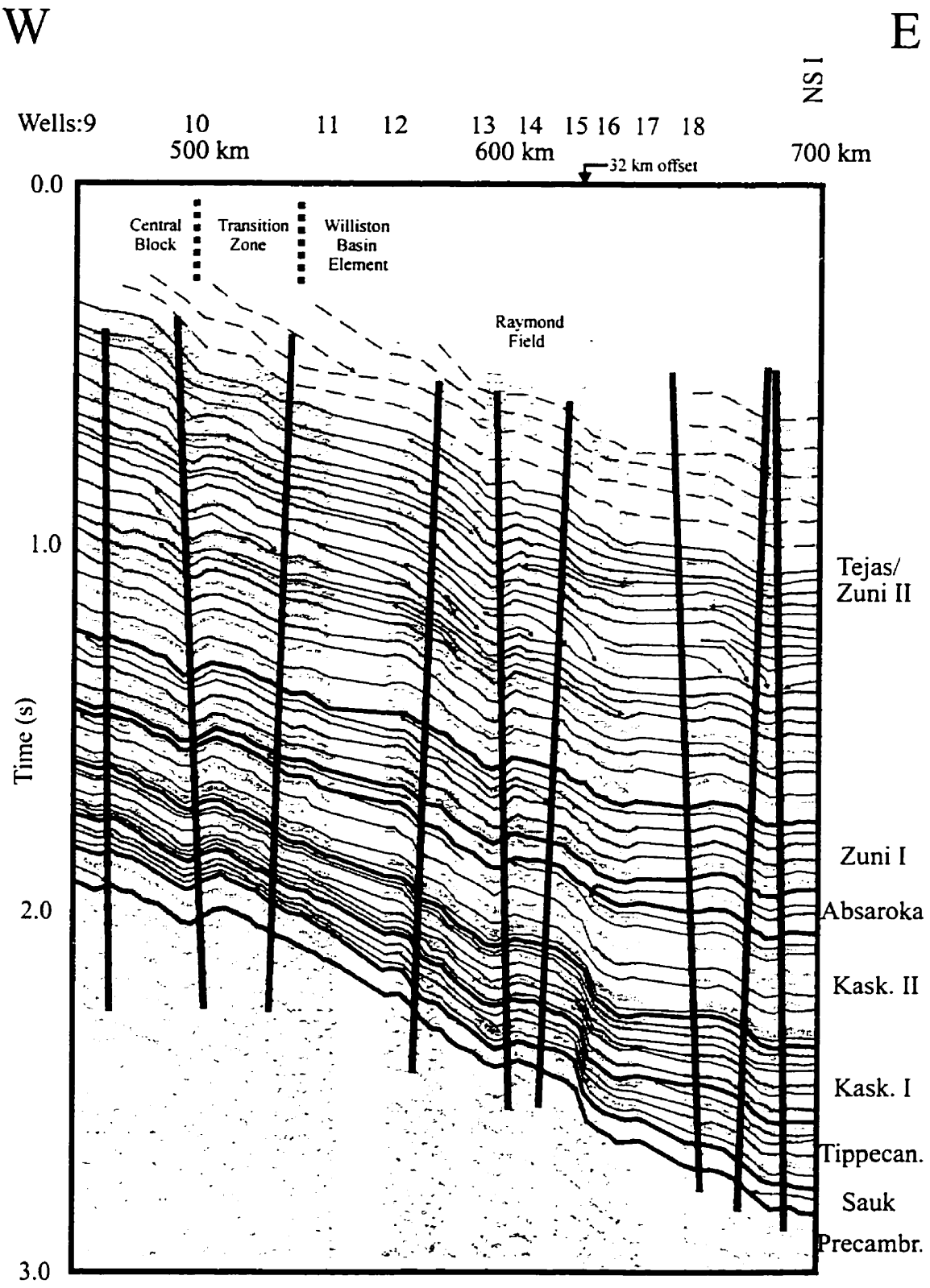

Fig. 6.4.b Line WE II, Williston Basin - western part , interpretation.

km between Well 15 and Well 16. The general pattern of the reflections is subparallel and divergent, with significant thickening toward the center of the basin. Some deep wells along this stretch helped to identify the geology of the area with greater certainty.

The *basement* reflector has a moderate positive amplitude and moderate continuity. Some westerly terminating reflections in the overlying Sauk Sequence can be identified against the basement reflector.

The *Sauk Sequence* itself is fairly thin in the central part of the interval and thickens slightly away from it. The upper boundary of the Sauk Sequence is sometimes difficult to trace. It has weak-moderate positive amplitude and moderate continuity.

The lowermost reflection of the *Tippecanoe Sequence* represents the surface between the sandstones of the Winnipeg Formation and the carbonates of the overlying Red River Formation. The petrophysical differences yield excellent reflection characteristics, manifested in high negative amplitude and excellent reflection continuity. The rest of the reflections of the Tippecanoe sequence exhibit a subparallel pattern, with moderate-to-good reflection properties. One reflection termination (truncation) can be identified against the upper boundary of the Tippecanoe Sequence between Well 17 and Well 18. The upper sequence boundary represents a major erosional surface which is in accord with the regional geology.

The reflections in the *Kaskaskia I Sequence* do not exhibit reflection terminations in this section. This underlines gainthe fact that the major transgressive–regressive direction was oriented at a high angle to the profile (i.e., that of Elk Point Basin). The reflection characteristics range from good to excellent, allowing an easy identification of seismic stratigraphic horizons. The reflection facies pattern is subparallel and even, corresponding to a generally low-energy sedimentary environment. Lithological units refer to higher-order sequence boundaries in this interval. The lower part of the sequence corresponds to the Elk Point Group. The Prairie

Evaporite is clearly resolvable in the eastern, deep part of the basin and still detectable in the west, where the thickness decreased significantly. This excellent resolution is due to the high reflection coefficient between the evaporites and the overlying Second Red Bed shales and between the evaporites and the underlying Winnipegosis carbonates. The upper boundary of the Prairie Evaporite appears with a strong negative reflection, while its lower boundary (top of the Winnipegosis Formation) appears with a strong positive reflection. Where minor discontinuity is present, Winnipegosis mounds can be inferred; however, identification of those can be made with more certainty on local seismic profiles. The reflections of the Manitoba Group formations can be identified reliably. The top of the Souris River Formation appears with a moderate-to-good, continuous negative reflection, while the top of the Dawson Bay Formation exhibits high, continuous positive reflection throughout the area. The reflections from the top of the Duperow and Birdbear (Nisku) formations have moderate amplitude and good continuity. The upper sequence boundary is virtually the top of the Three Forks Formation which exhibits moderate, positive amplitude and good continuity.

The reflections of the overlying *Kaskaskia II Sequence* are somewhat different from those in the sequence below. The strong negative reflection with excellent continuity representing the top of the Bakken Formation makes it easier to separate the two Kaskaskia sequences. The Bakken is clearly detectable, due to the significant petrophysical differences from the overlying Lodgepole Formation, but can not be resolved because of its limited thickness. The reflections above the Bakken Formation have high amplitude, but due to their hummocky character their continuity is not always good. This probably reflects the lateral facies changes in the Madison Group. Toward the west some erosional truncation type reflection termination can be observed against the upper sequence boundary of the Kaskaskia II Sequence. The interval in the eastern part of the area, below the upper sequence boundary and above the Madison reflections, represents the Three Fork Formation. Truncation-type reflection termination against the upper sequence boundary can be detected from this interval.

The overlying *Absaroka Sequence* is fairly thin all over the area; however, it thickens toward the east. Three higher-order sequences can be identified by reflection terminations. The lower one terminates with onlap against the erosional lower sequence boundary, probably representing the Pennsylvanian sediments, which are restricted to the central part of the basin. Even more limited is the extent of the overlying middle sequence (~Permian), which terminates with onlap against the upper boundary of the lower sequence, east of Well 18. The upper sequence within the Absaroka Sequence oversteps the lower sequences and is present all over the section. This sequence corresponds to the Triassic Spearfish Formation. Truncation can be identified against the upper sequence boundary of the Absaroka Sequence, representing again an erosional period.

Similarly to the area to the west, the reflections of the *Zuni I Sequence* show two distinct types of general charactersistics. The lower part exhibits continuous, high-amplitude subparallel reflections, reflecting low-energy depositional environments (Piper–Rierdon interval); while the upper part displays medium-amplitude reflections with limited continuity and some easterly dipping clinoforms, suggesting a westerly clastic sediment source (Swift interval).

The lower part of the overlying *Zuni II – Tejas* interval exhibits alternating continuous, subparallel, high-amplitude reflectors with moderately continuous, medium-amplitude shingled clinoform reflections. The alternation of the seismic facies mirrors the transgressive–regressive phases of this interval. The upper part of the interval shows a similar alternating pattern; however, the intervals, especially those containing clinoforms, exhibit progressively larger thickness upsection. This observation conforms with the increasing terrigenous sedimentation in the Western Interior Seaway with time. The extended thickness of the sequences containing clinoform reflection patterns allows for identifing the internal structures of the eastward prograding delta-type deposition.

The **structure** of this area is significantly different from the areas to the west. Folding is apparent throughout the interval, with increasing amplitude toward the center of the basin. The tripartite nature of the western end of the section is distinguishable. These three subregions are clearly the continuation of the "Central Block", the "Transition Zone" and the "Williston Basin Element", which was recognized in the Fort Peck Indian Reservation area, just south of the section ***(Section 2.2.1.2; Fig. 2.10)***.

The continuation of the "Central Block" crosses the seismic profile between Well 9 and Well 10 and the extension of the "Transition Zone" is located between Well 10 and Well 11. The area east of Well 11 belongs to the "Williston Basin Element". Fault-related folding is apparent at the boundary zone between the "Central Block" and the "Transition Zone". The axial plane of the major fold in this segment strikes roughly NNW-SSE, based on geological information. What the regional section reveals here is that the fold-bounding faults on both sides of this fold dip toward the axial plane of the fold, exhibiting a tightening of the fold downward in cross section.

Further to the east, the series of NW-SE striking folds can be identified on the section, in accord with the structural maps of the area ***(Fig. 2.11)***. The regional seismic section reinforces the downward tightening character of these folds, which are apparently asymmetric in this section which crosses the folds at an angle.

The oil fields of this area are clearly related to these folds. In the eastern end of this interval, the folds show a similar character and a higher amplitude.

6.1.4 Williston Basin, eastern part

The easternmost segment of the WE II line covers ~240 km ***(Figs. 6.5.a, b)***. It stretches from the deepest part of the basin to its eastern flanks. The gross character of the reflections of this region is subparallel and divergent to the west, showing a general thickening in that direction. Most of the wells reached the Sauk Sequence and some of

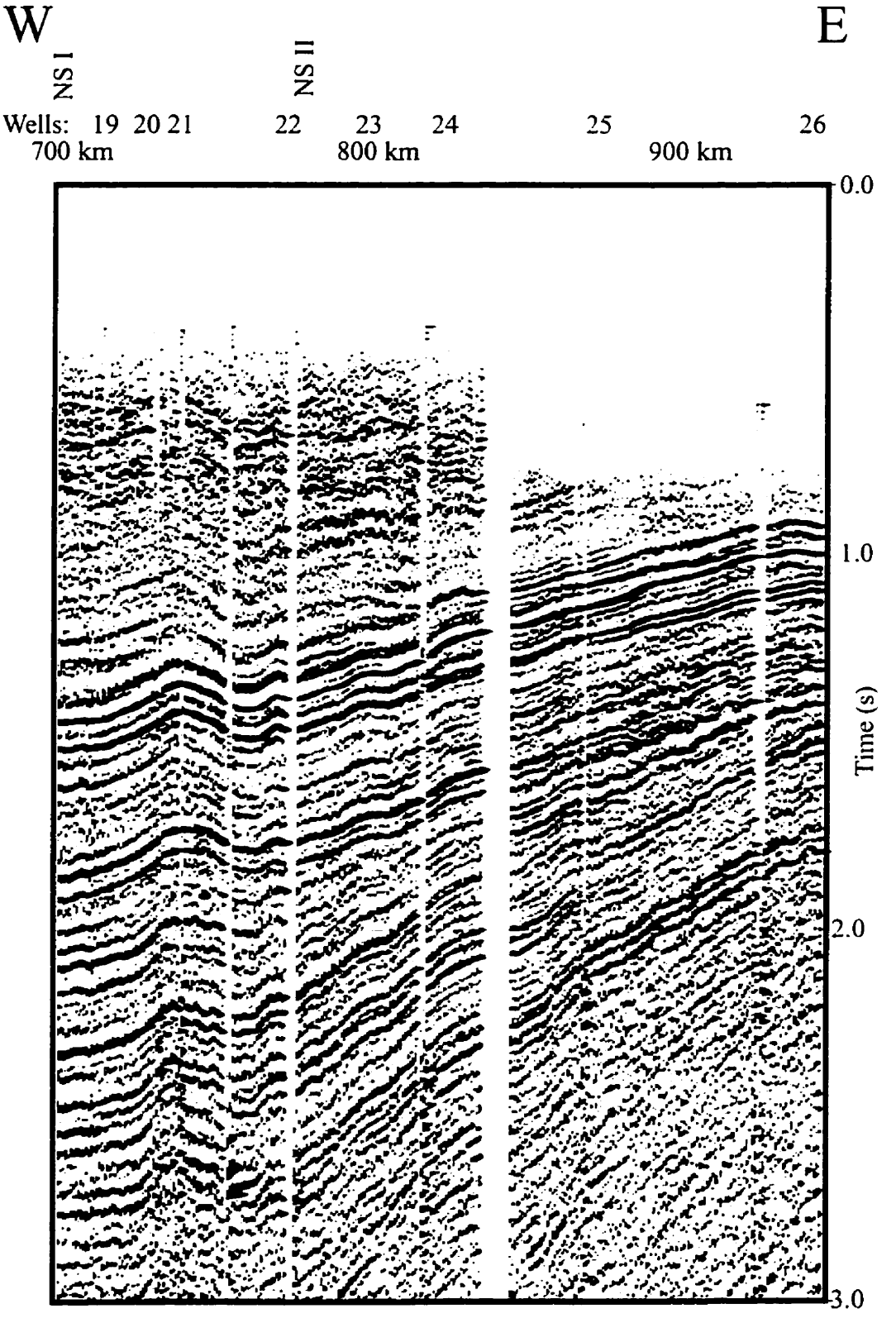

Fig. 6.5.a Line WE II, Williston Basin - eastern part, uninterpreted section.

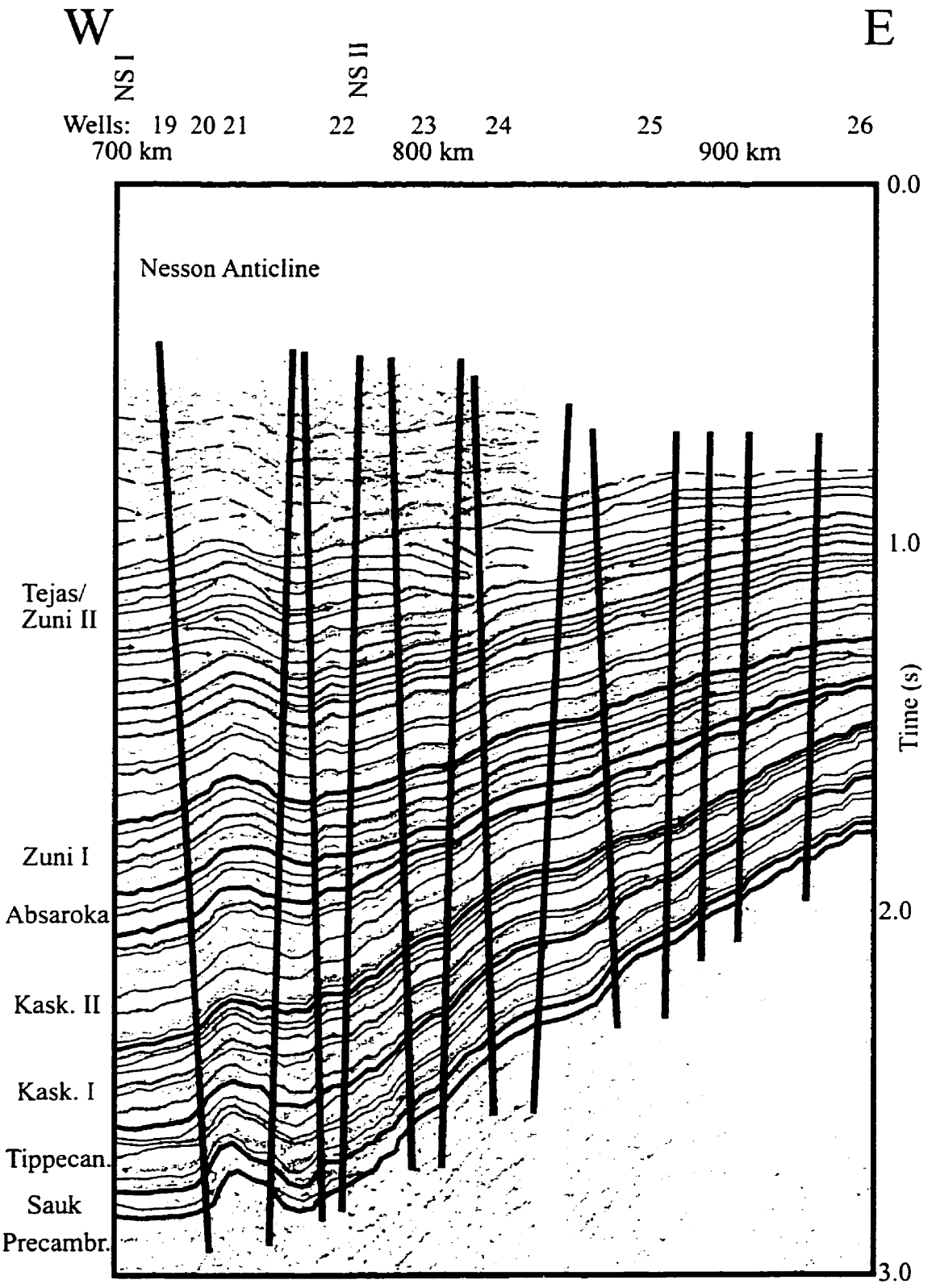

Fig. 6.5.b Line WE II, Williston Basin - eastern part, interpretation.

them penetrated the basement. This information coupled with the two north-south regional seismic lines allowed reliable interpretation.

The *basement* reflector in this side of the basin has variable, weak-to-moderate positive amplitude and continuity.

Reflections in the *Sauk Sequence* are weak and in some places show easterly onlap reflection termination representing the relative direction of transgression. The sequence itself is gradually thins toward the east; however, above the central, high-amplitude fold (Nesson Anticline) it shows some thinning and onlap reflection termination against both sides of the fold. This suggests that structural movements on this fold started at the very early stages of the basin's evolution or the earliest sediments were deposited on and around "islands" *(Lochman-Balk and Wilson, 1967)*. The upper boundary of the Sauk Sequence has a fairly weak, positive reflection.

It can be traced with the help of the lowermost reflection of the overlying *Tippecanoe Sequence*. The reflection from the Winnipegosis–Red River boundary continues to exhibit excellent reflection characteristics in this area, too. Other Tippecanoe reflections have moderate signal continuity and medium-to-high reflection amplitude. Reflection terminations against the upper boundary of the sequence can be identified east of Well 24.

Similarly to the western flank of the basin, the successive *Kaskaskia I Sequence* does not exhibit reflection terminations against its lower sequence boundary in this section, due to the almost perpendicular transgressional direction (SSE). The reflection from the top of the lowermost series (Ashern–Winnipegosis) shows a continuous, positive, high-amplitude reflection character. At the location of occasional discontinuities, mound buildup can be suspected. The strong negative, continuous reflection from the top of the Prairie Evaporite terminates with an offlap against the top of the Winnipegosis Formation, which mirrors the regressive phase of the Elk Point

Group. A medium-to-strong positive reflection can be detected within the Prairie Evaporite in the central part of the basin. The reflections in the upper part of the Kaskaskia I Sequence have moderate-to-good continuity, and medium-to-high amplitude. The reflection from the top of the Dawson Bay Formation continues to show the best seismic properties in this interval representing the Saskatchewan–Jefferson and the Manitoba groups. The upper sequence boundary of the Kaskaskia I is the reflection from the top of the Three Forks Formation, which exhibits high amplitude and excellent reflection continuity, especially where the Bakken Formation is present above. Where the Bakken is missing (east of Well 25), the reflection characteristics of this reflection are somewhat decreased.

The lowermost reflection in the *Kaskaskia II Sequence* is from the top of the Bakken Formation. It has excellent reflection characteristics up to the area where it terminates with an easterly onlap against the lower sequence boundary east of Well 25. Reflections from the internal part of the overlying Madison Group have moderate-good continuity, reflecting facies changes in relatively short distances in this area. In the east, where the successive Big Snowy sediments are not present, truncation-type terminations of the Madison reflections are identified against the upper sequence boundary. In the central part, reflections of the Big Snowy Group terminate against the upper sequence boundary, exhibiting an overall regressive pattern.

The *Absaroka Sequence*, which is thin all over the area thins even more to the east. The three higher-order sequences identified on the previous section can be traced to this area, too. The lower sequence (~Pennsylvanian) terminates with an onlap against the lower boundary of the Absaroka Sequence between Well 23 and Well 24. The middle sequence (~Permian) has a more limited extent and terminates with an onlap against the upper boundary of the lower sequence around Well 22. Erosion after the first two sequences is apparent. The thin, upper sequence within the Absaroka Sequence covers the whole area and no clear reflection can be identified in it; consequently, no reflection termination can be detected.

The overlying *Zuni I Sequence* continues to show two distinct types of seismic facies. Reflections of the lower, Piper–Rierdon series have a high-amplitude, continuous character; while the upper, Swift interval has a weaker, less continuous pattern.

The alternating pattern of the *Zuni II – Tejas* interval, observed in the western part, is extended to this region. The relative thickness and extent of these transgressive–regressive intervals changes, however. Generally, the intervals get thinner toward the east, making their delineation based on reflection termination more difficult. The lower series exhibit better continuity, higher amplitude, and subparallel reflections, even in the intervals which show a more clinoform internal pattern. This configuration suggests a lower-energy offshore environment away from the coarse material carried by the deltas from the west. Lithologically this interval in the east is represented by the Pierre Shale, which spreads over sedimentary sequences. Here, the sequence stratigraphic approach underlines the importance of its use in basin-evolution studies. The upper series show more clinoforms, which mirrors that final retreat of the sea and the increasing terrigenous sedimentation from the westerly source of the emerging Rockies.

The **structure** of this interval, at least in part, is the mirror image of the western part. Folds are apparent also on this side of the basin. The highest-amplitude fold (Nesson Anticline) is situated in the deepest part of the basin. The amplitudes of the folds decrease toward the flank, to the east. The central fold (Nesson Anticline) is bounded by faults (or fault system) on both its sides.

This regional seismic profile reveals that these bounding faults dip toward the fold's axial trace, resulting in a downward-tightening fold in cross section. These faults clearly show reverse displacement, suggesting compressive origin.

East of the major folds other, smaller folds can be observed between Well 22 and Well 25. These folds are asymmetric in cross section and also tighten downward.

The asymmetry folds (structural noses) in this cross section is the consequence of their NE-SW strike in this area ***(Figs. 2.13, 14)***.

The more easterly are the folds located on the profile, the more asymmetric they are in cross section. The bounding faults also show reverse displacement. This regional section reveals clearly their regional relationship. Interestingly enough, the faults east of Well 25, contrary to the region west of it, show dominantly normal displacement.

6.2 WE III line

The WE III regional seismic line covers over 400 km distance across the deepest part of the Williston Basin ***(Fig. 6.6)***. The basin in this section is roughly symmetrical and "bowl"-shaped, but it exhibits a slight westerly tilt. Two large-scale folds are apparent in the west (Poplar Dome) and in the central part (Nesson Anticline). Other smaller folds are also present on this regional cross section. For interpretation purposes the section can be subdivided into a ***"Western part"*** and an ***"Eastern part"***.

6.2.1 Western part

This interval is ~220 km long and dominated by the presence of the Poplar Dome in the west and the Nesson Anticline in the east ***(Figs. 6.7.a, b)***. There is a ~52 km gap in the regional profile west of the center of the basin.

The top of the *basement* reflector has a medium-to-high positive amplitude and good continuity in the western part of the section. East of the Poplar Dome the reflection characteristics deteriorate and the interpretation is less certain there.

The reflections of the *Sauk Sequence* are weak-to-moderate and onlap terminations against the basement can be inferred only in some places. The top of the Sauk Sequence appears with a medium-high positive amplitude reflection with moderate-good continuity.

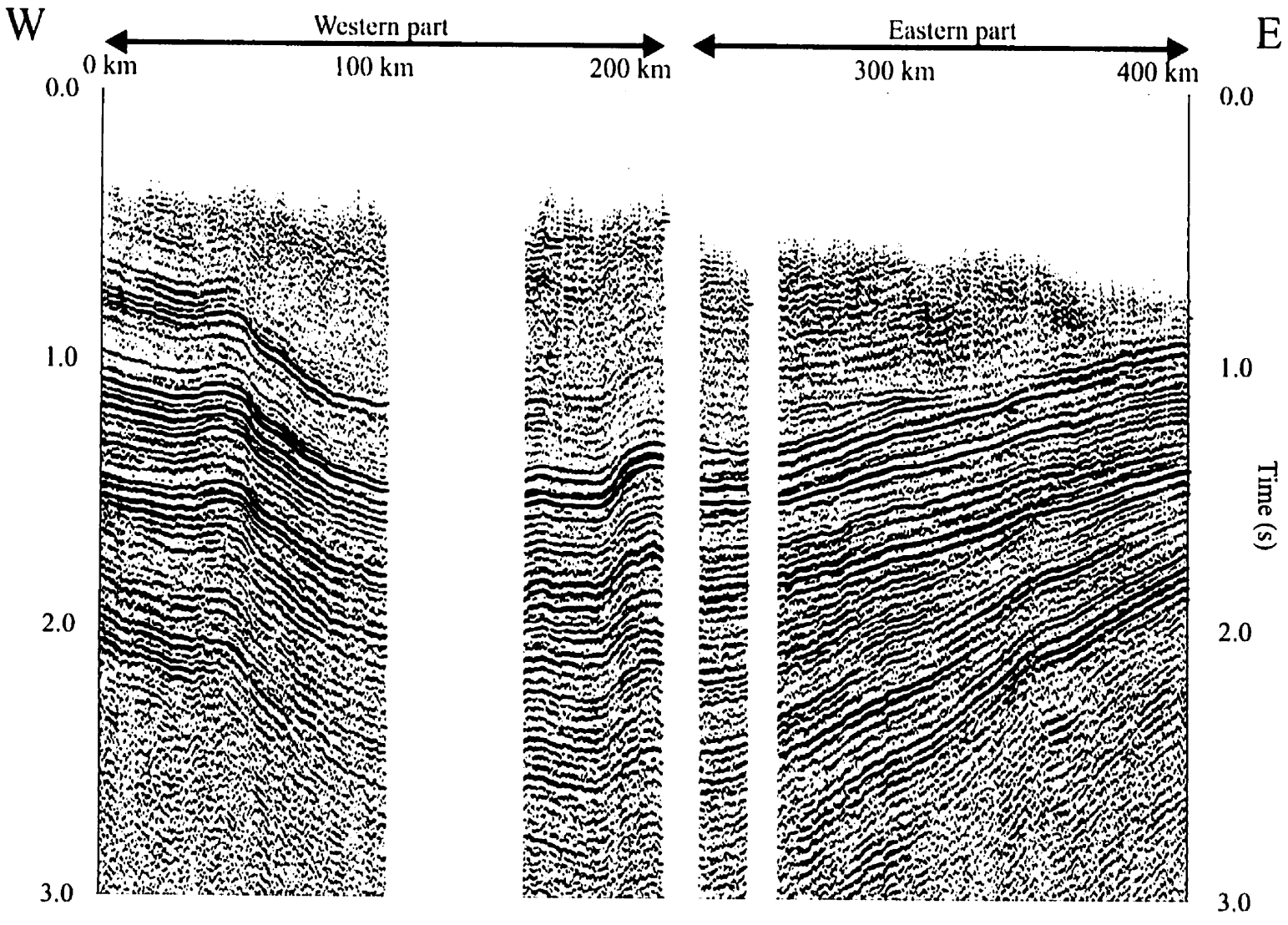

Fig. 6.6 WE III line.

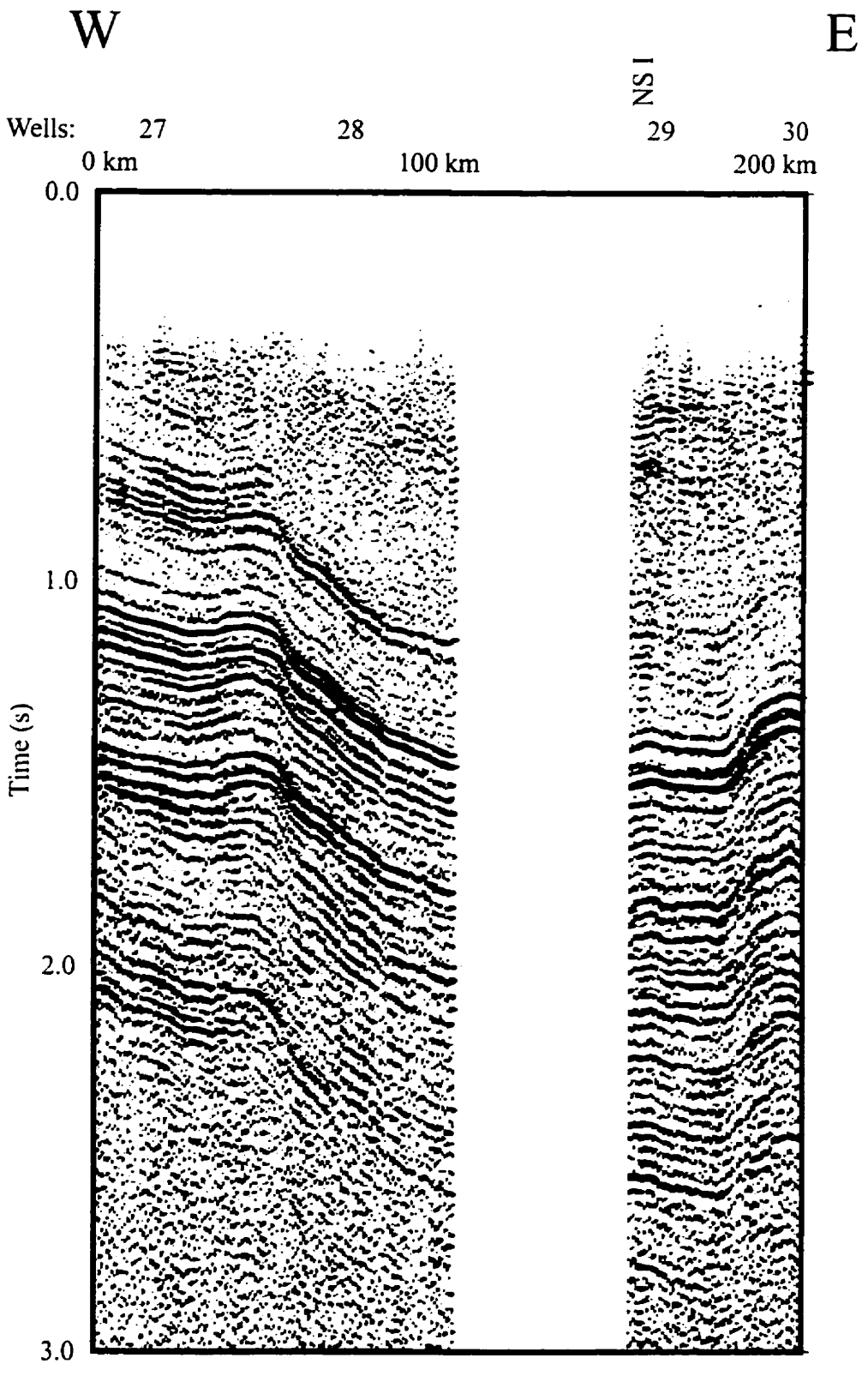

Fig. 6.7.a Line WE III, Williston Basin - western part, uninterpreted section.

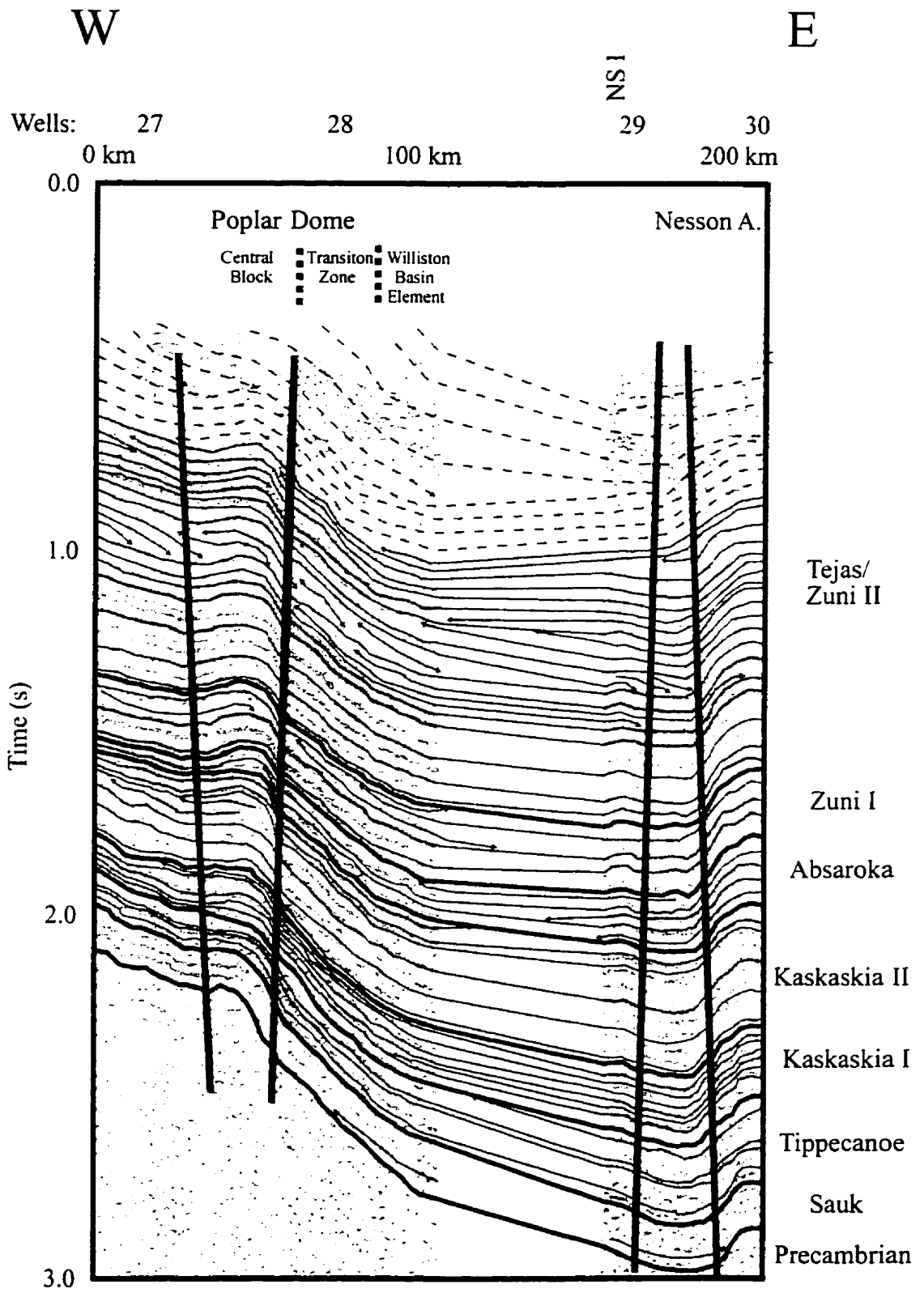

Fig. 6.7.b Line WE III, Williston Basin - western part, interpretation.

Similarly to the previous section, the lowermost reflection of the *Tippecanoe Sequence* from the Winnipeg–Red River boundary has excellent reflection characteristics in this area. The reflections of this sequence have medium-high amplitude and moderate-good continuity. Truncation type reflection terminations can be detected against the upper boundary of the Tippecanoe Sequence.

In the overlying *Kaskaskia I Sequence* the reflections are subparallel with good reflection characteristics. The extent of the Prairie Evaporite can be traced due to the strong reflections from its top and bottom. The reflection from its top terminates with an onlap just east of Well 28. Another reflection termination can be identified against the upper sequence boundary, which represents the erosional edge of the Three Forks Formation east of Well 27.

The *Kaskaskia II Sequence* is fairly thick in this block, even in the west, where the line is entering into the east-west trending Central Montana Trough. The excellent reflection from the top of the Bakken Formation is present all over this segment of the section. Numerous continuous, high-amplitude reflections can be distinguished from the overlying Madison interval. Some disrupted reflections could indicate the lateral facies changes in this succession. The topmost reflection terminations of the Madison interval can be seen at the base of the overlying Big Snowy Group in the west, suggesting erosional truncation. The Big Snowy Group strata thickens to the west showing the increasing sedimentation in the western part, in the Central Montana Trough. A truncation type reflection termination can be detected against the upper boundary of the Kaskaskia II Sequence between Well 28 and Well 29. This indicates again an erosion after the deposition of the Big Snowy Group. The location of the reflection truncation probably delineates the eastern limit of the late Mississippian Heath Formation in this section.

The *Absaroka Sequence* is thicker in this section than in the previous line. The lower subsequence within the Absaroka (~Pennsylvanian) is present throughout the line.

The reflection from its upper boundary has fairly good continuity. A westerly directed onlap type reflection termination, against the lower boundary of the Absaroka Sequence, just west of Well 29, suggests a transgression in that direction above the erosional surface. The middle sequence (~Permian) is present only east of the Poplar Dome, where its upper boundary terminates with an onlap against the lower sequence. Another onlap termination of the middle sequence can be suspected between Well 28 and Well 29. The middle sequence also exhibits an overall transgressive pattern toward the west. The upper sequence (~Triassic) oversteps the middle sequence and blankets the whole area. A truncation type upper termination against the top boundary of the Absaroka Sequence reinforces the regressive deposition and the erosion that follows.

The *Zuni I* reflections exhibit dual characteristics in this area, like they did in the areas to the north. Reflections of the lower unit (Piper–Rierdon) are subparallel and have excellent continuity and high amplitude. The unit is thicker in the western part indicating the shift in the depocenter at this time. This is in accord with the general character of the "Sundance Sea". The upper unit of the Zuni I Sequence has weak reflections which exhibit clinoformal configurations. These are the regressive, mostly clastic sediments of the Swift–Morrison interval, which are deposited from the western source of the emerging Sevier Orogeny.

The lower part of the overlying *Zuni II – Tejas* interval is dominated by subparallel reflections, where high-amplitude, continuous reflectivities alternate with shingled clinoforms. This arrangement represents shale/sandstone dominated transgressive–regressive cycles. This alternating pattern is preserved in the upper part of the interval; however, here the clinoforms became more sigmoid and definitely thicker than the subparallel, high-amplitude reflections. The internal structure (topsets, forsets) of the regressive delta sedimentation is visible and progradational patterns can be recognized. The increased terrigenous sediments mirror the effects of the increasing activity of the Laramide Orogeny west of the area.

The **structure** of this interval is dominated by the Poplar Dome in the west and the Nesson Anticline in the east. The structural subdivision of the area recognized in the Fort Peck Indian Reservation can be extended south to the WE III regional seismic line ***(Fig. 2.10)***. The Poplar Dome is a NW-SE trending major fold and is located in the "Central Block" ***(Fig. 2.10)***.

The WE III reveals that the Poplar Dome is also bounded by faults, which dip toward the fold's axial trace and exhibit reverse displacement. Asymmetry of the fold in the profile is probably the consequence of the non-perpendicular orientation of the fold. The eastern boundary fault marks the border between the "Central Block" and the "Transition Zone". The layers in the "Transition Zone" dip at a higher angle to the east than do those in the "Williston Basin Element" in the east.

East of the gap, in the eastern part of this stretch, the large Nesson Anticline dominates. Only the western boundary fault is covered by the seismic line, but similarly to the WE II profile, it dips toward the fold's axial trace, exhibiting a downward tightening pattern and a reverse displacement. It is important to mention that the Nesson Anticline is narrower and higher in this profile than in WE III, and the boundary fault is steeper. Another fault with reverse displacement can be observed west of the Nesson Anticline. Reverse displacement suggests an overall contractional deformation of the area. The nature and direction of the compressional forces can be established after analyzing the structures in 3D with the help of maps and the additional north-south seismic profiles.

6.2.2 Eastern part

This stretch of the WE III line covers ~180 km, from the eastern flanks of the Nesson Anticline to the eastern margin of the Williston Basin ***(Figs. 6.8.a, b)***. The reflections on a large scale exhibit a subparallel divergent pattern toward the west. Both wells along this interval reached the basement allowing a reliable interpretation even of the lowest sedimentary reflections.

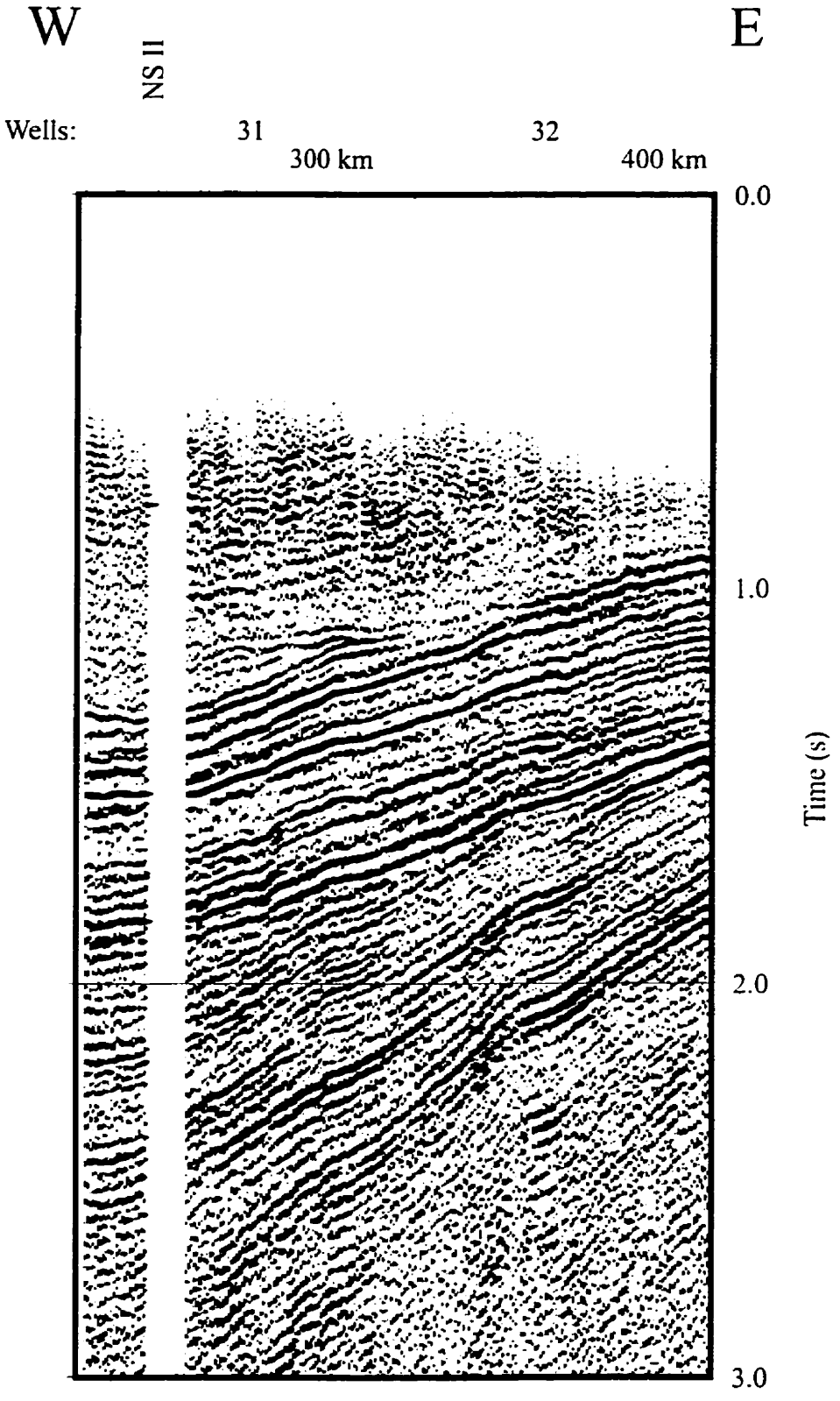

Fig. 6.8.a Line WE III, Williston Basin - eastern part, uninterpreted section.

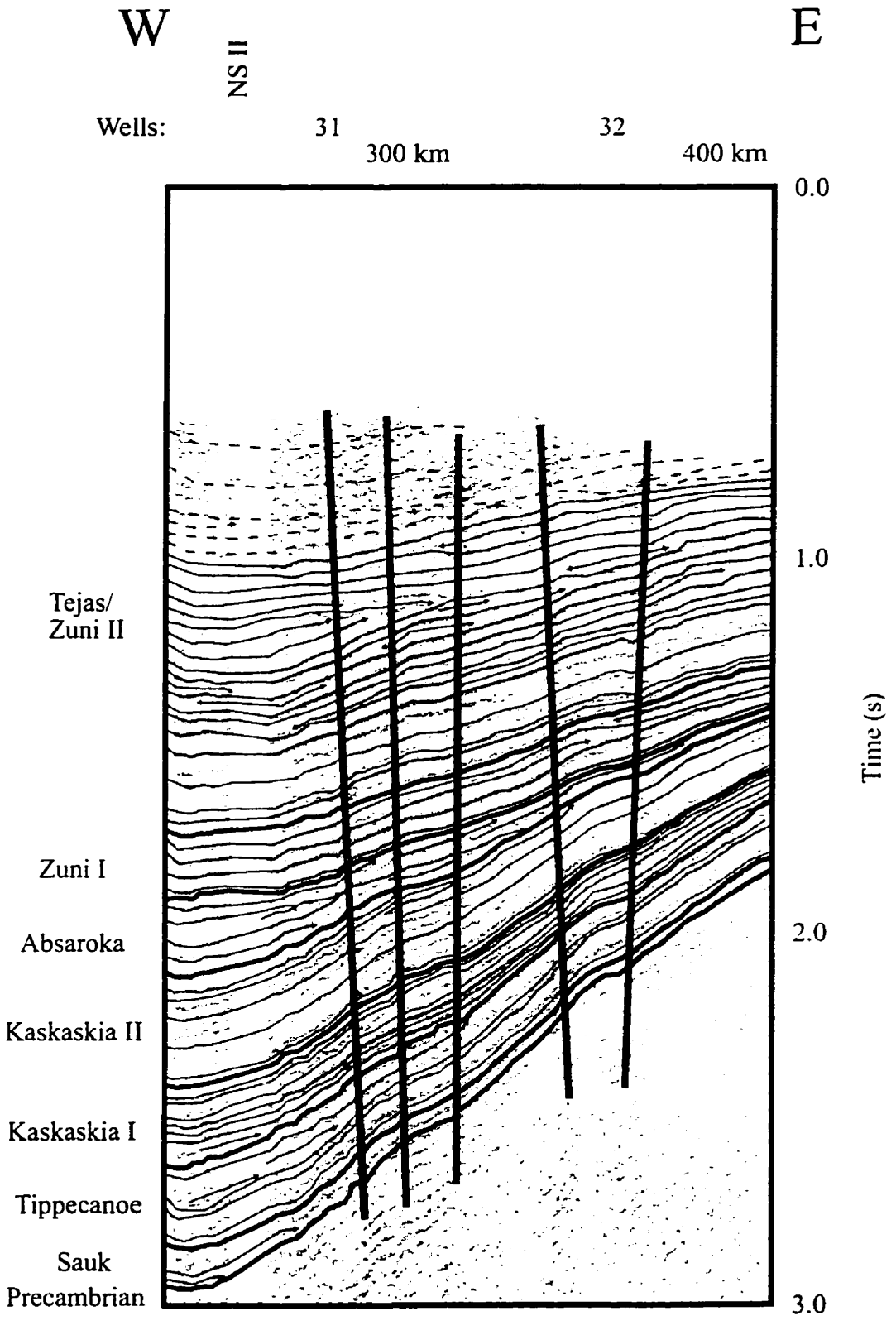

Fig. 6.8.b Line WE III, Williston Basin - eastern part, interpretation.

The *basement* reflection is a moderately continuous, medium amplitude positive reflection, which can be traced in the area.

Reflections of the *Sauk Sequence* terminate with eastward onlaps against the basement reflector, indicating the direction of the transgression. The Sauk Sequence itself thins considerably toward the east. The upper boundary of the sequence is a medium-to-high amplitude positive reflection with good-to-excellent continuity. Its continuity is somewhat decreased at the deepest part in the west.

Like in other areas, the lowest reflection of the *Tippecanoe Sequence* (Winnipeg–Red River boundary) appears with superb reflection characteristics. The rest of the Tippecanoe reflections in the area have good continuity and medium-high amplitude. Within the upper part of the sequence some eastward onlap reflection terminations can be observed, which represent the transgressive character of the sedimentation. Reflection termination against the upper sequence boundary indicates erosional truncation.

Contrary to the WE II line, onlap reflection terminations against the lower boundary of the *Kaskaskia I Sequence* can be identified in this section. This is the consequence of the orientation of this line at the southeastern margin of the Elk Point Basin, where transgressional features can be identified on profiles with this strike. The Prairie Evaporite is clearly detectable but fairly thin in this area, and the top reflector terminates against the bottom one with an onlap west of Well 32. The rest of the Kaskaskia I reflections show moderate-high amplitude and good reflection continuity. The reflection from the top of the Dawson Bay Formation exhibits again the best reflection characteristics.

The lowermost reflection of the overlying *Kaskaskia II Sequence* represents the Bakken Formation. The formation itself is very thin, but due to its excellent reflection

characteristics it is easily identifiable and can help to locate the lower boundary of the Kaskaskia II Sequence. Reflections of the successive Madison interval have moderate continuity and medium-high amplitude. As it was observed in other places, discontinuities of reflections in this series indicate facies changes. Some upper reflection terminations can be detected against the lower boundary of the upper part of the Kaskaskia II Sequence. This upper part represents the eastward thinning of the Big Snowy Group which is present here with the Kibbey and Otter formations. Truncation type reflection terminations against the upper sequence boundary delineate their extent to the east and indicate a widespread erosion.

The tripartite pattern of the overlying *Absaroka Sequence* is observable again in the western end of the profile. The reflections of the lower (~Pennsylvanian) and middle (~Permian) parts terminate against the lower boundary of the upper sequence, indicating a major erosional period after the middle sequence. The reflection from the top of the middle sequence terminates with an onlap against the lower sequence. The upper sequence (~Triassic) is present in the whole area. Its reflections are disrupted in places and show terminations against the upper boundary of the Absaroka Sequence, indicating again a major erosional surface.

The lower two reflections of the successive *Zuni I Sequence*, representing the Piper–Rierdon interval, are subparallel and have excellent reflection characteristics with high amplitude and good continuity. The reflections of the upper part (Swift) are less continuous and exhibit clinoforms with truncation-type terminations against the upper sequence boundary.

The lower part of the *Zuni II – Tejas* interval has again overwhelmingly subparallel reflections, with high amplitude and excellent continuity, which alternate with less continuous reflections. The upper part can be described by the less continuous reflections with a clinoform pattern and sharp reflection terminations. This indicates an increasingly clastic sedimentation upsection.

The **structures** of this flank of the basin seem more gentle than in other areas including the eastern part of the WE II line. This is because the axial plane folds of this area are at a very low angle to or parallel with the strike of the seismic profile ***(Fig. 2.17)***. Nevertheless, at least two folds can be identified in this area. The asymmetry and the apparent width of these folds are the consequences of the geometric relationship mentioned above. Both folds are bounded by faults which dip toward the fold's axial trace. The folds tighten downward. Reverse displacement can be observed on the fold-bounding faults, like on other similar structural elements of the central part of the basin, suggesting an overall compressive type deformation in the area.

6.3 NS I line

The NS I regional seismic line extends ~440 km from Saskatchewan to South Dakota ***(Fig. 6.9)***. It traverses the deepest part of the Williston Basin and exhibits an asymmetrical pattern. This section can also be subdivided into two subsections. The apparent stratigraphic dip in the shorter ***"Northern part"*** is larger than in the longer ***"Southern part"***. This is because this section closes the longer axis of the slightly NNW-SSE elongated Williston Basin at an angle ***(Fig. 4.1)***. Folding is apparent in both of the flanks, but the highest-amplitude fold is located in the central part. Unfortunately there are two ~15-20 km gaps in this regional section.

6.3.1 Northern part

The northern part of the NS I line stretches along ~220 km with a ~20 km gap in the deep part of the basin ***(Figs. 6.10.a, b)***. All the wells along this interval were drilled into the Sauk Sequence; however, they did not reach the Precambrian basement.

Nevertheless, the top of the *basement* reflector could be identified by correlation from the two east-west profiles and by the onlapping reflection terminations within the Sauk Sequence.

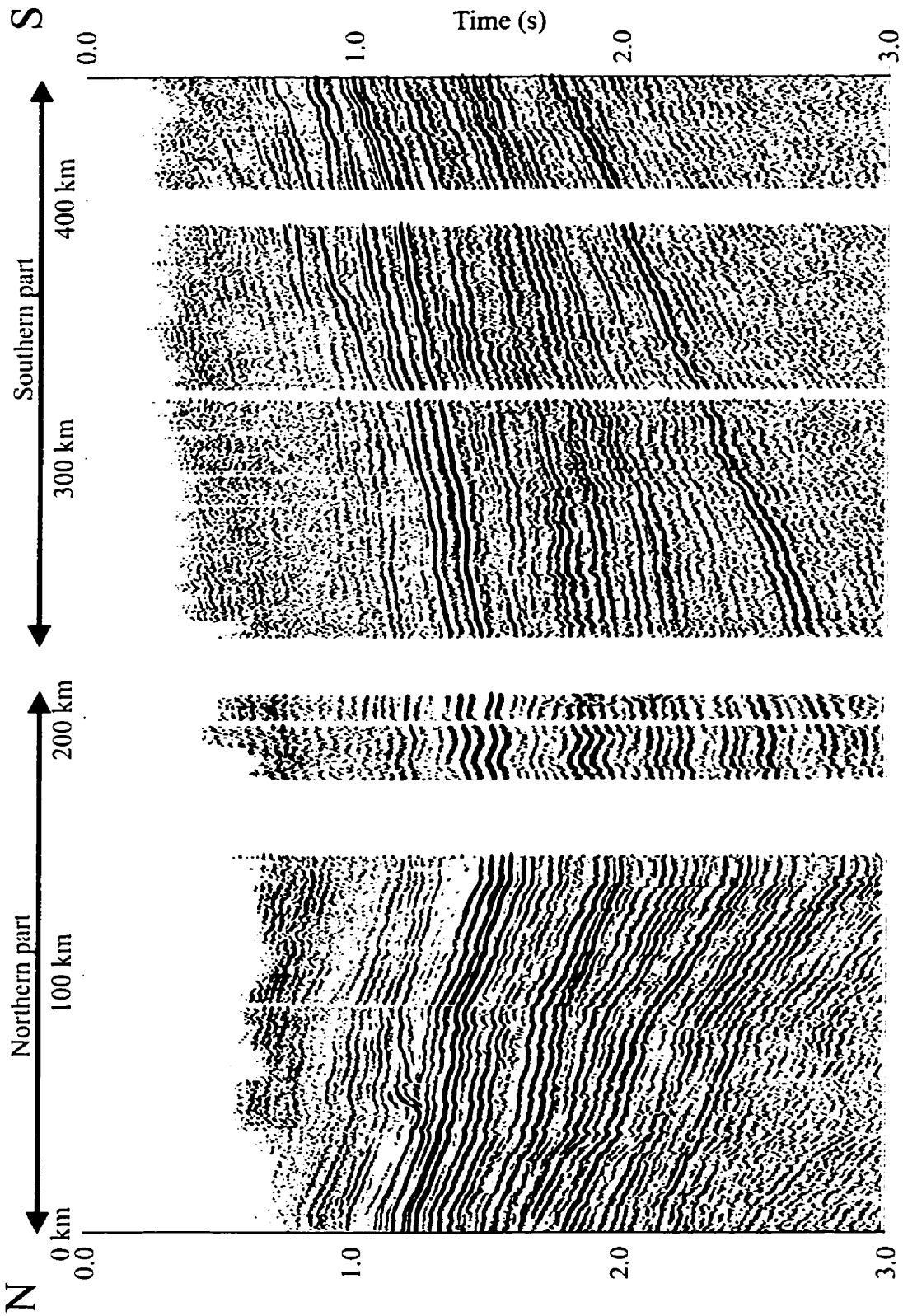

Fig. 6.9 NS I line.

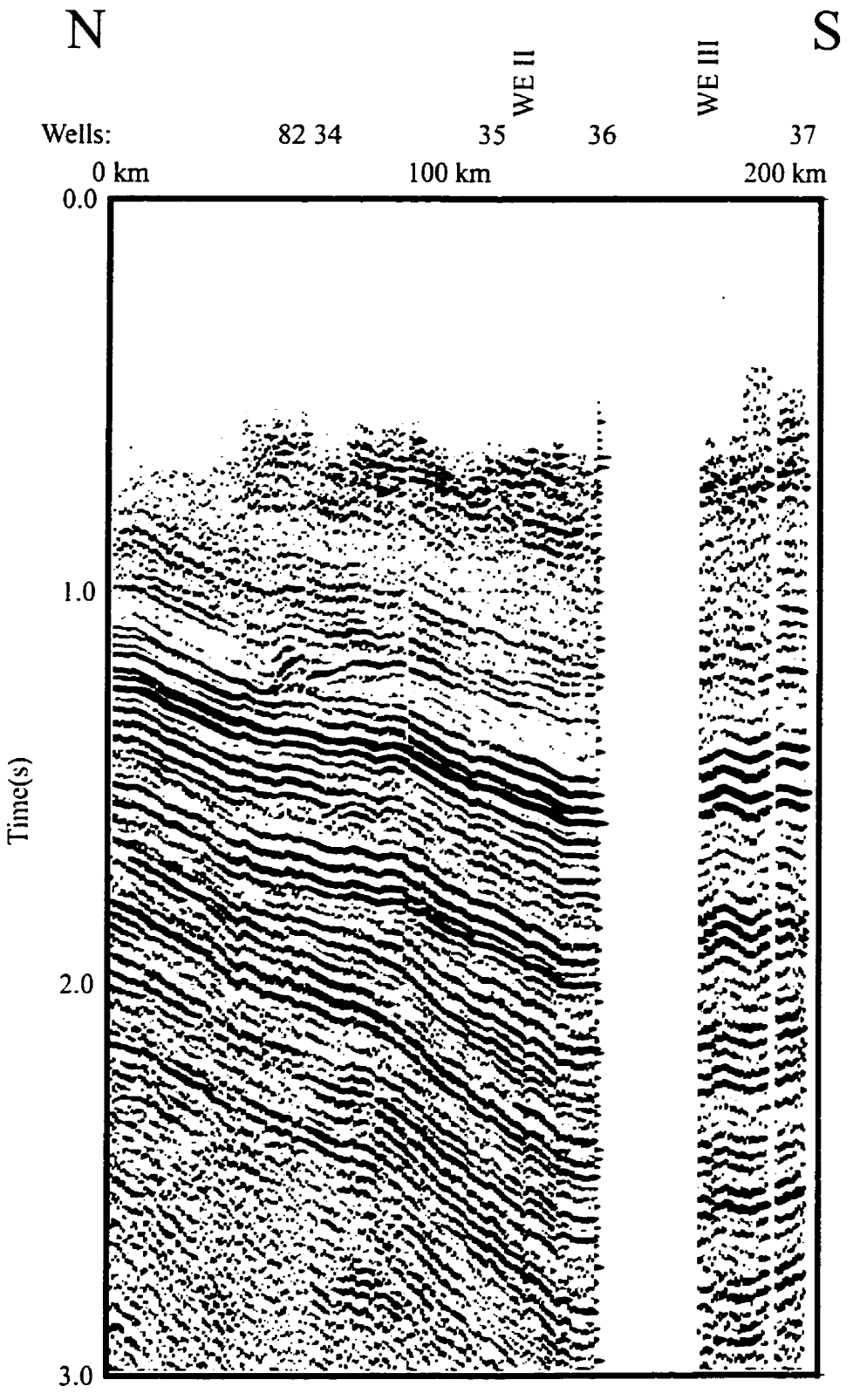

Fig. 6.10.a Line NS I, Williston Basin - northern part, uninterpreted section.

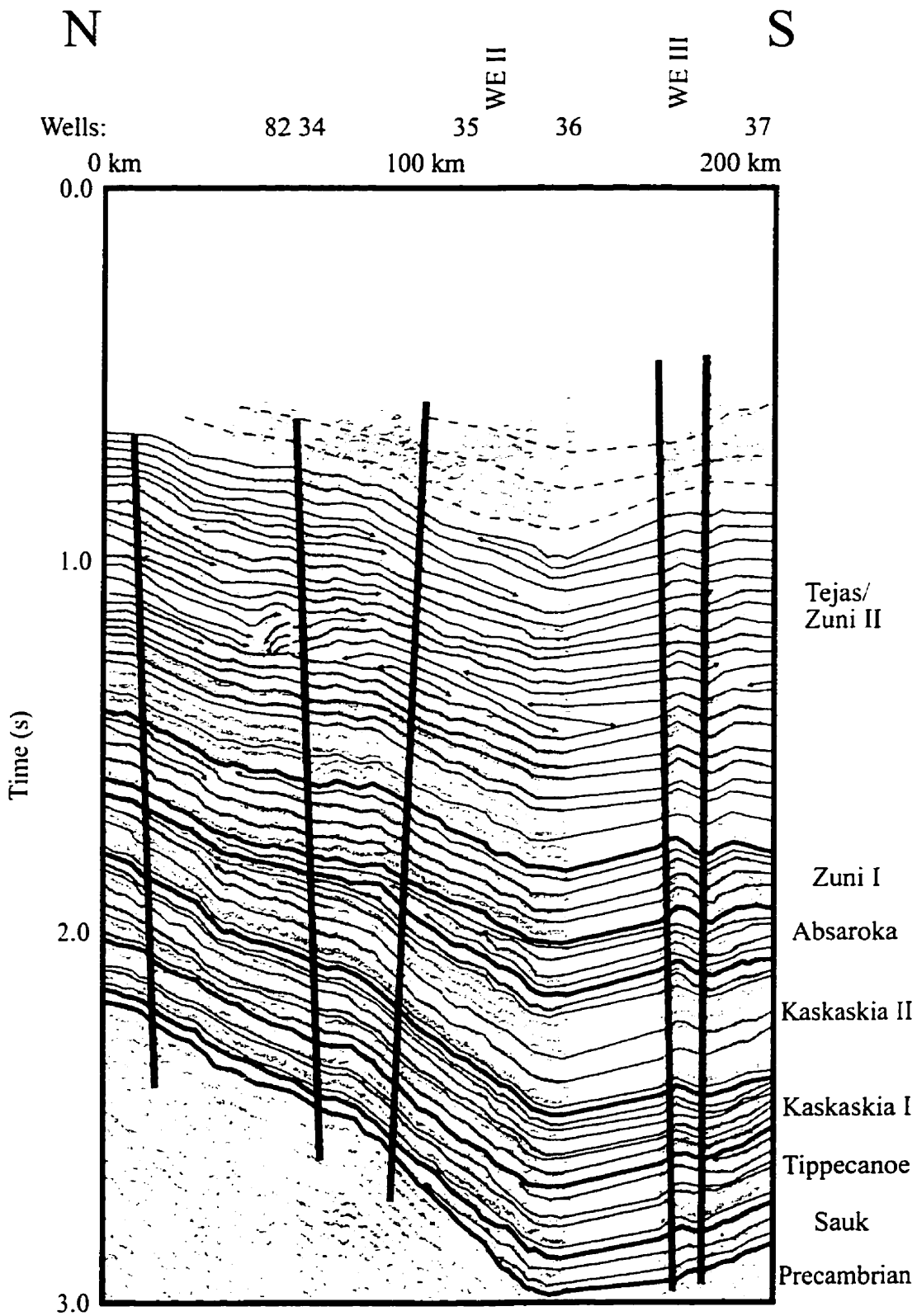

Fig. 6.10.b Line NS I, Williston Basin - northern part, interpretation.

The *Sauk Sequence* itself is thicker in the central part of the basin; however, north of the reflection terminations its thickness is fairly uniform. The reflection representing the upper sequence boundary of the Sauk has high, positive amplitude and good continuity.

The lowest *Tippecanoe* reflection (Winnipeg–Red River boundary) has again excellent reflection characteristics. The later reflections have moderate continuity and medium-good amplitude. Truncation-type reflection termination against the upper sequence boundary shows an apparent erosional surface.

Intervals of the overlying *Kaskaskia I Sequence* and the sequence as a whole thin toward the south approaching the southern limits of the sedimentation in the Elk Point Basin. Kaskaskia I reflections do not exhibit terminations in this interval. Their general reflection characteristics are good. In the case of the Prairie Evaporite, the reflection characteristics are excellent and its upper and lower boundaries are clearly distinguishable.

Based on reflection characteristics and correlation from other lines, the lower boundary of the overlying *Kaskaskia II Sequence* is easy to identify. The Bakken Formation appears again unmistakably with a strong, continuous negative reflection. Reflections of the lower part of the Madison Group (Lodgepole–Mission Canyon) are moderate and show discontinuity, reinforcing the lateral facies changes in this interval. The upper part of the Madison Group (~Charles) shows a strong, subparallel, continuous reflection pattern, which is probably due to the layered anhydritic lithology of the succession. These reflections terminate upward against the bottom of the overlying Big Snowy Group. The reflection from the Big Snowy Group itself terminates against the upper boundary of the Kaskaskia II Sequence.

The tripartite system of the *Absaroka Sequence* can be analyzed nicely in this section, too. The reflection from the top of the lower unit (~Pennsylvanian) terminates

against the lower sequence boundary with an onlap, and so does the middle unit (~Permian) against the top of the lower unit. The upper unit (~Triassic) oversteps the lower two units and covers the whole section. One truncation-type reflection termination against the upper boundary of the Absaroka Sequence indicates the presence of an erosional surface.

The lower part of the *Zuni I Sequence* (Piper–Rierdon interval) has subparallel, high-amplitude, continuous reflections. The upper part (Swift interval) exhibits shingled clinoforms with upper and lower reflection terminations, which indicate increasing terrigenous clastic input. The contorted internal character suggests that the direction of the sediment source is at a high angle with the strike of the section (from west).

The lower part of the overlying *Zuni II – Tejas* interval has high-amplitude, continuous reflections interbedded with less continuous ones, indicating a fluctuating transgressive–regressive sedimentation pattern. The upper part exhibits an alternating pattern, too; however, the intervals with less continuous reflections are thicker upsection and the reflections are contorted or sometimes sigmoid. Like in the sequence below, it represents increased clastic, delta-type sedimentation from a source out of the plane of the seismic section (from west). Strong downlap features are clearly visible in the area of Well 82 and Well 34. The apparent disruption of the downlapping reflection is an artifact of the offset in the section at Well 82 ***(Fig. 2.19)***.

The **structures** of this area appear to be less dramatic than those in the previous sections. This is partly because the folds are virtually parallel with the profile, especially in the northern end of the section ***(Fig. 2.19)***. Nevertheless, a fault with normal displacement can be observed close to the northern end of the section.

Further south however, downward tightening folds can be identified. These folds are also bounded by faults with reverse displacement and the faults dip toward the axial plane of the folds. The fold between Well 34 and Well 35 is apparently wider than the

one west of Well 37. This is mostly because the plane of the profile crosses the axial plane of the first fold at a smaller angle than it does the axial plane of the second fold. This profile ends just on the Red Wing Creek structure ***(Fig. 2.21)***, which was originally interpreted as a meteoritic impact structure *(Bridges, 1978)*, and later as an intersection of two major regional faults *(Bridges, 1987)*. Due to the lack of total coverage of the structure, it can not be differentiated satisfactorily.

6.3.2 Southern part

The southern part covers ~220 km distance from the deepest part of the Williston Basin to its southern flank ***(Figs. 6.11.a, b)***. Two out of four wells drilled along this interval reached the basement, which allows a reliable interpretation.

The top of the *basement* reflector has a medium-to-high positive reflection with good continuity.

The thickness of the *Sauk Sequence* is fairly uniform; however, some thickening–thinning, indicated by onlap reflection terminations can be observed against the basement reflector. This could indicate early tectonic activity and/or that the earliest sediments were deposited on and around "islands" *(Lochman-Balk and Wilson, 1967)*. The reflection from the top of the Sauk Sequence has excellent continuity and high amplitude.

The Winnipeg–Red River interface in the lower part of the overlying *Tippecanoe Sequence* continues to exhibit excellent reflection characteristics. The continuity of the rest of the Tippecanoe reflections is moderate and their amplitudes are high. Truncation-type reflection terminations can be identified against the upper sequence boundary.

Reflections of the overlying *Kaskaskia I Sequence* terminate with southerly progressive onlap against the same boundary. It reflects the southward transgression of the Elk Point Sea. The southern edge of the Prairie Evaporite is delineated by an onlap

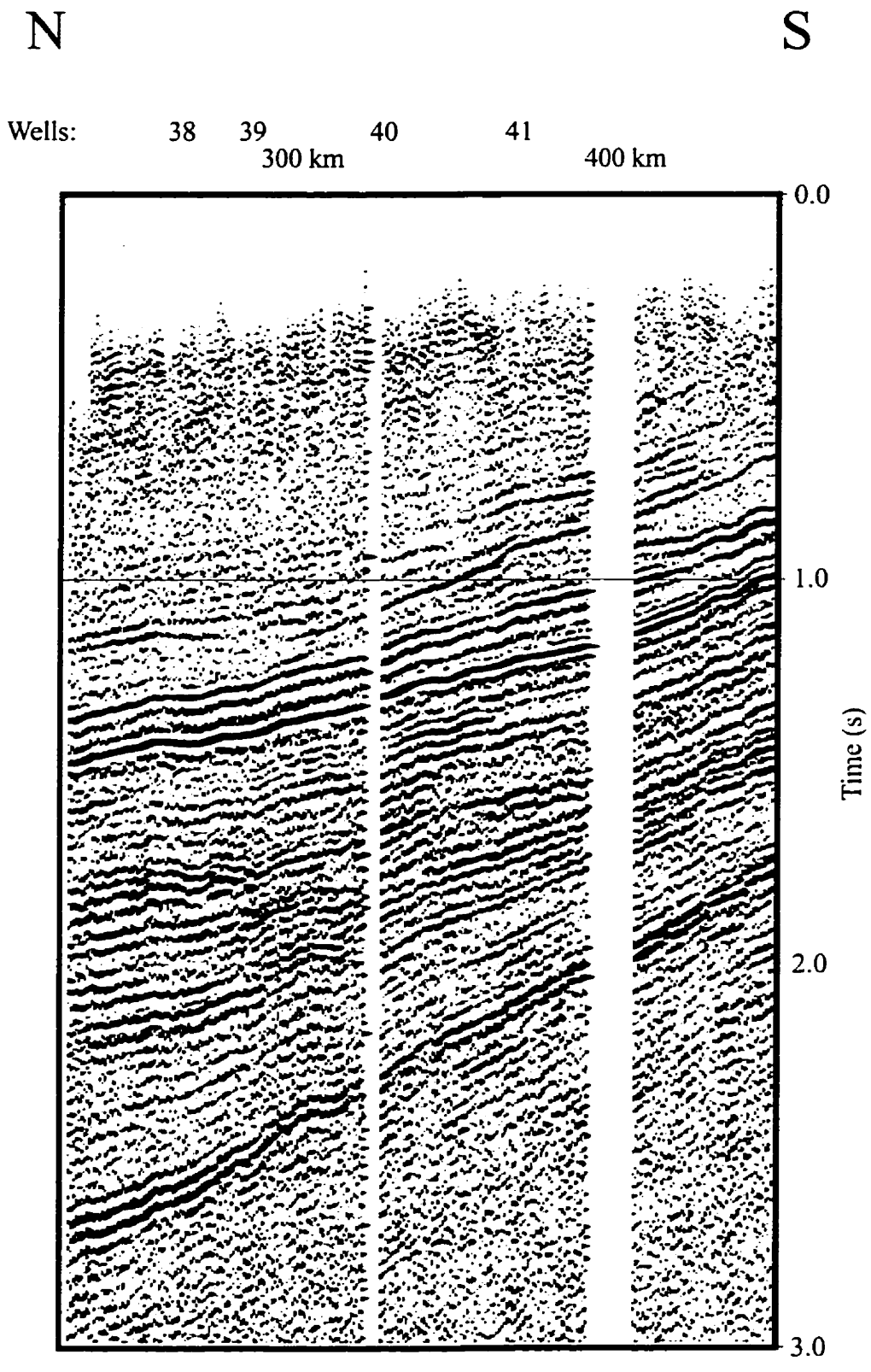

Fig. 6.11.a Line NS I, Williston Basin - southern part, uninterpreted section.

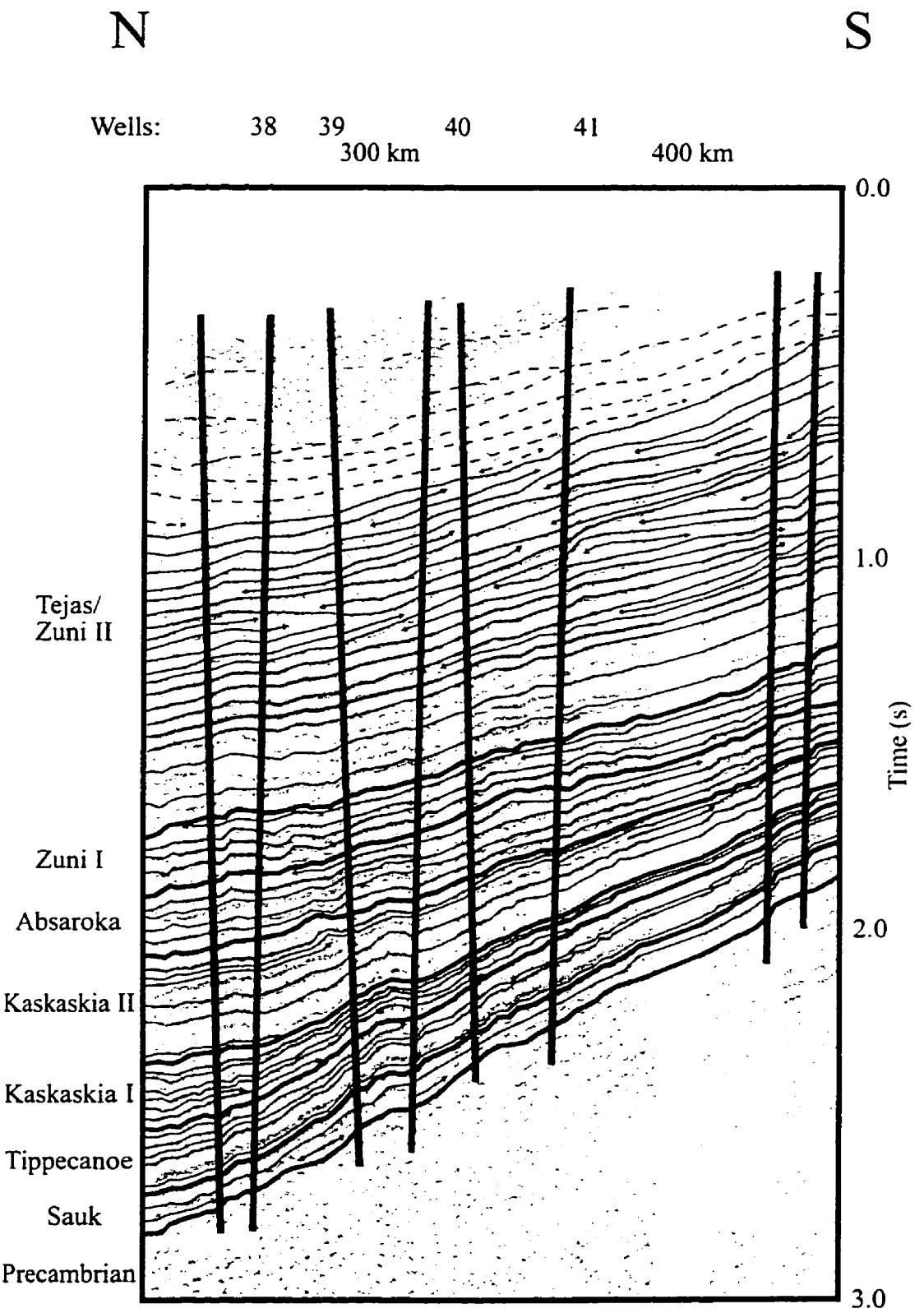

Fig. 6.11.b Line NS I, Williston Basin - southern part, interpretation.

reflection termination against the reflection from the top of the Winnipegosis Formation. The lack of the usual excellent reflection characteristics of the Prairie Evaporite reflection can be attributed to the increased amount of Winnipegosis buildups at the region close to the erosional edge. At the southern end, the Kaskaskia I Sequence thins considerably and the still present reflection from the Saskatchewan–Jefferson and Three Forks groups have moderate-good continuity and medium-high amplitude.

The typically excellent reflection characteristics of the Bakken Formation, in the lowest part of the *Kaskaskia II Sequence*, are degenerated close to its erosional edge at Well 38. Reflections from the lower and middle part of the Madison Group (Lodgepole–Mission Canyon interval) have medium-good amplitude and are discontinuous in places. The nature of these reflections again suggests facies changes in this series. Reflections from the overlying Charles interval of the Madison Group have excellent reflection characteristics and they can be traced until they terminate with truncation against the reflection of the overlying Big Horn Group. The Big Horn Group itself, appears with good, continuous reflections, which terminate against the upper sequence boundary, indicating erosion in this area, too.

The successive *Absaroka Sequence* is considerably thicker than on the other profiles, and thins only moderately to the south. All three subsequences can be identified in this area. The lower sequence (~Pennsylvanian) has good reflection characteristics, but no obvious reflection termination can be detected. Similar attributes characterize the middle sequence (~Permian). The thickest, upper sequence (~Triassic) has medium-high amplitude reflections with moderate-good continuity. Some onlap termination can be observed, which indicates the relative direction of the transgression in this section.

The lower part of the next *Zuni I Sequence* exhibits subparallel reflections, with high amplitudes and excellent continuity reflection characteristics. No reflection termination is apparent in this interval. The upper part (Swift) can be described by weak

continuity and medium-high amplitude reflecting high-energy, terrigenous sedimentation. Occasional reflection terminations are detectable, but their directions are not consistent, indicating out-of-plane sediment sources.

The lower part of the overlying *Zuni II – Tejas* interval shows, similarly to other areas, an alternating pattern; however, the thickness of the individual transgressive and regressive intervals changed. The transgressive intervals with subparallel, high amplitude, continuous reflections are thinner than the regressive intervals with moderate-high reflection amplitudes and weaker continuities. In the upper part, major differences can be observed in addition to the increased thickness of the regressive intervals with clinoforms. Within one specific regressive interval, where increasing terrigenous sediment influx is assumed, the internal pattern of the unit is complex, with a complicated reflection termination arrangement. Beyond the fact that the primary sedimentary source is from out of the plane of the profile (from the west), two major source directions can be identified.

The **structure** of this stretch of the NS I regional profile is fairly simple. Like at its northern end, the strikes of the structural noses and fold axes are generally parallel with the strike of the profile ***(Fig. 2.20)***. Nevertheless, wherever folds cross the section at a low angle they can be detected, with variable asymmetry. Downward tightening folds can be observed in the region around Well 38, between Well 39 and Well 40 and around Well 41. The fold-bounding faults exhibit reverse displacement, which was also observed on the previous regional profiles.

Additionally, faults with normal displacement can be detected at the southern end of the line. This tectonic configuration (i.e., compression in the center and extension in the flanks) was also observed in previous profiles.

6.4 CA I line

The CA I regional seismic profile covers almost 500 km ***(Fig. 6.12)***. It also can be subdivided into a ***"Northern part"*** and a "Southern part". Its northern end in Canada runs parallel with NS I ***(Fig. 2.19)***, but south of the international border it is identical with NS I; consequently, only the northern part will be discussed. Obviously the profile exhibits the same large-scale asymmetric character with a steeper northern flank. Since this profile extends further toward the north, it reveals more of the structures of this flank of the basin.

6.4.1 Northern part

The northern part of the CA I regional line is ~190 km long ***(Figs. 6.13.a, b)***. Only the northernmost 100 km section, which runs through Canadian territory, differs from the northern part of NS I. This profile traverses Zhu's *(1992)* east-west regional seismic section of the northern Williston Basin.

No additional onlap termination against the *basement* reflector could be identified in this 100 km interval.

The *Sauk Sequence* itself is fairly uniform here and shows only minor thinning toward the north.

The reflection from the *Tippecanoe* Winnipeg–Red River interface continues to exhibit excellent seismic characteristics. A minor decrease in amplitude and continuity can be observed on the later Tippecanoe reflections. An additional truncation type reflection termination against the upper sequence boundary shows that the post-Tippecanoe erosion affected this area as well.

Reflections of the successive *Kaskaskia I Sequence* have superb reflection characteristics and actually they are somewhat better than they were in the areas to the south. The Prairie Evaporite stands out prominently. No reflection terminations of this

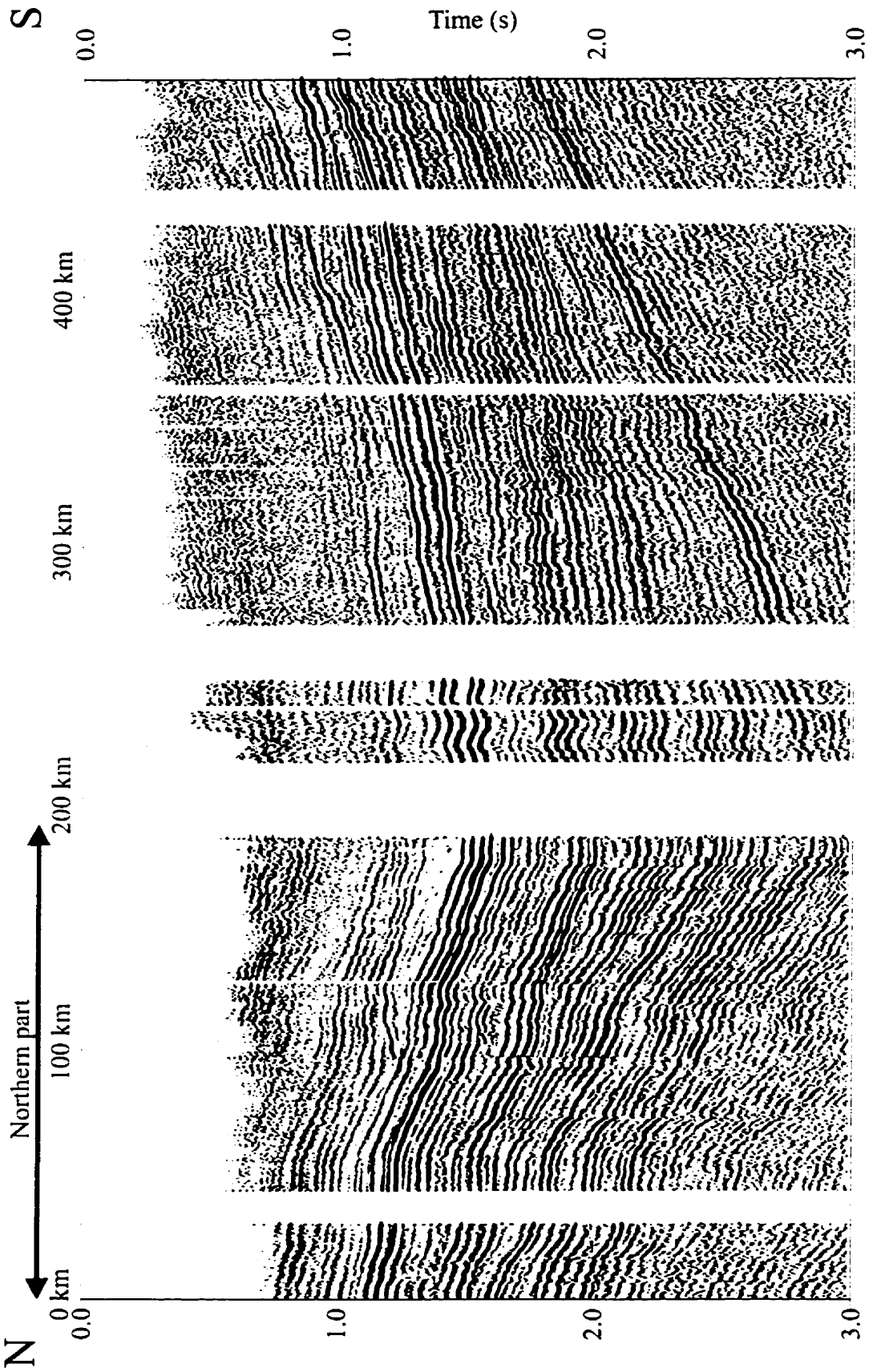

Fig. 6.12 CA1 line.

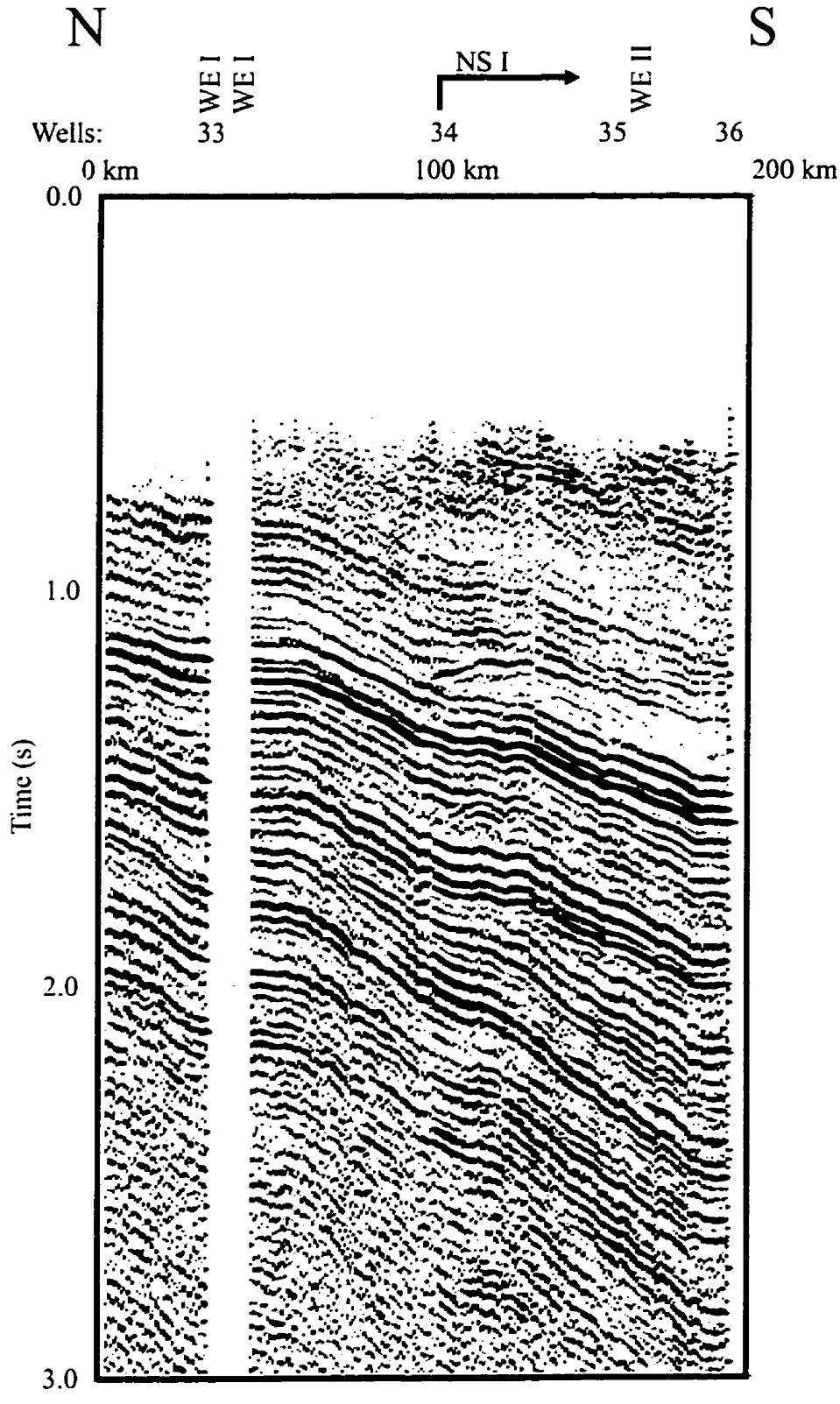

Fig. 6.13.a Line CA I, Williston Basin - northern part, uninterpreted section.

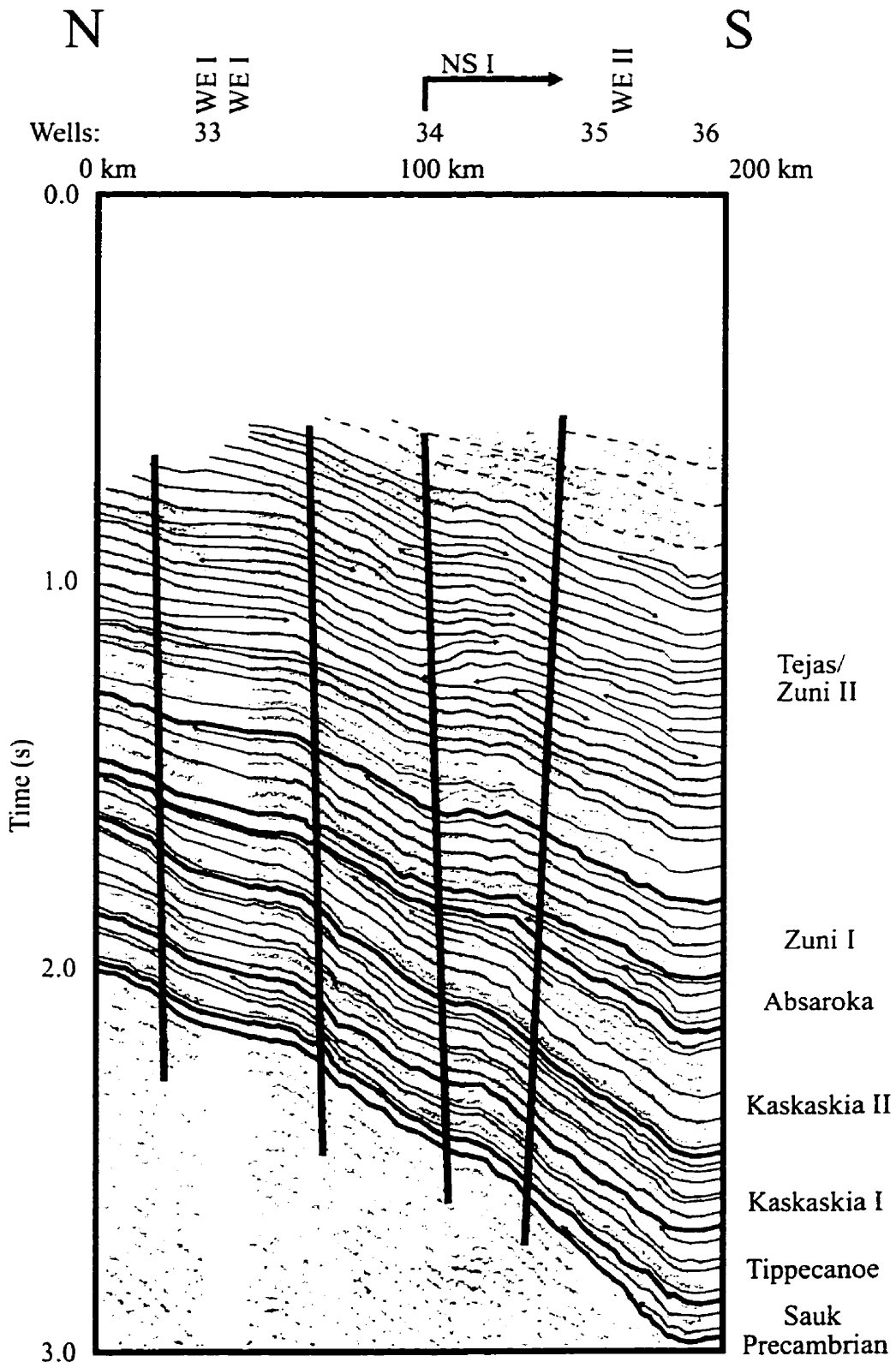

Fig. 6.13.b Line CA I, Williston Basin - northern part, interpretation.

sequence can be identified, however. This is probably because this part of the section is getting further away from the erosional edges of the Elk Point Basin.

The reflection from the Bakken Formation of the overlying *Kaskaskia II Sequence* preserves the excellent reflection quality in this area. The Madison Group reflections continue with similar characteristics to those in the south and west. There are more reflection terminations against the upper sequence boundary as compared to the parallel running NS I line. The observable limit of the Charles salts indicates that the section approaches the northern erosional edge of this interval. The northern erosional limit of the Big Snowy Group, as identified on the NS I line, is around Well 34.

The lower two sequences (~Pennsylvanian and Permian) of the *Absaroka Sequence* are not present north of the international border, along this section. The upper sequence (~Triassic) thins progressively toward the north. Additional truncation type termination against the upper boundary of the Absaroka Sequence suggests large-scale erosion in this northern area.

The *Zuni I Sequence* continues to exhibit a dual character. Although the whole sequence thins toward the north, the lower unit with high amplitude, continuous reflection progressively thickens relative to the upper unit in that direction. Moreover the northern extremes of the reflections of the lower unit have a somewhat decreased continuity, which could indicate an increasing marginal marine environment to the north. Reflection terminations of the reflections of the upper unit (~Swift) can be detected in this stretch as well.

The *Zuni II – Tejas* interval preserves the general dual character; however, the gross thickness of the succession is significantly less than to the south. Both lower and upper units exhibit a typically alternating transgressive–regressive character. In the lower part, the seismic representation of the two sedimentary environments appears more or less of equal thickness. In the upper part, the regressive environment with

occasional clinoforms and less continuous reflections get thicker relative to the transgressive interval, mirroring the increasing terrigenous material in the basin.

The **structure** of this area is obviously similar to that of the neighboring part of the NS I section. North of the asymmetric, downward tightening fold, a normal fault can be detected. This fault appears also on the parallel part of the NS I line, suggesting an east-west striking and southerly dipping fault.

An additional fault, with similar normal displacement can be clearly identified close to the northern end of the profile. This arrangement of faults underlines the extensional nature of the faults in the flanks of the basin.

6.5 NS II line

The last 400-km long NS II regional seismic profile ***(Fig. 6.14)***, like its NS I counterpart, exhibits a similar asymmetric character, with a steeper northern flank. It runs right from the American side of the international border, traversing the state of North Dakota, to South Dakota. Overall, the basin in this cross section is narrower and the total sedimentary column is thinner than in the previous north-south profile. This is due to the relatively more marginal position of this profile. Nevertheless, the structures along this profile are apparently larger than those in NS I or CA I. Unfortunately, there is a 62-km gap in the deepest part of the section. The section can be divided into a ***"Northern part"*** and ***"Southern part"*** relative to this gap.

6.5.1 Northern part

This part in the northern flank of the basin covers ~110 km distance ***(Figs. 6.15.a, b)***. Correlation from the two east-west profiles and the three deep wells along this interval allow a reliable interpretation.

The top of the *basement* can be identified as a continuous, positive, high-amplitude reflector throughout the area.

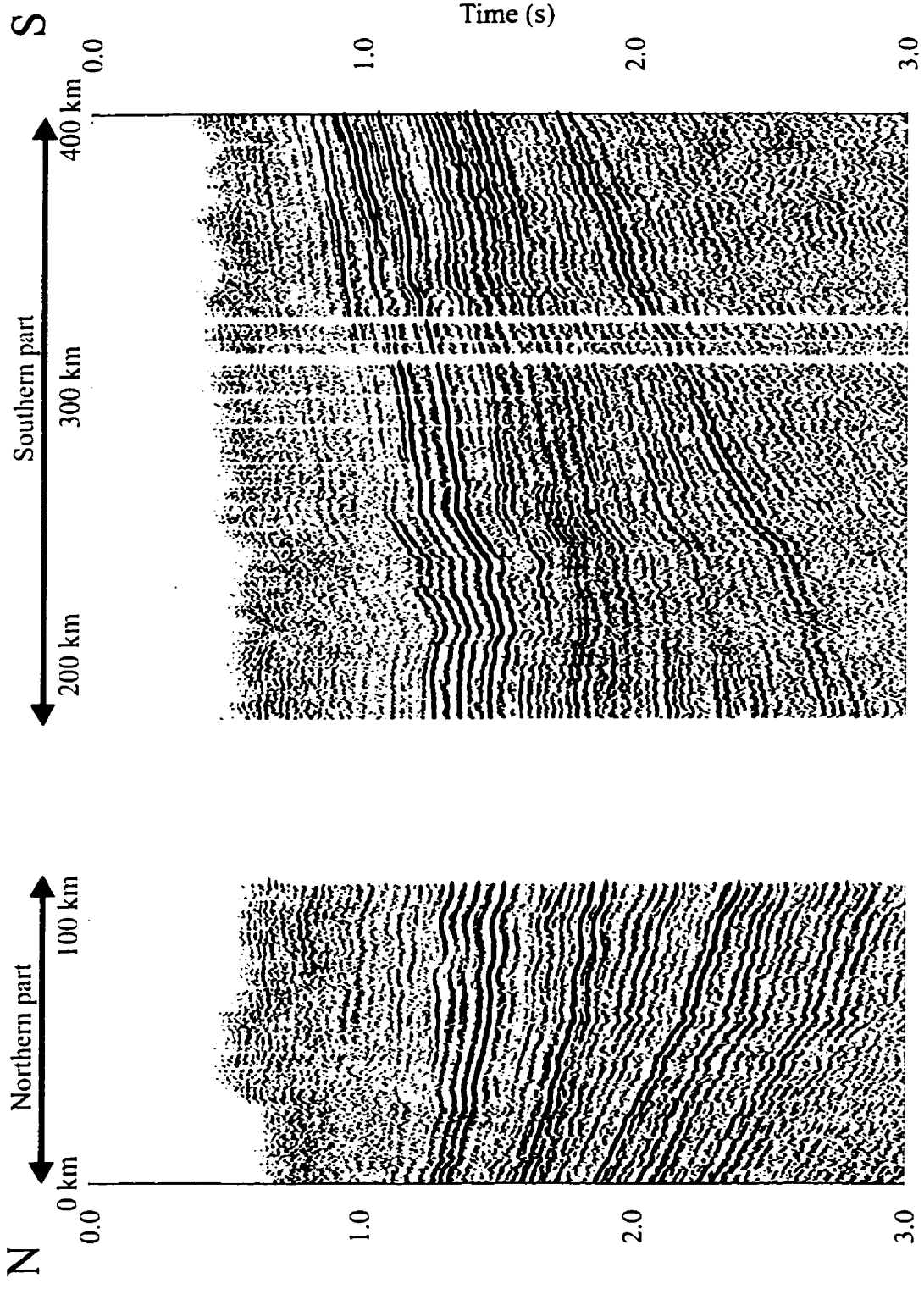

Fig. 6.14 NS II line.

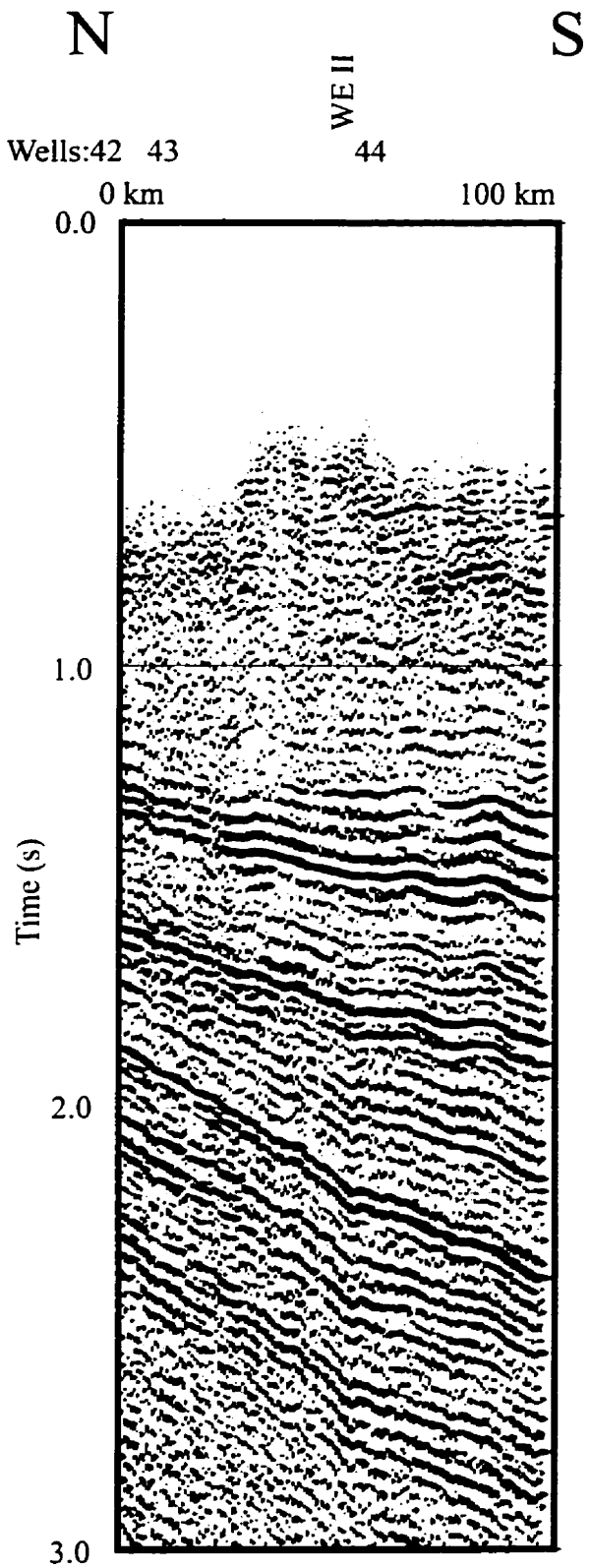

Fig. 6.15.a Line NS II, Williston Basin - northern part, uninterpreted section.

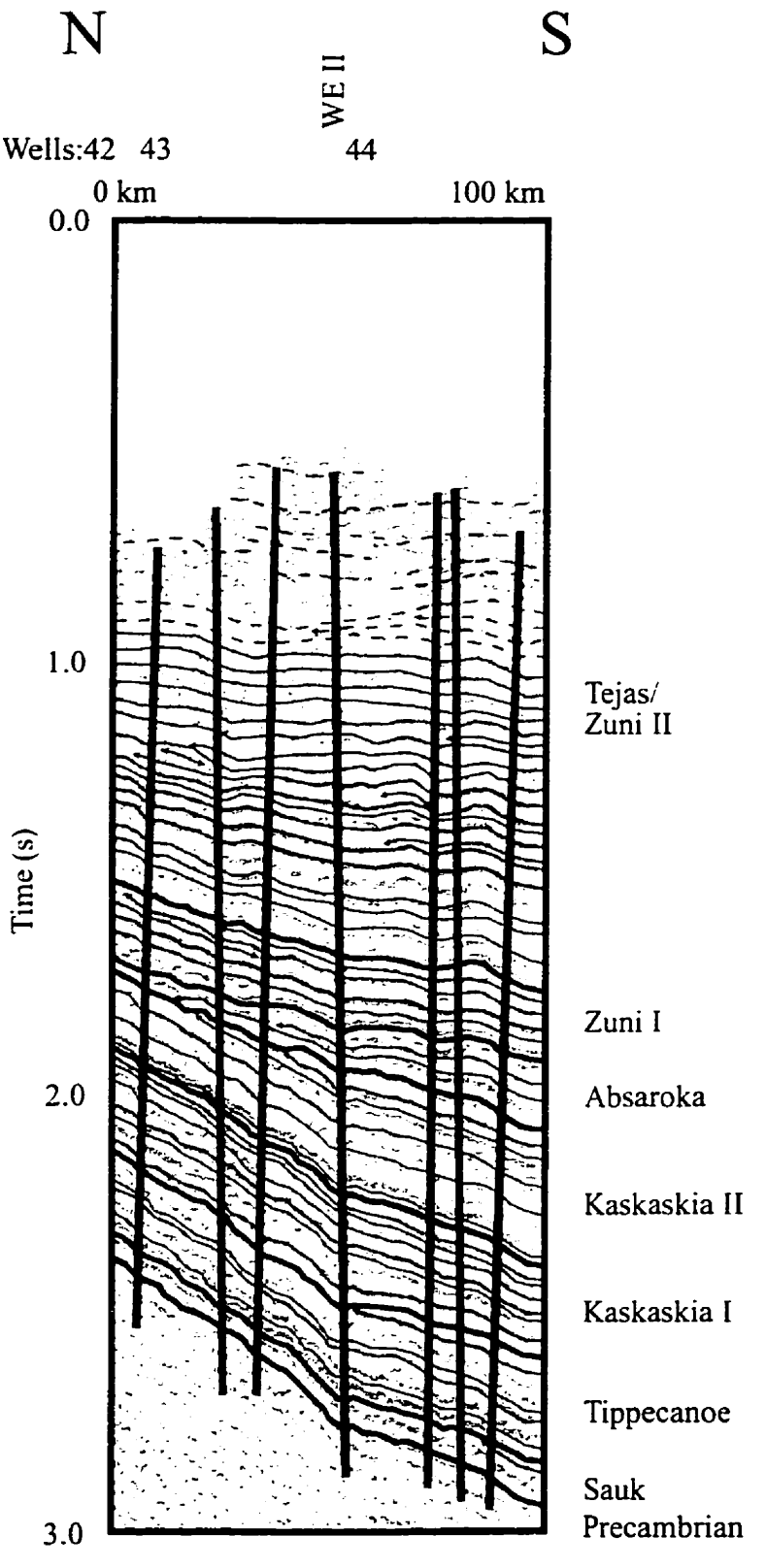

Fig. 6.15.b Line NS II, Williston Basin - northern part, interpretation.

Reflections of the *Sauk Sequence* have good reflection characteristics, but contrary to the other lines, here no onlap termination is apparent against the lower sequence boundary. A truncation type upper reflection termination is detectable in the deeper part suggesting an erosional surface.

The northward thinning *Tippecanoe Sequence* exhibits again an excellent reflection from the Winnipeg–Red River interface. The later reflections have lower continuity and smaller amplitude. Reflection termination against the upper boundary of the Tippecanoe Sequence can be identified in the vicinity of Well 44.

The southward thickening character of the overlying *Kaskaskia I Sequence* reflects well the different tectonic framework of the Elk Point Basin sedimentation. The lower part, the Elk Point Group, appears with superb reflection characteristics. The upper and lower boundaries of the Prairie Evaporite are clearly visible. Reflections from the rest of the sequence exhibit medium-high amplitude character with moderate-good continuity. No apparent reflection termination suggests considerable distance from the erosional edges.

The lowest reflection from the top of the Bakken Formation of the *Kaskaskia II Sequence* is unmistakable. The overlying Madison Group appears with reflections with moderate amplitude and weak-medium continuity, suggesting lateral facies changes in this area as well. Reflections of the upper, Big Snowy part of the sequence terminate against the upper sequence boundary, indicating the erosional edges of the formations of this interval.

The successive *Absaroka Sequence* shows a general wedge shape, with the thicker part to the south. The three units identified elsewhere can be traced in this section as well. The lower unit (~Pennsylvanian) terminates against the lower sequence boundary at Well 43, while the middle unit (~Permian) terminates against the lower unit

south of the same well. The upper unit (~Triassic) covers the whole area thinly and exhibits truncation type reflection terminations against the upper sequence boundary.

The lower part (Piper–Rierdon interval) of the overlying *Zuni I Sequence* displays subparallel, continuous reflections with high amplitude. The upper part (~Swift) exhibits shingled clinoforms with upper and lower reflection terminations, indicating terrigenous input. No obvious source direction can be deduced from this section.

The lower part of the overlying *Zuni II – Tejas* interval shows a subparallel gross character, with alternating continuous, high-amplitude and moderately continuous, medium-amplitude reflections. The upper part is progressively dominated by units with clinoform and less continuous reflections (regressive series). The two major terrigenous sediment source directions, out of the plane of the section (from west), which were identified on NS I, are detectable, but not as apparent as they were there.

The **structures** of this north-south line are more apparent. This is because the folds and structural noses traverse the section at higher angles ***(Figs. 2.13 and 2.23)***, making those structures more obvious. The downward tightening character of these folds is distinct. The fold-bounding faults, as in other central areas of the basin, dip toward the folds' axes and exhibit reverse displacement. The apparently progressively narrower and less asymmetric folds toward the south are the consequence of gradually higher intersection angle of the seismic section and the otherwise basin-center plunging folds.

6.5.2 Southern part

South of the gap, the regional profile stretches across ~220 km ***(Figs. 6.16.a and b)***. Three out of four wells along this section reach the basement. This advantageous information helps to identify the otherwise weak *basement* reflector.

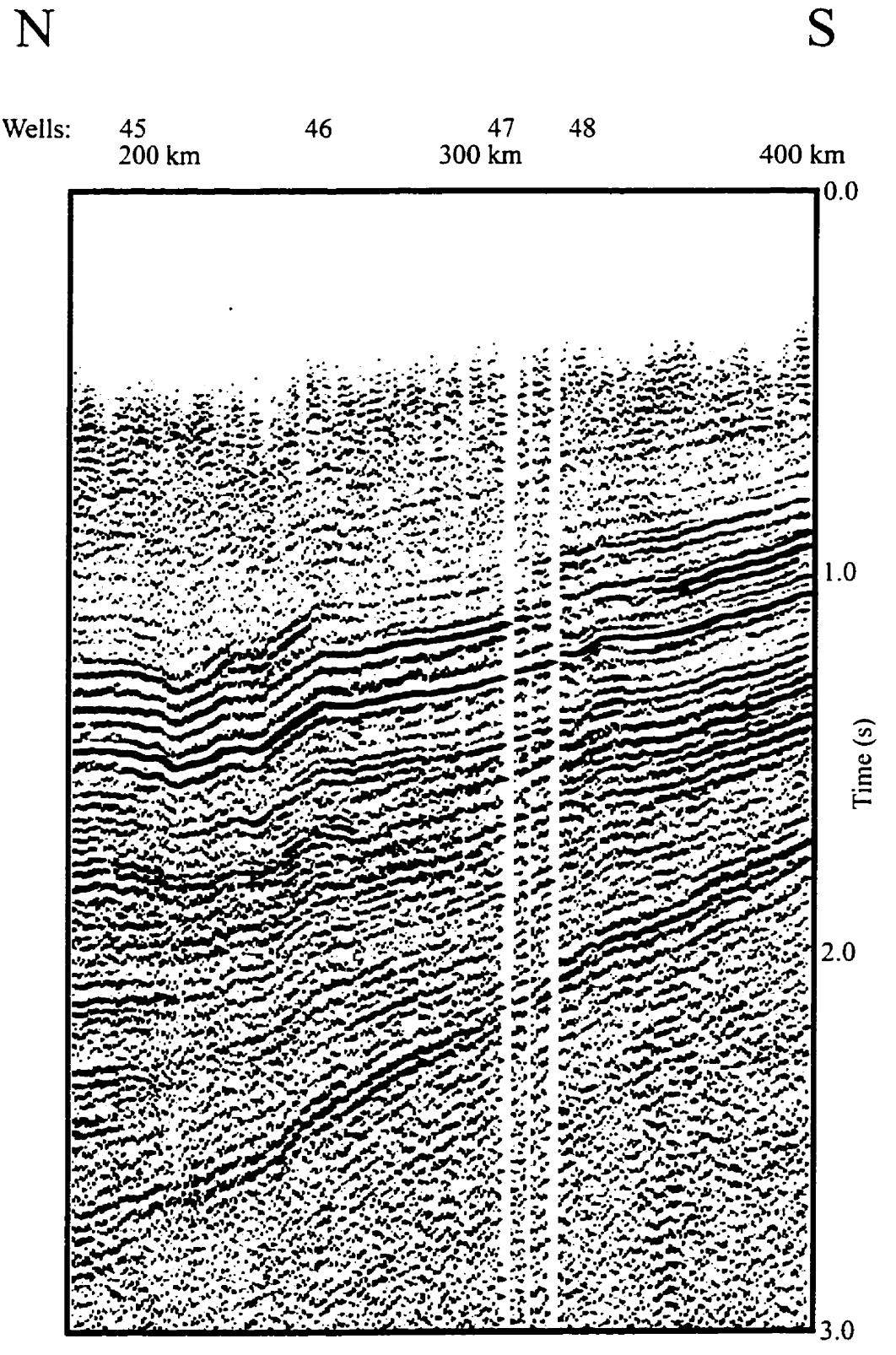

Fig. 6.16.a Line NS II, Williston Basin - southern part, uninterpreted section.

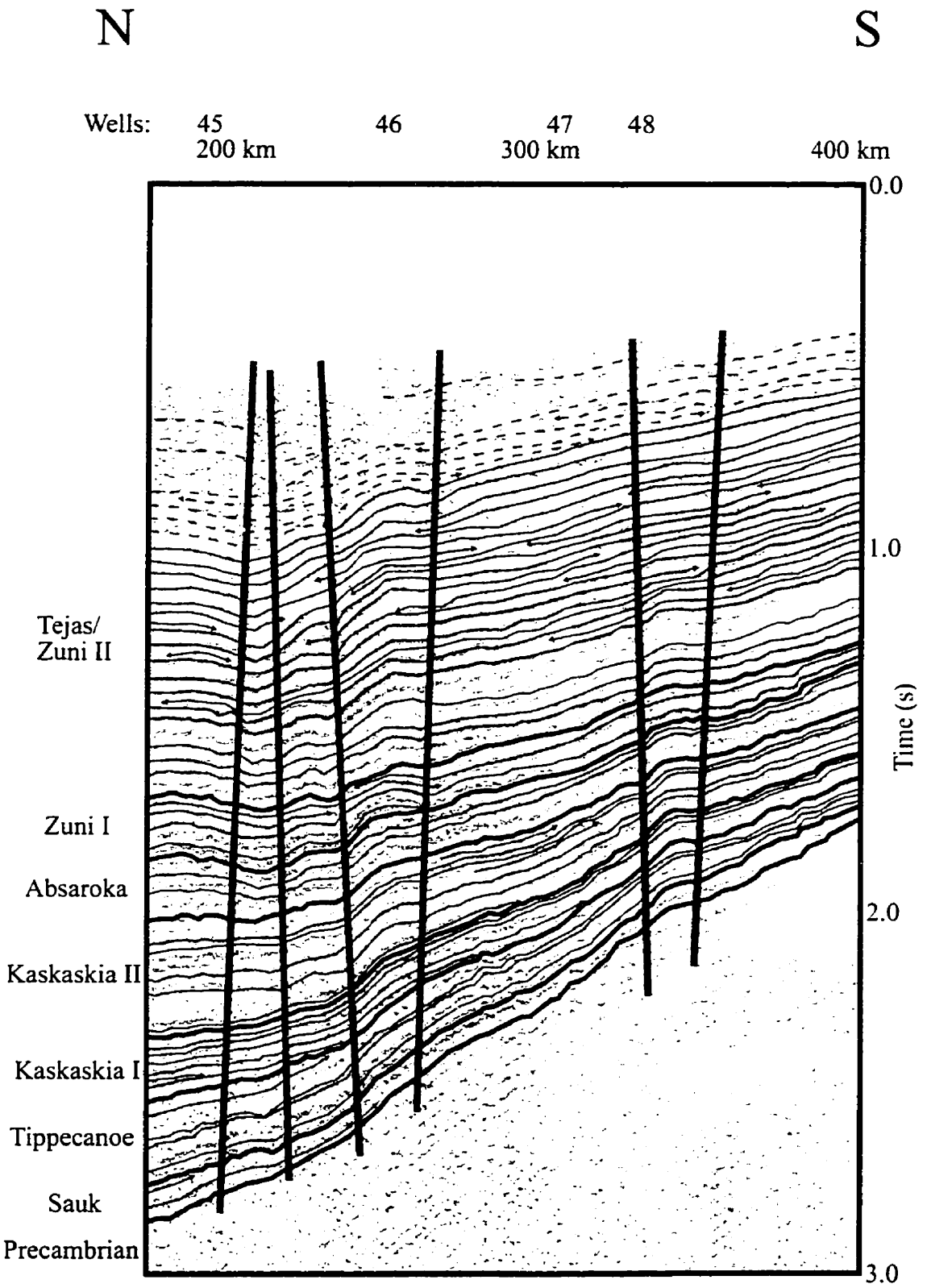

Fig. 6.16.b Line NS II, Williston Basin - southern part, interpretation.

The *Sauk Sequence* contains fairly weak reflections; however, onlap reflection termination against the basement is clearly detectable north of Well 46.

The reflection characteristics of the Winnipeg–Red River interface of the *Tippecanoe Sequence* are still excellent, but toward the south the reflection is somewhat less continuous. The subsequent Tippecanoe reflections have weak continuity and moderate amplitude. Reflection terminations against the upper sequence boundary are detectable in the central part.

The overlying *Kaskaskia I Sequence* thins dramatically toward the south. The lowermost Elk Point Group is present only in the deepest part. The reflection from the top of the Winnipegosis Formation terminates with onlap against the lower sequence boundary north of Well 46. The Prairie Evaporite reflection terminates against the Winnipeg reflection with onlap south of Well 45. The rest of the Kaskaskia I reflections have variable amplitude with medium continuity.

The lower boundary of the successive *Kaskaskia II Sequence* can be easily defined with the help of the reflection from the top of the Bakken Formation. South of the erosional edge of the Bakken (south of Well 47), identification of the sequence boundary is more difficult. Reflections from the Madison part of the sequence are discontinuous and have medium-high amplitudes. Higher amplitudes can be observed in the central part from the interfaces within the Charles Formation. The upper, Big Snowy reflections show a similar range of amplitudes but better continuities than the Madison reflections do. Occasional reflection terminations against the upper sequence boundary indicate an erosional phase.

The three units of the overlying *Absaroka Sequence* can be identified in this area as well; however, no reflection terminations can be identified in this section. The sequence itself gradually thins toward the southern flank of the basin. The reflections have medium-high amplitude and moderate-good continuity.

The *Zuni I Sequence* again exhibits two different characters. The lower part appears with subparallel, high-amplitude, continuous reflectors. Onlap termination is observable against the lower sequence boundary just south of Well 46. The upper part shows up with moderately continuous, good reflections, with clinoforms. Non-directional arrangement of the clinoforms suggests out-of-plane primary sediment influx.

The lower part of the *Zuni II – Tejas* interval exhibits a subparallel reflection pattern. Contrary to the areas to the west of here, the transgressive units dominate and the regressive intervals with shingled clinoforms are subordinate. This arrangement is due to the fact that during this time the area was further away from the terrigenous sediment sources in the west. In the upper part the thickness relation of the transgressive and regressive intervals switched. The regressive units with large clinoforms indicate the final fill up of the basin with sediments eroded from the emerging Rockies.

The **structure** of this stretch is similar to the rest of the areas. Downward tightening folds are recognizable and the fold-bounding faults have reverse displacement.

6.6 Summary of general reflection characteristics in the study area

In large scale, the Paleozoic (~Sauk–Absaroka) strata appear in subparallel, sheet-like continuous reflections indicating a primarily low-energy environment. The reflections virtually coincide with lithostratigraphic units. The Zuni – Tejas interval shows increasing terrigenous influx with a growing amount of clinoform. Reflections do not coincide with lithostratigraphic units. Obviously, within these two mega-scale subdivisions there are intervals which deviate from the general character of the given unit.

The Precambrian *basement* reflector is variable in the study area. In some places it is fairly easy to trace, in other places it can be identified with the help of synthetic seismograms and correlation from traversing sections.

The *Sauk* reflections are distinguishable and they exhibit numerous onlaps against the basement. These indicate the general direction of the transgression and in some places delineate "islands" *(Lochman-Balk and Wilson, 1967)*. The upper sequence boundary is more easily identified in the western part where there is a sharp lithic contact between the strata above and below the boundary (Deadwood–Winnipeg). In the east where the lithology is similar *(Lochman-Balk and Wilson, 1967)*, the upper sequence boundary can be delineated with the help of the lowermost Tippecanoe reflection.

This *Tippecanoe* reflection is the Winnipeg–Red River interface, which exhibits excellent reflection characteristics where it is present. The rest of the Tippecanoe reflections are fairly continuous and reflection terminations against the upper sequence boundary in the central part of the basin are frequent in most profiles.

The different paleotectonic configuration of the *Kaskaskia I Sequence* is identifiable on the regional profiles. The southeasterly direction of the transgression of the Elk Point Sea is clearly traceable with progressive onlaps in this direction. Reflections, in general, have good continuity and high amplitude. Exceptionally good reflections can be detected from the upper and lower boundaries of the Prairie Evaporite.

The lower sequence boundary of the overlying *Kaskaskia II Sequence* is easily traceable where the Bakken Formation is present, with its superb reflection characteristics. Where the Bakken is not present, the identification of the sequence boundary is somewhat more difficult; however, synthetic seismograms help a great deal. Reflections of the Lodgepole and Mission Canyon parts of the Madison Group are less

continuous in most places. Contrary to the lower parts of the Madison, the upper part (Charles Formation) appears with high amplitude, continuous reflections. Reflections of the uppermost part of the Kaskaskia II Sequence, the Big Snowy Group, are distinguishable from the Madison reflections by the different nature of their reflections and by onlap reflection terminations against a surface separating the Big Snowy and Madison units. The extent and the transgression direction of the Big Snowy Group are clearly identifiable and its increased thickness in the Central Montana Trough is apparent.

The *Absaroka Sequence* is fairly thin in the whole area, but its tripartite system is identifiable especially in the central part of the Williston Basin. There is no internal reflection distinguishable from the lowermost two units (~Pennsylvanian, Permian) and they are limited to the very central and southern areas of the basin. The upper unit (~Triassic) covers a much larger area and exhibits numerous truncation type reflection terminations against the upper sequence boundary, indicating widespread erosion.

The pattern of sedimentation changes in the *Zuni I* interval. No clear correlation can be made between reflections and lithological boundaries. Reflection terminations delineate transgressive and regressive intervals. In the Zuni I the thickness ratio of these intervals is more or less equal. The transgressive series are identified with more continuous and higher-amplitude reflections, while the regressive series show a primarily shingled clinoform character.

The *Zuni II – Tejas* interval is similar to Zuni I; however, in the upper part the regressive units are increasingly thicker. In some of the regressive series, the internal seismic characteristics (clinoforms) suggest a prograding-delta sedimentary environment. In large scale, the source direction from the west is apparent and in an interval two major sources can be distinguished with the help of north-south profiles.

6.7 Summary of the structures in the study area

Regional seismic profiles are fundamental to establishing the regional character of folds and faults. Additional regional seismic profiles in different directions further improve the understanding of the structural interrelationships by supplying a quasi-three-dimensional framework.

The fundamental importance of the structural interpretation of the regional sections is that in the central part of the basin all of them show contractional deformation expressed by folds, which are bounded by faults with reverse displacement. These faults dip toward the axial traces of the folds they bound ***(Figs. 6.4.a and b; 6.5.a and b; 6.7.a and b; 6.8.a and b; 6.10.a and b; 6.11.a and b; 6.13.a and b; 6.14.a and b; 6.15.a and b)***.

The directions of the folds are in accord with the structural maps of the area. The folds generally plunge toward the basement center. Asymmetry of the folds on the seismic profiles is apparent, due to the varying angle between the folds' axes and profile directions.

Another interesting finding is that, in the flanks of the basin, extensional faults can be identified. For instance, where two regional lines are close and parallel (northern end of NS I and CA I), the same normal fault can be identified on both sections ***(Figs. 6.10.a and b; 6.13.a and b)***. This indicates that the strike of this normal fault is actually circumferential with the oval-shaped Williston Basin.

In the western end of WE II, where no other regional profile runs close, no quasi-three-dimensional picture can be given. Nevertheless, the interpretation is in harmony with the regional geology. Thrust faults in the Foothills, major regional trends (Pendroy fault, Scapegoat–Bannatyne trend) and structures (Sweetgrass Arch, Bearpaw Mountains) are all identified.

CHAPTER 7

TECTONOSTRATIGRAPHIC SYNTHESIS AND BASIN EVOLUTION MODEL

A synthesis of the interpretation will be conducted in two main steps. The first addresses the large-scale tectonic evolution of the basin as a whole. The model proposed here is based primarily on the reprocessed regional seismic sections obtained in this study and the available (public domain) structural information of the basin at various scales (local, sub-regional structural and thickness maps, earthquake data, etc.). The second will elucidate the gross sequence stratigraphic character of the Zuni – Tejas interval, which represents the significantly larger part of the Phanerozoic sedimentary succession of the Williston Basin and its adjacent areas.

7.1 Tectonic evolution of the Williston Basin area

It is widely recognized that the tectonic evolution of the Williston Basin area can be subdivided into two major phases: the Sauk–Absaroka intracratonic basin phase, and the Zuni–Tejas foreland basin phase. These two phases left fundamentally different structural marks on the basin as a whole. Their structural expressions (faults, folds and structural noses) can be observed in the basin. Analysis of the structural attitudes of these features can shed light on the tectonic forces which caused them. ***Fig. 7.1*** shows a compilation of axial traces of folds and structural noses in the basin. Most of the folds and noses experienced recurrent movement throughout the Phanerozoic.Clearly the map is not complete. During the compilation from numerous public-domain sources (oilfield maps, sub-regional maps, scientific papers, etc.), effort was made to collect the original data. Special attention was given to exclude interpreted data since in many instances the

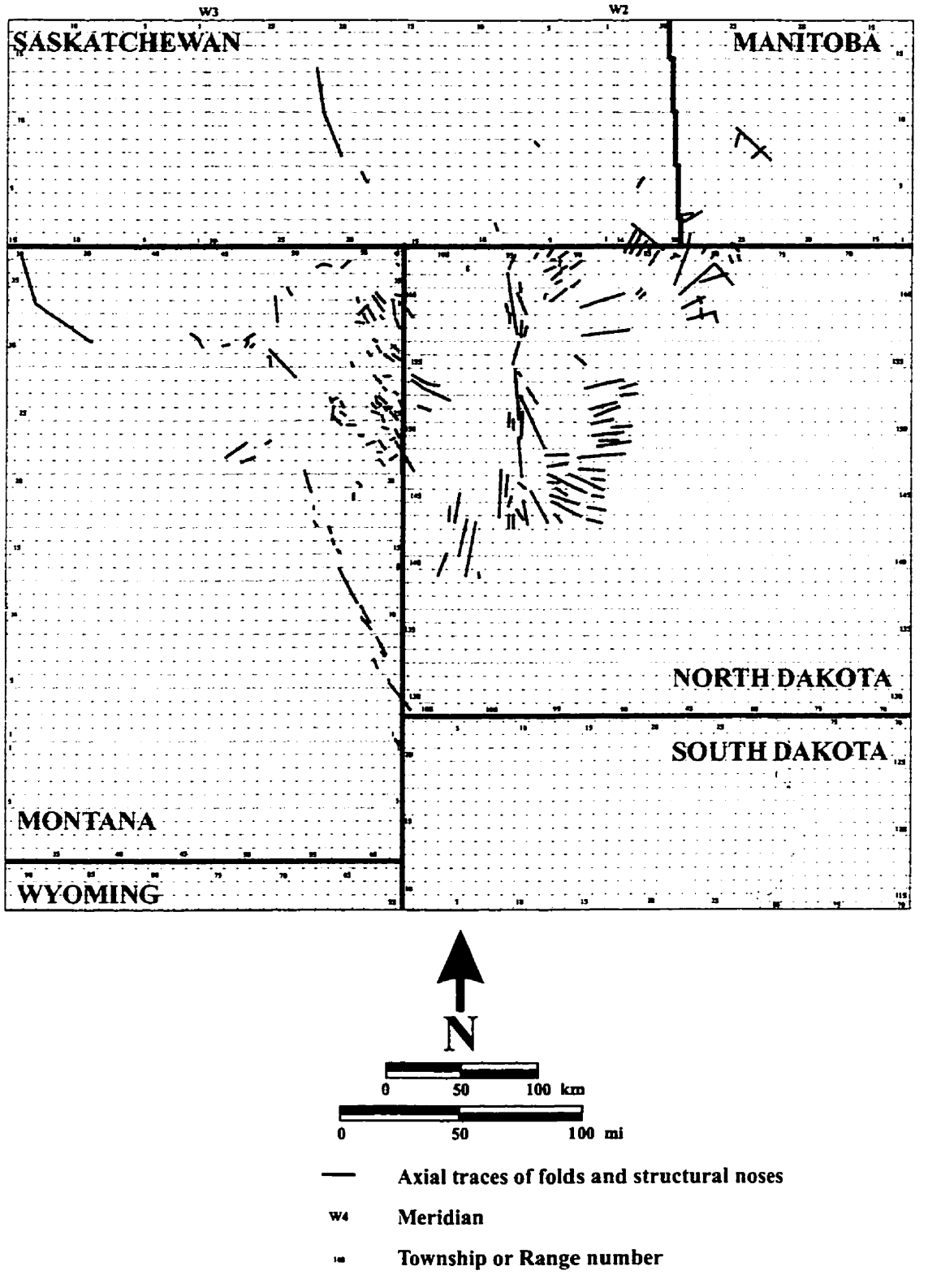

Fig. 7.1 A compilation of fold trends in the Williston Basin.

indicated structural directions had been modified to fit a given tectonic model. Clearly, the structural directions show a complex pattern, and hence cannot be described as a simple structural consequence of the NW-SE/NE-SW conjugate set of basement faults. More careful analysis reveals that the gross pattern of the axial traces of these structures shows a recognizable radial pattern centered in west-central North Dakota. This should not be surprising, since this area is located in the deepest part of the generally oval-shaped, axisymmetric Williston Basin. It is necessary, therefore, to address the problem of axisymmetric deformation and its applicability in basin-scale studies, especially in intracratonic basins.

7.1.1 Axisymmetric deformation

Stress states are described conventionally by their components in a Cartesian coordinate system *(Anderson 1951)*. These stress components are the ***vertical stress*** (σ_v), the ***greatest horizontal stress*** (σ_H) and the ***least horizontal stress*** (σ_h). Based on the relative magnitudes of stress components in such a system, three, different arrangements of the stresses are possible resulting in three different stress regimes (normal fault regime, strike-slip fault regime and the thrust fault regime).

In an area subjected to axisymmetric deformation this approach can not fully describe the internal deformation of the whole affected area. In this case the polar coordinate system should be used instead of the Cartesian system. Thus the three stresses are the ***vertical stress*** (σ_v), the ***radial stress*** (σ_ψ) and the ***hoop [circumferential, tangential] stress*** (σ_ϕ). The stress directions on a spherical surface, such as the face of the Earth, are shown in ***Fig. 7.2***. Obviously the stress regimes in this system depend on the magnitude of these principal stresses; however, the structural directions are different. A simple example of axisymmetric deformations is the "bar-stool effect" *(Lisle et al., 1990)*, which is the production of radially arranged wrinkles in the upholstery cover when depressed into a basin by the weight of the occupier ***(Fig. 7.3)***. Obviously a more sophisticated analysis is required to apply this effect to cratonic basin subsidence.

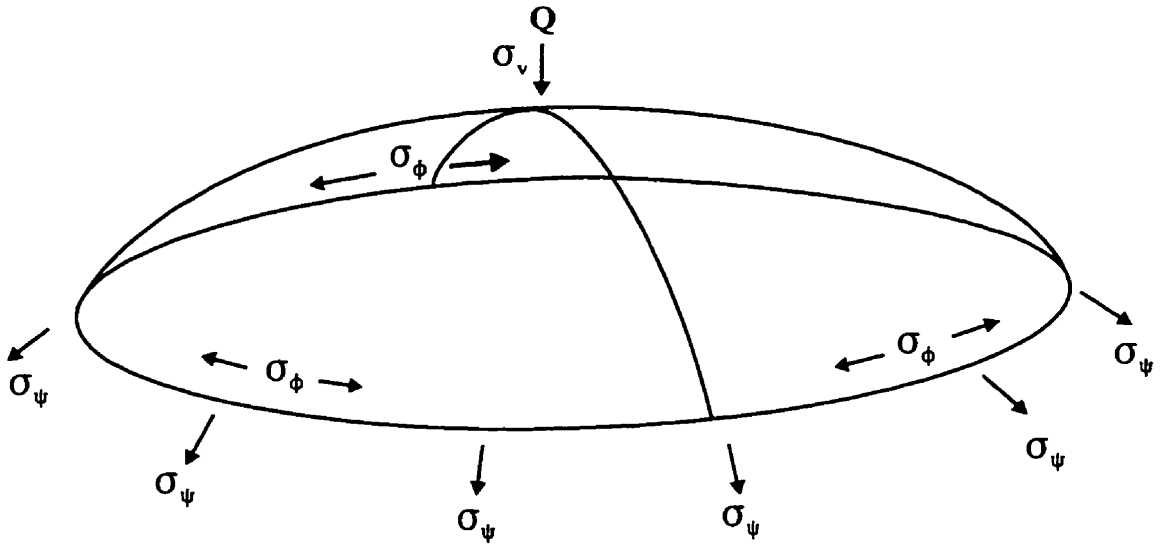

σ_v Vertical stress

σ_ψ Radial stress

σ_ϕ Hoop (circumferential, tangential) stress

Q Axisymmetric load

Fig. 7.2 Stresses in a spherical shell during axisymmetric loading.

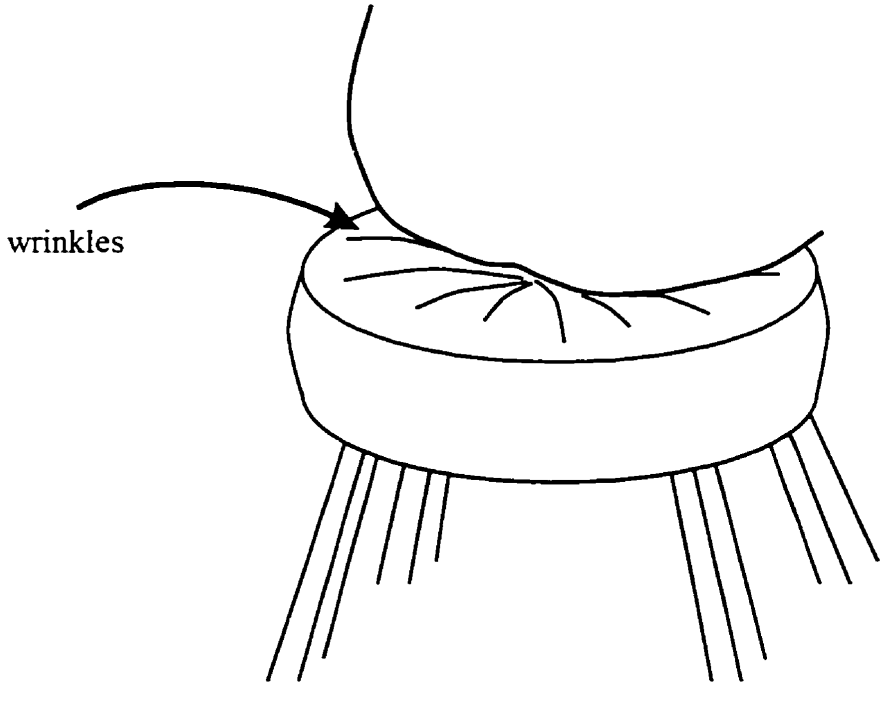

Fig. 7.3 "Bar-stool effect".

7.1.1.1 Similar structures in different environments

Tanimoto *(1997)* showed that unlike displacement, the state of stress is significantly affected by the Earth's sphericity. He also demonstrated that large compressional stresses are produced in subduction zones in the trench-strike direction when the spherical shell is bent downward. These compressional features, consisting of a series of arcs and cusps ***(Fig. 7.4)***, have previously been observed and modeled *(Bayly, 1982; Yamaoka et al., 1986; Yamaoka and Fukao, 1987; Fukao et al., 1987, Yamaoka, 1988)*. These worker all considered these cusps, which strike perpendicularly to the trench, as compressional features that result in buckling of a spherical shells. The compressive stress is largest at the deepest level. A different, extensional stress state occurs in the region where the subducting lithospheric plate is bent down and extended. Normal faults of this region strike parallel to the trench ***(Fig. 7.4)***.

The Earth's sphericity can influence the structural evolution of other tectonic environments. In the continental lithosphere, due to the extended thickness, the effects of sphericity are subtle but identifiable. In the Rocky Mountains Foreland Basin, during the later phases of the Laramide Orogeny, east-west trending uplifts, due to north-south compression, were observed in a general east-west compressional environment *(Gries, 1983)*. Gries *(1983)* ruled out the possibility of the role of strike-slip lineaments on these structural features in Wyoming, Utah and Colorado. The east-west trending uplifts, which in many cases contain hydrocarbons, are generally bounded by reverse (contractional) faults on their northern and southern sides, which dip toward the axial trace of the uplifts (folds). These uplifts can be also considered as buckling longitudinally along the strike of the foreland basin. The uplift and east-west extension of the forebulge area represent a bending-related extensional zone similar to that observed in the oceanic lithosphere ***(Fig. 7.4)***.

Similar to linear or quasi-linear subduction zones and forelands, structural analog can be found in the axisymmetric intracratonic environment. Compressional

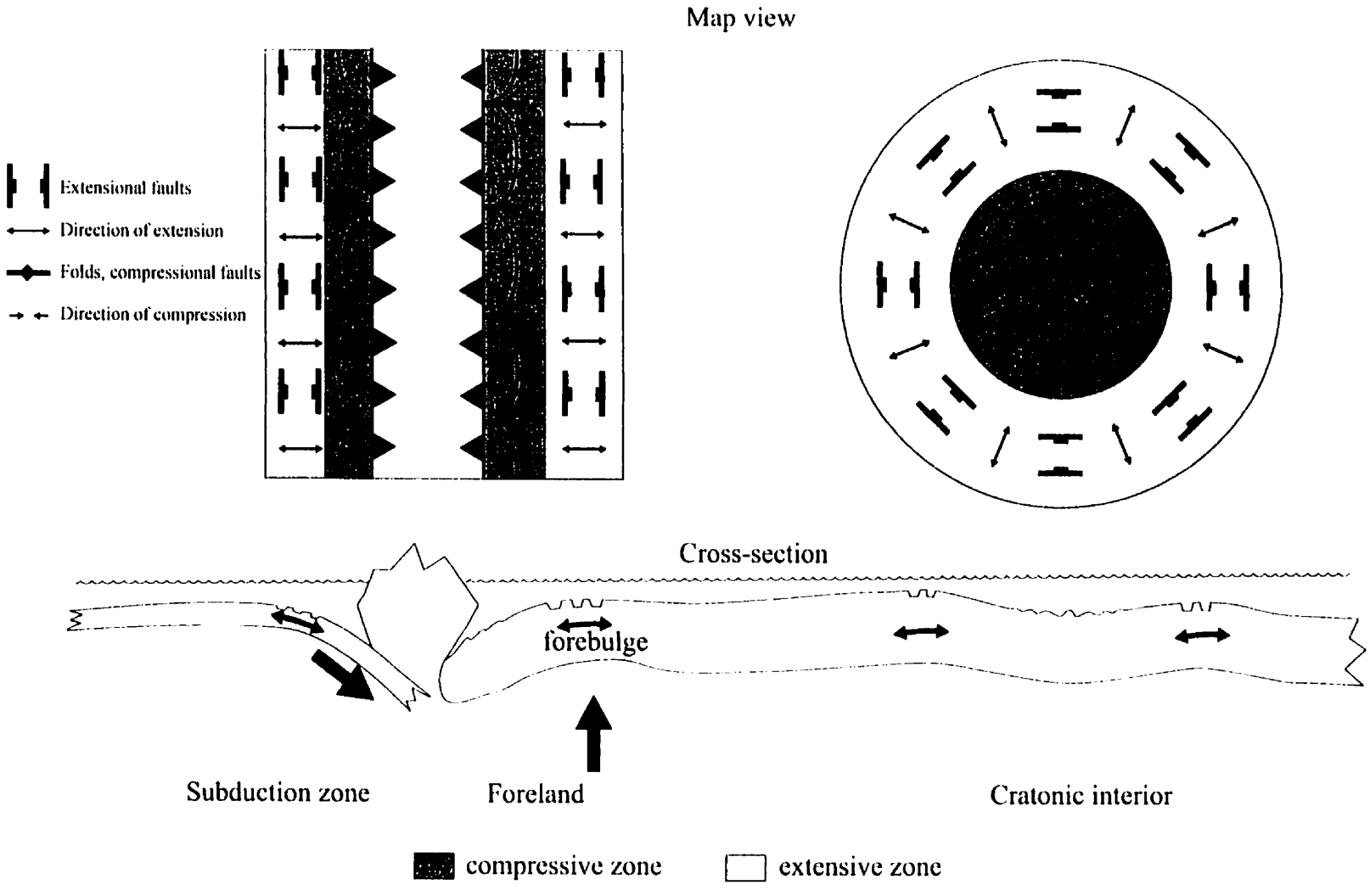

Fig. 7.4 Arrangement of compressive and extensive zones in various tectonic environments.

cusps and uplifts, trending perpendicularly to the subduction zone and foreland, are analogous to the radially arranged folds in the cratonic environment ***(Fig. 7.4)***. The extensional faults striking parallel to a subduction zone and a foreland basin, are analogous to the circularly arranged extensional features at the flanks of a cratonic basins (***Fig. 7.4***; cf. "dynamic rim" of Dallmus *[1958]*, ***Fig. 3.1.b***). The magnitude and extent of these structures in cratonic basins are smaller than those in the foreland (tens of meters vs hundreds of meters).

Both compressional and extensional structural styles are observed in the regional seismic profiles of the Williston Basin. Compressional features in the central region and extensional structures in the flanks can be attributed primarily to axisymmetric deformation. This statement, however, requires further explanation. Numerous mathematical models and analog experiments have addressed the question of deformation due to axisymmetric loading. Axisymmetrically deformed structures are readily observed both on a small/medium scale (domes) and on a planetary scale. On the scale of a large, terrestrial basin, however, this type of deformation was not recognized. The reason for this failure will be described below.

7.1.1.2 Mathematical models of axisymmetric deformation

Mathematical analysis of fault patterns associated with circular domes has shown that radially striking normal faults are expected in the central area, while circumferentially striking thrust faulting is predicted along the flanks together with a zone of intervening strike-slip faults ***(Figs. 7.5.a & b)*** *(Withjack and Scheiner, 1982)*. Janes and Melosh *(1990)* also arrived at the same conclusion and extended the analysis to axisymmetric subsidence. In that case the same structural features are predicted, but in the opposite sense (i.e., radially arranged reverse faults in the central part which are separated by strike-slip faults from the circumferentially arranged normal faults along the flanks ***(Fig. 7.5)***.

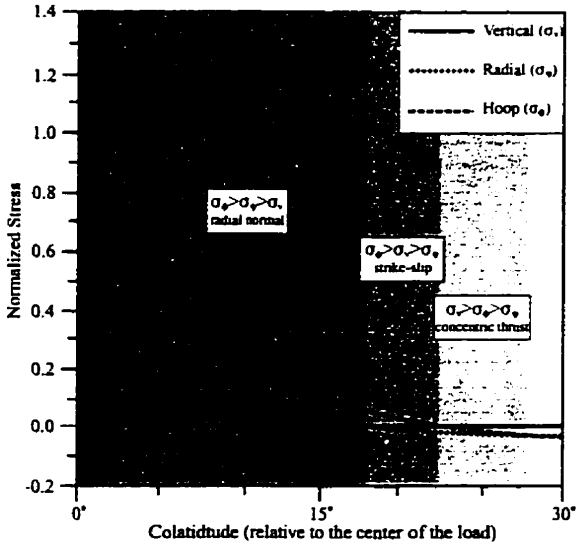

(a)

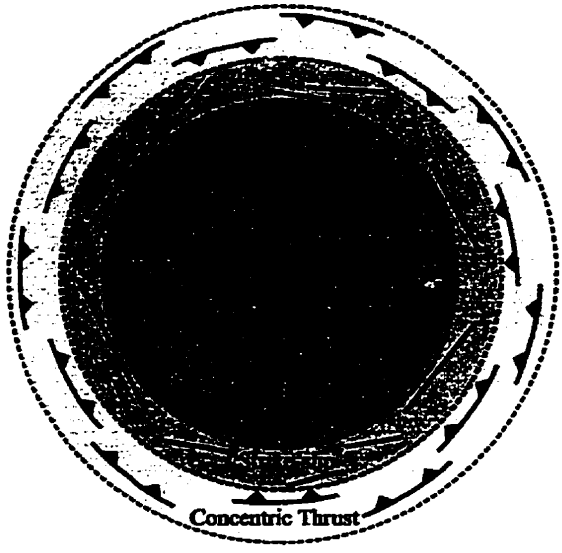

+ : center of the axisymmetric load (uplift)

(b)

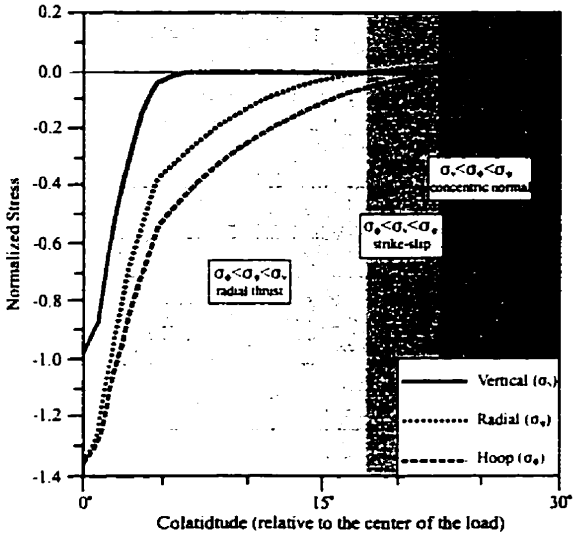

(c)

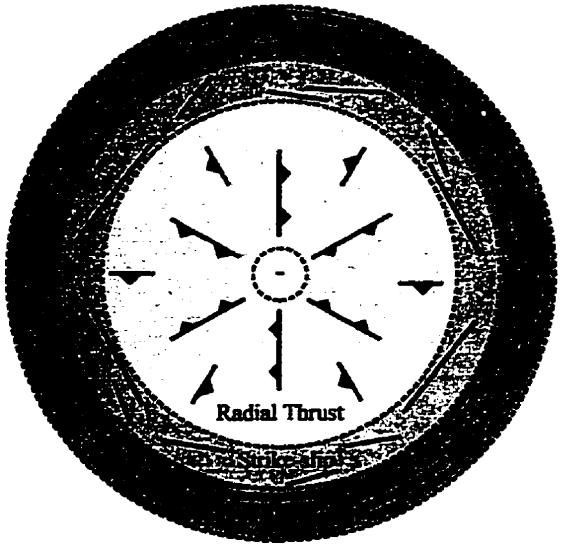

- : center of the axisymmetric load (subsidence)

(d)

Fig. 7.5 Conceptual model for development of structural features due to axisymmetric lithospheric load (adapted from Janes and Melosh, 1990); (a) Lithospheric uplift, surface stresses [positive-extension], (b) Tectonic styles associated with axisymmetric uplift, (c) Subsidence, surface stresses [negative-compression], (d) Tectonic styles associated with axisymmetric subsidence.

Schultz and Zuber *(1994)* showed theoretically that the annular zone of strike-slip faults around an axisymmetric load cannot exist. Planetary studies confirm this conclusion. They emphasized that a lithosphere with faults should be treated as a plastic material, because the elastic equations are not applicable to a fractured lithosphere.

7.1.1.3 Experimental models of axisymmetric deformation

Experimental models of axisymmetric uplift exhibit radially arranged extensional faults in the central part of the model *(Withjack and Scheiner, 1982)*, but do not show any strike-slip deformation zone, thus confirming the above stated conclusion of Schultz and Zuber (1994). The closest analog experiment to axisymmetric subsidence was conducted by Ghosh and Ramberg *(1968)* and Ghosh et al. *(1995)*.

7.1.1.4 Planetary analogs for axisymmetric deformation and comparison with the Earth

There are numerous planetary analogs of radial and circumferential structures associated with both compressional and extensional stress states due to axisymmetric loading. The well-studied gigantic Tharsis Rise on Mars exhibits radially arranged extensional features due to lithospheric processes ***(Fig. 7.6)***. On Venus, 163 large (radius > 100 km) radial lineament systems of grabens, fissures and fractures have been revealed *(Grosfils and Head, 1994; Ernst et al., 1995)*. According to Grosfils and Head *(1994)*, these radial features were formed by subsurface dyke-swarm emplacement and/or through uplift, while others *(Janes and Squyres, 1993; Koch, 1994; Watters and Janes, 1995)* attribute their existence to structural emplacements above ascending mantle diapirs or mantle blobs. One such example is shown on ***Fig. 7.7***, which illustrates the general radial and circumferential arrangements of the structural features in the central part and in the flanks, respectively. Several comparisons were made by these authors with respect to the Earth. Although numerous large-scale dyke swarms can be found on Earth, they are often dismembered and distorted by plate-tectonic rifting events. Radially fractured domes, on the scale observed on Venus, are virtually unknown on Earth *(Janes and Squyres, 1993)*. One major difference between the two

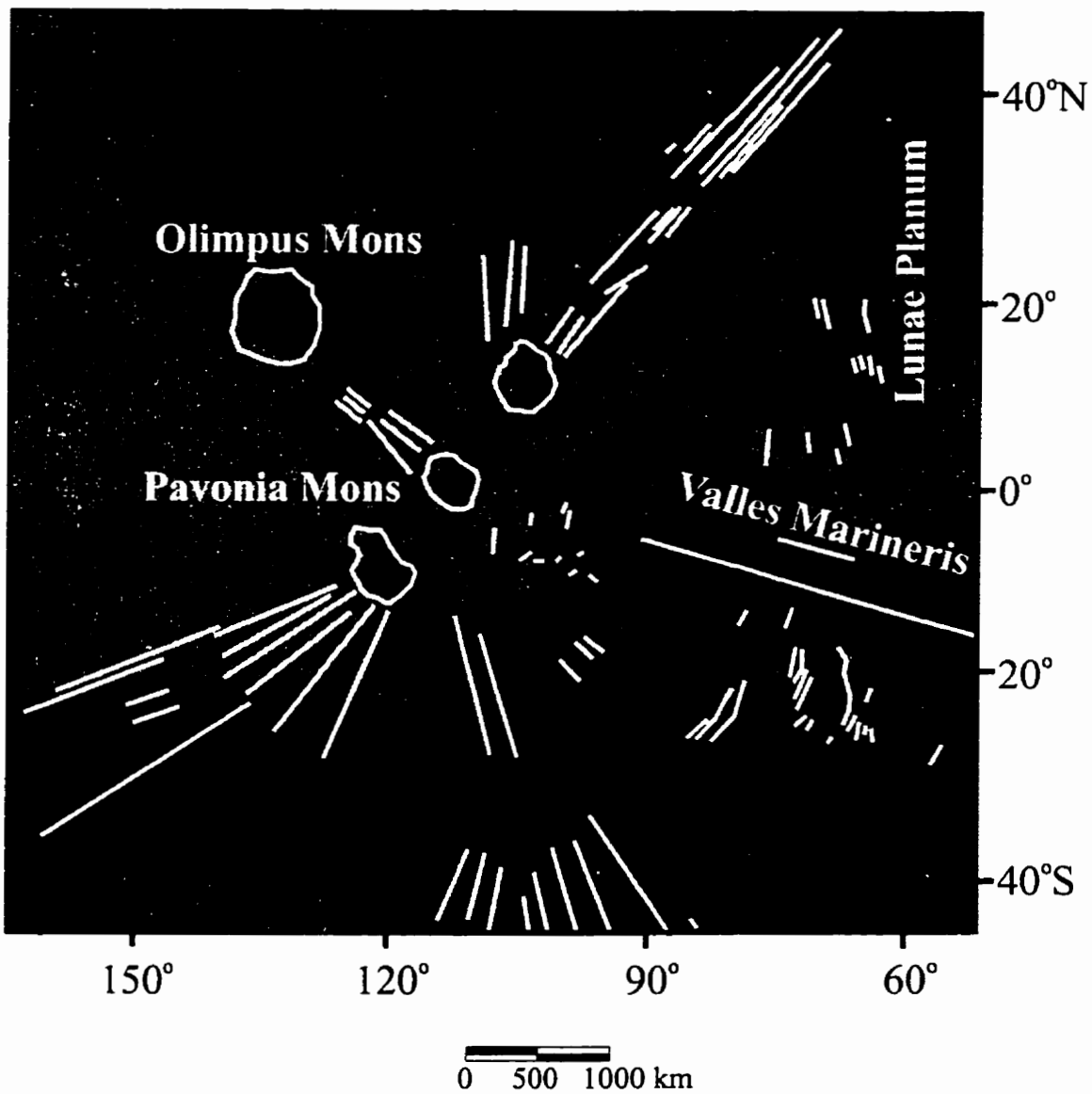

Fig. 7.6 Structures of the Tharsis region, Mars.
(Sleep and Phillips, 1985; Picture source: NASA).

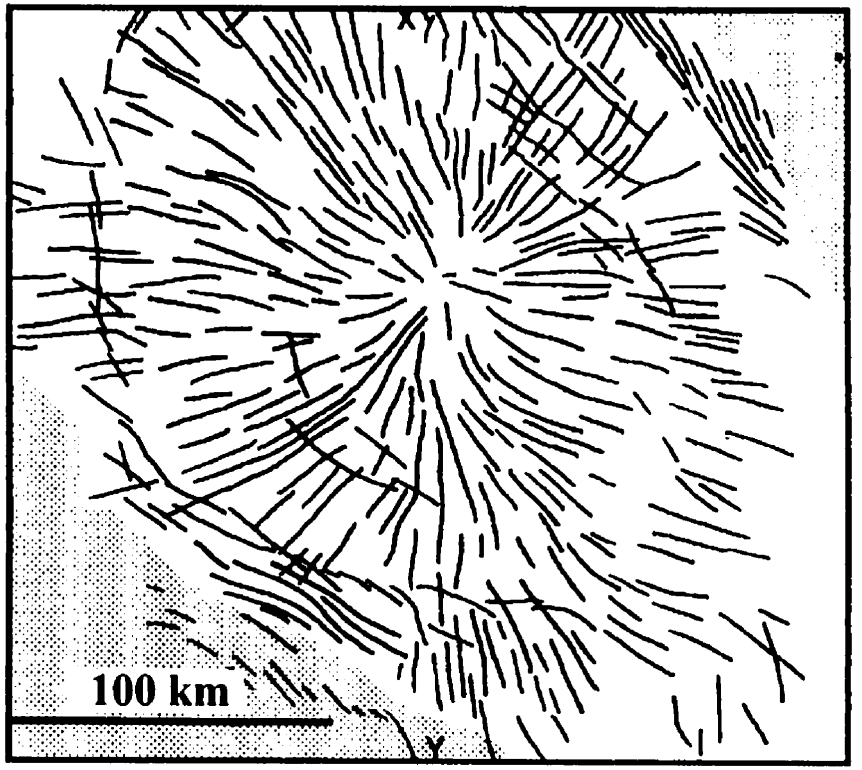

Fig. 7.7 Radial lineament system formed through uplift on Venus. (Grosfils and Head, 1994).

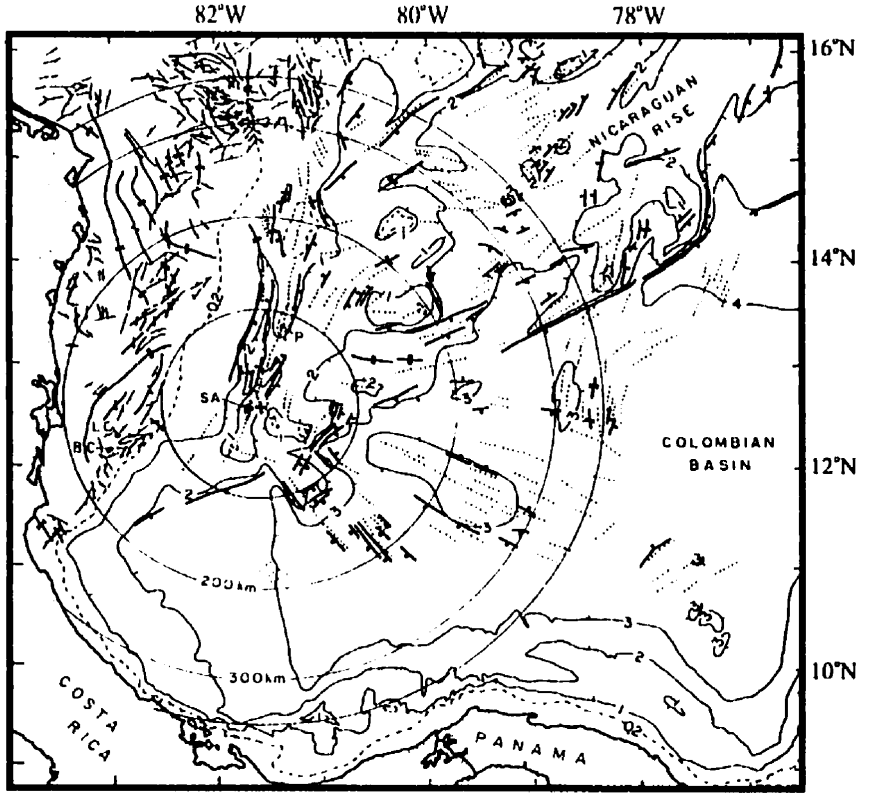

Fig. 7.8 Radial structures in the southwestern Caribbean Sea. (Christofferson and Hamil, 1978).

planets is that Venus was entirely resurfaced 0.5 G.a. ago and lacks any plate tectonic processes (one plate only). This has made it possible to preserve these features, while on Earth the continuous creation and destruction of the crust has erased the remnants of similar structures. Another reason is that, ironically, only 5% of the oceanic sea floor of the Earth, where these structures are primarily expected, has been imaged at a resolution comparable to that obtained for Venus. To date only one area in the oceanic lithosphere (southwestern Caribbean Sea) has been identified as a radially fractured dome *(Christofferson and Hamil, 1978)* ***(Fig.7.8)***.

The obvious locations where these kinds of structural features should be preserved are the intracratonic areas, far from plate tectonically active zones. Here, erosion and the sedimentary cover make it difficult to identify these features. Most of the cratonic basin models require some kind of mantle involvement and uplift for the origin of the cratonic basin ***(Section 3.1)***. The general axisymmetric geometry of these basins is revealed by their oval shape. During cratonic basin subsidence, radial compressive and concentric extensional structures can be expected, due to axisymmetric lithospheric loading *(D.M. Janes, personal communication)*. One of the rare exceptions of radial and circumferential structures is identified by Schultz-Ela et al. *(1994)*. At the Upheaval Dome in Utah they decribed peripheral extensional features and compressive stuctures (radial thrusts) in the core area.

Axisymmetric deformation of cratonic basins must be put in the context of the whole evolution of the basin. First of all, in the present case, it should be determined whether or not the axisymmetric theory is applicable to the Williston Basin. In other words, how circular (axisymmetric) has the basin been throughout its history?

7.1.1.5 Bivariate normal-probability surface approximation of the geometry of the Williston Basin

Establishing the exact limit of the Williston Basin – or, in fact, of any basin – is elusive because of recurrent erosion. This problem of erosion and the resultant

ambiguity concerning the extent of the Williston Basin can be avoided by studying the basin geometry as was done by Scherer *(1973)*, Sloss and Scherer *(1974)* and Sloss *(1987; 1991)*.

Their basic idea (i.e., applying a bivariate normal-probability (or Gaussian) surface to thickness values) was stated in ***Section 3.1.6***. The advantage of this approach is that it is not necessary to know the extent of the basin. Using the basin descriptors, especially the changes in the inflection ellipse, the variations in the shape and extent of the basin for each sequence can be monitored. Here a similar approach has been adopted; however, some important modifications have been incorporated.

Previous workers used digitized thickness maps as the input data, whereas in this study the input data are the thickness values taken directly from the wells, thereby reducing the errors that occur during map creation. Furthermore, the model is extended to each of the major stratigraphic sequences. In contrast, the earlier studies were limited to the Kaskaskia I (Devonian) sequence only. Yet another addition is the inclusion of a linear function to simulate the tilting of the basin area – a step not incorporated in the earlier work cited above.

The primary goal here is to determine both the center of the basin (position of maximum thickness) and the inflection ellipse of a given sequence. The inflection ellipse is considered to be the deformation ellipse, which helps to define how circular (axisymmetric) the basin was during a given stratigraphic sequence. A circle would reflect that axisymmetric deformation is the primary cause of the deformation of the basin; an ellipse would indicate that external (lateral) forces were applied to the basin, and had overprinted and/or replaced the axisymmetric load. The relative changes of the ellipses' parameters for consecutive sequences that are the important measures of tectonic evolution.

Some important points should be stated here. This robust approach yields a rough estimate of the shape of the basin as a whole and should therefore be considered as semi-quantitative. Effects of the internal structures mentioned earlier are obviously disregarded, since the aim here is to determine the change of shape of the basin in a plan view. Using a "flat Earth" model, instead of a spherical surface model is unlikely to pose a problem. The differences are probably minimal, in the range of kilometers.

A special effort was made to collect a reasonable number of thickness values from the map area and as uniformly as possible ***(Fig. 7.9)***. Zero-thickness values, from areas where a given sequence is absent or eroded, are ignored to avoid creating artifacts. Numerous sources, including those in the public domain, were used to obtain these thickness values. These data were then referenced to a rectangular (north-south/west-east) coordinate system.

The bivariate normal-probability (Gaussian) function *(Yule and Kendall, 1950)* with a linear function added is:

$$w = f(x,y) = \frac{1}{2\pi\sigma_1\sigma_2\sqrt{1-\rho^2}}\exp\left\{-\frac{1}{2(1-\rho^2)}\left[\frac{(x-a_1)^2}{\sigma_1^2} - 2\rho\frac{(x-a_1)(y-a_2)}{\sigma_1\sigma_2} + \frac{(y-a_2)^2}{\sigma_2^2}\right]\right\}$$
$$+b_1x+b_2y+c \qquad \text{(Eq. 7.1)}$$

where w is the thickness value; a_1 and a_2 are the x and y coordinates of the center of the subsidence; σ_1 and σ_2 are the distances of the center of the basin and the inflection points in the x and y directions; ϱ is the parameter which indicates the rotation of the principal axes from the x-y coordinate system; b_1 and b_2 are the tilt of the plane in x and y direction and c is a constant. The values are determined by a trial and error forward modelling procedure. The primary goal is to find the parameters of the inflection ellipse, namely the location of the center of the ellipse, the lengths of the principal axes and the angle of rotation of the principal axes with respect to the coordinate system. The location of the center of the ellipse is readily available from ***Eq. 7.1*** as a_1 and a_2. The

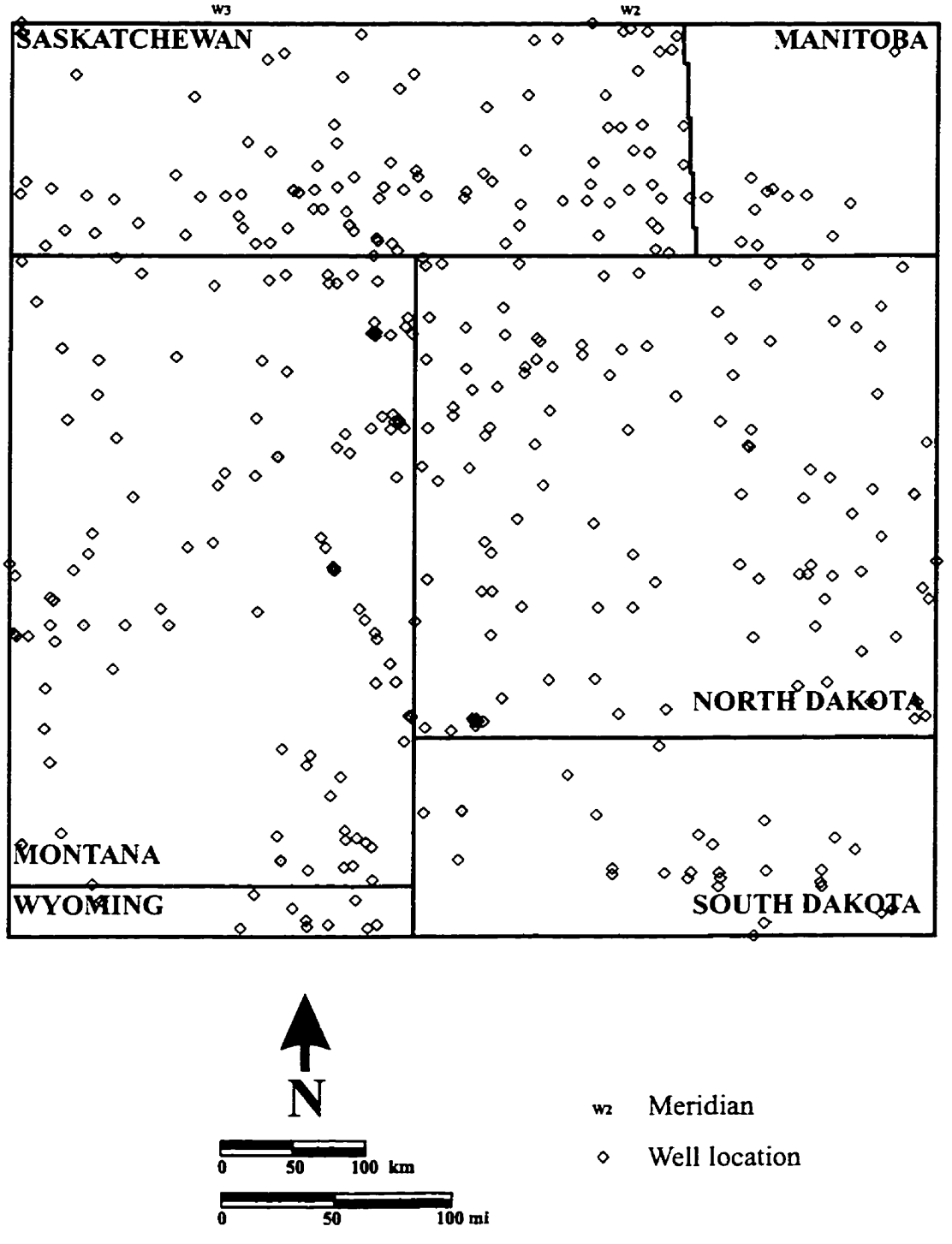

Fig. 7.9 Wells used for normal-probablity basin modeling.

other three parameters can be calculated from the following equations *(Yule and Kendall, 1950)*. The two principal axes (Z_1 and Z_2) of the ellipse and the angle of rotation (Θ) are:

$$Z_1 = \frac{\sqrt{\sigma_1^2 + \sigma_2^2 - 2\sigma_1\sigma_2\sqrt{(1-\rho^2)}} + \sqrt{\sigma_1^2 + \sigma_2^2 + 2\sigma_1\sigma_2\sqrt{(1-\rho^2)}}}{2} \qquad \text{(Eq. 7.2)}$$

$$Z_2 = \frac{\sqrt{\sigma_1^2 + \sigma_2^2 + 2\sigma_1\sigma_2\sqrt{(1-\rho^2)}} - \sqrt{\sigma_1^2 + \sigma_2^2 - 2\sigma_1\sigma_2\sqrt{(1-\rho^2)}}}{2} \qquad \text{(Eq. 7.3)}$$

$$\tan\Theta = \frac{2\rho\sigma_1\sigma_2}{\sigma_1^2 - \sigma_2^2} \qquad \text{(Eq. 7.4)}$$

The results for the seven stratigraphic sequences are shown in ***Figs. 7.10. a-g.*** and ***Fig. 7.11***. When analyzing the results some important observations should be made. As expected, the resulting thickness distributions of the calculated intervals do not show dramatic differences from the thickness maps ***(Figs. 2.3 and 2.4)***. Nevertheless, the results have produce a semi-quantitative solution, which allows some general conclusions to be made concerning the shape of the basin throughout its evolution.

It is obvious that the center of the basin during the Sauk - Absaroka interval, with the notable exception of Kaskaskia I, is located within a small area in west-central North Dakota. This agrees with the results obtained by Ahern and Mrkvicka *(1984)*. The maximum sedimentation in the Zuni I and Zuni II - Tejas sequences is offset to the northwest ***(Figs. 2.4.b-d)***. Nevertheless, the Williston Basin still preserved its character even after it became part of the foreland basin. The principal axes of the ellipses are more or less equal in the Sauk – Absaroka interval, again with the exception of Kaskaskia I. Consequently, the basin shape is circular and the angle of rotation of the principal axes becomes irrevelant. Circularity also means that the primary cause of subsidence during this interval was axisymmetric and no significant lateral force was

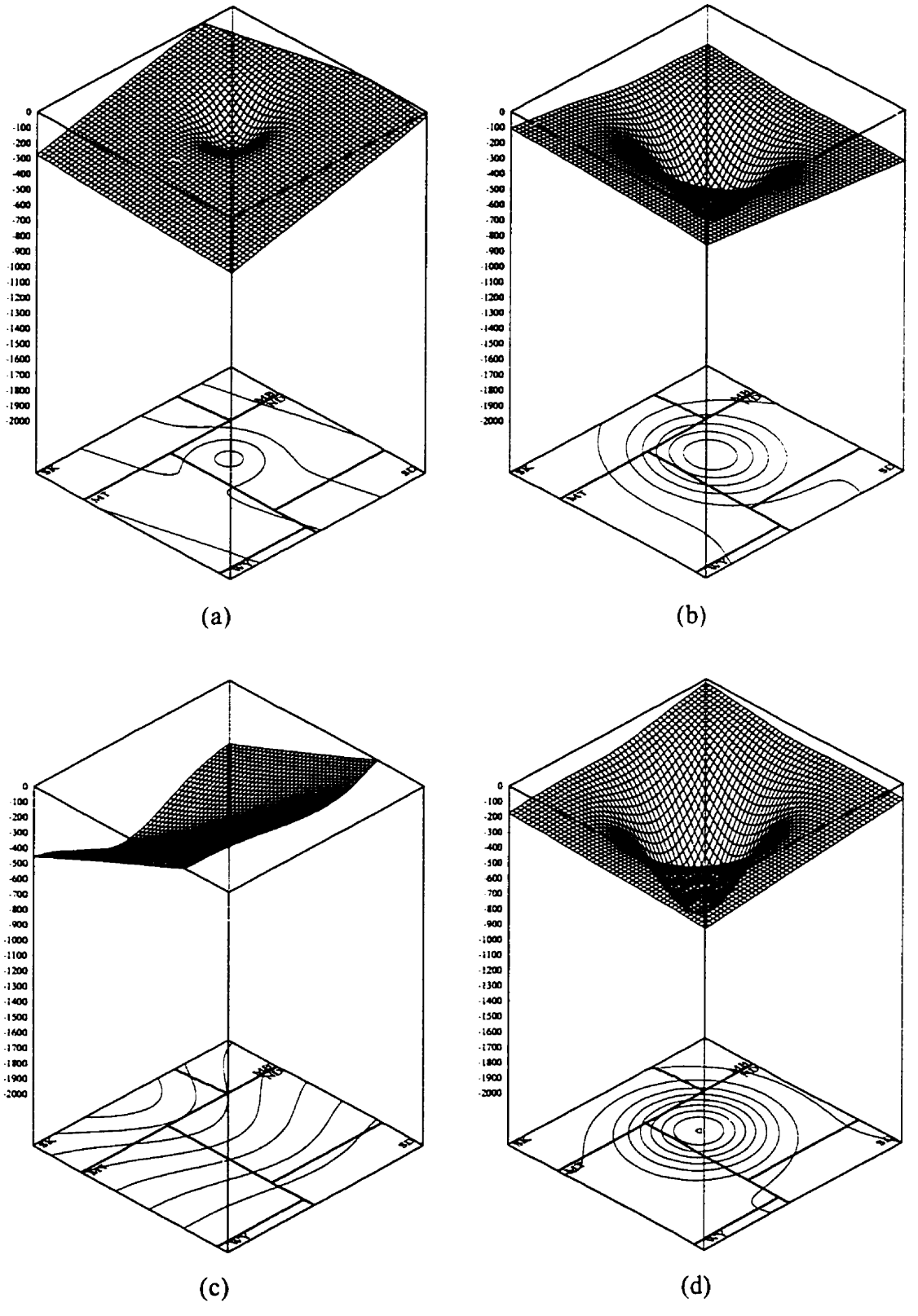

Fig. 7.10 Bivariate normal distribution of the sequences in the Williston Basin. (a) Sauk Sequence; (b) Tippecanoe Sequence; (c) Kaskaskia I Sequence; (d) Kaskaskia II Sequence.

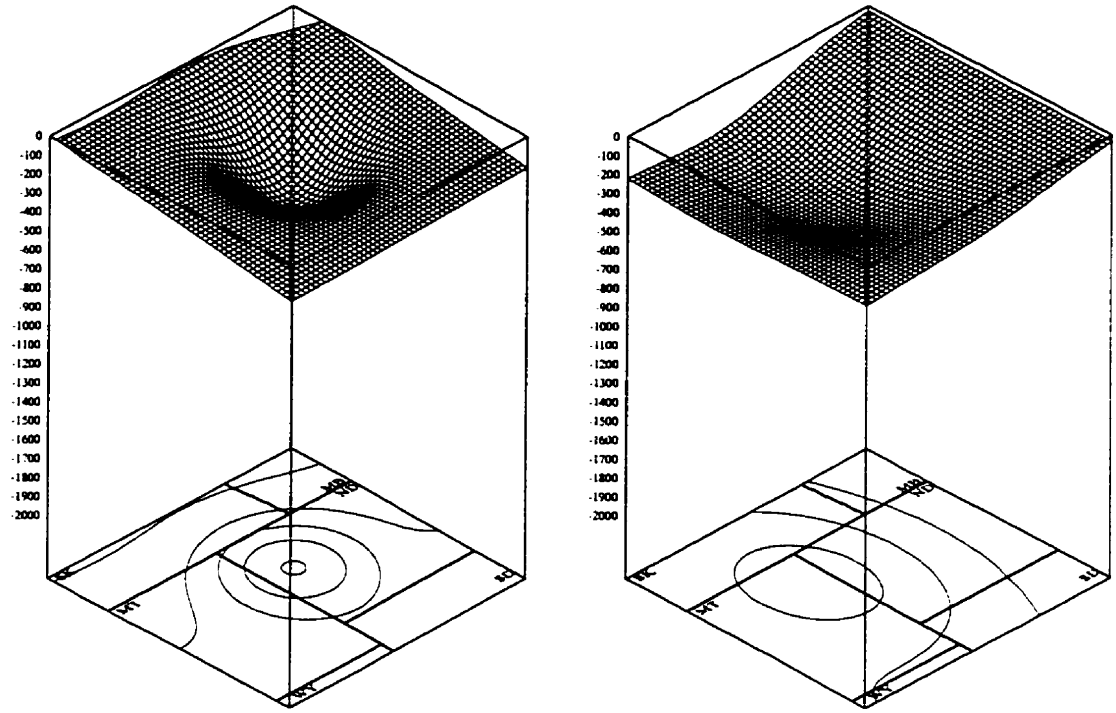

(e) (f)

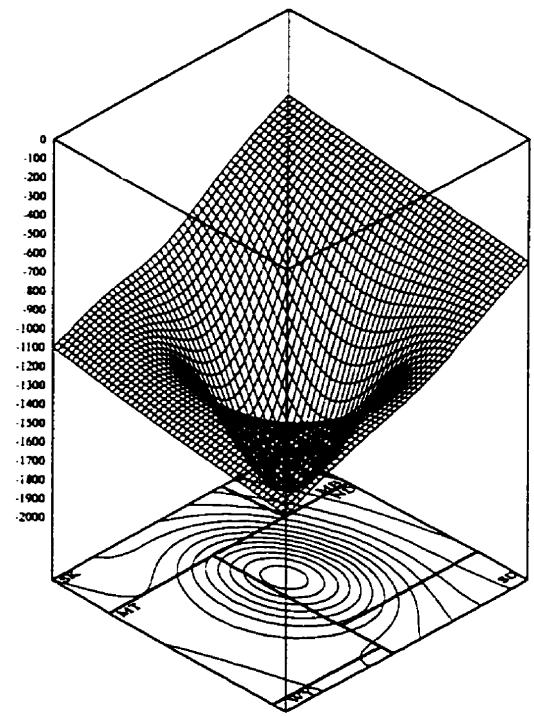

(g)

Fig. 7.10 Bivariate normal distribution of the sequences in the Willston Basin (cont.). (e) Absaroka Sequence; (f) Zuni I Sequence; (g) Zuni II - Tejas interval.

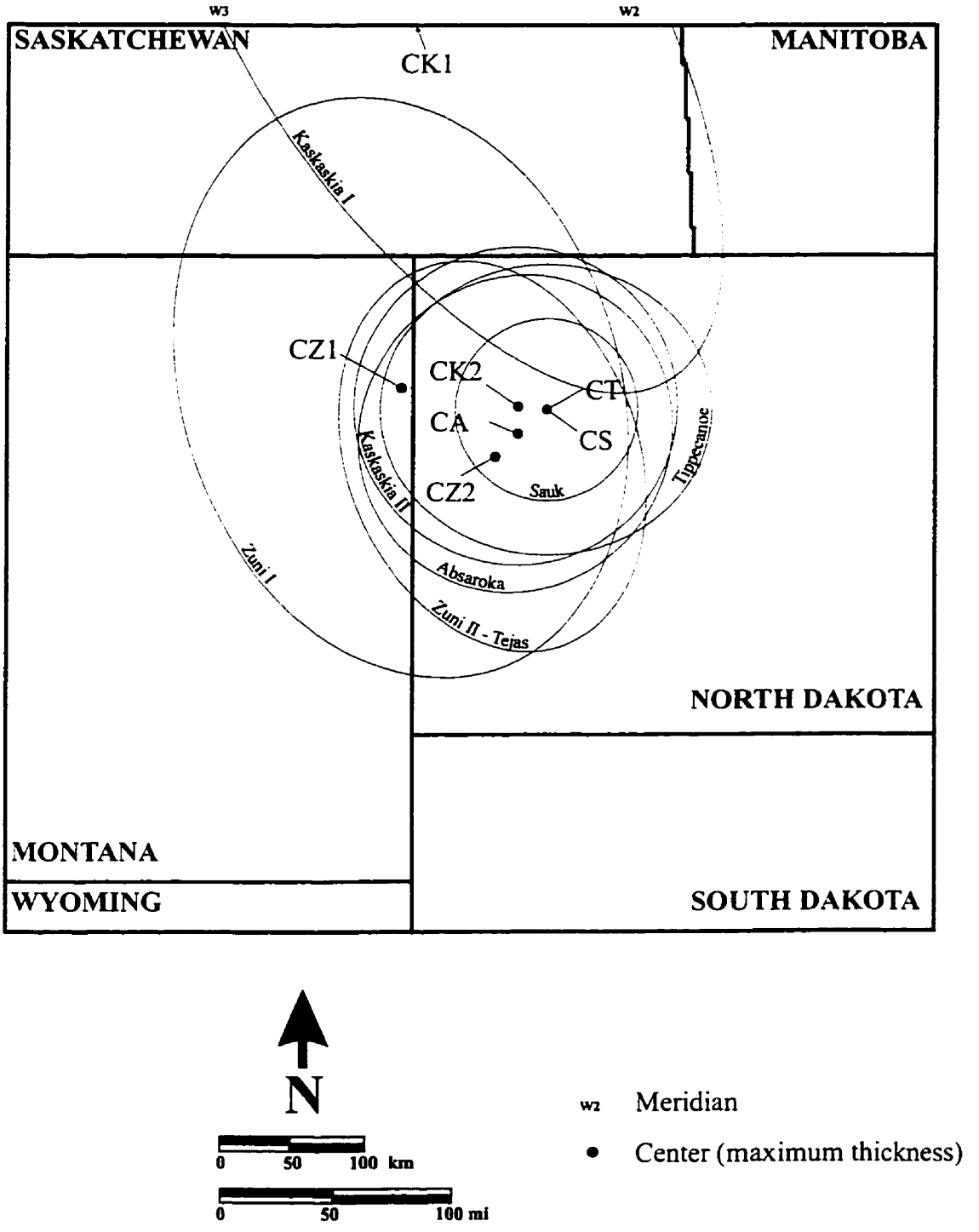

Fig. 7.11 Centers and inflection ellipses of the modeled sequences in the Williston Basin.

applied to the basin. The significant result is that the model invoking a NW/SE – SW/NE set of vertical faults is not applicable during the duration of these sequences.

The notable exception is, of course, the Kaskaskia I Sequence (Devonian), when the basin's configuration is fundamentally different from the bounding sequences. The larger, plate-tectonic causes of the geometry of this "Elk Point Basin" ***(Section 2.1.2.3)*** will not be addressed here, because it requires an analysis of a dataset covering an area far beyond that involved in this study. Nevertheless, uplift of the "Transcontinental Arch" southeast of the basin and/or the accelerated subsidence of the northwestern part of the Elk Point Basin were important in shaping the basin in the study area. These forces overprinted the axisymmetric primary style of the subsidence, which was re-established during the Kaskaskia II Sequence.

Fundamentally different geometry, with a NNW-SSE elongated inflection ellipse during the Zuni I and Zuni II – Tejas intervals, suggests that lateral forces did play an important role in the basin's geometric evolution. These forces are the manifestation of the Sevier and Laramide orogenies, which were accompanied by widespread NW/SE and SW/NE striking faults and a significant tilt of the basin to a WSW direction.

In summary, this modeling exercise has revealed that the primary cause of the subsidence in the Williston Basin area was axisymmetric loading in the Sauk – Absaroka interval (except during Kaskaskia I). This was overprinted by WSW-ENE compressional forces during the Zuni – Tejas period.

7.1.2 Earth-curvature correction of regional profiles

Janes and Melosh *(1990)* showed that the continental lithosphere, deformed by an axisymmetric load, can be described by the "flat Earth" approach for a region up to a 1500-2000 km wide, which gives the same structural zonation as the spherical shell approximation. Nevertheless, the "flat Earth" assumption gives a false perception of large geological structures, like intracratonic basins. These cover considerable areas of

the Earth's surface so that, in a geometrical sense, its curvature cannot be ignored ***(Fig. 3.2)***. ***Figs. 7.12 and 7.13*** give the general shape of a circular basin's basement/sediment contact in two and three dimensions, respectively.

Earth-curvature-corrected regional cross sections across a cratonic basin reveal its true form, which is a crescent shape with the convex side up. This was emphasized by Dallmus *(1958; 1964)* ***(Section 3.1.6)***. For example, in a basin with a 1000-km diameter [~9° of geocentric arc] (range of the Williston Basin) the chord between the opposite ends of the basin at the central part is approximately 20 km below the surface. In contrast, the Williston Basin is ~5.5 km deep in the central part. For this reason all the regional cross sections were depth migrated and corrected for the Earth's curvature. These profiles, with obvious vertical and angular exaggeration ('overcorrected"), are included in the ***Attachment (1-5)*** in the back pocket.

This display of the regional profiles reveals that the sediment/basement contact is actually shorter than the higher horizons and subject to compression during subsidence ***(Fig 3.1.a and b)***. The location of contrasting structural areas (i.e., compression in the central part, extension at the flanks) is apparent in these displays.

Mereu *(1967)* noted that in upper-mantle seismic refraction surveys, neglecting the curvature correction can produce erroneous results for refractors deeper than 10 km. He emphasized that the source of the problem is the incompatibility of "flat Earth" solutions with spherical ray theory.

Earth-curvature-corrected regional cross sections, other than those of Dallmus *(1958)*, are rare. One of the exceptions is the cross section of Nelson et al. *(1964)*. Although it stretches from the British Columbian Pacific margin to the Canadian Shield in Manitoba, no structural conclusion was drawn from the intracratonic portion representing the basin.

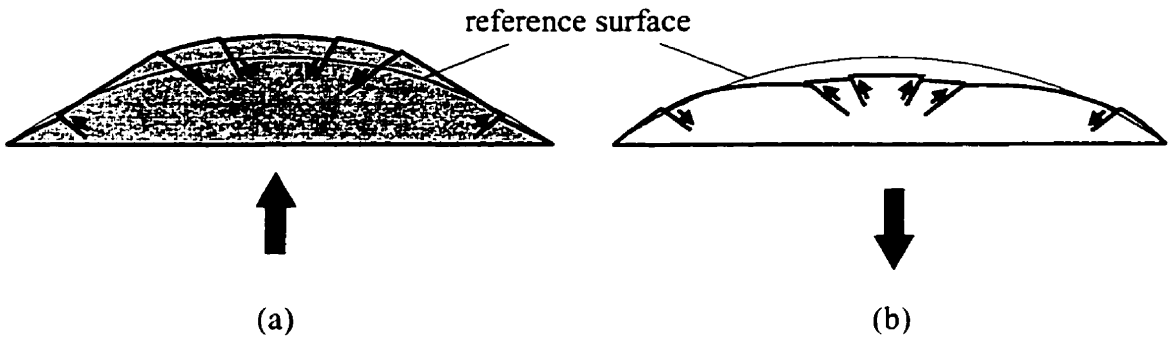

Fig. 7.12 Two-dimensional geometric deformation of a spherical surface.
(a) Uplift; (b) Subsidence.

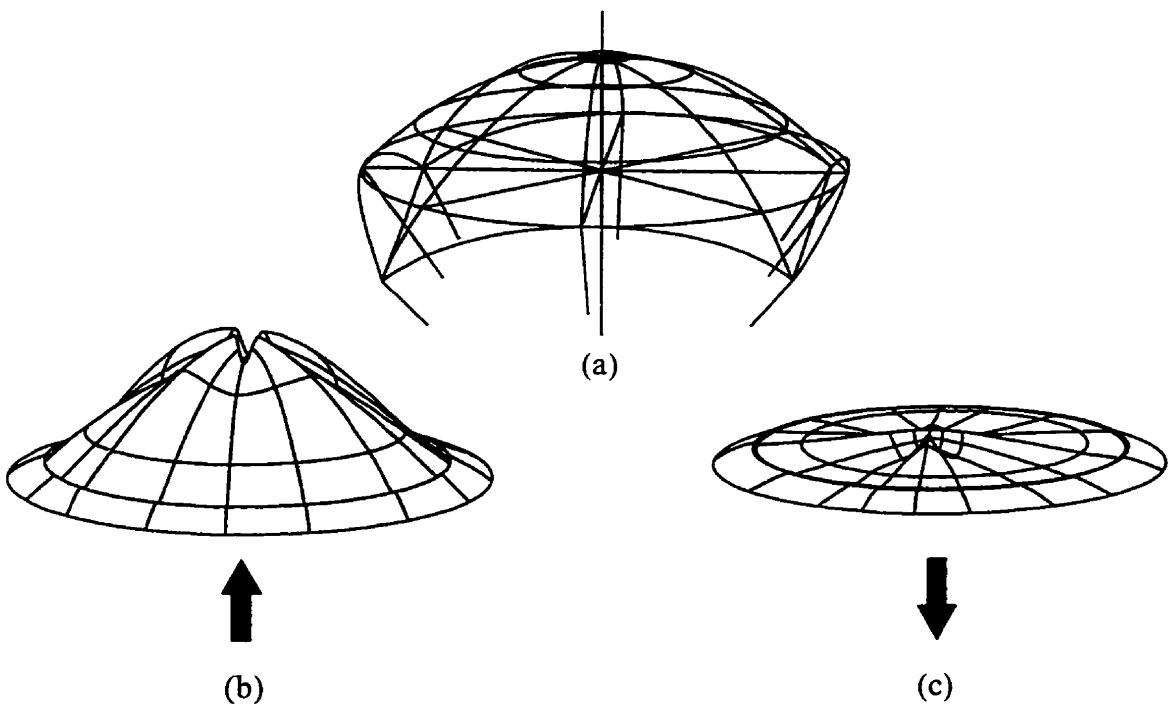

Fig. 7.13 Development of folding on a spherical surface.
(a) Slice of a sphere before uplift or subsidence. (b) Uplift. (c)Subsidence.

It should be emphasized that this study has not only yielded probably the most extensive regional seismic coverage of a cratonic basin but also provided most likely the first regional seismic section across the sedimentary portion of a cratonic basin corrected for the curvature of the Earth.

7.1.3 Interpretation of structures in the Williston Basin

An important result from the bivariate normal distribution modeling of the basin is that the consecutive inflection ellipses during the Sauk – Absaroka interval show a concentric pattern. These ellipses, regarded as tectonic hinge lines by Scherer *(1974)*, can be perceived as the limit of the (radial) compressional central deformation zone and the (concentric) extensional zone at the flanks during axisymmetric deformation. Consequently, there are areas which experienced both types of deformations during the Sauk – Absaroka interval.

7.1.3.1 Compressional structures

The compressional structures (folds, structural noses), which can be observed in the central part of the basin, and identified on maps and regional seismic profiles, plunge to the center of the basin and exhibit a narrowing shape toward that direction ***(Fig. 7.14.a)***. This is to be expected in axisymmetric deformation, since the difference between the more compressive hoop stress (σ_ϕ) and the less compressive radial stress (σ_ψ) increases towards the basin center ***(Figs. 7.5.c, d)***. In cross section, these features are bounded by faults dipping towards the axial plane ***(Fig. 7.14.b)***. In 3D, these bounding faults form helicoidal surfaces ***(Fig. 7.14.c)***. Most of the structures in the central part of the basin are compressional. An example showing these features from the Dwyer Field area (T32N, R58E-R59E) is shown on ***Fig. 7.14.d***.

The largest structure in the basin, the Nesson Anticline, is also considered a radial compressional structure ***(Figs. 7.15; 6.5.a, b; 6.7.a, b)***. The more central part of the Nesson Anticline (on WE III line) is narrower, has higher amplitude and the two bounding fault zones in the west and east (West Nesson Fault and East Nesson Fault),

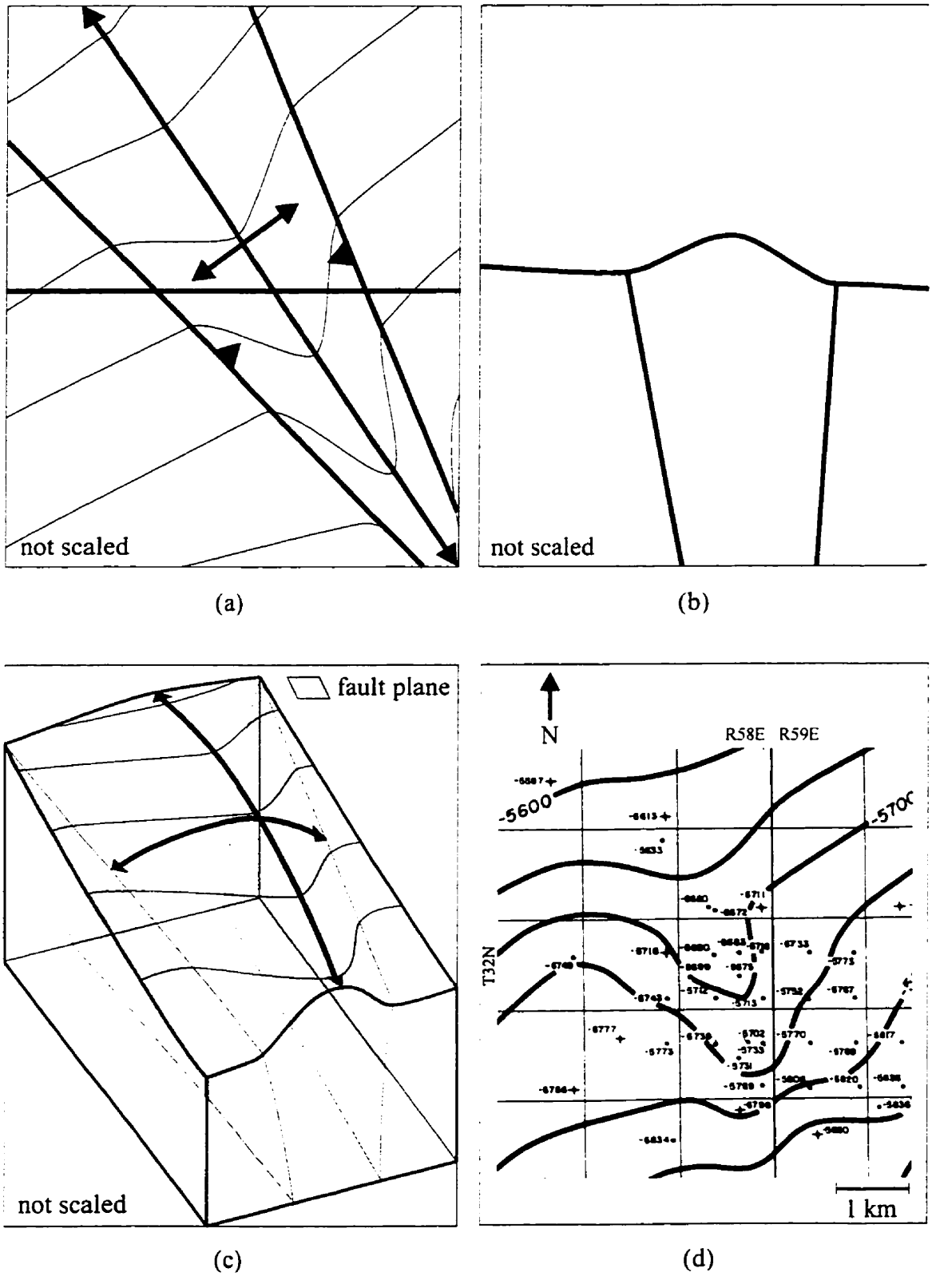

Fig. 7.14 Radial folds (structural 'noses'). (a) Map view; (b) Cross section; (c) 3D diagram; (d) Example; Dwyer Field, Montana (Rayne, 1985).

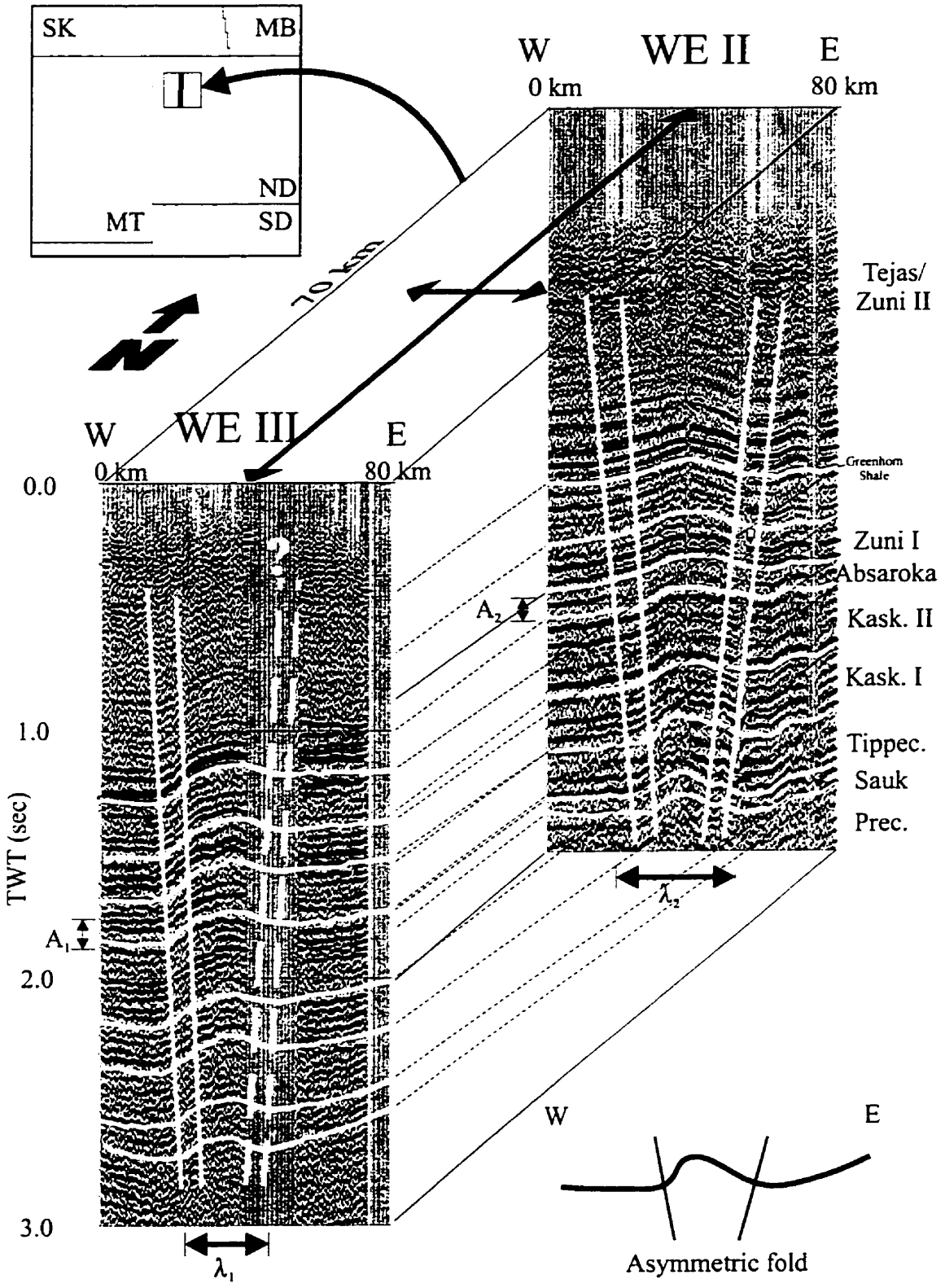

Fig. 7.15 North-South block diagram along the Nesson Anticline.
A_1 and A_2 : representative fold amplitude; λ_1 and ,λ_2: representative fold wavelengths.

which dip toward the hinge line of the anticline, are steeper. This observation reinforces the results of the detailed thickness and structural mapping of the Nesson Anticline conducted by Famakinwa *(1989)*, who concluded that the stratigraphic throw on the bounding faults decreases from south to north. He recognized numerous active periods on the faults; however, the dip direction on the faults was not clarified and they were interpreted as vertical faults. This shows the inherent limit of structural interpretation based on well data alone.

Fault interpretation relies on differences in thickness of a given geological unit between two wells, which does not allow determination of the nature of the fault (i.e. normal or reverse). Generally, faults so identified are interpreted as normal faults or vertical faults to accommodate the changing direction of the movement on the fault. A regional seismic profile gives a better understanding of the fault dip direction and can be interpreted in a basin-wide context.

LeFever and Crashell *(1991)* analyzed the timing of the structural movements of some anticlinal features in the southern part of the Williston Basin. By constructing subsidence curves from borehole data they concluded that the subsidence patterns of the folds are similar, except that the amount of calculated subsidence increases somewhat toward the basin center and is slightly less for wells on structural highs. This supports the present hypothesis that there is greater deformation on radial folds closer to the basin center ***(Fig. 7.13.c)***. The highest amplitude of the Nesson Anticline, therefore, is the consequence of its central position in the basin.

Radial arrangement of the folds and structural noses can also be identified in other segments of the basin. ***Fig. 7.16*** displays two different interpretations of the same map ***(Fig. 2.17)***. The map shows the structure of the Sherwood subinterval of the Mississippian Mission Canyon Formation (in the Kaskaskia II sequence). The limit between the white area in the northwestern (central) part and the grey area in the southern, southeastern and eastern parts (flanks) separates the regions with anhydrite

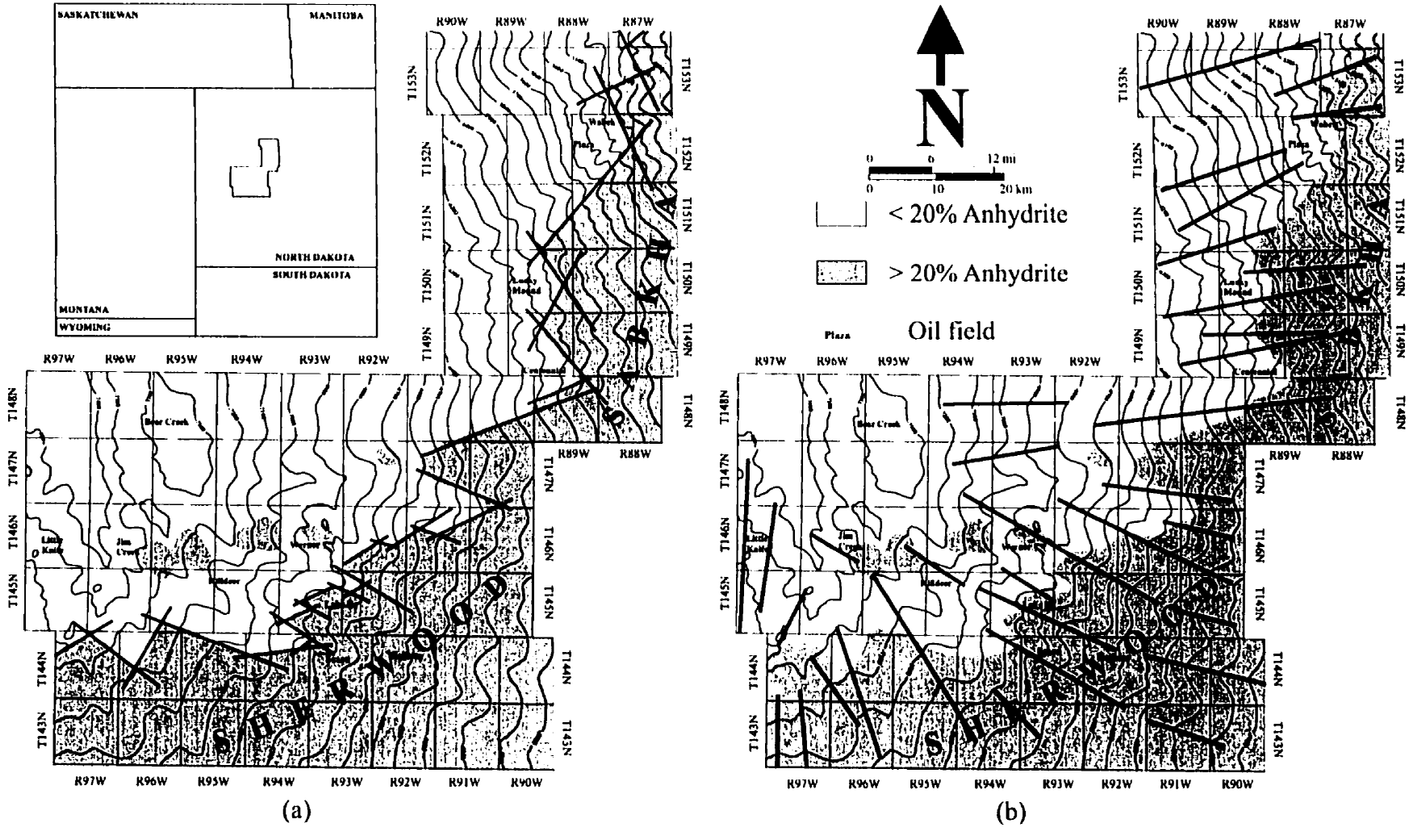

Fig. 7.16 Sherwood subinterval (Mississippian Mission Canyon Formation) structure, McLean, Mountrail and Dunn counties in west-central North Dakota (McClellan, 1995). (a) lineament interpretation, (b) radial folding.

content below and above 20 percent. This zigzag line indicates average shoreline position *(McClellan, 1995)*. The zigzag pattern of this shoreline is widely attributed to the expression of the assumed Precambrian blocks limited by a NW-SE/SW-NE set of faults *(McClellan, 1995)*.

The lineament interpretation is shown in ***Fig. 7.16.a***. There is no proven direct structural control in these directions on the lithologic boundary (based on anhydrite content). Although the eastern part of the map shows the assumed fault pattern, it deviates more and more from it as the shoreline continues to the southern areas.

If, instead of the assumed fault pattern, the real structural directions (e.g., axial traces of folds and structural noses) are followed, a general radial pattern can be observed which originates from the central part of the basin ***(Fig. 7.16.b)***. A zigzag pattern of the lithologic boundary can be easily envisaged, which actually follows the pattern of these radially arranged features in a better way.

Seismic evidence from the regional lines crossing this area underlines the directions and compressive nature of these structures ***(Figs. 6.8.a, b and 6.16.a, b)***. Further to the east, McCaslin *(1982)* concluded that the structural noses generally point toward the center of the basin.

7.1.3.2 Extensional structures

Extensional structures (normal faults) occur mostly in the flanks of the basin, and have been identified both on thickness and structural maps as well as regional seismic profiles. The strikes of these faults delineate the circumference of the basin with a dominant dip toward the basin's center ***(Figs. 7.12.b and 7.13.c)***. These structures are consistent with axisymmetric deformation, wherein the magnitude of the extensive hoop stress (σ_ϕ) is less than its radial counterpart (σ_ψ) ***(Figs. 7.5.c, d)***. The extensional structures in the flanks are significantly smaller than the compressive ones in the central part since the differential stresses decrease away from the center. These

structures can be recognized on the map by their step-like pattern ***(Fig. 7.17.a)***. Their cross-sectional and 3D view are shown in ***Figs. 7.17.b and c***, respectively. An example from southwestern Saskatchewan is displayed on ***Fig. 7.17.d***.

Since most of the regional seismic profiles cross the central part of the basin, it is primarily the compressive structures which are revealed on them. Nevertheless, in parts of the sections the extensional features are apparent. Normal faults can be seen in the easternmost part of the WE II line ***(Figs. 6.5.a, b)***, and also at the northern and southern extremes of NS I and CA I lines ***(Figs. 6.10.a, b; 6.11.a, b; 6.13.a, b)***. At the northern end of the NS I and CA I, where they run close to each other, the same normal fault can be identified on both sections, underlining its circumferential (E-W) strike ***(Figs. 6.10.a, b; 6.13.a, b)***.

7.1.3.3 Zuni rotation of the structures in the basin

It was shown previously that during the Zuni – Tejas interval, significant lateral forces effected a fundamental change in the shape of the Williston Basin. The original circular geometry in map view was deformed into an ellipse ***(Fig. 7.11)***. This dramatic change is the consequence of the Sevier and Laramide orogenies in the plate margin to the west ***(Figs. 2.4.b-d)***. The NNW-SSE elongation of the Zuni – Tejas inflection ellipses suggests a primarily WSW-ENE-directed compressional regime, which led to the present shape of the basin. Evidently, changes in the orientations of the previous radial and circumferential arranged structures are to be expected ***(Fig. 7.18)***.

The limit of the compressional and extensional deformations in the basin, as illustrated by ***Fig. 7.18***, represents a mean value, since the locations of the inflection ellipses vary with each sequence ***(Fig. 7.11)***. Nevertheless, the present WNW-ESE to NE-SW orientation of basin structures is attributed to this late deformation of the earlier radial and circular structures. Depending on their position in the basin, these structures were rotated in different directions ***(Fig. 7.19)***. The displacement took place along the pre-existing faults in a strike-slip sense. Dragging of the radial folds in the center of the

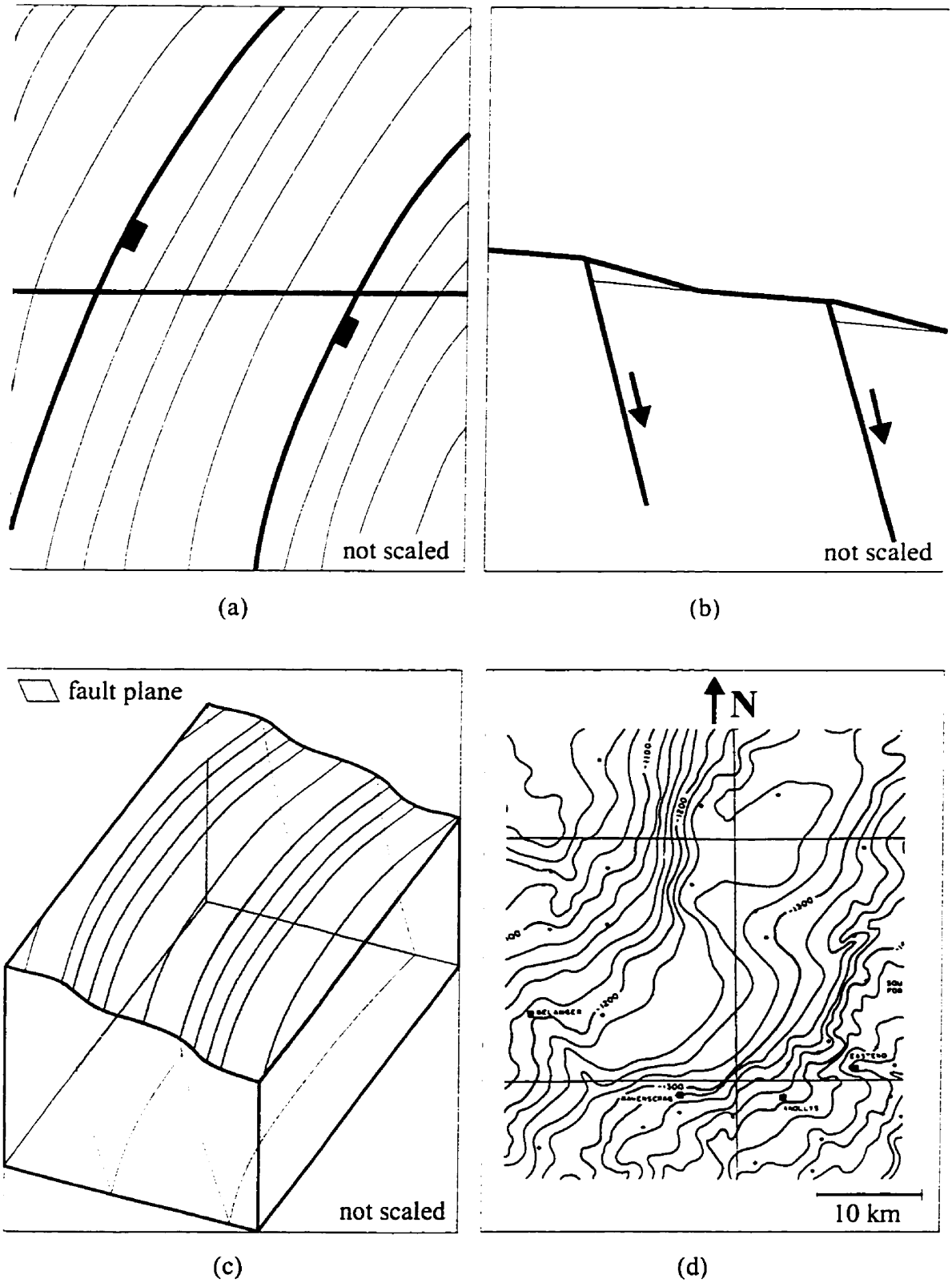

Fig. 7.17 Circular extensional structures. (a) Map view; (b) Cross section; (c) 3D diagram; (d) Example; SW Saskatchewan (Cristopher, 1987).

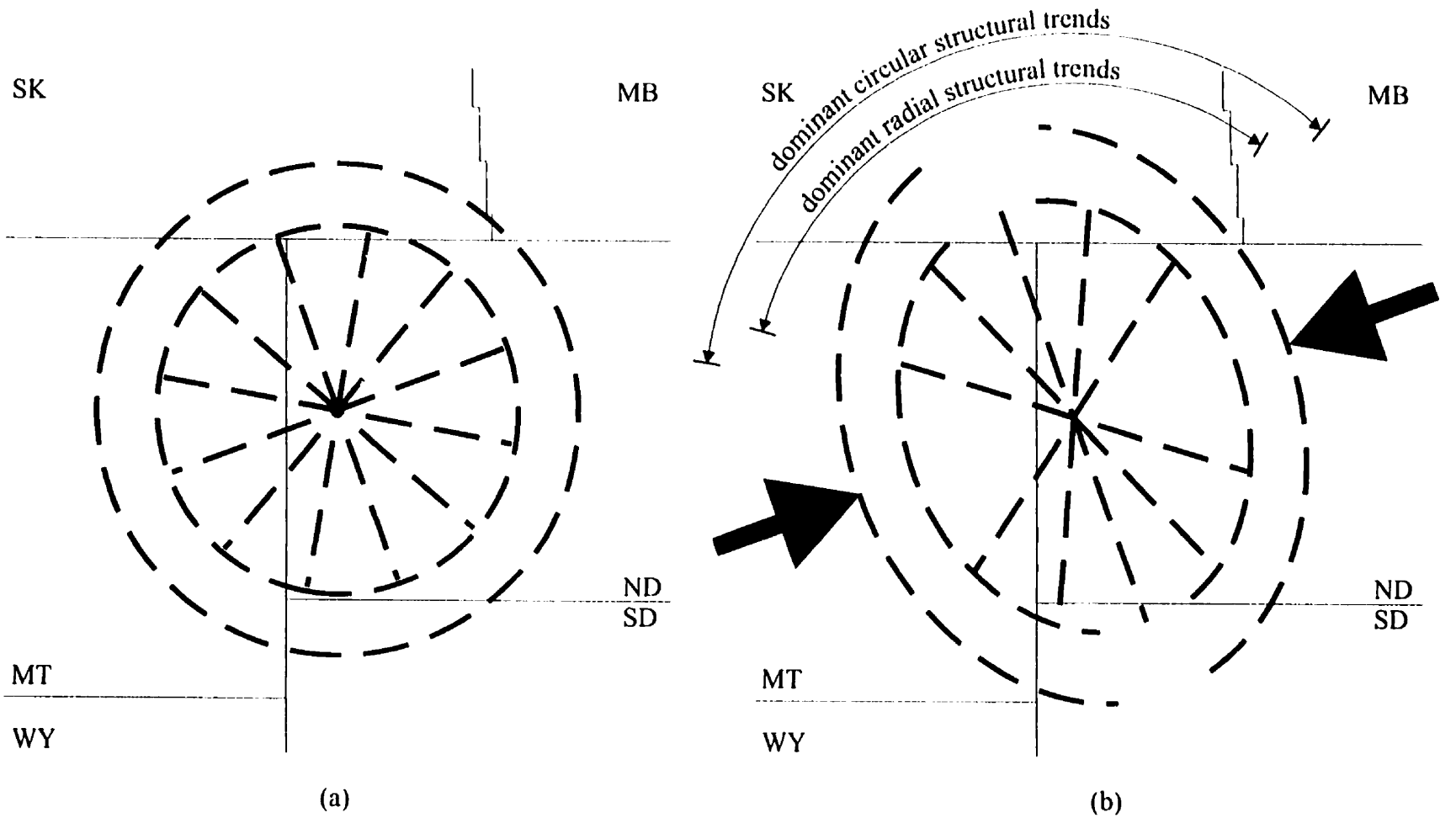

Fig. 7.18 Development model for structural orientations in the Williston Basin. (a) Pre-Zuni structural orientations [Kaskaskia I ?]. (b) Zuni-Tejas structural orientations. —— —— preferred structural trends (radial folds, reverse faults; circumfenetial normal faults).

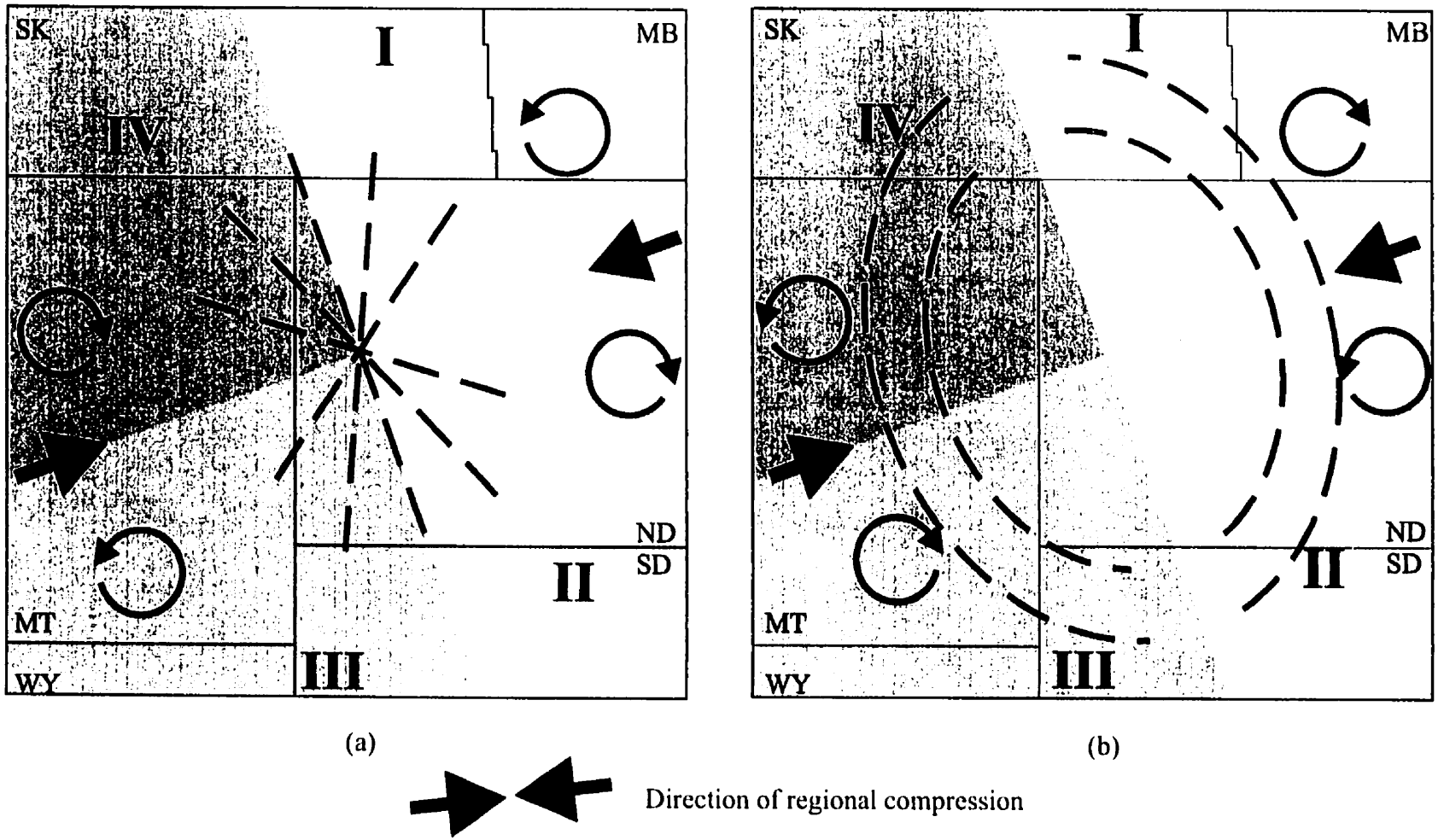

Fig. 7.19 Zuni rotation of radial and circular structures in the Williston Basin. (a) Radial folds. (b) Circular structures.
— — preferred structural trends; I, II, III, IV quadrants (with different shading).

basin resulted in asymmetry in their final shape. Again, depending on their original location in the basin, the asymmetry varies ***(Fig. 7.20)***.

The Nesson Anticline is located in the northeastern segment (Quadrant I) where the radial folds were rotated counterclockwise, resulting in a steeper western side ***(Figs 6.5.a, b; 6.7.a, b; 7.15)***. Probably this is the reason that the East Nesson Fault, identified by Famakinwa *(1989)*, is not as apparent as the West Nesson Fault. In Quadrant II (e.g., Little Knife area) ***(Fig. 7.20)***, the radial folds were rotated clockwise again causing steeper western sides, whereas in the Knutson-Fryburg area (Quadrant III) the folds were rotated counterclockwise causing the steeper flanks to occur on the east. A similar steeper eastern side in Quadrant IV (e.g., Poplar Dome) is the result of clockwise rotation of the folds there.

One result of these rotations is that the observed asymmetric profile of the folds on the regional seismic profiles is due not only to their apparent dip in the plane of the sections, but also to their real asymmetry caused by the Zuni – Tejas deformation ***(Figs. 6.5.a, b; 6.7.a, b; 7.15 for the Nesson Anticline and Figs 6.7.a, b for the Poplar Dome)***.

7.1.4 Relationship of natural earthquakes and river directions to the major tectonic trends in the Williston Basin area

It is widely accepted that earthquakes usually occur along weak structural zones; thus their locations delineate these zones. Consequently, it is important to incorporate any available earthquake information when trying to establish the structural framework of an area. The historic earthquakes of the Montana, North Dakota and Saskatchewan regions of the study area are shown in ***Fig. 7.21*** and listed in ***Table 7.1***.

It is evident from ***Fig. 7.21*** that the earthquake locations are sparse in the Williston Basin area but increase toward the mobile belt in the west. Nevertheless, some important conclusions can be drawn from the earthquake data.

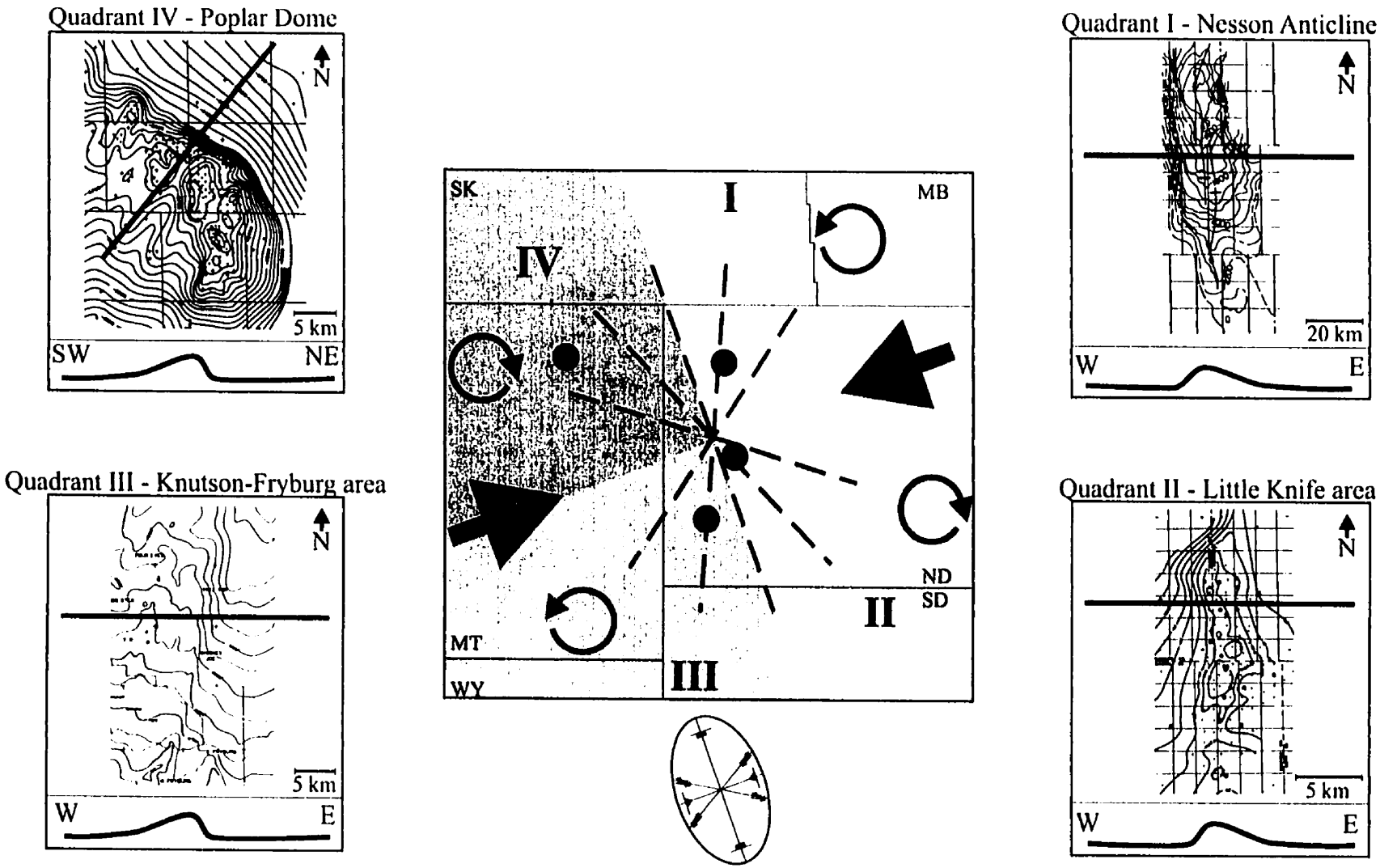

Fig. 7.20 Asymmetry of radial folds due to Zuni deformation. I,II,III,IV quadrants; ● location of map areas within a quadrant; — — fold trends; Maps from Orchard (1987), LeFever et al. (1987a), Bogle and Hansen (1987), Narr and Burrus (1984).

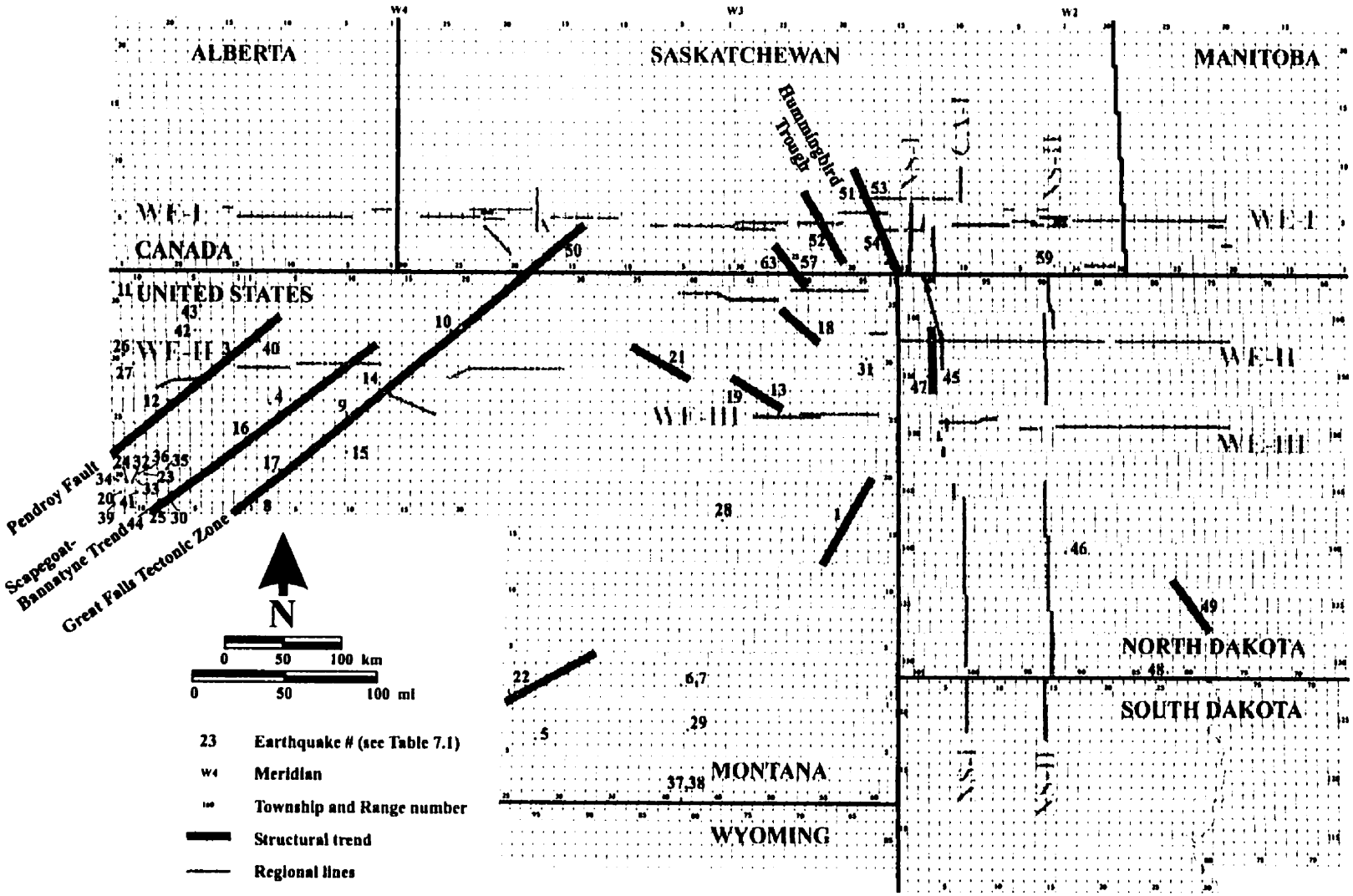

Fig. 7.21 Historic natural earthquakes in Montana, North Dakota and Saskatchewan.

Table 7.1 Historic natural earthquake locations in Montana (map area only), North Dakota and Saskatchewan.

	Date	Time (UTC) H:M:S	Lat. N	Long. W	Area	Depth km	Hypocenter Quality (A-I)	Magnitude (1-12)	Intensity (I-XII)	Comment
					MONTANA (1805 - 1985) [Qamar and Stickney, 1983; Reagor et al., 1985]					
1	1878 APR 15		47.10	104.70	Glendive		G		IV	
2	1909 MAY 16	04:15:00.0	49.00	104.00	MT/ND/SK			5.5		
3	1915 MAR 04	08:30:00.0	48.35	111.90	Shelby		G		III	
4	1915 MAR 04	15:00:00.0	48.00	111.40			G		III	
5	1928 MAR 02	05:25:00.0	45.47	108.29	Billings		G			
6	1932 JAN 10	06:40:00.0	45.86	106.63	Colstrip		G		IV	
7	1932 JAN 10	06:46:00.0	45.86	106.63	Colstrip		G		IV	
8	1934 AUG 08	02:20:00.0	47.30	111.70			G		IV	
9	1935 MAY 11	11:00:00.0	47.95	110.50	Loma		F		II	
10	1935 OCT 16	07:50:00.0	48.58	109.23	Chinook		G		II	
11	1935 OCT 24	01:30:00.0	48.91	113.25	Whitlash		G		III	
12	1935 OCT 31		48.02	112.65	Blackleaf		G		III	
13	1935 OCT 31	07:00:00.0	48.08	105.66	Wolf Point		G		IV	
14	1935 OCT 31	15:10:00.0	48.18	110.11	Big Sandy				III	
15	1935 OCT 31	19:18:00.0	47.66	110.45	Montague		F		III	
16	1935 OCT 31	19:40:00.0	47.82	111.66	Ft. Benton		F		III	
17	1936 JAN 11	18:02:00.0	47.50	111.30			G		V	
18	1943 JUN 25	04:25:00.0	48.50	105.00	Froid			4.0	VI	
19	1946 OCT 26	20:45:00.0	48.10	105.70	NE Montana		I		IV	
20	1950 AUG 20	01:44:55.0	47.25	113.25	Seeley Lake		D		VI	
21	1956 DEC 02	21:30:00.0	48.35	106.90	Vandalia		I		IV	
22	1958 JUL 13	01:45:32.0	45.80	108.50	Billings		H		III	
23	1959 MAY 17	10:56:52.0	47.50	113.00	NE of Seeley Lake		D		V	
24	1965 OCT 26	11:28:04.1	47.40	113.20	Seeley Lake	32.0	D	4.0	V	
25	1968 NOV 21	01:06:47.3	47.31	112.75		33.0	C	3.8		
26	1970 DEC 16	02:36:30.9	48.38	113.22		15.0	C	4.8		
27	1971 JUN 24	14:05:45.6	48.34	113.12		5.0	C	4.0		
28	1973 SEP 26	18:38:26.6	47.12	106.13		25.0	C	2.8		
29	1973 NOV 13	05:59:50.1	45.59	106.56		10.0	C			
30	1975 MAR 18	06:19:18.1	47.27	112.65			A	2.6		
31	1975 SEP 05	20:47:40.7	48.37	104.38		5.0	C	3.5		
32	1975 DEC 11	11:50:36.6	47.35	113.15		1.0	C	2.7	III	
33	1975 DEC 11	16:01:07.0	47.39	113.13		10.0	C	2.8	III	
34	1976 APR 27	15:37:38.5	47.39	113.33			A	2.5		
35	1976 JUL 28	05:06:16.9	47.55	112.73	Augusta	5.0	C	3.5	IV	
36	1976 AUG 01	23:15:09.8	47.46	113.06			A	2.5		
37	1976 AUG 10	13:54:57.5	45.03	106.57		5.0	C	3.4		
38	1976 OCT 08	13:54:00.0	45.03	106.57			C	3.5		
39	1978 MAR 24	18:35:03.3	47.22	113.33		5.0	B	3.8		
40	1978 AUG 30	16:33:21.2	48.49	111.48		5.0	B	3.5		
41	1979 JAN 04	14:51:24.8	47.31	113.14	N of Ovando	5.0	B	3.0		
42	1979 APR 14	09:39:06.4	48.59	112.41	SW of Cutbank	5.0	B	3.2		
43	1980 APR 14	03:27:33.8	48.79	112.34	N of Cutbank	5.0	B	3.6		
44	1980 AUG 24	08:32:22.5	47.19	112.92		5.0	B	3.4		
					NORTH DAKOTA (1915 - 1981) [Reagor et al., 1981]					
45	1915 AUG 08	15:15:00.0	48.20	103.60			G		IV	
46	1927 APR 30	02:15:00.0	46.90	102.10			G		III	
47	1946 OCT 26	20:37:00.0	48.20	103.70			G		IV	
48	1947 MAY 14	05:02:00.0	46.00	100.90			H		IV	
49	1968 JUL 08	16:50:12.0	46.50	100.60		33.0	B	4.4	IV	
					SASKATCHEWAN (1965 - 1997) [Horner and Hasegawa, 1978; D.Gendzwill personal communication]					
50	1968 SEP 11	12:00:06.0	49.25	108.14	Val Marie			2.7		
51	1968 OCT 11	12:28:04.0	49.61	104.49	Radville			2.8		
52	1972 JUL 26	03:58:19.0	49.35	104.93	Bengough			3.7	V	
53	1976 MAR 23	22:31:47.0	49.56	104.37	Radville			3.2	V	
54	1976 MAR 25	00:12:16.0	49.39	104.27	Radville			3.5	IV	
55	1976 MAY 15	06:21:12.0	52.45	105.44	Humbolt			2.3		Not on the map
56	1981 JAN 10	08:34:31.0	51.91	103.44	Kuroki			3.1		Not on the map
57	1982 AUG 17	04:50:31.0	49.01	105.27	Big Beaver			3.9		
58	1984 FEB 05	04:30:14.0	52.70	106.95	Redberry Lake			2.3		Not on the map
59	1985 OCT 10	12:43:37.0	49.07	102.17	Northgate			2.9		
60	1991 APR 25	20:53:53.0	51.90	103.48	Kuroki			3.1		Not on the map
61	1991 APR 26	00:02:26.0	51.90	103.48	Kuroki			2.5		Not on the map
62	1993 NOV 08	16:20:44.0	52.70	107.30	Redberry Lake			2.6		Not on the map
63	1997 APR 18	00:25:39.0	49.08	105.38	Coronach			3.0		

At the western end of WE II, three major NE-SW trending dextral strike-slip fault zones are delineated by earthquakes. The westernmost, the Pendroy Fault, which can be seen on the regional seismic profile ***(Figs. 6.2.a, b)***, is the location of earthquakes 3, 12 and 40. To the east, the Scapegoat–Bannatyne Trend ***(Figs. 6.2.a, b)*** marks the source location of earthquakes 4, 16, 25, 30 and 44. The major Great Falls Tectonic Zone, which involves the Bearpaw Mountains ***(Figs. 6.3.a, b)***, can be traced over the largest distance by the epicenters of earthquakes numbered 8, 9, 10, 14, 15, 17 and 50.

In the Williston Basin area it is more difficult to correlate the sparsely located earthquakes to the fault zones identified in an independent manner. Brown and Reilinger *(1986)* indicated that the stable interior areas pose special problems since it is extremely difficult to associate intraplate earthquakes, even large ones, with specific faults. Nevertheless, due to the proximity of some known faults to earthquake locations in the Williston Basin area, some assumptions can be made. Earthquake 21 is located close to the Bowdoin Dome, which was active throughout the Phanerozoic ***(Section 2.2.1.1)***. The Poplar Dome is in close proximity to earthquakes 13 and 19, while earthquake 18 is on the line separating the "Transition Zone" from the "Williston Basin Element" in the Fort Peck Indian Reservation ***(Section 2.2.1.2)***.

In southern Saskatchewan earthquakes line up roughly along three NNW-SSE zones. The eastern two lines roughly delineate the Hummingbird Trough. Some of these earthquakes are located in areas where the Prairie Evaporite is present. Earthquakes in areas where the Prairie Evaporite is present can be attributed to a salt dissolution/collapse mechanism. Due to limitations of the recording instrumentation, the computed position of an epicenter can be as much as 20 km off from its true position. It is, therefore, difficult to establish the involvement of the Prairie salts in these earthquakes. Nevertheless, whether salt collapse was involved or not, the fundamental causes of the earthquakes here are most probably related to basement structures *(D.*

Gendzwill, personal communication). Other earthquakes south of the Hummingbird Trough are probably fault related, too, and appear along major rivers: earthquakes 1 and 22 along the Yellowstone River, 45 and 47 along the Little Muddy River, and 49 along the Missouri River.

Numerous claims have been made that river streams in the Williston Basin area delineate a NE-SW/NW-SE pattern which could corroborate these structural directions. Detailed analysis of tributaries showed that this concept is undoubtedly true for younger (Zuni) structural directions *(Stauffer and Gendzwill, 1987)*. Presumably the major rivers delineate the older, larger stuctural directions. A short look at the river patterns, at least in the central part of the basin, reveals radial structural pattern along the major rivers ***(Fig. 7.22)***. The Missouri River in northeastern Montana runs E-W, while in west-central North Dakota it runs WNW-ESE. The Yellowstone River in eastern Montana delineates a NE-SW zone, while the Little Missouri River in western North Dakota shows a roughly N-S orientation. Two shorter rivers in northwest North Dakota, the Little Muddy River and the Little Knife River run N-S and NNE-SSW, respectively. The radial pattern in the central region of the basin, originates from an area in northwest North Dakota. This area is located above the deepest part of the basin. and emphasizes the radial structural framework of the basin.

7.1.5 Summary of the structural evolution of the Williston Basin

The structural evolution model of the Williston Basin presented here is based upon an extensive set of sources; namely, geological data, terrestrial and planetary analogs, mathematical and experimental models and, most importantly, the recently compiled regional seismic lines. Based on the syntheses of these data sets, the tectonic history of the Williston Basin area can be subdivided into three main periods, during which the present overall shape of the basin and its internal structure developed:

1. "Pre-Williston" phase

2. Sauk–Absaroka intracratonic phase (except Kaskaskia I)

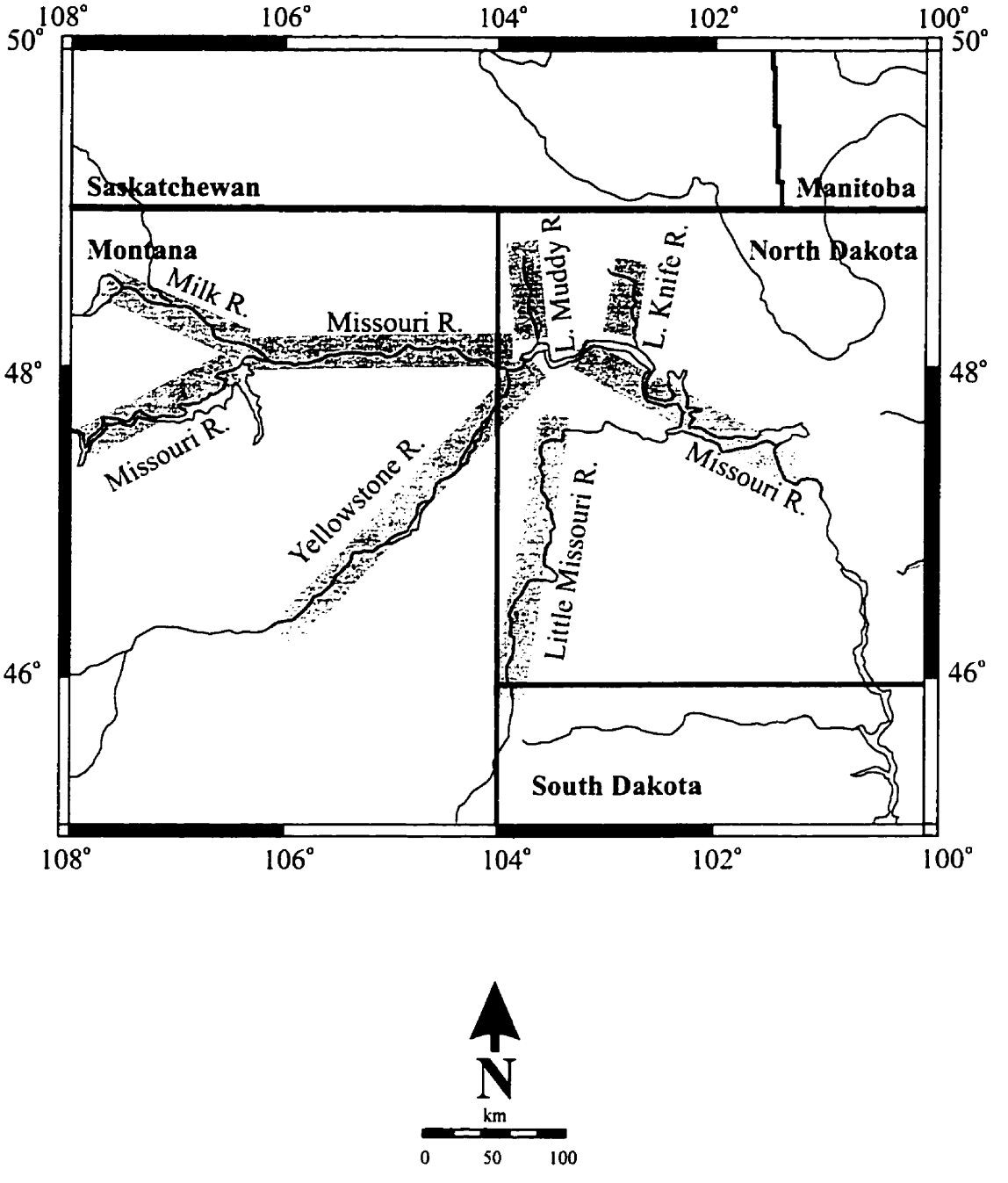

Fig. 7.22 Rivers and radial structural trends in the Williston Basin area.

3. Zuni–Tejas foreland phase

The first, ***"pre-Williston" phase***, obviously cannot be deduced directly from the sedimentary record. Nevertheless, some important observations lead to the following conclusion. The Williston Basin is not underlain by a rift, but by the Archean Dakota Block, which suggests different tectonic behavior than the surrounding areas. The Williston Basin area was thermally uplifted, probably in the early Cambrian, and was then subjected to 3 km of pre-subsidence erosion *(Crowley et al., 1985)*. The uplift was probably caused by a mantle intrusion. Erosion was accompanied by cooling and/or phase change of the mantle material which caused overall subsidence. The geometry of the mantle intrusion was axisymmetric and resulted in radially arranged extensional fractures and faults of the crust in the central part of the basin, and circumferentially arranged compressive structures at the flanks ***(Figs. 7.5.a, b)***. This arrangement is responsible for the widely recognized oval shape of the basin. Furthermore these structural trends were rejuvenated throughout the Phanerozoic history of the basin.

It is interesting to note that the evolution of the Bearpaw Mountains described by Reeves *(1946; 1953)*, although on a smaller scale, is basically similar to the first phase (i.e., magmatic intrusion causing an axisymmetric uplift, accompanied by radially arranged extensional faulting in the central part and circumferentially arranged reverse faults due to plainsward sliding on the flanks ***[Figs. 2.8.a, b]***).

The first Paleozoic sedimentary records of the basin were deposited in the beginning of the second, ***Sauk–Absaroka intracratonic phase***. The "pre-existing" radial and circumferential structural trends, set by the earlier pre-subsidence uplift, were reactivated and inverted ***(Figs. 7.5.c, d)***. Radially arranged compressional structures dominated the central part, and circumferential extensional structures occupied the flanks. The earliest Deadwood Sea transgressed from the west, covering a rough terrain spotted by "islands" *(Lochman-Balk and Wilson, 1967)*, which are the structural remnants of the earlier phase. The subsidence continued in an axisymmetric manner and

recurrent active phases were detected in the basin. The generalized subsidence curve of the Williston Basin can be subdivided into shorter exponentially decreasing periods *(**Fig. 7.23**)*. The inherent limit of subsidence curves is that the curves are generated from information of the sedimentary record available. Only 10-25% of the geological history is represented by rocks in the Williston Basin area *(Fig. 2.2)* and the remaining intervals are interpolated. These periods are assumed to be the more active tectonic intervals and can represent additional subsidence/sedimentation and uplift/erosion. E.g., during the Cretaceous kilometers of sediments were eroded from the area. The active phases are not coincident with the orogenic events elsewhere in North America *(LeFever, 1988; LeFever and Crashell, 1987)* and cannot be correlated with similar phases in other North American cratonic basins. Consequently this type of periodicity, ranging from 30-50 M.a., seems to be part of the very nature of subsidence in a cratonic basin. During this period, the Kaskaskia I Sequence exhibited a fundamentally different configuration, due to large-scale structural activity on the Transcontinental Arch southwest of the basin and/or due to the increased subsidence of the northwest part of the Elk Point Basin. The axisymmetric nature of the basin's subsidence was overprinted by this tectonic event. The cause of this cratonwide tectonic event requires a larger synthesis and no explanation can confidently be given based on this dataset. Nevertheless, the axisymmetric character of the basin was re-established in the Kaskaskia II Sequence and continued into the Absaroka Sequence.

The third, ***Zuni–Tejas foreland phase*** indicates a fundamental change in the tectonic character of the Williston Basin; however, its unique character is still recognizable. The increasing structural activity of the Sevier and Laramide orogenies to the west was accompanied by a dominant compressive force in a WSW-ENE direction across the basin. These events caused an NNW-SSE elongation of the circular basin, which then became increasingly elliptical. The deformations were accompanied by the rotation and dragging of the pre-existing structures and caused their asymmetry. Wide NW-SE/NE-SW sets of fracturing related to this phase are prevalent and well documented *(Stauffer and Gendzwill, 1987; Narr and Burrus, 1984)*. The meticulous

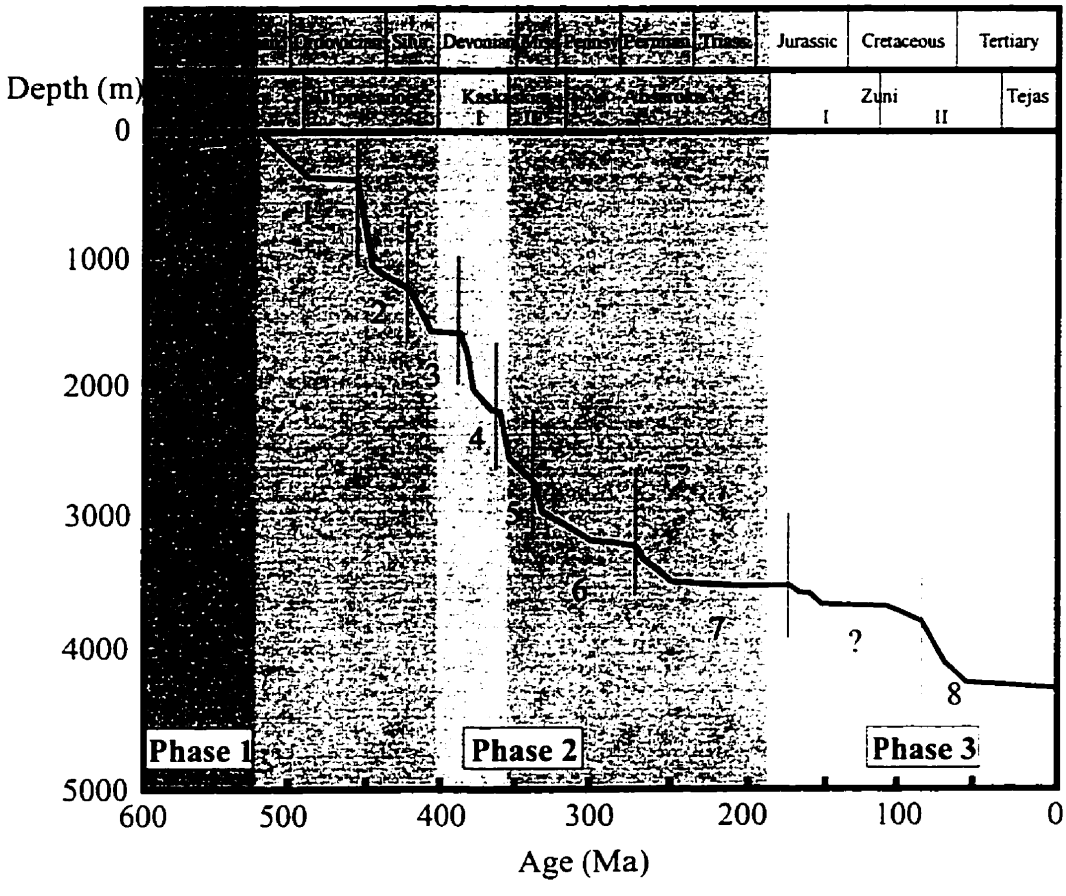

Fig. 7.23 Secondary cycles on the generalized tectonic subsidence curve of the Williston Basin (modified from Haid, 1991).

study of Schurr et al. *(1989a)*, on a larger scale, also concluded a radial arrangement of the Zuni structures ***(Fig. 7.24)***; however no tectonic explanation was given.

7.1.6 Applicability of the model for other cratonic basins

Detailed review in ***Chapter 3*** revealed that circular shape is more a rule than an exception in cratonic basins.

Basins with proven coeval compressional and extensional stress regimes in their central part and their flanks, respectively, are prime candidates for further studies (e.g., Michigan Basin, Paris Basin, West Siberian Basin). Also cratonic basins with triple junctions beneath them can be the location of radially arranged structures (e.g., Paris Basin, Illinois Basin). Evidently more advanced lateral forces can make the originally radial and circumferentially arranged structures unrecognizable (e.g., Amadeus Basin, Sichuan Basin).

Still, probably the closest "cousin" of the Williston Basin is the Michigan Basin. Brown and Reilinger *(1986)* noted that features such as the Michigan Basin and the similarly circular but positive structure, the Adirondack Dome, constitute incontrovertible evidence that cratons were subjected to major vertical motions in the past that lack clear connections to the plate-tectonic scenarios of those times. This is particularly true not only for the Michigan Basin, but also for the Williston Basin, as was shown earlier. Beyond the generally circular shape, the radial intrabasinal structures, with downward tightening character and bounding faults dipping toward the axial traces of the folds accompanied by reverse faulting in the central part of the basin, is well documented ***(Section 3.2.1.2)***. Similarly, compression in the central part, extension in the flanks and late-stage shear movements due to lateral forces (Appalachian Orogeny) along the pre-existing radial faults were detected.

The Michigan Basin and the Williston Basin are the most explored cratonic basins in the world. They show remarkable similarities in their evolution, which to a

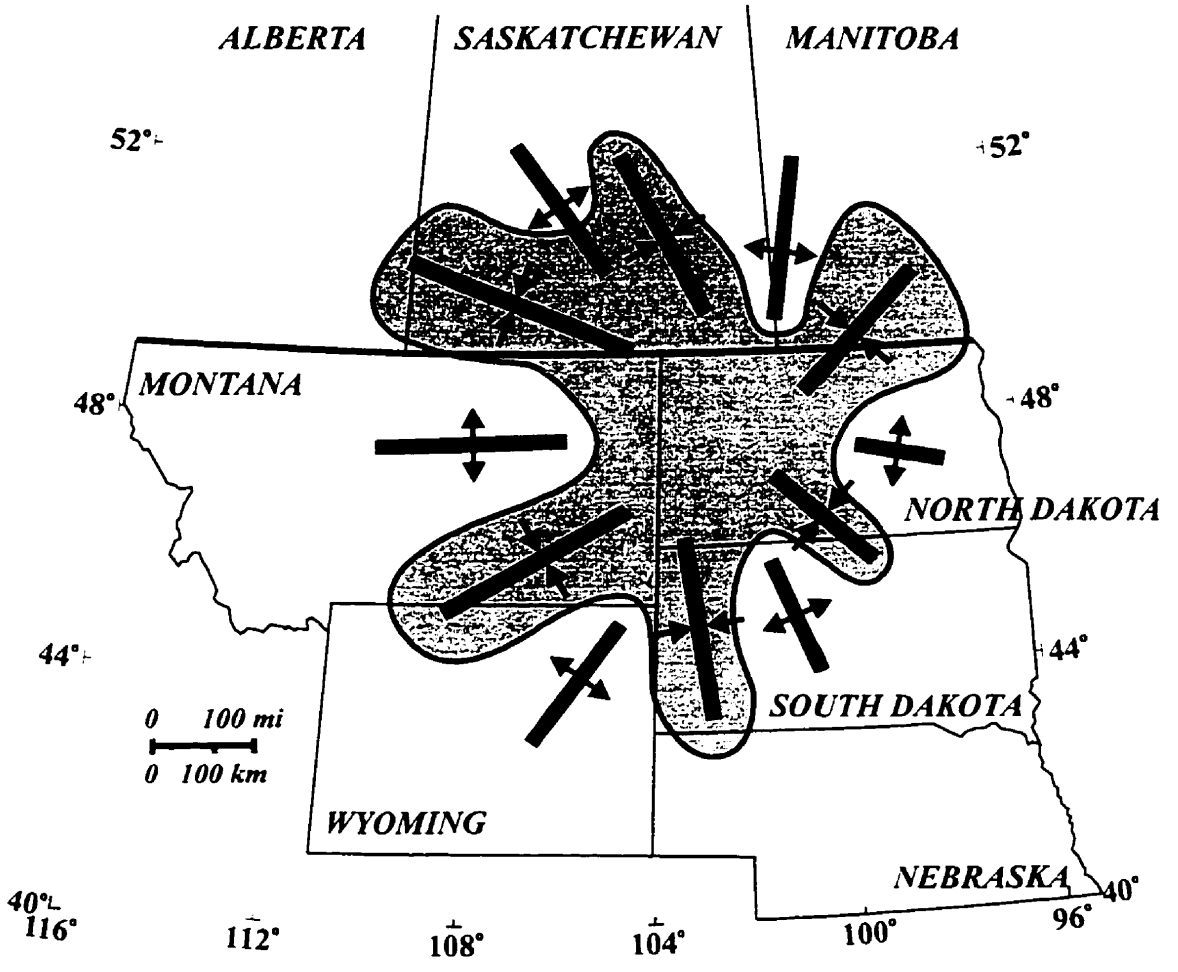

Fig. 7.24 Zuni marginal paleotectonic elements surrounding the center of the Williston Basin (modified from Shurr et al., 1989a).

certain degree we could expect to find in other cratonic basins, if enough data were available. As noted earlier, not all cratonic basins share a similar history; however, most of them exhibit a circular or oval shape. One probable scenario is that most of them are caused by some type of mantle upwelling. The final basement character and evolution probably depend on how advanced the mantle intrusion was (i.e., from what phase the subsidence starts).

The Williston Basin can be seen to represent the type of cratonic basin, where the mantle material intruded, uplifted and fractured the upper crust; but the uplift did not continue, and the erosion and subsidence started from this stage (pre-Williston phase – intracratonic basin phase).

Other cratonic basins, which are underlain by clear triple rift junctions (e.g., Paris Basin, Illinois Basin) could represent a more advanced stage of magmatic intrusion. This approach is more or less the same as that suggested by Burke and Dewey *(1973)* as a model for plume-generated triple junctions.

An even further stage could be represented by cratonic basins which are located above ancient rifts. This hypothesis requires further studies with datasets similar to that available for the Williston Basin.

7.2 Zuni sequence stratigraphy of the Williston Basin area

Deposits of the Zuni – Tejas interval occupy by far the largest segment of the Phanerozoic sedimentary record of the Williston Basin area. The structural framework of the sedimentation is fairly well established. The Zuni sedimentation took place in a foreland environment, as opposed to an intracratonic platform as was the case in the Sauk–Absaroka interval; however, the Williston Basin still exhibited a certain degree of distinctness ***(previous section)***. The lithology of this interval is dominated by clastic sediments which were derived from sediment sources primarily to the west. In Zuni–

Tejas times, the area was part of the roughly north-south trending Western Interior Seaway. Together with the tectonic activity of the emerging Sevier and Laramide orogenies, the eustatic sea-level changes and the quantity of the sediments define primarily the sediment accommodation potential of the area. Consequently, sequence stratigraphic analysis reveals the composite of these factors.

7.2.1 Seismic stratigraphy of the regional profiles

Large-scale sequences can be identified with greater confidence by applying regional seismic profiles. The five regional profiles of this thesis supply a unique and novel dataset for a foreland basin of this scale. Due to the tectonic processes and the extended thickness of the Zuni – Tejas interval in the area, the interpretation is easier in profiles with datum correction. The most convenient datum is the Greenhorn Shale (Second White Speckled Shale in Canada) due to its presence all over the area and its excellent seismic characteristics. The datum-corrected sections are displayed in ***Figs. A.1-6 in the Appendix***. The same profiles are shown in two fence diagrams to enhance the three dimensionality of the Zuni–Tejas depositional system ***(Figs 7.25 and 7.26)***. The standard seismic stratigraphic interpretation procedure, discussed in ***Section 5.2***, was used by identifying seismic reflection terminations, seismic surfaces, seismic packages/units, etc. Although the regional reflection profiles are considered to be a sufficient base for large-scale interpretation, some limitations should be observed. The first is that the decreasing number of seismic traces containing information from the upper part leads to increasing uncertainties upsection, due to lower-quality stacking. The second limitation is the scarcity of well-log information. This is not necessarily due to the number of wells used (49), but to the general insufficiency of logging of the Cretaceous sediments in the whole area. It is reiterated that the large-scale interpretation is reliable, although in smaller scale, well-log based sequence stratigraphic analysis should be incorporated.

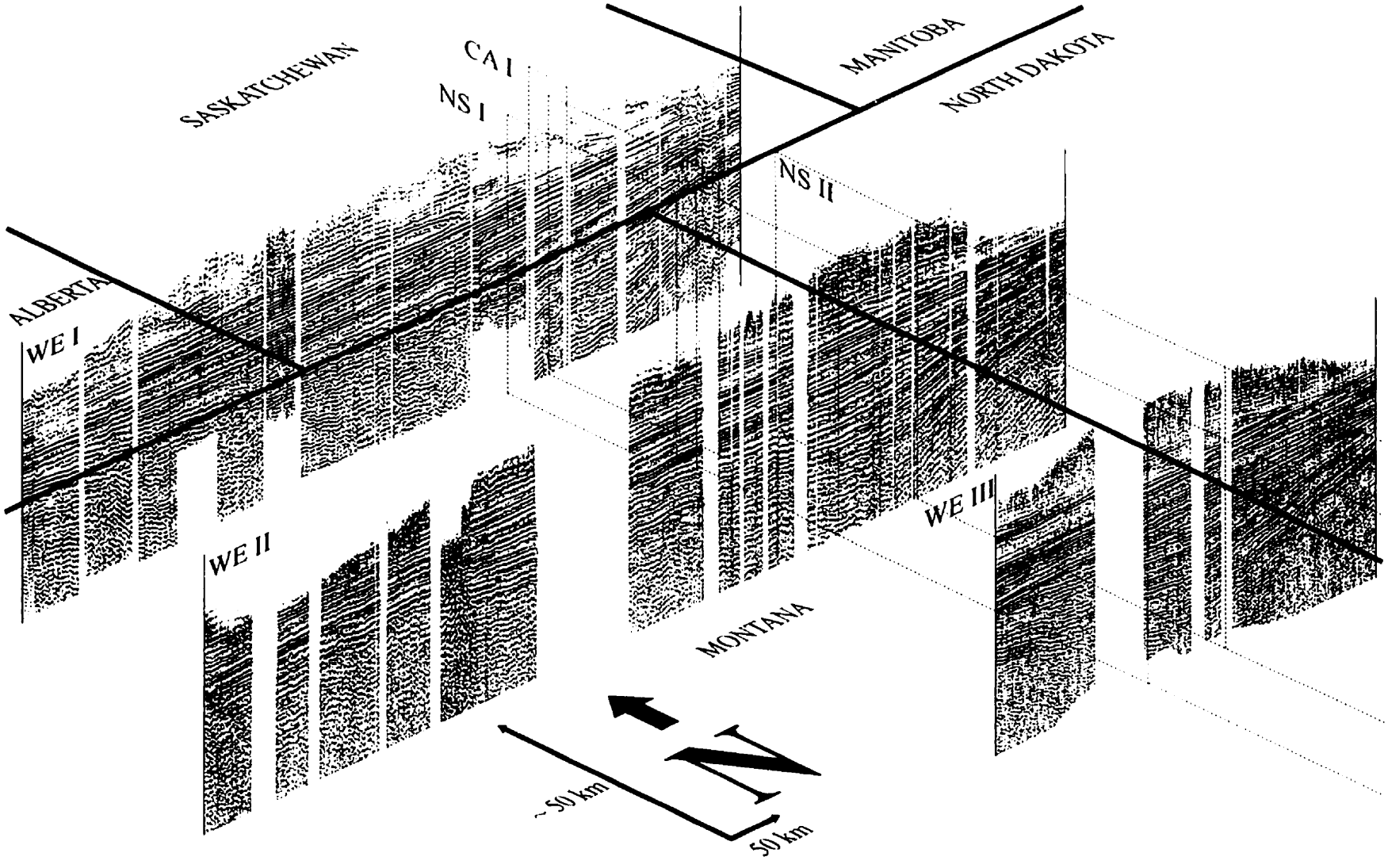

Fig. 7.25 Fence diagram of the east-west profiles.

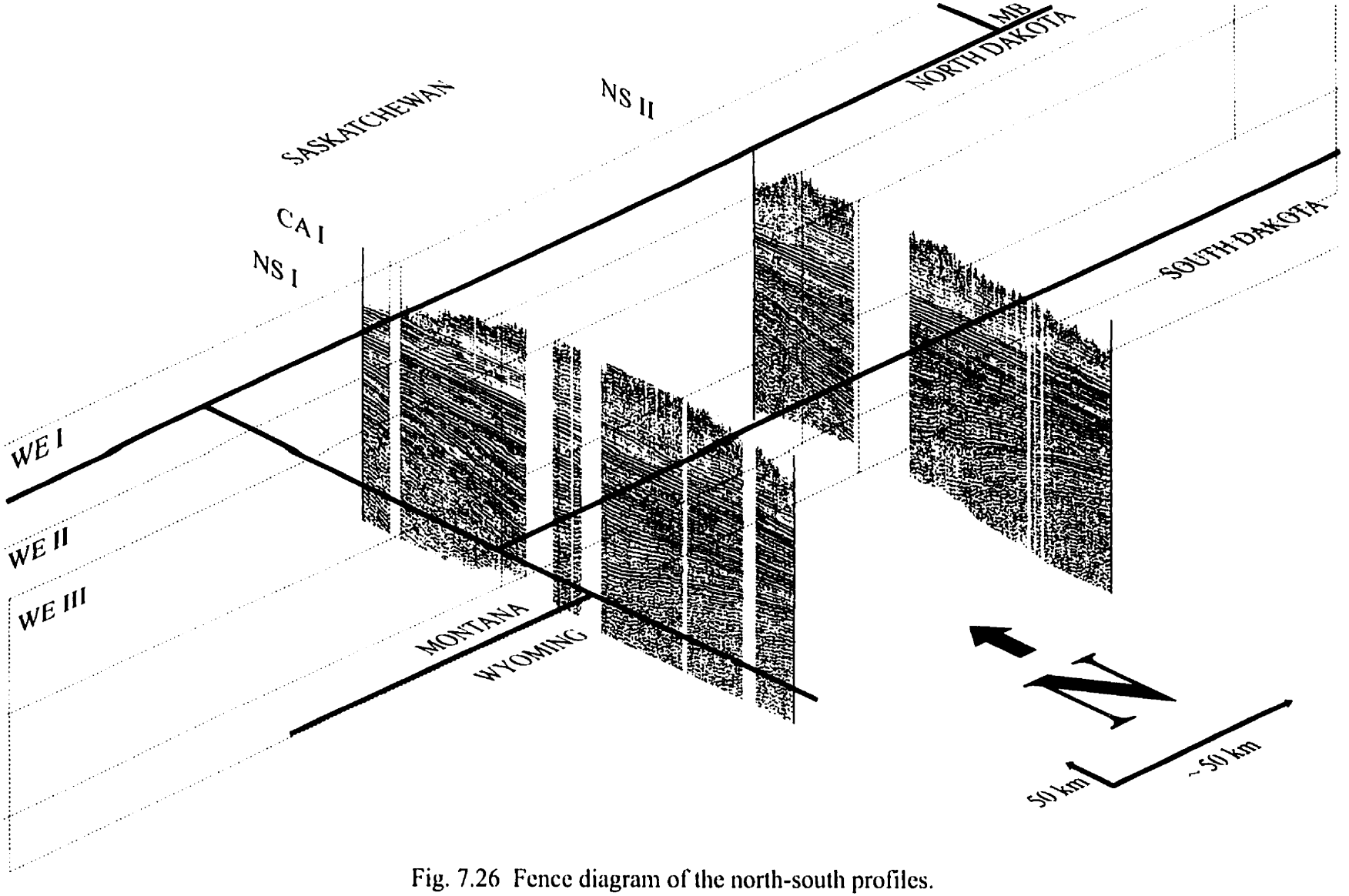

Fig. 7.26 Fence diagram of the north-south profiles.

7.2.2 Sequence stratigraphic framework of the Zuni sediments

Sequence stratigraphic interpretations of the regional lines, without the seismic profiles, are shown in ***Figs. 7.27 and 7.28***. In the light of the four additional profiles, Zhu's *(1992)* profile (WE I) was reinterpreted. Reflection terminations delineate unconformity surfaces, which in turn bound sedimentary packages/units. Altogether, sixteen sequence stratigraphic units were identified. In the east-west profiles ***(Fig. 7.27)*** the lower units are fairly thin with uniform thickness, while in the upper parts the units exhibit wedge shapes, with thinning toward the east. Units are increasingly thicker upsection. This general configuration shows well the general shallowing and final fill-up of the Western Interior Seaway. In the north-south direction the units show a similar pattern; however, the wedge shape of the upper units is not observable because the sediment source is at a high angle to the plane of the profiles.

7.2.2.1 Sequential subdivision of the Zuni Sequence in the study area

Zhu *(1992)* subdivided the Zuni part of the WE I profile into Zuni I (Jurassic), Mannville, Lower Colorado, Upper Colorado and Montana sequences. Within the Montana sequence seven subsequences were identified (A-G). Naming stratigraphic sequences with accepted lithostratigraphic unit names used in the area is unfortunate, since it can lead to misunderstandings. It is necessary therefore to find other nomenclature which explicitly refers to stratigraphic sequences. Stratigraphic sequences and transgressive-regressive cycles are both indicators of cyclic changes of the accommodation potential of a given area and of sea-level changes, although they are not synonymous. Nine transgressive-regressive cycles were identified in the late Zuni times by Kauffman and Caldwell *(1993)* and all of them are defined again with lithostratigraphic names:

	Cycle	Approximate age (M.a.):
IX	Fox Hill cycle	72 – 65
VIII	Bearpaw cycle	78 – 72

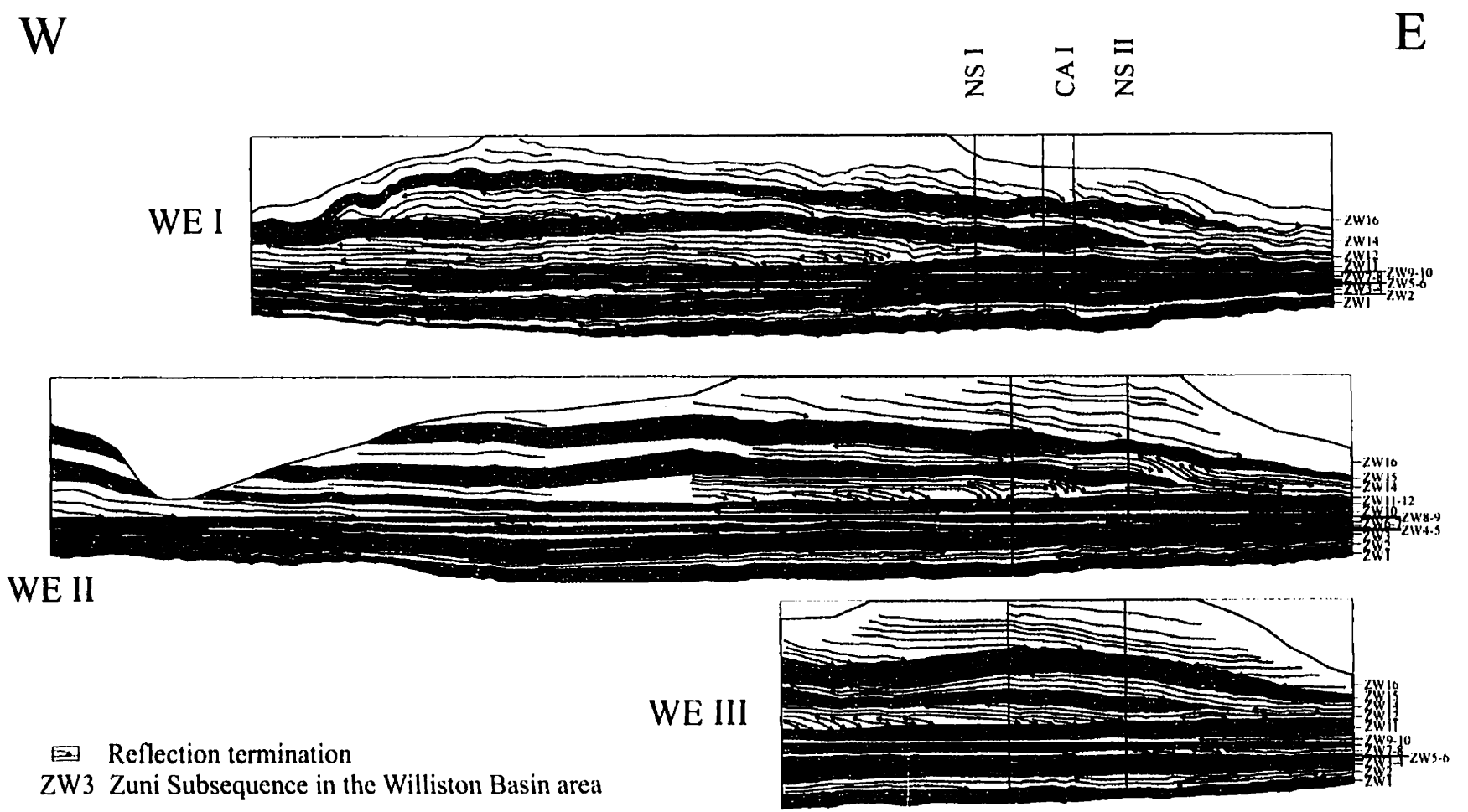

Fig. 7.27 Zuni sequence stratigraphy of the west-east lines.

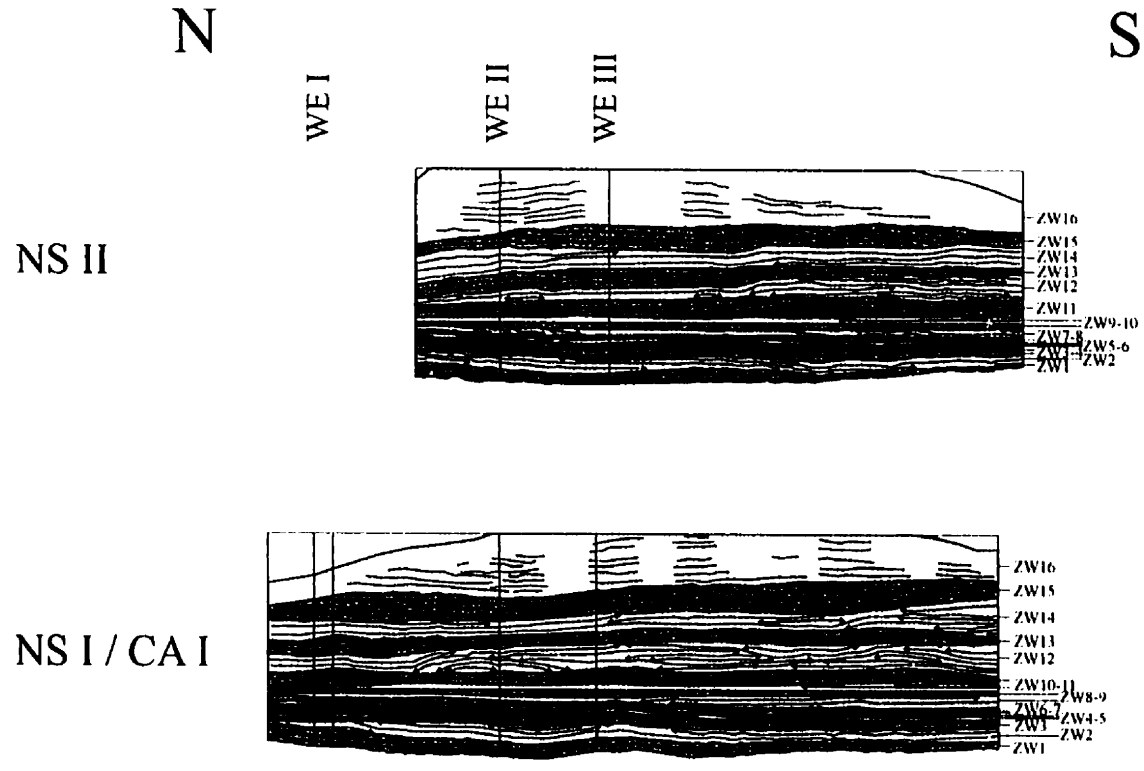

Reflection termination
ZW3 Zuni Subsequence in the Williston Basin area

Fig. 7.28 Zuni sequence stratigraphy of the north-south lines.

VII	Claggett cycle	81 – 78
VI	Niobrara cycle	90 – 81
V	Greenhorn cycle	99 – 90
IV	Skull Creek cycle	109 – 99
III	Clearwater	112 – 109
II	Mount Goodenough cycle	129 – 112
I	Betty Peaks cycle	139 – 129

This nomenclature is also to be avoided for sequence stratigraphic subdivision for the aforementioned reason. Sequence stratigraphic subdivision of Haq et al. *(1988b)* cannot be used either, because they indicate only the assumed 'eustatic' sea level changes. The interpreted subsequences overlap in some places with the sequences of Haq et al. *(1988b)*, which shows that the sequential development (sediment accommodation potential) in the Western Interior Seaway is dependent not only on eustatic sea-level variations, but tectonic and sediment supply, as well. Based on the concept of sequence stratigraphy, therefore, sixteen Zuni Williston Basin Subsequences (ZW) can be identified in the regional seismic sections ***(Fig. 7.29)***. Kauffman and Caldwell *(1993)* noted that in the Western Interior Seaway lowstand and transgressive system tracts show restricted development or commonly are absent altogether, whereas highstand system tracts dominate the sequences. A more refined subdivision, identifying system tracts, would require a denser seismic grid and more well-log information.

7.2.2.2 Progradational pattern of the ZW12 subsequence

Due to the limited thickness of the individual sequence-stratigraphic units, detailed interpretation of the internal structure can be made only for a few units. The best example is the lowstand part of the ZW12 subsequence. It is not surprising that Zhu *(1992)* was bale to subdivide this part into several subsequences (~A-E subsequences of his Montana sequence). Three-dimensional investigation allowed by the extra regional profiles of the present study leads to the recognition that the lower part of Zhu's *(1992)* Montana sequence (~A-E) is part of a progradational sequence. The finer subdivisions

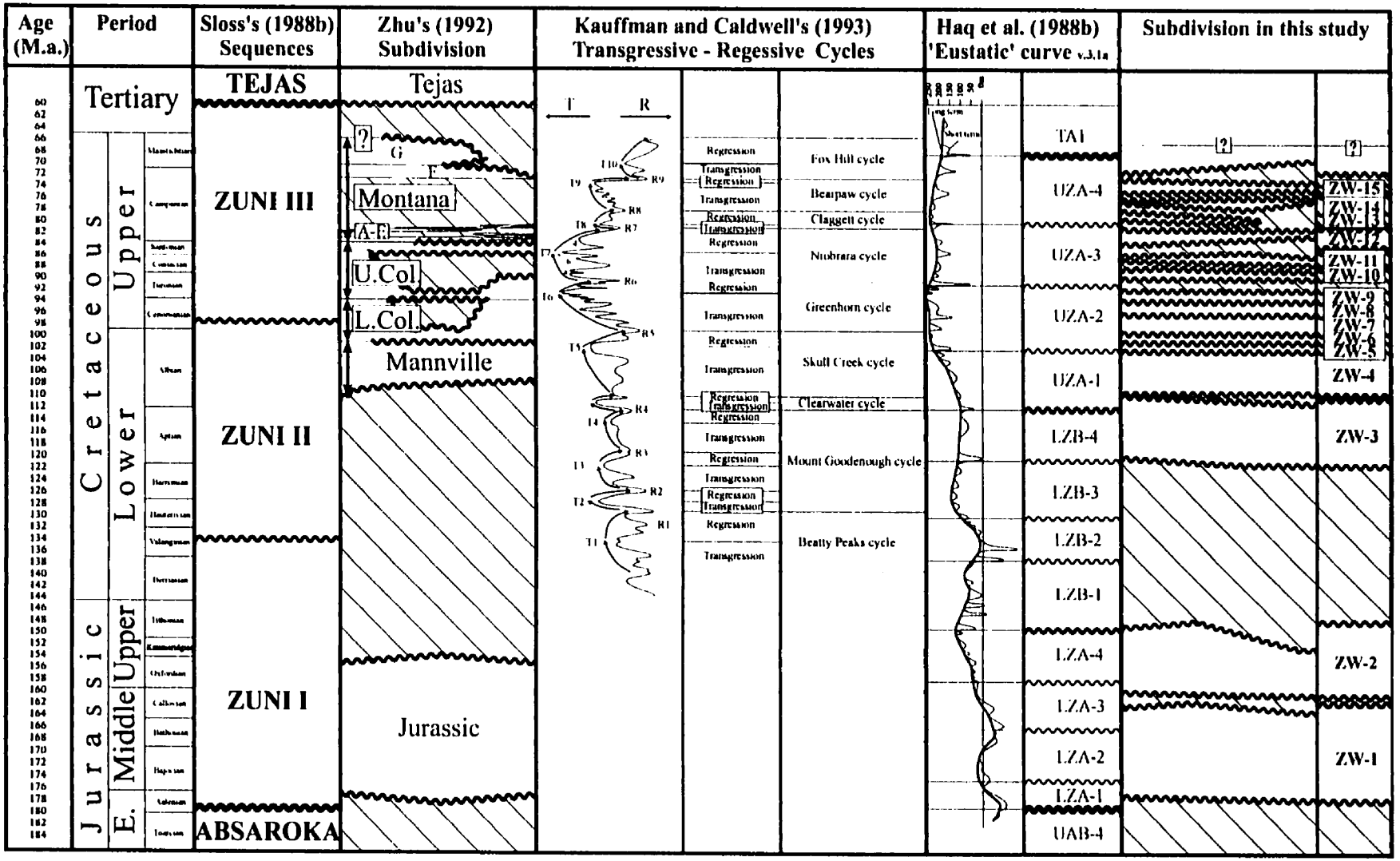

Fig. 7.29 Various sequential subdivisions of the Zuni Sequence in the Williston Basin area.

of by Zhu (1992) are actually the higher- (fourth-?) order sequences representing phases of progradation. Although higher-order sequences of this lowstand can be identified on the other regional seismic sections, the regional profiles are not reliable for correlation of fourth- and higher-order sequences. For this, a denser seismic grid is required. The ZW12 subsequence refers to the regressive phase of the Niobrara cycle ***(Fig. 7.29)***. Lithologically, the Eagle Sandstone and its equivalents occupy most of this interval. Within the Eagle Sandstone, Hanson and Little *(1987)* identified seven fourth-order progradational sequences around Billings, MT. Gill and Cobban *(1973)* and Rice *(1980)* defined the strandlines and the seaward limits of the Eagle coastal and shelf sandstones of the regressive phase of the Niobrara Sea ***(Fig. 7.30)***. The numbers in ***Fig. 7.30*** indicate an eastward moving shoreline position. The shorelines exhibit a wavy character with "bays" and "peninsulas". The eastern limits of the Eagle coastal and shelf sandstones generally follow this shoreline pattern. Consecutive downlap surfaces of the eastward thinning ZW12 subsequence delineate a similar wavy pattern which also mimics the shoreline ~500 km from it! Especially the downlap termination of the oldest traceable reflection, labeled ***a***, is clearly recognizable on the regional sections. The north-south sections, primarily NS I, unmistakeably exhibit two western sediment sources ***(Fig. 7.30)***. Of the two, the northern source (northern arrow in ***Fig. 7.30***) is probably the deltas located southeast of the Bearpaw Mountains, which spread their clastic sediments toward the ENE, expressed by the "peninsula" extended in that direction. The southern source (southern arrow in ***Fig. 7.30***) is located around south-central Montana and north-central Wyoming. Sediments from this source area reached the Williston Basin area in southwestern North Dakota and northwestern South Dakota ***(Fig. 7.30)***. Further to the east the successive downlap limits ***(b, c, d)*** still show the two sediment sources, however with decreasing resolution. Although a similar correlation in other progradational units of the sediment sources and the depositional structures in the central part of the study area was expected, no clear indication allowed a comparable interpretation.

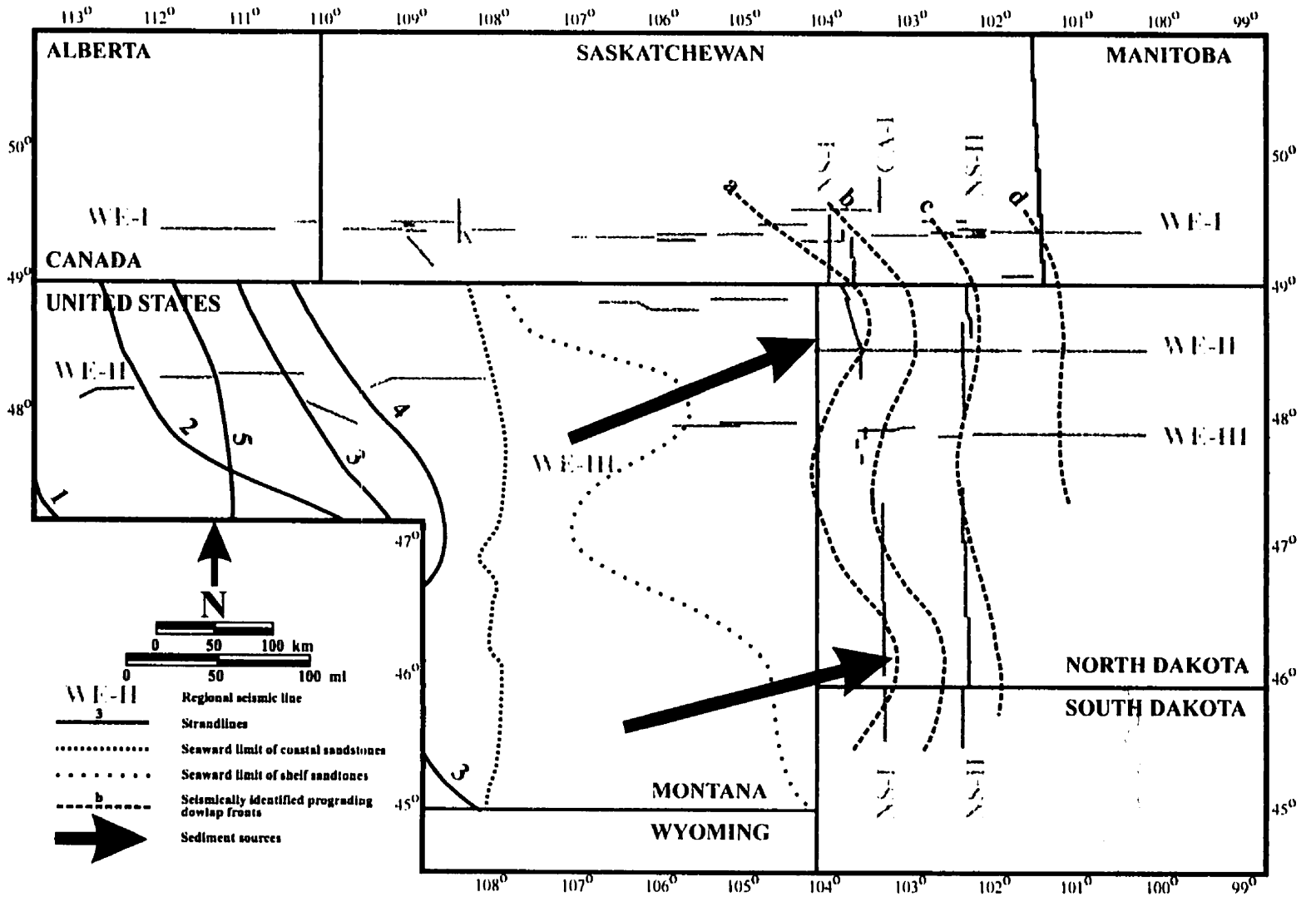

Fig. 7.30 Progradation during the ZW12 sequence. [~Eagle Formation and equivalents] (extended from Rice, 1980).

CHAPTER 8

SUMMARY AND SUGGESTED DIRECTIONS FOR FUTURE RESEARCH

8.1 Summary

The Williston Basin is one of the most researched cratonic basins of the world. Despite the vast amount of data from the basin, the current basin-evolution models still can not describe satisfactorily the primary cause of the subsidence and the deformation of the basin throughout its history. This investigation essentially addresses the second aspect, although the possibilities of the basin's origin are narrowed down by the additional insights provided by the results.

Some of the previous models for the internal deformation of the basin are considered here to be inadequate, some of them partly applicable and others, often the most popular ones, are highly speculative and found to be occasionally unsubstantiated by real data.

In this thesis, a different approach was chosen. Instead of a model-based basin-evolution theory, compilation of an extensive dataset supplied the factual background for the evolution model of the Williston Basin presented here.

The primary source of the interpretation is the ~3090 km of seismic information incorporating the 790-km section of Zhu's *(1992)* study. The total data length includes the gaps of the profiles as described previously. The new dataset represents four more

regional seismic profiles, resulting in probably the best and most extensive regional seismic coverage of the a cratonic basin.

All the new seismic data were reprocessed from field tapes. A standard seismic processing scheme was applied, with special consideration of the requirements of regional profiling. An additional step, the "Earth-curvature" correction, was executed for display reasons, to enhance general character the of the Williston Basin.

Synthetic seismograms were generated, from wells along the seismic lines, to aid in the identification and interpretation of the seismic reflections.

The rigorous seismic interpretation was based on the principles of seismic stratigraphy. A sequence stratigrapic framework of the Phanerozoic strata was supplied, which is the basis of analysis of the Williston Basin.

The new and extensive seismic interpretation, combined with well information and existing thickness and structural maps supplied a solid base for the new tectonostratigraphic model of the Williston Basin.

The evolution of the Williston Basin area can be subdivided into three major periods, representing different structural characters.

The first, **"pre-Williston" phase**, took part before the beginning of the basin subsidence, around the early-middle Cambrian. Indirect information from later structural directions and subsidence studies suggests that the area of the Williston Basin, underlain by an Archean cratonic block, was axisymmetrically uplifted probably by a mantle intrusion, and eroded prior to the subsidence. The axisymmetric uplift was accompanied by radially arranged extensional faults and fractures in the basement below the subsequent location of the basin and presumably circumferentially arranged compressional faults at its flanks.

The second phase is the **intracratonic phase**, which is represented in the Williston Basin by the interval ranging from the Sauk Sequence to the Absaroka Sequence. The subsidence was presumably caused and maintained by cooling and/or phase change of the mantle material. This mantle source was located beneath the central part of the basin and the subsidence resulted in recurrent reactivation of the pre-existing, axisymmetric radial and circumferential faults in a way that was the opposite to how they acted in the first phase. The radial faults in the central part became compressional, while the circumferential faults became extensional. Distribution of the sequences in this phase shows that, without significant lateral forces, the axisymmetric deformation dominated the basin's tectonics. This underlines other observations; namely that the structural activities in the basin do not coincide and, therefore, are not related to tectonic processes on the plate margins. The recurrent active periods are considered here the very consequence of cratonic basin subsidence. The oval shape of the basin, and probably of other cratonic basins, is the result of axisymmetric subsidence. A notable exception in the second phase is the tectonic framework of the Kaskaskia I Sequence (Devonian), when the area was tilted to the northwest and the axisymmetric deformation was overprinted by this effect. The axisymmetric framework of the basin's subsidence was reestablished in the Kaskaskia II and continued into the Absaroka.

During the third, **foreland phase**, in the Zuni – Tejas interval, the Williston Basin became part of the Western Canada Sedimentary Basin. ENE-WSW-oriented compressional forces, related to the Sevier and Laramide orogenies, resulted in a NNW-SSE elliptical elongation of the basin. Prevalent NE-SW/SE-NW-oriented faulting and fracturing with rotation and dragging of the earlier radial and circumferential structural features accompanied these forces. The earlier dominantly axisymmetric deformation in the basin was overprinted by this lateral compression; although, as the distribution of the sequences shows, the Williston Basin can still be considered as a separate structural entity.

Seismic/sequence stratigraphic analysis confirmed that major sequence boundaries generally coincide with lithostratigraphic boundaries during the Sauk–Absaroka interval.

In the Zuni–Tejas interval, where the clastic sedimentation was dominant, these boundaries are not identical. Some 16 sequence stratigraphic units were identified, reflecting cycles of sediment accommodation potential (composite of tectonics, eustatic sea-level changes, sediment influx, etc.) of the area. Out of the 16 sequence stratigraphic units, only one, that containing the Eagle Sandstone and its equivalents, allowed a finer analysis. The basin-scale three-dimensionality of the seismic profiles revealed two distinct western sources of sediments. In the central part of the Williston Basin, more than 500 km from the shorelines, sediment structures from deltas, located in central Montana in the north and north-central Wyoming in the south, are still recognizable.

8.2 Suggested directions for future research

As noted in the ***Introduction***, the dataset has far more information that can fit into one thesis and this type of study can never be finished. This thesis, based on the new seismic dataset, challenges some earlier interpretations of the basin's evolution. The suggested direction for future research points out the important areas where additional data could prove or supersede the model presented in this thesis.

The latest crustal seismic data of the Trans-Hudsonian system, as noted in the thesis, show a northern, Archean "Sask Craton" and a southern, Archean "Dakota Block". The latter is located beneath the Williston Basin. The undefined boundary between the two blocks and the bend in the Central Plains Conductive Anomaly suggest some kind of structural zone. Additional crustal seismic profiling is needed to reveal the exact nature of this boundary. This is a complex part of the Trans-Hudson Orogen and is not imaged by the recent crustal seismic data in satisfactory detail.

A related issue is the clarification of the southern extent of the Tabbernor Fault. Recent interpretations, mainly based on air and satellite images, suggesting its continuation south of the assumed line, is questioned here. This problem could be addressed with a subregional study in southeast Saskatchewan and southwest Manitoba – which is actually underway due to the cooperation of the Geological Survey of Canada (Calgary) and the University of Saskatchewan. A denser seismic grid of this area could test the ideas of the thesis in this structurally complicated area, which was affected by both the radial and circumferential structural features throughout the history of the basin. A subregional seismic grid, coupled with extended well information from the Jurassic–Cretaceous interval could help to fine-tune the recently identified Zuni–Tejas seismic/sequence stratigraphic boundaries and identify higher-order (fourth-fifth) stratigraphic sequences. This could lead to a better Zuni–Tejas subdivision of that part of the Williston Basin tied to the Sevier–Laramide structural activity.

REFERENCES

Ahern, J.L. and Mrkvicka, S.R. 1984. A mechanical and thermal model for the evolution of the Williston basin. *Tectonics, 3, 79-102.*

Ahern, J.L. and Ditmars, R.C. 1985. Rejuvenation of continental lithosphere beneath an intracratonic basin. *Tectonophysics, 120, 21-35.*

Ahern, J.L. and Dikeou, P.J. 1989. Evolution of the lithosphere beneath the Michigan Basin. *Earth and Planetary Science Letters, 95, 73-84.*

Aleinikov, A.L., Bellavin, O.V., Bulashevich, Y.P., Tarvin, I.F., Maksimov, E.M., Rudkevich, M.Y., Nalivkin, V.D., Shoblinskoyo, N.V. and Surkov, V.S. 1980. Dynamics of the Russian and West Siberian platforms. *In: Bally, A.W., Bender, P.L., McGetchin, R.I. (eds.) Dynamics of plate interiors. Geodynamic Series, 1, 53-71.*

Allum, J.A.E. 1978. Lineament, linear, lineation: some proposed new standards for old terms: Discussion *Geological Society of America Bulletin, 88(1), 159.*

Altschuld, N. and Kerr, S.D.Jr. 1982. Mission Canyon and Duperow reservoirs of the Billings Nose, Billings County, North Dakota. *In: Christopher, J.E. and Kaldi, J. (eds.) Fourth International Williston Basin Symposium, Saskatchewan Geological Society, Special Publication 6, 89-93.*

Anderson, E.M. 1951. The dynamics of faulting and dyke formations with application to Britain. *2nd ed., Edinburgh, Oliver and Boyd. 206p.*

Anderson, S.B., Hansen, D.E., Easwood, W.P., Hansen, M. Johnson, D.S. and Folsom, C.B. 1960. Oil fields in the Burke County area, North Dakota. *North Dakota Geological Survey, Report of investigation 36, 71p.*

Andrew, J.A., Edwards, D.M., Graf, R.J. and Wold, R.J. 1991. Empirical observations relating near-surface magnetic anomalies to high- frequency seismic data and Landsat data in eastern Sheridan County, Montana. *Geophysics, 56(10), 1553-1570.*

Ansdell, K.M., Lucas, S.B., Connors, K.A. and Stern, R.A. 1995. Kisseynew metasedimentary gneiss belt, Trans-Hudson Orogen (Canada): back-arc origin and collisional inversion. *Geology, 23, 1039-1043.*

Avbovbo, A.A., Ayoola, E.O. and Osahon, G.A. 1986. Depositional and structural styles in Chad Basin of northeastern Nigeria. *American Association of Petroleum Geologists Bulletin, 70(12), 1787-1798.*

Badley, M.E. 1985. Practical seismic interpretation. *International Human Resources Corporation, 266p.*

Baird, D.J., Knapp, J.H., Steer, D.N., Brown, L.D. and Nelson, K.D. 1995. Upper-mantle reflectivity beneath the Williston basin, phase-change Moho, and the origin of intracratonic basins. *Geology, 23(5), 431-434.*

Baird, D.J., Nelson, K.D., Knapp, J.H., Walters, .J. and Brown, L.D. 1996. Crustal structure and evolution of the Trans-Hudson orogen: Results from seismic reflection profiling. *Tectonics, 15(2), 416-426.*

Ballard, W.W. 1985. Ledger Field. *In: Tonnsen, J.J. (ed.) Montana oil and gas field symposium 1985. Montana Geological Society, v.2., 685-688.*

Bally, A.W. 1982. Musing over sedimentary basin evolution. *Philosophical Transactions of the Royal Society, London, Series A, 305, 325-338.*

Bally, A.W. 1989. Phanerozoic basins of North America. *In: Bally, A.W. and Palmer, A.R. (eds.) Geological Society of America, The geology of North America, A, 221-241.*

Basinski, P.M. 1985. Outlook, Middle Field. *In: Tonnsen, J.J. (ed.) Montana oil and gas field symposium 1985. Montana Geological Society, v.1., 573-576.*

Bayly, B. 1982. Geometry of subducted plates and island arcs viewed as a buckling problem. *Geology, 10(12), 629-632.*

Beaumont, C., Quinlan, G.M. and Stockmal, G.S. 1993. The evolution of the Western Interior Basin: causes, consequences and unsolved problems. *In: Caldwell, W.G.E. and Kauffman, E.G. (eds.) Evolution of the Western Interior Basin. Geological Association of Canada, Special Paper 39, 97-117.*

Bogle, R.W. and Hansen, W.B. 1987. Knutson Field and its relationship to the Mission Canyon Oil play, south-central Williston Basin. *In: Carlson, C.G. and Christopher, J.E. (eds.) Fifth International Williston Basin Symposium, Saskatchewan Geological Society, Special Publiaction 9, 242-252.*

Bond, G.C. and Kominz, M.A. 1991. Disentangling Middle Paleozoic sea level and tectonic events in cratonic margins and cratonic basins of North America. *Journal of Geophysical Research, 96(B4), 6619-6639.*

Braille, L.W., Keller, G.R., Hinze, W.J. and Lidiak, E.G. 1982. An ancient rift complex and its relation to contemporary seismicity in the New Madrid seismic zone. *Tectonics, 1, 225-237.*

Braille, L.W., Keller, G.R., Hinze, W.J., Lidiak, E.G. and Sexton, J.L. 1986. Tectonic development of the New Madrid Rift complex, Mississippi embayment, North America. *Tectonophysics, 131, 1-21.*

Bridges, L.W.D 1978. Red Wing Creek field, North Dakota: a concentricline of structural origin. *In: Estelle, D. and Miller, R. (eds.) The economic geology of the Williston Basin. Montana Geological Society, 315-326.*

Bridges, L.W.D. 1987. Red Wing Creek field, North Dakota: a growth faulted or meteoritic impact structure. *In: Peterson, J.A., Kent, D.M., Anderson, S.B., Piladzke, R.H. and Longman, M.W. (eds.) Williston Basin: anatomy of a cratonic oil province. Rocky Mountains Association of Geologists, 433-440.*

Bronner, G., Roussel, J., Trompette, R. and Clauer, N. 1980. Genesis and geodynamic evolution of the Taoudeni cratonic basin (Upper Precambrian and Paleozoic), Western Africa. *In: Bally, A.W., Bender, P.L., McGetchin, T.R. and Walcott, R.I. (eds.) Dynamics of plate interiors. Geodynamics Series, 1, 81-90.*

Brown, Donald L. and Brown, Darren L. 1987. Wrench-style deformation and paleostructural influence on sedimentation in and around a cratonic basin. *In: Peterson, J.A., Kent, D.M., Anderson, S.B., Piladzke, R.H. and Longman, M.W. (eds.) Williston Basin: anatomy of a cratonic oil province. Rocky Mountains Association of Geologists, 57-70.*

Brown, L.D. and Reilinger, R.E. 1986. Epeirogenic and intraplate movements. *In: Wallace, R.E. (chairperson) Active tectonics. Studies in geophysics, National Academy Press, 30-44.*

Burke, K. and Dewey, .F. 1973. Plume generated triple junctions; key indicators in applying plate tectonics to old rocks. *Journal of Geology, 81(4), 406-433.*

Burke, K. 1976. The Chad Basin: an active intra-continental basin. *Tectonophysics, 36, 197-206.*

Burke, K. 1977. Aulacogens and continental breakup. *Annual Review of Earth and Planetary Sciences, 5, 371-396.*

Burke, R.B. 1991. Mississippian oil production in part of Burke, Mountrail and Ward counties, North Dakota. *In: Christopher, J.E. and Haidl, F.M. (eds.) Sixth International Williston Basin Symposium. Saskatchewan Geological Society, Special Publication 11, 130-134.*

Burton, R., Kendall, C.G.St.C. and Lerche, I. 1987. Out of our depth: on the impossibility of fathoming eustasy from the stratigraphic record. *Earth-Science Reviews, 24, 237-277.*

Buschbach, T.C. and Kolata, D.R. 1991. Regional setting of Illinois Basin. *In: Leighton, M.W., Kolata, D.R., Oltz, D.F. and Eidel, J.J. (eds.) Interior cratonic basins. American Association of Petroleum Geologists, Memoir 51, 29-55.*

Butterfield, G.E. 1985. Laredo Field. *In: Tonnsen, J.J. (ed.) Montana oil and gas field symposium 1985. Montana Geological Society, v.2., 681-684.*

Carlson, C.G. 1960. Stratigraphy of the Winnipeg and Deadwood formations in North Dakota. *North Dakota Geological Survey Bulletin, 35, 149 p.*

Carlson, C.G. and Thompson, S.C. 1987. Stratigraphy of the Deadwood Formation and Winnipeg Group in the Williston Basin. *In: Peterson, J.A., Kent, D.M., Anderson, S.B., Piladzke, R.H. and Longman, M.W. (eds.) Williston Basin: anatomy of a cratonic oil province. Rocky Mountains Association of Geologists, 71-81.*

Catacosinos, P.A., Harrison, W.B. and Daniels, P.R. 1991. Structure, stratigraphy, and petroleum geology of the Michigan Basin. *In: Leighton, M.W., Kolata, D.R., Oltz, D.F. and Eidel, J.J. (eds.) Interior cratonic basins. American Association of Petroleum Geologists, Memoir 51, 561-601.*

Cercone, K.R. 1984. Thermal history of Michigan Basin. *American Association of Petroleum Geologists Bulletin, 68(2), 130-136.*

Chamberlain, V.R. 1985. Gypsy Basin Field. *In: Tonnsen, J.J. (ed.) Montana oil and gas field symposium 1985. Montana Geological Society, v.1., 573-576.*

Chow, N. 1991. Dolomitization in Middle Devonian platform carbonates, Elm Point Formation, Interlake area, Manitoba. *In: Christopher, J.E. and Haidl, F.M. (eds.) Sixth International Williston Basin Symposium. Saskatchewan Geological Society, Special Publication 11, 34-39.*

Christie-Blick, N., Mountain, G.S. and Miller, K.G. 1990. Seismic stratigraphic record of sea-level change. *In: Revelle, R.R. (panel chairman), Sea-level change. National Academy of Sciences, Studies in Geophysics, 116-140.*

Christofferson, E. and Hamil, M. 1978. A radial pattern of sea-floor deformation in the southwestern Caribbean Sea. *Geology, 6, 341-344.*

Christopher, J.E. 1987. Depositional patterns and oil field trends in the lower Mesozoic of the northern Williston Basin, Canada. *In: Peterson, J.A., Kent, D.M., Anderson, S.B., Piladzke, R.H. and Longman, M.W. (eds.) Williston Basin: anatomy of a cratonic oil province. Rocky Mountains Association of Geologists, 223-243.*

Cloetingh, S. 1986. Intraplate stresses: A new tectonic mechanism for fluctuations of relative sea level. *Geology, 14, 617-620.*

Cloetingh, S. 1988. Intraplate stresses: A new element in basin analysis. *In: Kleinspehn, K.L. and Paola, C. (eds.) New perspectives in basin analysis. Springer., 205-230.*

Coakley, B.J., Nadon, G.C. and Wang, H.F. 1994. Spatial variations in tectonic subsidence during Tippecanoe I in the Michigan Basin. *Basin Research, 6, 131-140.*

Collinson, C., Sargent, H.L. and Jennings, J.R. 1988. Illinois Basin region. *In: Sloss, L.L. (ed.) Sedimentary cover - North American craton, U.S. Geological Society of America, The geology of North America, D-2, 383-426.*

Cross, T.A. and Lessenger, M.A. 1988. Seismic stratigraphy. *Annual Review of Earth and Planetary Sciences, 16, 319-354.*

Crowley, K.D., Ahern, J.L. and Naeser, C.W. 1985. Origin and epeirogenic history of the Williston Basin: Evidence from fission-track analysis of apatite. *Geology, 13, 620-623.*

Dallmus, K.F. 1958. Mechanics of basin evolution and its relation to the habitat of oil in the basin. *In: Weeks,L.G. (ed.) Habitat of oil. American Association of Petroleum Geologists, Tulsa. 883-931.*

Dallmus, K.F. 1964. Discussion of "Strain energy in rocks". *In: Judd, W.R. (ed.) State of stress in the earth's crust - Proceedings of the International Conference, Santa Monica, CA, 1963. American Elsevier, 261-269.*

Daly, M.C., Lawrance,S.R., Diemu-Tshiband,K. and Matouana,B. 1992. Tectonic evolution of the Cuvette Centrale, Zaire. *Journal of the Geological Society of London, 149, 539-546.*

Day, J., Uyeno, T., Norris, W. Witzke, B. and Bunker, B.J. 1996. Middle- Upper Devonian realtive sea-ievel histories of central and western North American interior basins. *In: Witzke, B.J., Ludvigson, G.A. and Day, J. (eds.) Paleozoic sequence stratigraphy: views from the North American craton. Geological Society of America Special Paper 306, 425-434.*

Dean, K. 1982. Devonian Dawson Bay Formation in northwestern North Dakota. *In: Christopher, J.E. and Kaldi, J. (eds.) Fourth International Williston Basin Symposium, Saskatchewan Geological Society, Special Publication 6, 89-92.*

Dean, K. 1987. Mississippian Ratcliffe and Nesson reservoirs, Rosebud Field, Williams County, North Dakota. *Mountain Geologist, 24(4), 95-106.*

De Brito-Neves, B.B., Fuck, R.A., Cordani, U.G. and Thomaz, A. (1984) Influence of basement structures on the evolution of the major sedimentary basins of Brazil: a case of tectonic heritage. *Journal of Geodynamics, 1, 495-510.*

De Caritat, P. and Braun, J. 1992. Cyclic development of sedimentary basins at convergent plate margins - 1. Structural and tectono-thermal evolution of some Gondwana basins of eastern Australia. *Journal of Geodynamics, 16(4), 241-282.*

De Matos, R.M.D. and Brown, L.D. 1992. Deep seismic profile of the Amazonian craton (northern Brazil). *Tectonics, 11(3), 621-633.*

DeRito, R.F., Cozzarelli, F.A. and Hodge, D.S. 1983. Mechanism of subsidence of ancient cratonic rift basins. *Tectonophysics, 94, 141-168.*

Dolson, J. Muller, D. Evetts, M.J. and Stein, J.A. 1991. Regional paleotopographic trends and production, Muddy Sandstone (Lower Cretaceous), central and northern Rocky Mountains. *American Association of Petroleum Geologists Bulletin, 75(3), 409-435.*

Dolson, J., Piombino, J., Franklin, M. and Harwood, R. 1993. Devonian oil in Mississippian and Mesozoic reservoirs - unconformity controls on migration and accumulation, Sweetgrass Arch, Montana. *Mountain Geologist, 30(4), 125-146.*

Dunn, C.E. 1982. Geology of the Middle Devonian Dawson Bay Fromation in the northern part of the Williston Basin. *In: Christopher, J.E. and Kaldi, J. (eds.) Fourth International Williston Basin Symposium, Saskatchewan Geological Society, Special Publication 6, 29-42.*

Ellingson, J.B. and LeFever, R.D. 1995. Depositional environments and history of the Winnipeg Group (Ordovician), Williston Basin North Dakota. *In: Vern Hunter, L.D. and Schalla, R.A. (eds.) Seventh International Williston Basin Symposium Guidebook, 129-139.*

Elliott, C.G. 1996. The Tabbernor Fault in four dimensions. *In: Hajnal, Z. and Lewry, J. (eds.) LITHOPRPOBE Trans-Hudson Orogen Transect. Report of sixth transect meeting. LITHOPROBE Report 55, 5-9.*

Emery, D. and Myers, K.J. 1996. Sequence stratigraphy. *Blackwell Science, 297p.*

Ernst, R.E., Head, J.W., Parfitt, E., Grosfils, E. and Wilson, L. 1995. Giant radiating dyke swarms on Earth and Venus. *Earth Science Reviews, 39, 1-58.*

Famakinwa, S.B. 1989. Structural and tectonic study of the central Williston Basin, northeast Montana and northwest North Dakota. *Unpublished Ph.D. Thesis. Colorado School of Mines. 212 p.*

Finlayson, D.M., Leven, J.H. and Wake-Dyster, K.D. 1989. Large-scale lenticles in the lower crust under an intra-continental basin in eastern Australia. *In: Mereu, R.F., Mueller, S. and Fountain, D.M. (eds.) Properties and processes of the Earth's lower crust. American Geophysical Union, Geophysical Monograph 51, IUGG Volume 6, 3-16.*

Fisher, J.H. and Barratt, M.W. 1985. Exploration in Ordovician of central Michigan Basin. *American Association of Petroleum Geologists Bulletin, 69(12), 2065-2076.*

Fisher, J.H., Barratt, M.W., Droste, J.B. and Shaver, R.H. 1988. Michigan Basin. *In: Sloss, L.L. (ed.) Sedimentary cover - North American craton, U.S. Geological Society of America, The geology of North America, D-2, 361-382.*

Fowler, C.M.R. and Nisbet, E.G. 1985. The subsidence of the Williston Basin. *Canadian Journal of Earth Sciences, 22, 408-415.*

Freisatz, W.B. 1995. Fracture-enhanced porosity and permeability trends in the Bakken Formation, Williston Basin, western North Dakota. *In: Vern Hunter, L.D. and Schalla, R.A. (eds.) Seventh International Williston Basin Symposium Guidebook, 389-398.*

Fukao, Y., Yamaoka, K. and Sakura, T. 1987. Spherical shell tectonics: buckling of subducting lithosphere. *Physics of the Earth and Planetary Interiors, 45, 59-67.*

Gallagher, K. and Lambeck, K. 1989. Subsidence, sedimentation and sea- level changes in the Eromanga Basin, Australia. *Basin Research, 2, 115-131.*

Galloway, W.E. 1989. Genetic stratigraphic sequences in basin analysis I: Architecture and genesis of flooding-surface bounded depositional units. *American Association of Petroleum Geologists Bulletin, 73(2), 125-142*

Gendzwill, D.J. 1978. Winnipegosis mounds and Prairie Evaporite Formation of Saskatchewan - seismic study. *American Association of Petroleum Geologists Bulletin, 62, 73-86.*

Gendzwill, D.J. and Wilson, N.L. 1987. Form and distribution of Winnipegosis mounds in Saskatchewan. *In: Peterson, J.A., Kent, D.M., Anderson, S.B., Piladzke, R.H. and Longman, M.W. (eds.) Williston Basin: anatomy of a cratonic oil province. Rocky Mountains Association of Geologists, 9-43.*

Gerhard, L.C., Anderson, S.B., LeFever, J.A. and Carlson, C.G. 1982. Geological development, origin and energy mineral resources of the Williston Basin, North Dakota. *American Association of Petroleum Geologists Bulletin, 66, 989-1020.*

Gerhard, L.C., Anderson, S.B. and LeFever, J.A. 1987. Structural history of the Nesson Anticline, North Dakota. *In: Peterson, J.A., Kent, D.M., Anderson, S.B., Piladzke, R.H. and Longman, M.W. (eds.) Williston Basin: anatomy of a cratonic oil province. Rocky Mountains Association of Geologists, 337-354.*

Gerhard, L.C. and Anderson, S.B. 1988. Geology of the Williston Basin (United States portion). *In: Sloss, L.L. (ed.) Sedimentary cover - North American craton, U.S. Geological Society of America, The geology of North America, D-2, 221-241.*

Gerhard, L.C., Anderson, S.B. and Fischer, D.W. 1991. Petroleum geology of the Williston Basin. *In: Leighton, M.W., Kolata, D.R., Oltz, D.F. and Eidel, J.J. (eds.) Interior cratonic basins. American Association of Petroleum Geologists, Memoir 51, 507-559.*

Gerhard, L.C., Anderson, S.B. Olea, R. and Robertson, L. 1995. Western Cold Turkey Creek field anomaly: a meteorite impact crater - NOT! *In: Vern Hunter, L.D. and Schalla, R.A. (eds.) Seventh International Williston Basin Symposium Guidebook, 179-185.*

Ghosh, S.K. and Ramberg, H. 1968. Buckling experiment on intersecting fold patterns. *Tectonophysics, 5(2), 89-105.*

Ghosh, S.K., Khan, D. and Sengupta, S. 1995. Interfering folds in constrictional deformation. *Journal of Structural Geology, 17(10), 1361-1373.*

Gibson, R.I. 1995. Basement tectonics and hydrocarbon production in the Williston Basin: an interpretive overview. *In: Vern Hunter, L.D. and Schalla, R.A. (eds.) Seventh International Williston Basin Symposium Guidebook, 3-9.*

Gill, J.R. and Cobban, W.A. 1973. Stratigraphy and geologic history of the Montana Group and equivalent rocks, Montana, Wyoming, and North and South Dakota. *United States Geological Survey, Professional Paper 776. 37p.*

Giroux, D.L. 1995. Location and Phanerozoic history of the Tabbernor Fault. *In: Macdonald, R., Sibbald, T.I.I., Harper C.T., Paterson, D.F. and Guliov, P. (eds.) Summary of investigations 1995, Saskatchewan Geological Survey, Saskatchewan Energy and Mines Miscellaneous Report, 95-4, 153-155.*

Gradstein, F.M., Agterberg, F.P., Ogg, J.G., Hardenbol, J., van Veen, P., Thierry, J. and Huang, Z. 1995. A Triassic, Jurassic and Cretaceous time scale. *In: Berggren, W.A., Kent, D.V., Aubry,M-P. and Hardenbol, J. (eds.) Geochronology, time scales and global stratigraphic correlation. Society for Sedimentary Geology, Special Publications, 54, 95-128.*

Grosfils, E.B. and Head, J.W. 1994. The global distribution of giant radiation dike swarms on the Venus: Implications for the global stress state. *Geophysical Research Letters, 21(8), 701-704.*

Gries, R. 1983. North-south compression of the Rocky Mountain Foreland structures. *In: Lowell, J.D. (ed.) Rocky Mountain Foreland basins and uplifts. Rocky Mountain Association of Geologists, 9-32.*

Haid, J. 1991. Tectonic subsidence analysis of the Williston Basin. *Unpublished M.Sc. Thesis, University of Saskatchewan, 118p.*

Hajnal, Z., Fowler, C.M.R., Mereu, R.F., Kanasewich, E.R., Cumming, G.L., Green, A.G. and Mair, A. 1984. An initial analysis of the Earth's crust under the Williston Basin: 1979 COCRUST experiment. *Journal of Geophysical Research, 89(B11), 9381-9400.*

Halabura, S. 1982. Depositional environments of the Upper Devonian Birdbear Formation, Saskatchewan. *In: Christopher,J.E. and Kaldi,J. (eds.) Fourth International Williston Basin Symposium, Saskatchewan Geological Society, Special Publication 6, 29-42.*

Hamdani, Y., Mareschal, J-C. and Arkani-Hamed, J. 1991. Phase change and thermal subsidence in intracontinental sedimentary basins. *Geophysical Journal International, 106, 657-665.*

Hamdani, Y., Mareschal, J-C. and Arkani-Hamed, J. 1994. Phase change and thermal subsidence of the Williston basin. *Geophysical Journal International, 116, 585-597.*

Hanson, M.S. and Little, L.D. 1987. Genetic sequence analysis and its application to chronostratigraphic correlation, Eagle Sandstone (Campanian), Montana. *Geological Society of America Rocky Mountain Section, 40th Annual Meeting, Abstracts with Programs, 19(5), 281.*

Haq, B.U., Vail, P.R., Hardenbol, J. and Van Wagoner, J.C. 1988a. Sea level history. *Science, 241, 596-602.*

Haq, B.U., Hardenbol, J. and Vail, P.R. 1988b. Mesozoic and Cenozoic chronostratigraphy and eustatic cycles. *In: Wilgus, C.K., Hastings, B.S., Kendall, C.G.St.C., Posamentier, H.W., Ross, C.A. and Van Wagoner, J.C. (eds.) Sea-level changes: an integrated approach. Society of Economic Paleontologists and Mineralogists, Special Publication 42, 71-108.*

Hardage, R.A. 1987. Seismic stratigraphy. *Geophysical Press, 432p.*

Hartley, R.W. and Allen, P.A. 1994. Interior cratonic basins of Africa: relation to continental break-up and role of mantle convection. *Basin Research, 6, 95-113.*

Hartling, A., Brewster, A. and Posehn, G. 1982. The geology and hydrocarbon trapping mechanisms of the Mississippian Oungre Zone (Ratcliffe Beds) of the Williston Basin. *In: Christopher, J.E. and Kaldi, J. (eds.) Fourth International Williston Basin Symposium, Saskatchewan Geological Society, Special Publication 6, 217-223.*

Haxby, W.F., Turcotte, D.L. and Bird, J.M. 1976. Thermal and mechanical evolution of the Michigan Basin. *Tectonophysics, 36, 57-75.*

Heidlauf, D.T., Hsui, A.T. and Klein, G.deV. 1986. Tectonic subsidence analysis of the Illinois basin. *Journal of Geology, 94(6), 779-794.*

Hill, A.T. 1985. Sioux Pass Field. *In: Tonnsen, J.J. (ed.) Montana oil and gas field symposium 1985. Montana Geological Society, v.2., 1045-1049.*

Hoffman, P.F. 1988. United Plates of America, the birth of a craton: Early Proterozoic assembly and growth of Laurentia. *Annual Review of Earth and Planetary Sciences, 16, 543-603.*

Horner, J.R. 1984. Three ecologically distinct vertebrae faunal communities from the Late Cretaceous Two Medicine Formation of Montana, with discussion of evolutionary pressures induced by Interior Seaway fluctuations. *In: McBane, J.D. and Garrison, P.B. (eds.) Northwest Montana and adjacent Canada. Montana Geological Society 1984 Field Conference and Symposium, 299-303.*

Horner, R.B. and Hasegawa, H.S. 1978. The seismotectonics of southern Saskatchewan. *Canadian Journal of Earth Sciences, 15, 1341-1355.*

Howell, P.D. and van der Pluijm, B.A. 1990. Early history of the Michigan Basin: subsidence and Appalachian tectonics. *Geology, 18(12), 1195-1198.*

Inden, R.A. and Burke, R.B. 1995. Fault control and late stage diagenetic creation and enhancement of reservoirs. *In: Vern Hunter, L.D. and Schalla, R.A. (eds.) Seventh International Williston Basin Symposium Guidebook, 351-366.*

Indorf, C.P. and Norwood, E.E. 1987. Development of structure and porosity at Medicine Lake field in the northeastern Montana Williston Basin. *In: Peterson, J.A., Kent, D.M., Anderson, S.B., Piladzke, R.H. and Longman, M.W. (eds.) Williston Basin: anatomy of a cratonic oil province. Rocky Mountains Association of Geologists, 407-422.*

James, R.A. 1995. Post-Jurassic tectonism in the West Siberian Basin, Russia. *Journal of Petroleum Geology, 18(2), 125-148.*

Janes, D.M. and Melosh, H.J. 1990. Tectonics of planetary loading: A general model and results. *Journal of Geophysical Research, 95(B13), 21,345-21,355.*

Janes, D.M. and Squyres, S.W. 1993. Radially fractured domes: a comparison of Venus and the Earth. *Geophysical Research Letters, 20(24), 2,961-2,964.*

Jervey, M.T. 1988. Quantitative geological modelling of siliciclastic rock sequences and their sesimic expression. *In: Wilgus, C.K., Hastings, B.S., Kendall, C.G.St.C., Posamentier, H.W., Ross, C.A. and Van Wagoner, J.C. (eds.) Sea-level changes: an integrated approach. Society of Economic Paleontologists and Mineralogists, Special Publication 42, 47-70.*

Johnson, E.H. 1984. Blackleaf Canyon Field and Knowlton Field, Teton County, Montana. *In: McBane J.D. and Garrison, P.B. (eds.) Northwest Montana and adjacent Canada. Montana Geological Society 1984 Field Conference and Symposium, 325-330.*

Kallweit, R.S. and Wood, L.C. 1982. The limits of resolution of zero-phase wavelets. *Geophysics, 47(7), 1035-1046.*

Kanasewich, E.R., Clowes, R.M. and McLoughan, C.H. 1969. A buried Precambrian rift in western Canada. *Tectonophysics, 8, 513-527.*

Kanasewich, E.R., Hajnal, Z., Green, A.G., Clumming, G.L., Mereu, R.F., Clowes, R.M., Morel-a-l'Huissier, P., Chiu, S., Macrides, C.G., Shahriar, M. and Congram, A.M. 1987. Seismic studies of the crust under the Williston Basin. *Canadian Journal of Earth Sciences, 24, 2160-2171.*

Karner, G.D. 1986. Effects of lithospheric in-plane stress on sedimentary basin stratigraphy. *Tectonics, 5(4), 573-588.*

Kauffman, E.G. and Caldwell, W.G.E. 1993. The Western Interior Basin in space and time. *In: Caldwell, W.G.E. and Kauffman, E.G. (eds.) Evolution of the Western Interior Basin. Geological Association of Canada, Special Paper 39, 1-30.*

Kent, D.M. and Minto, J. 1991. Growth patterns of the Middle Devonian Winnipegosis Formation, Bluff reef Dawson Bay area, Manitoba. *In: Christopher, J.E. and Haidl F.M. (eds.) Sixth International Williston Basin Symposium. Saskatchewan Geological Society, Special Publication 11, 34-39.*

Klasner, J.S. and King, E.R. 1990. A model of tectonic evolution of the Trans-Hudson orogen in North and South Dakota. *In: Lewry, J.F. and Stauffer, M.R. (eds.) The Early Proterozoic Trans-Hudson Orogen of North America. Geological Association of Canada, Special Paper, 37, 271-286.*

Klein, G. deV. 1991. Origin and evolution of North American cratonic basins. *South African Journal of Geology, 94(1), 3-18.*

Klein, G. deV. and Hsui, A.T. 1987. Origin of cratonic basins. *Geology, 15(12), 1094-1098.*

Koch, D.M. 1994. A spreading drop model for plumes on Venus. *Journal of Geophysical Research, 99(E1), 2,035-2,052.*

Kogbe, C.A. 1991. Stratigraphy and tectonic history of the Iullemedden Basin in West Africa. *South African Journal of Geology, 94(1), 19-32.*

Kominz, M.A. and Bond, G.C. 1991. Unusually large subsidence and sea- level events during middle Paleozoic time: New evidence supporting mantle convection models for supercontinent assembly. *Geology, 19, 56-60.*

Korsch, R.J., Huazhao, M., Zhaocai, S. and Gorter, J.D. 1991. The Sichuan Basin, southwest China: a Late Proterozoic (Sinian) petroleum province. *Precambrian Research, 54, 45-64.*

Kupsch, W.O. and Wild, J. 1958. Lineaments in Avonlea area, Saskatchewan. *American Association of Petroleum Geologists Bulletin, 41(1), 127-134.*

Lambeck, K. 1983. Structure and evolution of the intracratonic basins of central Australia. *Geophysical Journal of the Royal Astronomical Society, 74, 843-886.*

Langtry, T.M. 1982. Carbonate sand bodies within the basal Swift Formation (Upper Jurassic) of northwestern North Dakota. Dakota. *In: Christopher, J.E. and Kaldi, J. (eds.) Fourth International Williston Basin Symposium, Saskatchewan Geological Society, Special Publication 6, 263-275.*

Lawrance, S.R. and Makazu, M.M. 1988. Zaire's Central basin: prospectivity and outlook. *Oil and Gas Journal, September 19, 1988, 105-108.*

Leckie, D. and Krystinik, L. 1989. Does paleocurrent data support storm-generated geostropic flow in an epeiric seaway. *28th International Geological Congress, Abstracts v. 2, 2,272-2,273.*

LeFever, J.A. and Anderson, S.B. 1986. Structure and stratigraphy of the Frobisher-Alida intervals, Mississippian Madison Group, north-central North Dakota. *North Dakota Geological Survey, Report of investigation 84. 17p.*

LeFever, J.A., LeFever, R.D. and Anderson, S.B. 1987a. Structural evolution of the central and southern portion of the Nesson Anticline, North Dakota. *In: Carlson, C.G. and Christopher, J.E. (eds.) Fifth International Williston Basin Symposium, Saskatchewan Geological Society, Special Publication 9, 147-156.*

LeFever, R.D. 1988. Subsidence history of the Williston Basin in North Dakota (abstract). *American Association of Petroleum Geologists Bulletin, 72, 875.*

LeFever, R.D., Thompson, S.C. and Anderson, D.B. 1987b. Earliest Paleozoic history of the Williston Basin in North Dakota. *In: Carlson, C.G. and Christopher, J.E. (eds.) Fifth International Williston Basin Symposium, Saskatchewan Geological Society, Special Publication 9, 22-36.*

LeFever, R.D. and Crashell, J.J. 1991. Structural development of the Williston Basin in southwestern North Dakota. *In: Christopher, J.E. and Haidl, F.M. (eds.) Sixth International Williston Basin Symposium, 222-233.*

LeFever, R.D. and McCloskey, J.G. 1995. Depositional history of the Newcastle Formation (Lower Cretaceous), Williston Basin, North Dakota, South Dakota and eastern Montana. *In: Vern Hunter, L.D. and Schalla, R.A. (eds.) Seventh International Williston Basin Symposium Guidebook, 411-416.*

Leighton, M.W. 1991. Introduction to interior cratonic basins. *In: Leighton, M.W., Kolata, D.R., Oltz, D.F. and Eidel, J.J. (eds.) Interior cratonic basins. American Association of Petroleum Geologists, Memoir 51, 1-24.*

Lewry, J.F., Thomas, D.J., Macdonals, R. and Chiarenzelli, J. 1990. Structural relations in accreted terranes of the Trans-Hudson Orogen, Saskatchewan: Telescoping in a collisional regime? *In: Lewry, J.F. and Stauffer, M.R. (eds.) The Early Proterozoic Trans-Hudson Orogen of North America. Geological Association of Canada, Special Paper, 37, 75-94.*

Lima, C., Nascimento, E. and Assumcao, M. 1997. Stress orientation in Brazilian basins from breakout analysis: implications for force models in the South American plate. *Geophysical Journal International, 130, 112-124.*

Lindsay, J.F. and Korsch, R.J. 1989. Interplay of tectonic and sea-level changes in basin evolution: an example from intracratonic Amadeus Basin, central Australia. *Basin Research, 2, 3-25.*

Lindsey, J.P. 1989. The Fresnel zone and its interpretive significance. *The Leading Edge, 8(10), 33-39.*

Lisle, R.J., Styles, P. and Freeth, S.J. 1990. Fold interference structures: the influence of layer competence contrast. *Tectonophysics, 172, 197-200.*

Liu, H.-S. and Bostrom, R.C. 1980. Mantle convection and subcrustal stress under the United States. *Modern Geology, 7, 81-93.*

Lobdell, F.K. 1984. Age and depositional history of the Middle Devonian Ashern Formation in the Williston Basin, Saskatchewan and North Dakota. *In: Lorsong, J.A. and Wilson, M.A. (eds.) Oil and Gas in Saskatchewan. Saskatchewan Geological Society, Special Publication 7, 5-12.*

LoBue, C. 1982. Depositional environments and diagenesis of the Silurian Interlake Formation, Williston Basin, western North Dakota. *In: Christopher, J.E. and Kaldi, J. (eds.) Fourth International Williston Basin Symposium, Saskatchewan Geological Society, Special Publication 6, 29-42.*

Lochman-Balk, C. 1972. Cambrian system. In: Mallory,W.W. (ed.) Geologic Atlas of the Rocky Mountain region. *Rocky Mountains Association of Geologists, 60-75.*

Lochman-Balk, C. and Wilson, J.L. 1967. Stratigraphy of Upper Cambrian - Lower Ordovician subsurface sequence in Williston Basin. *American Association of Petroleum Geologists Bulletin, 51(6), 883-917.*

Lopez, D.A. 1995. Geology of the Sweet Grass Hills north-central Montana. *Montana Bureau of Mines and Geology Memoir 68, 35p.*

Lorenz, J.C. 1982. Lithospheric flexure and the history of the Sweetgrass Arch northwestern Montana. *In: Powers, R.B. (ed.) Geologic studies of the Cordilleran thrust belt. Volume I., 77-98.*

Loup, B. and Wildi, W. 1994. Subsidence analysis in the Paris Basin: a key to Northwest European intracontinental basins? *Basin Research, 6, 159-177.*

Lucas, S.B., White, D., Bleeker, W., Hajnal, Z., Lewry, J. and Weber, W. 1996. Crustal structure of the Superior Boundary Zone (Thompson Belt) from new LITHOPROBE seismic reflection data. *Trans-Hudson Orogen Transect, LITHOPROBE Report, 55, 82-94.*

Marechal, J-C. and Lee, C-K. 1983. Initiation of subsidence in a sedimentary basin underlain by a phase change. *Geophysical Journal of the Royal Astronomical Society, 74, 689-712.*

Martindale, W., Erkmen, U., Metcalfe, D. and Potts, E. 1991. Winnipegosis buildups of the Hichcock area, southeastern Saskatchewan - a case study. *In: Christopher, J.E. and Haidl, F.M. (eds.) Sixth International Williston Basin Symposium. Saskatchewan Geological Society, Special Publication 11, 47-63.*

Martiniuk, C.D., Young, H.R. and LeFever,J .A. 1995. Lithofacies and petroleum potential of the Birdbear Formation (Upper Devonian), southwestern Manitoba and north-central North Dakota. *In: Vern Hunter, L.D. and Schalla, R.A. (eds.) Seventh International Williston Basin Symposium Guidebook, 89-102.*

Marvin, R.F., Hearn, B.C.Jr., Mehnert, H.H., Naeser, C.W., Zartman, R.E. and Lindsey, D.A. 1980. Late Cretaceous-Paleocene-Eocene igneous activity in north-central Montana. *Isochron/West 29, 5-25.*

Maughan, E.K. 1984. Paleogeographic setting of Pennsylvanian Tyler Formation and relation to underlying Mississippian rocks in Montana and North Dakota. *American Association of Petroleum Geologists Bulletin, 68(2), 178-195.*

Mayer, J.D. 1987. Geology of the Indian Hill Field area, central Williston Basin, North Dakota - a multiple-pay field developed in the 1980s. *In: Carlson, C.G. and Christopher, J.E. (eds.) Fifth International Williston Basin Symposium. Saskatchewan Geological Society, Special Publication 9, 197-211.*

McCaslin, J.C. 1982. Remote east Williston wildcat reported. *Oil & Gas Journal, 80, 38(Sept 20), 189-191.*

McClellan, W.A. 1995. Sherwood subinterval of the Mission Canyon Formation in central western North Dakota. *North Dakota Geological Survey, Report of investigation 97, 11p. 7pl.*

McTavish, G.J. 1991. Role of salt dissolution in controlling outcrop distribution in south-central Saskatchewan. *In: Christopher, J.E. and Haidl, F.M. (eds.) Sixth International Williston Basin Symposium. Saskatchewan Geological Society, Special Publication 11, 244-249.*

McTavish, G.J. and Vigrass, L.W. 1987. Salt dissolution and tectonics, south-central Saskatchewan. *In: Carlson, C.G. and Christopher, J.E. (eds.) Fifth International Williston Basin Symposium. Saskatchewan Geological Society, Special Publication 9, 157-168.*

Megnien, C. and Pomerol, C. 1980. Subsidence of the Paris basin from Lias to the Late Cretaceous. *In: Bally, A.W., Bender, P.L., McGetchin, R.I. (eds.) Dynamics of plate interiors. Geodynamic Series, 1, 91-92.*

Mereu, R.F. 1967. Curvature corrections to upper mantle seismic refraction surveys. *Earth and Planetary Science Letters 3, 469-475.*

Mesner, J.C. and Wooldridge, L.C.P. 1964. Maranhao Paleozoic basin and Cretaceous coastal basins, north Brazil. *American Association of Petroleum Geologists Bulletin, 48(9), 1475-1512.*

Miall, A.D. 1992. Exxon global cycle chart: An event for every occasion? *Geology, 20(9), 787-790.*

Miall, A.D. 1997. The geology of stratigraphic sequences. *Springer. 433p.*

Middleton, M.F. 1980. A model of intracratonic basin formation, entailing deep crustal metamorphism. *Geophysical Journal of the Royal Astronomical Society, 62, 1-14.*

Middleton, M.F. 1989. A model for the formation of intracratonic sag basins. *Geophysical Journal International, 99, 665-676.*

Mitchum, R.M., Vail, P.R. and Sangree, J.B. 1977a. Seismic stratigraphy and global changes of sea level; Part 6 Stratigraphic interpretation of seismic reflection patterns in depositional sequences. *In: Payton, C.E. (ed.) Seismic stratigraphy - application to hydrocarbon exploration. American Association of Petroleum Geologists, Memoir 26, 117-133.*

Mitchum, R.M., Vail, P.R. and Thompson, S. 1977b. The depositional sequence as a basic unit for stratigraphic analysis. *In: Payton, C.E. (ed.) Seismic stratigraphy - application to hydrocarbon exploration. American Association of Petroleum Geologists, Memoir 26, 53-62.*

Monson, L.M. 1996. Cretaceous system stratigraphy and shallow gas resources on the Fort Peck Reservation, northeastern Montana. *In: Vern Hunter, L.D. and Schalla, R.A. (eds.) Seventh International Williston Basin Symposium Guidebook, 163-176.*

Monson, L.M. and Lund, D.F. 1991. Breaking into Bakken potential on the Fort Peck Reservation in northeastern Montana. *In: Christopher, J.E. and Haidl, F.M. (eds.) Sixth International Williston Basin Symposium. Saskatchewan Geological Society, Special Publication 11, 47-52.*

Morel-a-l'Huissier, P., Green, A.G. and Pike, C.J. 1987. Crustal refraction surveys across the Trans-Hudson Orogen/Williston Basin of South Central Canada. *Journal of Geophysical Research, 92(B7), 6403-6420.*

Naimark, B.M. and Ismail-Zadeh, A.T. 1995. Numerical models of a subsidence mechanism in intracratonic basins: application to North American basins. *Geophysical Journal International, 123, 149-160.*

Napier, N.J. 1982. Knowlton gas field, Teton County, Montana. *In: Powers, R.B. (ed.) Geological studies of the Cordilleran thrust belt. Rocky Mountains Geological Society Guidebook, v.2., 575-579.*

Narr, W. and Burruss, R.C. 1984. Origin and reservoir fractures in Little Knife Field, North Dakota. *American Association of Petroleum Geologists Bulletin, 68(9), 1087-1100.*

Nelson, S.J., Glaister, R.P. and McCrossan, R.G. 1964. Chapter 1 - Introduction. *In: McCrossan, R.G. and Glaister, R.P. (eds.) Geological History of Western Canada. Alberta Society of Petroleum Geologists, 1-13.*

North American Commission on Stratigraphic Nomenclature 1983. North American Stratigraphic Code. *American Association of Petroleum Geologists Bulletin, 67(5), 841-875.*

Nunn, J.A. 1994. Free thermal convection beneath intracratonic basins: thermal and subsidence effects. *Basin Research, 6, 115-130.*

Nunn, J.A. and Sleep, N.H. 1984. Thermal contraction and flexure of intracratonical basins: a three-dimensional study of the Michigan basin. *Geophysical Journal of the Royal Astronomical Society, 76, 587-635.*

Nunn, J.A., Sleep, N.H. and Moore, W.E. 1984. Thermal subsidence and generation of hydrocarbons in Michigan Basin. *American Association of Petroleum Geologists Bulletin, 68(3), 296-315.*

Nydegger, G.L., Rice, D.D. and Brown, C.A. 1980. Analysis of shallow gas development from low-permeability reservoirs of Late Cretaceous age, Bowdoin Dome area. *Journal of Petroleum Technology, 32(12), 2111-2120.*

Oglesby, C.A. 1991. Distinguishing between depositional and dissolution thinning: Devonian Prairie Formation, Williston Basin, North America. *In: Christopher, J.E. and Haidl, F.M. (eds.) Sixth International Williston Basin Symposium. Saskatchewan Geological Society, Special Publication 11, 47-52.*

O'Leary, D.W., Friedman, J.D. and Pohn, H.A. 1976. Lineament, linear, lineation: some proposed new standards for old terms *Geological Society of America Bulletin, 87(10), 1463-1469.*

O'Leary, D.W., Friedman, J.D. and Pohn, H.A. 1978. Lineament, linear, lineation: some proposed new standards for old terms: reply *Geological Society of America Bulletin, 88(1), 159-160.*

O'Neill, J.M. and Lopez, D.A. 1985. Character and regional significance of Great Falls tectonic zone, east-central Idaho and west-central Montana. *American Association of Petroleum Geologists Bulletin, 69, 437-447.*

Orchard, D.M. 1987. Structural history of Poplar Dome and the dissolution of Charles Formation salt, Roosevelt County, Montana. *In: Carlson, C.G. and Christopher, J.E. (eds.) Fifth International Williston Basin Symposium, Saskatchewan Geological Society, Special Publication 9, 169-177.*

Parker, J.M. 1967. Salt solution and subsurface structures, Wyoming, North Dakota, and Montana. *American Association of Petroleum Geologists Bulletin, 51(10). 1929-1947.*

Parker, T.S. and Powe, W.H. 1982. Geology of the Raymond Field area Sheridan County, Montana. *In: Christopher, J.E. and Kaldi, J. (eds.) Fourth International Williston Basin Symposium, Saskatchewan Geological Society, Special Publication 6, 225-234.*

Payton, C.E. (ed.) 1977. Seismic stratigraphy - application to hydrocarbon exploration. *American Association of Petroleum Geologists, Memoir 26, 516p.*

Peper, T. 1993. Quantitative subsidence analysis of the Western Canada foreland basin with implications for short-term facies changes. *Tectonophysics, 226, 301-318.*

Perrin, N.A. 1982. Environments of deposition and daigenesis of the Winnipegosis Formation (Middle Devonian), Williston Basin, North Dakota. *In: Christopher, J.E. and Kaldi, J. (eds.) Fourth International Williston Basin Symposium, Saskatchewan Geological Society, Special Publication 6, 51-74.*

Perrodon, A. and Zabek, J. 1991. Paris Basin. *In: Leighton, M.W., Kolata, D.R., Oltz, D.F. and Eidel, J.J. (eds.) Interior cratonic basins. American Association of Petroleum Geologists, Memoir 51, 633-679.*

Peterson, J.A. 1984. Stratigraphy and sedimentary facies of the Madison limestone and associated rocks in parts of Montana, Nebraska, North Dakota, South Dakota, and Wyoming. *United States Geological Survey Professional Paper 1273-A. 34p.*

Peterson, J.A. 1988. Phanerozoic stratigraphy of the northern Rocky Mountains region. *In: Sloss, L.L. (ed.) Sedimentary cover - North American craton, U.S. Geological Society of America, The geology of North America, D-2, 83-107.*

Peterson, J.A. and MacCary, L.M. 1987. Regional stratigraphy of the U.S. portion of the Williston Basin and adjacent areas. *In: Peterson, J.A., Kent, D.M., Anderson, S.B., Piladzke, R.H. and Longman, M.W. (eds.) Williston Basin: anatomy of a cratonic oil province. Rocky Mountains Association of Geologists, 9-43.*

Peterson, J.A. and Clarke, J.W. 1991. Geology and hydrocarbon habitat of the West Siberian Basin. *American Association of Petroleum Geologists, Studies in Geology 32, 96p.*

Petters, S.W. 1979. West African cratonic sequences. *Geology, 7(11), 528-531.*

Porter, J.W., Price, R.A. and McCrossan, R.G. 1982. The Western Canada sedimentary basin. *Philosophical Transaction of the Royal Society of London, Series A 305, 169-192.*

Precht, W.F. and Shepard, W. 1989. Waulsortian carbonate buildups of Mississippian age from Montana and relations to rifting. *In: French, D.E. and Grabb, R.F. (eds.) Geologic Resources of Montana. Volume I. Montana Geological Society, 1989 Field Conference Guidebook, 65-68.*

Prouty, C.E. 1986. Tectonic development of the Michigan Basin [abstract]. *American Association of Petroleum Geologists Bulletin, 70(8), 1069-1070.*

Prouty, C.E. 1988. Trenton exploration and wrenching tectonics - Michigan Basin and environs. *In: Keith,B.D. (ed.) The Trenton Group (Upper Ordovician Series) of eastern North America - deposition, diagenesis, and petroleum. American Association of Petroleum Geologists, Studies in Geology 29, 207-236.*

Qamar, A.I. and Stickney, M.C. 1983. Montana earthquakes 1869-1979. *Montana Bureau of Mines and Geology, Memoir 51, 79p.*

Quinlan, G. 1987. Models of subsidence mechanisms in intracratonic basins, and their applicability to North American examples. *In: Beaumont, C. and Tankard, A.J. (eds.) Sedimentary basins and basin-forming mechanisms. Canadian Society of Petroleum Geologists, Memoir 12, 463-481.*

Quinlan, G.M. and Beaumont, C. 1984. Appalachian thrusting, lithospheric flexure, and the Paleozoic stratigraphy of the Eastern Interior of North America. *Canadian Journal of Earth Sciences, 21, 973-996.*

Rayne, T.W. 1985. Dwyer Field. *In: Tonnsen, J.J. (ed.) Montana oil and gas field symposium 1985. Montana Geological Society, v.1., 457-461.*

Reagor, B.G., Stover, C.W. and Algermissen, S.T. 1981. Seismicity map of the State of North Dakota. *United States Geological Survey Miscellaneous Field Studies Map MF-1326.*

Reagor, B.G., Stover, C.W. and Algermissen, S.T. 1981. Seismicity map of the State of Montana. *United States Geological Survey Miscellaneous Field Studies Map MF-1819.*

Reeves, F. 1924. Geology and possible oil and gas resources of the faulted area south of the Bearpaw Mountains. *United States Geological Survey Bulletin, 751-C, 71-114.*

Reeves, F. 1925. Shallow folding and faulting around the Bearpaw Mountains. *American Journal of Science, 10, 187-200.*

Reeves, F. 1946. Origin and mechanics of the thrust faults adjacent to the Bearpaw Mountains, Montana. *Bulletin of the Geological Society of America, 57, 1033-1047.*

Reeves, F. 1953. Bearpaw thrust-faulted area. *In: Parker, J.M. (ed.) Billing Geological Society 4th Annual Field Conference Guidebook, 114-117.*

Rice, D.D. 1980. Coastal and deltaic sedimentation of Upper Cretaceous Eagle Sandstone: relation to shallow gas accumulations, north- central Montana. *American Association of Petroleum Geologists Bulletin, 64(3), 316-338.*

Roksandić, M.M. 1987. The tectonics and evolution of the Hudson Bay region. *In: Beaumont, C. and Tankard, A.J. (eds.) Sedimentary basins and basin-forming mechanisms. Canadian Society of Petroleum Geologists, Memoir 12, 507-518.*

Rosenthal, L.R., 1987. The Winnipegosis Formation of the northeastern margin of the Williston Basin. *In: Carlson, C.G. and Christopher, J.E. (eds.) Fifth International Williston Basin Symposium, Saskatchewan Geological Society, Special Publication 9, 37-46.*

Ross, G. and Parrish, R.R. 1991. Detrital zircon geochronology of metasedimentary rocks in the southern Omineca Belt, Canadian Cordillera. *Canadian Journal of Earth Science, 28, 1254-1270.*

Ross, G., Parrish, R.R., Villeneuve, M.E. and Bowring, S.A. 1991. Geophysics and geochronology of the crystalline basement of the Alberta Basin, western Canada. *Canadian Journal of Earth Sciences, 28, 512-522.*

Ross, G. and Stephenson, R.A. 1989. Crystalline basement: the foundation of Western Canada Sedimentary Basin. *In: Ricketts, B.D. (ed.) Western Canada Sedimentary Basin. A case history. Canadian Society of Petroleum Geologists, 33-45.*

Rumsey, I.A.P. 1971. Relationship of fractures in unconsolidated superficial deposits to those in the underlying bedrock. *Modern Geology, 3, 25-44.*

Sanford, B.V. 1987. Paleozoic geology of the Hudson Platform. *In: Beaumont, C. and Tankard, A.J. (eds.) Sedimentary basins and basin-forming mechanisms. Canadian Society of Petroleum Geologists, Memoir 12, 483-505.*

Sangree, J.B. and Widimer, J.M. 1977. Seismic stratigraphy and global changes of sea level - Part 9: Seismic interpretation of clastic depositional facies. *In: Payton, C.E. (ed.) Seismic stratigraphy - application to hydrocarbon exploration. American Association of Petroleum Geologists, Memoir 26, 165-184.*

Scherer, W. 1973. A mathematical model for the differential subsidence of intra-cratonic basins. *Unpublished Ph.D. Thesis, Northwestern University, 59p.*

Schlager, W. 1992. Sedimentology and sequence stratigraphy of reefs and carbonate platforms. *American Association of Petroleum Geologists, Continuing Education Course Note Series #34, 71p.*

Schöder-Adams, C.J., Leckie, D.A., Bloch, J., Craig, J., McIntyre, D.J. and Adams, P.J. 1996. Paleoenvironmental changes in the Cretaceous (Albian to Turonian) Colorado Group of western Canada: microfossil, sedimentological and geochemical evidence. *Cretaceous Research, 17, 311-365.*

Schultz-Ela, D.D., Jackson, M.P., Hudec, M.R., Fletcher, R.C., Porter, M.L. and Watson, I.A. 1994. Structures formed by radial contraction at Upheaval Dome, Utah. *Geological Society of America, Abstract with Programs, 26(7), 72.*

Schultz, R.A. and Zuber, M.T. 1994. Observation, models, and mechanisms of failure of surface rocks surrounding planetary surface loads. *Journal of Geophysical Research, 99(E7), 14,691-14,702.*

Shepard, W. and Bartow, B. 1986. Tectonic history of the Sweetgrass Arch, a key to finding new hydrocarbons, Montana and Alberta. *In: Noll, H.(ed.) Wyoming Geological Association Symposium, Rocky Mountain Oil and Gas Fields, 9-19.*

Sheriff, R.E. 1980. Seismic stratigraphy. *International Human Resources Corporation, 227p.*

Sheriff, R.E. 1991. Encyclopedic dictionary of exploration geophysics. *Third edition. Society of Exploration Geophysicists, Geophysical Reference Series 1, 376p.*

Sheriff, R.E. and Geldart, L.P. 1982. Exploration seismology. Volume 1. *Cambridge University Press, Cambridge, 253p.*

Shouldice, J.R. 1963. Gravity slide faulting on Bowes Dome, Bearpaw Mountains area, Montana. *Geological Society of America Bulletin, 47(11), 1943-1951.*

Shurr, G.W. 1995. Tectonic setting of horizontal Bakken production in southwestern North Dakota. *In: Vern Hunter, L.D. and Schalla, R.A. (eds.) Seventh International Williston Basin Symposium Guidebook, 23-39.*

Shurr, G.W., Anna, L.O. and Peterson, J.A. 1989a. Zuni sequence in Williston Basin - evidence for Mesozoic paleotectonism. *American Association of Petroleum Geologists Bulletin, 73(1), 68-87.*

Shurr, G.W., Larson, B.S. and Watkins, I.W. 1989b. The basement block mosaic beneath the Montana plains. *In: French, D.E. and Grabb, R.F. (eds.) Geologic Resources of Montana. Volume I. Montana Geological Society, 1989 Field Conference Guidebook, 299-309.*

Shurr, G.W. and Monson, L.M. 1995. Tectonic setting and paleotectonic history of Fort Peck Reservation in northeastern Montana. *In: Vern Hunter, L.D. and Schalla, R.A. (eds.) Seventh International Williston Basin Symposium Guidebook, 11-22.*

Shurr, G.W., Ashworth, A.C., Burke, R.B. and Diehl, P.E. 1995. Tectonic controls on the Lodgepole play in northern Stark County, North Dakota - perspectives from surface and subsurface studies. *In: Vern Hunter, L.D. and Schalla, R.A. (eds.) Seventh International Williston Basin Symposium Guidebook, 203-208.*

Sleep, N.H., Nunn, J.A. and Chou, L. 1980. Platform basins. *Annual Review of Earth and Planetary Sciences, 8, 17-34.*

Sleep, N.H. and Phillips, R.J. 1985. Gravity and lithospheric stress on the terrestrial planets with reference to the Tharsis Region of Mars. *Journal of Geophysical Research, 90(B6), 4,469-4,489.*

Sloss, L.L. 1963. Sequences in the cratonic interior of North America. *Geological Society of America Bulletin, 74, 93-114.*

Sloss, L.L. 1987. The Williston Basin in the family of cratonic basins. *In: Peterson, J.A., Kent, D.M., Anderson, S.B., Piladzke, R.H. and Longman, M.W. (eds.) Williston Basin: anatomy of a cratonic oil province. Rocky Mountains Association of Geologists, 209-221.*

Sloss, L.L. 1988a. Introduction. *In: Sloss, L.L. (ed.) Sedimentary cover - North American craton, U.S. Geological Society of America, The geology of North America, D-2, 1-3.*

Sloss, L.L. 1988b. Tectonic evolution of the craton in Phanerozoic time. *In: Sloss, L.L. (ed.) Sedimentary cover - North American craton, U.S. Geological Society of America, The geology of North America, D-2, 221-241.*

Sloss, L.L. 1991. The tectonic factor in sea level change: a countervailing view. *Journal of Geophysical Research, 96(B4), 6,609-6,617.*

Sloss, L.L. 1996. Sequence stratigraphy on the craton: caveat emptor. *In: Witzke, B.J., Ludvigson, G.A. and Day, J. (eds.) Paleozoic sequence stratigraphy: views from the North American craton. Geological Society of America Special Paper 306, 425-434.*

Sloss, L.L. and Scherer, W. 1975. Geometry of sedimentary basins: application to Devonian of North America and Europe. *In: Whitte, E.H.T. (ed.) Quantitative studies in the geological sciences. Geological Society of America, Memoir 142, 71-88.*

Soares, P.C, Landim, P.M.B. and Fulfaro, V.J. 1978. Tectonic cycles and sedimentary sequences in the Brazilian intracratonic basins. *Geological Society of America Bulletin, 89(2), 181-191.*

Smith, M.G., Bustin, R.M. and Caplan, M.L. 1995. Sedimentology of the Late Devonian and Early Mississippian Bakken Formation, Williston Basin. *In: Vern Hunter, L.D. and Schalla, R.A. (eds.) Seventh International Williston Basin Symposium Guidebook, 129-139.*

Stafleu, J. and Schlager, W. 1993. Pseudo-toplap in seismic models of the Schlern-Raibl contact (Sella platform, northern Italy). *Basin Research, 5, 55-65.*

Stauffer, M.R. and Gendzwill, D.J. 1987. Fractures in the northern plains, stream patterns, and the midcontinent stress field. *Canadian Journal of Earth Sciences, 24, 1086-1097.*

Steckler, M.S. and Watts, A.B. 1978. Subsidence of the Atlantic-type margin off New York. *Earth and Planetary Science Letters, 41, 1-13.*

Stel, H., Cloething, S., Heeremans, M. and van de Beek, P. 1993. Anorogenic granites, magmatic underplating and the origin of intracratonic basins in non-extensional setting. *Tectonophysics, 226, 285-299.*

Stone, D.S. 1991. Analysis of scale exaggeration on seismic profiles. *American Association of Petroleum Geologists Bulletin, 75(7), 1161-1177.*

Sturm, S.D. 1978. Depositional history and cyclicity in the Tyler Formation (Pennsylvanian), southwesetrn North Dakota. *In: Peterson, J.A., Kent, D.M., Anderson, S.B., Piladzke, R.H. and Longman, M.W. (eds.) Williston Basin: anatomy of a cratonic oil province. Rocky Mountains Association of Geologists, 209-221.*

Tanimoto, T. 1997. Bending of spherical lithosphere - axisymmetric case. *Geophysical Journal International, 129, 305-310.*

Telford, W.M., Geldart, L.P. and Sheriff, R.E. 1990. Applied Geophysics. *Second edition. Cambridge University Press, 770p.*

Thomas, G.E. 1974. Lineament-block tectonics: Williston-Blood Creek basin. *American Association of Petroleum Geologists Bulletin, 58(7), 1305-1322.*

Thomas, M.D., Sharpton, V.L. and Grieve, R.A.F. 1987. Gravity patterns and Precambrian structure in the North American Central Plains. *Geology, 15(6), 489-492.*

Thorne, J.A. 1992. An analysis of the implicit assumptions of the methodolgy of seismic sequence stratigraphy. *In: Watkins, J.S., Zhinqiang, F. and McMillen, K.J. (eds.) Geology and geophysics of continental margins. American Association of Petroleum Geologists, Memoir 52, 375-396.*

Tipper, J.C. 1993. Do seismic reflections necessarily have chronostratigraphic significance? *Geological Magazine, 130(1), 47-55.*

Vail, P.R., Mitchum, R.M.Jr. and Thompson, S.III. 1977a. Global cycles of relative changes of sea level. *In: Payton, C.E. (ed.) Seismic stratigraphy - application to hydrocarbon exploration. American Association of Petroleum Geologists, Memoir 26, 83-97.*

Vail, P.R., Todd, R.G. and Sangree, J.B. 1977b. Seismic stratigraphy and global changes of sea level, Part 5: Chronostratigraphic significance of sea level. *In: Payton, C.E. (ed.) Seismic stratigraphy - application to hydrocarbon exploration. American Association of Petroleum Geologists, Memoir 26, 99-116.*

Vail, P.R. and Cramez, C. 1990. Seismic interpretation - sequence stratigraphy. *Short Course Notes with French and Spanish glossary, 313p.*

Van Wagoner, J.C., Posamentier, H.W., Mitchum, R.M., Vail, P.R., Sarg, J.F., Loutit, T.S. and Hardenbol, J. 1988. An overview of the fundamentals of sequence stratigraphy and key definitions. *In: Wilgus, C.K., Hastings, B.S., Kendall, C.G.St.C., Posamentier, H.W., Ross, C.A. and Van Wagoner, J.C. (eds.) Sea-level changes: an integrated approach. Society of Economic Paleontologists and Mineralogists, Special Publication 42, 39-45.*

Van Wagoner, J.C., Posamentier, H.W. and Hardenbol, J. 1990. Siliciclastic sequence stratigraphy in well logs, cores, and outcrops: concept for high-resolution correlation of time and facies. *American Association of Petroleum Geologists, Methods in Exploration Series, 7, 55p.*

Veevers, J.J. 1994. Case for the Gamburtsev Subglacial Mountains of East Antarctica originating by mid-Carboniferous shortening of an intracratonic basin. *Geology, 22(7), 593-596.*

Wetters, T.R. and Janes, D.M. 1995. Coronae on Venus and Mars: implications for similar structures on Earth. *Geology 23(3), 200-204.*

Widess, M.B. 1973. How thin is a thin bed? *Geophysics, 38(6), 1176-1180.*

Williams, H., Hoffman, P.F., Lewry, J.F., Monger, J.W.H. and Rivers, T. 1991. Anatomy of North America: thematic geologic portrayals of the continent. *Tectonophysics, 187, 117-134.*

Wilson, J.L. and Piladzke, R.H. 1987. Carbonate-evaporite cycles in Lower Duperow Formation of the Williston Basin. *In: Peterson, J.A., Kent, D.M., Anderson, S.B., Piladzke, R.H. and Longman, M.W. (eds.) Williston Basin: anatomy of a cratonic oil province. Rocky Mountains Association of Geologists, 9-43.*

Withjack, M.O. and Scheiner, C. 1982. Fault patterns associated with domes - an experimental and analytical study. *American Association of Petroleum Geologists Bulletin, 66(3), 302-316.*

Yamaoka, K. 1988. Spherical shell tectonics: on the buckling of the lithosphere at subduction zones. *Tectonophysics, 147, 179-191.*

Yamaoka, K., Fukao, Y. and Kumazawa, M. 1986. Sperical shell tectonics: effects of sphericity and inextensibility on the geometry of the descending lithosphere. *Reviews of Geophysics, 24(1), 27-53.*

Yamaoka, K. and Fukao, Y. 1987. Why do island arcs for cusps at their junctions? *Geology, 15(1), 34-36.*

Yilmaz, O. 1987. Seismic data processing. *Society of Exploration Geophysicists, Investigations in Geophysics, Volume 2, 526p.*

Yule, G.U. and Kendall, M.G. 1950. An introduction to the theory of statistics. *14th edition, Griffin & Co., New York, 701p.*

Zalan, P.V., Wolff, S., Astolfi, M.A.M., Vieira, I.S., Concelcao, J.C.J., Appi, V.T., Neto, E.V.S., Cerqueira, J.R. and Marques, A. 1991. The Parana Basin, Brazil. *In: Leighton, M.W., Kolata, D.R., Oltz, D.F. and Eidel, J.J. (eds.) Interior cratonic basins. American Association of Petroleum Geologists, Memoir 51, 681-708.*

Zhu, C. 1992. A seismic study of the northern Williston Basin. *Unpublished Ph.D. Thesis. University of Saskatchewan. 394p.*

Zhu, T. and Brown, L.D. 1986. Consortium for Continental Reflection Profiling Michigan surveys: reprocessing and results. *Journal of Geophysical Research, 91(B11), 11477-11495.*

Ziegler, P.A. 1988. Evolution of the Arctic-North Atlantic and the Western Tethys. *American Association of Petroleum Geologists, Memoir 43, 198p.*

APPENDIX

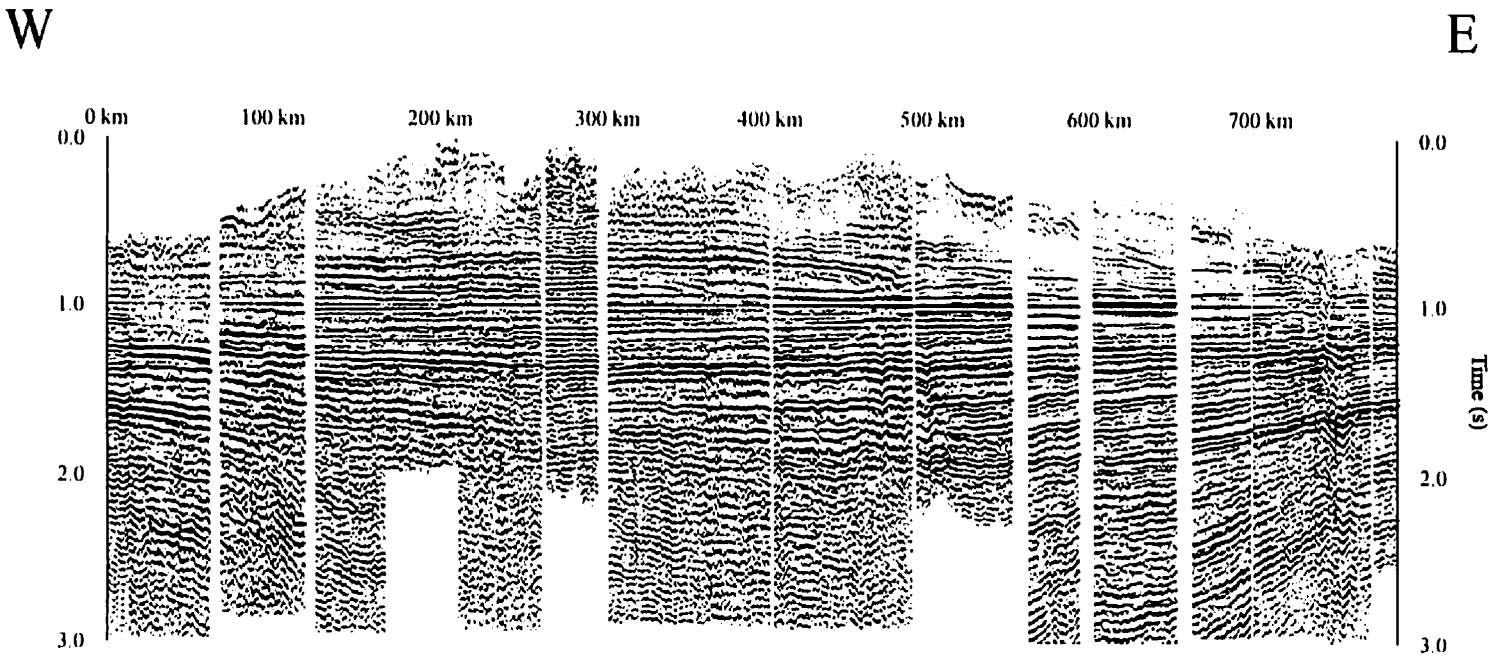

Datum: Greenhorn Shale @ 1.0 sec

Fig. A.1 WE 1 line (datum-corrected) (Zhu, 1992).

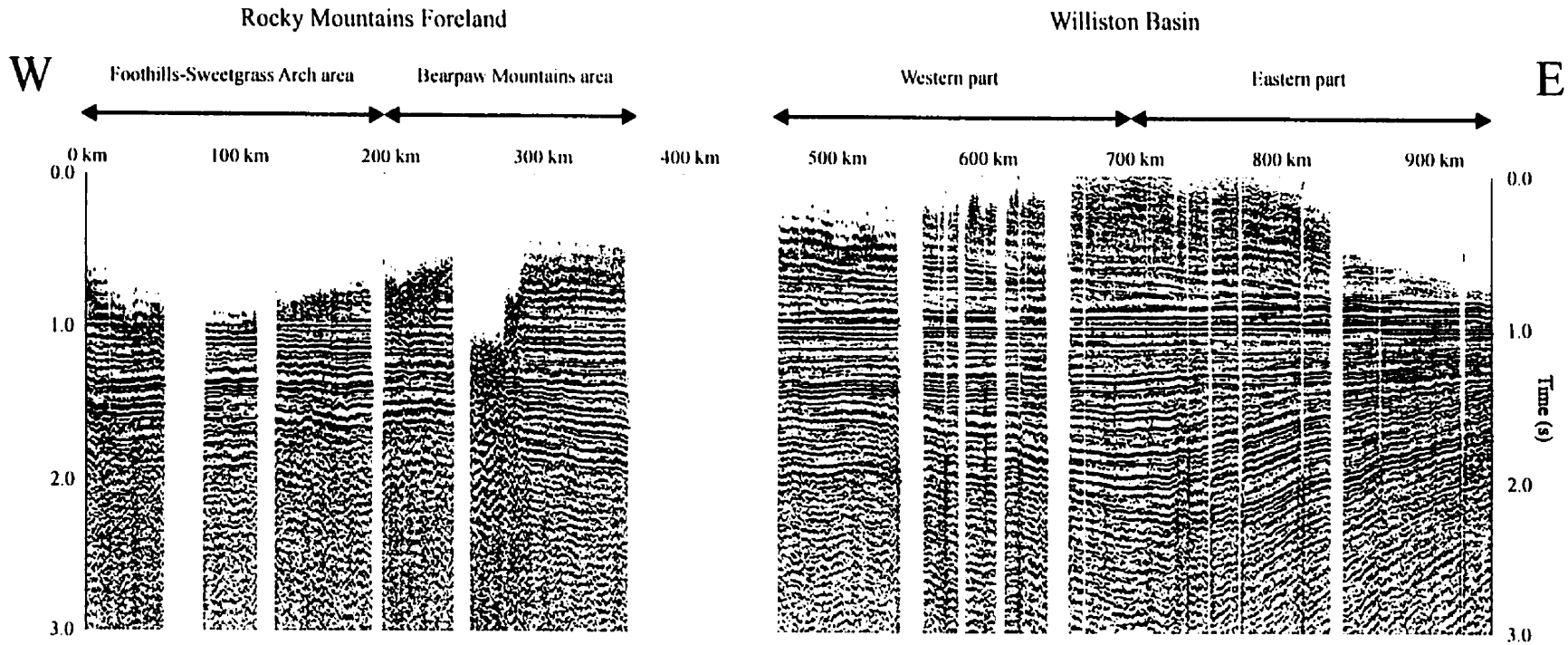

Datum: Greenhorn Shale @ 1.0 sec

Fig. A.2 WE II line (datum-corrected).

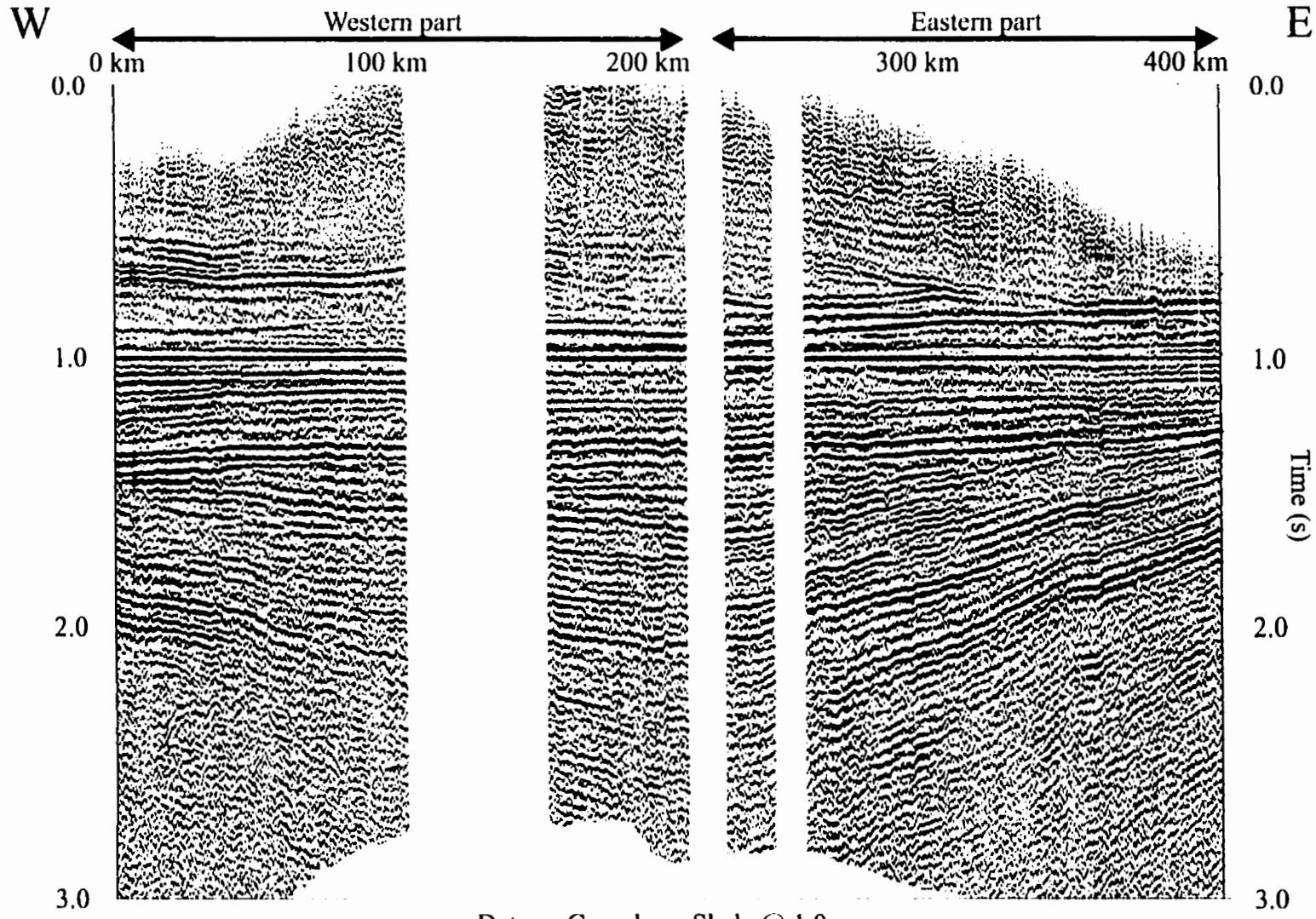

Datum: Greenhorn Shale @ 1.0 sec

Fig. A.3 WE III line (datum-corrected).

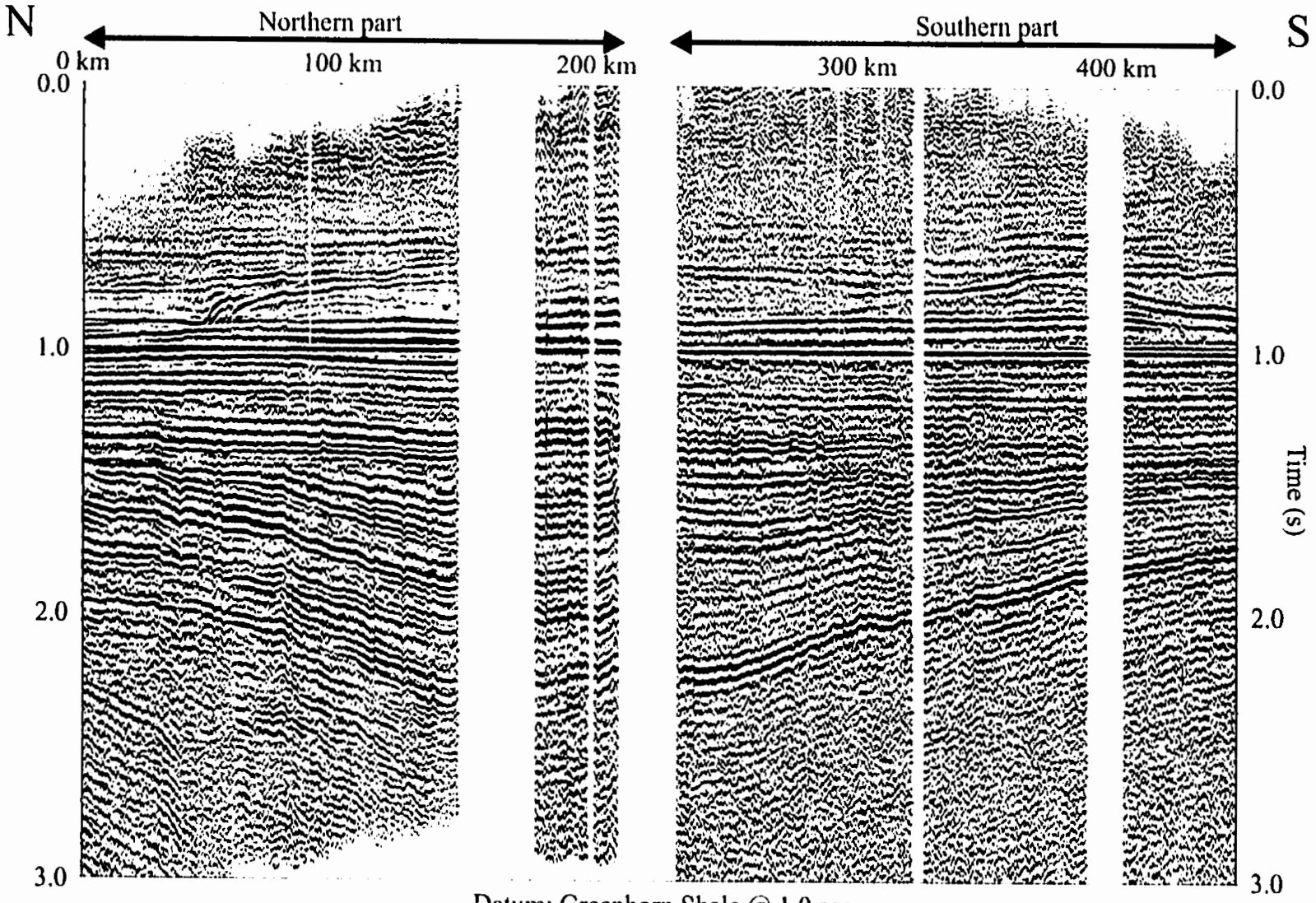

Datum: Greenhorn Shale @ 1.0 sec

Fig. A.4 NS I line (datum-corrected).

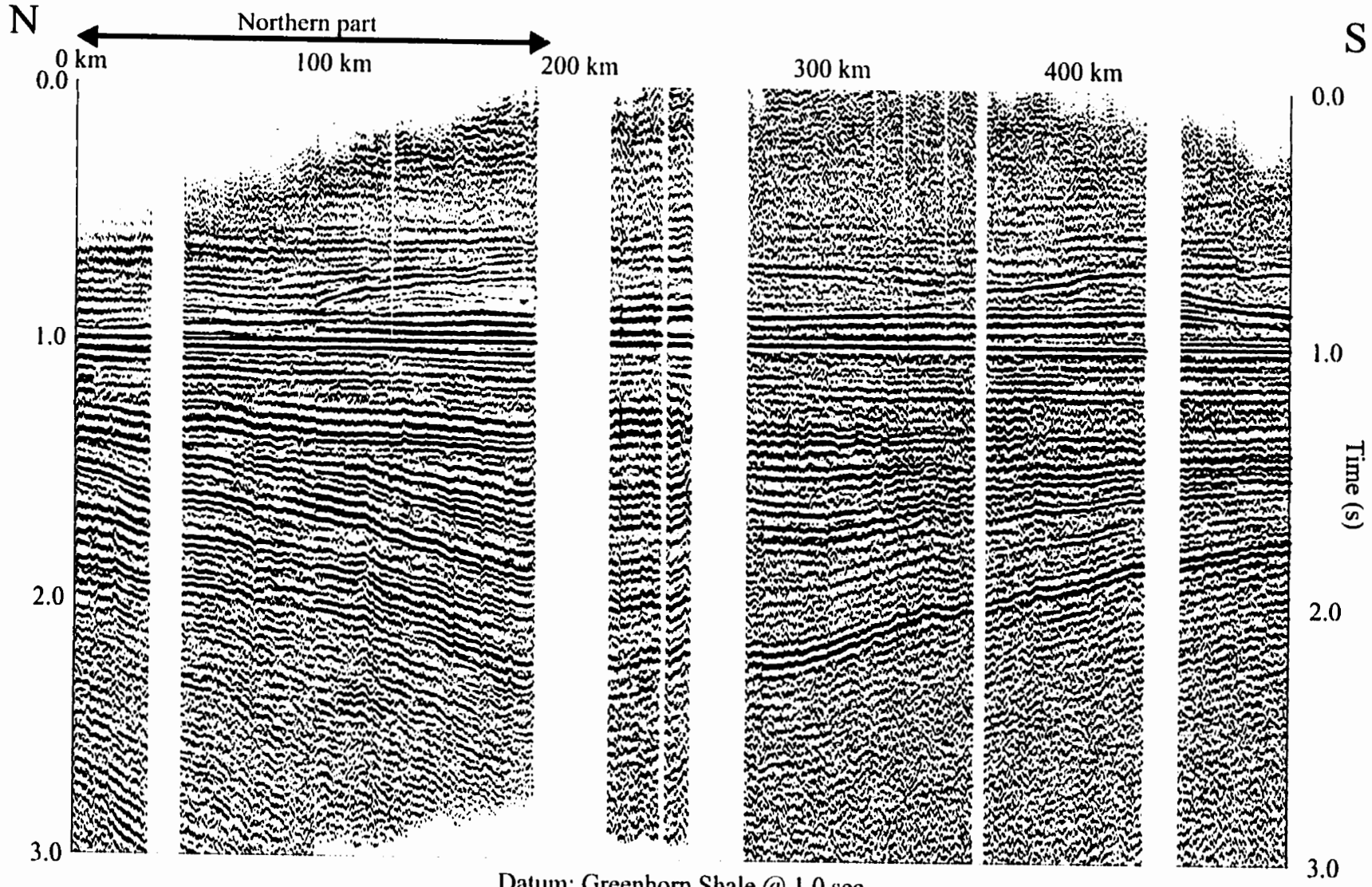

Datum: Greenhorn Shale @ 1.0 sec

Fig. A.5 CA I line (datum-corrected).

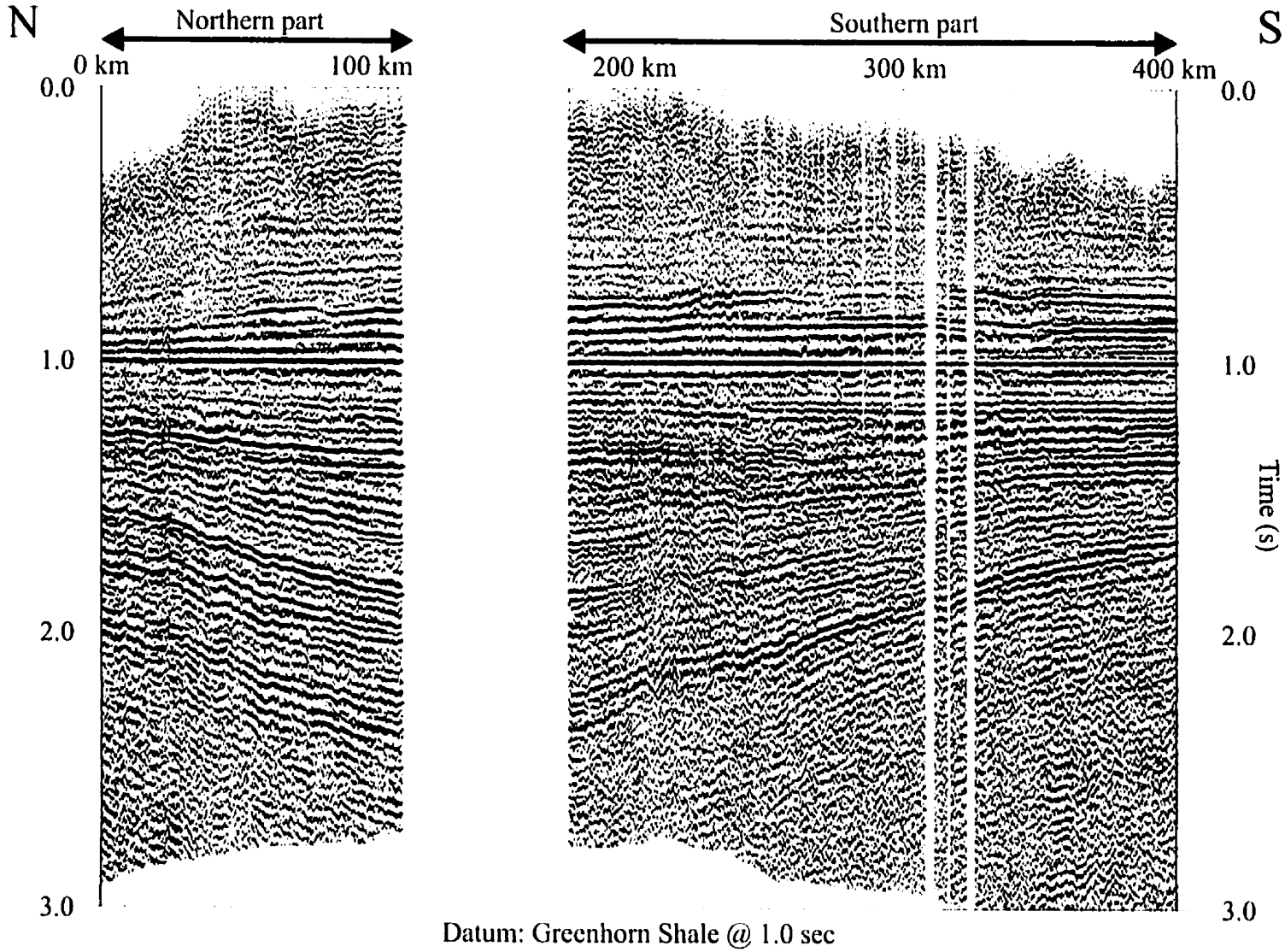

Datum: Greenhorn Shale @ 1.0 sec

Fig. A.6 NS II line (datum-corrected).

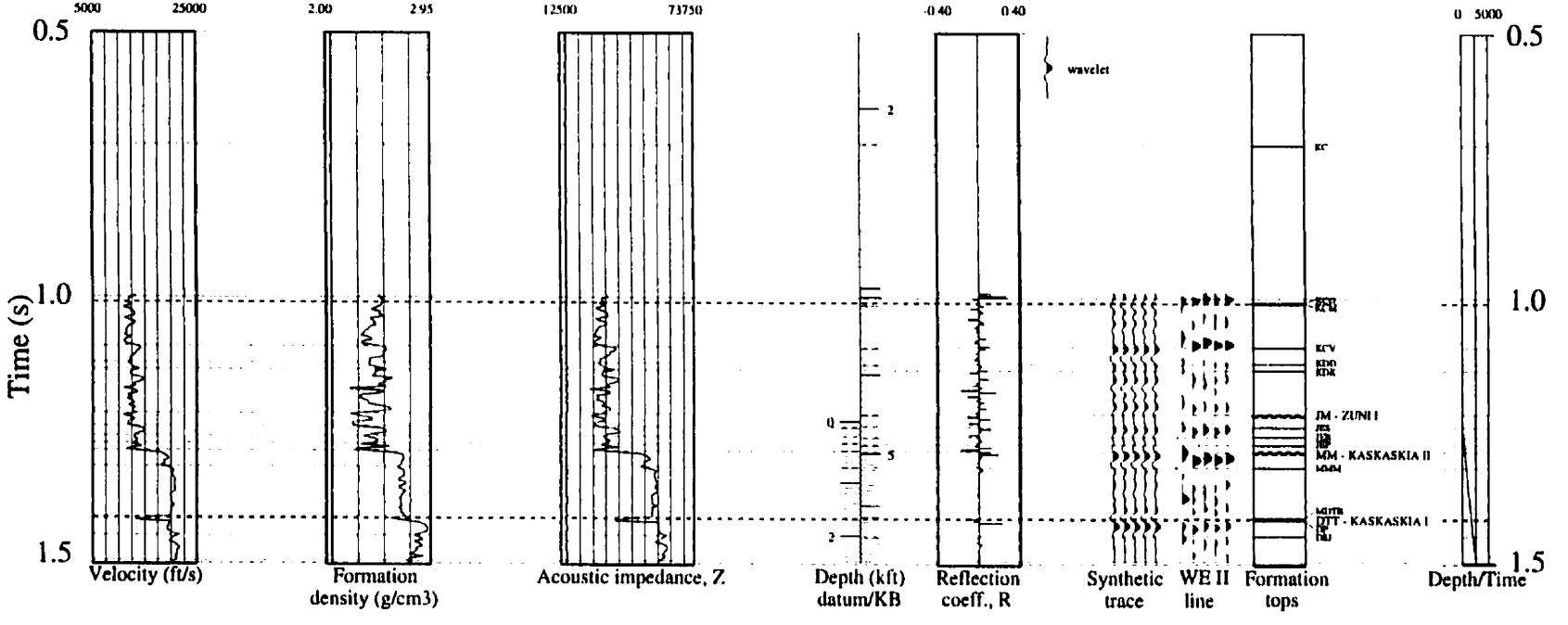

Fig. A.7 Well 1 - Synthetic seismogram.

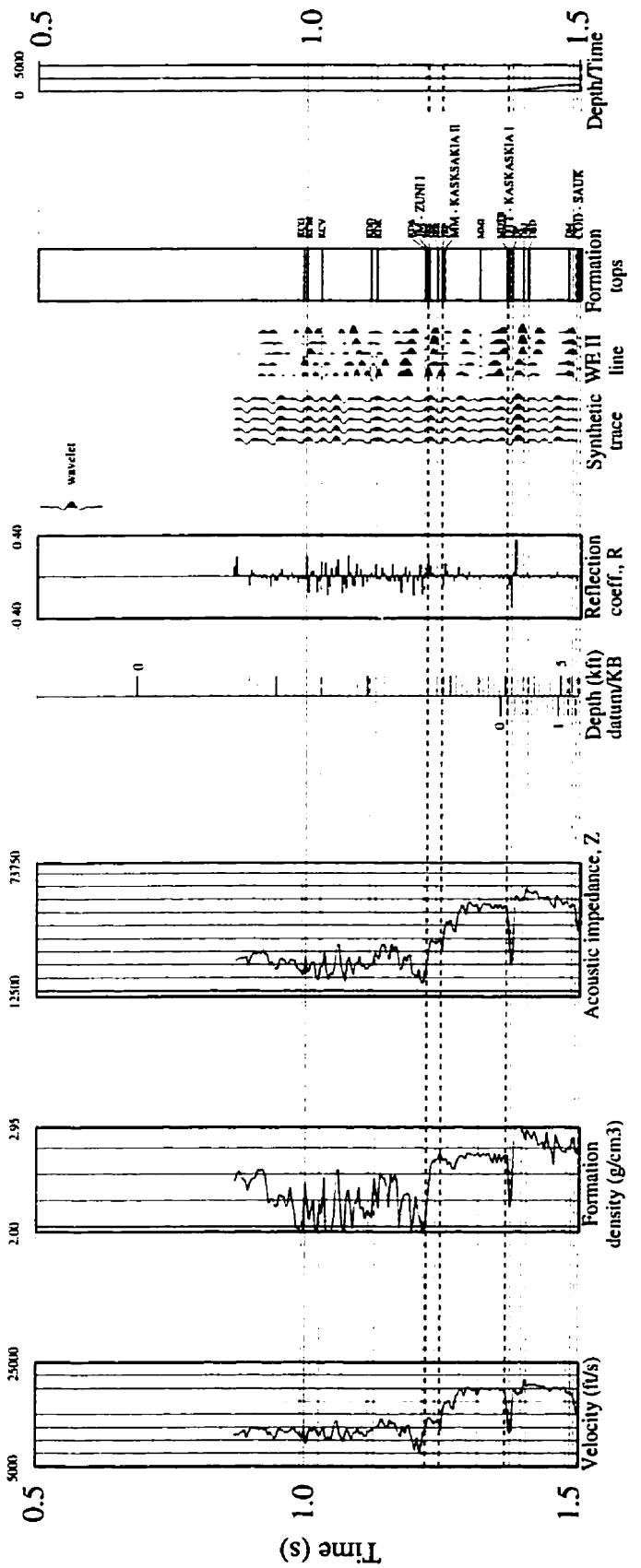

Fig. A.8 Well 2 - Synthetic seismogram.

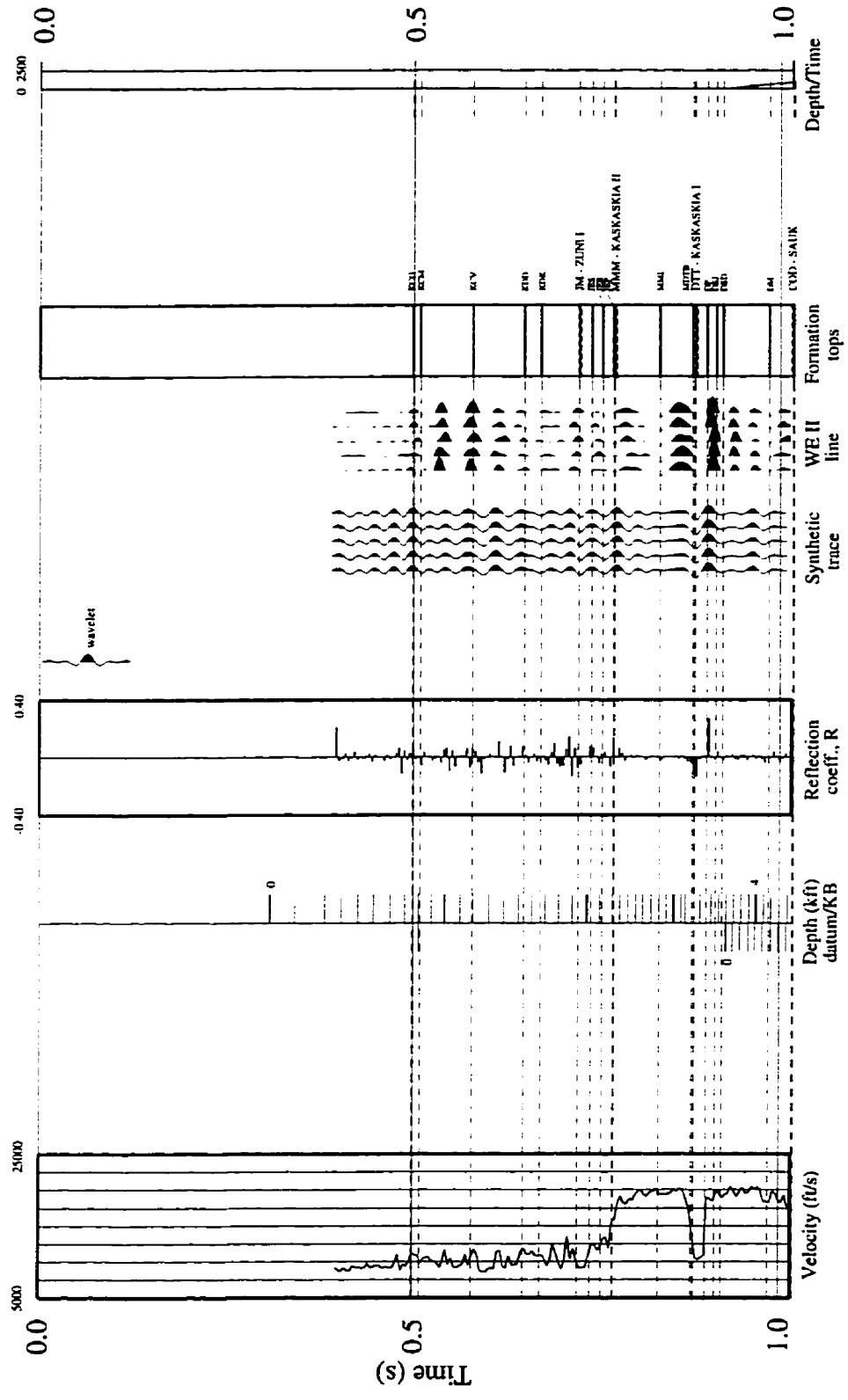

Fig. A.9 Well 3 - Synthetic seismogram.

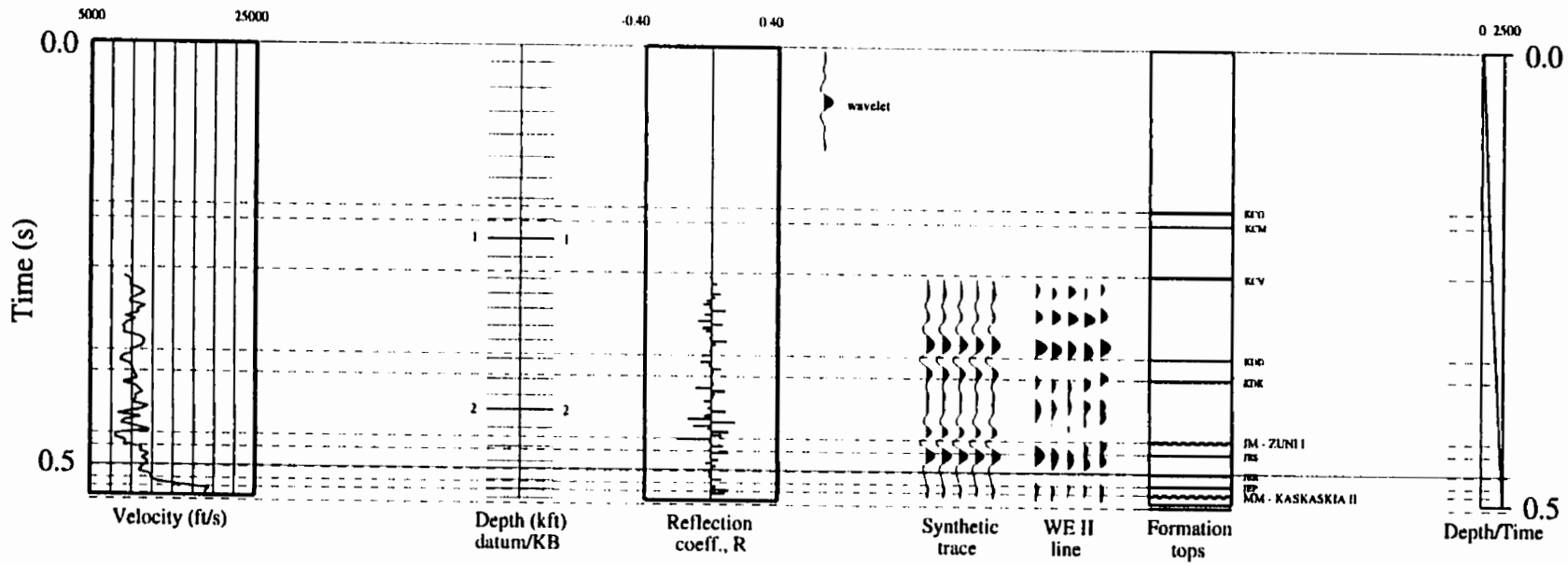

Fig. A.10 Well 4 - Synthetic seismogram.

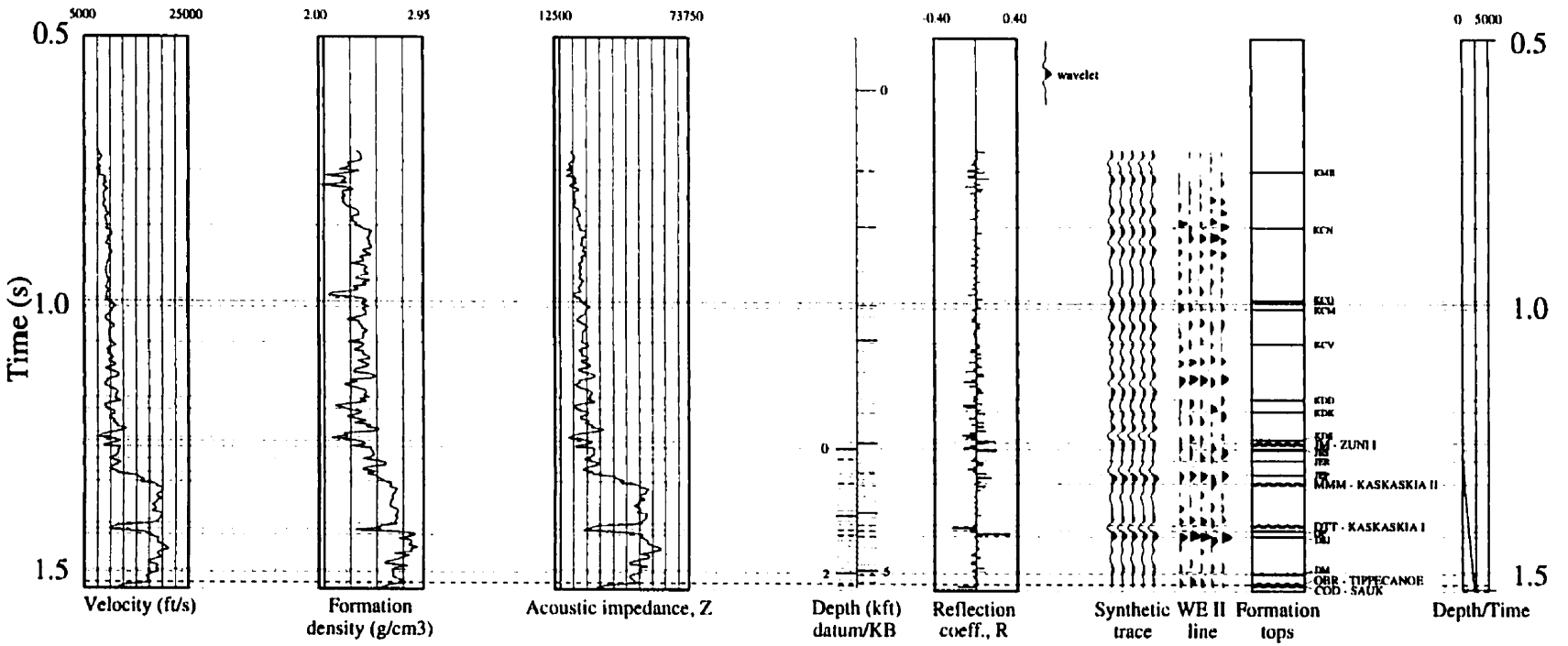

Fig. A.11 Well 5 - Synthetic seismogram.

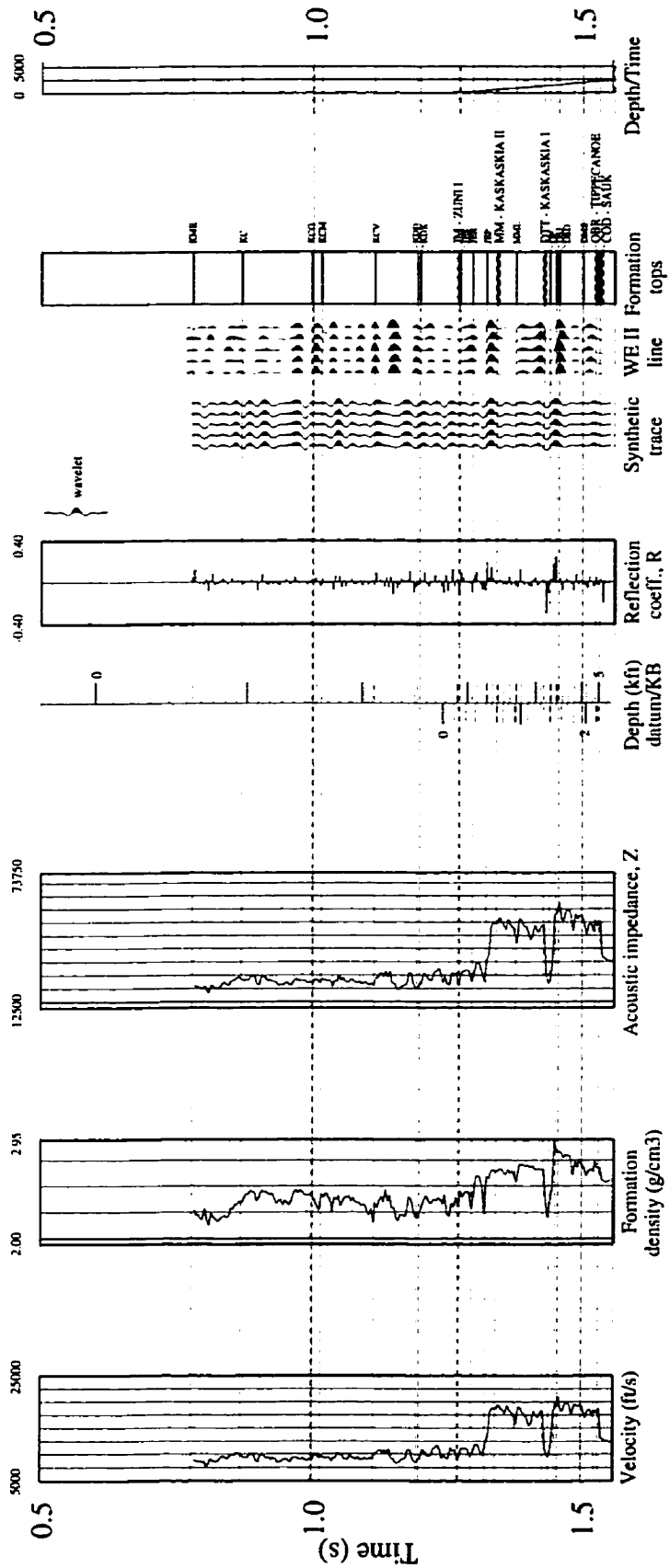

Fig. A.12 Well 6 - Synthetic seismogram.

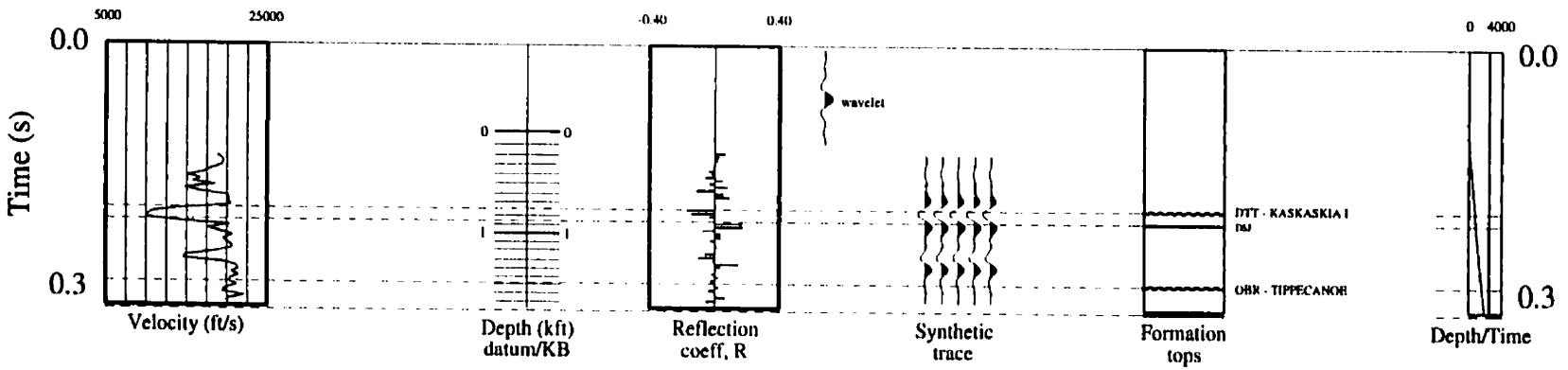

Fig. A.13 Well 7 - Synthetic seismogram.

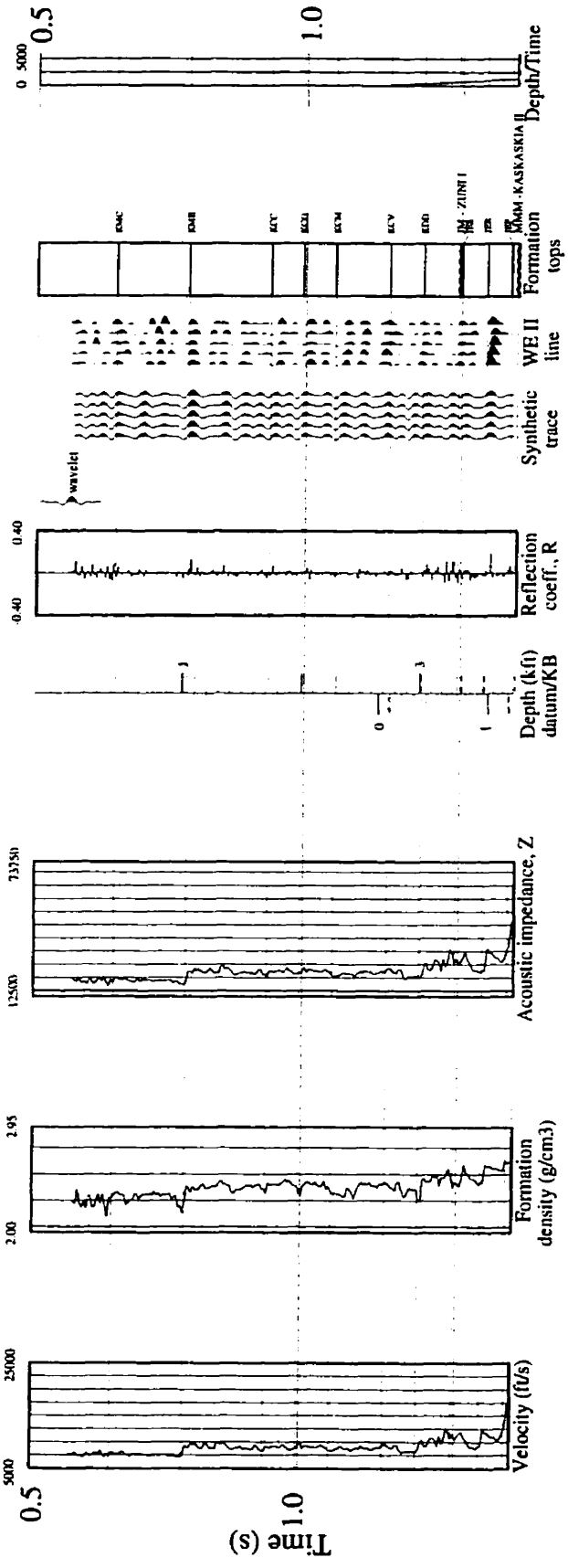

Fig. A.14 Well 8 - Synthetic seismogram.

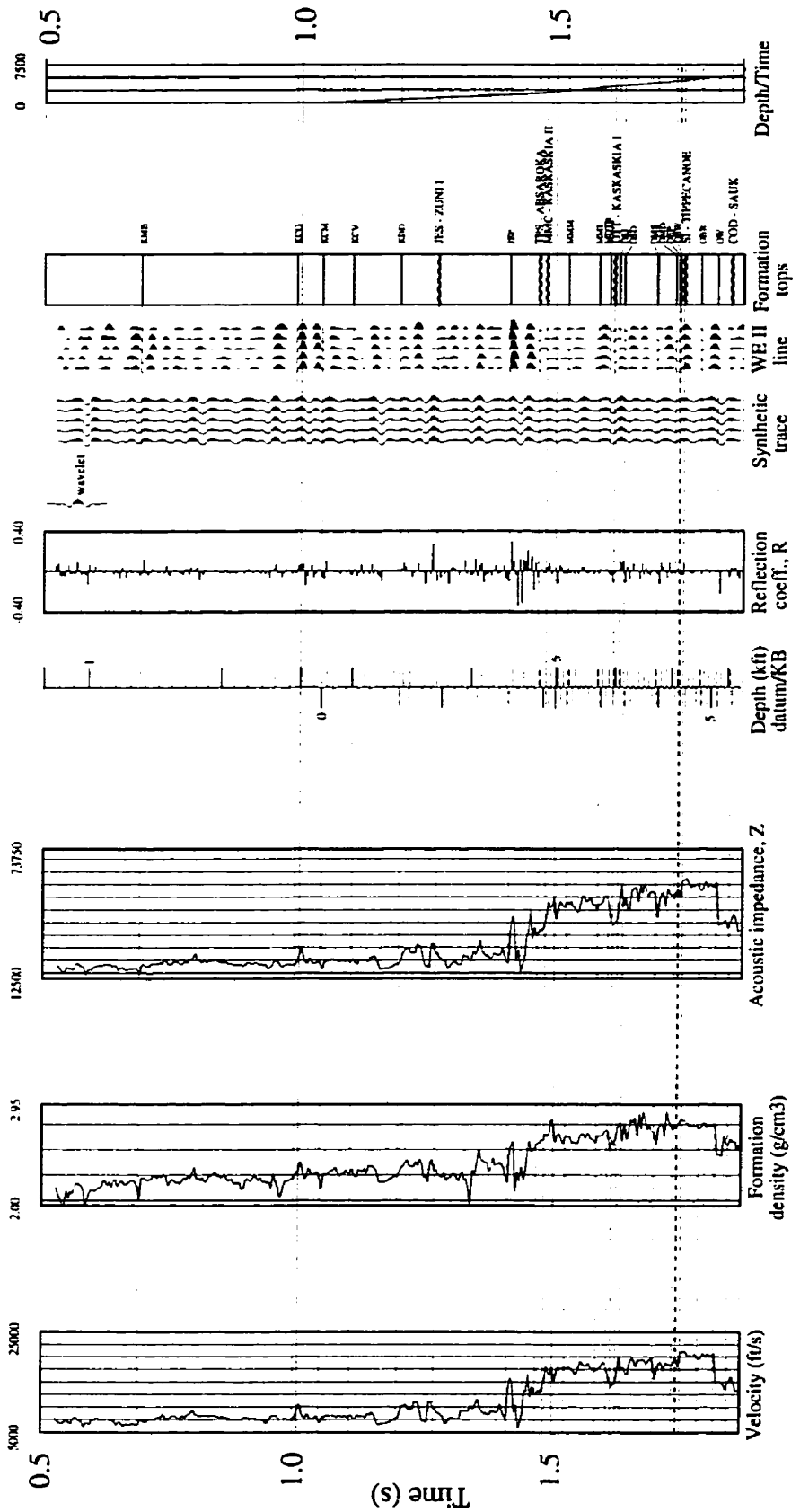

Fig. A.15 Well 9 - Synthetic seismogram.

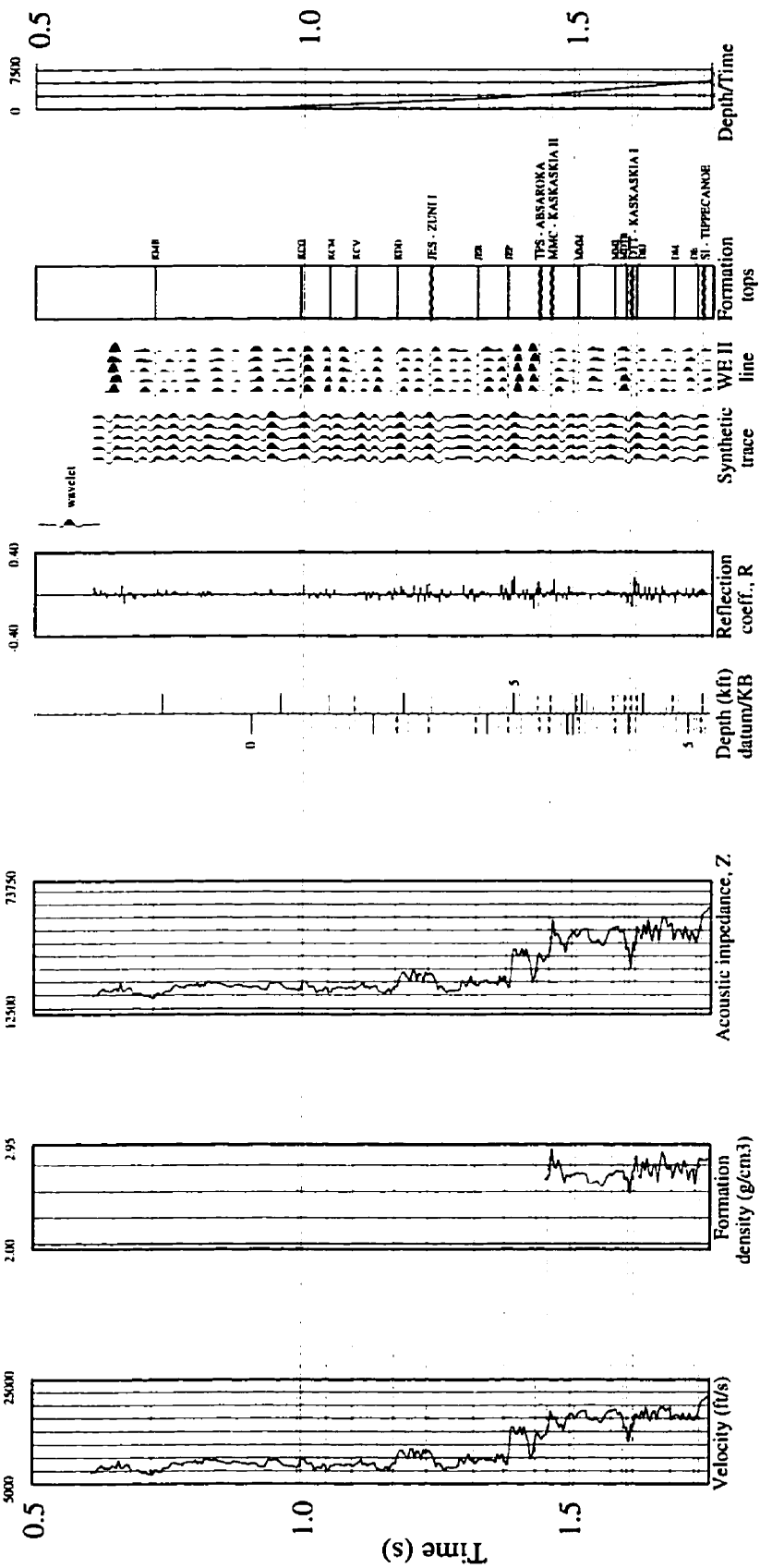

Fig. A.16 Well 10 - Synthetic seismogram.

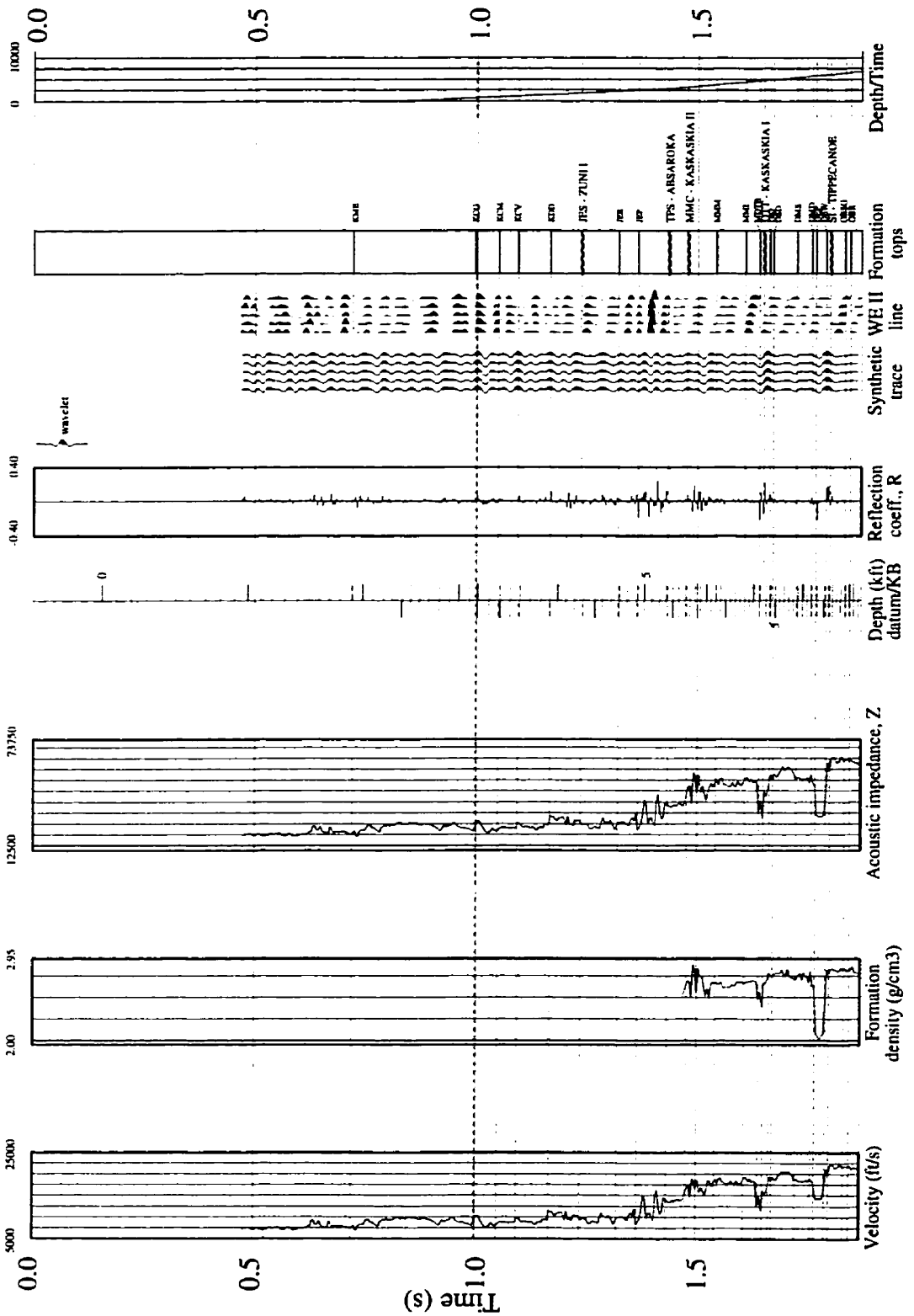

Fig. A.17 Well 11 - Synthetic seismogram.

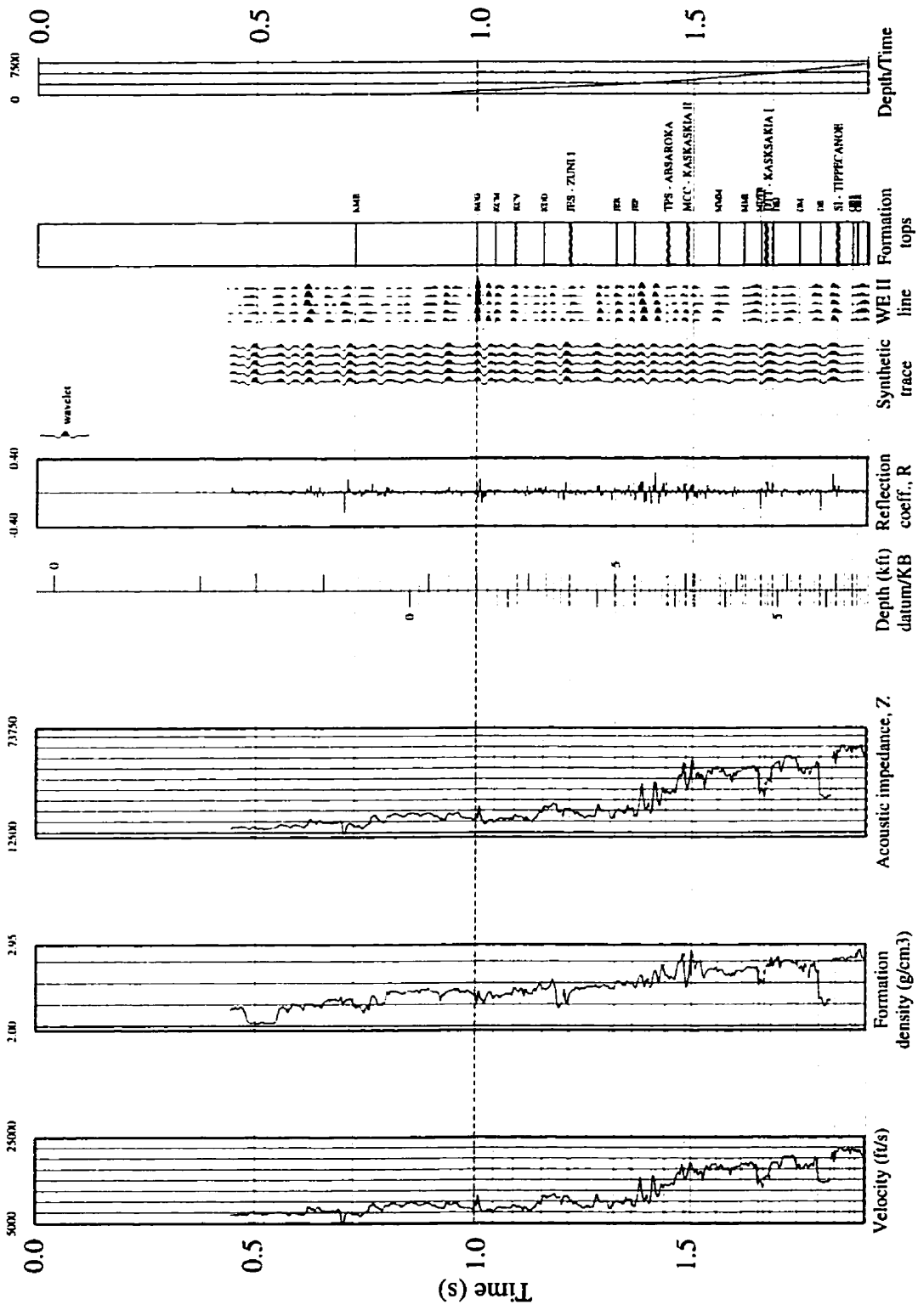

Fig. A.18 Well 12 - Synthetic seismogram.

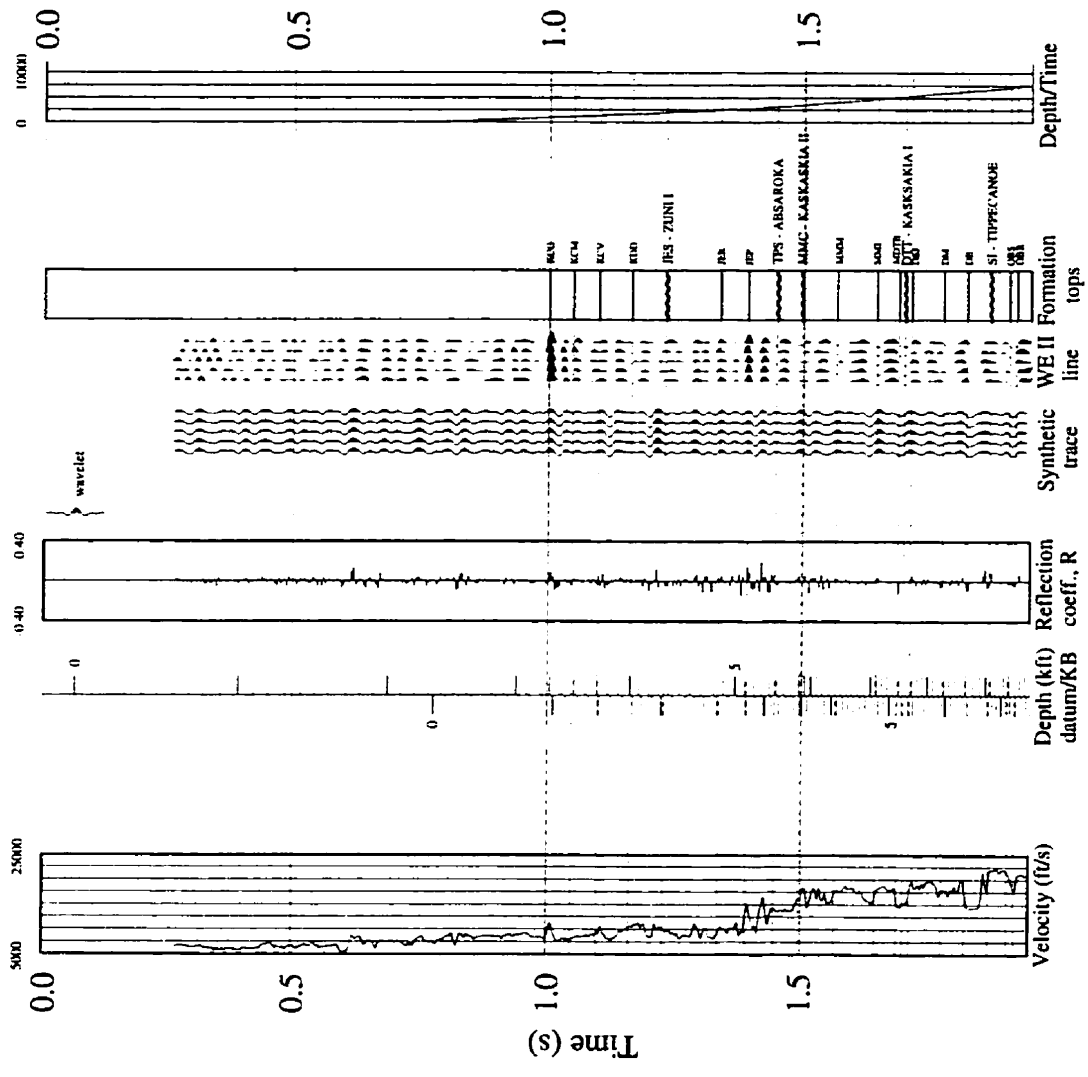

Fig. A.19 Well 13 - Synthetic seismogram.

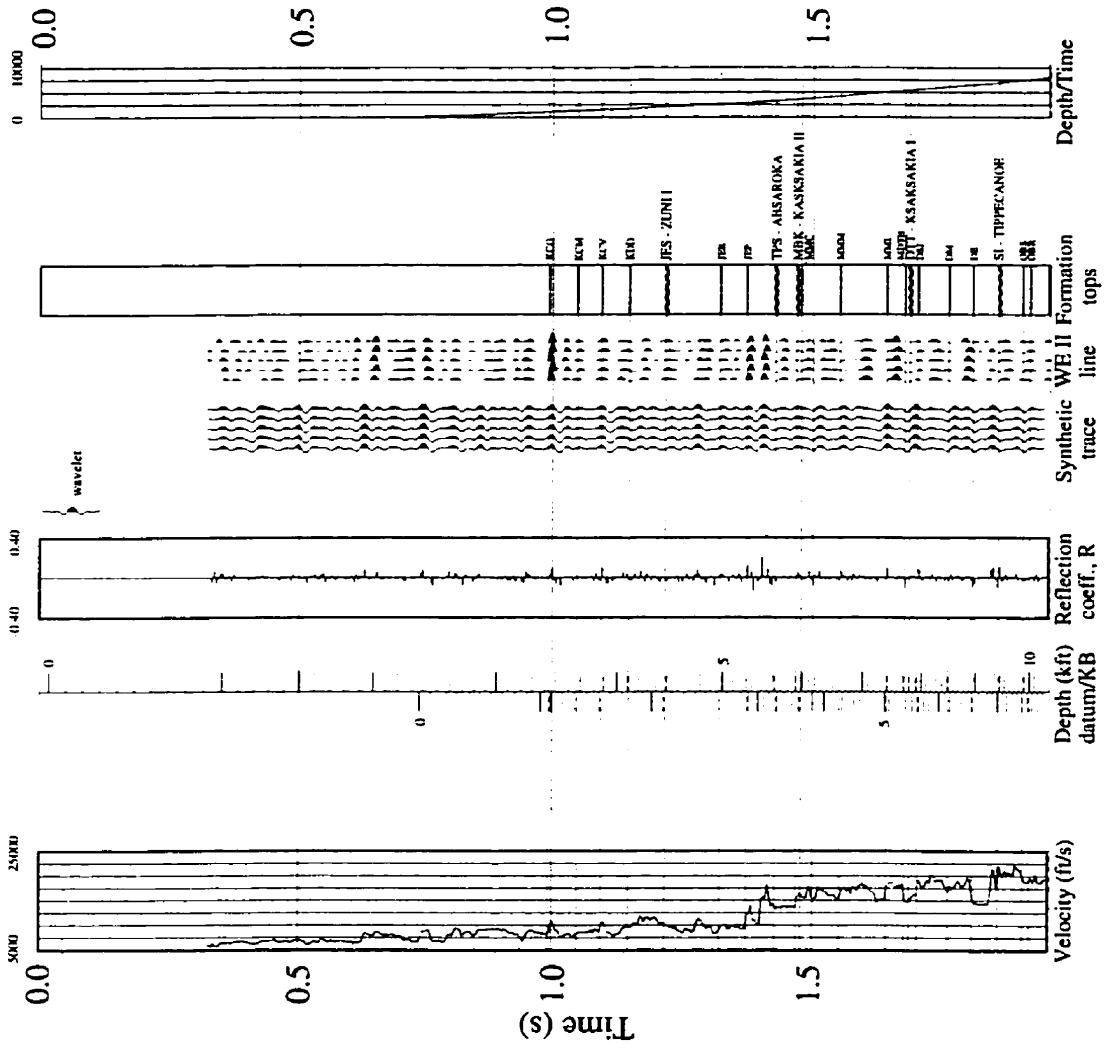

Fig. A.20 Well 14 - Synthetic seismogram.

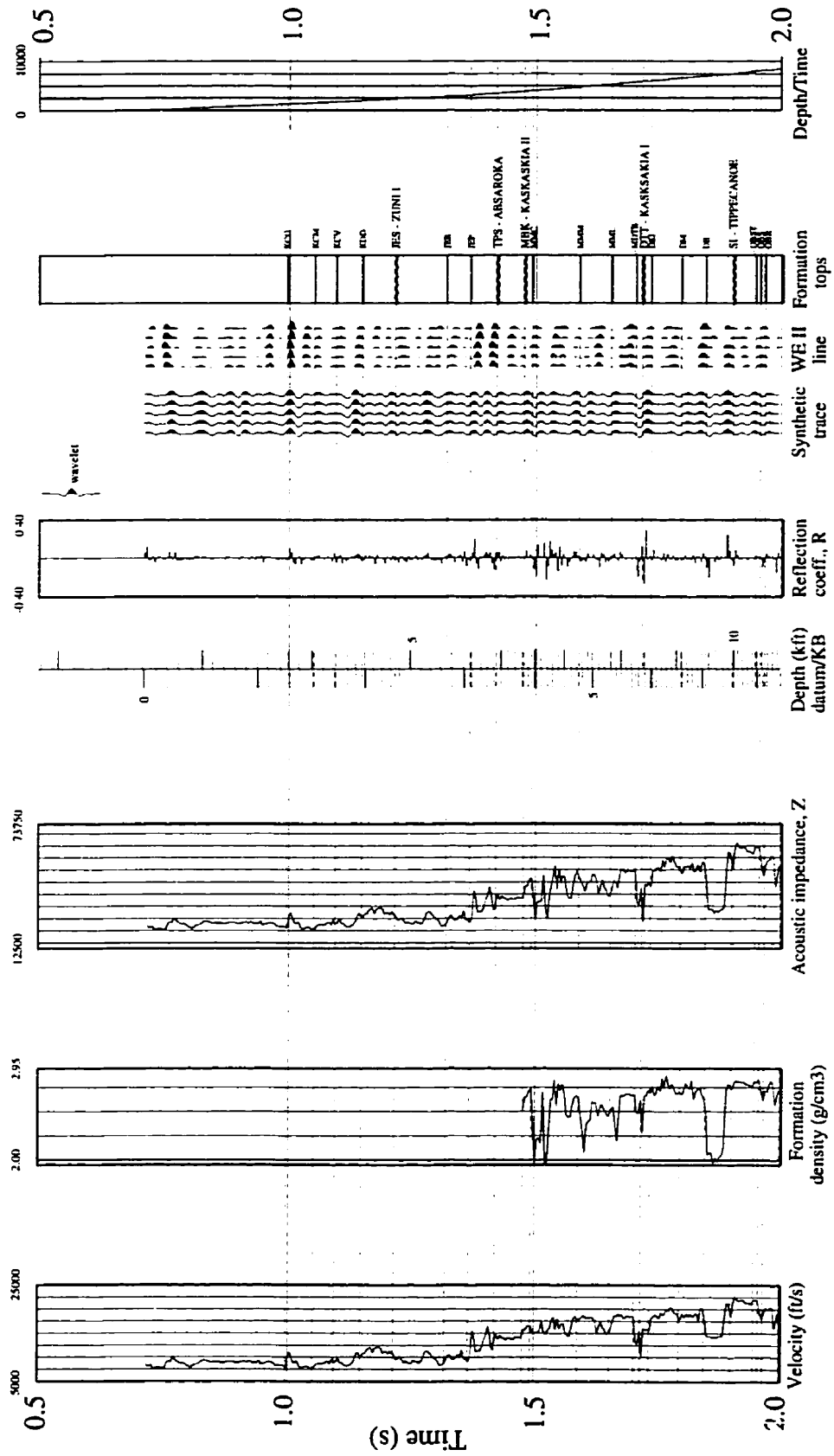

Fig. A.21 Well 15 - Synthetic seismogram.

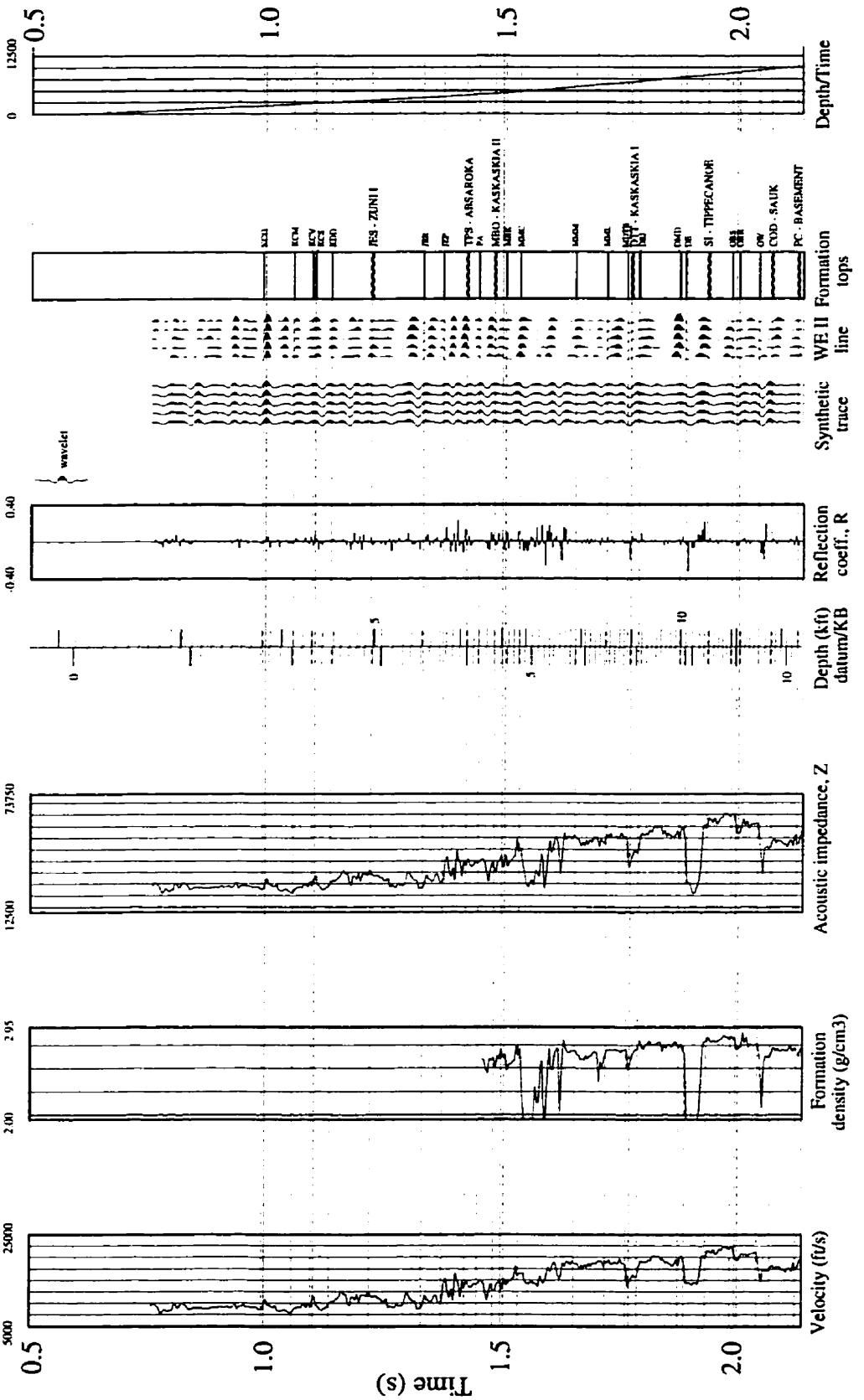

Fig. A.22 Well 16 - Synthetic seismogram.

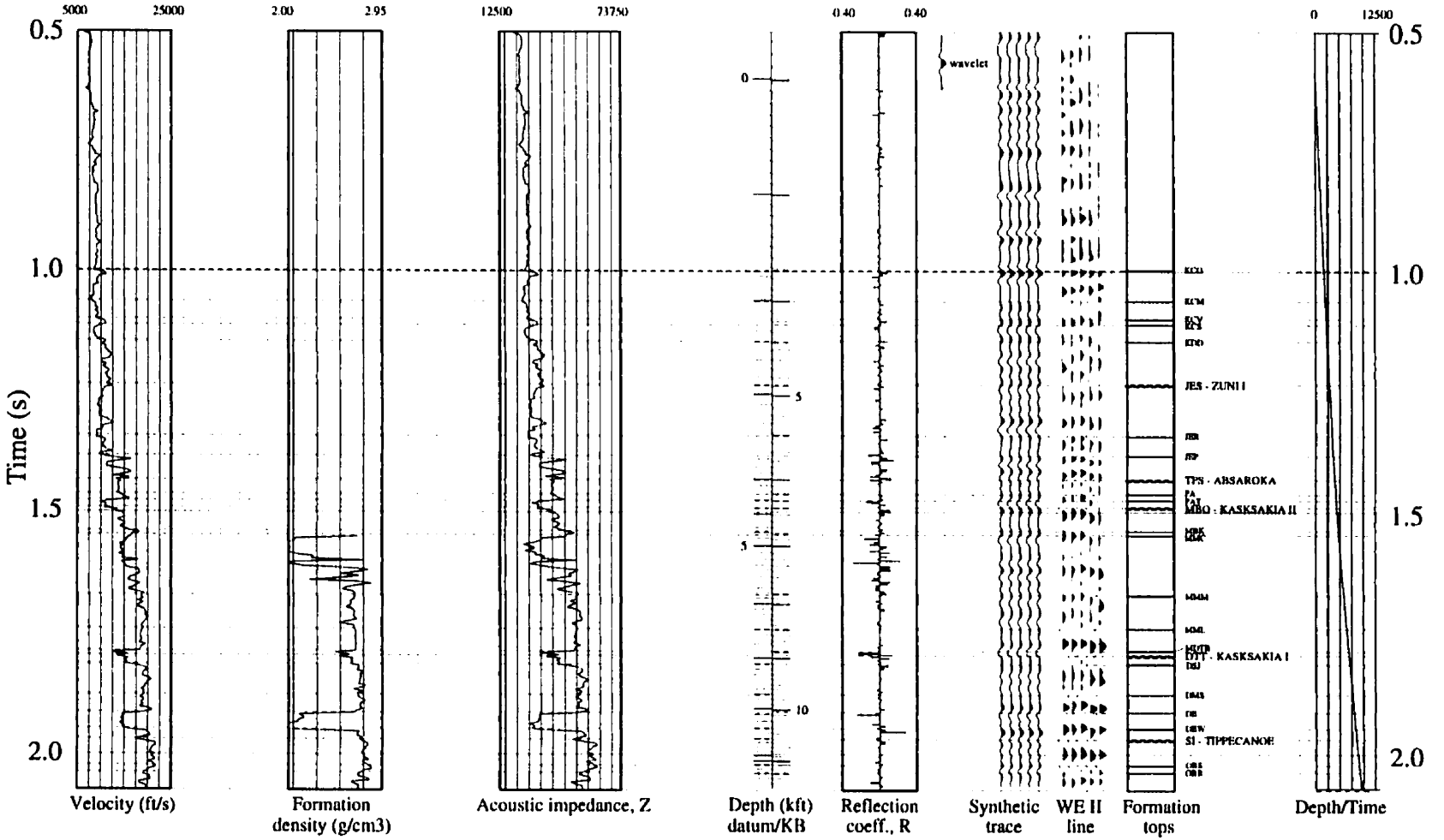

Fig. A.23 Well 17 - Synthetic seismogram.

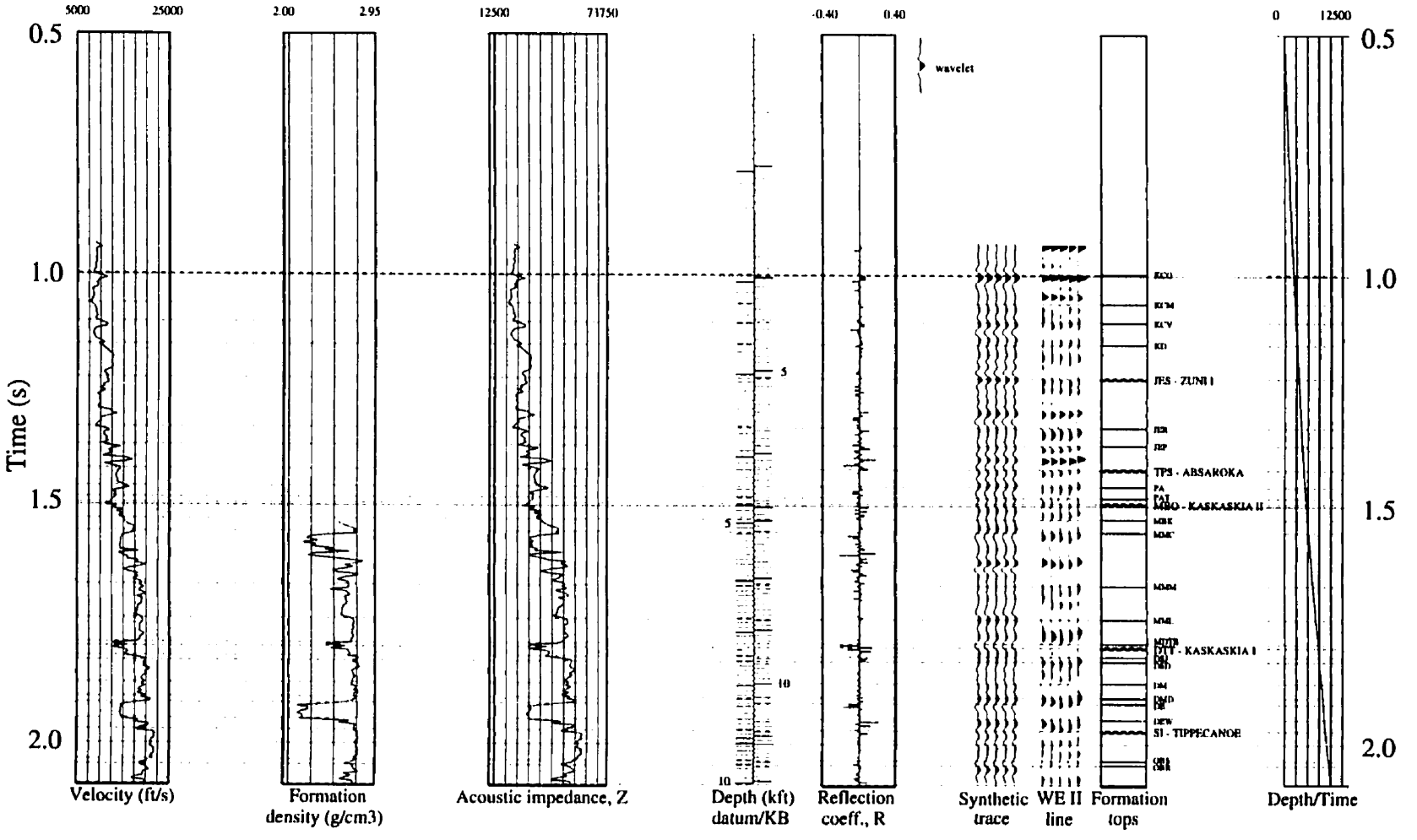

Fig. A.24 Well 18 - Synthetic seismogram.

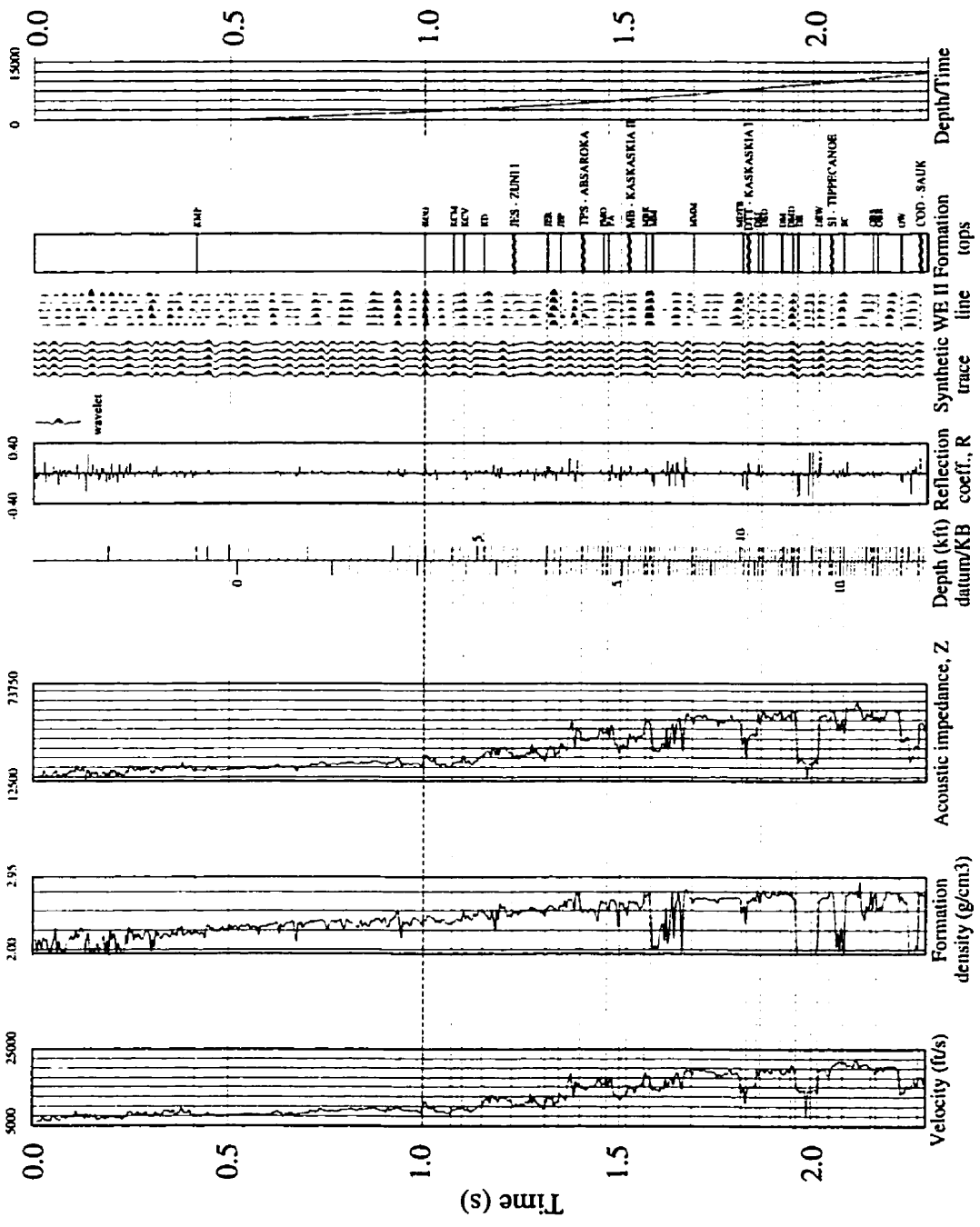

Fig. A.25 Well 19 - Synthetic seismogram.

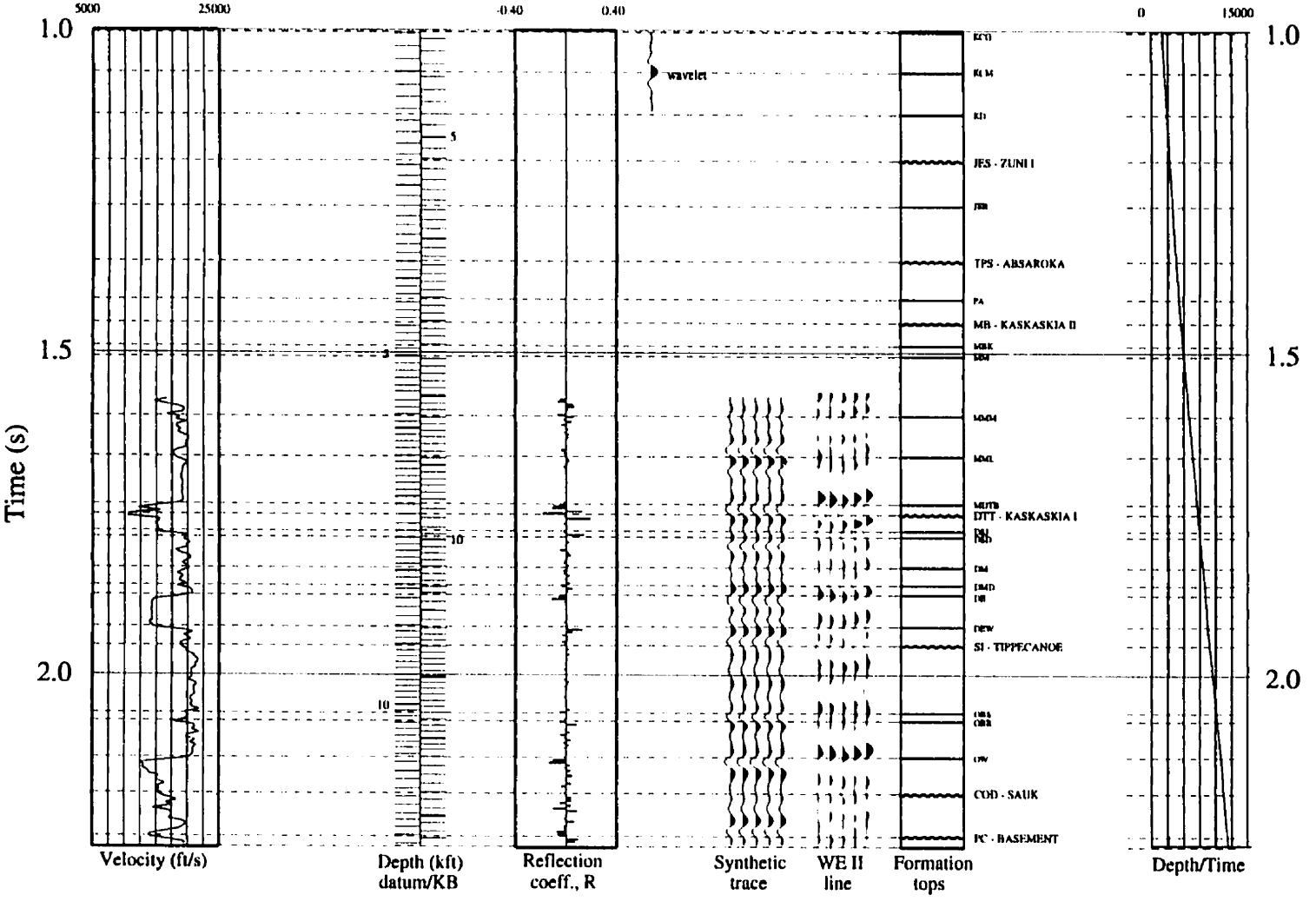

Fig. A.26 Well 20 - Synthetic seismogram.

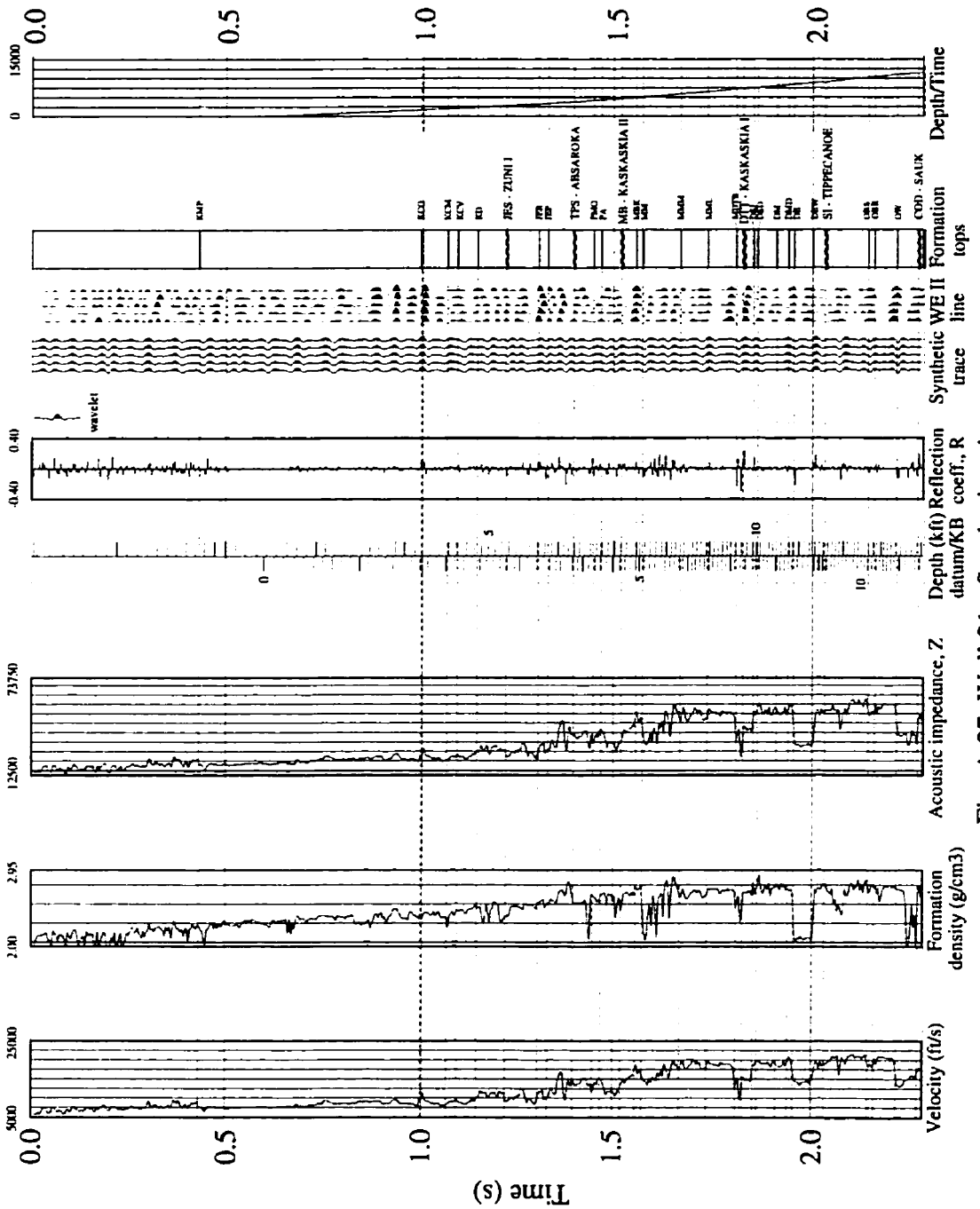

Fig. A.27 Well 21 - Synthetic seismogram.

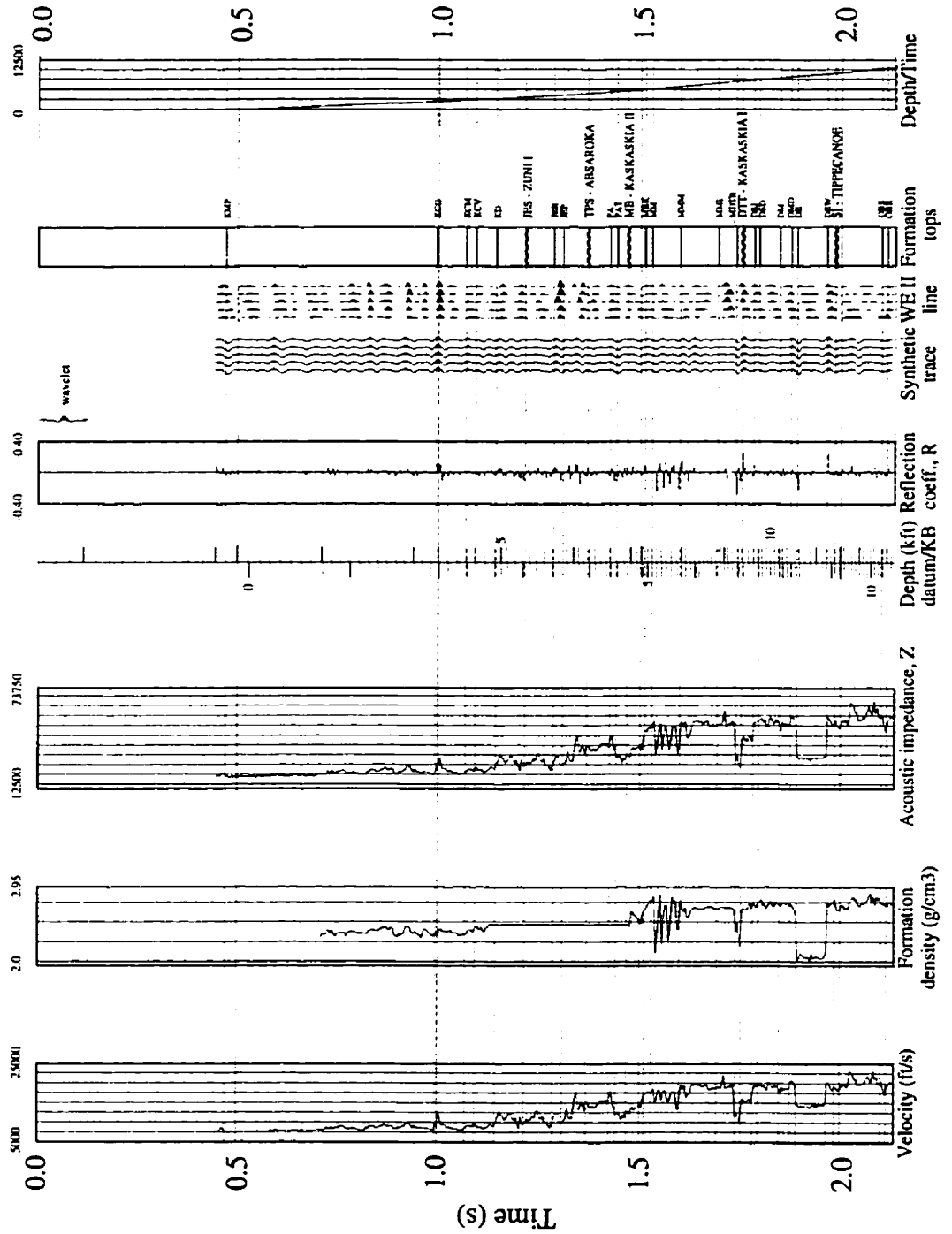

Fig. A.28 Well 22 - Synthetic seismogram.

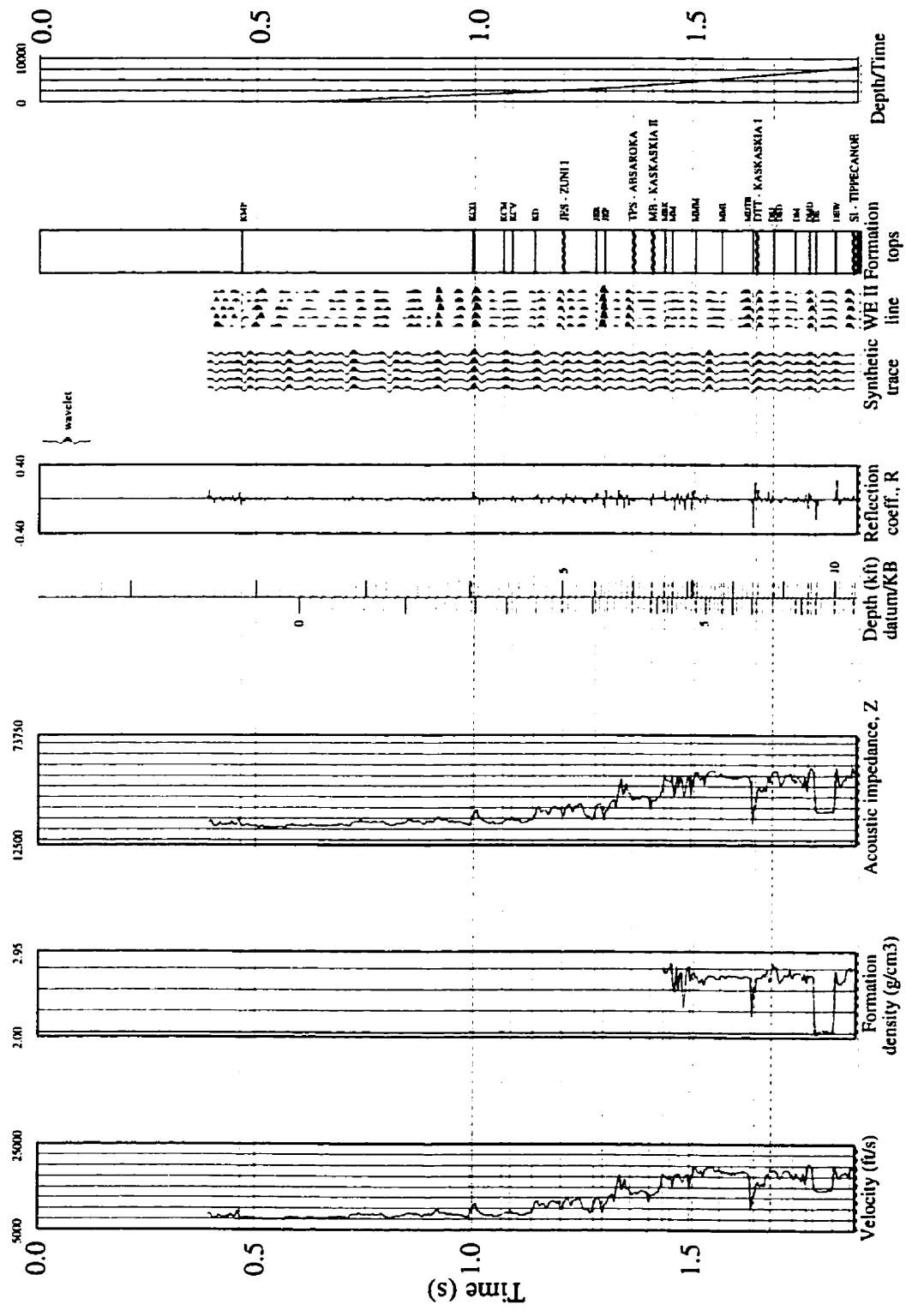

Fig. A.29 Well 23 - Synthetic seismogram.

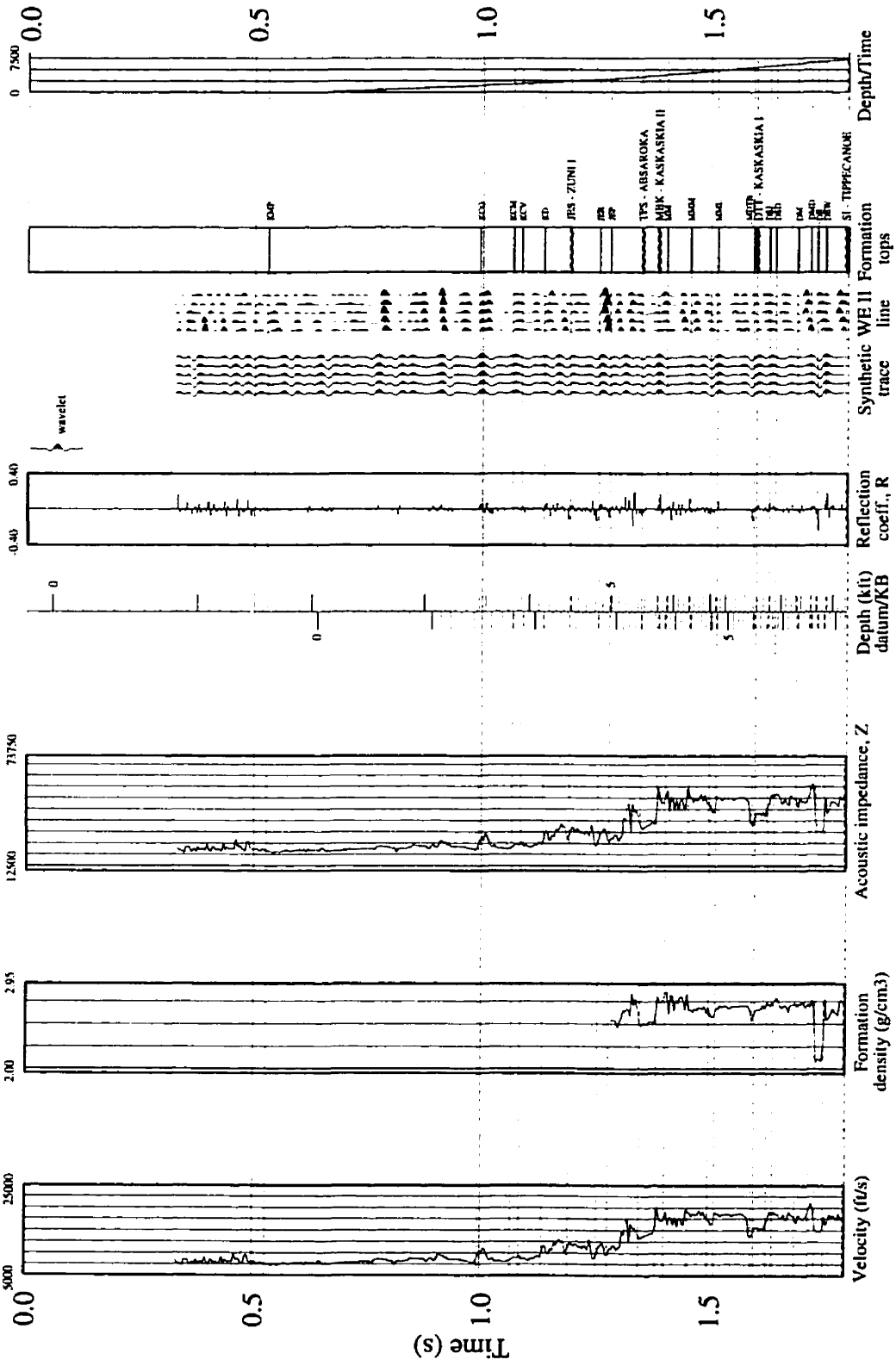

Fig. A.30 Well 24 - Synthetic seismogram.

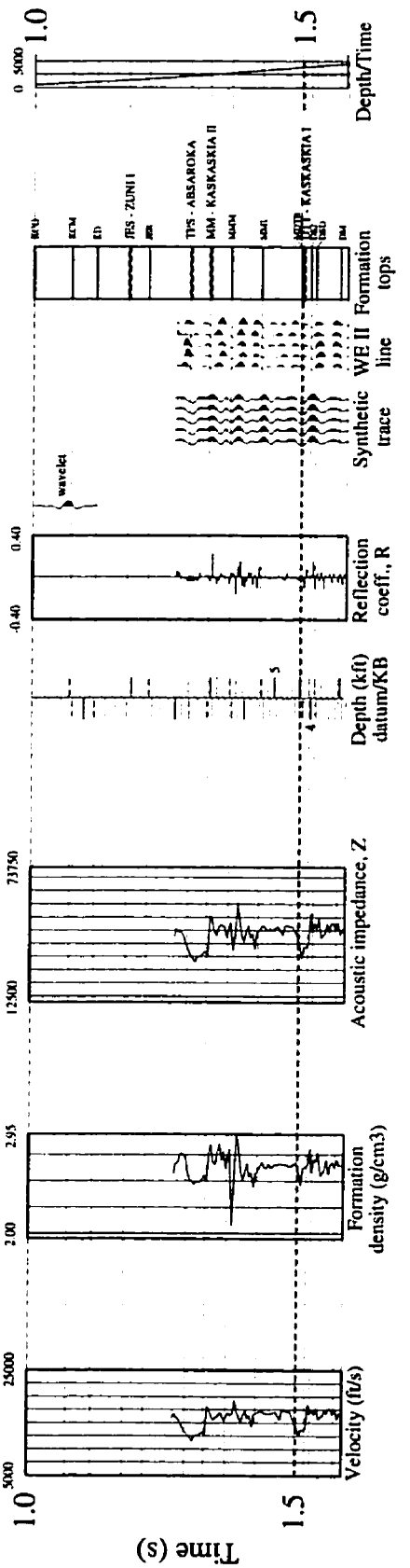

Fig. A.31 Well 25 - Synthetic seismogram.

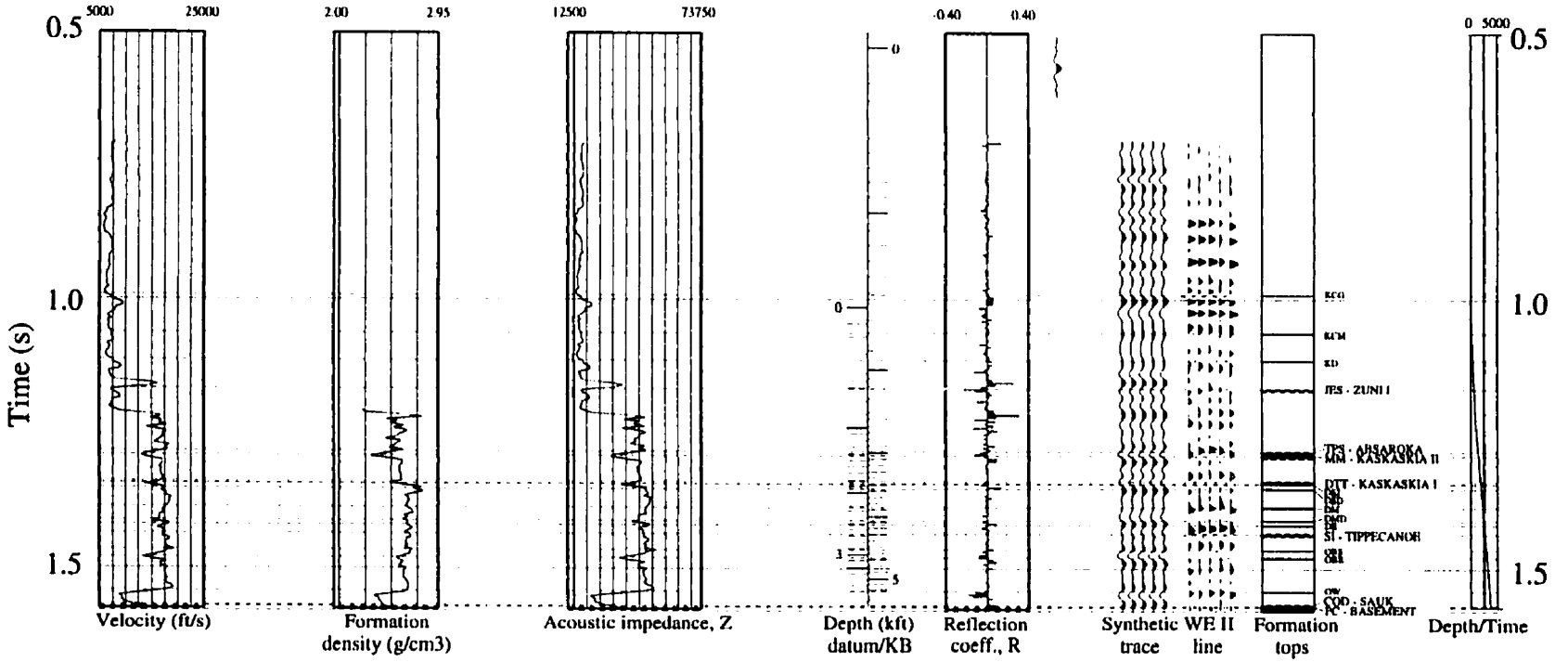

Fig. A.32 Well 26 - Synthetic seismogram.

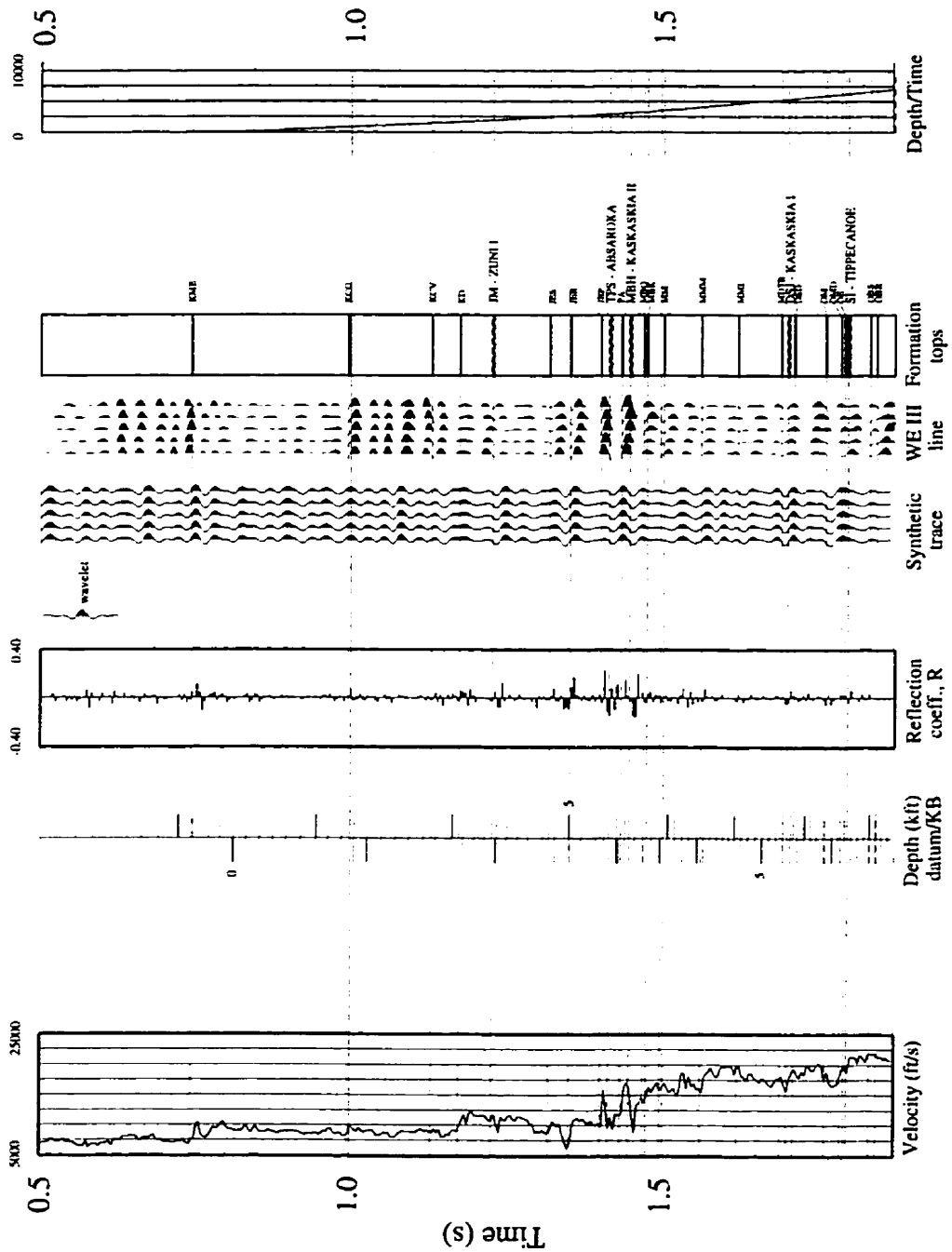

Fig. A.33 Well 27 - Synthetic seismogram.

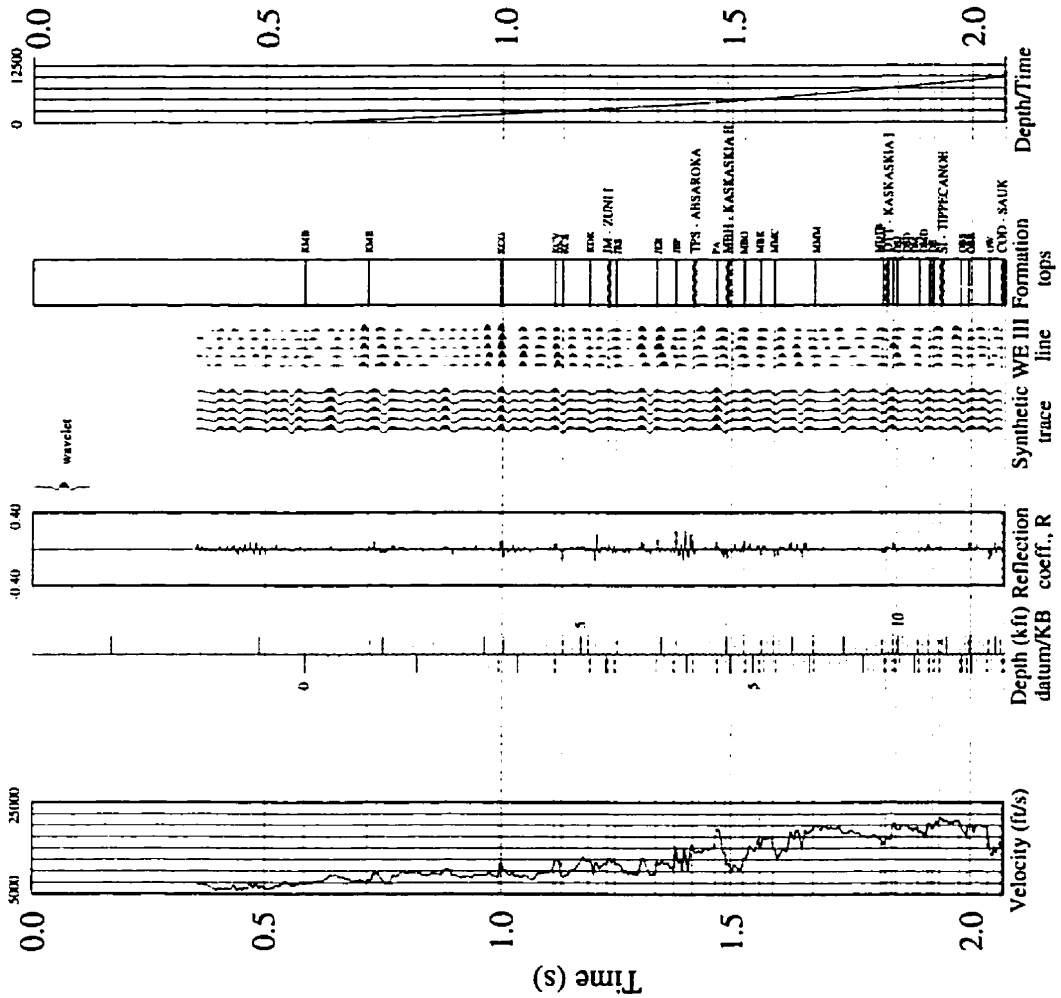

Fig. A.34 Well 28 - Synthetic seismogram.

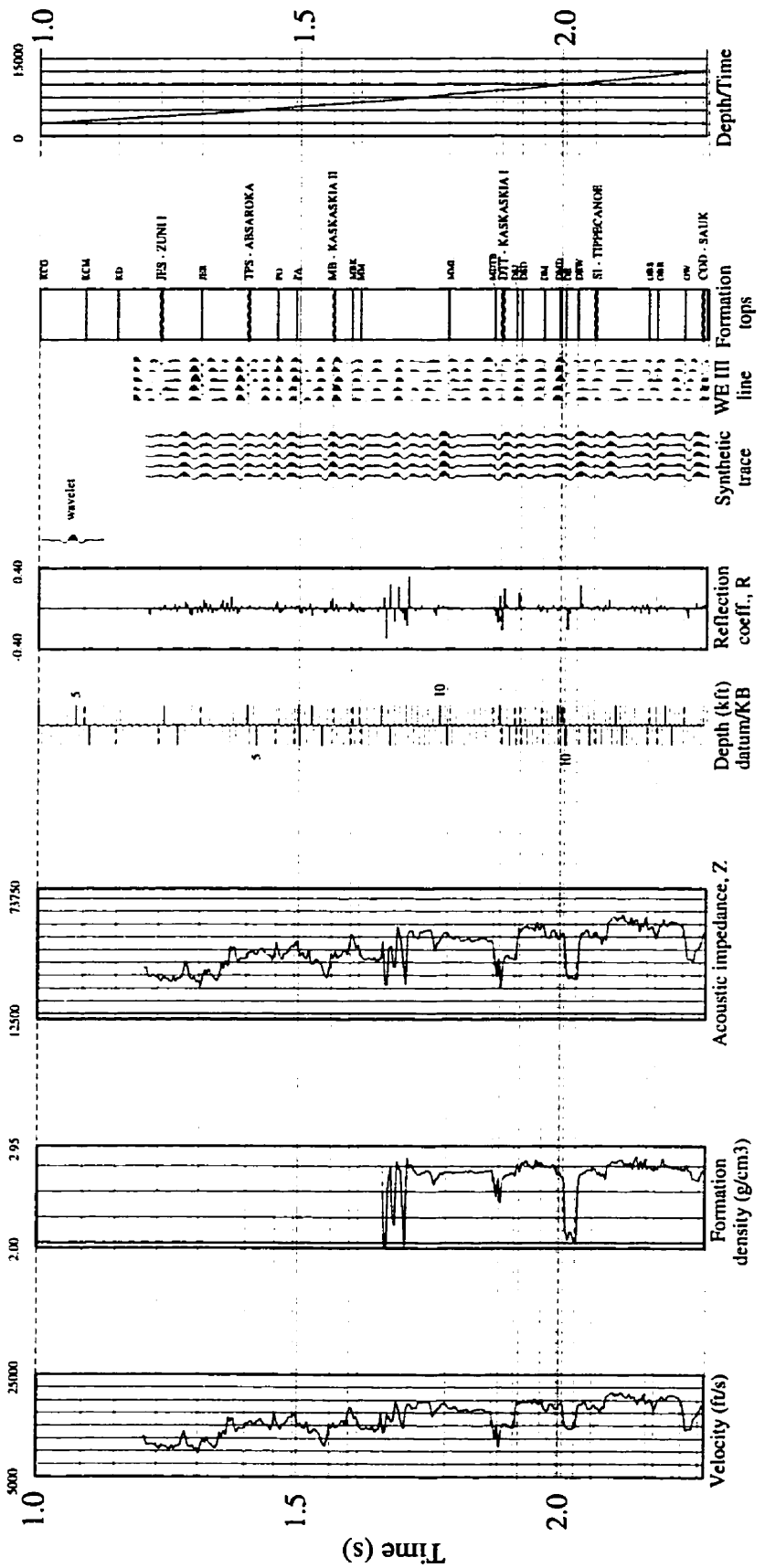

Fig. A.35 Well 29 - Synthetic seismogram.

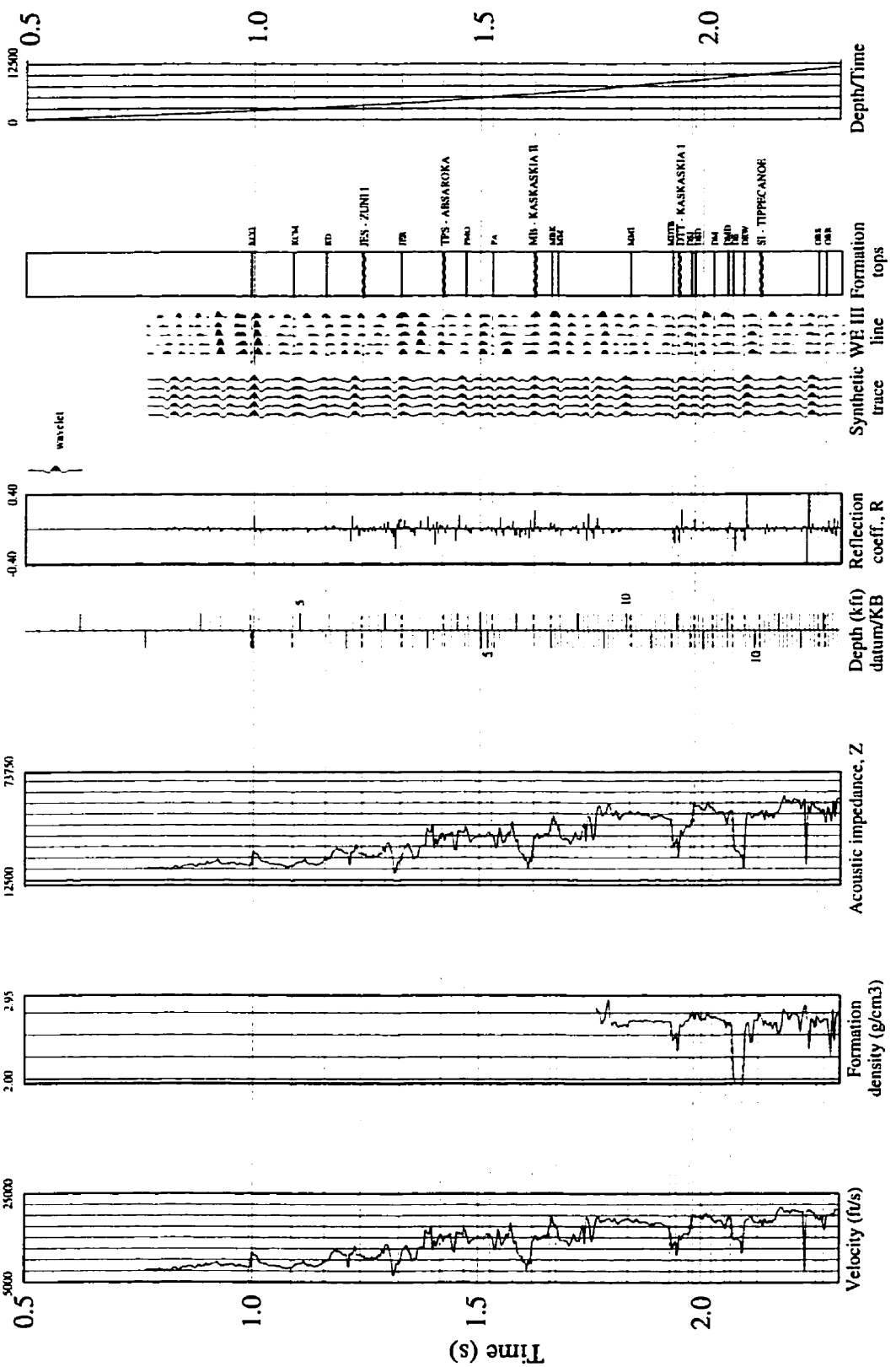

Fig. A.36 Well 30 - Synthetic seismogram.

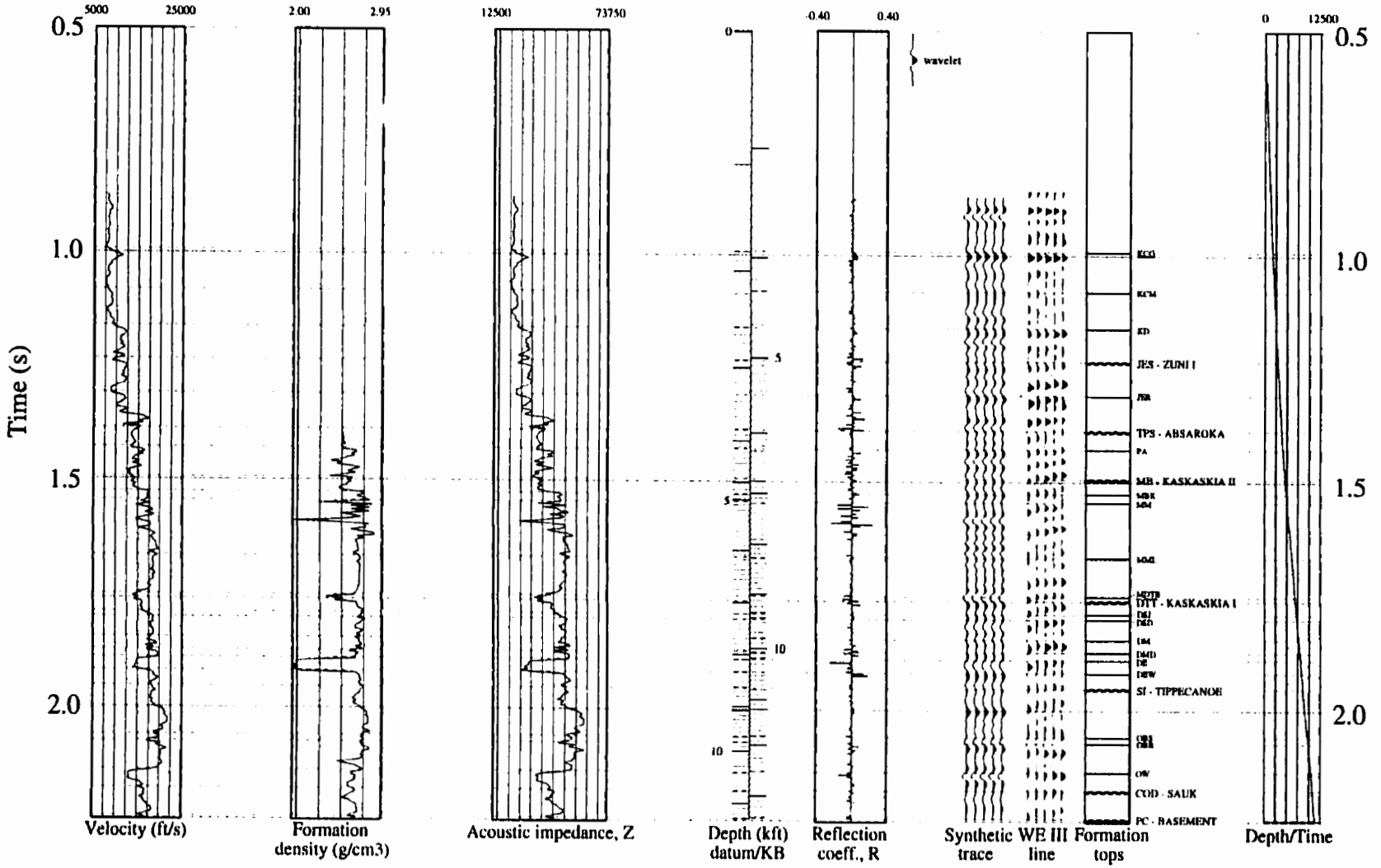

Fig. A.37 Well 31 - Synthetic seismogram.

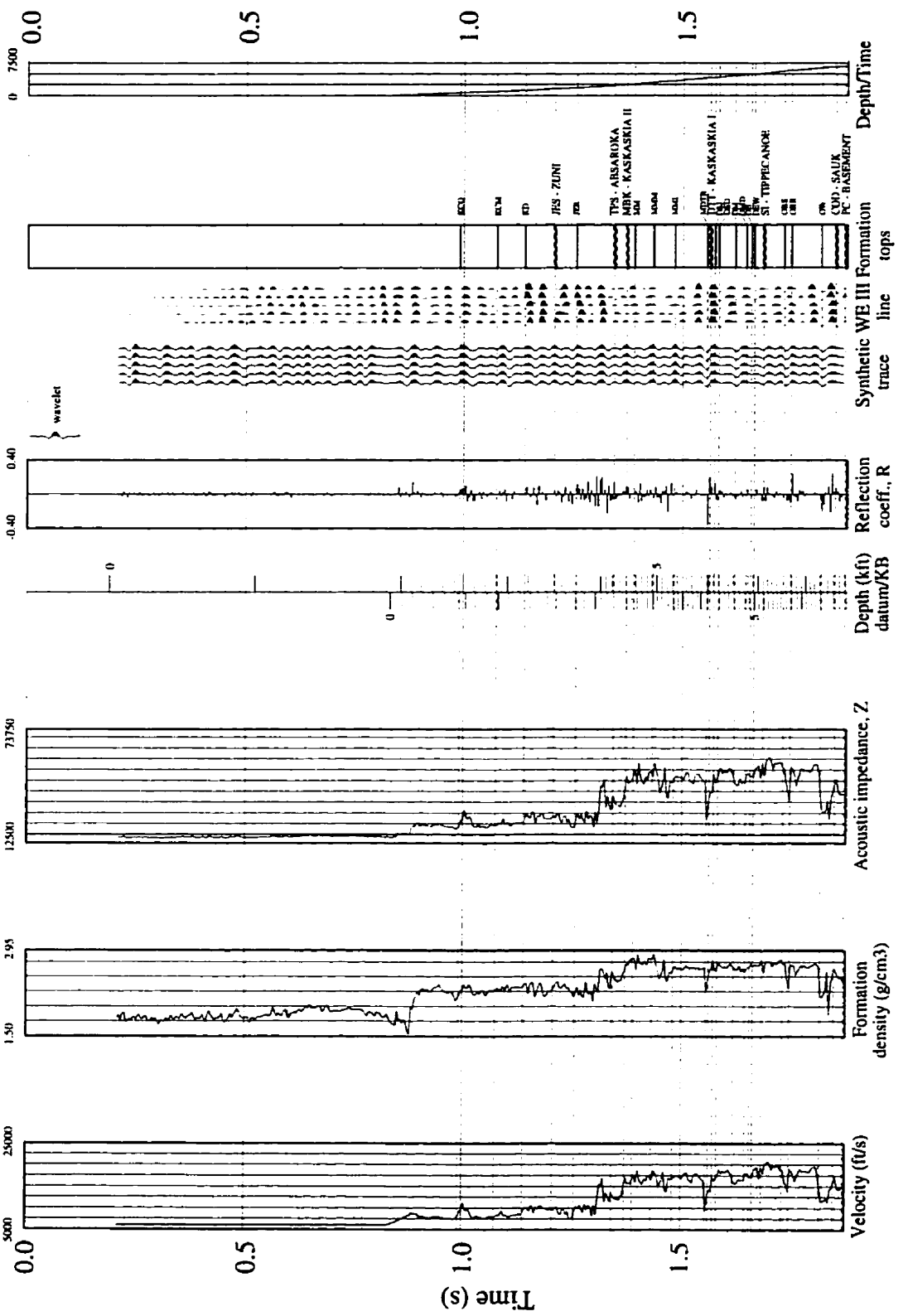

Fig. A.38 Well 32 - Synthetic seismogram.

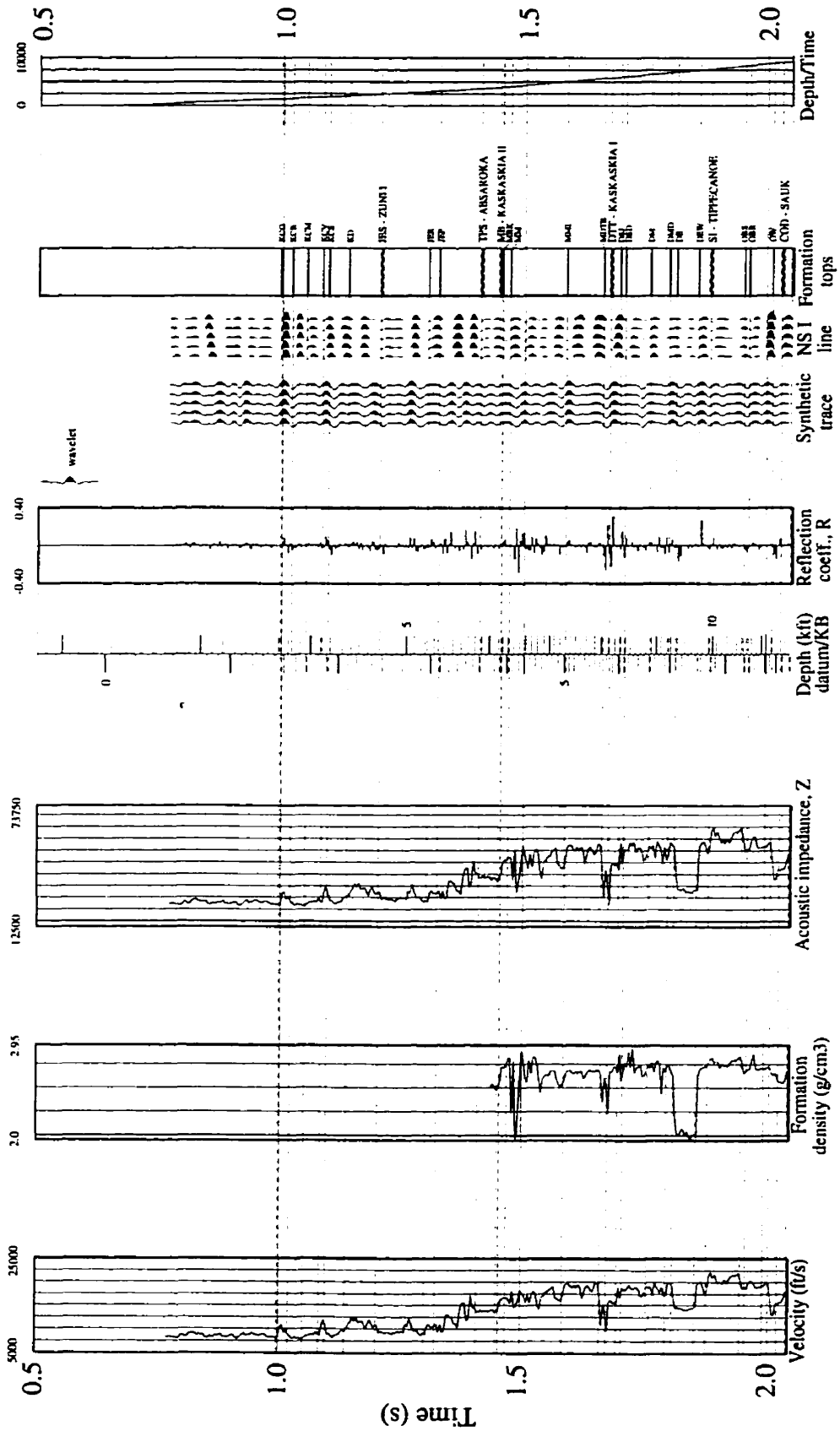

Fig. A.39 Well 34 - Synthetic seismogram.

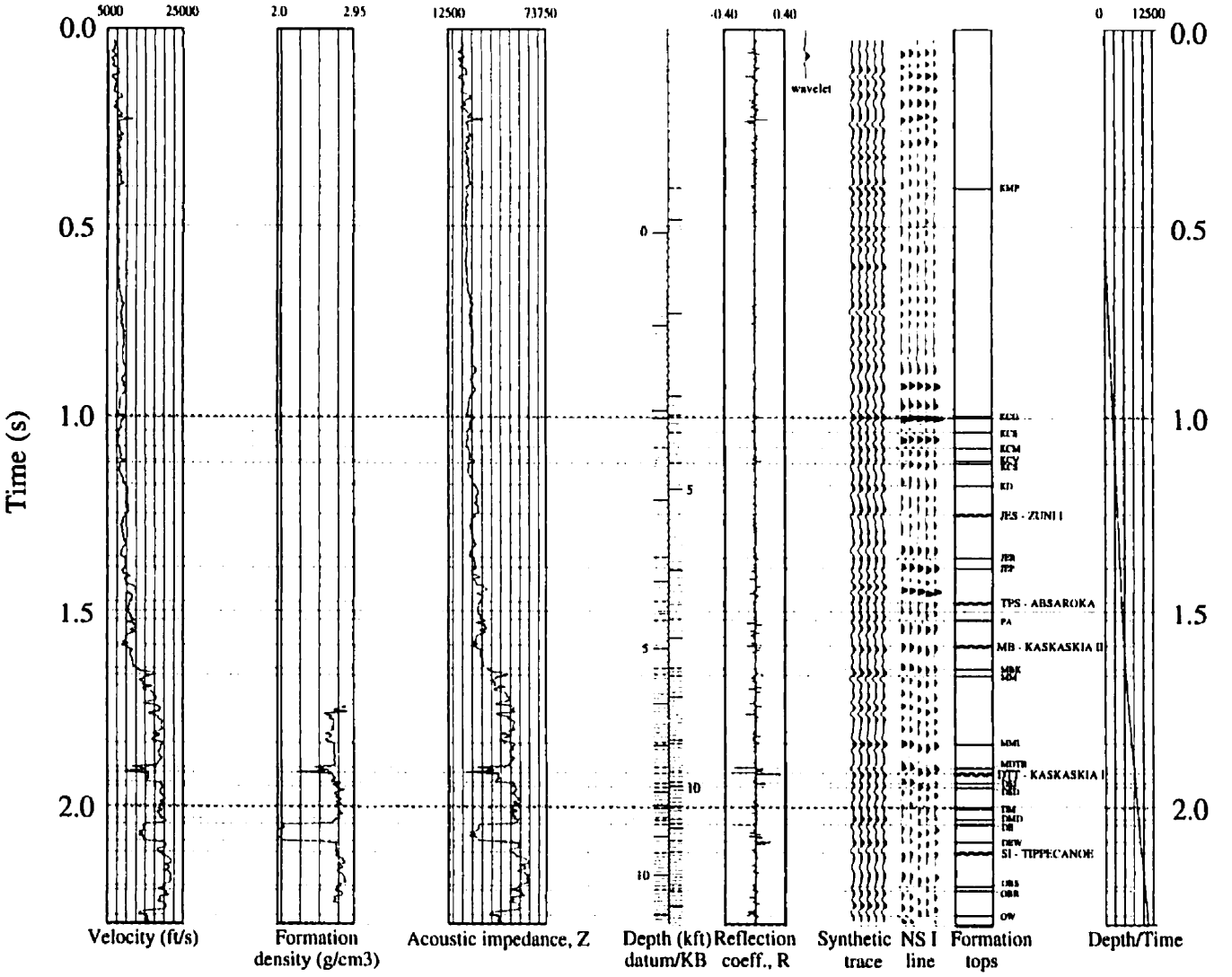

Fig. A.40 Well 35 - Synthetic seismogram.

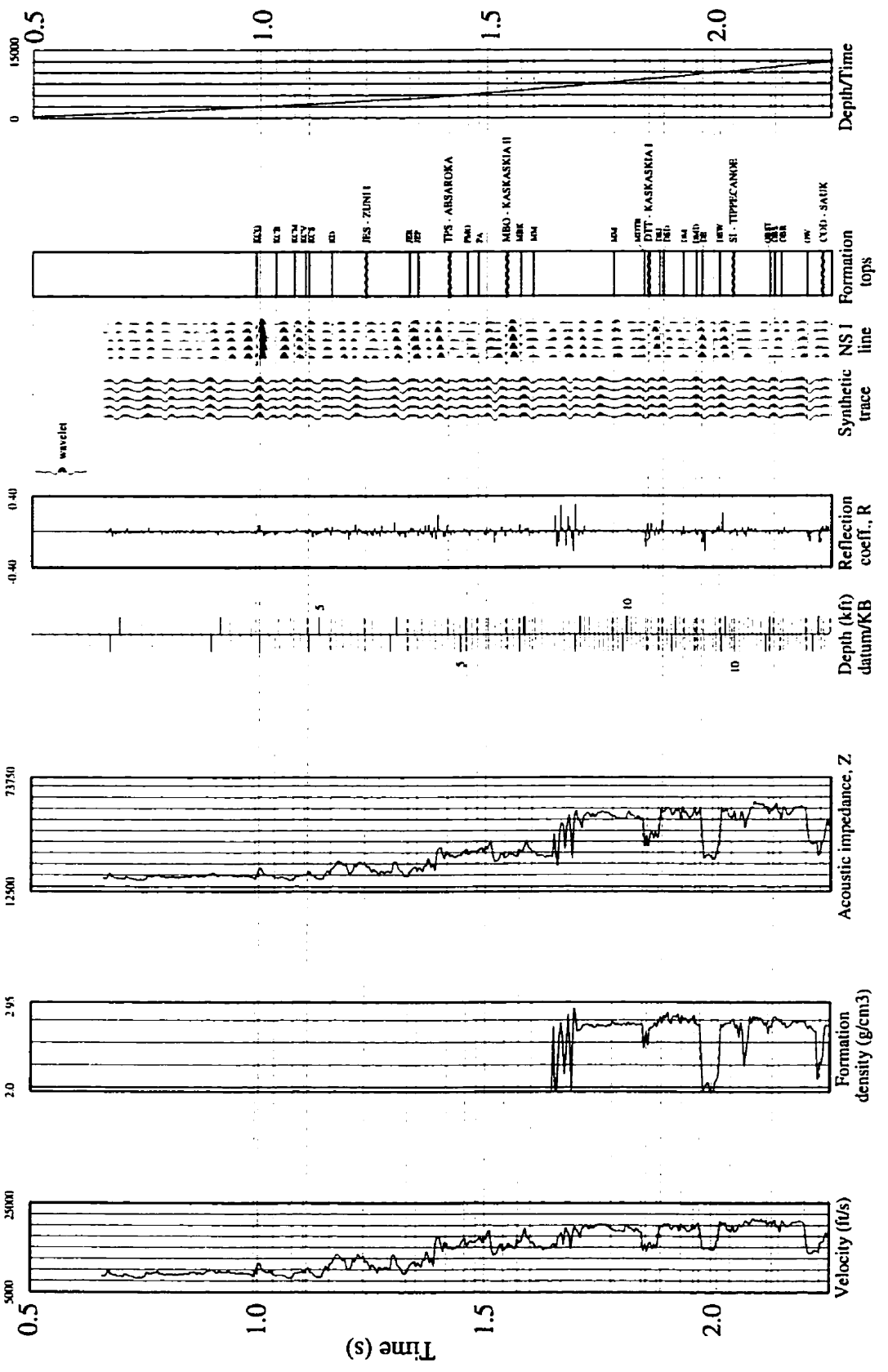

Fig. A.41 Well 36 - Synthetic seismogram.

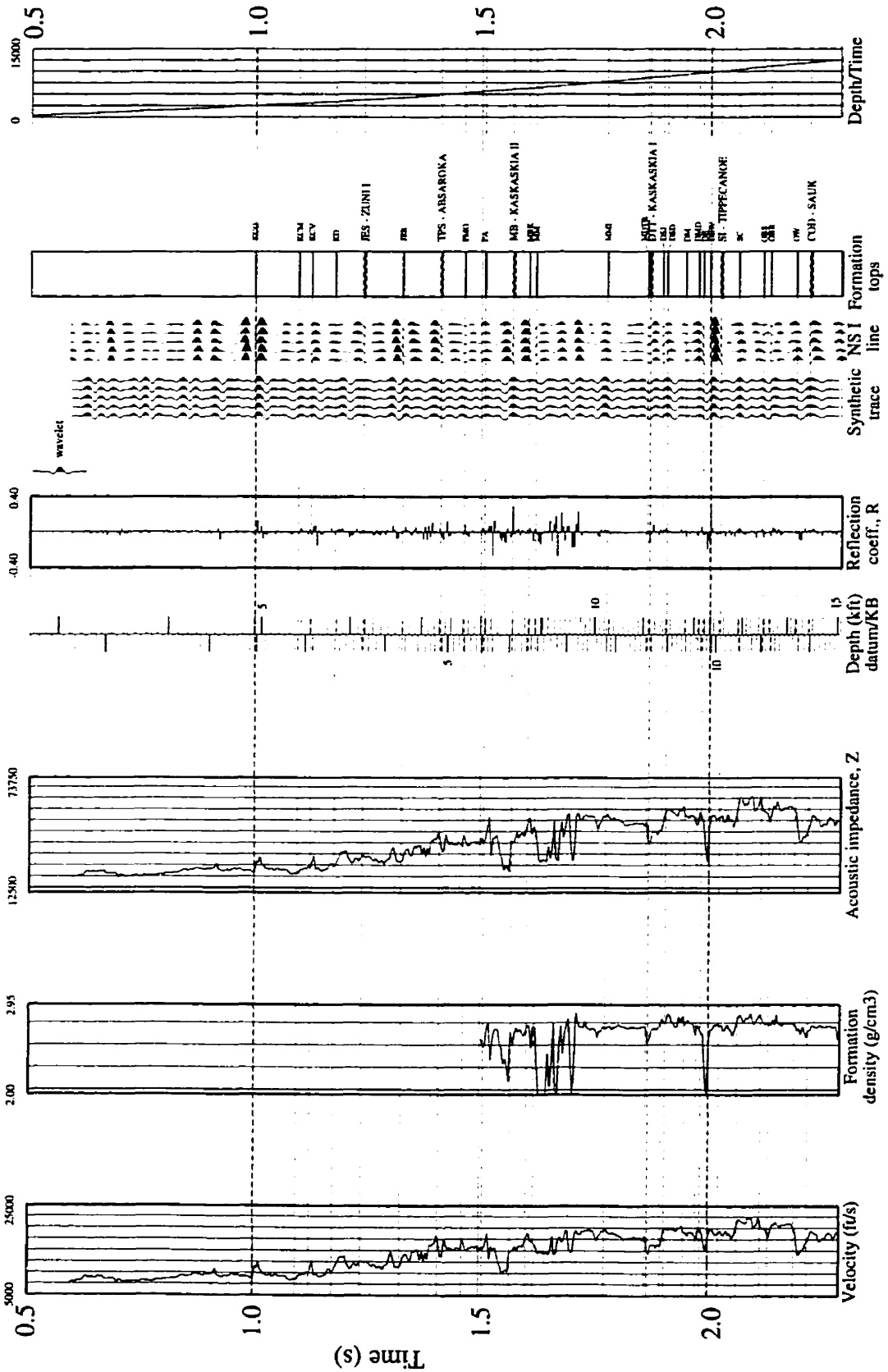

Fig. A.42 Well 37 - Synthetic seismogram.

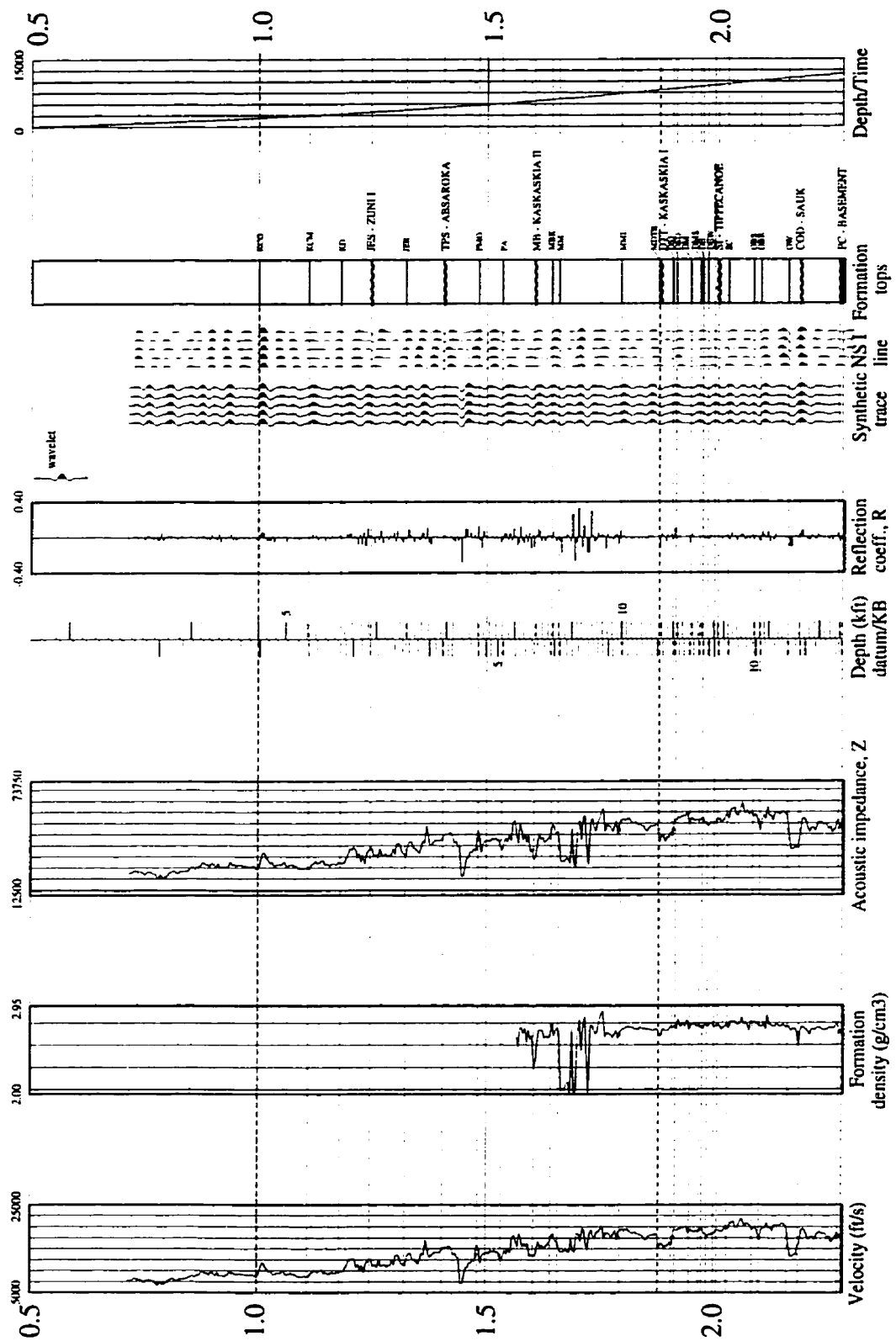

Fig. A.43 Well 38 - Synthetic seismogram.

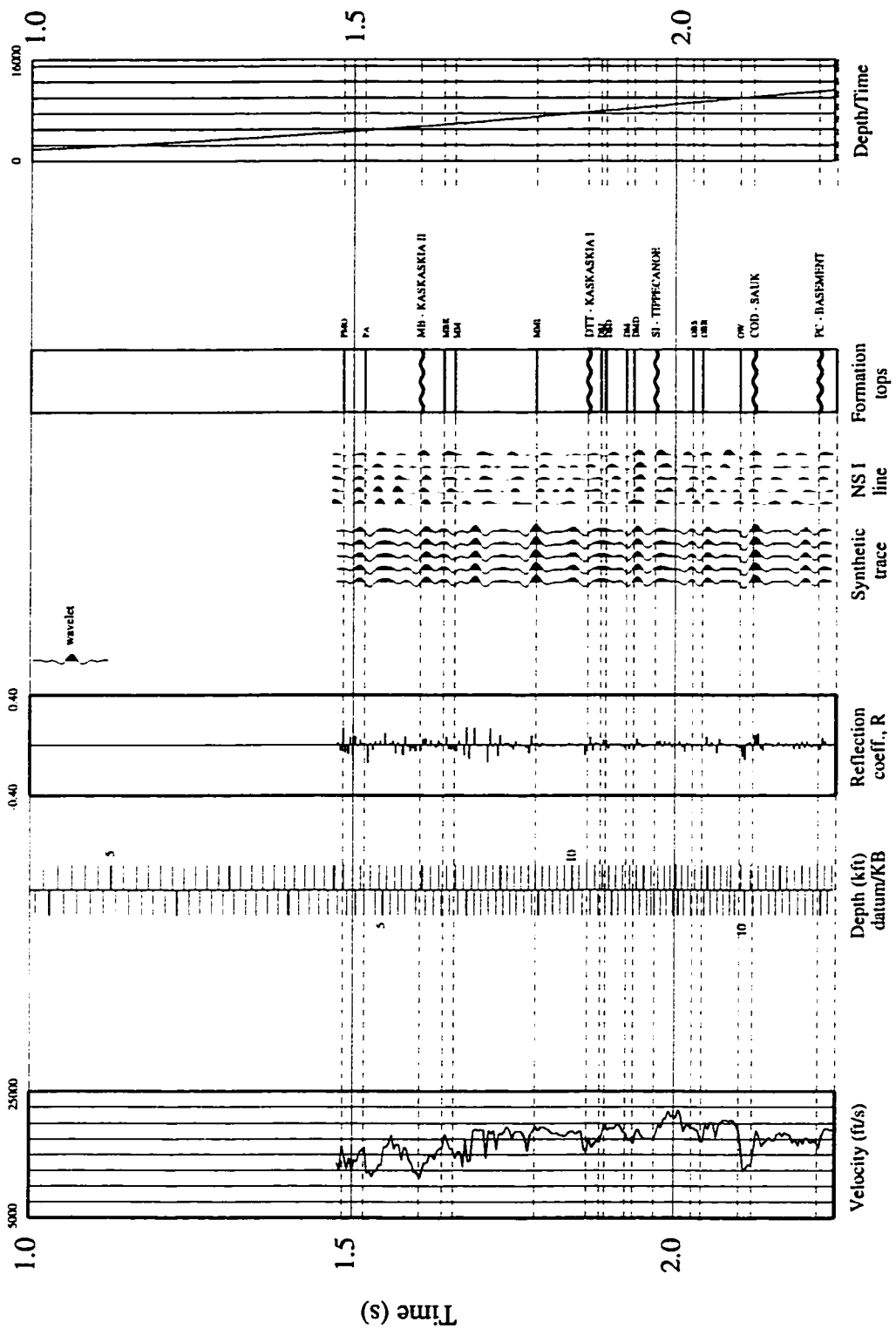

Fig. A.44 Well 39 - Synthetic seismogram.

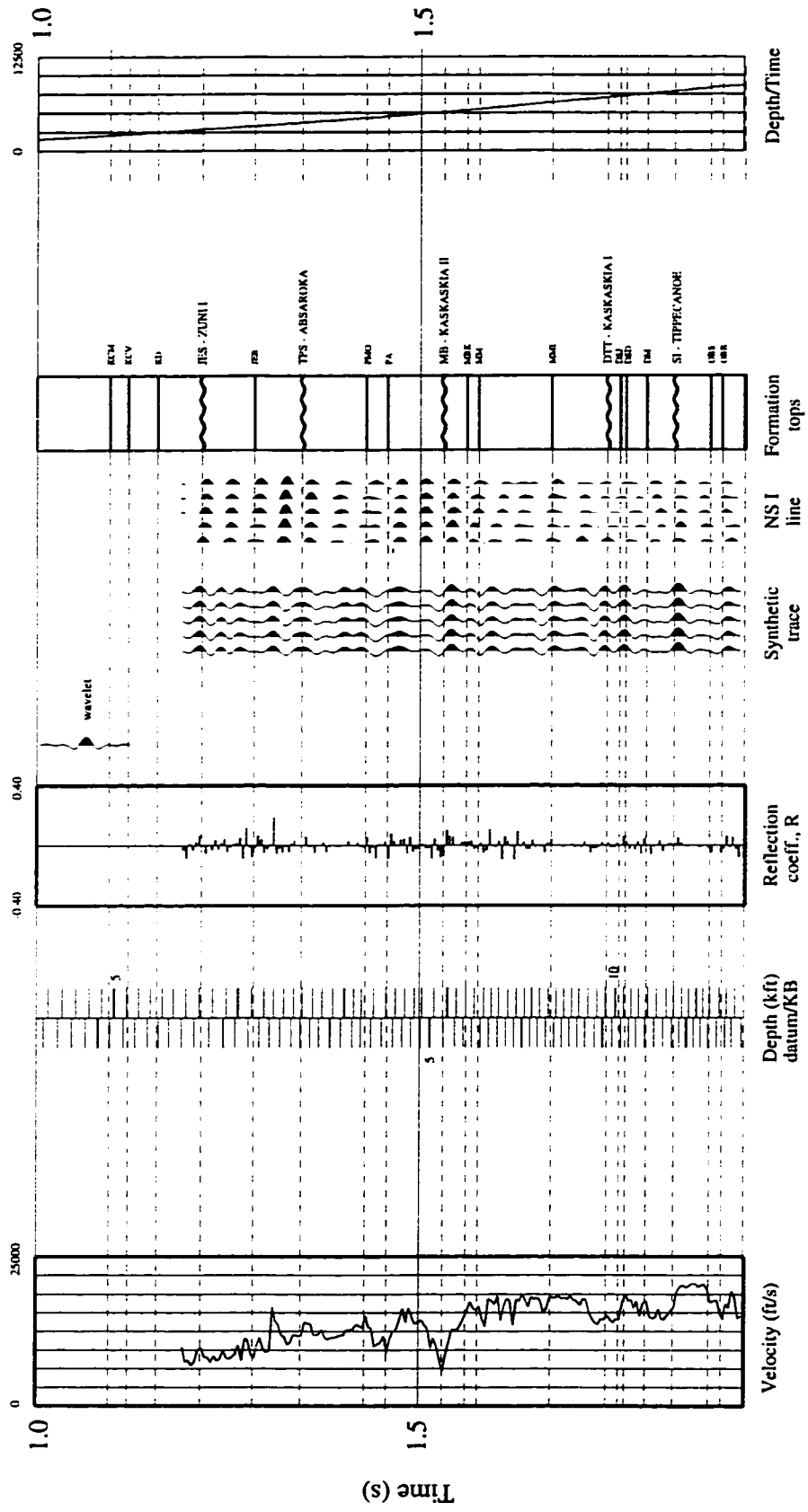

Fig. A.45 Well 40 - Synthetic seismogram.

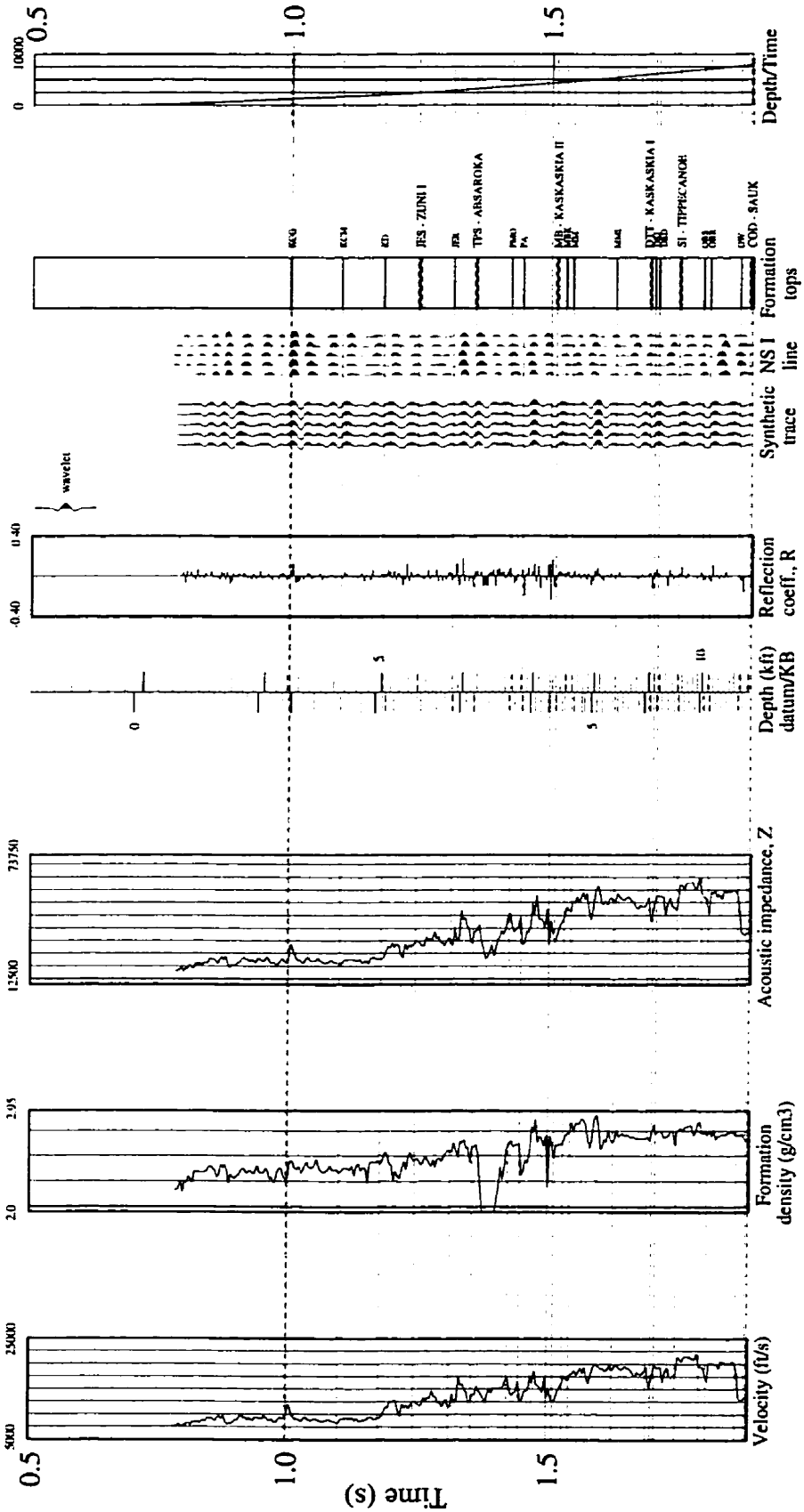

Fig. A.46 Well 41 - Synthetic seismogram.

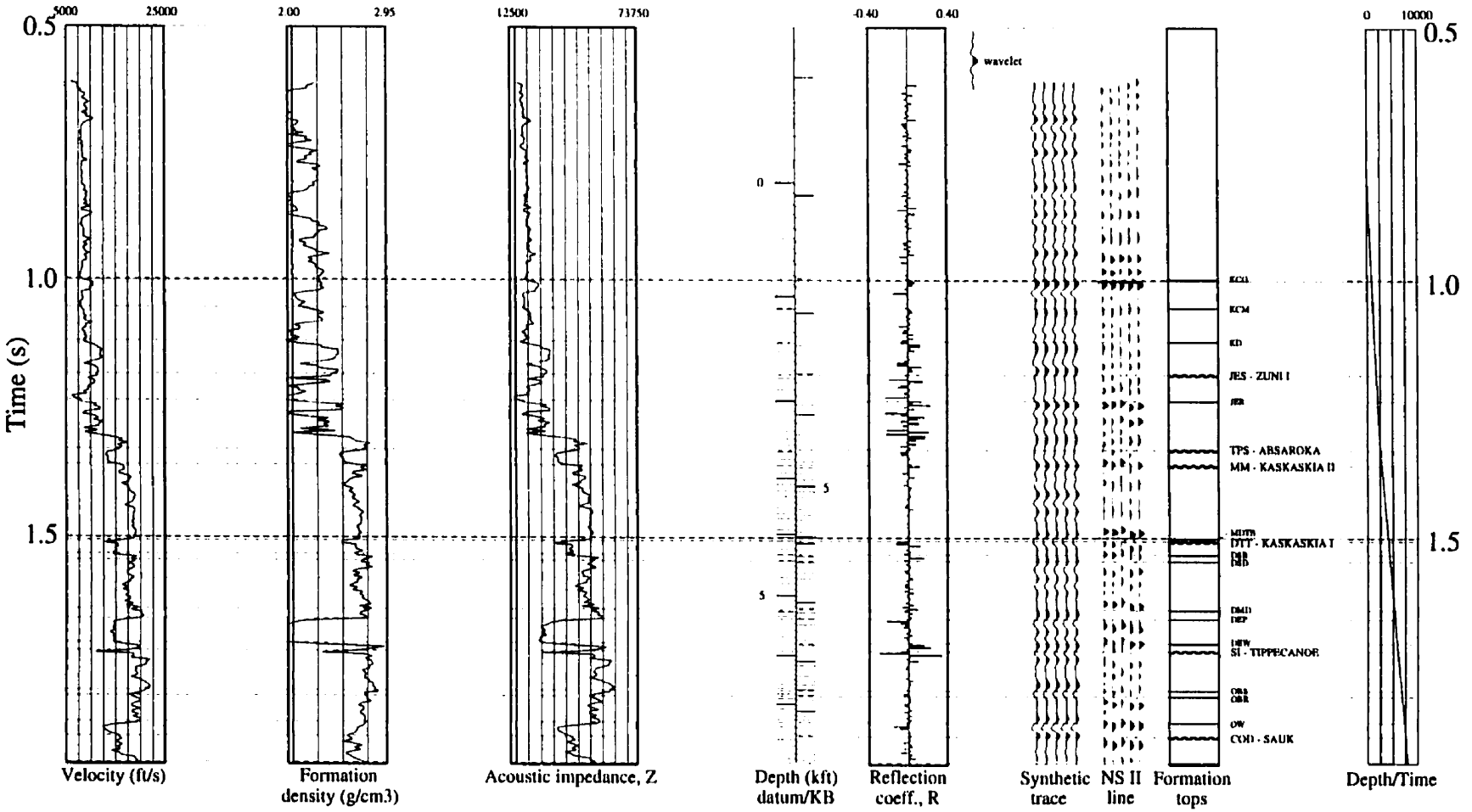

Fig. A.47 Well 42 - Synthetic seismogram.

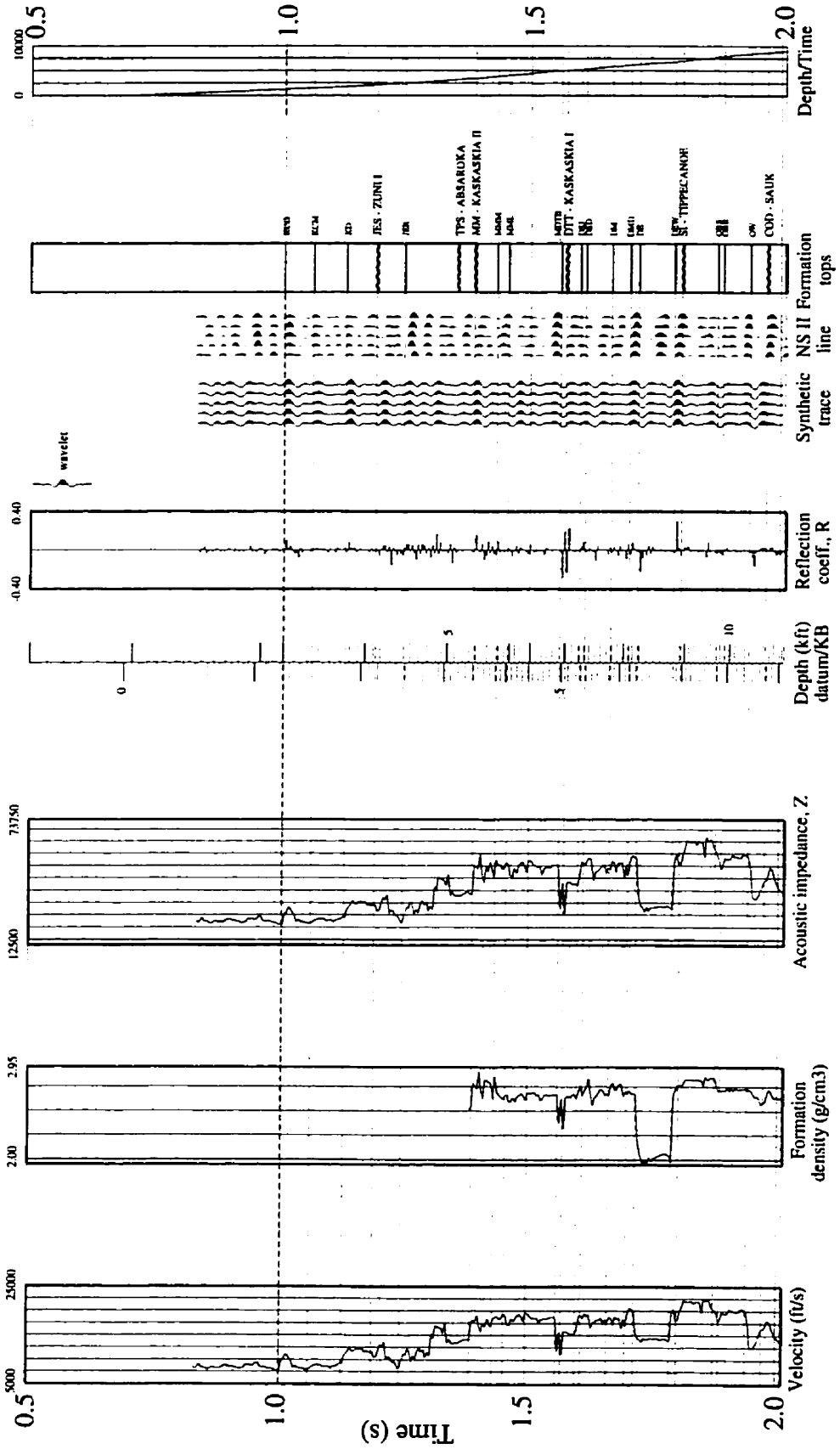

Fig. A.48 Well 43 - Synthetic seismogram.

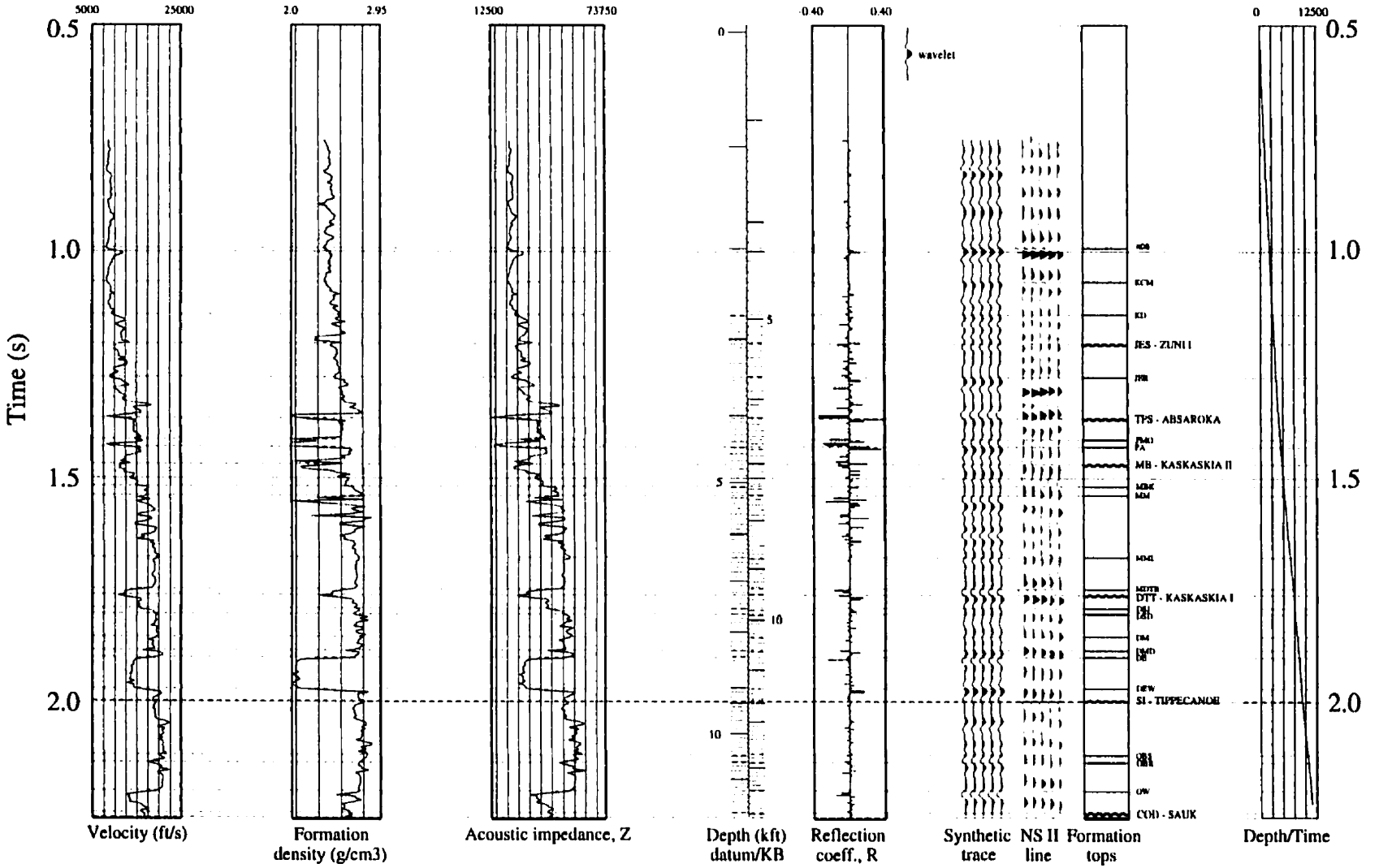

Fig. A.49 Well 44 - Synthetic seismogram.

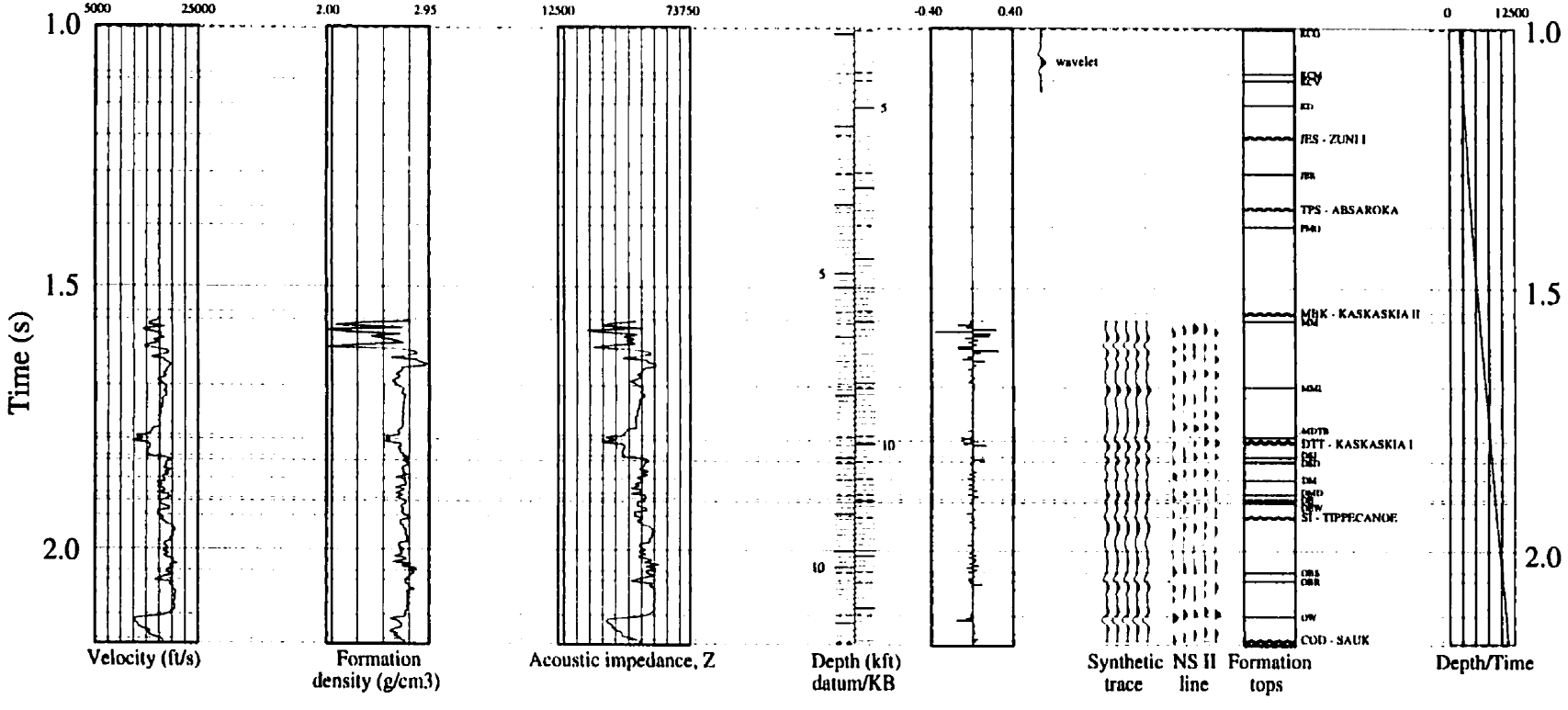

Fig. A.50 Well 45 - Synthetic seismogram.

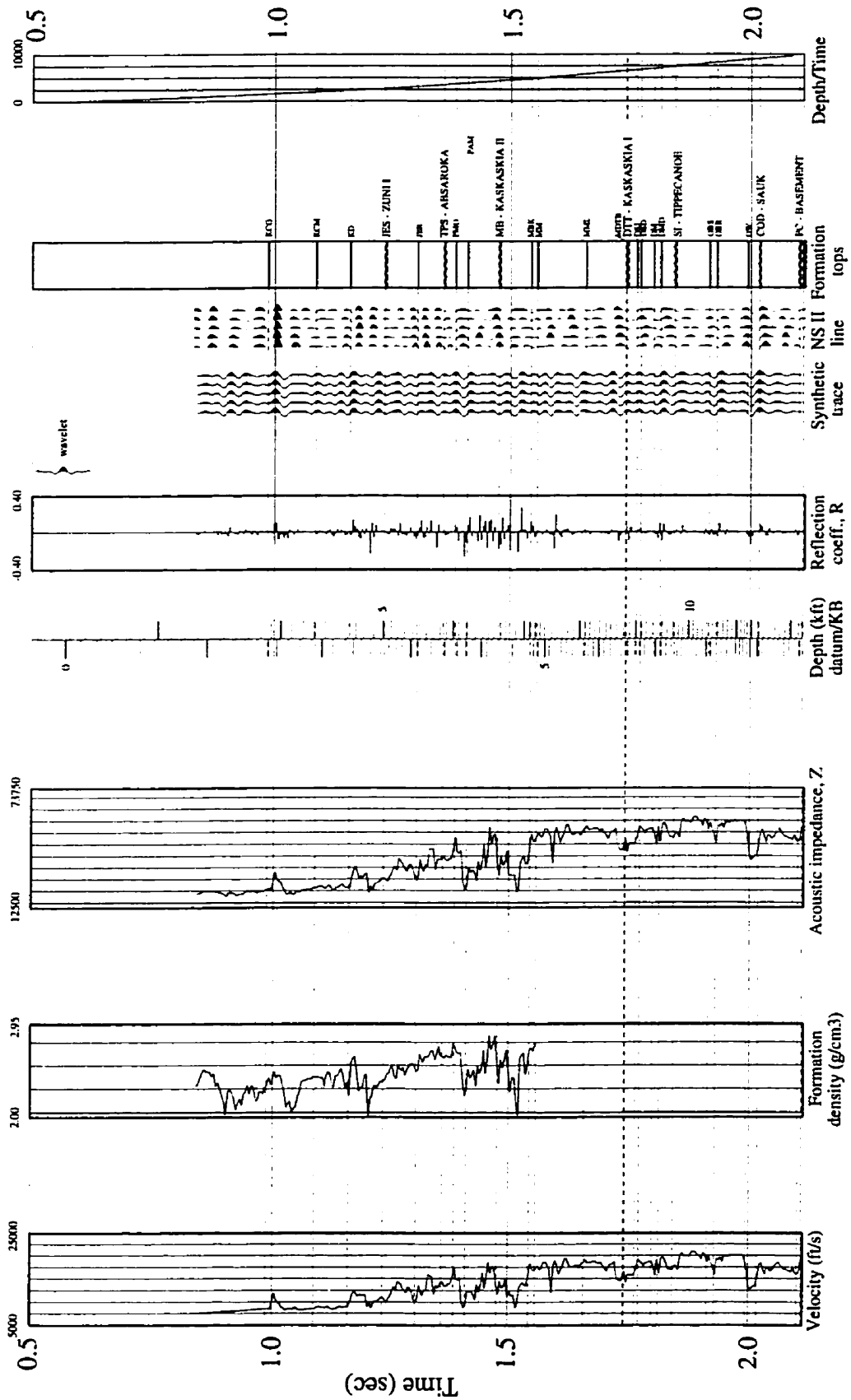

Fig. A.51 Well 46 - Synthetic seismogram.

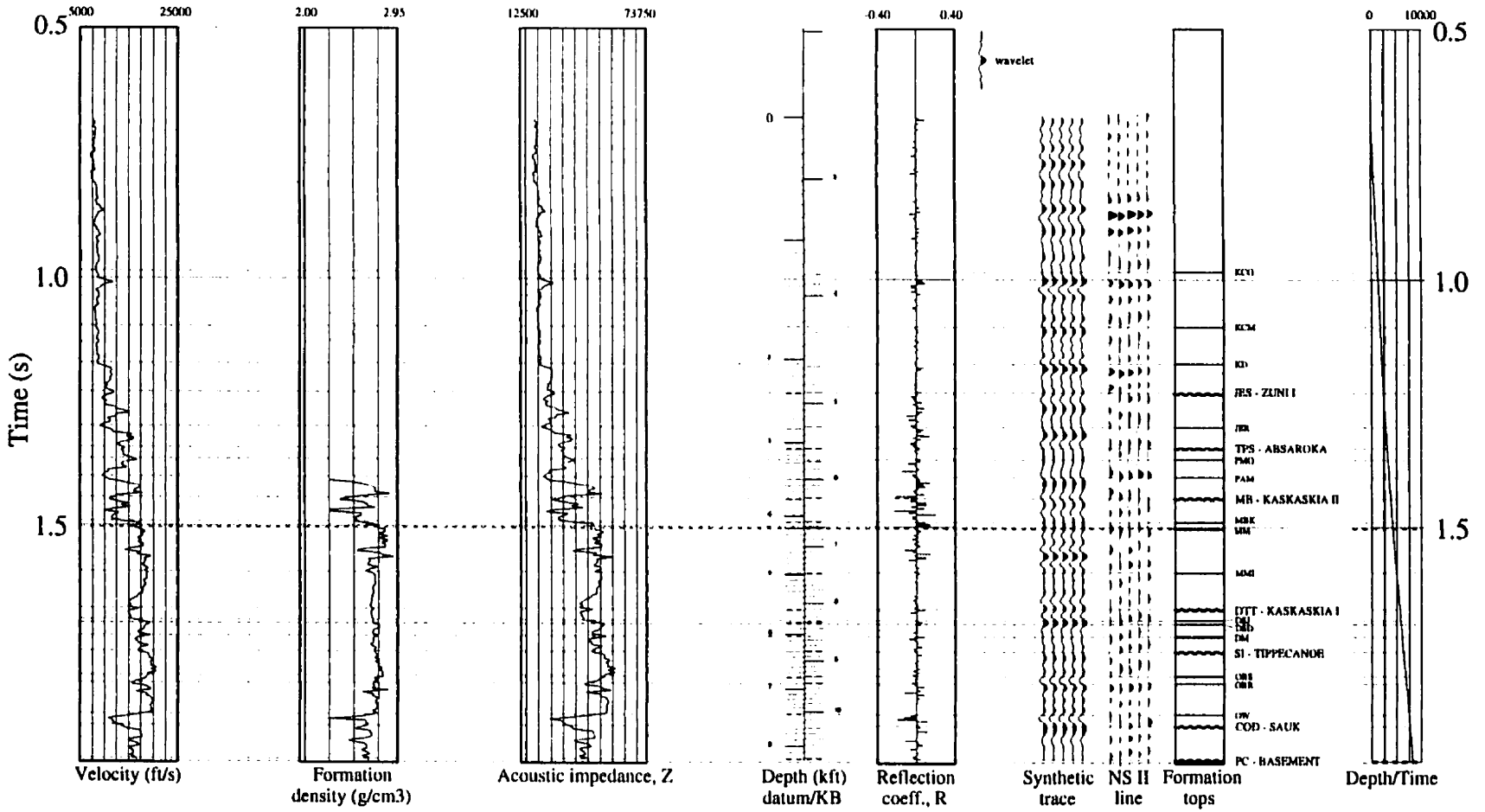

Fig. A.52 Well 47 - Synthetic seismogram.

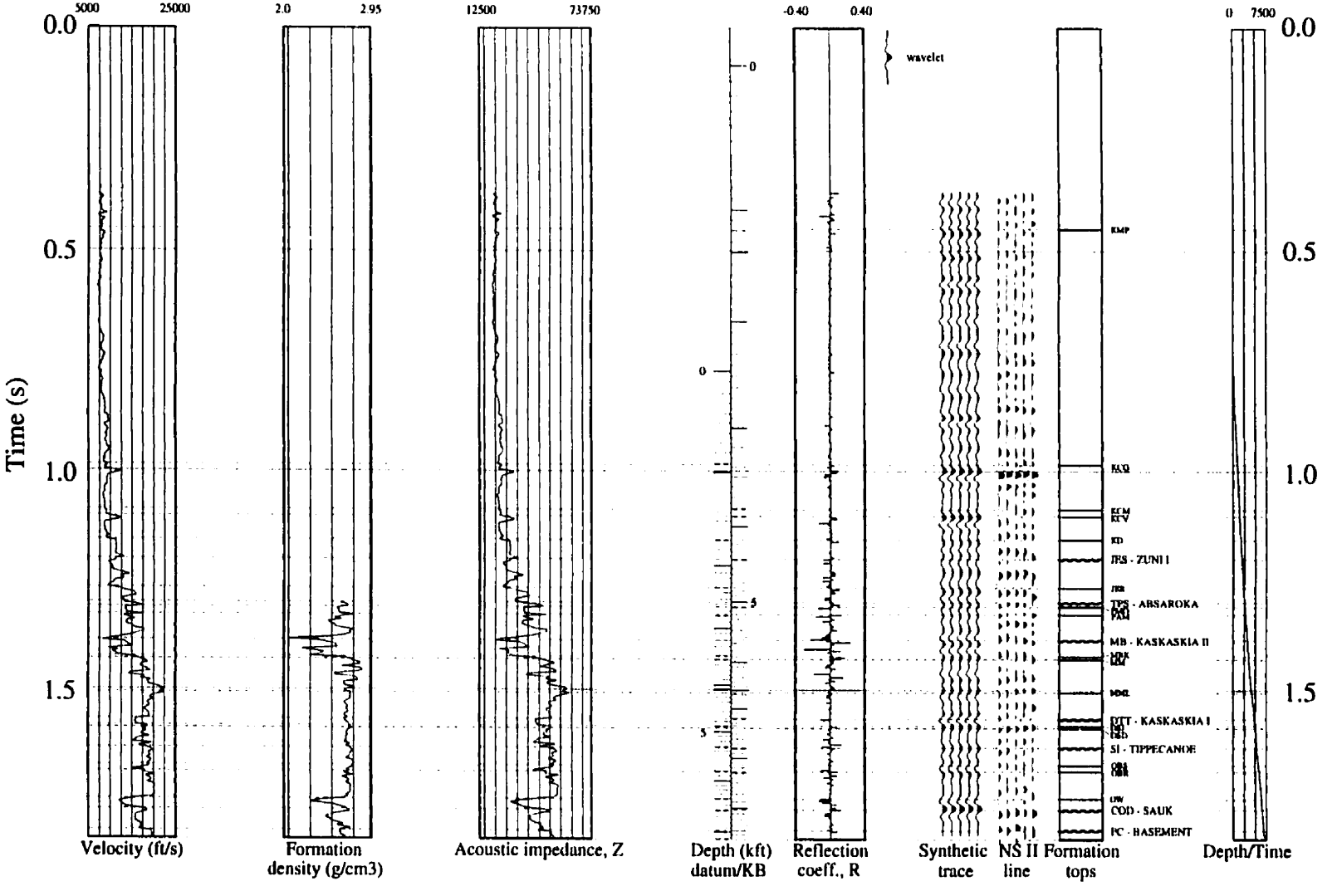

Fig. A.53 Well 48 - Synthetic seismogram.

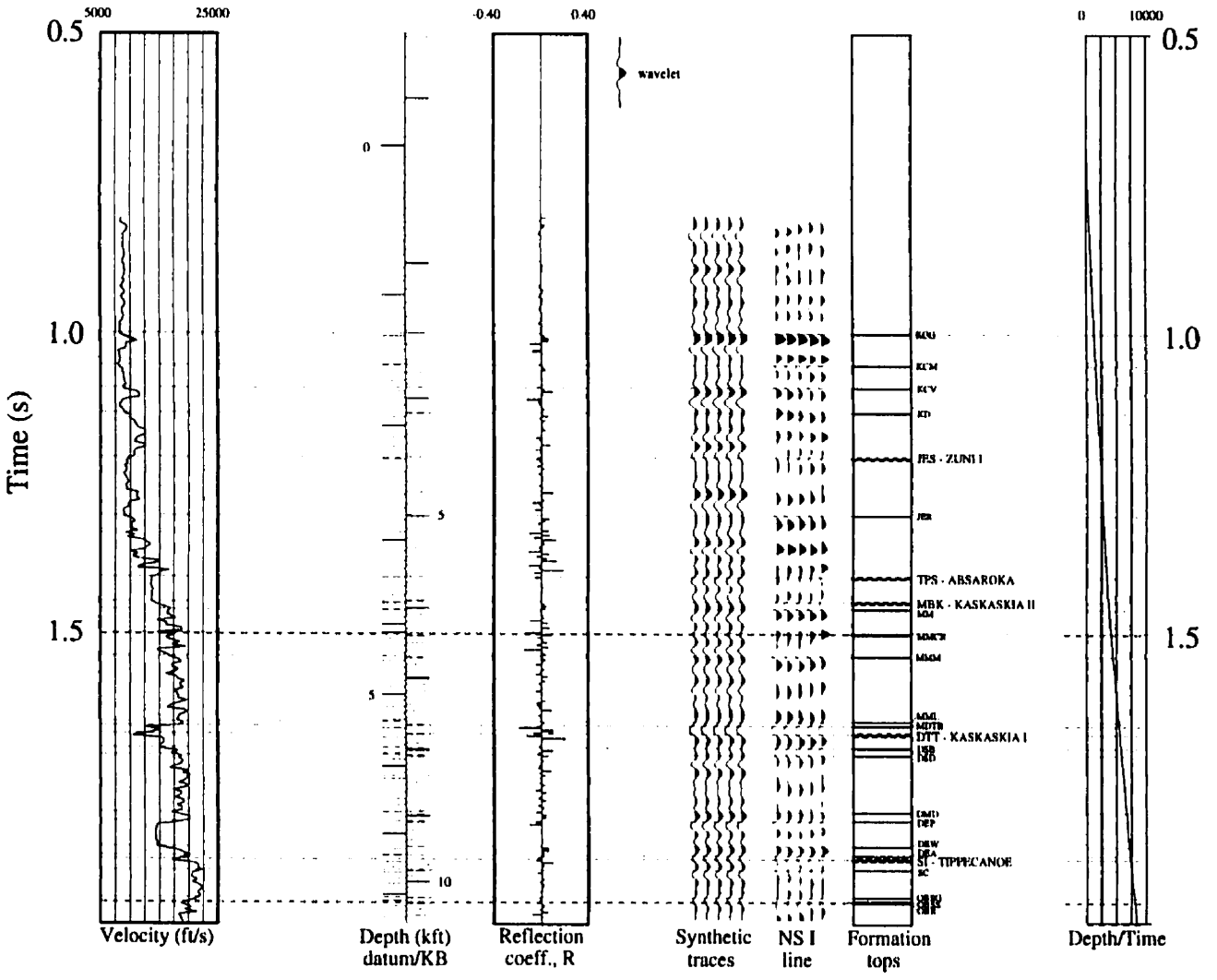

Fig. A.54 Well 82 - Synthetic seismogram.

Table A.1 Stratigraphic picks

		Well 1		Well 2		Well 3		Well 4		Well 5	
		m.	ft.	m.	ft.	m.	ft.	m.	ft.	m.	ft.
Kelly Bushing	KB	1388.1	4554.0	1205.8	3956.0	1093.3	3587.0	918.1	3012.0	933.9	3064.0
Ground Level	GL	1384.1	4541.0	1202.7	3946.0	1090.3	3577.0	915.6	3004.0	929.9	3051.0
ZUNI II											
Cretaceous											
Montana Group	KM										
Pierre Shale/Riding Mountain	KMP										
Bearpaw	KMB										
Judith River/Belly River	KMJ										
Claggett/Lea Park	KMC										
Eagle/Milk River/ Virgelle	KME									154.2	506.0
Colorado Group	KC	673.9	2211.0								
Niobrara/1st WS/Kevin sh.	KCN									302.4	992.0
Carlile/Bowd/Ferdig/U.Col Sh	KCC										
Greenhorn Shale/2nd White Specks	KCG	966.5	3171.0	395.6	1298.0	228.6	750.0	256.0	840.0	513.6	1685.0
Belle Fou./Graneros/L.Color.	KCB										
Blackleaf/Mowry/Fish Scale Z.	KCM	966.5	3171.0	395.6	1298.0	246.9	810.0	277.4	910.0	527.3	1730.0
Newcl./Muddy/Bow Is./Viking	KCV	1118.6	3670.0	456.0	1496.0	360.6	1183.0	358.1	1175.0	617.8	2027.0
Skull Cr./Joli Fou/Thermopolis	KCS										
Mannville/Inyan Kara/Dakota Gp.	KD										
Dakota/Fall R./Pense/Swan R.	KDD	1178.4	3866.0	620.6	2036.0	467.3	1533.0	509.0	1670.0	780.9	2562.0
Kootenai/Fuson/Cantaur	KDK	1204.6	3952.0	641.3	2104.0	506.9	1663.0	544.1	1785.0	815.3	2675.0
Sunburst	KDS			808.6	2653.0					901.0	2956.0
ZUNI I											
Jurassic											
Morrison	JM	**1367.9**	**4488.0**	**816.9**	**2680.0**	**592.8**	**1945.0**	**656.8**	**2155.0**	**914.4**	**3000.0**
Ellis Group	JE										
Swift/Vang./Sund./Masefield	JES	1412.4	4634.0	822.0	2697.0	618.1	2028.0	676.7	2220.0	930.9	3054.0
Rierdon/Melita	JER	1455.1	4774.0	857.4	2813.0	644.7	2115.0	718.4	2357.0	967.4	3174.0
Piper/Sawtooth/Shaunavon	JEP	1486.2	4876.0	874.8	2870.0	676.7	2220.0	743.7	2440.0	1011.9	3320.0
ABSAROKA											
Triassic-Permian											
Spearfish/L.Watrou./L.Amaranth	TPS										
Permian											
Minnekahta/Opeche	PMO										
Pennsylvanian											
Amsden-Minnel.-Broom Cr. Gr.	PA										
KASKASKIA II											
Mississippian-Devonian											
Big Snowy Group	MB										
Heath	MBH										
Otter	MBO										
Kibbey (Sandstone/Limestone)	MBK										
Madison Group	MM										
Charles/Castle Reef D./Sun R.	MMC	**1512.1**	**4961.0**	**878.4**	**2882.0**						
Mission Canyon	MMM	1598.7	5245.0			**679.7**	**2230.0**	**765.0**	**2510.0**	**1052.2**	**3452.0**
Lodgepole/Banff/Souris Val.	MML			1075.6	3529.0	853.4	2800.0				
Three Forks Group	MDT										
Bakken/Exshaw (Miss/Dev)	MDTB	1895.6	6219.0	1229.6	4034.0	984.5	3230.0				
KASKASKIA I											
Devonian											
Three Forks/Torquay/Lyeton	*DTT*	**1897.4**	**6225.0**	**1234.1**	**4049.0**	**991.8**	**3254.0**			**1286.9**	**4222.0**
Potlatch	DP	1906.2	6254.0	1251.5	4106.0	1020.2	3347.0			1305.5	4283.0
Saskatchewan-Jefferson Gr.	DSJ										
Birdbear/Nisku/Calmar	DSB			1307.9	4291.0	1053.1	3455.0			1334.4	4378.0
Duperow	DSD	1995.2	6546.0	1338.1	4390.0	1080.2	3544.0			1354.5	4444.0
Manitoba Group	DM										
Souris River/Maywood	DMS			1566.4	5139.0	1268.3	4161.0			1542.9	5062.0
Dawson Bay	DMD										
Elk Point Group	DE										
Prairie Evaporite	DEP										
Winnipegosis	DEW										
Ashern	DEA										
TIPPECANOE											
Silurian											
Interlake/Cedar Lake	SI										
Ordovician											
Big Horn Group	OB										
Stonewall Formation	OBST										
Stony Mountain	OBS										
Red River	OBR									**1592.3**	**5224.0**
Winnipeg Group	OW										
SAUK											
Cambrain/Ordovician											
Deadwood	COD			**1607.2**	**5273.0**	**1356.4**	**4450.0**			**1595.6**	**5235.0**
PRECAMBRIAN	PC										
Total Depth	TD	2161.9	7093.0	1620.9	5318.0	1362.8	4471.0	810.8	2660.0	1616.4	5303.0

Table A.1 Stratigraphic picks (continued)

		Well 6		Well 7		Well 8		Well 9		Well 10	
		m.	ft.	m.	ft.	m.	ft.	m.	ft.	m.	ft.
Kelly Bushing	KB	822.3	2780.0	1218.0	3996.0	808.9	2654.0	839.1	2753.0	841.6	2761.0
Ground Level	GL	818.1	2766.0	1214.9	3986.0	806.2	2645.0	833.9	2736.0	836.4	2744.0
ZUNI II											
Cretaceous											
Montana Group	KM										
Pierre Shale/Riding Mountain	KMP										
Bearpaw	KMB										
Judith River/Belly River	KMJ										
Claggett/Lea Park	KMC					161.5	530.0				
Eagle/Milk River/ Virgelle	KME	158.8	537.0			315.8	1036.0	416.1	1365.0	594.4	1950.0
Colorado Group	KC	281.9	953.0								
Niobrara/1st WS/Kevin sh.	KCN										
Carlile/Bowd/Ferdig/U.Col Sh	KCC					526.7	1728.0				
Greenhorn Shale/2nd White Specks	KCG	467.3	1580.0			609.0	1998.0	779.1	2556.0	961.0	3153.0
Belle Fou. Graneros/L.Color.	KCB										
Blackleaf/Mowry/Fish Scale Z.	KCM	485.1	1640.0			694.9	2280.0	841.2	2760.0	1036.3	3400.0
Newcl./Muddy/Bow Is./Viking	KCV	627.4	2121.0			833.9	2736.0	914.4	3000.0	1098.8	3605.0
Skull Cr./Joli Fou/Thermopolis	KCS										
Mannville/Inyan Kara/Dakota Gp.	KD										
Dakota/Fall R./Pense/Swan R.	KDD	746.0	2522.0			918.4	3013.0	1024.1	3360.0	1200.3	3938.0
Kootenai/Fuson/Cantuar	KDK	753.7	2548.0								
Sunburst	KDS										
ZUNI I											
Jurassic											
Morrison	JM	**860.7**	**2910.0**			**1021.1**	**3350.0**				
Ellis Group	JE										
Swift/Vang./Sund./Masefield	JES	866.1	2928.0			1030.8	3382.0	**1130.8**	**3710.0**	**1302.4**	**4273.0**
Rierdon/Melita	JER	901.6	3048.0			1100.9	3612.0			1423.4	4670.0
Piper/Sawtooth/Shaunavon	JEP	944.7	3194.0			1179.0	3868.0	1325.0	4347.0	1503.9	4934.0
ABSAROKA											
Triassic-Permian											
Spearfish/L.Watrou./L.Amaranth	TPS							**1430.1**	**4692.0**	**1624.0**	**5328.0**
Permian											
Minnekahta/Opeche	PMO										
Pennsylvanian											
Amsden-Minnel.-Broom Cr. Gr.	PA										
KASKASKIA II											
Mississippian-Devonian											
Big Snowy Group	MB										
Heath	MBH										
Otter	MBO										
Kibbey (Sandstone/Limestone)	MBK										
Madison Group	MM										
Charles/Castle Reef D./Sun R.	MMC							**1464.3**	**4804.0**	**1672.1**	**5486.0**
Mission Canyon	MMM	**995.9**	**3367.0**			**1205.2**	**3954.0**	1575.8	5170.0	1806.2	5926.0
Lodgepole/Banff/Souris Val.	MML	1091.4	3690.0					1741.9	5715.0	1987.9	6522.0
Three Forks Group	MDT										
Bakken/Exshaw (Miss/Dev)	MDTB							1803.5	5917.0	2050.1	6726.0
KASKASKIA I											
Devonian											
Three Forks/Torquay/Lyeton	DTT	**1220.7**	**4127.0**	**237.1**	**778.0**			**1821.5**	**5976.0**	**2067.8**	**6784.0**
Potlatch	DP	1238.4	4187.0								
Saskatchewan-Jefferson Gr.	DSJ										
Birdbear/Nisku/Calmar	DSB	1267.7	4286.0	264.6	868.0			1844.6	6052.0	2093.4	6868.0
Duperow	DSD	1282.8	4337.0	289.0	948.0			1871.5	6140.0	2118.4	6950.0
Manitoba Group	DM										
Souris River/Maywood	DMS	1399.1	4730.0					2048.3	6720.0	2290.6	7515.0
Dawson Bay	DMD							2148.8	7050.0	2386.3	7829.0
Elk Point Group	DE										
Prairie Evaporite	DEP							2167.1	7110.0	2407.6	7899.0
Winnipegosis	DEW							2174.7	7135.0	2414.3	7921.0
Ashern	DEA									2425.9	7959.0
TIPPECANOE											
Silurian											
Interlake/Cedar Lake	SI							**2194.6**	**7200.0**	**2437.2**	**7996.0**
Ordovician											
Big Horn Group	OB										
Stonewall Formation	OBST										
Stony Mountain	OBS										
Red River	OBR	**1462.4**	**4944.0**	**481.6**	**1580.0**			2295.1	7530.0		
Winnipeg Group	OW							2390.2	7842.0		
SAUK											
Cambrain/Ordovician											
Deadwood	COD	**1480.1**	**5004.0**					**2445.7**	**8024.0**		
PRECAMBRIAN	PC										
Total Depth	TD	1528.6	5168.0	581.9	1909.0	1206.4	3958.0	2496.0	8189.0	2499.4	8200.0

Table A.1 Stratigraphic picks (continued)

		Well 11		Well 12		Well 13		Well 14		Well 15	
		m.	ft.	m.	ft.	m.	ft.	m.	ft.	m.	ft
Kelly Bushing	KB	729.7	2394.0	852.8	2798.0	710.8	2332.0	717.2	2353.0	764.1	2507.0
Ground Level	GL	724.8	2378.0	849.8	2788.0	707.4	2321.0	717.2	2353.0	760.5	2495.0
ZUNI II											
Cretaceous											
Montana Group	KM										
Pierre Shale/Riding Mountain	KMP										
Bearpaw	KMB										
Judith River/Belly River	KMJ										
Claggett/Lea Park	KMC										
Eagle/Milk River/ Virgelle	KME	582.2	1910.0	691.9	2270.0						
Colorado Group	KC										
Niobrara/1st WS/Kevin sh.	KCN										
Carlile/Bowd/Ferdig/U.Col Sh	KCC										
Greenhorn Shale/2nd White Specks	KCG	961.0	3153.0	1062.2	3485.0	997.9	3274.0	1046.7	3434.0	1150.9	3776.0
Belle Fou. Graneros/L.Color.	KCB										
Blackleaf/Mowry/Fish Scale Z.	KCM	1030.2	3380.0	1118.6	3670.0	1060.7	3480.0	1118.6	3670.0	1225.3	4020.0
Newcl./Muddy/Bow Is./Viking	KCV	1088.1	3570.0	1179.6	3870.0	1130.2	3708.0	1180.2	3872.0	1286.3	4220.0
Skull Cr./Joli Fou/Thermopolis	KCS										
Mannville/Inyan Kara/Dakota Gp.	KD										
Dakota/Fall R./Pense/Swan R.	KDD	1188.7	3900.0	1268.0	4160.0	1220.1	4003.0	1252.7	4110.0	1362.5	4470.0
Kootenai/Fuson/Cantaur	KDK										
Sunburst	KDS										
ZUNI I											
Jurassic											
Morrison	JM										
Ellis Group	JE										
Swift/Vang./Sund./Masefield	JES	**1301.5**	**4270.0**	**1386.8**	**4550.0**	**1325.9**	**4350.0**	**1365.5**	**4480.0**	**1478.3**	**4850.0**
Rierdon/Melita	JER	1426.5	4680.0	1527.0	5010.0	1478.3	4850.0	1517.9	4980.0	1630.7	5350.0
Piper/Sawtooth/Shaunavon	JEP	1496.6	4910.0	1591.1	5220.0	1558.4	5113.0	1592.9	5226.0	1702.3	5585.0
ABSAROKA											
Triassic-Permian											
Spearfish/L.Watrou./L.Amaranth	TPS	**1624.6**	**5330.0**	**1728.2**	**5670.0**	**1670.9**	**5482.0**	**1713.9**	**5623.0**	**1810.5**	**5940.0**
Permian											
Minnekahta/Opeche	PMO										
Pennsylvanian											
Amsden-Minnel.-Broom Cr. Gr.	PA										
KASKASKIA II											
Mississippian-Devonian											
Big Snowy Group	MB										
Heath	MBH										
Otter	MBO										
Kibbey (Sandstone/Limestone)	MBK							**1802.6**	**5914.0**	**1930.0**	**6332.0**
Madison Group	MM										
Charles/Castle Reef D./Sun R.	MMC	**1718.2**	**5637.0**	**1836.7**	**6026.0**	**1773.3**	**5818.0**	1823.6	5983.0	1971.4	6468.0
Mission Canyon	MMM	1888.8	6197.0	2027.5	6652.0	1950.1	6398.0	2011.7	6600.0	2208.6	7246.0
Lodgepole/Banff/Souris Val.	MML	2072.6	6800.0	2178.7	7148.0	2158.0	7080.0	2254.0	7395.0	2379.9	7808.0
Three Forks Group	MDT										
Bakken/Exshaw (Miss/Dev)	MDTB	2161.0	7090.0	2281.1	7484.0	2277.8	7473.0	2356.1	7730.0	2523.1	8278.0
KASKASKIA I											
Devonian											
Three Forks/Torquay/Lyeton	DTT	**2182.4**	**7160.0**	**2305.5**	**7564.0**	**2305.5**	**7564.0**	**2379.3**	**7806.0**	**2548.1**	**8360.0**
Potlatch	DP										
Saskatchewan-Jefferson Gr.	DSJ										
Birdbear/Nisku/Calmar	DSB	2216.5	7272.0	2342.1	7684.0	2337.8	7670.0	2416.5	7928.0	2590.8	8500.0
Duperow	DSD	2238.8	7345.0	2367.1	7766.0	2371.3	7780.0	2446.0	8025.0	2621.9	8602.0
Manitoba Group	DM										
Souris River/Maywood	DMS	2397.3	7865.0	2518.3	8262.0	2521.3	8272.0	2596.0	8517.0	2771.9	9094.0
Dawson Bay	DMD	2496.9	8192.0	2626.2	8616.0	2622.2	8603.0	2696.6	8847.0	2877.3	9440.0
Elk Point Group	DE										
Prairie Evaporite	DEP	2522.2	8275.0	2653.6	8706.0	2650.2	8695.0	2730.4	8958.0	2912.1	9554.0
Winnipegosis	DEW	2573.1	8442.0	2718.8	8920.0	2723.4	8935.0	2809.0	9216.0	2996.8	9832.0
Ashern	DEA			2740.2	8990.0	2747.8	9015.0			3030.3	9942.0
TIPPECANOE											
Silurian											
Interlake/Cedar Lake	SI	**2599.9**	**8530.0**	**2748.7**	**9018.0**	**2761.5**	**9060.0**	**2852.9**	**9360.0**	**3044.3**	**9988.0**
Ordovician											
Big Horn Group	OB										
Stonewall Formation	OBST									3190.0	10466.0
Stony Mountain	OBS			2862.1	9390.0	2888.0	9475.0	3005.9	9862.0	3219.0	10561.0
Red River	OBR	2745.3	9007.0	2898.6	9510.0	2930.7	9615.0	3048.0	10000.0	3244.9	10646.0
Winnipeg Group	OW										
SAUK											
Cambrain/Ordovician											
Deadwood	COD										
PRECAMBRIAN	PC										
Total Depth	TD	2824.0	9265.0	2977.9	9770.0	3020.3	9909.0	3161.7	10373.0	3337.6	10950.0

Table A.1 Stratigraphic picks (continued)

		Well 16		Well 17		Well 18		Well 19		Well 20	
		m.	ft.	m.	ft.	m.	ft.	m.	ft.	m.	ft.
Kelly Bushing	KB	636.7	2089.0	605.6	1987.0	623.3	2045.0	694.0	2277.0	748.9	2457.0
Ground Level	GL	630.6	2069.0	599.2	1966.0	617.2	2025.0	687.3	2255.0	744.6	2443.0
ZUNI II											
Cretaceous											
Montana Group	KM										
Pierre Shale/Riding Mountain	KMP							576.1	1890.0		
Bearpaw	KMB										
Judith River/Belly River	KMJ										
Claggett/Lea Park	KMC										
Eagle/Milk River/ Virgelle	KME										
Colorado Group	KC										
Niobrara/1st WS./Kevin sh.	KCN										
Carlile/Bowd/Ferdig/U.Col Sh	KCC										
Greenhorn Shale/2nd White Specks	KCG	1161.3	3810.0	1131.7	3713.0	1206.7	3959.0	1332.0	4370.0	1264.0	4147.0
Belle Fou.-Graneros-L.Color.	KCB										
Blackleaf/Mowry/Fish Scale Z.	KCM	1252.7	4110.0	1219.2	4000.0	1295.4	4250.0	1437.1	4715.0	1360.6	4464.0
Newel-Muddy/Bow Is.-Viking	KCV	1308.8	4294.0	1271.6	4172.0	1350.3	4430.0	1475.2	4840.0		
Skull Cr.-Joli Fou/Thermopolis	KCS	1319.8	4330.0	1290.8	4235.0						
Mannville/Inyan Kara/Dakota Gp.	KD							1549.3	5083.0	1463.0	4800.0
Dakota/Fall R.-Pense/Swan R.	KDD	1367.3	4486.0	1336.5	4385.0	1420.4	4660.0				
Kootenai/Fuson/Cantaur	KDK										
Sunburst	KDS										
ZUNI I											
Jurassic											
Morrison	JM										
Ellis Group	JE										
Swift/Vang.-Sund.-Masefield	JES	**1514.9**	**4970.0**	**1487.4**	**4880.0**	**1554.5**	**5100.0**	**1688.6**	**5540.0**	**1589.5**	**5215.0**
Rierdon/Melita	JER	1681.3	5516.0	1650.2	5414.0	1726.7	5665.0	1826.7	5993.0	1724.3	5657.0
Piper/Sawtooth/Shaunavon	JEP	1752.6	5750.0	1719.1	5640.0	1792.2	5880.0	1885.2	6185.0		
ABSAROKA											
Triassic-Permian											
Spearfish/L.Watrou.-L.Amarath	TPS	**1856.5**	**6091.0**	**1829.4**	**6002.0**	**1902.0**	**6240.0**	**2007.1**	**6585.0**	**1905.3**	**6251.0**
Permian											
Minnekahta/Opeche	PMO							2138.5	7016.0		
Pennsylvanian											
Amsden-Minnel.-Broom Cr. Gr.	PA	1911.1	6270.0	1892.8	6210.0	1981.2	6500.0	2167.1	7110.0	2046.1	6713.0
KASKASKIA II											
Mississippian-Devonian											
Big Snowy Group	MB							**2276.9**	**7470.0**	**2139.7**	**7020.0**
Heath	MBH										
Otter	MBO	**1981.2**	**6500.0**	**1947.4**	**6389.0**	**2054.4**	**6740.0**				
Kibbey (Sandstone/Limestone)	MBK	2032.4	6668.0	2058.9	6755.0	2166.8	7109.0	2382.6	7817.0	2229.6	7315.0
Madison Group	MM							2423.8	7952.0	2273.8	7460.0
Charles-Castle Reef D.-Sun R.	MMC	2104.3	6904.0	2081.8	6830.0	2196.1	7205.0			2438.4	8000.0
Mission Canyon	MMM	2406.1	7894.0	2386.9	7831.0	2480.5	8138.0	2690.2	8826.0	2523.7	8280.0
Lodgepole/Banff/Souris Val.	MML	2603.0	8540.0	2581.7	8470.0	2676.1	8780.0			2702.4	8866.0
Three Forks Group	MDT										
Bakken/Exshaw (Miss/Dev)	MDTB	2726.1	8944.0	2708.1	8885.0	2817.3	9243.0	3065.7	10058.0	2913.3	9558.0
KASKASKIA I											
Devonian											
Three Forks-Torquay/Lyeton	DTT	**2745.6**	**9008.0**	**2728.0**	**8950.0**	**2835.9**	**9304.0**	**3095.9**	**10157.0**	**2944.4**	**9660.0**
Potlatch	DP										
Saskatchewan-Jefferson Gr.	DSJ										
Birdbear/Nisku-Calmar	DSB	2786.5	9142.0	2772.8	9097.0	2883.7	9461.0	3157.7	10360.0	3003.2	9853.0
Duperow	DSD	2815.1	9236.0	2801.7	9192.0	2912.4	9555.0	3189.4	10464.0	3031.5	9946.0
Manitoba Group	DM										
Souris River/Maywood	DMS	2929.1	9610.0	2956.6	9700.0	3045.9	9993.0	3339.1	10955.0	3172.4	10408.0
Dawson Bay	DMD	3043.1	9984.0			3165.7	10386.0	3422.9	11230.0	3254.7	10678.0
Elk Point Group	DE										
Prairie Evaporite	DEP	3077.3	10096.0	3063.2	10050.0	3171.1	10404.0	3463.7	11364.0	3298.5	10822.0
Winnipegosis	DEW	3144.0	10315.0	3140.7	10304.0	3246.7	10652.0	3579.3	11743.0	3408.3	11182.0
Ashern	DEA	3174.8	10416.0			3291.2	10798.0				
TIPPECANOE											
Silurian											
Interlake/Cedar Lake	SI	**3189.4**	**10464.0**	**3202.2**	**10506.0**	**3313.5**	**10871.0**	**3665.2**	**12025.0**	**3499.1**	**11480.0**
Ordovician											
Big Horn Group	OB										
Stonewall Formation	OBST										
Stony Mountain	OBS	3359.2	11021.0	3383.3	11100.0	3524.7	11564.0	4008.4	13151.0	3840.2	12599.0
Red River	OBR	3405.5	11173.0	3431.4	11258.0	3555.2	11664.0	4045.9	13274.0	3878.9	12726.0
Winnipeg Group	OW	3536.3	11602.0					4225.4	13863.0	4056.9	13310.0
SAUK											
Cambrain/Ordovician											
Deadwood	COD	**3602.1**	**11818.0**					**4331.2**	**14210.0**	**4178.8**	**13710.0**
PRECAMBRIAN	PC	**3747.8**	**12296.0**							**4350.1**	**14272.0**
Total Depth	TD	3783.5	12413.0	3541.8	11620.0	3680.5	12075.0	4399.2	14433.0	4397.0	14426.0

Table A.1 Stratigraphic picks (continued)

		Well 21		Well 22		Well 23		Well 24		Well 25	
		m.	ft.	m.	ft.	m.	ft.	m.	ft.	m.	ft.
Kelly Bushing	KB	754.1	2474.0	704.1	2310.0	724.8	2378.0	626.4	2055.0	467.0	1532.0
Ground Level	GL	748.6	2456.0	697.7	2289.0	721.2	2366.0	622.7	2043.0	463.3	1520.0
ZUNI II											
Cretaceous											
Montana Group	KM										
Pierre Shale/Riding Mountain	KMP	562.4	1845.0	640.1	2100.0	566.9	1860.0	498.3	1635.0		
Bearpaw	KMB										
Judith River/Belly River	KMJ										
Claggett/Lea Park	KMC										
Eagle/Milk River/ Virgelle	KME										
Colorado Group	KC										
Niobrara/1st WS/Kevin sh.	KCN										
Carlile/Bowd/Ferdig/U.Col Sh	KCC										
Greenhorn Shale/2nd White Specks	KCG	1272.5	4175.0	1297.2	4256.0	1225.9	4022.0	1072.3	3518.0	641.9	2106.0
Belle Fou./Graneros/L.Color.	KCB										
Blackleaf/Mowry/Fish Scale Z.	KCM	1369.2	4492.0	1400.3	4594.0	1323.7	4343.0	1172.3	3846.0	734.6	2410.0
Newcl./Muddy/Bow Is./Viking	KCV	1404.5	4608.0	1432.6	4700.0	1350.3	4430.0	1197.9	3930.0		
Skull Cr./Joli Fou/Thermopolis	KCS										
Mannville/Inyan Kara/Dakota Gp.	KD	1474.6	4838.0	1505.1	4938.0	1417.3	4650.0	1264.9	4150.0	804.7	2640.0
Dakota/Fall R./Pense/Swan R.	KDD										
Kootenai/Fuson/Cantaur	KDK										
Sunburst	KDS										
ZUNI I											
Jurassic											
Morrison	JM										
Ellis Group	JE										
Swift/Vang./Sund./Masefield	JES	**1604.5**	**5264.0**	**1626.4**	**5336.0**	**1527.7**	**5012.0**	**1366.7**	**4484.0**	**901.0**	**2956.0**
Rierdon/Melita	JER	1738.6	5704.0	1741.3	5713.0	1653.2	5424.0	1480.1	4856.0	969.3	3180.0
Piper/Sawtooth/Shaunavon	JEP	1783.1	5850.0	1783.1	5850.0	1690.1	5545.0	1521.0	4990.0		
ABSAROKA											
Triassic-Permian											
Spearfish/L.Watrou./L.Amaranth	TPS	**1918.1**	**6293.0**	**1912.0**	**6273.0**	**1824.8**	**5987.0**	**1663.0**	**5456.0**	**1135.1**	**3724.0**
Permian											
Minnekahta/Opeche	PMO	2026.0	6647.0								
Pennsylvanian											
Amsden-Minnel.-Broom Cr. Gr.	PA	2067.8	6784.0	2033.0	6670.0						
KASKASKIA II											
Mississippian-Devonian											
Big Snowy Group	MB	**2165.6**	**7105.0**	**2118.4**	**6950.0**	**1918.7**	**6295.0**				
Heath	MBH										
Otter	MBO										
Kibbey (Sandstone/Limestone)	MBK	2252.5	7390.0	2208.6	7246.0	1984.2	6510.0	**1741.6**	**5714.0**		
Madison Group	MM	2301.2	7550.0	2255.5	7400.0	2033.0	6670.0	1791.0	5876.0	**1208.8**	**3966.0**
Charles/Castle Reef/D. Sun R.	MMC										
Mission Canyon	MMM	2532.9	8310.0	2429.9	7972.0	2177.2	7143.0	1927.6	6324.0	1311.6	4303.0
Lodgepole/Banff/Souris Val.	MML	2726.1	8944.0	2699.6	8857.0	2360.1	7743.0	2084.8	6840.0	1454.8	4773.0
Three Forks Group	MDT										
Bakken Exshaw (Miss/Dev)	MDTB	2932.5	9621.0	2833.4	9296.0	2561.8	8405.0	2299.7	7545.0	1644.4	5395.0
KASKASKIA I											
Devonian											
Three Forks/Torquay/Lyeton	DTT	**2964.8**	**9727.0**	**2859.0**	**9380.0**	**2579.2**	**8462.0**	**2312.2**	**7586.0**	**1648.1**	**5407.0**
Potlatch	DP										
Saskatchewan-Jefferson Gr.	DSJ										
Birdbear/Nisku/Calmar	DSB	3024.8	9924.0	2930.3	9614.0	2674.9	8776.0	2374.4	7790.0	1679.1	5509.0
Duperow	DSD	3054.1	10020.0	2965.1	9728.0	2678.0	8786.0	2406.4	7895.0	1705.1	5594.0
Manitoba Group	DM										
Souris River/Maywood	DMS	3198.6	10494.0	3116.0	10223.0	2819.4	9250.0	2539.3	8331.0	1822.7	5980.0
Dawson Bay	DMD	3282.7	10770.0	3200.4	10500.0	2899.9	9514.0	2618.2	8590.0		
Elk Point Group	DE										
Prairie Evaporite	DEP	3325.4	10910.0	3249.2	10660.0	2946.8	9668.0	2660.9	8730.0		
Winnipegosis	DEW	3430.8	11256.0	3415.0	11204.0	3047.4	9998.0	2702.7	8867.0		
Ashern	DEA										
TIPPECANOE											
Silurian											
Interlake/Cedar Lake	SI	**3518.6**	**11544.0**	**3478.1**	**11411.0**	**3152.9**	**10344.0**	**2818.8**	**9248.0**		
Ordovician											
Big Horn Group	OB										
Stonewall Formation	OBST										
Stony Mountain	OBS	3866.4	12685.0	3833.8	12578.0						
Red River	OBR	3912.4	12836.0	3873.4	12708.0						
Winnipeg Group	OW	4097.7	13444.0								
SAUK											
Cambrain/Ordovician											
Deadwood	COD	**4218.4**	**13840.0**								
PRECAMBRIAN	PC										
Total Depth	TD	4264.2	13990.0	3936.8	12916.0	3198.0	10492.0	2831.0	9288.0	1859.3	6100.0

Table A.1 Stratigraphic picks (continued)

		Well 26		Well 27		Well 28		Well 29		Well 30	
		m.	ft.	m.	ft.	m.	ft.	m.	ft.	m.	ft.
Kelly Bushing	KB	494.4	1622.0	729.7	2394.0	712.6	2338.0	651.4	2137.0	766.3	2514.0
Ground Level	GL	490.7	1610.0	726.3	2383.0	709.0	2326.0	643.7	2112.0	759.9	2493.0
ZUNI II											
Cretaceous											
Montana Group	KM										
Pierre Shale/Riding Mountain	KMP										
Bearpaw	KMB					712.6	2338.0				
Judith River/Belly River	KMJ										
Claggett/Lea Park	KMC										
Eagle/Milk River/ Virgelle	KME			637.0	2090.0	876.9	2877.0				
Colorado Group	KC										
Niobrara/1st WS/Kevin sh.	KCN										
Carlile/Bowd/Ferdig/U.Col Sh	KCC										
Greenhorn Shale/2nd White Specks	KCG	461.5	1514.0	988.8	3244.0	1264.0	4147.0	1402.1	4600.0	1371.6	4500.0
Belle Fou./Graneros/L.Color.	KCB										
Blackleaf/Mowry/Fish Scale Z.	KCM	545.6	1790.0					1551.4	5090.0	1501.1	4925.0
Newcl./Muddy/Bow Is./Viking	KCV			1178.1	3865.0	1431.6	4697.0				
Skull Cr./Joli Fou/Thermopolis	KCS					1462.1	4797.0				
Mannville/Inyan Kara/Dakota Gp.	KD	598.9	1965.0	1237.5	4060.0			1662.7	5455.0	1604.5	5264.0
Dakota/Fall R./Pense/Swan R.	KDD										
Kootenai/Fuson/Cantuar	KDK					1559.7	5117.0				
Sunburst	KDS										
ZUNI I											
Jurassic											
Morrison	JM			**1331.1**	**4367.0**	**1632.2**	**5355.0**				
Ellis Group	JE										
Swift/Vang./Sund./Masefield	JES	**676.7**	**2220.0**	1479.5	4854.0	1666.0	5466.0	**1813.6**	**5950.0**	**1744.4**	**5723.0**
Rierdon/Melita	JER			1524.3	5001.0	1808.4	5933.0	1946.8	6387.0	1882.1	6175.0
Piper/Sawtooth/Shaunavon	JEP			1601.1	5253.0	1879.4	6166.0				
ABSAROKA											
Triassic-Permian											
Spearfish/L.Watrou./L.Amaranth	TPS	**914.4**	**3000.0**	**1627.6**	**5340.0**	**1959.9**	**6430.0**	**2131.5**	**6993.0**	**2063.5**	**6770.0**
Permian											
Minnekahta/Opeche	PMO							2273.8	7460.0	2180.5	7154.0
Pennsylvanian											
Amsden-Minnel.-Broom Cr. Gr.	PA			1659.9	5446.0	2073.6	6803.0	2364.3	7757.0	2314.3	7593.0
KASKASKIA II											
Mississippian-Devonian											
Big Snowy Group	MB							**2520.1**	**8268.0**	**2505.5**	**8220.0**
Heath	MBH			**1691.6**	**5550.0**	**2132.1**	**6995.0**				
Otter	MBO			1736.4	5697.0	2193.6	7197.0				
Kibbey (Sandstone/Limestone)	MBK			1748.3	5736.0	2274.7	7463.0	2607.9	8556.0	2597.2	8521.0
Madison Group	MM	**931.8**	**3057.0**	1813.6	5950.0			2652.7	8703.0	2638.3	8656.0
Charles/Castle Reef D./Sun R.	MMC					2349.1	7707.0				
Mission Canyon	MMM			1966.6	6452.0	2567.9	8425.0				
Lodgepole/Banff/Souris Val.	MML			2147.6	7046.0			3093.7	10150.0	3072.1	10079.0
Three Forks Group	MDT										
Bakken/Exshaw (Miss/Dev)	MDTB			2334.2	7658.0	2953.8	9691.0	3332.7	10934.0	3331.2	10929.0
KASKASKIA I											
Devonian											
Three Forks/Torquay/Lyeton	DTT	**1052.5**	**3453.0**			**2975.5**	**9762.0**	**3357.4**	**11015.0**	**3358.0**	**11017.0**
Potlatch	DP										
Saskatchewan-Jefferson Gr.	DSJ										
Birdbear/Nisku/Calmar	DSB	1062.5	3486.0	**2361.0**	**7746.0**	3011.1	9879.0	3422.0	11227.0	3426.0	11240.0
Duperow	DSD	1083.9	3556.0	2390.9	7844.0	3037.6	9966.0	3450.6	11321.0	3451.9	11325.0
Manitoba Group	DM										
Souris River/Maywood	DMS	1176.5	3860.0	2537.5	8325.0	3174.8	10416.0	3575.6	11731.0	3574.1	11726.0
Dawson Bay	DMD	1240.5	4070.0	2601.2	8534.0	3236.7	10619.0	3661.9	12014.0	3657.9	12001.0
Elk Point Group	DE					3259.2	10693.0				
Prairie Evaporite	DEP	1264.9	4150.0					3697.2	12130.0	3691.1	12110.0
Winnipegosis	DEW							3747.5	12295.0	3741.4	12275.0
Ashern	DEA			2618.2	8590.0						
TIPPECANOE											
Silurian											
Interlake/Cedar Lake	SI	**1307.6**	**4290.0**	**2632.9**	**8638.0**	**3307.1**	**10850.0**	**3840.8**	**12601.0**	**3841.1**	**12602.0**
Ordovician											
Big Horn Group	OB										
Stonewall Formation	OBST										
Stony Mountain	OBS	1389.0	4557.0	2742.0	8996.0	3441.8	11292.0	4164.8	13664.0	4230.6	13880.0
Red River	OBR	1424.6	4674.0	2777.9	9114.0	3490.6	11452.0	4211.1	13816.0	4282.1	14049.0
Winnipeg Group	OW	1589.8	5216.0			3623.2	11887.0	4384.9	14386.0	4485.1	14715.0
SAUK											
Cambrain/Ordovician											
Deadwood	COD	**1633.7**	**5360.0**			**3690.2**	**12107.0**	**4465.9**	**14652.0**	**4575.0**	**15010.0**
PRECAMBRIAN	PC	**1641.7**	**5386.0**								
Total Depth	TD	1657.2	5437.0	2861.8	9389.0	3707.3	12163.0	4504.6	14779.0	4614.7	15140.0

Table A.1 Stratigraphic picks (continued)

		Well 31		Well 32		Well 33		Well 34		Well 35	
		m.	ft.	m.	ft.	m.	ft.	m.	ft.	m.	ft.
Kelly Bushing	KB	650.1	2133.0	583.7	1915.0	611.4	2006.0	688.8	2260.0	652.3	2140.0
Ground Level	GL	645.3	2117.0	580.3	1904.0	606.6	1990.0	682.8	2240.0	645.9	2119.0
ZUNI II											
Cretaceous											
Montana Group	KM										
Pierre Shale/Riding Mountain	KMP									515.1	1690.0
Bearpaw	KMB										
Judith River/Belly River	KMJ										
Claggett/Lea Park	KMC										
Eagle/Milk River/ Virgelle	KME					493.8	1620.0				
Colorado Group	KC					715.4	2347.0				
Niobrara/1st WS/Kevin sh.	KCN										
Carlile/Bowd/Ferdig/U.Col Sh	KCC										
Greenhorn Shale/2nd White Specks	KCG	1195.4	3922.0	775.1	2543.0	796.1	2612.0	1131.1	3711.0	1282.6	4208.0
Belle Fou./Graneros/L.Color.	KCB					819.9	2690.0	1167.4	3830.0	1336.5	4385.0
Blackleaf/Mowry/Fish Scale Z.	KCM	1311.9	4304.0	882.7	2896.0			1206.4	3958.0	1383.8	4540.0
Newcl./Muddy/Bow Is./Viking	KCV					891.5	2925.0	1251.2	4105.0	1424.9	4675.0
Skull Cr./Joli Fou/Thermopolis	KCS					914.4	3000.0	1272.5	4175.0	1435.6	4710.0
Mannville/Inyan Kara/Dakota Gp.	KD	1415.2	4643.0	962.3	3157.0	969.3	3180.0	1328.9	4360.0	1507.5	4946.0
Dakota/Fall R./Pense/Swan R.	KDD										
Kootenai/Fuson/Cantaur	KDK										
Sunburst	KDS										
ZUNI I											
Jurassic											
Morrison	JM										
Ellis Group	JE										
Swift/Vang./Sund./Masefield	JES	**1538.3**	**5047.0**	**1065.0**	**3494.0**	**1090.3**	**3577.0**	**1443.5**	**4736.0**	**1624.6**	**5330.0**
Rierdon/Melita	JER	1663.9	5459.0	1133.2	3718.0			1592.6	5225.0	1783.1	5850.0
Piper/Sawtooth/Shaunavon	JEP					1177.4	3863.0	1627.6	5340.0	1822.7	5980.0
ABSAROKA											
Triassic-Permian											
Spearfish/L.Watrou./L.Amaranth	TPS	**1816.6**	**5960.0**	**1284.7**	**4215.0**	**1292.4**	**4240.0**	**1789.8**	**5872.0**	**1970.5**	**6465.0**
Permian											
Minnekahta/Opeche	PMO										
Pennsylvanian											
Amsden-Minnel.-Broom Cr. Gr.	PA	1908.0	6260.0							2051.3	6730.0
KASKASKIA II											
Mississippian-Devonian											
Big Snowy Group	MB	**2060.8**	**6761.0**					**1871.5**	**6140.0**	**2164.7**	**7102.0**
Heath	MBH										
Otter	MBO										
Kibbey (Sandstone/Limestone)	MBK	2135.1	7005.0	**1342.0**	**4403.0**			1883.7	6180.0	2268.6	7443.0
Madison Group	MM	2185.4	7170.0	1387.4	4552.0			1924.5	6314.0	2309.8	7578.0
Charles/Castle Reef D./Sun R.	MMC					**1379.2**	**4525.0**				
Mission Canyon	MMM			1498.4	4916.0	1488.9	4885.0				
Lodgepole/Banff/Souris Val.	MML	2522.2	8275.0	1625.8	5334.0	1611.8	5288.0	2225.0	7300.0	2770.9	9091.0
Three Forks Group	MDT										
Bakken/Exshaw (Miss/Dev)	MDTB	2752.6	9031.0	1828.8	6000.0	1749.6	5740.0	2444.8	8021.0	2941.0	9649.0
KASKASKIA I											
Devonian											
Three Forks/Torquay/Lyeton	DTT	**2774.0**	**9101.0**	**1842.2**	**6044.0**	**1770.9**	**5810.0**	**2473.8**	**8116.0**	**2967.5**	**9736.0**
Poulatch	DP										
Saskatchewan-Jefferson Gr.	DSJ										
Birdbear/Nisku/Calmar	DSB	2842.3	9325.0	1864.8	6118.0	1826.4	5992.0	2525.0	8284.0	3025.1	9925.0
Duperow	DSD	2873.0	9426.0	1888.5	6196.0	1859.3	6100.0	2555.4	8384.0	3054.7	10022.0
Manitoba Group	DM										
Souris River/Maywood	DMS	2997.7	9835.0	1990.3	6530.0	2023.9	6640.0	2703.0	8868.0	3208.9	10528.0
Dawson Bay	DMD	3070.6	10074.0	2056.2	6746.0	2144.3	7035.0	2815.7	9238.0	3289.4	10792.0
Elk Point Group	DE										
Prairie Evaporite	DEP	3117.8	10229.0	2088.2	6851.0	2197.3	7209.0	2857.2	9374.0	3330.2	10926.0
Winnipegosis	DEW	3182.7	10442.0	2107.1	6913.0	2353.1	7720.0	2957.2	9702.0	3427.8	11246.0
Ashern	DEA					2373.8	7788.0				
TIPPECANOE											
Silurian											
Interlake/Cedar Lake	SI	**3277.8**	**10754.0**	**2162.6**	**7095.0**	**2383.5**	**7820.0**	**3026.7**	**9930.0**	**3510.4**	**11517.0**
Ordovician											
Big Horn Group	OB										
Stonewall Formation	OBST					2554.8	8382.0				
Stony Mountain	OBS	3599.1	11808.0	2301.2	7550.0	2580.7	8467.0	3246.1	10650.0	3792.9	12444.0
Red River	OBR	3642.4	11950.0	2342.1	7684.0	2618.2	8590.0	3274.8	10744.0	3827.4	12557.0
Winnipeg Group	OW	3842.0	12605.0	2535.9	8320.0	2740.2	8990.0	3415.9	11207.0	3988.0	13084.0
SAUK											
Cambrain/Ordovician											
Deadwood	COD	**3932.5**	**12901.0**	**2600.6**	**8532.0**	**2802.6**	**9195.0**	**3457.0**	**11342.0**	**4304.1**	**14121.0**
PRECAMBRIAN	PC	**4091.9**	**13425.0**	**2648.1**	**8688.0**	**2901.7**	**9520.0**				
Total Depth	TD	4107.8	13477.0	2679.8	8792.0			3505.2	11500.0	4074.3	13367.0

Table A.1 Stratigraphic picks (continued)

		Well 36		Well 37		Well 38		Well 39		Well 40	
		m.	ft.	m.	ft.	m.	ft.	m.	ft.	m.	ft.
Kelly Bushing	KB	582.2	1910.0	744.9	2444.0	830.9	2726.0	774.2	2540.0	874.2	2868.0
Ground Level	GL	576.4	1891.0	737.6	2420.0	823.6	2702.0	769.6	2525.0	870.2	2855.0
ZUNI II											
Cretaceous											
Montana Group	KM										
Pierre Shale/Riding Mountain	KMP	600.5	1970.0							532.5	1747.0
Bearpaw	KMB										
Judith River/Belly River	KMJ										
Claggett/Les Park	KMC										
Eagle/Milk River/ Virgelle	KME										
Colorado Group	KC										
Niobrara/1st WS/Kevin sh.	KCN										
Carlile/Bowd/Ferdig/U.Col Sh.	KCC										
Greenhorn Shale/2nd White Specks	KCG	1328.9	4360.0	1496.9	4911.0	1432.6	4700.0			1345.7	4415.0
Belle Fou./Graneros/L.Color.	KCB	1392.6	4569.0								
Blackleaf/Mowry/Fish Scale Z.	KCM	1444.4	4738.8	1638.0	5374.0	1592.0	5223.0			1512.4	4962.0
NewcL/Muddy/Bow Is./Viking	KCV	1487.4	4880.0	1682.2	5519.0					1556.6	5107.0
Skull Cr./Joli Fou/Thermopolis	KCS	1494.1	4902.0								
Mannville/Inyan Kara/Dakota Gp.	KD	1556.6	5107.0	1761.7	5780.0	1695.9	5564.0			1631.0	5351.0
Dakota/Fall R./Pense/Swan R.	KDD										
Kootenai/Fuson/Cantaur	KDK										
Sunburst	KDS										
ZUNI I											
Jurassic											
Morrison	JM										
Ellis Group	JE										
Swift/Vang./Sund./Masefield	JES	**1711.5**	**5615.0**	**1881.8**	**6174.0**	**1808.7**	**5934.0**			**1740.7**	**5711.0**
Rierdon/Melita	JER	1868.1	6129.0	2040.3	6694.0	1943.4	6376.0			1865.4	6120.0
Piper/Sawtooth/Shaunavon	JEP	1902.6	6242.0								
ABSAROKA											
Triassic-Permian											
Spearfish/L.Watrou./L.Amaranth	TPS	**2051.9**	**6732.0**	**2231.7**	**7322.0**	**2115.6**	**6941.0**	?	?	**2004.4**	**6576.0**
Permian											
Minnekahta/Opeche	PMO	2137.9	7014.0	2356.1	7730.0	2264.7	7430.0	2162.6	7095.0	2199.7	7217.0
Pennsylvanian											
Amsden-Minnel.-Broom Cr. Gr.	PA	2230.5	7318.0	2462.8	8080.0	2377.4	7800.0	2237.2	7340.0	2260.1	7415.0
KASKASKIA II											
Mississippian-Devonian											
Big Snowy Group	MB			**2589.0**	**8494.0**	**2550.0**	**8366.0**	**2431.1**	**7976.0**	**2427.7**	**7965.0**
Heath	MBH										
Otter	MBO	**2339.3**	**7675.0**								
Kibbey (Sandstone/Limestone)	MBK	2443.3	8016.0	2674.3	8774.0	2641.1	8665.0	2514.6	8250.0	2499.1	8199.0
Madison Group	MM	2487.2	8160.0	2715.8	8910.0	2684.1	8806.0	2557.3	8390.0	2542.0	8340.0
Charles/Castle Reef D./Sun R.	MMC										
Mission Canyon	MMM										
Lodgepole/Banff/Souris Val.	MML	2961.1	9715.0	3127.2	10260.0	3043.7	9986.0	2893.5	9493.0	2813.3	9230.0
Three Forks Group	MDT										
Bakken/Exshaw (Miss/Dev)	MDTB	3157.4	10359.0	3375.7	11075.0	3276.3	10749.0				
KASKASKIA I											
Devonian											
Three Forks/Torquay/Lyeton	DTT	**3180.0**	**10433.0**	**3387.2**	**11113.0**	**3282.4**	**10769.0**	**3109.6**	**10202.0**	**3019.7**	**9907.0**
Potlatch	DP										
Saskatchewan-Jefferson Gr.	DSJ										
Birdbear/Nisku/Calmar	DSB	3240.0	10630.0	3455.8	11338.0	3347.6	10983.0	3159.9	10367.0	3061.4	10044.0
Duperow	DSD	3266.5	10717.0	3482.0	11424.0	3371.1	11060.0	3181.8	10439.0	3083.1	10115.0
Manitoba Group	DM										
Souris River/Maywood	DMS	3426.0	11240.0	3603.7	11823.0	3463.7	11364.0	3273.6	10740.0	3163.8	10380.0
Dawson Bay	DMD	3486.9	11440.0	3684.4	12088.0	3519.5	11547.0	3306.2	10847.0		
Elk Point Group	DE										
Prairie Evaporite	DEP	3524.7	11564.0	3714.3	12186.0	3536.6	11603.0				
Winnipegosis	DEW	3615.5	11862.0	3752.1	12310.0	3566.2	11700.0				
Ashern	DEA	3669.8	12040.0								
TIPPECANOE											
Silurian											
Interlake/Cedar Lake	SI	**3698.1**	**12133.0**	**3823.1**	**12543.0**	**3630.2**	**11910.0**	**3396.7**	**11144.0**	**3258.9**	**10692.0**
Ordovician											
Big Horn Group	OB										
Stonewall Formation	OBST	3961.5	12997.0								
Stony Mountain	OBS	4000.8	13126.0	4109.6	13483.0	3861.8	12670.0	3584.4	11760.0	3409.2	11185.0
Red River	OBR	4037.4	13246.0	4156.3	13636.0	3907.2	12819.0	3627.4	11901.0	3451.9	11325.0
Winnipeg Group	OW	4210.2	13813.0	4331.2	14210.0	4094.7	13434.0	3804.8	12483.0		
SAUK											
Cambrain/Ordovician											
Deadwood	COD	**4304.1**	**14121.0**	**4401.3**	**14440.0**	**4146.5**	**13604.0**	**3848.1**	**12625.0**		
PRECAMBRIAN	PC					**4380.6**	**14372.0**	**4116.3**	**13505.0**		
Total Depth	TD	4334.6	14221.0	4590.0	15059.0	4401.3	14440.0	4191.0	13750.0	3532.0	11588.0

Table A.1 Stratigraphic picks (continued)

		Well 41		Well 42		Well 43		Well 44		Well 45	
		m.	ft.	m.	ft.	m.	ft.	m.	ft.	m.	ft
Kelly Bushing	KB	897.6	2945.0	570.0	1870.0	594.4	1950.0	690.7	2266.0	677.9	2224.0
Ground Level	GL	891.2	2924.0			590.4	1937.0	684.9	2247.0	672.1	2205.0
ZUNI II											
Cretaceous											
Montana Group	KM										
Pierre Shale/Riding Mountain	KMP										
Bearpaw	KMB										
Judith River/Belly River	KMJ										
Claggett/Lea Park	KMC										
Eagle/Milk River/ Virgelle	KME										
Colorado Group	KC										
Niobrara/1st WS/Kevin sh.	KCN										
Carlile/Bowd/Ferdig/U.Col Sh	KCC										
Greenhorn Shale/2nd White Specks	KCG	1282.6	4208.0	829.1	2720.0	971.4	3187.0	1297.2	4256.0	1274.7	4182.0
Belle Fou./Graneros/L.Color.	KCB										
Blackleaf/Mowry/Fish Scale Z.	KCM	1422.2	4666.0	903.7	2965.0	1052.5	3453.0	1402.1	4600.0	1407.0	4616.0
Newcl./Muddy/Bow Is./Viking	KCV									1429.5	4690.0
Skull Cr./Joli Fou/Thermopolis	KCS										
Mannville/Inyan Kara/Dakota Gp.	KD	1529.2	5017.0	993.0	3258.0	1144.8	3756.0	1508.8	4950.0	1513.0	4964.0
Dakota/Fall R./Pense/Swan R.	KDD										
Kootenai/Fuson/Cantuar	KDK										
Sunburst	KDS										
ZUNI I											
Jurassic											
Morrison	JM										
Ellis Group	JE										
Swift/Vang./Sund./Masefield	JES	**1647.1**	**5404.0**	**1102.2**	**3616.0**	**1257.3**	**4125.0**	**1622.8**	**5324.0**	**1629.8**	**5347.0**
Rierdon/Melita	JER	1780.0	5840.0	1176.5	3860.0	1351.2	4433.0	1745.9	5728.0	1770.9	5810.0
Piper/Sawtooth/Shaunavon	JEP										
ABSAROKA											
Triassic-Permian											
Spearfish/L.Watrou./L.Amaranth	TPS	**1875.1**	**6152.0**	**1354.5**	**4444.0**	**1531.6**	**5025.0**	**1922.7**	**6308.0**	**1909.3**	**6264.0**
Permian											
Minnekahta/Opeche	PMO	2033.3	6671.0					2028.4	6655.0	1988.5	6524.0
Pennsylvanian											
Amsden-Minnel.-Broom Cr. Gr.	PA	2082.4	6832.0					2058.9	6755.0		
KASKASKIA II											
Mississippian-Devonian											
Big Snowy Group	MB	**2236.6**	**7338.0**					**2137.6**	**7013.0**	**2282.6**	**7489.0**
Heath	MBH										
Otter	MBO										
Kibbey (Sandstone/Limestone)	MBK	2281.7	7486.0					2247.6	7374.0	2387.8	7834.0
Madison Group	MM	2318.3	7606.0	**1417.3**	**4650.0**	**1635.6**	**5366.0**	2293.0	7523.0	2429.9	7972.0
Charles/Castle Reef D./Sun R.	MMC										
Mission Canyon	MMM					1756.9	5764.0				
Lodgepole/Banff/Souris Val.	MML	2559.1	8396.0			1821.8	5977.0	2668.8	8756.0	2763.0	9065.0
Three Forks Group	MDT										
Bakken/Exshaw (Miss/Dev)	MDTB			1806.2	5926.0	2115.3	6940.0	2875.2	9433.0	3020.9	9911.0
KASKASKIA I											
Devonian											
Three Forks/Torquay/Lyeton	DTT	**2747.2**	**9013.0**	**1819.7**	**5970.0**	**2135.4**	**7006.0**	**2901.1**	**9518.0**	**3037.0**	**9964.0**
Potlatch	DP										
Saskatchewan-Jefferson Gr.	DSJ										
Birdbear/Nisku/Calmar	DSB	2772.5	9096.0	1880.0	6168.0	2199.1	7215.0	2974.8	9760.0	3109.0	10200.0
Duperow	DSD	2793.2	9164.0	1914.8	6282.0	2231.4	7321.0	3010.5	9877.0	3136.4	10290.0
Manitoba Group	DM										
Souris River/Maywood	DMS					2372.9	7785.0	3159.9	10367.0	3237.0	10620.0
Dawson Bay	DMD			2174.4	7134.0	2472.8	8113.0	3246.1	10650.0	3315.6	10878.0
Elk Point Group	DE										
Prairie Evaporite	DEP			2226.9	7306.0	2523.7	8280.0	3291.8	10800.0	3346.7	10980.0
Winnipegosis	DEW			2336.6	7666.0	2680.7	8795.0	3441.2	11290.0	3361.9	11030.0
Ashern	DEA										
TIPPECANOE											
Silurian											
Interlake/Cedar Lake	SI	**2901.7**	**9520.0**	**2379.3**	**7806.0**	**2722.2**	**8931.0**	**3518.3**	**11543.0**	**3437.5**	**11278.0**
Ordovician											
Big Horn Group	OB										
Stonewall Formation	OBST										
Stony Mountain	OBS	3048.0	10000.0	2626.8	8618.0	2968.8	9740.0	3883.2	12740.0	3753.6	12315.0
Red River	OBR	3087.6	10130.0	2657.9	8720.0	3002.3	9850.0	3929.2	12891.0	3799.0	12464.0
Winnipeg Group	OW	3255.6	10681.0	2812.7	9228.0	3168.7	10396.0	4118.5	13512.0	4006.6	13145.0
SAUK											
Cambrain/Ordovician											
Deadwood	COD	**3291.2**	**10798.0**	**2871.8**	**9422.0**	**3243.7**	**10642.0**	**4229.4**	**13876.0**	**4110.5**	**13486.0**
PRECAMBRIAN	PC										
Total Depth	TD	3299.2	10824.0	3002.6	9851.0	3331.5	10930.0	4252.0	13950.0	4130.0	13550.0

Table A.1 Stratigraphic picks (continued)

		Well 46		Well 47		Well 48		Well 82	
		m.	ft.	m.	ft.	m.	ft.	m.	ft.
Kelly Bushing	KB	723.0	2372.0	767.2	2517.0	747.7	2453.0	682.1	2238.0
Ground Level	GL	716.3	2350.0	762.0	2500.0	743.7	2440.0	676.0	2218.0
ZUNI II									
Cretaceous									
Montana Group	KM								
Pierre Shale/Riding Mountain	KMP					359.7	1180.0		
Bearpaw	KMB								
Judith River/Belly River	KMJ								
Claggett/Lea Park	KMC								
Eagle/Milk River/ Virgelle	KME								
Colorado Group	KC							1064.4	3492.0
Niobrara/1st WS/Kevin sh.	KCN								
Carlile/Bowd/Ferdig/U.Col Sh	KCC								
Greenhorn Shale/2nd White Specks	KCG	1179.3	3869.0	1151.5	3778.0	1026.3	3367.0	1070.8	3513.0
Belle Fou./Graneros/L.Color.	KCB								
Blackleaf/Mowry/Fish Scale Z.	KCM	1313.7	4310.0	1296.6	4254.0	1164.6	3821.0	1141.5	3745.0
Newcl./Muddy/Bow Is./Viking	KCV					1185.7	3890.0	1189.9	3904.0
Skull Cr./Joli Fou/Thermopolis	KCS								
Mannville/Inyan Kara/Dakota Gp.	KD	1410.6	4628.0	1393.9	4573.0	1263.1	4144.0	1250.9	4104.0
Dakota/Fall R./Pense/Swan R.	KDD								
Kootenai/Fuson/Cantaur	KDK								
Sunburst	KDS								
ZUNI I									
Jurassic									
Morrison	JM								
Ellis Group	JE								
Swift/Vang./Sund./Masefield	JES	**1530.7**	**5022.0**	**1495.0**	**4905.0**	**1339.6**	**4395.0**	**1379.2**	**4525.0**
Rierdon/Melita	JER	1665.4	5464.0	1616.4	5303.0	1450.8	4760.0	1522.2	4994.0
Piper/Sawtooth/Shaunavon	JEP								
ABSAROKA									
Triassic-Permian									
Spearfish/L.Watrou./L.Amaranth	TPS	**1782.5**	**5848.0**	**1706.9**	**5600.0**	**1524.0**	**5000.0**	**1717.5**	**5635.0**
Permian									
Minnekahta/Opeche	PMO	1840.1	6037.0	1757.5	5766.0	1549.6	5084.0		
Pennsylvanian									
Amsden-Minnel.-Broom Cr. Gr.	PA	1889.8	6200.0	1824.5	5986.0	1588.0	5210.0		
KASKASKIA II									
Mississippian-Devonian									
Big Snowy Group	MB	**2033.0**	**6670.0**	**1920.8**	**6302.0**	**1724.6**	**5658.0**		
Heath	MBH								
Otter	MBO								
Kibbey (Sandstone/Limestone)	MBK	2169.0	7116.0	2015.9	6614.0	1796.8	5895.0	**1804.4**	**5920.0**
Madison Group	MM	2204.9	7234.0	2049.5	6724.0	1812.0	5945.0		
Charles/Castle Reef/D. Sun R.	MMC							1834.3	6018.0
Mission Canyon	MMM								
Lodgepole/Banff/Souris Val.	MML	2472.8	8113.0	2278.1	7474.0	2026.0	6647.0	2332.6	7653.0
Three Forks Group	MDT								
Bakken/Exshaw (Miss/Dev)	MDTB	2692.6	8834.0					2350.3	7711.0
KASKASKIA I									
Devonian									
Three Forks/Torquay/Lyeton	DTT	**2695.0**	**8842.0**	**2468.3**	**8098.0**	**2200.7**	**7220.0**	**2375.9**	**7795.0**
Potlatch	DP								
Saskatchewan-Jefferson Gr.	DSJ								
Birdbear/Nisku/Calmar	DSB	2745.9	9009.0	2519.2	8265.0	2238.1	7343.0	2427.7	7965.0
Duperow	DSD	2767.6	9080.0	2538.7	8329.0	2255.8	7401.0	2460.3	8072.0
Manitoba Group	DM								
Souris River/Maywood	DMS	2845.0	9334.0	2606.6	8552.0			2614.9	8579.0
Dawson Bay	DMD	2881.9	9455.0					2726.7	8946.0
Elk Point Group	DE								
Prairie Evaporite	DEP							2767.9	9081.0
Winnipegosis	DEW							2864.5	9398.0
Ashern	DEA							2909.3	9545.0
TIPPECANOE									
Silurian									
Interlake/Cedar Lake	SI	**2966.6**	**9733.0**	**2686.5**	**8814.0**	**2370.4**	**7777.0**	**2925.5**	**9598.0**
Ordovician									
Big Horn Group	OB								
Stonewall Formation	OBST								
Stony Mountain	OBS	3179.1	10430.0	2831.0	9288.0	2485.0	8153.0	3060.2	10040.0
Red River	OBR	3221.7	10570.0	2869.7	9415.0	2520.1	8268.0	3164.1	10381.0
Winnipeg Group	OW	3422.6	11229.0	3056.2	10027.0	2699.0	8855.0	3118.1	10230.0
SAUK									
Cambrain/Ordovician									
Deadwood	COD	**3474.4**	**11399.0**	**3180.4**	**10172.0**	**2747.5**	**9014.0**	**3157.7**	**10360.0**
PRECAMBRIAN	PC	**3700.6**	**12141.0**	**3269.0**	**10725.0**	**2863.9**	**9396.0**		
Total Depth	TD	3724.0	12218.0	3287.0	10784.0	2921.2	9584.0	3269.9	10728.0

UNIVERSITY OF SASKATCHEWAN

College of Graduate Studies and Research

SUMMARY OF DISSERTATION

Submitted in partial fulfillment

of the requirements for the

DEGREE OF DOCTOR OF PHILOSOPHY

by

Pál Rédly

Department of Geological Sciences

University of Saskatchewan

Spring 1998

Examining Committee:

Dr. D. de Boer	Dean/Associate Dean, Dean's Designate, Chair College of Graduate Studies and Research
Dr. James Basinger	Chair of Advisory Committee, Department of Geological Sciences
Dr. Zoltán Hajnal	Supervisor, Department of Geological Sciences
Dr. Mel Stauffer	Department of Geological Sciences
Dr. Don Gendzwill	Department of Geological Sciences
Dr. Brian Pratt	Department of Geological Sciences
Dr. George Sofko	Department of Physics

External Examiner:

Dr. James Brown

Department of Geology and Geophysics

University of Calgary

2500 University Drive N.W.

Calgary, Alberta T2N 1N4

Tectonostratigraphic Evolution of the Williston Basin

In the Williston Basin five regional seismic profiles, covering ~3090 km were utilized for a comprehensive study of this complex geologic feature. 2300 km field data were added to the existing 790 km profile. The novel seismic information in conjunction with a sizeable number of wireline data and incorporation of stuctural and isopach maps provided a unique data environment for development of a new elaborate tectonostratigraphic model of this major continental depression.

Standard reflection seismic processing procedures were implemented with special emphasis on regional perspectives, including "Earth curvature correction", to generate images of the basin fill. The latter helped to reveal the true nature of this large scale cratonic basin. This novel information permitted new approaches in establishing the deformation styles in the Williston Basin.

Structural studies of the newly reprocessed regional seismic profiles revealed the compressional nature of the radially arranged tectonic elements in the center of the basin, and the extensional character of the peripheral regions. The results suggest that axisymmetric deformation controlled the early stages of the Williston Basin area, and was the causal factor of the oval shape of the basin.

In the first, "pre-Williston" phase, the region was uplifted by an axisymmetric lithospheric intrusion creating radial extensional signatures in the central zone and compressional structures in the surroundings. Erosion and thermal cooling and/or phase change of the mantle material led to the initiation of the basin subsidence.
Consequently, in the "intracratonic phase" (Sauk – Absaroka), the pre-existing radial and circumferentially arranged structures were periodically reactivated in the opposite sense. The active periods were unrelated to global orogenic events of the continent. The exception is the Kaskaskia I (Devonian) interval, when the territory was tilted to the northwest and the axisymmetric cause of the subsidence was overprinted.

The subsequent "foreland phase" (Zuni – Tejas), was dominated by lateral forces of the Sevier and Laramide orogenies. This plate-margin-related major tectonic development was associated with the NNW-SSE elliptical elongation of the basin and the related highly prevalent NE-SW/NW-SE faulting and fracturing. Additional consequences of this process were offsetting and rotation of the pre-existing radial and circumferential structural features. These radial and circumferential structural features of the Williston Basin may be recognizable in comparable cratonic environments (e.g., Michigan Basin, Paris Basin).

Comprehensive seismic/sequence stratigraphiy was developed throughout the basin. In the Sauk – Absaroka interval the sequence stratigraphic and the lithostratigraphic boundaries are generally identical. In the Zuni – Tejas interval, when the clastic sedimentation was dominant, the two subdivisions are not identical. In these younger strata 16 sequence stratigraphic units were identified. More detailed subdivision of the interval containing the Eagle Sandstone revealed that two major sources of the terrigenous sediments are directly recognizable on the seismic profiles, beyond 500 km east of the shorelines.

BIOGRAPHICAL

August, 1963	Born in Budapest, Hungary
June, 1987	M.Sc. in Geology, Eötvös Loránd University

HONOURS

Graduate Scholarship, University of Saskatchewan, 1995-1997
Füzessy Award, Saskatchewan Geological Society, 1995
Graduate Teaching Fellowship, University of Saskatchewan, 1994-1995
Scholarship, Canadian Institute of Mines and Metallurgy, 1994
Sholarship, Wascana Energy Resources, Ltd., 1992-1995

PUBLICATIONS

Rédly, P. and Hajnal, Z. (1997) Interpretation of regional seismic sections from the Williston Basin – a 'Slossian' approach (abstract), *Canadian Society of Petroleum Geologists and Society for Economic Paleontologists, Joint Convention 1997, Program with Abstracts, p. 235*

Rédly, P. and Hajnal, Z. (1996) Phanerozoic basinwide folding in the Williston and the Rocky Mountain Foreland basins (abstract), *Geological Society of Canada and Mineralogical Society of Canada, Annual Meeting, 1996, Program with Abstracts, v. 21., p. A-78.*

Rédly, P. and Hajnal, Z. (1996) Basinwide fold evolution and geometric development of cratonic – foreland basin interaction (abstract), *1996 AAPG Annual Convention, Official Program and Abstracts, p. A118.*

Rédly, P. and Hajnal, Z. (1995) Earth-curvature based interpretation of intracratonic and foreland basin evolution. A regional seismic study from Western Canada (abstract), *Geological Society of America, Abstracts with Program, v. 27(6), p. A-392*

Rédly, P. and Hajnal, Z. (1995) Tectono-stratigraphic evolution of the Williston Basin: A regional seismic stratigraphic study, **in** *L.D.V. Hunter and R.A. Schalla, eds., 7th International Williston Basin Symposium, p. 341-350.*

Attachment # 1

Pál Rédly

Tectonostratigraphic Evolution of the Williston Basin

Ph.D. Thesis, 1998
University of Saskatchewan

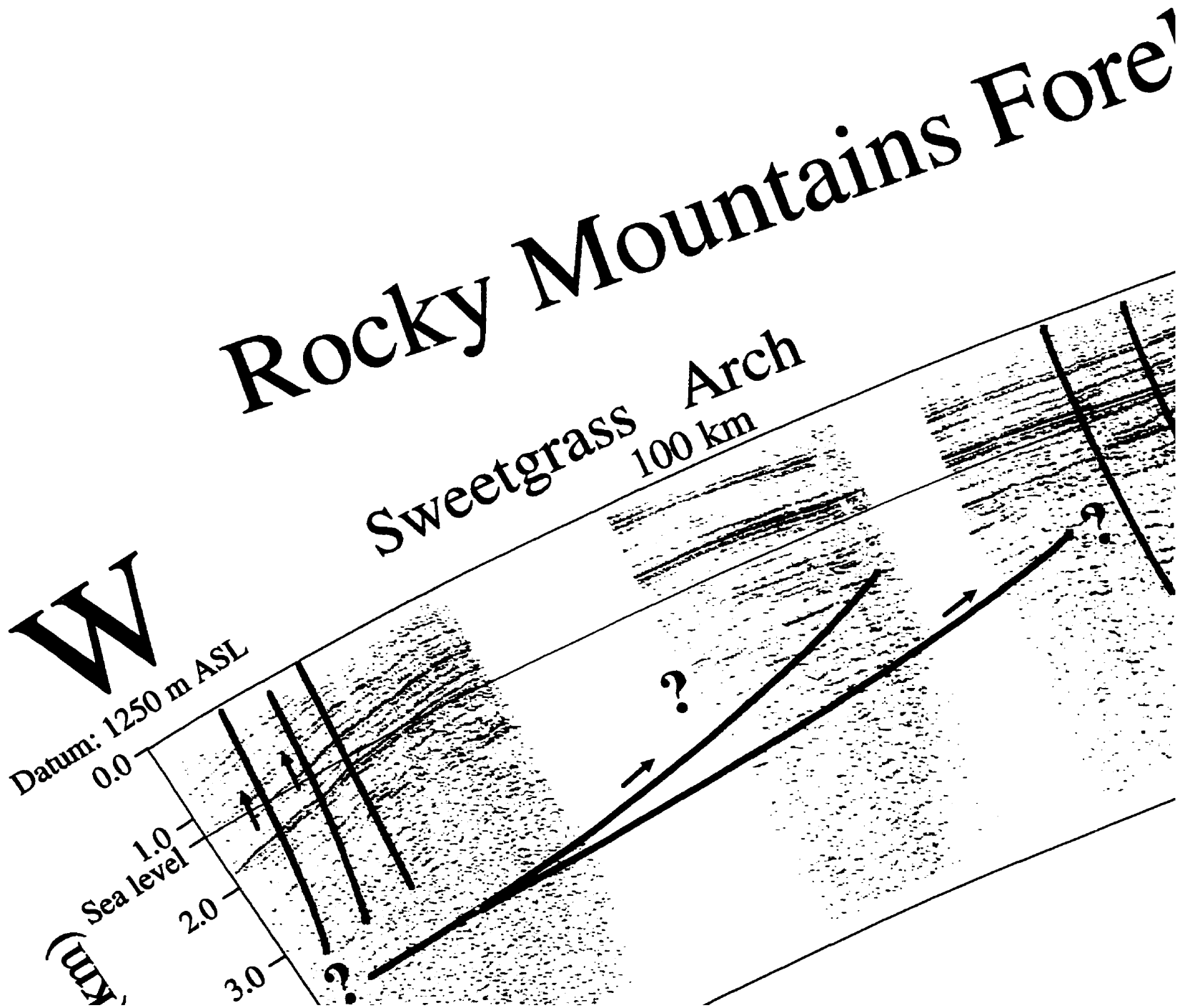

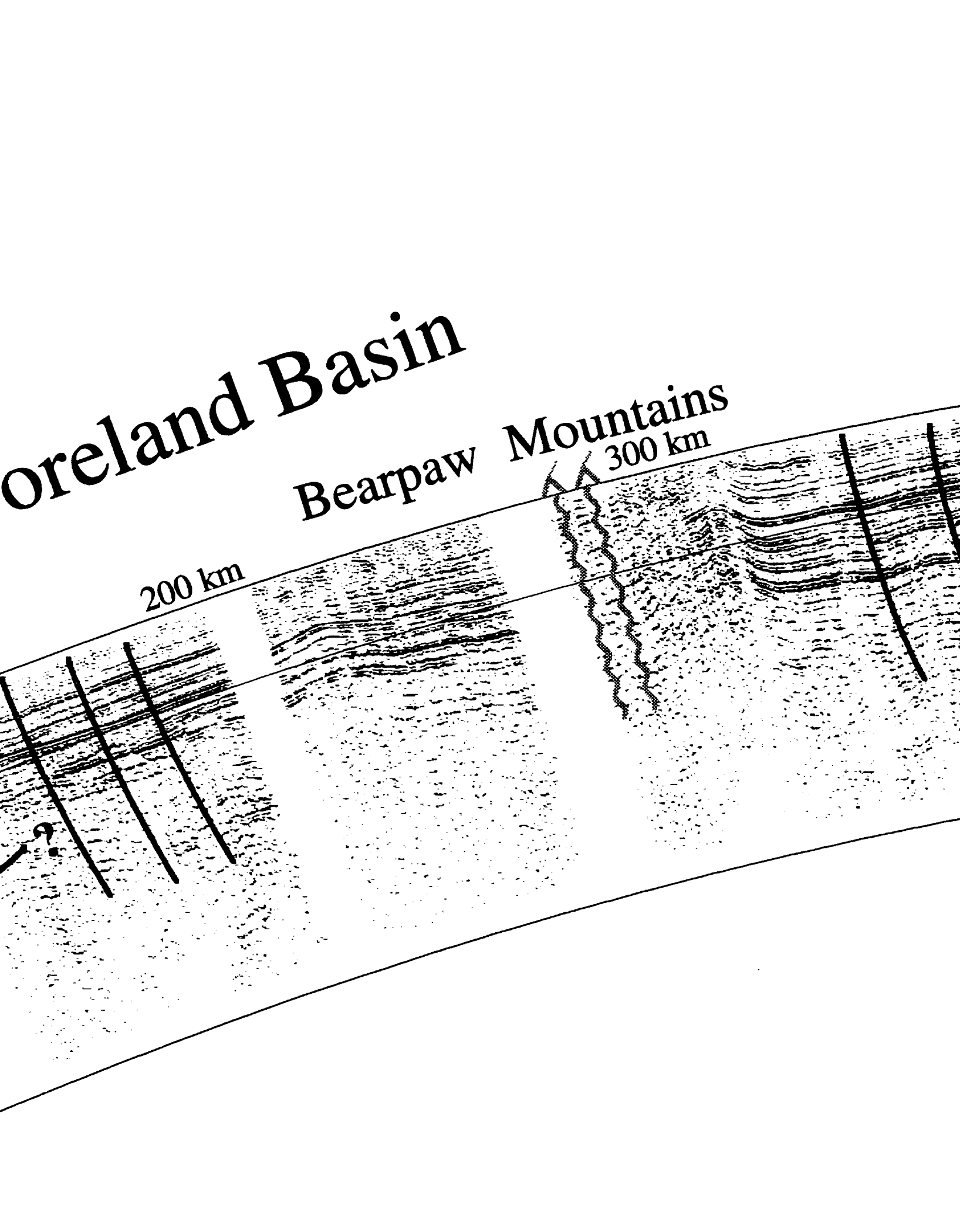
oreland Basin
Bearpaw Mountains
300 km
200 km
?

WE

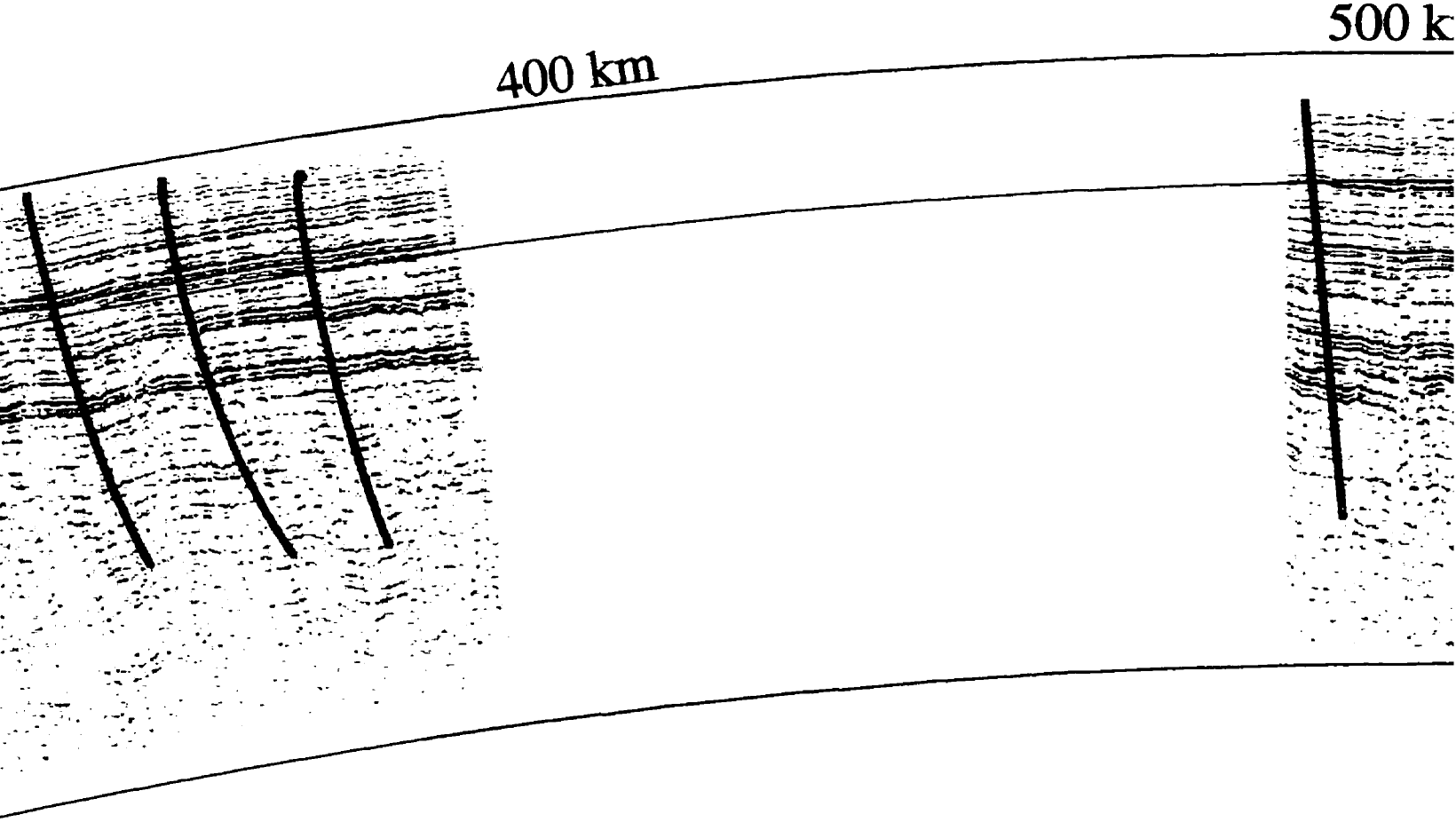

II Line

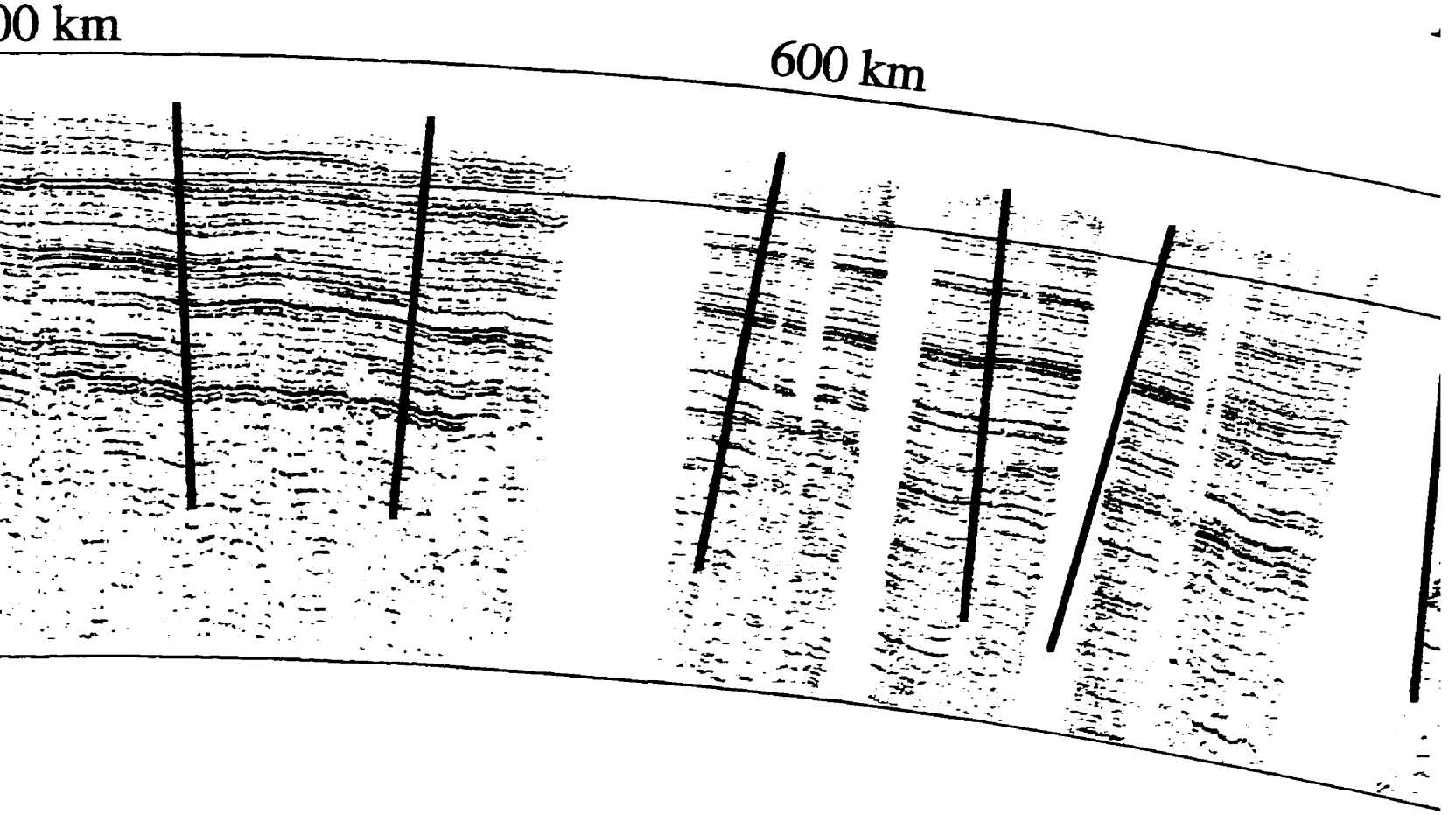

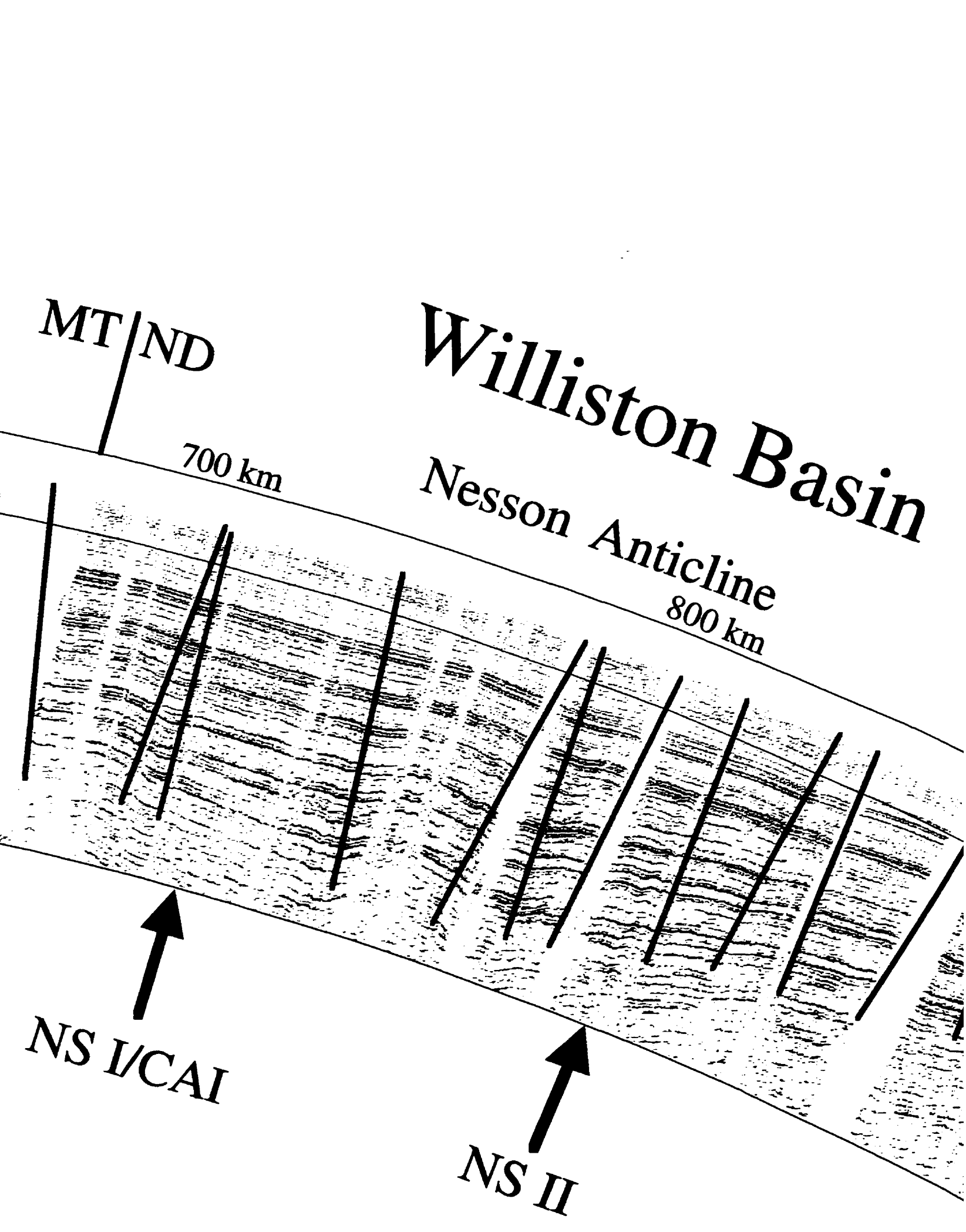
MT
ND
Williston Basin
700 km
Nesson Anticline
800 km
NS I/CAI
NS II

ton Basin
nticline
800 km
900 km
E
Datum: 1250 m ASL
0.0
1.0
Sea level
2.0

Sea level
2.0
3.0
4.0
5.0
6.0
Depth (km)
?


NS II

ea level
2.0
3.0
4.0
5.0
6.0
Depth (km)

Attachment # 2

Pál Rédly

Tectonostratigraphic Evolution of the Williston Basin

Ph.D. Thesis, 1998
University of Saskatchewan

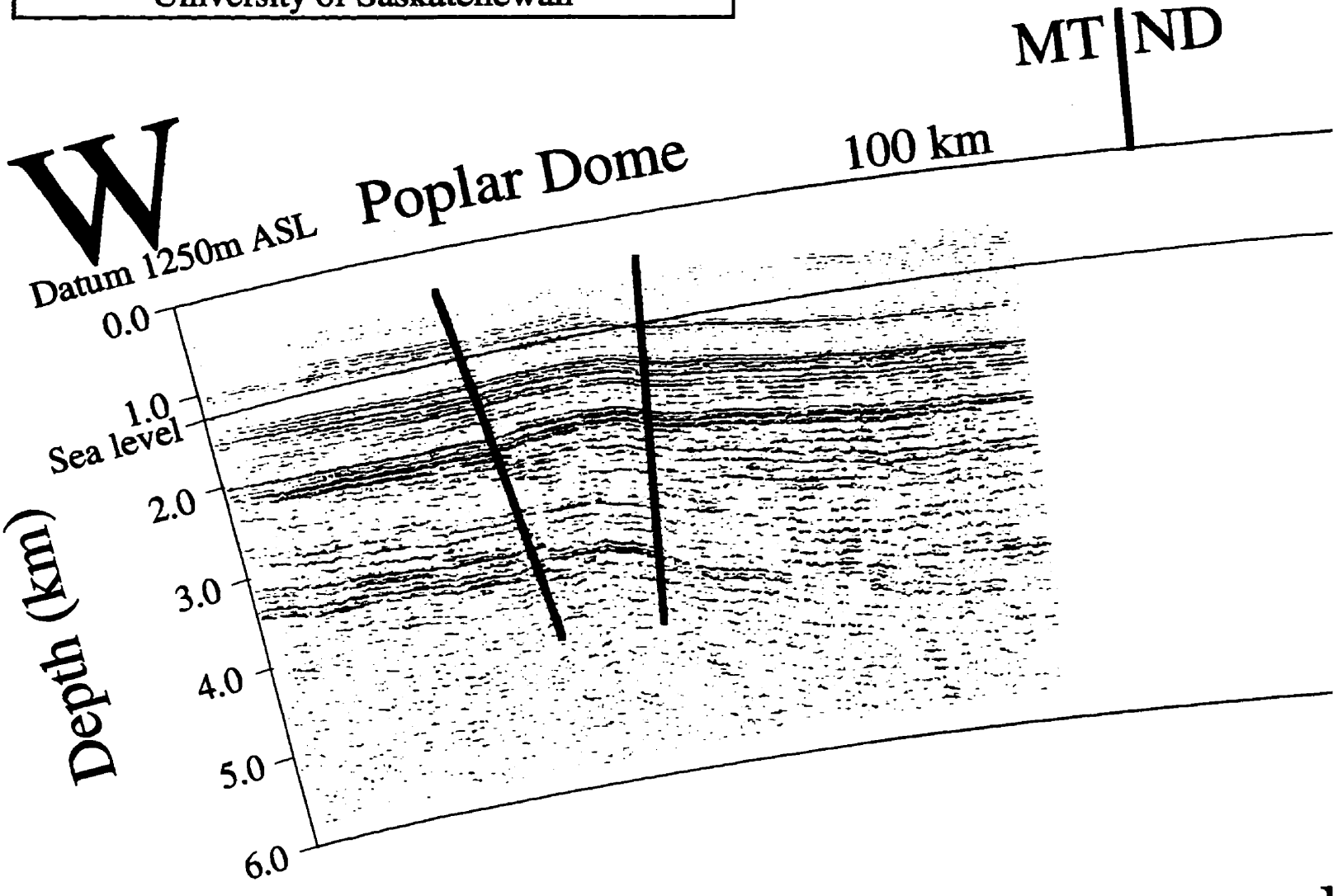

WE III Line

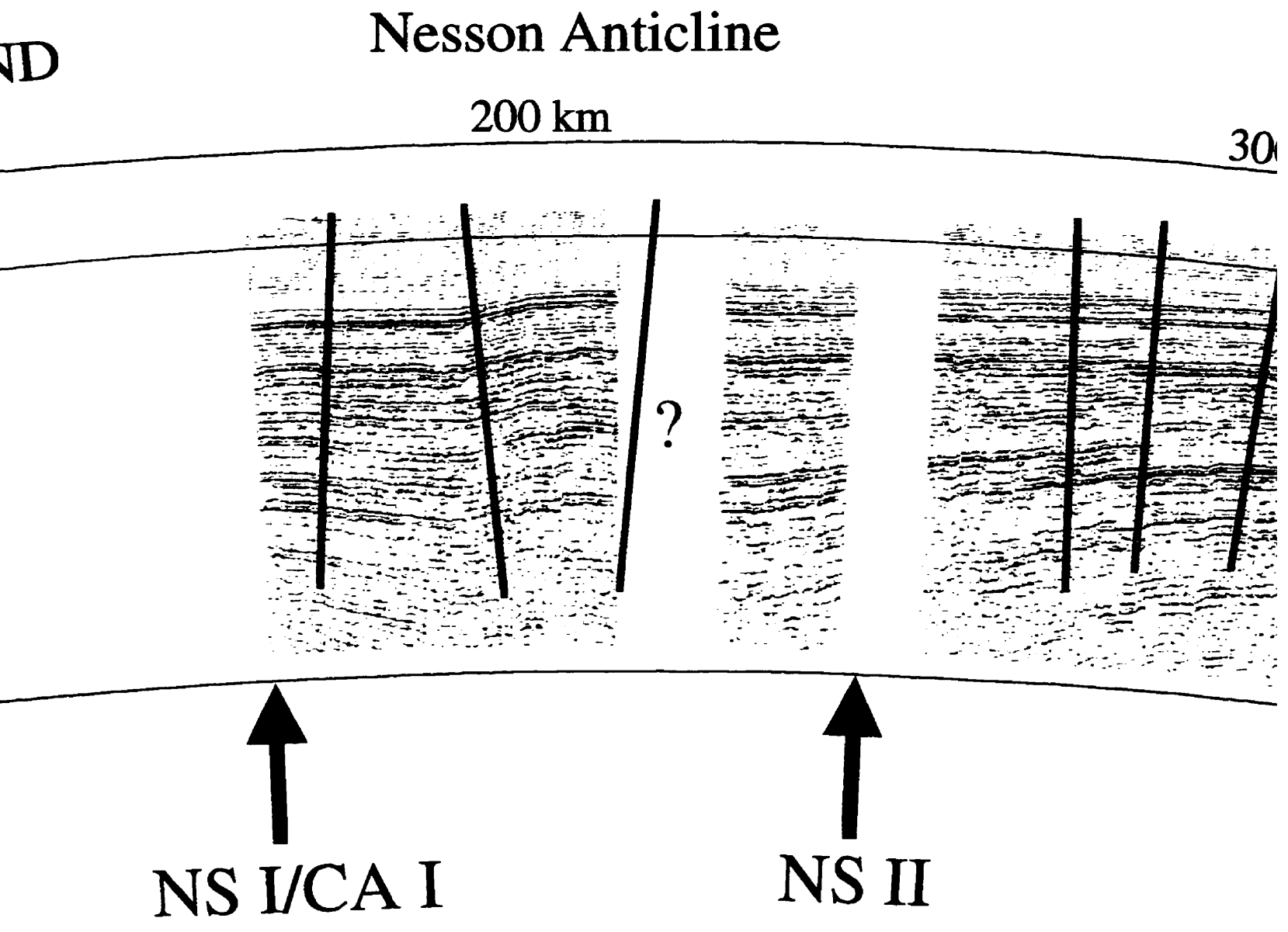

e

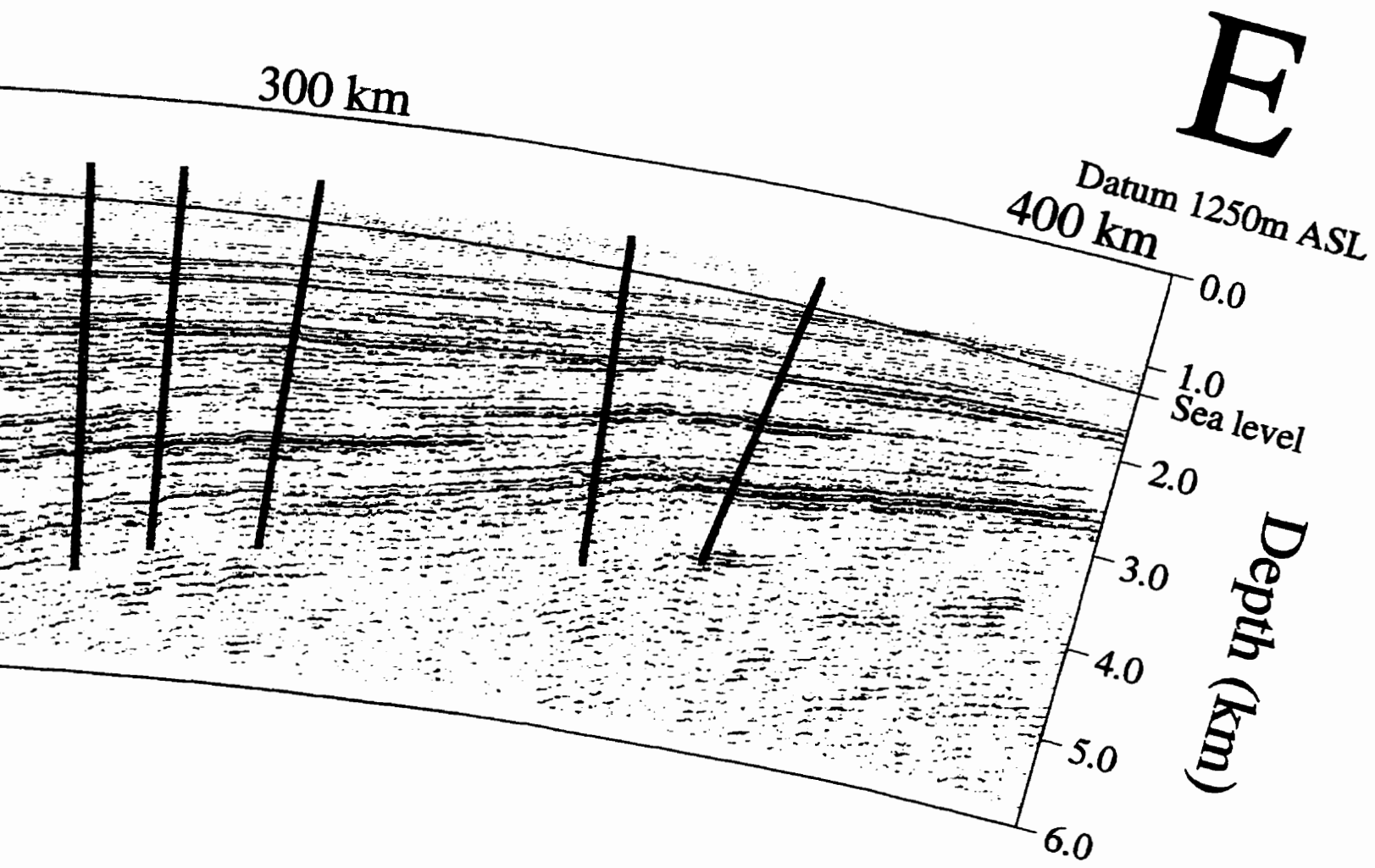
300 km
E
Datum 1250m ASL
400 km
0.0
1.0
Sea level
2.0
3.0
4.0
5.0
6.0
Depth (km)

Attachment # 3

Pál Rédly

Tectonostratigraphic Evolution of the Williston Basin

Ph.D. Thesis, 1998
University of Saskatchewan

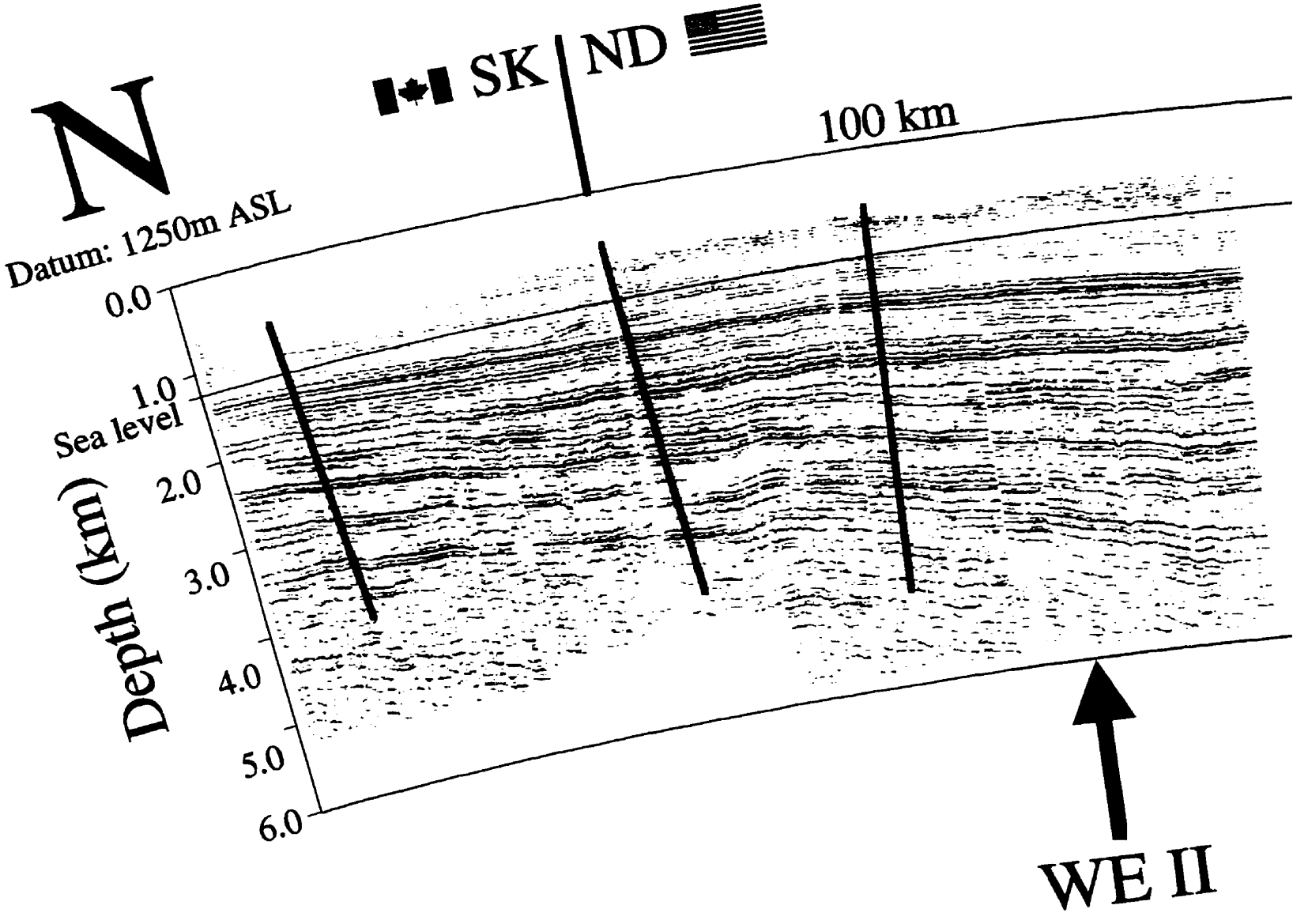

NS I Line

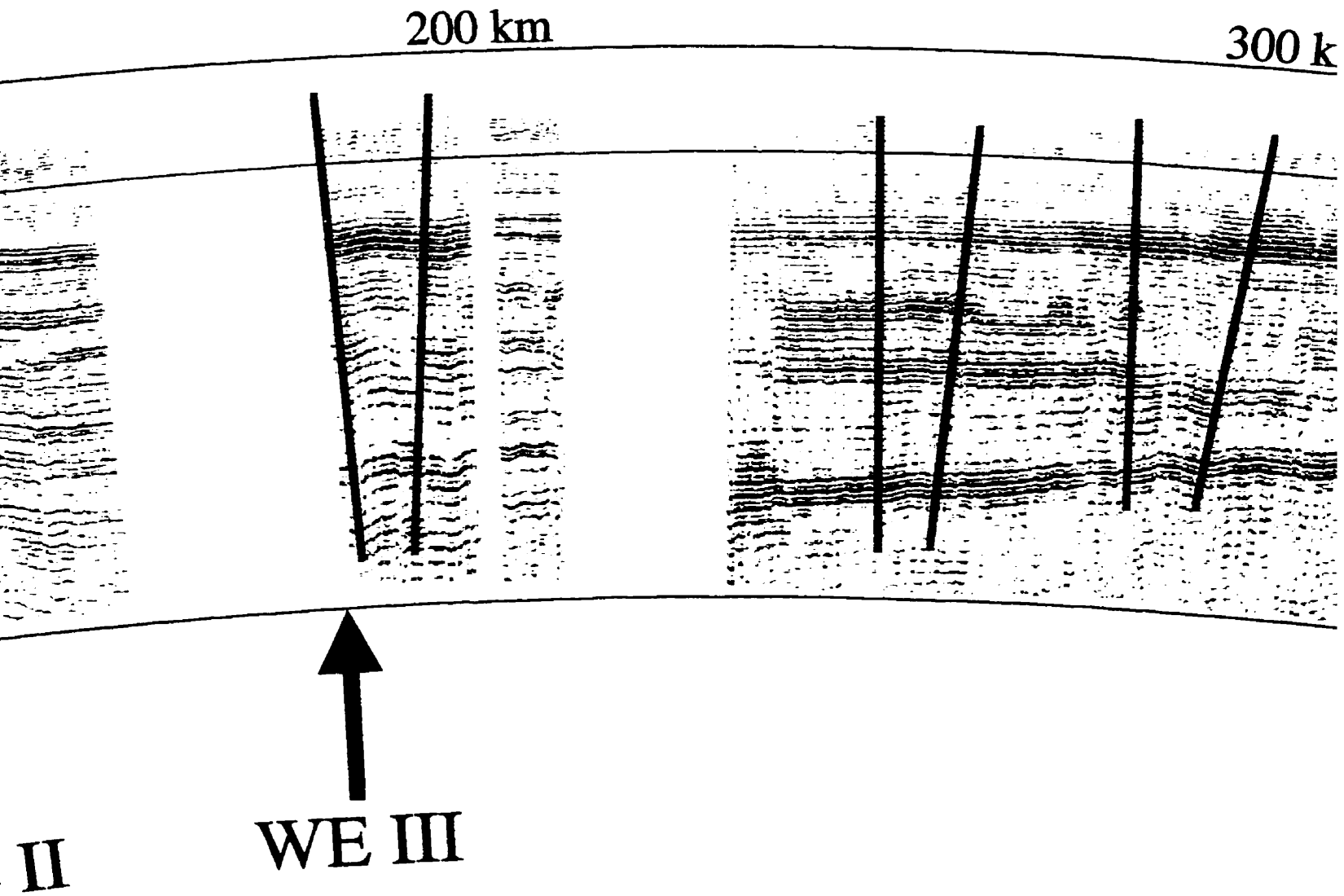

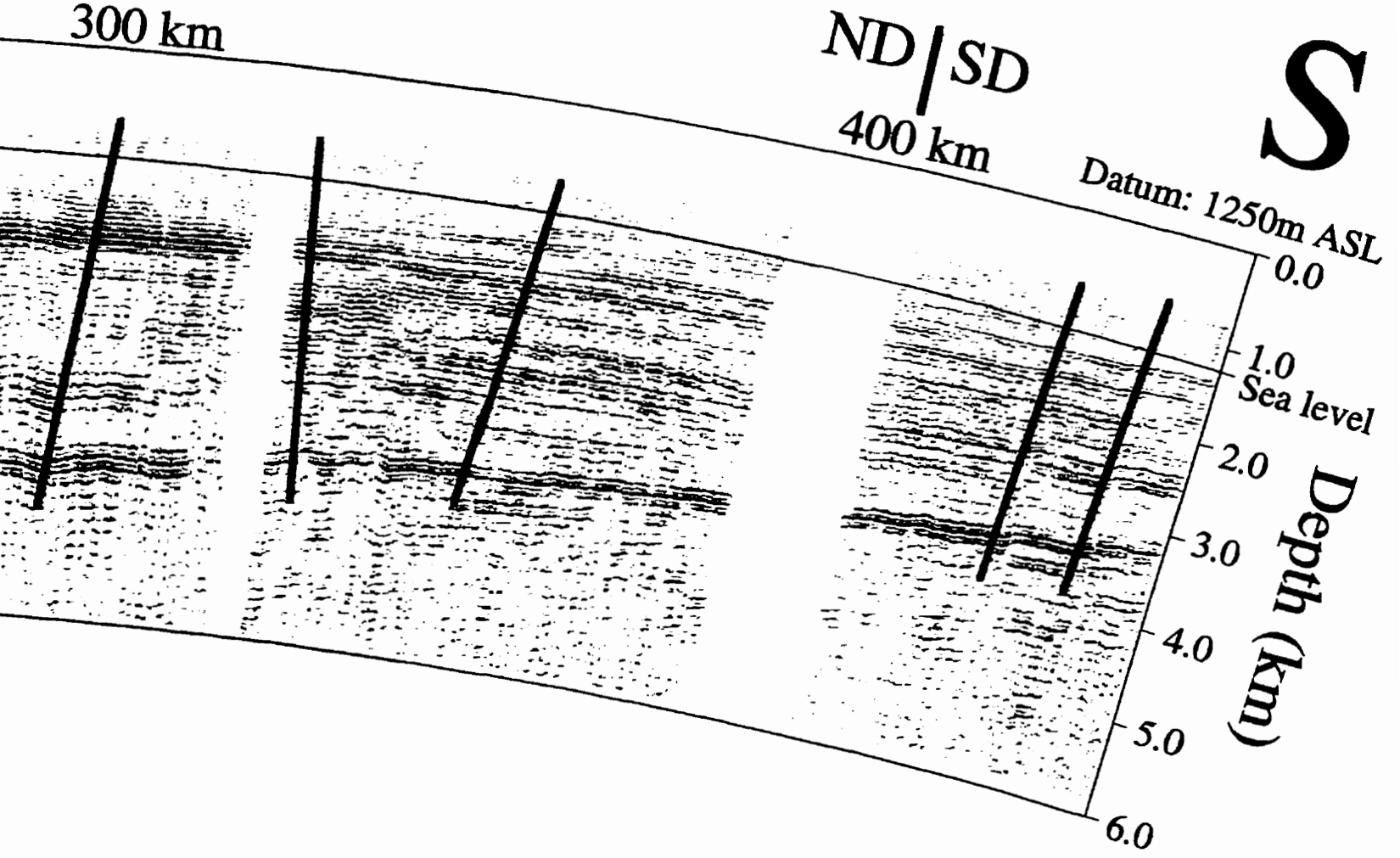
300 km
ND
SD
400 km
S
Datum: 1250m ASL
0.0
1.0
Sea level
2.0
3.0
4.0
5.0
6.0
Depth (km)

NOTE TO USERS

Oversize maps and charts are microfilmed in sections in the following manner:

LEFT TO RIGHT, TOP TO BOTTOM, WITH SMALL OVERLAPS

The following map or chart has been microfilmed in its entirety at the end of this manuscript (not available on microfiche). A xerographic reproduction has been provided for paper copies and is inserted into the inside of the back cover.

Black and white photographic prints (17"x 23") are available for an additional charge.

UMI

Attachment # 4

Pál Rédly

Tectonostratigraphic Evolution of the Williston Basin

Ph.D. Thesis, 1998
University of Saskatchewan

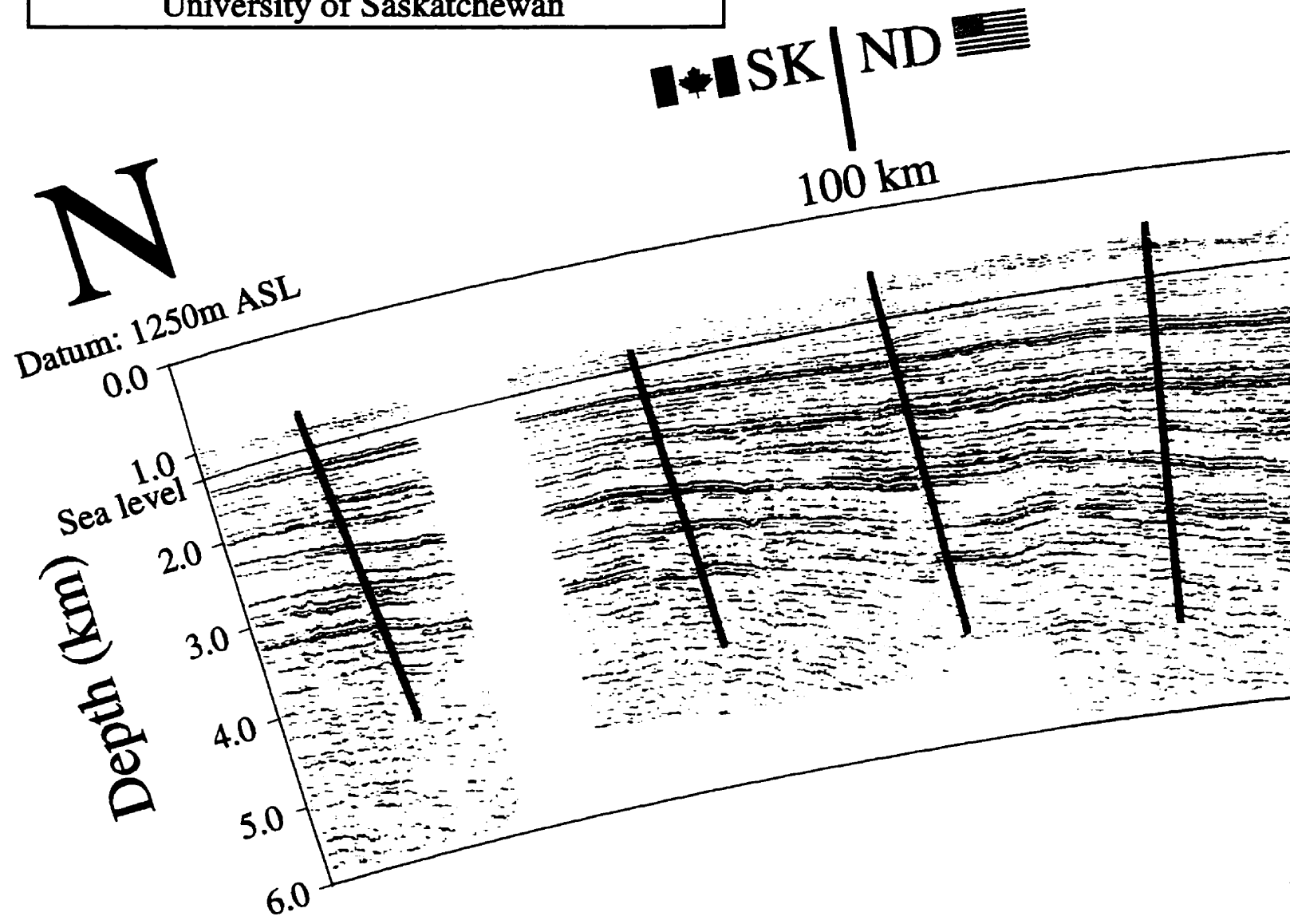

CA I Line

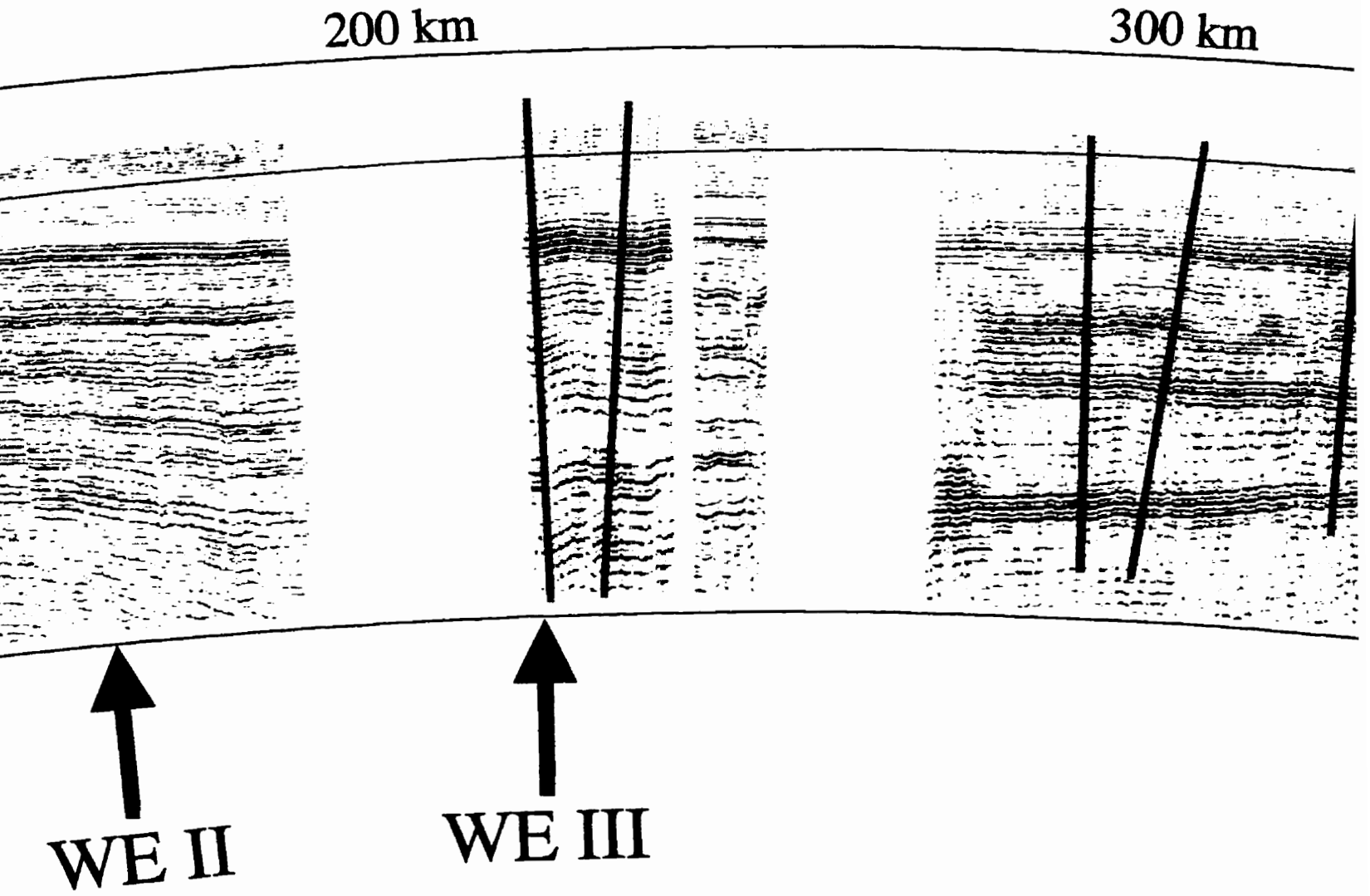

Line

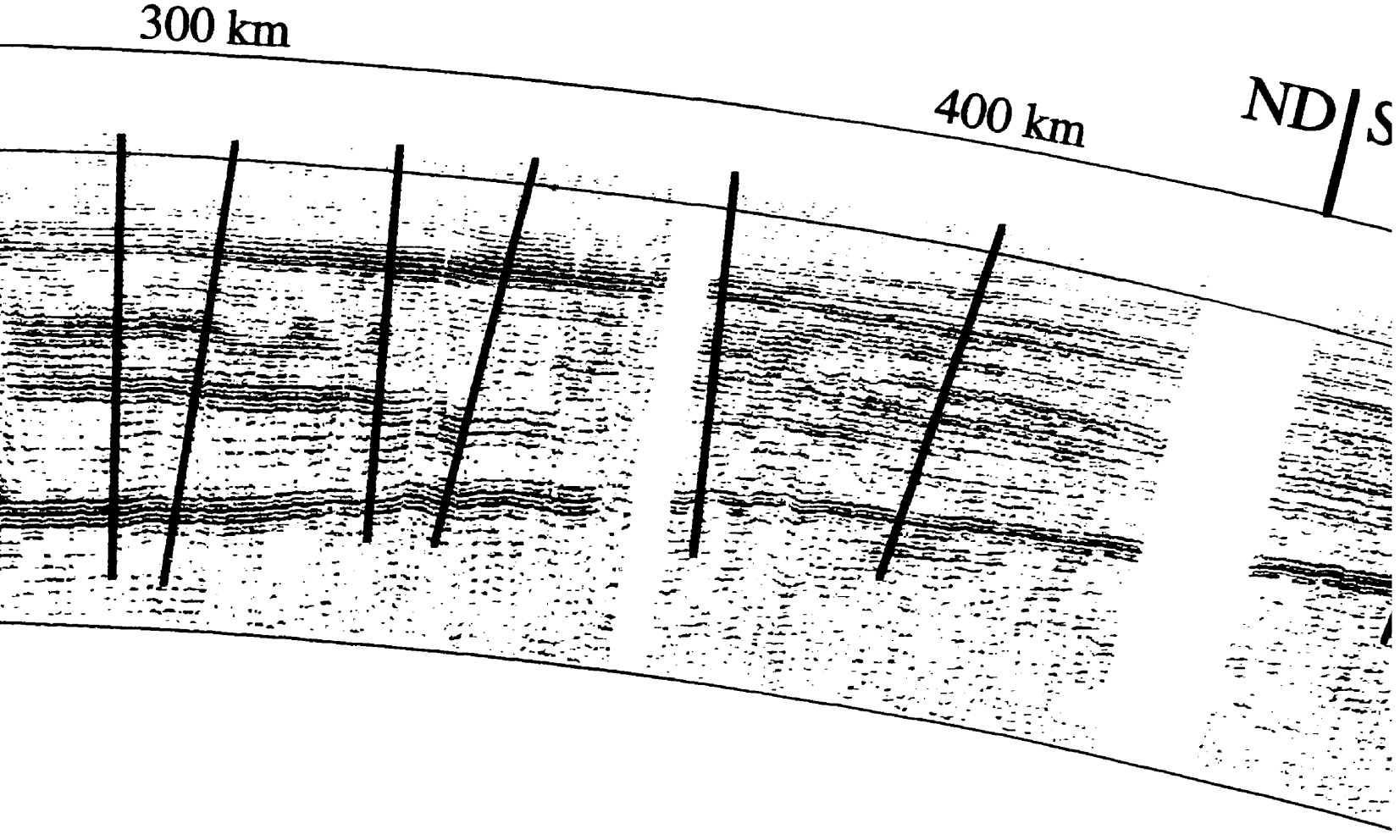

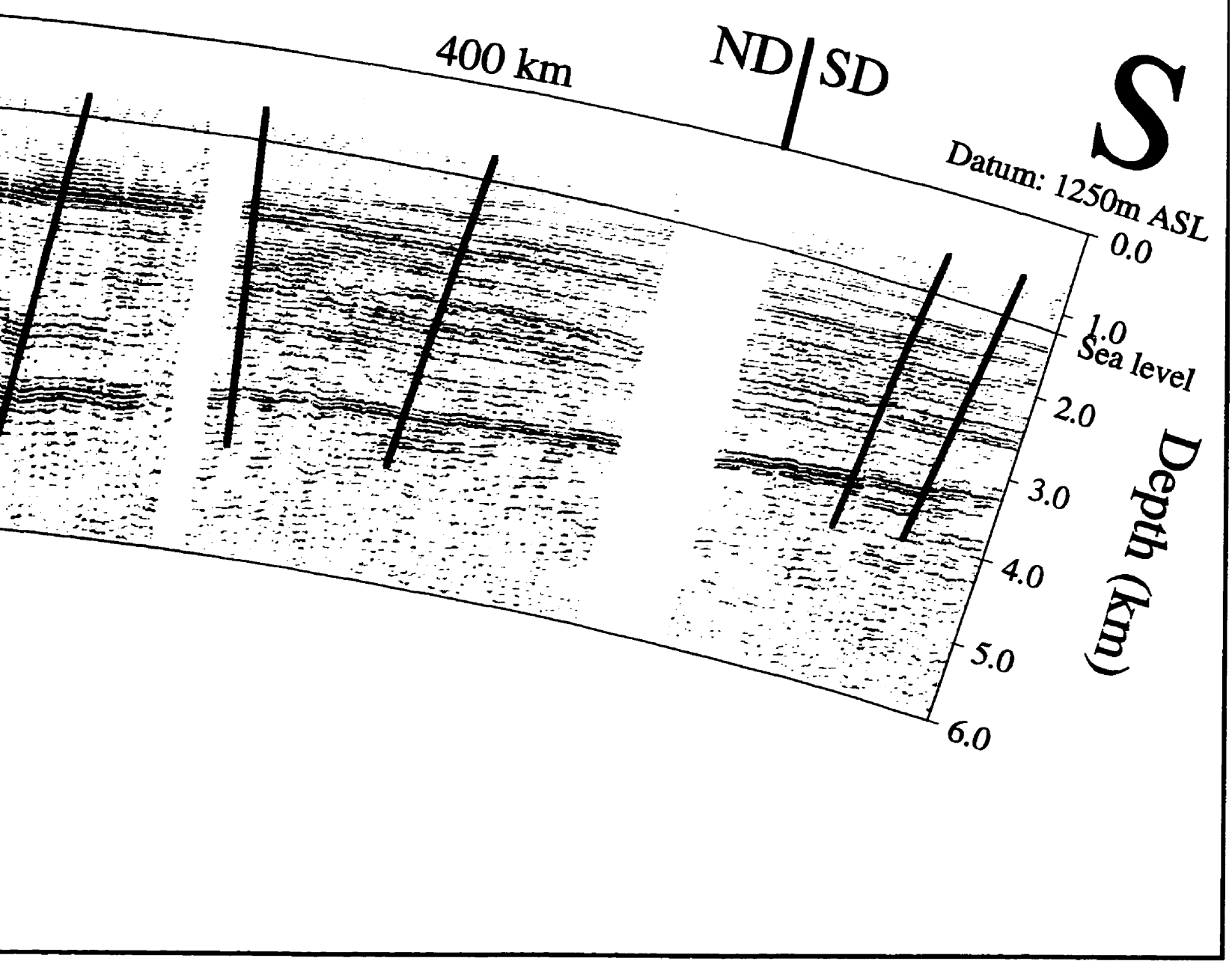
400 km
ND
SD
S
Datum: 1250m ASL
0.0
1.0
Sea level
2.0
3.0
4.0
5.0
6.0
Depth (km)

Attachment # 5

Pál Rédly

Tectonostratigraphic Evolution of the Williston Basin

Ph.D. Thesis, 1998
University of Saskatchewan

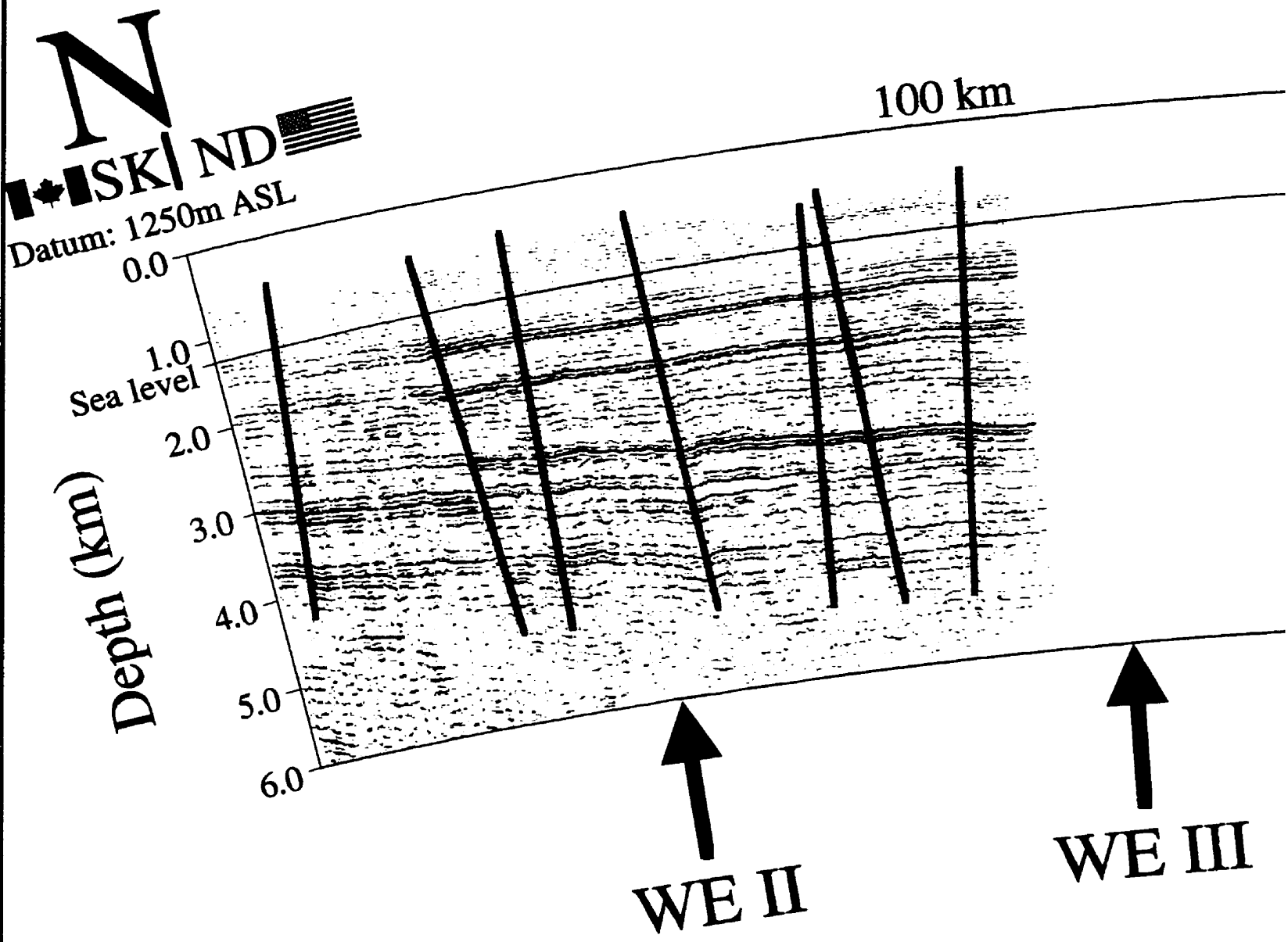

NS II Line

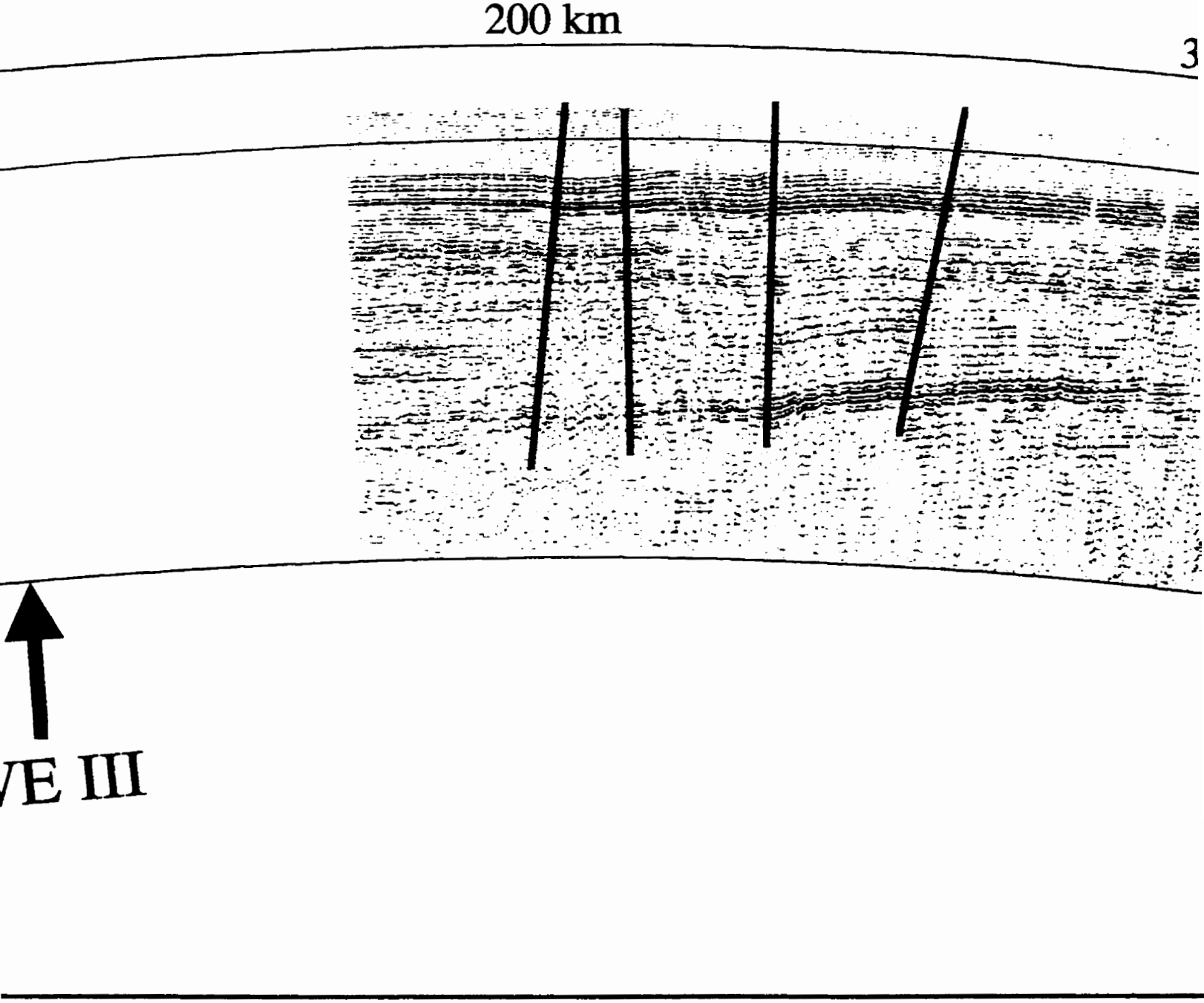

e

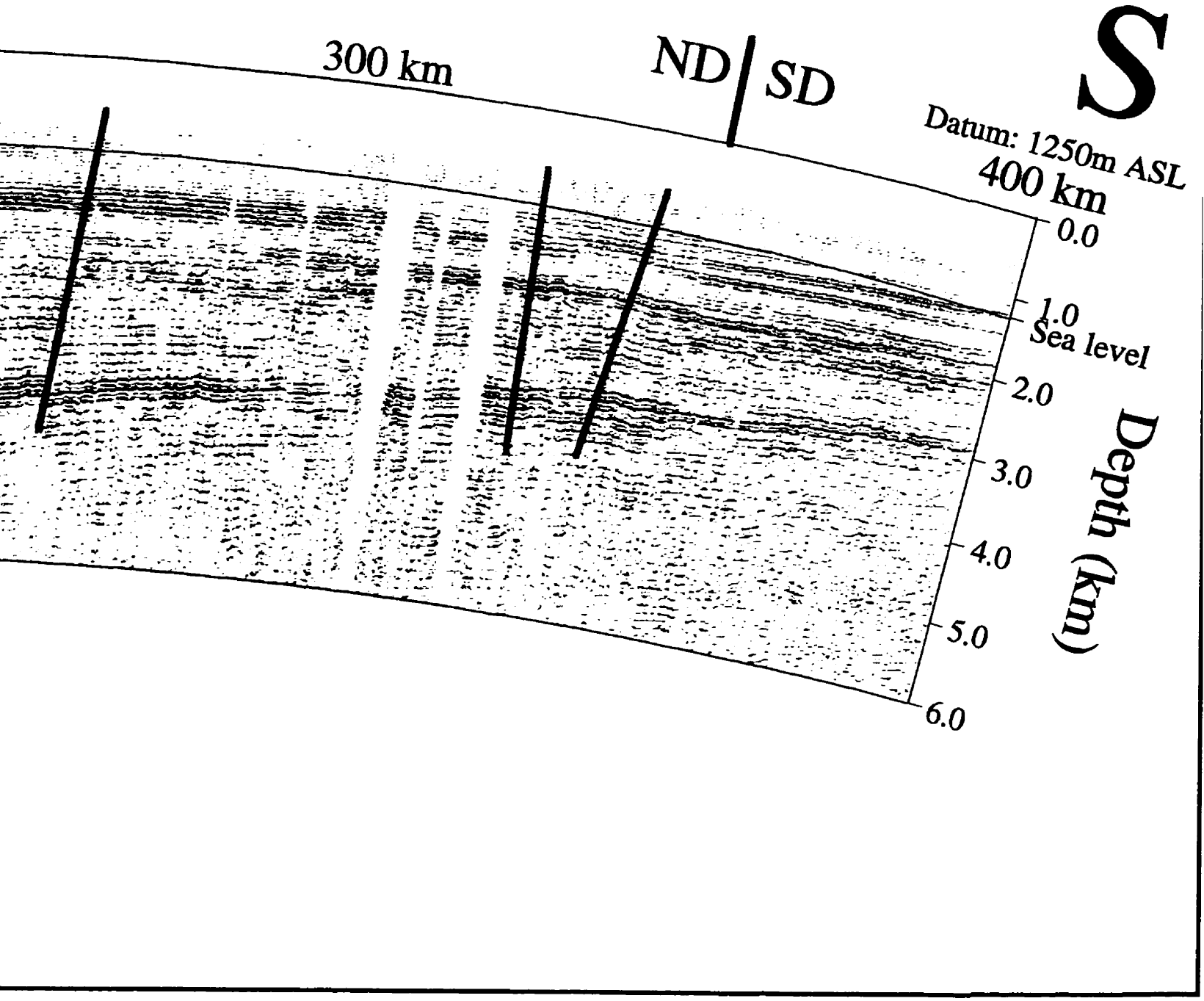
300 km
ND
SD
S
Datum: 1250m ASL
400 km
0.0
1.0
Sea level
2.0
3.0
4.0
5.0
6.0
Depth (km)

IMAGE EVALUATION TEST TARGET (QA-3)

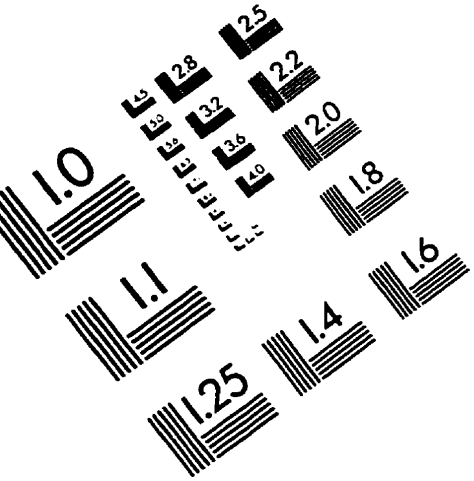

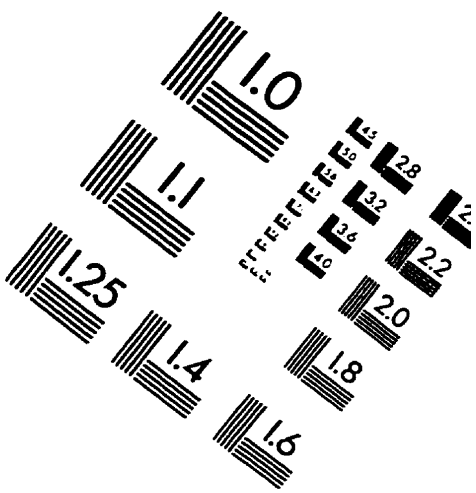

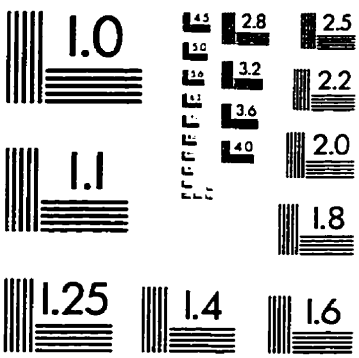

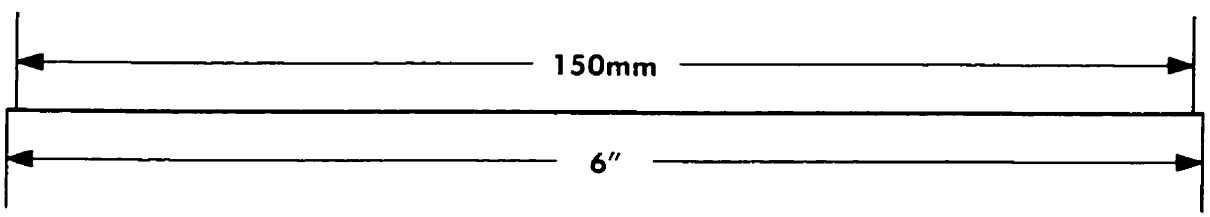

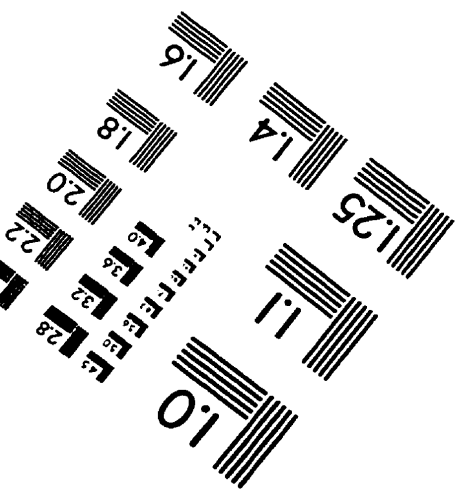

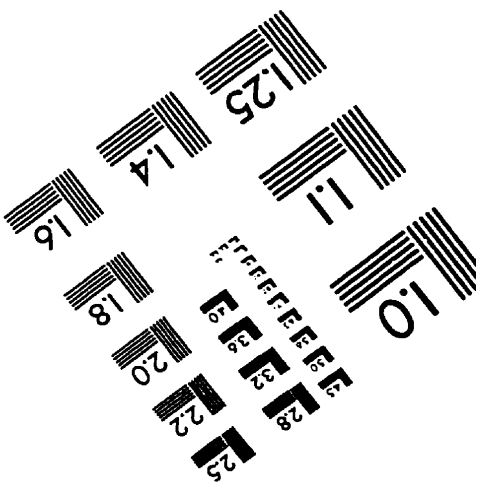

APPLIED IMAGE, Inc
1653 East Main Street
Rochester, NY 14609 USA
Phone: 716/482-0300
Fax: 716/288-5989